Non-Linear Dynamics and Fundamental Interactions

Edited by

Faqir Khanna and Davron Matrasulov

Non-Linear Dynamics and
Fundamental Interactions

NATO Science Series

A Series presenting the results of scientific meetings supported under the NATO Science Programme.

The Series is published by IOS Press, Amsterdam, and Springer (formerly Kluwer Academic Publishers) in conjunction with the NATO Public Diplomacy Division.

Sub-Series

I. **Life and Behavioural Sciences**	IOS Press
II. **Mathematics, Physics and Chemistry**	Springer (formerly Kluwer Academic Publishers)
III. **Computer and Systems Science**	IOS Press
IV. **Earth and Environmental Sciences**	Springer (formerly Kluwer Academic Publishers)

The NATO Science Series continues the series of books published formerly as the NATO ASI Series.

The NATO Science Programme offers support for collaboration in civil science between scientists of countries of the Euro-Atlantic Partnership Council. The types of scientific meeting generally supported are "Advanced Study Institutes" and "Advanced Research Workshops", and the NATO Science Series collects together the results of these meetings. The meetings are co-organized by scientists from NATO countries and scientists from NATO's Partner countries — countries of the CIS and Central and Eastern Europe.

Advanced Study Institutes are high-level tutorial courses offering in-depth study of latest advances in a field.
Advanced Research Workshops are expert meetings aimed at critical assessment of a field, and identification of directions for future action.

As a consequence of the restructuring of the NATO Science Programme in 1999, the NATO Science Series was re-organized to the four sub-series noted above. Please consult the following web sites for information on previous volumes published in the Series.

http://www.nato.int/science
http://www.springer.com
http://www.iospress.nl

Series II: Mathematics, Physics and Chemistry – Vol. 213

Non-Linear Dynamics and Fundamental Interactions

edited by

Faqir Khanna

University of Alberta,
Edmonton, AB, Canada

and

Davron Matrasulov

Uzbek Academy of Sciences,
Tashkent, Uzbekistan

PREFACE

This volume contains the papers presented at the NATO Advanced Research Institute on "Non-Linear Dynamics and Fundamental Interactions" held in Tashkent, Uzbekistan, from Oct.10-16,2004.

The main objective of the Workshop was to bring together people working in areas of Fundamental physics relating to Quantum Field Theory, Finite Temperature Field theory and their applications to problems in particle physics, phase transitions and overlap regions with the areas of Quantum Chaos. The other important area is related to aspects of Non-Linear Dynamics which has been considered with the topic of chaology. The applications of such techniques are to mesoscopic systems, nanostructures, quantum information, particle physics and cosmology. All this forms a very rich area to review critically and then find aspects that still need careful consideration with possible new developments to find appropriate solutions.

There were 29 one-hour talks and a total of seven half-hour talks, mostly by the students. In addition two round table discussions were organised to bring the important topics that still need careful consideration. One was devoted to questions and unsolved problems in Chaos, in particular Quantum Chaos. The other round table discussion considered the outstanding problems in Fundamental Interactions. There were extensive discussions during the two hours devoted to each area. Applications and development of new and diverse techniques was the real focus of these discussions.

The conference was ably organised by the local committee consisting of D.U. Matrasulov, M.M. Musakhanov, Kh.Yu. Rakhimov, A.A. Saidov, B.S. Yuldashev with P.K. Khabibullaev as the chair. A whole cadre of students helped with many detailed jobs. Our thanks go to Olga V. Karpova for help with the secretarial duties before, during and after the conference. The task of getting the proceedings ready for publication was carried out by Olga Karpova and Lee Grimard (University of Alberta). We thank them for their help.

The conference was held at the Grand Mir hotel in Tashkent. The hotel management provided every assistance possible to make the conference run smoothly.

Finally we wish to thank NATO Science Program for their financial assistance. Additional assistance was provided by Science and Technology center of Uzbekistan, Heat Physics department of Uzbek Academy of Sciences.

<div align="right">

Faqir Khanna
Davron Matrasulov

</div>

CONTENTS

Nonlinear Dynamics

Heat conduction in one dimensional systems: Fourier law, chaos, and heat control

Giulio Casati[(a,b)] and Baowen Li [(b)]

a) Center for Nonlinear and Complex Systems,
Universita' degli studi dell'Insubria, Como
Istituto Nazionale di Fisica della Materia,
Unita' di Como, and Istituto Nazionale di Fisica Nucleare,
sezione di Milano, Milano, Italy
b) Department of Physics, National University of Singapore,
Singapore 117542, Republic of Singapore

1. Introduction

"It seems there is no problem in modern physics for which there are on record as many false starts, and as many theories which overlook some essential feature, as in the problem of the thermal conductivity of non-conducting crystals" (Peierls, 1961). This statement by R. Peierls goes back to almost 50 years ago, yet it appears to be still valid. Compared with charge flow (electric current), much less is known about the heat flow.

Nevertheless, encouraging results have been obtained in recent years (see reviews(Bonetto et al, 1961) and the references therein). For example it is now known that in one dimensional systems of the Fermi-Pasta-Ulam (FPU) type (Lepri et al, 1998), heat conduction is anomalous and the coefficient of thermal conductivity κ diverges with the system size L as $\kappa \sim L^{2/5}$ (when the transverse motion is considered $\kappa \sim L^{1/3}$ (?)). The connection between anomalous conductivity and anomalous diffusion has been also established(Li and Wang, 2003; Li et al, 2005), which implies in particular that a subdiffusive system is an insulator in the thermodynamic limit and a ballistic system is a perfect thermal conductor, the Fourier law being therefore valid only when phonons undergo a normal diffusive motion. More profoundly, it has been clarified that exponential dynamical instability is a sufficient(Casati et al, 2005; Alonso et al, 2005) but not a necessary condition for the validity of Fourier law (Li et al, 2005; Alonso et al, 2002; Li et al, 2003; Li et al, 2004). These basic studies not only enrich our knowledge of the fundamental transport laws in statistical mechanics, but also open the way for applications such as designing novel thermal materials and/or

devices such as the thermal rectifier(Terrano et al, 2002; Li Wang Casati, 2004) and the thermal transistor(Li Wang Casati, 2004).

In this paper we give a brief review of the relation between microscopic dynamical properties and the Fourier law of heat conduction as well as the connection between anomalous conduction and anomalous diffusion. We then discuss the possibility to control the heat flow.

2. Microscopic dynamics and the Fourier heat law

In spite of several years of investigation, so far there is neither phenomenological nor fundamental transport theory which can predict whether or not a given classical, many-body Hamiltonian system, yields an energy transport governed by the Fourier heat law. It is known that heat flow obeys a simple diffusion equation which can be regarded as the continuum limit of a discrete random walk. However, modern ergodic theory tells us that for K-systems, a sequence of measurements with finite precision mimics a truly random sequence and therefore these systems appear precisely those deterministically random systems tacitly required by transport theory. It is therefore interesting to establish which class, if any, of many-body systems satisfy the necessary stringent requirements for the validity of Fourier law of heat conduction.

2.1. DYNAMICAL CHAOS IS A SUFFICIENT CONDITION FOR THE FOURIER LAW

2.1.1. *Ding-a-ling model*
The first example for which convincing evidence has been provided that Fourier law can be derived on purely dynamical grounds, without any additional statistical assumptions, is the so-called ding-a-ling model proposed in (Casati et al, 2005).

The Hamiltonian of the ding-a-ling model is:

$$H = \frac{1}{2} \sum \left(p_k^2 + \omega_k^2 q_k^2 \right) + \text{hard point core} \tag{1}$$

where ω_k equals ω for even k and zero for odd k and where all particles have unit mass. It can be shown that it is possible to fix the energy per particle ($E = 1$) and the half of the lattice distance between two bound particles ($l_0 = 1$). After this the dynamics is uniquely determined by the frequency ω which becomes therefore the only adjustable parameter.

As shown in Fig 1. the model is a one-dimensional array of equal mass, hard-point particles, the even-numbered particles form a set of
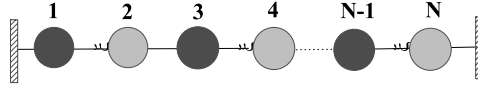
Figure 1. The N-particle ding-a-ling model. Odd particles can move freely in between two collisions, while even particles are bounded by a harmonic spring.

equally spaced harmonic oscillators with each oscillator bound to its individual lattice site and with all oscillators vibrating with the same frequency ω. The odd-numbered particles are free particles constrained only by the two adjacent even-numbered oscillators.

This model has been chosen in order to meet two requirements. First, it is necessary to select a deterministically random system, and second, the system must be sufficiently simple to allow efficient numerical analysis. Let us also recall that even systems obeying the Fourier heat law can transport energy in the form of slowly decaying coherent excitations such as soundlike pulses. In numerical experiments, which unavoidably consider only a small number of particles, this phenomenon is quite troublesome. Though K or almost K-system guarantees that these soundlike solutions will eventually decay, one needs to find a small chaotic system in which this decay rate is sufficiently rapid(Li Wang Casati, 1979). The selected model (1) is a many-body system which exhibits, as the frequency is varied, the full range of behaviour from integrable to almost K and which at the same time has no problem with energy-bearing, long-lived, solitonlike pulses. Indeed, it can be shown that as ω is increased from zero (which is the well known integrable 1-d hard point gas), the system undergoes a transition from integrable to almost fully chaotic. This fact makes this model ideal to study the connection between Fourier law and microscopic dynamical chaos.

Heat conductivity has been studied by placing the end particles in contact with two thermal reservoirs at different temperatures (see (Casati et al, 2005) for details)and then integrating the equations of motion. Numerical results (Casati et al, 2005) demonstrated that, in the small ω regime, the heat conductivity is system size dependent, while at large ω, when the system becomes almost fully chaotic, the heat conductivity becomes independent of the system size (if the size is large enough). This means that Fourier law is obeyed in the chaotic regime.

Figure 2. The geometry of the Lorentz gas channel model. The two heat reservoirs at temperatures T_L and T_R are indicated.

2.1.2. *Lorentz gas channel*
The above conclusions have been nicely confirmed and clarified in (Alonso et al, 2005) where the heat conduction has been studied in a Lorentz gas channel - a quasi one dimensional billiard with circular scatterers. The model (see Fig. 2) consists of two parallel lines and a series of semicircles of radius R placed in a triangular lattice along the channel. By construction no particle can move along the horizontal direction without colliding with the disks. The dynamics in the Lorentz gas is rigorously known to be mixing and all trajectories with nonzero projection on the horizontal direction are of hyperbolic type; further it has positive Kolmogorov-Sinai entropy and a well defined diffusive behavior. Very accurate numerical evidence has been provided (Alonso et al, 2005) which shows that heat conduction in this model obeys the Fourier law. This result therefore clearly indicates that mixing with positive Lyapounov exponents is a sufficient condition to ensure Fourier law of heat conduction.

2.2. CHAOS IS NOT A NECESSARY CONDITION

2.2.1. *Triangle billiard gas channel*
Quite naturally, the next question which arises is whether strong, exponential unstable chaos, being sufficient, is also necessary.

In this connection let us remark that in spite of several efforts, the relation between Lyapounov exponents, correlations decay, diffusive and transport properties is still not completely clear. For example a model has been presented (Casati Prosen, 2000) which has zero Lyapounov exponent and yet it exhibits unbounded Gaussian diffusive behavior. Since diffusive behavior is at the root of normal heat transport then the above result(Casati Prosen, 2000) constitutes a strong suggestion that normal heat conduction can take place even without the strong requirement of exponential instability.

The above problem has been addressed in (Li et al, 2003), where we have considered a quasi-one dimensional billiard model which consists of two parallel lines and a series of triangular scatterers (see Fig.3). In this geometry, no particle can move between the two reservoirs without suffering elastic collisions with the triangles. Therefore this model is
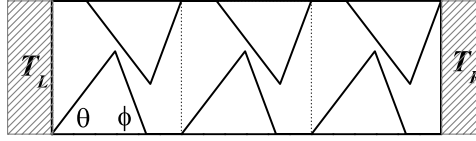
Figure 3. The geometry of the triangle billiard gas channel. Particles move in the region outside the triangular scatterers. The two heat reservoirs at temperatures T_L and T_R are indicated.

analogous to the previous Lorentz gas channel with triangles instead of discs: the essential difference is that in the triangular model the dynamical instability is linear and therefore the Lyapounov exponent is zero.

Strong numerical evidence has been given (Casati and Prosen, 1999) that the motion inside a triangular billiard, with all angles irrational with π is mixing, without any time scale. It is therefore reasonable to expect that the motion inside the irrational polygonal area of Fig 3 is diffusive thus leading to normal conductivity.

Indeed, numerical results in (Li et al, 2003) show that in the irrational case (when the ratio θ/π and ϕ/π are irrational numbers) the system in Fig 3 exhibits normal diffusion and the heat conduction obeys the Fourier law. In the rational case instead, the system shows a superdiffusive behavior, $\langle\sigma^2\rangle = 2Dt^{1.178}$ (Li et al, 2003)and the heat conductivity diverges with the system size as $\kappa \approx N^{0.25\pm0.01}$.

2.2.2. *Alternate mass-core hard potential channel*

In the two billiard gas models just discussed there is no local thermal equilibrium. Even though the internal temperature can be clearly defined at any position(Alonso et al, 2005), the above property may be considered unsatisfactory(Dhars, 1999). In order to overcome this problem, we have recently introduced a similar model which however exhibits local thermal equilibrium, normal diffusion, and zero Lyapunov exponent(Li et al, 2004).

This model consists of a one-dimensional chain of elastically colliding particles with alternate masses m and M. In order to prevent total momentum conservation we confine the motion of particles of mass M (bars) inside separate cells. Schematically the model is shown in Fig.4: particles with mass m move horizontally and collide with bars of mass M which, besides suffering collisions with the particles, are elastically reflected back at the edges of their cells. In between collisions, particles and bars move freely.
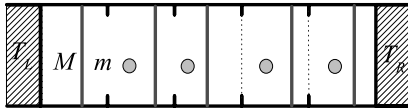
Figure 4. The geometry of the alternate mass-core hard potential channel. The elementary cell is indicated by the two dotted lines. The bars have mass $M = 1$, and the particles have mass $m = (\sqrt{5} - 1)/2$. The two heat baths at temperatures T_L and T_R are indicated.

Numerical results(Li et al, 2004) clearly indicate that this model also obeys the Fourier law.

3. Anomalous heat conduction

Numerical experiments have shown that in many one dimensional systems with total momentum conservation, the heat conduction does not obey the Fourier law and the heat conductivity depends on the system size. For example, in the so-called FPU model, $\kappa \sim L^\beta$, with $\beta = 2/5$, and if the transverse motion is introduced, $\beta = 1/3$. Moreover, in the billiard gas channels (with conserved total momentum), the value of β differs from model to model(Li and Wang, 2003). The question is whether one can relate β to the dynamical and statistical properties of the system.

Recently, a simple formula has been found (Li and Wang, 2003) which connects anomalous heat conductivity with anomalous diffusion. More precisely, it has been shown that for a one dimensional system, if the energy diffusion can be described by

$$\langle \sigma^2 \rangle = 2Dt^\alpha, \quad (0 < \alpha \le 2) \tag{2}$$

then the heat conductivity is given by

$$\kappa = -j/\nabla T \propto L^\beta \tag{3}$$

where the exponent β is

$$\beta = 2 - 2/\alpha. \tag{4}$$

This relation connects heat conduction and diffusion, quantitatively. As expected, normal diffusion ($\alpha = 1$) corresponds to the size-independent ($\beta = 0$) heat conduction obeying the Fourier law. Moreover, a ballistic motion ($\alpha = 2$) implies that the thermal conductivity is proportional to
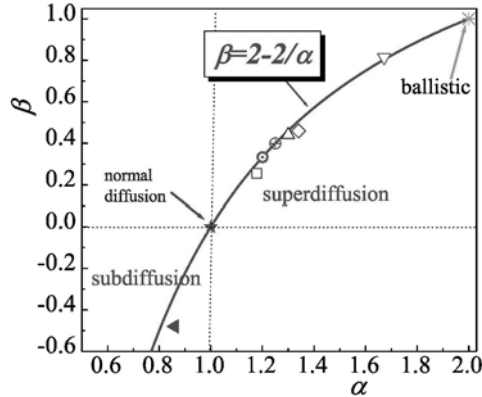
Figure 5. Comparison of prediction (4) with numerical data. Normal diffusion ($\star$). The ballistic motion ($*$). Superdiffusion: 1D Ehrenfest gas channel (Li et al, 2005)($\bigtriangledown$); the rational triangle channel (Li et al, 2003) (empty box); the polygonal billiard channel with ($\phi_1 = (\sqrt{5}-1)\pi/4$), and $\phi_2 = \pi/3$ (Alonso et al, 2002)($\triangle$); the triangle-square channel gas(Li et al, 2005) ($\Diamond$). β values are obtained from system size $L \in [192, 384]$ for all channels except Ehrenfest channel (Li et al, 2005). The FPU lattice model at high temperature regime (Li et al, 2005)($\odot$), and the single walled nanotubes at room temperature ($\oplus$). Subdiffusion: model from Ref. (Alonso et al, 2002) (solid left triangle). The solid curve is $\beta = 2 - 2/\alpha$.

the system size L, a superdiffusive behavior($1 < \alpha < 2$) implies a divergent thermal conductivity ($\beta > 0$), and a subdiffusive behavior ($\alpha < 1$) implies zero thermal conductivity ($\beta < 0$) in the thermodynamic limit.

The simple relation (4) is in good agreement with existing data from billiard gas channels to nonlinear lattices, and even single walled nanotubes(Li et al, 2005). This is shown in Fig. 5, where we compare the theoretical prediction (4) with existing data in different models.

We should mention here the one dimensional hard point gas model for which anomalous heat conduction has been found by several authors (Dhar, 2003; Grassberger et al, 2002). However it seems there is no agreement on the numerical value of the exponent β. Indeed in Ref.(Dhar, 2003), the value $\beta \approx 0.25$ has been found, while the value $\beta \approx 0.33$ is reported in (Grassberger et al, 2002).

4. Control of heat flow

While in the previous sections we have discussed the relation between dynamical chaos and heat conductivity, in the following we will turn our attention to the possibility to control heat flow. Actually a model of thermal rectifier has been recently proposed(Terrano et al, 2002) in
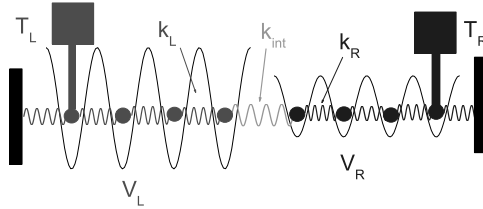
Figure 6. Configuration of the thermal diode model based on two coupled FK chains.

which the heat can flow preferentially in one direction. Although this model is far away from a prototype realization, it is based on a mechanism of very general nature and, as such, is suitable of improvement and may eventually lead to real applications. This problem is discussed in the next section.

4.1. THERMAL DIODE

In a recent paper(Li Wang Casati, 2004), a thermal diode model has been proposed in which, even though the underlying physical mechanism is similar to the one in Ref.(Terrano et al, 2002), there is a new crucial element which allows to improve the efficiency by more than two orders of magnitude.

The diode model consists of two segments of nonlinear lattices coupled together by a harmonic spring with constant strength k_{int} (see Fig. 6). Each segment is described by the (dimensionless) Hamiltonian:

$$H = \sum \frac{p_i^2}{2m} + \frac{1}{2}k(x_i - x_{i+1} - a)^2 - \frac{V}{(2\pi)^2}\cos 2\pi x_i. \qquad (5)$$

The two ends of the system are put into contact with thermal baths at temperature T_L and T_R for left and right bath, respectively. In fact, Eq. (5) is the Hamiltonian of the Frenkel-Kontorova (FK) model which is known to have normal heat conduction(Hu Li Zhao, 1998). For simplicity we set the mass of the particles and the lattice constant $m = a = 1$. Thus the adjustable parameters are $(k_L, k_{int}, k_R, V_L, V_R, T_L, T_R)$, where the letter L/R indicates the left/right segment. In order to reduce the number of adjustable parameters, we set $V_R = \lambda V_L$, $k_R = \lambda k_L$, $T_L = T_0(1 + \Delta), T_R = T_0(1 - \Delta)$ and, unless otherwise stated, we fix $V_L = 5$, $k_L = 1$ so that the adjustable parameters are reduced to four, $(\Delta, \lambda, k_{int}, T_0)$. Notice that when $\Delta > 0$, the left bath is at higher temperature and vice versa when $\Delta < 0$.

In Fig. 7 we plot the heat current J versus Δ for different temperatures T_0. It is clearly seen that when $\Delta > 0$ the heat current (J_+)
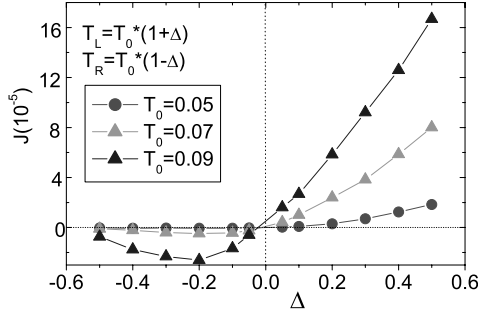
Figure 7. Heat current J versus the dimensionless temperature difference Δ for different values of T_0. Here the total number of particles $N = 100$, $k_{int} = 0.05$, $\lambda = 0.2$. The lines are drawn to guide the eye.

increases with Δ, while in the region $\Delta < 0$ the heat current (J_-) is almost zero, i.e. the system behaves as a thermal insulator. The results in Fig. 7 show that our model has the rectifying effect in a wide range of temperatures. The rectifying efficiency, defined as $|J_+/J_-|$, could be as high as few hundreds times, depending on temperature as well as on other parameters.

4.1.1. *Rectifying mechanism*

To understand the underlying rectifying mechanism, let's start from the energy spectrum of the interface particles. Fig. 8 shows the phonon spectra of the left and right interface particles at different temperature when the two lattices are decoupled ($k_{int} = 0$).

The match/mismatch of the energy spectra of the two interface particles controls the heat current. It is clearly seen from Fig. 8 that, if the left end is in contact with the high temperature bath T_L, and the right end with the low temperature bath T_R ($< T_L$), then the phonon spectra of the two particles at interface overlap in a large range of frequencies, thus the heat current can easily go through the system from the left end to the right end. However, if the left end is at lower temperature T_L and the right end is at higher temperature T_R ($> T_L$), then the phonon spectrum of the right interface particle is mainly in the low frequency part, while the left interface particle is in the high frequency part. Then there is almost no overlap in phonon frequency, and the heat current can hardly go through from right to left, and the system behaves as an insulator. Why the left and right particles at the interface have so different phonon spectra? This can be understood from the following analysis on temperature dependent phonon spectra, due to the nonlinearity.
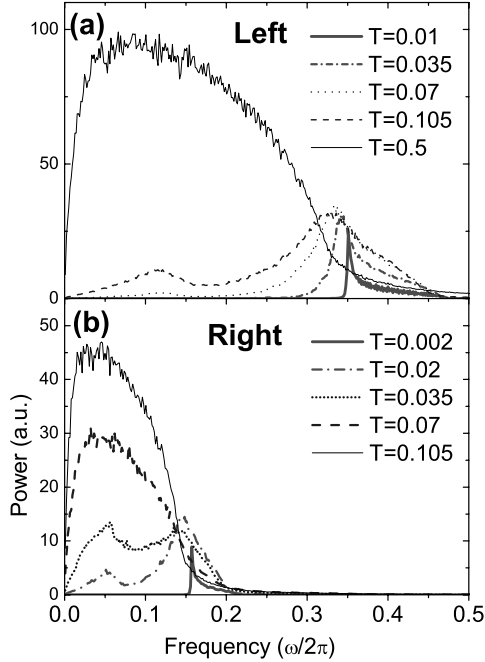
Figure 8. Spectra of the two particles at the interface for different temperatures at $k_{int} = 0$. (a) particle at the left side of the interface, (b) particle at the right side of the interface. Here $\lambda = 0.2$, $N = 100$.

(1) *Low temperature limit.* At low temperature, the particle is confined in the valley of the on-site potential. By linearizing the equation of motion one can easily obtain the frequency band(Li Wang Casati, 2004):

$$\sqrt{V} < \omega < \sqrt{V + 4k}. \qquad (6)$$

For the case of Fig.7 with T=0.01 (left) and T=0.002 (right), this corresponds to $0.36 < \omega/2\pi < 0.48$ for the left particle and to $0.16 < \omega/2\pi < 0.21$ for the right particle.

As the temperature is increased, the interparticle potential $kx^2/2$ becomes more and more important until a critical value $T_{cr} \approx V/(2\pi)^2$ is reached (we take the Boltzman constant equal to unity), when the kinetic energy is large enough to overcome the on-site potential barrier. At this point low frequency appears and this happens at the critical temperatures $T_{cr} = 0.13$ for $V = 5$ (left), and $T_{cr} = 0.025$ for $V = 1$ (right). This is in quite good agreement with the data of Fig.8.

(2) *High temperature limit.* In the high temperature limit the on-site potential can be neglected, the system is close to two coupled harmonic

chains, and the phonon band is given by(Kittel, 1996) :

$$0 < \omega < 2\sqrt{k}, \tag{7}$$

which gives $0 < \omega/2\pi < 0.32$ for the left particle and $0 < \omega/2\pi < 0.14$ for the right particle, again in good agreement with Fig.8.

In fact, in order to optimize the rectifying effect, one should avoid the overlapping of the phonon bands in the low temperature limit (Eq.6) and that in the high temperature limit (Eq.7) for each segment of the system. According to the above estimates, one should have $V > 4k$, which is satisfied for the case of Fig.8.

We should stress that it is the nonlinearity of the potential that makes phonon spectra temperature dependent, and thus the rectifying effect possible. Therefore it is reasonable to expect the rectifying effect to be present, in different degrees, in typical nonlinear lattices.

4.2. Negative Differential Thermal Conductance

Apart from the "one-way heat flow", the *negative differential thermal resistance* phenomenon observed in a certain temperature intervals in the thermal diode is of particular interest. As illustrated in Fig.7 for $\Delta < -0.2$, a smaller temperature difference (Δ), can induce a larger heat current since, due to nonlinearity, it can result in a better match in phonon bands.

The same phenomenon is shown for different inter-face coupling constants k_{int} in Fig. 9(a), and different system size in Fig. 9(b).

4.3. Thermal Transistor

The phenomenon of negative differential thermal resistance allows us to propose a "thermal transistor"(Li Wang Casati, 2004). The configuration of the thermal transistor is shown in Fig.10(a). It consists of three segments, D, S and G. The names D, S and G follow the ones used in a MOSFET (Metal-Oxide-Semiconductor Field-Effect-Transistor) that is the most important device for very large scale integrated chips such as microprocessors and semiconductor memories. Segment D (from D to O) has a negative differential thermal resistance in a certain temperature regime while segment S is a normal heat conductor, i.e., heat current inside this segment is positively dependent on temperature difference. Segment G is the control segment, which is connected to the junction particle between segments S and D. Temperature T_G will be used to control temperature T_o (at the junction O) so as to control the heat current from D to S. In analogy to the MOSFET, in which the electronic current in the electrode G is very small, we require here that
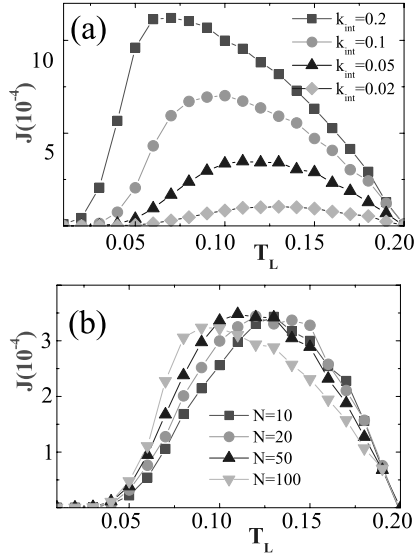
Figure 9. (a) Heat current versus temperature T_L (at fixed $T_R = 0.2$) for different coupling constants, k_{int}, with lattice size $N = 50$. The system parameters are: $V_L = 5$, $V_R = 1$, $k_L = 1$, $k_R = 0.2$. (b) Same as (a) but for different system size N. $k_{int} = 0.05$. Notice that when $T_L \leq 0.1$ the heat current increases with decreasing the external temperature difference.

the heat current J_G through segment G to be as small as possible, (otherwise it is hard to set T_G to a required value in experiment). Moreover the heat resistance of segment G must be small enough in order to well control the temperature T_o by changing T_G so that $T_o \approx T_G$.

Notice that, in typical situations, the differential heat resistance, $R_S = \left(\frac{\partial J_S}{\partial T_o}\right)^{-1}_{T_S=\text{const}}$ in segment S, and $R_D = -\left(\frac{\partial J_D}{\partial T_o}\right)^{-1}_{T_D=\text{const}}$ in segment D, are both positive and therefore there exists only one value of T_o for which $J_S = J_D$ so that $J_G = 0$, Since $J_S = J_D + J_G$, the "*current amplification factor*", $\alpha = \left|\frac{\partial J_D}{\partial J_G}\right| = \left|\frac{R_S}{R_S+R_D}\right| < 1$, namely in order to make a change ΔJ_D, the control heat bath has to provide a larger ΔJ_G. This means that the "transistor" can never work!

The key point of our transistor model is the "*negative differential heat resistance*" as we observed in the diode model(Li Wang Casati, 2004). It provides the possibility that when T_o changes both J_S and J_D change simultaneously in the same way. Therefore $J_S = J_D$ (or $J_s \approx J_D$) can be achieved for several different values of T_o or even in a wide region of T_o as shown in Figs.10 and 11. In this situation heat switch and heat modulator/amplifier are possible. In the ideal, limiting
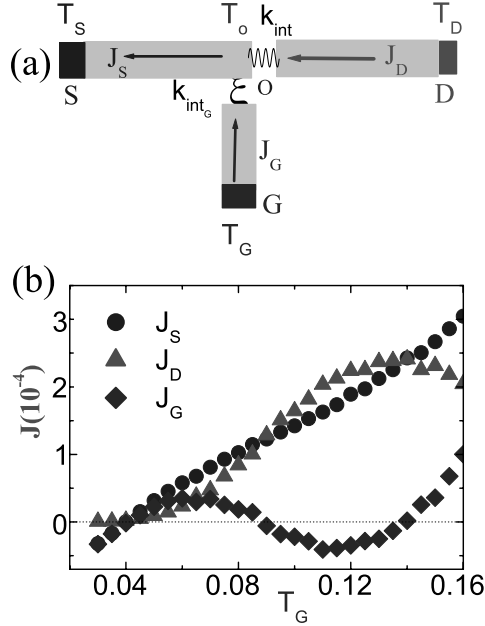
Figure 10. (a) Configuration of the thermal transistor. (b) Heat current versus the control temperature T_G. Parameters are: $T_D = 0.2, , V_D = 1.0, k_D = 0.2,$ $k_{int} = 0.05; T_S = 0.04, V_S = 5, k_S = 0.2, V_G = 5, k_G = 1, k_{int_G} = 1$. Notice that both J_S and J_D increase when the temperature T_G is increased.

case of $R_S = -R_D$ which, in principle, can be obtained by adjusting parameters, the transistor works perfectly.

4.3.1. *Thermal switch*

We first demonstrate the "*switch*" function of our transistor, namely we show that the system can act like a good heat conductor or an insulator depending on the control temperature. This is illustrated in Fig.10(b), where we plot J_G, J_S, and J_D versus T_G. When T_G increases from 0.03 to 0.135, both J_D and J_S increase. In particular, at three points: $T_G \approx 0.04, 0.09$ and $0.135, J_D = J_S$ thus J_G is exactly zero. These three points correspond to "off", "semi-on" and "on" states, at which J_D is $2.4 \times 10^{-6}, 1.2 \times 10^{-4}$ and 2.3×10^{-4}, respectively. The ratio of the heat current at the "on" state and that at the "off" state is about 100, hence our model displays one important function - switch - just like the function of a MOSFET used in a digital circuit.
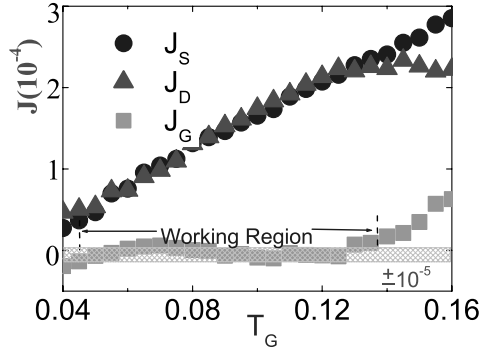
Figure 11. Heat current versus the control temperature T_G. Here: $T_D = 0.2, V_D = 1.0, k_D = 0.2, T_S = 0.04, V_S = 5, k_S = 0.2, k_{int} = 0.05, V_G = 5, k_G = 1, k_{intG} = 0.1$. The shadow region is the range of variation of J_G in the temperature interval $T_G \in (0.05, 0.135)$.

4.3.2. *Thermal modulator/amplifier*

As demonstrated above, the heat current from D to S can be switched between different values. However, in many cases, like in an analog circuit, we need to continuously adjust the current J_S and/or J_D in a wide range by adjusting the control temperature T_G. In Fig.11 we demonstrate this "modulator/amplifier" function of our transistor. The basic mechanism of such "modulator/amplifier" is the same as that of the "switch" but we consider here different parameter values. It is seen that in the temperature interval $T_G \in (0.05, 0.135)$, the heat current through the segment G remains very small $((-10^{-5} \sim 10^{-5})$, within the shadow strip in Fig.10, while the heat currents J_S and J_G continuously increase from 5×10^{-5} to 2×10^{-4}.

5.   Conclusions and discussions

In this paper, we have given a brief summary of our recent work on heat conduction in one dimensional systems. We have shown that strong chaos is sufficient but not strictly necessary for the validity of the Fourier heat law. Indeed linear mixing can be sufficient to induce a diffusive process which ensures normal heat conductivity.

For systems with total momentum conservation one typically finds anomalous conductivity, namely the thermal conductivity is divergent with the system size. Anomalous conductivity has been connected with anomalous diffusion via the very simple formula (4).

Finally we have shown the possibility to build a thermal diode which exhibits a very significant rectifying effect in a very wide range of system parameters. Moreover, based on the phenomenon of *negative differential thermal resistance* observed in the thermal diode, we have built a theoretical model for a thermal transistor. The model displays two basic functions of a transistor: switch and modulator/amplifier. Although at present it is just a model we believe that, sooner or later, it can be realized in a nanoscale system experiment. After all the Frenkel-Kontorova model used in our simulation is a very popular model in condensed matter physics(Braun and Kivshar, 1998).

6. Acknowledgment

References

Peierls, R. E.. Theoretical Physics in the Twentieth Century. *edited by M. Fiera and V. F. Weisskopf*, Wiley, New York, 1961

Bonetto F. Mathematical Physics 2000. *edited by A. Fokas et al*, Imperial College Press, London, 2000 Wiley, New York, 1961; S. Lepri et al. *Phys. Rep.*, 377, 1 (2003).

H. Kaburaki and M. Machida, Phys. Lett. A 181, 85 (1993); S. Lepri et al. Europhys. Lett. 43, 271 (1998); S. Lepri, Phys. Rev. E 58, 7165 (1998); S. Lepri et al, Phys. Rev. Lett. 78, 1896 (1997); B. Hu, B. Li, and H. Zhao, Phys. Rev. E 61, 3828 (2000); A. Pereverzev, Phys. Rev. E, 68, 056124 (2003).

J.-S Wang and B. Li, Phys. Rev. Lett.92, 074302 (2004); Phys. Rev. E, 70, 021204 (2004).

Li B., and Wang J. B. Li and J. Wang, Phys. Rev. Lett. 91, 044301 (2003); 92, 089402 (2004).

Li B., Wang J., Wang L., Zhang G. CHAOS, xxx(2005); cond-mat/0410355.

G. Casati, J. Ford, F Vivaldi, and W. M. Visscher, Phys. Rev. Lett, 52, 1861 (1984).

D. Alonso, R. Artuso, G. Casati, and I. Guarneri, Phys. Rev. Lett 82, 1859 (1999).

B. Li, L Wang, and B Hu, Phys. Rev. Lett. 88, 223901 (2002)

D. Alonso et al. Phys. Rev. E 66, 066131 (2002).

B. Li, G. Casati, and J. Wang, Phys. Rev. E 67, 021204 (2003)

B. Li, G. Casati, J. Wang, and T. Prosen, Phys. Rev. Lett. 92, 254301 (2004)

M. Terraneo, M. Peyrard, and G. Casati, Phys. Rev. Lett 88, 094302 (2002).

B. Li, L. Wang, and G. Casati, Phys. Rev. Lett. 93, 184301 (2004).

B. Li, L Wang, and G. Casati, cond-mat/0410173

B. V. Chirikov, Phys. Rep. 52, 263, 335 (1979).

G. Casati and T. Prosen, Phys.Rev. Lett. 85, 4261 (2000).

G. Casati, and T. Prosen, Phys. Rev. Lett. 83, 4729 (1999)

A. Dhar and D. Dhar, Phys. Rev. Lett. 82, 480 (1999).

A. Dhar, Phys. Rev. Lett., 86, 3554 (2001); G. Casati and T. Prosen, Phys. Rev. E **67**, 015203(R) (2003).

P. Grassberger, W. Nadler, and L. Yang,   ibid. **89**, 180601 (2002); H. Li and H. Zhao, ibid **89**, 079401 (2002).

J. Bardeen and W. H. Brattain, Phys. Rev. 74, 230 (1948).

B. Hu, B. Li, and H. Zhao, Phys. Rev. E 57, 2992 (1998).

C. Kittel, Introduction to Solid State Physics   7'th edition, John Wiley & Sons, Inc. New York), 1996.

O. M. Braun and Y. S. Kivshar, Phys. Rep. **306**, 1 (1998).

Quantum graphs which sound the same

Talia Shapira and Uzy Smilansky
Department of Physics of Complex Systems,
The Weizmann Institute of Science, Rehovot 76100, Israel

Abstract. We present a method to construct pairs of isospectral quantum graphs which are not isometric. These graphs are the analogues of the family of isospectral domains in $\mathbb{R}^2$ which were first introduced by Gordon, Webb and Wolpert (C. Gordon et.al., 1992), recently enlarged by P. Buser *et. al.* (P. Buser et.al., 1994), and discussed further by Okada *et. al.* (Y. Okada et.al., 2001).

Keywords: Quantum graphs, isospectrality

1. Introduction

In response to M. Kac's classical paper "Can one hear the shape of a drum?" (M. Kac, 1966), much research effort was invested in two complementary problems - to identify classes of systems for which Kac's question is answered in the affirmative, or to find examples which are isospectral but not isometric. In the present paper we shall focus our attention to quantum graphs and in the following lines will review the subject of isospectrality from this intentionally narrowed point of view. The interested reader is referred to (T. Sunada, 1985; C. Gordon et.al., 1992; S. Chapman, 1995; P. Buser et.al., 1994; Y. Okada et.al., 2001; S. Zelditch, 2004) for a broader view of the field where spectral inversion and its uniqueness are discussed.

Spectral problems related to graphs emerge in two distinct ways. In the first, the spectrum of the connectivity (adjacency) matrix is considered. It represents a discrete version of the Laplacian, and for finite graphs, the spectrum is finite. This class of problems are often referred to as combinatorial graphs. *Quantum (metric) graphs* are obtained by associating the standard metric to the bonds which connect the vertices. The Schrödinger operator consists of the one-dimensional Laplacians on the bonds, complemented by appropriate boundary conditions at the vertices (see next section). The spectrum of quantum graphs is unbounded, and it displays many interesting features which made it a convenient paradigm in the study of quantum chaos (T. Kottos et.al., 1999).

Shortly after the appearance of Kac's paper, M. E. Fisher published his work "On hearing the shape of a drum" (M.E. Fisher, 1966), where

he addresses isospectrality for the discrete version of the Laplacian.
Since then, the study of isospectral combinatorial graphs made very
impressive progress. In particular, several methods to construct isospec-
tral yet different graphs were proposed. A review of this problem can
be found in (R. Brooks, 1999). In particular, a method which was origi-
nally put forward by Sunada (T. Sunada, 1985) to construct isospectral
Laplace-Beltrami operators on Riemann manifolds, was adapted for the
corresponding problem in the context of combinatorial graphs (L. Hal-
beisen et.al., 1999). Here we shall go one step further, and show that
it can be also adapted for quantum graphs.

The conditions under which the spectral inversion of *quantum graphs*
is unique was studied previously (R. Carlson, 1999; B. Gutkin et.al.,
2001). The main result is a theorem (B. Gutkin et.al., 2001) which
states:

Theorem(B. Gutkin and U. Smilansky): The connectivity and the bond
lengths of quantum graphs *whose bond lengths are rationally indepen-
dent* are determined *uniquely* by the spectrum.

That is the shape of the graph "can be heard". (Some technical con-
ditions which appear in the original statement of the theorem are
automatically satisfied for the Neumann graphs which will be consid-
ered here.) The uniqueness of the inversion follows from the existence of
an exact trace formula for quantum graphs (Jean-Pierre Roth, ; T. Kot-
tos et.al., 1999). Thus, isospectral pairs of different graphs, must have
rationally dependent bond lengths. The Sunada method, which is based
on constructing the isospectral domains by concatenating several copies
of a given building block, automatically provide us with graphs with
rationally dependent lengths. Such a pair was already discussed in
(B. Gutkin et.al., 2001). Here we shall show that all the known isospec-
tral domains in $\mathbb{R}^2$ (P. Buser et.al., 1994; Y. Okada et.al., 2001) have
corresponding isospectral pairs of quantum graphs.

The paper is organized in the following way. For the sake of com-
pleteness we shall give a short review of some elementary definitions and
facts on quantum graphs. We shall then show how pairs of isospectral
domains in $\mathbb{R}^2$ can be converted to isospectral pairs of quantum graphs,
and discuss their spectra and eigenfunctions.

1.1. A SHORT INTRODUCTION TO QUANTUM GRAPHS

We consider finite graphs consisting of V vertices connected by B
bonds. The $V \times V$ connectivity matrix will be denoted by $C_{i,j} : C_{i,j} = 1$
when the vertices i and j are connected, and it vanishes otherwise.
The bonds are endowed with the standard metric and the length of

the bonds will be denoted by $L_{i,j}$. The total length of the graph is $\mathcal{L} = \sum_{i>j} L_{i,j}$.

The domain of the Schrödinger operator on the graph is the $\mathbb{L}^2$ space of differentiable functions which are continuous at the vertices. The operator is constructed in the following way. On the bonds, it is identified as the one dimensional Laplacian $-\frac{\mathrm{d}^2}{\mathrm{d}x^2}$. It is supplemented by boundary conditions on the vertices which ensure that the resulting operator is self adjoint. We shall consider in this paper the Neumann boundary conditions:

$$\forall i \quad : \quad \sum_j C_{i,j} \left. \frac{\mathrm{d}}{\mathrm{d}x_{i,j}} \, \psi_{i,j}(x_{i,j}) \right|_{x_{i,j}=0} \quad = \quad 0 \; . \tag{1}$$

Here and elsewhere, the bonds are identified by the vertices that they connect, the coordinates along the bonds i, j are denoted by $x_{i,j}$, and the derivatives in (1) are directed out of the vertex i.

A wave function with a wave number k can be written as

$$\psi_{i,j}(x_{i,j}) = \frac{1}{\sin kL_{i,j}} \left(\phi_i \sin k(L_{i,j} - x_{i,j}) + \phi_j \sin kx_{i,j} \right) \tag{2}$$

where the ϕ_i are the values of the wave function at the vertices. The form (2) ensures continuity. The spectrum $\{k_n\}$ and the corresponding eigenfunctions are determined by substituting (2) in (1). The resulting homogeneous linear equations for the ϕ_i have a non trivial solution if the determinant of the coefficients vanishes, and this happens at $\{k_n^2\}$, which is a discrete positive and unbounded spectrum.

2. Isospectral quantum graphs

The first pair of isospectral planar domains which was introduced by Gordon, Web and Wolpert (C. Gordon et.al., 1992) is a member of a much larger set which was discussed in (P. Buser et.al., 1994; Y. Okada et.al., 2001). The important and distinctive features of these pairs are:

– The domains are built by concatenating an elementary "building block" in two different prescribed ways to form the two domains. A building block is joined to another by reflecting along the common boundary. The shape of the building block is constrained only by symmetry requirements, but otherwise it is quite general.

– The eigenfunctions corresponding to the same eigenvalue are related to each other by a *transplantation*. That is, the eigenfunction in a building block of one domain can be expressed as a linear

combination of the eigenfunction in several building blocks in the other domain. The transplantation matrix is independent of the considered eigenvalue.

— The construction of these pairs reflects an abstract algebraic structure which is due to T. Sunada (T. Sunada, 1985).
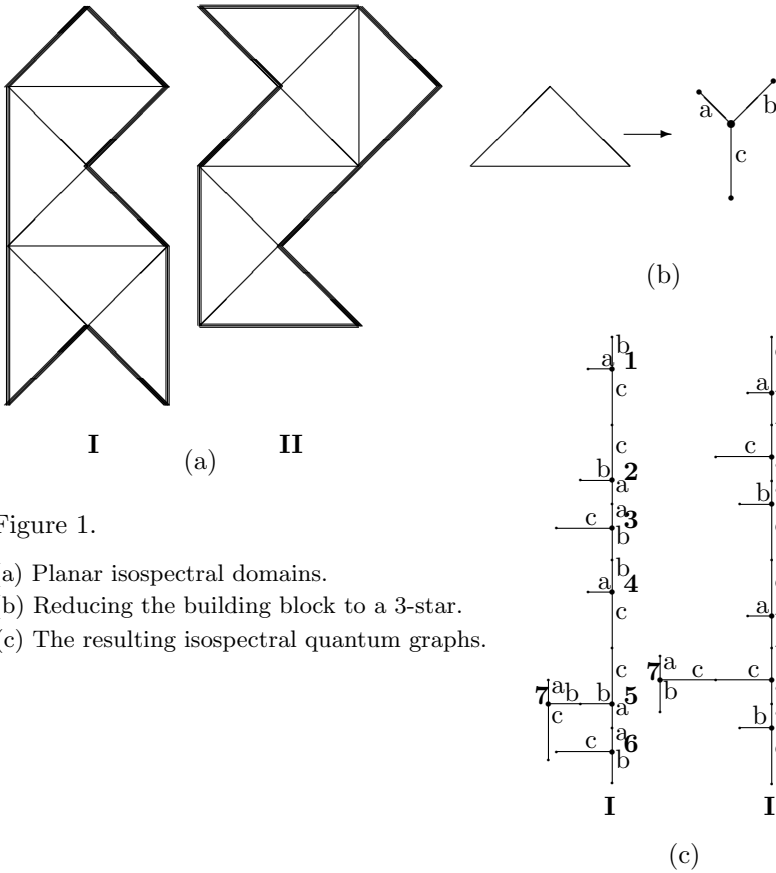
Figure 1.

(a) Planar isospectral domains.
(b) Reducing the building block to a 3-star.
(c) The resulting isospectral quantum graphs.

An example of an isospectral pair and its building block is given in figure 1.(a). Drawings of other examples are shown in e.g., (P. Buser et.al., 1994; S. Chapman, 1995). Okada and Shudo (Y. Okada et.al., 2001) analyzed these planar isospectral pairs, and showed that the construction process can be described in terms of a pair of three colored (not metric) graphs, one graph for each member of the pair. The vertices stand for the building blocks, and the connecting colored bonds denote the side about which the reflection is to be performed, each of the colors represents one of the sides of the basically triangular building block. This way, the colored graphs provide a systematic way to record and discuss the topology and related algebraic properties of the domains.

We can construct *metric* graphs analogues of the domains in $\mathbb{R}^2$, by replacing the building blocks by appropriate *metric* graphs which preserve the required symmetry. As an example, the triangular building block of figure 1.(a) can be replaced by a 3 - star with bonds of lengths a, b and c as shown in Figure 1(b). This yields the pair of isospectral but non isometric graphs shown in figure 1(c). (In drawing figure 1.(c) we took advantage of the fact that the "angles" between the bonds do not have any significance). Note that the two graphs shown in figure 1.(c). share the same connectivity matrix (they are topologically congruent) however they are not isometric. As a matter of fact the right and the left graphs are interchanged when the bonds "b" with "c" are switched. Thus, the lengths b and c must be different to ensure that the two graphs are not isometric. This is an example of the symmetry requirement mentioned above.

From here on we shall study the spectrum of the graphs shown in Figure 1.(c). Similar properties can be derived with only minor modifications for all the other examples in (P. Buser et.al., 1994).

The vertices in the graphs can be divided to three classes, according to their valency (cardinality) $v_i = \sum_j C_{i,j}$. It is easy to see that the values of the wave function at the 7 vertices with $v = 3$ (shown in Figure 1(c). as numbered large dots) determine the wave function on all the other vertices. We shall denote these values by $\vec{\phi}^{\,I,II} = (\phi_1^{I,II} \cdots, \phi_7^{I,II})^\top$ where the index I, II stand for the left or the right graph, and the vertices are enumerated as in Figure 3. We shall refer to the $\vec{\phi}^{\,I,II}$ as the the vertex wave functions. The value of the wave function on a $v = 1$ vertex connected to the i'th $v = 3$ vertex by a bond of length $t = a, b, c$ is

$$\phi_t^{v=1} = \frac{\phi_i}{\cos kt} \ . \tag{3}$$

Similarly, the value of the wave function on a $v = 2$ vertex which is a distances t from two $v = 3$ vertices, is

$$\phi_t^{v=2} = \frac{(\phi_i + \phi_j)}{2 \cos kt} \quad . \tag{4}$$

Using these relations we can construct the bond wave functions (2) and express the matching conditions (1) in terms of the vectors $\vec{\phi}^{\,I,II}$ only. The resulting quantization conditions can be expressed in terms of the matrix,

$$A(a, b, c; k) =$$

$$\begin{pmatrix} \xi - \gamma & \gamma & 0 & 0 & 0 & 0 & 0 \\ \gamma & \xi - \alpha - \gamma & \alpha & 0 & 0 & 0 & 0 \\ 0 & \alpha & \xi - \alpha - \beta & \beta & 0 & 0 & 0 \\ 0 & 0 & \beta & \xi - \beta - \gamma & \gamma & 0 & 0 \\ 0 & 0 & 0 & \gamma & \xi - \alpha - \beta - \gamma & \alpha & \beta \\ 0 & 0 & 0 & 0 & \alpha & \xi - \alpha & 0 \\ 0 & 0 & 0 & 0 & \beta & 0 & \xi - \beta \end{pmatrix} \tag{5}$$

with

$$\alpha(a; k) = \frac{1}{\sin 2ka} \quad ; \quad \beta(b; k) = \frac{1}{\sin 2kb} \quad ; \quad \gamma(a; k) = \frac{1}{\sin 2kc} \tag{6}$$

and

$$\xi(a, b, c; k) = \tan ak \ + \ \tan bk \ + \ \tan ck \ . \tag{7}$$

The secular equation for the graph (I) is

$$\det A(a, b, c; k_n) = 0 \tag{8}$$

The corresponding vertex eigenfunction $\vec{\phi}^{\,I}$ is the eigenvector of $A(a, b, c; k_n)$ with a vanishing eigenvalue. The secular equation for the graph II and the corresponding vertex eigenfunctions are obtained from the matrix $A(a, c, b; k_n)$. (c and b are interchanged). Explicit computation shows that $\det A(a, b, c; k) = \det A(a, c, b; k)$. This proves the isospectrality of the two graphs.

The sum of the elements of any of the columns of $A(a, b, c; k)$ is ξ. Hence the vector $\vec{1} = (1, 1, 1, 1, 1, 1, 1)$ is an eigenvector with an eigenvalue ξ. The values of k for which $\xi(a, b, c; k) = 0$ are in the spectrum of both graphs. They correspond to eigenfunctions which are the same on each of the 3-star - the building block of the complete graphs (figure 1.(b)). As a matter of fact, the condition $\xi(a, b, c; k) = 0$ is the secular equation for this 3-star with bond lengths a, b, c (T. Kottos et.al., 1999). This subset exhausts 1/7 of the spectrum of the graphs, and in this set the transplantation property is trivial.

The transplantation property which is basic to the proof of isospectrality for the $\mathbb{R}^2$ domains in (P. Buser et.al., 1994) can be explicitly formulated by the transplantation matrix

$$T = \begin{pmatrix} 0 & 0 & 0 & 1 & 1 & 1 & 0 \\ 0 & 0 & 1 & 0 & 0 & 1 & 1 \\ 0 & 1 & 0 & 0 & 1 & 0 & 1 \\ 1 & 0 & 0 & 1 & 0 & 0 & 1 \\ 1 & 0 & 1 & 0 & 1 & 0 & 0 \\ 1 & 1 & 0 & 0 & 0 & 1 & 0 \\ 0 & 1 & 1 & 1 & 0 & 0 & 0 \end{pmatrix} , \quad \text{so that} \quad \vec{\phi}^{\,II} = T\vec{\phi}^{\,I} . \tag{9}$$

We observe that the inverse transplantation is also effected by T: $\vec{\phi}^{\,I} = T\vec{\phi}^{\,II}$, even though T is not self inversive. The fact that T induces the transplantation in the two directions, implies that the vertex wave functions $\vec{\phi}$ must be eigenvectors of T^2. (The wave functions are defined up to normalization, and therefore the corresponding eigenvalues can be different than unity). The spectrum of T^2 consists of the eigenvalue 9 and the six-fold degenerate eigenvalue 2. Thus, the vertex wave functions are either proportional to $\vec{1}$, or belong to the 6 dimensional subspace of vectors orthogonal to $\vec{1}$.
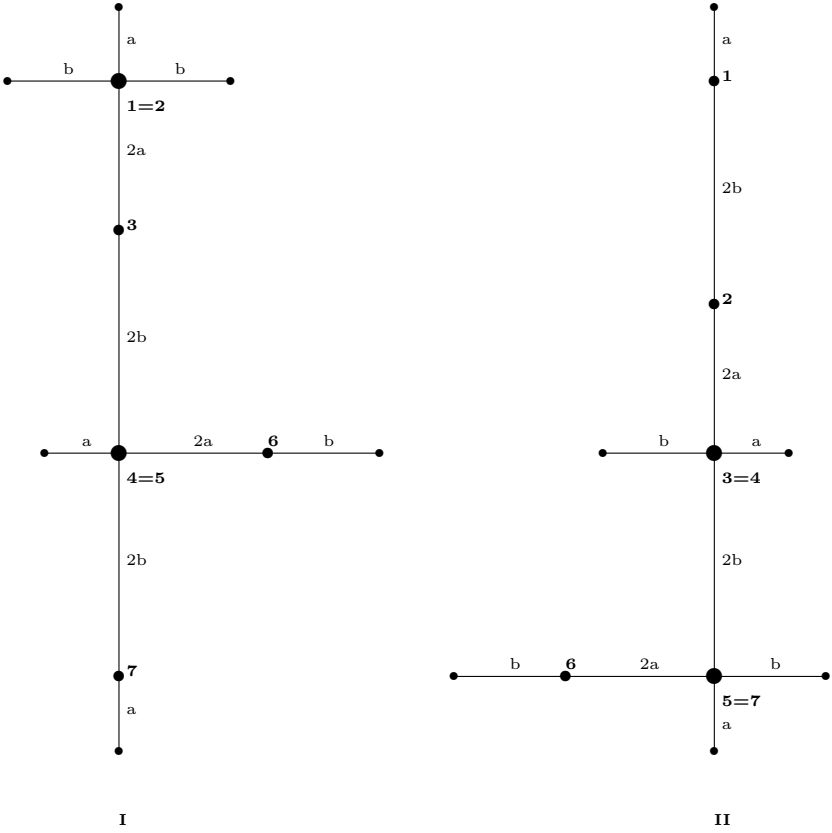
Figure 2. The isospectral quantum graphs of (B. Gutkin et.al., 2001)

The isospectral pair which was proposed in (B. Gutkin et.al., 2001) can be easily obtained from the example discussed above by taking the limit $c \to 0$. In this limit the vertices 1, 2 and 4, 5 on graph I, and 3, 4 and 5, 7 on graph II coalesce, and the remaining wave functions are completely specified in terms of the values on the 5 resulting vertices. This can be shown explicitly by expanding to leading order in $\epsilon = ck$ both the matrix A (5) and the eigenvector $\vec{\phi}$ which corresponds to a vanishing eigenvalue. We shall present the computation explicitly for the graph I.

$$A = \frac{1}{\epsilon}A_{-1} + A_0 + \epsilon A_1 \ \ ; \ \ \vec{\phi} = \vec{\phi}_0 + \epsilon \vec{\phi}_1 \ , \tag{10}$$

so that the secular condition reads

$$A\vec{\phi} = \frac{1}{\epsilon}A_{-1}\vec{\phi}_0 + \left[A_0\vec{\phi}_0 + A_{-1}\vec{\phi}_1\right] + \epsilon \left[A_1\vec{\phi}_0 + A_0\vec{\phi}_1\right] + \mathcal{O}(\epsilon^2) = 0 \ , \tag{11}$$

Where A_1 is the unit matrix, A_0 is obtained from A by replacing ξ by $\xi_0 = \tan ka + \tan kb$, and setting $\gamma = 0$.

$$A_{-1} = \frac{1}{2} \begin{pmatrix} -1 & 1 & 0 & 0 & 0 & 0 & 0 \\ 1 & -1 & 0 & 0 & 0 & 0 & 0 \\ 0 & 0 & 0 & 0 & 0 & 0 & 0 \\ 0 & 0 & 0 & -1 & 1 & 0 & 0 \\ 0 & 0 & 0 & 1 & -1 & 0 & 0 \\ 0 & 0 & 0 & 0 & 0 & 0 & 0 \\ 0 & 0 & 0 & 0 & 0 & 0 & 0 \end{pmatrix}. \tag{12}$$

The secular condition (11) has to be obeyed separately for the leading orders in ϵ. The diverging term implies that $\vec{\phi}_0 = (\phi_1, \phi_1, \phi_3, \phi_4, \phi_4, \phi_6, \phi_7)$, which follows from the coalescence of the vertices when $c \to 0$. The term proportional to ϵ requires $\vec{\phi}_0 = -A_0 \vec{\phi}_1$. The remaining condition can be expressed as $(-A_1 A_0^{-1} + A_0)\vec{\phi}_0 = 0$. This condition, in turn, can be reformulated for vectors of dimension 5 obtained from $\vec{\phi}_0$ above by disregarding the second and fifth components. The resulting 5×5 matrices for the two isospectral graphs are

$$A_I(a, b; k) =$$

$$\begin{pmatrix} 2\xi_0 - \alpha & \alpha & 0 & 0 & 0 \\ \alpha & \xi_0 - \alpha - \beta & \beta & 0 & 0 \\ 0 & \beta & 2\xi_0 - \alpha - 2\beta & \alpha & \beta \\ 0 & 0 & \alpha & \xi_0 - \alpha & 0 \\ 0 & 0 & \beta & 0 & \xi_0 - \beta \end{pmatrix},$$

$$A_{II}(a, b; k) =$$

$$\begin{pmatrix} \xi_0 - \beta & \beta & 0 & 0 & 0 \\ \beta & \xi_0 - \alpha - \beta & \alpha & 0 & 0 \\ 0 & \alpha & 2\xi_0 - \alpha - \beta & \beta & 0 \\ 0 & 0 & \beta & 2\xi_0 - \beta - \alpha & \alpha \\ 0 & 0 & 0 & \alpha & \xi_0 - \alpha \end{pmatrix}. \tag{13}$$

Direct computation shows that $\det A_I(a, b; k) = \det A_{II}(a, b; k)$ for all k, which proves isospectrality. The graphs which result from this contraction are rather different from the original ones (i.e., they have vertices with $v = 4$). They remain metrically distinct even when $a = b$. The above discussion shows that their isospectrality is based on the same algebraic roots,however, in some disguise. Note, that taking the limit $a \to 0$ gives two identical graphs.

Finally, it should be emphasized, that the skeleton of $v = 3$ vertices (shown by larger black dots and numbered in figure 3) form graphs which are identical to the topological, colored graphs which

were introduced in (Y. Okada et.al., 2001) to express the transplanta-
tion properties of the isospectral domains in $\mathbb{R}^2$. The quantum, metric
graphs can be obtained simply by completing each topological vertex to
a 3-vertex star graph with lengths a, b, c. Topological bonds are associ-
ated with lengths according to their colors, and bonds are added to the
topological vertices with valency less than three, to complete to 3- stars.
This implies that the computation carried out here can be repeated for
any of the topological graphs shown in (Y. Okada et.al., 2001). The
last example, where we constructed new metric graphs by eliminating
the c bonds, can also be applied for the entire set, to generate a richer
variety of isospectral but not isometric quantum graphs.

3. Scattering approach to quantization

The secular function det $A(a, b, c; k)$ (8) has poles on the real k axis,
which is not convenient for numerical work. In the present section we
use the scattering approach to quantization of graphs (T. Kottos et.al.,
1999), to derive a secular function which is finite on the real axis.

The scattering approach for quantization of graphs is explained in
detail in (T. Kottos et.al., 1999). In this method, to each vertex one
associates an elementary scattering matrix $\sigma^i_{d',d}$, where d labels a di-
rected bond which is incoming to the vertex i while d' labels a directed
bond which is outgoing from i. Denoting the valency of the vertex i
by v_i, then σ^i is a $v_i \times v_i$ unitary matrix. Using the σ matrices for all
the vertices on the graph, one constructs a $2B \times 2B$ unitary matrix,
$S^B_{d',d}$ in the space of all the directed bonds. Its elements vanish unless
d and d' are incoming and outgoing bonds from the same vertex i. In
this case

$$S^B_{d',d}(k) = \mathrm{e}^{ikL_{d'}} \sigma^i_{d',d} \;, \tag{14}$$

where L_d is the length of the bond d, and k the wave number. The
eigenvalues of the graph are the set $\{k_n^2\}$ where k_n are the solutions of
the secular equation

$$\det(\; I - S^B(k) \;) = 0 \tag{15}$$

and I is the $2B \times 2B$ unit matrix. The unitarity of $S^B(k)$ on the real
k line guarantees that the secular function is finite.

The main disadvantage of (15) is that the number of directed bonds
$2B$ may be quite large, (in the example discussed presently, $2B = 30$
while the matrix A has dimension 7. However, the tree structure of
most of the isospectral graphs under consideration here can be used
to obtain a much simplified, and almost explicit form of the secular
function. This simplification is the object of the present appendix.

Most of the graphs we deal with are trees- that is, they do not have any self tracing loops. Choose a vertex which will be the "root". In the example we consider here we shall take vertex 5 as the root (see figure 1.(c)). A wave which propagates from the root along a certain branch is reflected, and this reflection can be expressed by a reflection from the vertex which is next to the root. Once we know the reflection coefficient, which because of unitarity is a complex number with unit modulus, we can construct the $S^B(k)$ matrix. In the present cases, when the valency of the root is 3, we get

$$S^B(k) =$$

$$
\begin{pmatrix}
e^{2ika} & 0 & 0 & 0 & 0 & 0 \\
0 & e^{2ikb} & 0 & 0 & 0 & 0 \\
0 & 0 & e^{2ikc} & 0 & 0 & 0 \\
0 & 0 & 0 & e^{2ika} & 0 & 0 \\
0 & 0 & 0 & 0 & e^{2ikb} & 0 \\
0 & 0 & 0 & 0 & 0 & e^{2ikc}
\end{pmatrix}
\begin{pmatrix}
0 & 0 & 0 & \rho_a & 0 & 0 \\
0 & 0 & 0 & 0 & \rho_b & 0 \\
0 & 0 & 0 & 0 & 0 & \rho_c \\
-\frac{1}{3} & \frac{2}{3} & \frac{2}{3} & 0 & 0 & 0 \\
\frac{2}{3} & -\frac{1}{3} & \frac{2}{3} & 0 & 0 & 0 \\
\frac{2}{3} & \frac{2}{3} & -\frac{1}{3} & 0 & 0 & 0
\end{pmatrix}
.\quad(16)
$$

The columns and rows of S^B are arranged such that the bonds outgoing from the root occupy the first 1.(c) indices, while the incoming ones take the last ones. The first matrix on the left is just the exponentiated bond-length matrix. In the second matrix, the reflection coefficients are denoted by ρ with a suffix which labels the corresponding bond by its length. The 3×3 matrix at the lower left quadrant is the vertex scattering matrix for the root. After some algebra we get

$$\det(\, I - S^B(k)\,) =$$

$$\frac{1}{3}\left[4(1 - \tilde{\rho}_a(k)\tilde{\rho}_b(k)\tilde{\rho}_c(k) - (1 - \tilde{\rho}_a(k))(1 - \tilde{\rho}_b(k))(1 - \tilde{\rho}_c(k))\right]\quad(17)$$

where $\tilde{\rho}_a(k) = e^{4iak}\rho_a(k)$, *etc.* The secular equation can be made real by multiplying it with $[\det S^B(k)]^{\frac{1}{2}} = [-\tilde{\rho}_a(k)\tilde{\rho}_b(k)\tilde{\rho}_c(k)]^{\frac{1}{2}}$. This gives the desired form of the secular equation in real form, and the only task is to compute the reflection coefficients $\rho_{a,b,c}$.

The computation of ρ_a or ρ_b (for graph I in figure 1.(c)) is straight forward. It corresponds to scattering from a vertex from which emerge two bonds of lengths p and q and the line on which the wave is incoming and outgoing. The reflection coefficient is

$$r(p, q; k) = -\frac{\tan kp + \tan kq - i}{\tan kp + \tan kq + i}\quad(18)$$

Thus, $\rho_a(k) = r(b, c; k)$; $\rho_b(k) = r(a, c; k)$. The computation of the reflection coefficient of the more complex branch needs on more element.

Consider a $v = 3$ vertex out of which a bond of length p emerges and waves can imping on the vertex from two lines and be either transmitted or reflected. The vertex scattering matrix in this case is 2×2 and it reads

$$\sigma(k) = \begin{pmatrix} r(p;k) & t(p;k) \\ t(p;k) & r(p;k) \end{pmatrix} \quad ;$$

$$t(p;k) = \frac{1}{1 - \frac{i}{2}\tan kp} \quad ; \quad r(p;k) = \frac{\frac{i}{2}\tan kp}{1 - \frac{i}{2}\tan kp} \ . \tag{19}$$

Proceeding now along the branch from the root, we encounter 3 vertices with scattering matrices of the type (19) which are separated by and vertices of lengths $2c, 2b, 2a$ until we reach a vertex from which the reflection coefficient is of the type (18). The effective reflection coefficient can be computed iteratively, using

$$\rho_i = r_i + \frac{e^{2ikp_i}t_i^2}{1 - r_i e^{2ikp_i}\rho_{i-1}}\rho_{i-1} \ . \tag{20}$$

Here ρ_i is the reflection coefficient from the branch which starts at the i'th vertex. The length of the bond $i, i-1$ is p_i, the verex with $i = 0$ is the last $v = 3$ vertex (number 1 in graph I of figure 3) and for the computation here the iteration goes over $i = 1, 2, 3$. Clearly $\rho_0 = r(p = a, q = b; k)$. The mapping $\rho_{i-1} \to \rho_i$ is a Möbius transformation which preserves the unit circle.

Finally it should be noted that the tools developed above, can be directly applied for all but the pair 21_1 shown in figure 5 of (Y. Okada et.al., 2001).

4. Summary

We presented above a general method to construct isospectral pairs of quantum graphs, by converting each of the known pairs of domains in $\mathbb{R}^2$ to a corresponding pair of quantum graph. We demonstrated it by an explicit example, and provided two secular functions whose zeros are the spectrum of the graphs. One of these secular functions preserves in a transparent way the underlying algebraic structure which is responsible for the isospectrality. This is achieved at the cost of being less convenient for numerical work. The scattering approach provides another form of the secular function which is bounded on the real k axis. The tree structure of the graphs can be used to simplify the secular function, at the cost of obscuring the underlying algebraic structure.

However, the secular functions for the pairs of graphs coincide in both version - thus providing explicit proofs of isospectrality.

5.   Acknowledgments

References

Kac, M. *Amer. Math. Monthly*, 73:1, 1966.

Sunada, T. *Ann. of Math.*, 121:196, 1985.

Halbeisen, L., and N. Hungerbuhler. *J. Graph Theory*, 31:255, 1999.

Gordon, C., D. Webb and S. Wolpert. *Bull. Am. Math. Soc.*, 27:134, 1992.

Chapman, S. *Amer. Math. Mon.*, 102:124, 1995.

Buser, P., J. Conway, P. Doyle and K.-D. Semmler. *Int. Math. Res. Notices*, 9:391, 1994.

Okada Y., and A. Shudo. *J. Phys. A: Math. Gen.*, 34:5911, 2001.

Zelditch, S. Survey on the inverse spectral problem. *to appear in J. Diff. Geom. Surveys*, 2004.

Brooks, R. *Ann. Inst. Fouriere*, 49:707, 1999.

Kottos, T., and U. Smilansky. *Annals of Physics*, 274:76, 1999.

Fisher, M.E. *J. Combinatorial Theory*, 1:105, 1966.

Gutkin, B., and U. Smilansky. *J. Phys. A.*, 31:6061, 2001.

Carlson, R. *Trans. Amer. Math. Soc.*, 351:4069, 1999.

Jean-Pierre Roth. Lectures Notes in Mathematics: Theorie du Potentiel. *A. Dold and B. Eckmann, eds. (Springer–Verlag)*, 521.

Scarred states in strongly coupled quantum systems

Bala Sundaram

Graduate Faculty in Physics & Department of Mathematics,
City University of New York - CSI,
Staten Island, New York 10314

Abstract. Twenty years after they were first introduced, quantum wavefunctions scarred on classically unstable structures continue to appear in new and surprising contexts. Starting from the photoelectric effect in ultra-strong fields, the manuscript briefly reviews some of these and suggests a motivation for a more general understanding of this quantum phenomenon.

1. Introduction

In his 1987 Bakerian Lecture to the Royal Society in London, M. V. Berry defined quantum chaology as "the study of semiclassical, but nonclassical, behaviour characteristic of systems whose classical motion exhibits chaos" (M.V. Berry, 1987). For more than two decades prior to this, work on systems which exhibited such behavior had been ongoing under the nominal definition of 'quantum chaos' (G. Casati, et.al., 1995). Unfortunately, the very nature of quantum mechanics precludes many of the defining characteristics of classical chaos, making this latter definition burdensome. In fact it even led some researchers to ignore the unquestionable fact that there are quantifiable changes in the quantum dynamics when the limiting classical dynamics exhibits chaos, as compared with a nonchaotic counterpart. In this article, we focus on one specific manifestation, the phenomenon of "scarring" of quantum mechanical wavefunctions on unstable classical structures.

The concept of scarred quantum wavefunctions was introduced by Eric Heller (E.J. Heller, 1984) a little over 20 years ago in work that contradicted what appeared at the time to be a reasonable expectation. It had been conjectured (M.V. Berry, 1981) that a semiclassical eigenstate (when appropriately transformed) is concentrated on the region explored by a generic classical orbit over infinite times. Applied to classically chaotic systems, where a typical orbit was expected to uniformly cover the energetically allowed region, the corresponding typical eigenfunction was anticipated to be a superposition of plane

waves, i.e.

$$\psi = \sum_n A_n \exp\left(i\vec{k_n}.\vec{r}\right) , \tag{1}$$

with random amplitudes A_n and random orientation $\vec{k_n}$ though constant $|\vec{k_n}|$. Heller considered the system of the stadium or Bunimovich billiards, known to be classical chaotic, and numerically computed the excited states of the quantum problem. The surprise was that these states were not at all random but exhibited pronounced ridges along unstable classical periodic orbits. A heuristic explanation of this phenomenon can immediately be constructed by considering a quantum wavepacket centered on a classical unstable periodic orbit. The packet returns with frequency ω and a reduced amplitude characterized by the classical Lyapunov exponent λ and self-interferes. The ratio ω/λ controls the local density enhancement, favoring shorter period orbits and those that are less unstable. In general, states are associated with a combination of periodic orbits than with a specific orbit except in the deep semiclassical regime.

Semiclassical constructions of scarred wavefunctions, first in configuration space (E.B. Bogomolny, 1988) and then more conveniently in phase space (M.V. Berry, 1989), were quickly obtained. The phase space construction is particularly suggestive for our view given the clear analogy to the treatment of integrable systems. The result was a Wigner function peaked along a periodic orbit with interference fringes due to on- and off- energy shell effects. A few years later, a measure of the extent of scarring (along a periodic orbit) or 'scar weight' was proposed which once again reinforced the idea that lower period orbits are more prone to scarring (O. Agam, et.al., 1994).

In this article, we take the view that scarred states provide a basis for strongly coupled quantum systems, which typically exhibit non-integrable classical limits. We use a simple paradigm to support this view and cite other examples in the literature as evidence that the idea may be valid in applications outside the strict semiclassical regime and for open quantum systems. These are used to suggest the need for a more general understanding of the scarring phenomenon, even in the semiclassical regime (H. Schanz, et.al., 2003).

2. Photoeffect and stabilization

We were first introduced to the photoelectric effect as the emission of electrons when a surface is irradiated with light. The threshold is defined by $h\nu = W$ where ν is the frequency of the light and W a characteristic binding energy for the electron. It was soon realized that

a generalized multi-photon threshold $N_{th}h\nu = W$ was possible though the intensity of the light had to be considerably higher with increasing N_{th}. This principle was put into practice with the advent of the laser, with atoms and molecules as targets, and W taken to be the ionization or dissociation energy. Since that time, laser power has rapidly gone through the kilo-, mega-, giga-, and tera- prefixes and is now into the peta-Watt regime. This increase in intensity has brought with it new and manifestly non-perturbative phenomena such as above-threshold ionization (where the electron absorbs more photons than the minimum needed for ionization) and harmonic generation (the irradiated system scatters photons at frequencies which are large multiples of the incident frequency). These have led to a revision of the traditional analysis of multi-photon physics (P.W. Milonni, et.al., 1993). Most importantly, from our perspective, it has brought dynamics to the foreground.

Despite these changes in our understanding of the photoeffect, the one feature which had not been challenged was the fact that the probability of freeing the electron was still expected to *increase* with *increasing* intensity of the light. In other words, *the lifetime of the quantum state was expected to decrease* with growing intensity.

The phenomenon of 'stabilization' was reported in numerical experiments (Q. Su, et.al., 1990) with a model Hamiltonian for a 1-D atom:

$$H(x, p, t) = p^2/2 - 1/\sqrt{1 + x^2} + xF\cos(\omega t + \phi) , \qquad (2)$$

where F, ω, and ϕ are the field strength, frequency, and phase of the oscillating electric field (in atomic units). This 1-D model potential asymptotes to the Coulombic potential for large x, but eliminates the singular behavior at the origin. The solution of the time-dependent Schrodinger equation, yielded the surprising result that on *increasing F, the probability for freeing the electron decreased dramatically*, for fixed interaction time. The wavefunction at this time also exhibited peaks which were consistent with an effective double well potential (Q. Su, et.al., 1990). Both 'stabilization' and the distinct 'dichotomous' form of the residual wavefunction were soon confirmed in more realistic 3-D simulations (K.C. Kulander, et.al., 1991). However, introducing dynamics in the analysis shows that stabilization is an illustration of the effects of 'quantum chaology', which can then be used to predict both the extent of stabilization and the shape of the wavefunction (R.V. Jensen, et.al., 1990).

In the high-field limit ($F > 1$ atomic unit meaning that it is greater than the binding potential) the smoothed Coulomb potential in Eq. (2) can be treated as a perturbation on the regular, classical motion of a free electron in an oscillating field. So, let us first consider the Hamiltonian for the one-dimensional motion of a free electron in the

oscillating electric field $E = F cos(\omega t + \phi)$,

$$H_0(x, v, t) = v^2/2 - xF cos(\omega t + \phi) . \qquad (3)$$

The classical equations of motion can be integrated exactly and the solution for the position of the electron as a function of time,

$$x(t) = x_0 - \frac{F}{\omega^2}[\cos(\omega t + \phi) - \cos \phi] + [v_0 - \frac{F}{\omega} \sin \phi]t , \qquad (4)$$

describes a particle that oscillates back and forth in the electric field with frequency $\nu = \omega/2\pi$ and amplitude $\alpha = F/\omega^2$, and drifts away from its initial position, x_0, with velocity $v_d = v_0 - \frac{F}{\omega} \sin \phi$.

The classical motion is considerably simplified if we consider variables in the oscillating frame

$$q = x + \alpha[\cos(\omega t + \phi) - \cos \phi]$$

$$\qquad (5)$$

$$p = v - [\frac{F}{\omega} \sin(\omega t + \phi)] .$$

In the absence of any other forces $p = v_d$ is constant and the oscillation center drifts at the constant velocity $q(t) = x(0) + v_d t$. In particular, if $v_d = 0$ (eg. $v_0 = 0$ and $\phi = 0$ or π), then $q(t) = x_0$ is constant.

On adding a potential $V(x)$, we have in the transformed frame

$$H(q, p, t) = p^2/2 + V(q - \alpha[\cos(\omega t + \phi) - \cos \phi]) , \qquad (6)$$

which can be conveniently expanded in a discrete Fourier series

$$H(q, p, t) = p^2/2 + \sum_{n=-\infty}^{\infty} V_n(q)e^{in\omega t} , \qquad (7)$$

as the perturbation is periodic with period $T = 2\pi/\omega$. The Fourier coefficient $V_0(q)$ is simply the time-averaged potential which is all that is required in the high-frequency approximation. Away from this limit, the other coefficients $V_n(q)$ contain valuable dynamical information.

The ansatz that $V_n(q) \approx V_0(q)$ for a large number of n provides the other extreme. In this case, the Hamiltonian in the oscillating frame reduces to

$$H(q, p, t) \approx p^2/2 + V_0(q) \sum_{n=-\infty}^{\infty} \delta(t - nT + \phi T/2\pi) , \qquad (8)$$

using the Poisson sum rule. The phase ϕ can be set to zero with no loss of generality and integrating the classical equations of motion over one

period T leads to the nonlinear, area-preserving map,

$$q_{n+1} \; = \; q_n + Tp_{n+1}$$

$$(9)$$

$$p_{n+1} \; = \; p_n + G(q_n)$$

where q_n and p_n are the positions and momenta of the electron in the oscillating frame, evaluated once every period of the field. The total impulse of each kick $G(q_n)$ is the time-integral of the force over one period and can be simply expressed in terms of the space derivative of the time-integral of the oscillating potential,

$$G(q_n) = -\frac{d}{dq}TV_0(q)|_{q=q_n} \; . \qquad (10)$$

A more physical motivation for the map as well as the explicit conditions for its validity are discussed in Ref. (R.V. Jensen, et.al., 1990).
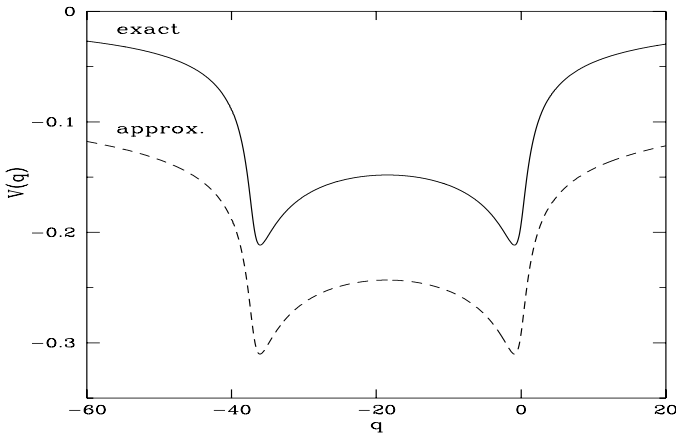
Figure 1. Kick potential as a function of q for $F = 5.0$ (a.u.) and $\omega = 0.52$ (a.u.), for both exact and approximate (evaluated only in the vicinity of the classical turning points) kicking terms. The curves clearly show that a simple constant shift is the only difference. Note that $F = 5$ means that the external field is five times larger than the binding field.

We now consider the smoothed Coulomb potential

$$V(x) = -Z/\sqrt{a^2 + x^2} \; , \qquad (11)$$

for which the time-average of the potential in the moving frame can be expressed exactly in terms of elliptic integrals. For our purposes it is enough to note that, as shown in Fig. 1, it is a double-welled potential
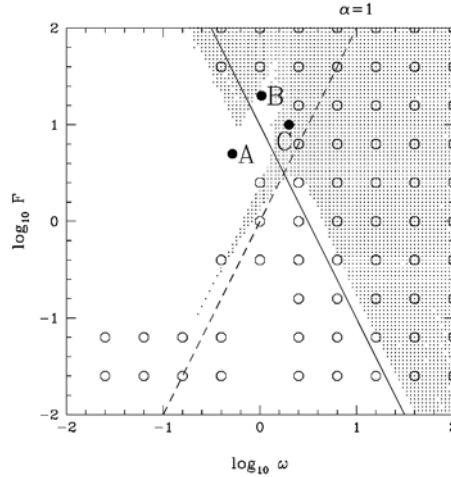
Figure 2. The classical stability of the map (dots) and the full differential dynamics (circles) was assessed by advancing the equations of motion 200 periods of the perturbation. If the trajectory returned to the vicinity of the nucleus a point was plotted in the $(\omega - F)$ parameter plane. The dividing line $\alpha = 1.0$ is indicated by the dotted line while the stability boundary is shown by the solid line.

with minima *near* the classical turning points at 0 and -2α for the free electron in the oscillating field. The map approximates the impulse only at these turning points and results in $G(q_n) = kF(q_n)$ where $k = \sqrt{8/F}$ and $F(x)$ involves complete elliptic integrals of the first and second kinds. The effective potential in the map approximation, also shown in Fig. 1, is simply shifted relative to the exact potential. The product $\kappa = kT$ is the *stochasticity parameter* and determines the nature (locally/globally/not chaotic) of the phase space of classical solutions. Both high field and high frequency limits lead to small κ, which implies 'linear' or integrable dynamics. The validity of the map approximation can be checked and shown to be more effective with increasing α (R.V. Jensen, et.al., 1990).

Using the mapping, a general stability analysis can be used to predict the classical parameter bounds for stabilization. These are *determined merely by the existence or not of stable regions (islands) in phase space.* The clearest representation of the parameter values for which regular regions exist in the classical phase space is a stability diagram in the space of $F - \omega$, shown in Fig. 2. The dotted line divides the overall parameter space into two regions where $\alpha < 1$ (on the right side) and $\alpha > 1$ (on the left side). When $\alpha << 1$ the map potential is a single well centered on a fixed point near $-\alpha$.

Increasing α leads to the effective double-well potential shown earlier with two elliptic (stable) and one hyperbolic (unstable) fixed points. The elliptic fixed points become unstable for parameter values below
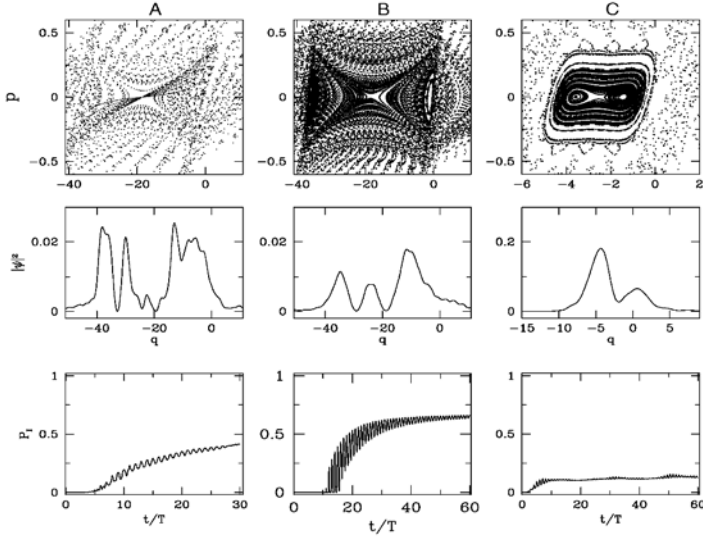
Figure 3. Classical phase portraits (upper panel), residual quantum wavefunctions (middle panel), and ionization probability versus time (in units of the period T) (bottom panel). The parameters are (A) $F = 5.0$, $\omega = 0.52$; (B) $F = 20$, $\omega = 1.04$; and (C) $F = 10$ and $\omega = 2.0$. Note that the peak structure of the final wavefunction reflects both stable and unstable classical fixed points. For case C, the peaks are beginning to coalesce reflecting the approach of the single-well effective potential (see text).

an analytically predicted stability border (solid line) after which *no classical mechanism for stabilization exists*. The predicted boundary is consistent with the existence of stable structures in both map dynamics (indicated by the dotted region) and the full differential dynamics (indicated by the open circles), as seen from Fig. 2. Note the region of low F and ω where map and differential dynamics disagree. In this regime, the relevant time scale is the internal period rather than the external field period we use. This results in a different stroboscopic approximation called the Kepler map (G. Casati, et.al., 1988).

We consider three parameter sets corresponding to the points A, B and C in the stability diagram. Purely classical stability arguments would suggest no stabilization for A and a larger fraction for C as compared with B. C is also closer to the line $\alpha = 1$ which means a near single-well effective potential. As we shall see, the quantum determination of stability is considerably more complicated.

For the quantum dynamics, we simply integrate the time-dependent Schrödinger equation (in atomic units)

$$i\frac{\partial \Psi(x,t)}{\partial t} = \left[-\frac{1}{2}\frac{\partial^2}{\partial x^2} - V(x) - xE(t) \right] \Psi(x,t) , \qquad (12)$$

on a space-time grid. The initial condition is the ground state of the undriven potential. Given our picture of the stabilization mechanism as resulting from a free-particle interacting periodically with trapping centers (in this case a double well potential), a simple measure of ionization is the fraction of wavefunction that is outside the "interaction volume". A smaller ionized fraction means increased stabilization. As the maximum spacing of the double-wells (averaging over an external period) is 4α, a suitable choice for this interaction volume (in one dimension) is $-4\alpha \le x \le 4\alpha$. Thus, a definition of ionization as

$$P_I(t) = \int_{|x|>4\alpha} |\Psi(x,t)|^2 dx \qquad (13)$$

is adequate to establish when stabilization is significant.

The results of the quantum simulations for cases A, B and C are shown in the lower two panels in Fig. 3. The corresponding classical phase portraits shown reinforce our inferences from the stability diagram; no stabilization for A while larger islands exist for C as compared with B. However, the ionized fraction as calculated from the quantum evolution supports the contrary result that there is *more stabilization for A as compared with B*. Case C is the most stable which is at least consistent with the classical prediction. What is the origin of this discrepancy?
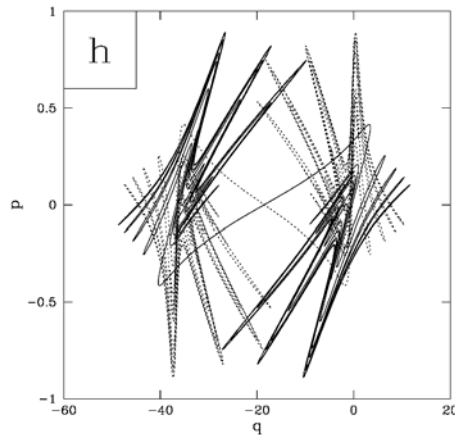
Figure 4. Homoclinic tangle associated with the fixed point at $(-\alpha, 0)$ for case A. Near the fixed point, the solid line gives the unstable direction while the dashed line is the stable direction. The size of Planck's constant h is shown to illustrate that several states can be supported by the single structure. An estimate of the number of states is given by the number of h boxes needed to cover the structure.

The resolution comes from the fact that the classical predictions were based entirely on the stability analysis of low-order fixed points.

Though a fixed point may be unstable, there remains an important dynamically invariant, but unstable, classical structure - the *homoclinic tangle*. Homoclinic tangles corresponding to cases A and B are shown in Figs. 4 and 5 respectively. The tangle emanates from unstable fixed points and its complicated appearance is simply a consequence of the area-preserving constraint of Hamiltonian evolution. The unstable tangle also provides support for quantum wavefunctions - an example of scarring. A simple estimate of the 'support' provided by the tangle for quantization is obtained by considering how the size (area) of the tangle compares with Planck's constant. This measure clearly shows that despite larger stable regions, the overall support   *stable and unstable*, is considerably less in case B as compared with case A. This is the reason for the reduced stabilization. However, the wavefunction at the end of the interaction time in case B exhibits three distinct peaks which clearly reflect the stable regions in the phase space, unlike A. Case C is one where the phase space is dominated by a large stable region and classical and quantum intuition agree. Thus, the discrepancy in cases A/B is a direct consequence of what was stated to be quantum chaology - "..nonclassical behaviour characteristic of systems whose classical motion exhibits chaos".
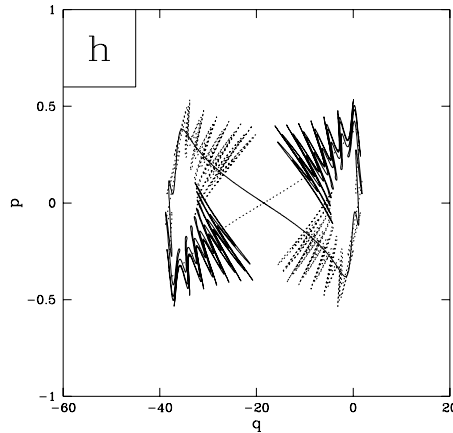
Figure 5. Same as Fig 4 but for case B. Note that the classical excursion $\alpha = F/\omega^2$ is the same in the two cases.

These considerations can be extended to the full 3-D system where scarring is once again a relevant feature (R.V. Jensen, et.al., 1993; F. Benvenuto, et.al., 1994). For those concerned by the large field strengths used in the illustrative cases, it should be noted that these results can be scaled to other frequency regimes and also to excited state initial conditions, where an experimental realization is more likely (R.R. Jones, et.al., 1991). However, our simple example is sufficient to

illustrate the fact that scarred states provide a compact description of the quantum behavior of this strongly coupled system.

3. Other examples and inferences

The system we just considered shows how the transfer of energy from the external field to the atomic system is severely hampered when scarred quantum states are excited. The very same effect was first experimentally seen and analyzed in the context of highly-excited (Rydberg) atoms in the presence of strong electric or magnetic fields. In particular, we cite the example of microwave ionization of Rydberg hydrogen atoms where it was observed that the field strengths required to ionize atoms prepared in $n = 62$ state was considerably higher than when the initial state was $n = 61$ (Van Leeuven, et.al., 1985; E.J. Galvez, et.al., 1988). On projecting the initial state onto a appropriately chosen basis, it was shown that the $n = 62$ projection was dominated by a single strongly scarred state (R.V. Jensen, et.al., 1989). By contrast, $n = 61$ was composed of several states none of which strongly inhibited excitation to higher levels. A detailed resolution to the question as to why the excitation of this particular state inhibited ionization was provided a few years later (J.G. Leopold, et.al., 1994) when it was shown that the scarred state was *less strongly coupled* to high lying states as contrasted with (energetically) adjacent states. Other instances of non-monotonic variation in the data could also be explained using this same idea.

This notion that scarred states may preferentially couple to other states was also suggested more recently in the context of deviations from random matrix theory (S. Jammalamadaka, et.al., 1999). The authors considered the case of a Rydberg atom in a magnetic field and looked for deviations in the statistics of transition probabilities from the predictions of random matrix theory. They found variation from the predicted distribution at large values of the (scaled) transition probability and related this to couplings among states scarred on classical unstable periodic orbits. On removing these states from the sample, the distribution reverted to the random matrix theory prediction. Thus, in this case, the scarred wavefunctions formed a strongly coupled subspace of states.

Another important contribution came in the form of a solution to an old problem, that of the semiclassical theory of Helium (G.S. Ezra, et.al., 1991). Besides demonstrating the necessity to include contributions from unstable dynamics in computing the energies, the work also showed that doubly excited resonances (corresponding to strongly

coupled electronic motion) are scarred states. Together, these examples (and others) appear to suggest that scarred states (when better characterized) may be an effective basis for dealing with strongly coupled quantum systems.

The stability of scarred states to external noise and other environmental disturbances was the next natural issue that was raised and partially addressed earlier (L. Sirko, et.al., 1993; R. Scharf, et.al., 1994). The main conclusion was that scarred states are quite robust to 'reasonable' levels of noise. This question took on added relevance with the coming of age of mesoscopic systems where, be it spontaneous emission in atom optics or leads or scattering and other forms of dissipation in heterostructures, the open nature of the system must be accounted for. These new experiments also provided non-ideal realizations of simple theoretical paradigms such as stadium billiards and the kicked rotor, with additional issues that had to be accounted for in the theory.

The role of leads in electronic realizations of billiard systems (C. M. Marcus, et. al., 1992) is of particular interest. Here, the usual assumption is that the coupling to the leads uniformly smears the (lead-free) level spectrum. However, recent work (R. Akis, et.al., 2002) challenges this notion, suggesting instead that level broadening is highly nonuniform and that individual states can stay resolved even when the leads are very wide. In particular, these 'long-lived' states were shown to be those scarred on periodic orbits which avoid the leads, suggesting situations under which some scarred states may survive an apparent strong coupling to the environment.

Our recent work on a semiclassical view of the quantum-classical transition in a class of open systems shows that environmental noise modifies both classical and quantum dynamics to arrive at agreement (B. D. Greenbaum, et. al.,). When the two dynamics match, the Wigner function clearly highlights the early time segments of the unstable classical manifold (with some fringing) suggesting a possible connection to the Berry construction for scars (M.V. Berry, 1989). Here again, the coupling to the environment is significant when this occurs.

In summary, the main point of this paper can be put in the following way. Integrable systems (classical and quantum) can be viewed as those with a preferred (diagonal) representation, a feature that no longer exists once the classical dynamics become nonintegrable or chaotic. Here, quantum mechanically, any expansion basis is as effective as any other. We have suggested (by considering just a few examples from a large literature on the topic) that scarred states may be the preferred basis for strongly coupled quantum systems and, as such, are worth characterizing more fully.

4. Acknowledgments

References

Berry, M.V. *Proc. Roy. Soc. London A*, 413:183, 1987.

Casati, G. and B.V. Chirkov. Quantum chaos: between order and disorder: a selection of papers. *Cambridge University Press, New York*, 1995.

Heller, E.J. *Phys. Rev. Lett.*, 53:1515, 1984.

Berry, M.V. Les Houches Lecture Series Session **XXXV**. *eds. Balian, R., Kle'man, M., and Poirier, J-P., (North-Holland, Amsterdam)*, 453, 1981.

Bogomolny, E.B. *Physica D*, 31:169, 1988.

Berry, M.V. *Proc. Roy. Soc. London A*, 423:219, 1989.

Agam, O., and S. Fishman. *Phys. Rev. Lett.*, 73:806, 1994.

Schanz, H., and T. Kottos. *Phys. Rev. Lett.*, 90:23401, 2003.

Milonni, P.W., and B. Sundaram. *Progress in Optics*, XXXI:3, 1993.

Su, Q., J.H. Eberly, and J. Javanainen. *Phys. Rev. Lett.*, 64:862, 1990.

Kulander, K.C., K.J. Schafer, and J.L. Krause. *in Multiphoton Processes, edited by G. Mainfray, and P. Agostini (CEA-Press, Paris)*, 1991; *ibid Phys. Rev. Lett.*, 66:2601, 1991.

Jensen, R.V., and B. Sundaram. *Phys. Rev. Lett.*, 65:1964, 1990; *ibid Phys. Rev. A*, 47:1415, 1993.

Casati, G., I. Guarneri, and D.L. Shepelyansky. *IEEE J. Quantum Electron*, 24:1420, 1988.

Jensen, R.V., and B. Sundaram. *Phys. Rev. A*, 47:1415, 1993; *Laser Physics*, 3:291, 1993.

Benvenuto, F., G. Casati, and D.L. Shepelyansky. *Z. Phys. B*, 94:481, 1994.

Jones. R.R., and P.H. Bucksbaum. *Phys. Rev. Lett.*, 67:3215, 1991; De Boer, M.P., J.H. Hoogenraad, R.B. Vrijen, L.D. Noordam, and H.G. Muller. *Phys. Rev. Lett.*, 71:3263, 1993.

Van Leeuwen, K. A. H., et.al. *Phys. Rev. Lett.*, 55:2231, 1985.

Galvez, E.J., B.E. Sauer, L. Moorman, P.M. Koch, and D. Richards. *Phys. Rev. Lett.*, 61:2011, 1988.

Jensen, R.V., M.M. Sanders, M. Saraceno, and B. Sundaram. *Phys. Rev. Lett.*, 63:2771, 1989.

Leopold, J.G., and D. Richards. *J. Phys. B*, 27:2169, 1994.

Jammalamadaka, S., J. Main, and G. Wunner. *Nonlinear Phenomena in Complex Systems*, 2:1, 1999.

Ezra, G.S., K. Richter, G. Tanner, and D. Wintgen. *J. Phys. B*, 24:L413, 1991.

Sirko, L., M.R.W. Bellermann, A. Haffmans, P.M. Koch, and D. Richards. *Phys. Rev. Lett.*, 71:2895, 1993.

Scharf, R., and B. Sundaram. *Phys. Rev. E*, 49:R2509, 1994.

Marcus, C.M., A.J. Rimberg, R.M. Westervelt, P.F. Hopkins, and A.C. Gossard. *Phys. Rev. Lett.*, 69:506, 1992; Marcus, C.M., R.M. Westervelt, P.F. Hopkins, and A.C. Gossard. *Chaos*, 3:643, 1993.

Akis, R., J.P. Bird, and D.K. Ferry. *Appl. Phys. Lett.*, 81:129, 2002.

Greenbaum, B.D., S. Habib, K. Shizume, and B. Sundaram. *quant-ph/0401174*.

Nonlinear quantum dynamics

Salman Habib
The University of California, Los Alamos National Laboratory,
Los Alamos, New Mexico, USA

Abstract. The vast majority of the literature dealing with quantum dynamics is concerned with linear evolution of the wave function or the density matrix. A complete dynamical description requires a full understanding of the evolution of measured quantum systems, necessary to explain actual experimental results. The dynamics of such systems is intrinsically nonlinear even at the level of distribution functions, both classically as well as quantum mechanically. Aside from being physically more complete, this treatment reveals the existence of dynamical regimes, such as chaos, that have no counterpart in the linear case. Here, we present a short introductory review of some of these aspects, with a few illustrative results and examples.

Keywords: chaos, conditioned evolution, continuous measurement, density matrix, quantum backaction, quantum feedback.

1. Introduction

It is hard to imagine a scientific discipline older than the study of dynamical systems. The remarkable history of the field testifies to nature's inexhaustible store of subtlety and ability to surprise. Ever since Galileo, remarkable experiments, deep theoretical insights, and powerful calculational tools have all contributed to creating the rich panorama that the field presents today.

From a theoretical perspective, dynamical systems are specified by the rules of evolution and the physical objects to which these rules apply. Our fundamental notions regarding both aspects have undergone radical changes in the past few hundred years. Classical mechanics has made way for quantum mechanics and absolute notions of space and time have been replaced by the unified viewpoint of classical general relativity. A key lesson to be drawn from these advances is that even the most basic notions regarding the nature of physical information must change as our overall understanding progresses.

The next step forward has yet to be taken: The clash between relativity and quantum mechanics – the choice between causality and unitarity – awaits resolution. However, on a less grand scale, the tension between fundamentally different points of view is already apparent in the discord between quantum and classical mechanics. Unlike special relativity, where $v/c \to 0$ smoothly transitions between Einstein and

Newton, the limit $\hbar \to 0$ is singular. The symmetries underlying quantum and classical dynamics – unitarity and symplecticity, respectively – are fundamentally incompatible with the opposing theory's notion of a physical state: quantum-mechanically, a positive semi-definite density matrix; classically, a positive phase-space distribution function.

Chaos provides an excellent illustration of this dichotomy of worldviews (A. Peres, 1993). Without question, chaos exists, can be experimentally probed, and is well-described by classical mechanics. But the classical picture does not simply translate to the quantum view; attempts to find chaos in the Schrodinger equation for the wave function, or, more generally, the quantum Liouville equation for the density matrix, have all failed. This failure is due not only to the linearity of the equations, but also the Hilbert space structure of quantum mechanics which, via the uncertainty principle, forbids the formation of fine-scale structure in phase space, and thus precludes chaos in the sense of classical trajectories. Consequently, some people have even wondered if quantum mechanics fundamentally cannot describe the (macroscopic) real world.

It is therefore clear that there is more than sufficient motivation for investigating the notion of nonlinearity in classical and quantum theories. The main point of this article is to provide an angle of vision which sets nonlinearity in its experimentally relevant context. Familiar to control theorists (P.S. Maybeck;Jacobs, 1993) – but much less so to most physicists – this perspective bridges the classical and quantum points of view and smoothly connects them with each other.

The ar ticle is organized as follows. We will begin with a discussion of the various possibilities of dynamical description, clarify what is meant by "nonlinear quantum dynamics", discuss its connection to nonlinear classical dynamics, and then study two experimentally relevant examples of quantum nonlinearity – (i) the existence of chaos in quantum dynamical systems far from the classical regime, and (ii) real-time quantum feedback control.

The results described here are due to the efforts of many people spread over the last thirty years or so, some results being even older. Unfortunately, space limitations prevent anywhere near an adequate job of referencing, for which a sympathetic understanding is begged in advance. Restrictions also meant the omission of important topics and explanations of derivations.

2. Evolution: isolated, open, and conditioned

How should one describe a dynamical system? Before settling on a definition, it is best to first ask some important physical questions. As an illustrative example, a situation worth learning from arose in the attempt to define a field-theoretic notion of a particle in a general spacetime (W.G. Unruh, 1976). In Minkowski space, the formal definition is simple: positive energy plane-waves, but this definition cannot be extended to arbitrary metrics. It soon became clear that the correct way to approach the problem was to give up the attempt to arrive at a formal definition and replace it with a physical definition: "A particle is what a particle detector detects." Thus, specifying a field theory Lagrangian is not sufficient to define the notion of a particle, additionally we must model the detector and how it couples to the field. Just what a physical 'particle' is depends on the design of the detector and the field-detector coupling.

Keeping the lesson of the above example in mind, we will explore three different dynamical possibilities below: *isolated* evolution, where the system evolves without any coupling to the external world, *unconditioned open* ev olution, where the system evolves coupled to an external environment but where no information regarding the system is extracted from the environment, and *conditioned open* evolution where such information is extracted. In the third case, the evolution of the physical state is driven by the system evolution, the coupling to the external world, and by the fact that observational information regarding the state has been obtained. This last aspect – system evolution *conditioned* on the measurement results via Bayesian inference – leads to an intrinsically nonlinear evolution for the system state. The conditioned evolution provides, in principle, the most realistic possible description of an experiment. To the extent that quantum and classical mechanics are eventually just methodological tools to explain and predict the results of experiments, this is the proper context in which to compare them.

2.1. Isolated and Open Evolution

Suppose we are given an arbitrary system Hamiltonian $H(x,p)$ in terms of the dynamical variables x and p; we will be more specific regarding the precise meaning of x and p later. The Hamiltonian is the generator of time evolution for the physical system state, provided there is no coupling to an environment or measurement device. In the classical case, we specify the initial state by a positive phase space distribution function $f_{Cl}(x,p)$; in the quantum case, by the (position-representation) positive

semi-definite density matrix $\rho(x_1, x_2)$ or, completely equivalently, by the Wigner distribution function $f_W(x, p)$ (M. Hillery et.al., 1984) (not positive).

The evolution of an *isolated* system is then given by the classical and quantum Liouville equations for the *fine-grained* distribution functions (i.e., the evolution is entropy-preserving):

$$\partial_t f_{Cl}(x, p) = -\left[\frac{p}{m}\partial_x - \partial_x V(x)\partial_p\right] f_{Cl}(x, p), \qquad (1)$$

$$\partial_t f_W(x, p) = -\left[\frac{p}{m}\partial_x - \partial_x V(x)\partial_p\right] f_W(x, p)$$
$$+ \sum_{\lambda=1}^{\infty} \frac{(\hbar/2i)^{2\lambda}}{(2\lambda+1)!} \partial_x^{2\lambda+1} V(x)\partial_p^{2\lambda+1} f_W(x, p), \qquad (2)$$

here we have assumed for simplicity that the potential $V(x)$ can be Taylor-expanded. Note that these evolutions are both linear in the respective distribution functions. Classically, the limit $f_{Cl}(x, p) = \delta(x - \bar{x})\delta(p - \bar{p})$ is allowed, and, on substitution in Eqn. (2), yields Newton's equations. These may then be interpreted as equations for the particle position and momentum, although this identification is only formal at this stage (as in the Minkowski space definition of a particle in the field theory example). Quantum mechanically, this ultralocal limit is not allowed as $f_W(x, p)$ must be square-integrable, therefore, even formally, no direct particle interpretation exists (an obstacle that arises as something new is added – just like the generalization to arbitrary metrics above).

The basic idea behind extension to open systems is simple to state but not easy to implement in practice. The complete Hamiltonian now includes a piece representing the environment and another, the system-environment coupling. If the environment is in principle unobservable, then a (nonlocal in time) linear master equation for the system's reduced density matrix is derivable by tracing over the environmental variables (in practice, tractable equations are impossible to obtain without drastic simplifying assumptions such as weak coupling, timescale separations, and simple forms for the environmental and coupling Hamiltonians). In any case, the important point to note is that the act of tracing over the environment does not change the linear nature of the equations. Generally speaking, master equations describing open evolution of *coarse-grained* distributions augment the RHS of Eqns. (2) and (2) with terms containing dissipation and diffusion kernels connected via generalized fluctuation-dissi pation relations (R. Zwanzig, 2001). While the classical diffusion term vanishes in the limit of zero

temperature for the environment, this is not true quantum mechanically due to the presence of zero-point fluctuations.

2.2. CONDITIONED EVOLUTION

Conditioned evolution of the type we are interested in here is fundamentally different from the equations discussed above. We assume that measurements are possible on the environment and ask what the evolution of the reduced density matrix of the system is, given that the results of these measurements are known (H.J. Carmichael, 2001). Let us consider an example. Suppose we wish to measure the position of a nanomechanical oscillator (Fig. 1). By electrostatically coupling the resonator to a single-electron transistor (SET), and measuring the (classical) SET current – the measurement record – we are in fact measuring the transverse displacement of the resonator. In this situation, the evolution of the reduced density matrix of the system must contain a term that reflects the gain in information arising from the measurement record ("innovation" in the language of control theory). This term, arising from applying a continuous analog of Bayes' theorem, is intrinsically nonlinear in the distribution function. The coupling to an external probe (and the associated environment) will also cause effects very similar to the open evolution considered earlier, and there can once again be dissipation and diffusion terms in the evolution equations. The primary differences between the classical and quantum treatments, aside from the kinematic constraints on the distribution functions, are the following: (i) the (nonlocal in p) quantum evolution term in Eqn. (2), and (ii) an irreducible diffusion contribution due to quantum backaction reflecting the *active* nature of quantum measurements.

We now consider a simple model of position measurement to provide a measure of concreteness. In this model, we will assume that there are no environmental channels aside from those associated with the measurement. Suppose we have a single quantum degree of freedom, position in this case, under a weak, ideal continuous measurement (C.M. Caves et.al., 1987). Here "ideal" refers to no loss of information during the measurement, i.e., a fine-grained evolution with no loss of unitarity. Then, we have two coupled equations, one for the measurement record $y(t)$,

$$dy = \langle x \rangle dt + dW/\sqrt{8k} \qquad (3)$$

where dy is the infinitesimal change in the output of the measurement device in time dt, the parameter k characterizes the rate at which the measurement extracts information about the observable, i.e., the *strength* of the measurement (A.C. Doherty et.al., 2001), and
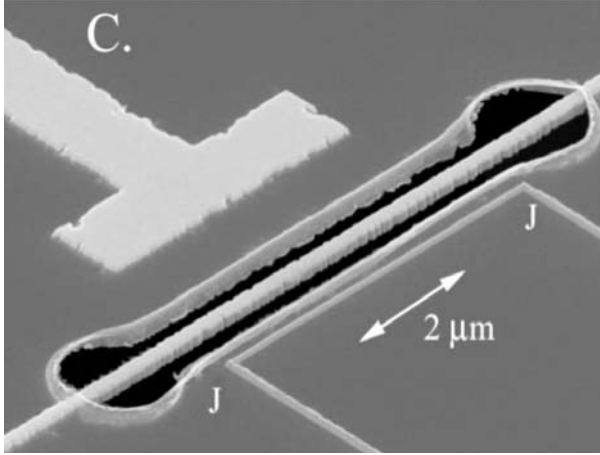
Figure 1. A nanomechanical resonator: the thin central bar is coated with a conductor (gold) which also forms the T-shaped control electrode to the left. The thin line parallel to the resonator is the central island of a single-electron transistor which serves as the position sensor.

dW is the Wiener increment describing driving by Gaussian white noise (D.T. Gillespie, 1996), the difference between the observed value and that expected. The other equation – the nonlinear stochastic master equation (SME) – specifies the resulting conditioned evolution of the system density matrix, given below in the Wigner representation,

$$
\begin{aligned}
f_W(x,p,t+dt) \; = \; & \left[1 + dt \left[-\frac{p}{m}\partial_x + \partial_x V(x)\partial_p + D_{BA}\partial_p^2 \right] \right. \\
& \left. + dt \sum_{\lambda=1}^{\infty} \frac{(\hbar/2i)^{2\lambda}}{(2\lambda+1)!} \partial_x^{2\lambda+1} V(x,t)\partial_p^{2\lambda+1} \right] f_W(x,p,t) \\
& + dt\sqrt{8k}(x - \langle x \rangle)f_W(x,p,t)dW,
\end{aligned} \tag{4}
$$

where $D_{BA} = \hbar^2 k$ is the diffusion coefficient arising from quantum backaction and the last (nonlinear) term represents the co nditioning due to the measurement. In principle, there is also a (generalized) damping term (D. Mozyrsky et.al., 2002), but if the measurement coupling is weak enough, it can be neglected. If we choose to average over all the measurement results, which is the same as ignoring them, then the conditioning term vanishes, but *not* the diffusion from the measurement backaction. Thus the resulting linear evolution of the coarse-grained quantum distribution is not the same as the linear fine-grained evolution (2), but yields a conventional open-system master equation. Moreover, for a given (coarse-grained) master equation, dif-

ferent underlying fine-grained SME's may exist, specifying different measurement possibilities.

The classical conditioned master equation [set $\hbar = 0$ in Eqn. (4), holding k fixed],

$$
\begin{aligned}
f_{Cl}(x, p, t + dt) \;=\; & \left[1 - dt \left[\frac{p}{m} \partial_x - \partial_x V(x) \partial_p \right] \right] f_{Cl}(x, p, t) \\
& + dt \sqrt{8k}(x - \langle x \rangle) f_{Cl}(x, p, t) dW,
\end{aligned}
\tag{5}
$$

does not have the backaction term as classical measurements are *passive*: Averaging over all measurements simply gives back the Liouville equation (2), and there is no difference between the fine-grained and coarse-grained evolutions in this special case. [In general, classical diffusion terms from ordinary open evolution can also co-exist, as in the more general *a posteriori* evolution specified by the Kushner-Stratonovich equation.] As a final point, we will delay our discussion of how the classical trajectory limit is incorporated in Eqn. (5), i.e., the precise sense in which the "the position of a particle is what a position-detector detects" to the next section.

3. QCT: The quantum-classical transition

As mentioned already, quantum and classical mechanics are fundamentally incompatible in many ways, yet the macroscopic world is well-described by classical dynamics. Physicists have struggled with this quandary ever since the laying of the foundations of quantum theory. It is fair to say that, even today, not everyone is satisfied with the state of affairs – including many seasoned practitioners of quantum mechanics.

If quantum mechanics is really the fundamental theory of our world, then an effectively classical description of macroscopic systems must emerge from it – the so-called quantum-classical transition (QCT). It turns out that this issue is inextricably connected with the question of the physical meaning of dynamical nonlinearity discussed in the Introduction. The central thesis is that real experimental systems are by definition not isolated, hence the QCT must be viewed in the relevant physical context.

Quantum mechanics is intrinsically probabilistic, but classical theory – as shown above by the existence of the delta-function limit for the classical distribution function – is not. Since Newton's equations provide an excellent description of observed classical systems, including chaotic systems, it is crucial to establish how such a localized description can arise quantum mechanically. We will call this the *strong* form of

the QCT. Of course, in many situations, only a statistical description is possible even classically, and here we will demand only the agreement of quantum and classical distributions and the associated dynamical averages. This defines the *weak* form of the QCT.

3.1. THE STRONG FORM OF THE QCT

It is clear that the strong form of the QCT is impossible to obtain from either the isolated or open evolution equations for the density matrix or Wigner function. For a generic dynamical system, a localized initial distribution tends to distribute itself over phase space and either continue to evolve in complicated ways (isolated system) or asymptote to an equilibrium state (open system) – whether classically or quantum mechanically. In the case of conditioned evolution, however, the distribution can be localized due to the information gained from the measurement. In order to quantify how this happ ens, let us first apply a cumulant expansion to the (fine-grained) conditioned classical evolution (5), resulting in the equations for the centroids ($\bar{x} \equiv \langle x \rangle$, $\bar{p} \equiv \langle p \rangle$),

$$d\bar{x} = \frac{\bar{p}}{m}dt + \sqrt{8k}C_{xx}dW, \quad d\bar{p} = \langle F(x) \rangle dt + \sqrt{8k}C_{xp}dW, \qquad (6)$$

where

$$F(x) = -\partial_x V(x), \quad C_{AB} = (\langle AB \rangle + \langle BA \rangle - 2\langle A \rangle \langle B \rangle)/2, \qquad (7)$$

along with a hierarchy of coupled equations for the time-evolution of the higher cumulants. These equations are the continuous measurement, real-world, analog of the formal ultralocal Newtonian limit of the distribution function in the classical Liouville equation (2). While Eqns. (6) always apply, our aim is to determine the conditions under which the cumulant expansion effectively truncates and brings their solution very close to that of Newton's equations. This will be true provided the noise terms are small (in an average sense) and the force term is localized, i.e., $\langle F(x) \rangle = F(\bar{x}) + \cdots$, the corrections being small. The required analysis involves higher cumulants and has been carried out in Ref. (T. Bhattacharya et.al., 2000;2003). (Ref. (T. Bhattacharya et.al., 2000;2003) also points to previous literature.) It turns out that the distribution will be localized provided

$$8k \gg \sqrt{\frac{(\partial_x^2 F)^2 |\partial_x F|}{2mF^2}} \qquad (8)$$

and the motion of the centroid will effectively define a smooth classical trajectory – the low-noise condition – as long as

$$k \gg \frac{2|\partial_x F|}{S} \tag{9}$$

where S is the action scale of the system. Note that this condition does not bound the measurement strength.

We now turn to the quantum version of these results. In this case, the analogous cumulant expansion gives exactly the same equations for the centroids as above, while the equations for the higher cumulants are different. We can again investigate whether a trajectory limit exists. Localization holds in the weakly nonlinear case if the classical condition above is satisfied. In the case of strong nonlinearity, the inequality becomes

$$8k \gg \frac{(\partial_x^2 F)^2 \hbar}{4mF^2}. \tag{10}$$

Because of the backaction, the low-noise condition is implemented in the quantum case by a double-sided inequality:

$$\frac{2|\partial_x F|}{s} \ll \hbar k \ll \frac{|\partial_x F| s}{4}, \tag{11}$$

where the action is measured in units of $\hbar$, s being dimensionless. The left inequality is the same as the classical one discussed above, however the right inequality is essentially quantum mechanical. The measurement strength cannot be made arbitrarily large as the backaction will result in too large a noise in the equations for the centroids. As the action s is made larger, both inequalities are satisfied for an ever wider range of k. For continuously measured quantum systems, trajectories that emerge in the macroscopic limit follow Newton's equations, and hence can be chaotic as shown in Ref. (T. Bhattacharya et.al., 2000;2003). Thus, as speculated in a prescient paper by Chirikov (B.V. Chirikov, 1991), measurement indeed provides the missing link between "quantum" and "chaos."

3.2. The Weak Form of the QCT

If the conditions enforcing the strong form of the QCT are satisfied, then the weak form follows automatically. The reverse is not true, however: results from a coarse-grained analysis cannot be applied to the fine-grained situation. Moreover, the violation of the strong inequalities (11) need not prevent a weak QCT: It does not matter if the distribution is too wide, as long as the classical and quantum distributions agree, and, even if the backaction noise is large, the coarse-grained distribution remains smooth and the weak quantum-classical

correspondence can still exist. Consequently, the weak form of the QCT has to be approached in a different manner. In fact, the weak version is just another way to state the con ventional decoherence idea; however, as discussed elsewhere (S. Habib et.al., 2002), mere suppression of quantum interference does not guarantee the QCT even in the weak form.

In a recent analysis carried out for a bounded open system with a classically chaotic Hamiltonian, it has been argued that the weak form of the QCT is achieved by two parallel processes (B. Greenbaum et.al.,), explaining earlier numerical results (S. Habib et.al., 1998). First, the semiclassical approximation for quantum dynamics, which breaks down for classically chaotic systems due to overwhelming nonlocal interference, is recovered as the environmental interaction filters these effects. Second, the environmental noise restricts the foliation of the unstable manifold (the set of points which approach a hyperbolic point in reverse time) allowing the semiclassical wavefunction to track this modified classical geometry.

It turns out that this analysis applies only to systems with a bounded phase space. It is possible that topological restrictions on the accessible phase space – and not only the form of the particular Hamiltonian – play a crucial role in determining when the weak form of the QCT actually applies. For example, this might explain why the open-system quantum delta-kicked rotor is a counter-example to naive expectations regarding the QCT (S. Habib et.al., 2002).

4. Chaos and quantum mechanics

The results of the previous section have already established that classical chaos and quantum mechanics are not incompatible in the macroscopic limit. The question then naturally arises whether observed quantum mechanical systems can be chaotic far from the classical limit? This question is particularly significant as closed quantum mechanical systems are not chaotic, at least in the conventional sense of dynamical systems theory (R. Kosloff et.al., 1981;1989). In the case of observed systems it has recently been shown, by defining and computing a maximal Lyapunov exponent applicable to quantum trajectories, that the answer is in the affirmative (S. Habib et.al., 1998). Thus, realistic quantum dynamical systems are chaotic in the conventional sense and there is no fundamental conflict between quantum mechanics and the existence of dynamical chaos.

The basic idea in Ref. (S. Habib et.al., 1998) is to focus attention on a single time-series, say, the expectation value $\langle x \rangle$, and analyze it for
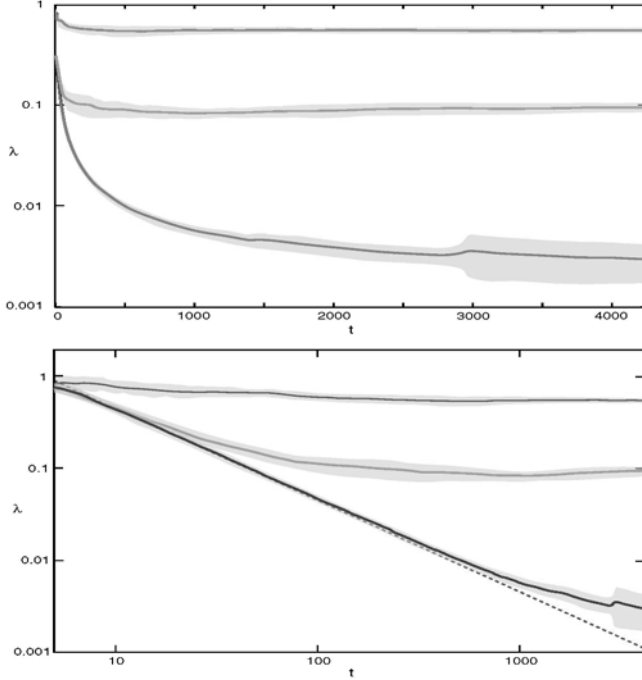
Figure 2. Finite-time Lyapunov exponents $\lambda(t)$ for a driven Duffing oscillator with measurement strengths $k = 5 \times 10^{-4}$, 0.01, 10, averaged over 32 trajectories (linear scale in time, top, and logarithmic scale, bottom; bands indicate the standard deviation over the 32 trajectories) (S. Habib et.al., 1998).The (analytic) $1/t$ fall-off at small k values (dashed red line), prior to the asymptotic regime, is evident in the bottom panel.

chaos. Following Ref. (S. Habib et.al., 1998) the Lyapunov exponent is defined to be

$$\lambda = \lim_{t \to \infty} \lim_{\Delta_s(0) \to 0} \frac{1}{t} \ln \Delta_s(t) \equiv \lim_{t \to \infty} \lambda_s(t) \tag{12}$$

where the subscript s denotes the particular noise realization and $\Delta(t) = |\langle x(t) \rangle - \langle x_{fid}(t) \rangle|$ defines the divergence between two "trajectories." The noise realization is kept fixed when calculating $\Delta(t)$. For isolated systems it is possible to prove that the Lyapunov exponent is zero, with the finite-time exponent vanishing as $1/t$, as $t \to \infty$ (S. Habib et.al., 1998). This is consistent with our expectation of not finding chaos for linear evolution. In the case of conditioned nonlinear evolution, however, the situation can be dramatically different as shown in Fig. 2. What we find is that for small k, $\lambda(t)$ first falls as $1/t$ (as for $k = 0$), but then stabilizes at an asymptotic value which is k-dependent, and different from the classical value. Even at values of k small enough

that the strong inequalities (11) are not satisfied, λ is finite, and the evolution is, thus, chaotic.

We stress that the chaos identified here is not merely a formal result - even deep in the quantum regime, the Lyapunov exponent can be obtained from measurements on a real system. Quantum predictions of this type can be tested in the near future, e.g., in cavity QED and nanomechanics experiments (H. Mabuch et.al., 2002;2004). Experimentally, one would use the known measurement record to integrate the SME; this provides the time evolution of the mean value of the position. From this fiducial trajectory, given the knowledge of the system Hamiltonian, the Lyapunov exponent can be obtained by following the procedure described above. It is important to keep in mind that these results form only a starting point for the further study of nonlinear quantum dynamics and its theoretical and experimental ramifications.

5. Quantum feedback control

To illustrate an application of nonlinear quantum dynamics, we now consider real-time control of quantum dynamical systems. Feedback control is essential for the operation of complex engineered systems, such as aircraft and industrial plants. As active manipulation and engineering of quantum systems becomes routine, quantum feedback control is expected to play a key role in applications such as precision measurement and quantum information processing. The primary difference between the quantum and classical situations, aside from dynamical differences, is the active nature of quantum measurements. As an example, in classical theory the more information one extracts from a system, the better one is potentially able to control it, but, due to backaction, this no longer holds true quantum mechanically.

Controlling quantum systems is possible using state-estimation ideas as pioneered by Belavkin (V.P. Belavkin et.al., 1992;2000) or direct feedback of the measured classical current (H.M. Wiseman et.al., 1993). Applications studied so far include controlling atomic (H.M. Wiseman et.al., 2002) and qubit (R. Ruskov et.al., 2002) states as well as active cooling of dynamical degrees of freedom. As one example, let us consider an atom trapped in a high-finesse optical cavity in the strong-coupling limit, with the output laser light monitored via homodyne detection. The resulting photocurrent provides information about the position of the atom in the cavity which, in turn, can be used to cool the atom's position degree of freedom by varying the intensity of the driving laser field (D.A. Steck et.al., 2004) (Fig. 3). Nanomechanical resonators can also be cooled by feedback. Here, the present state of the art has reached
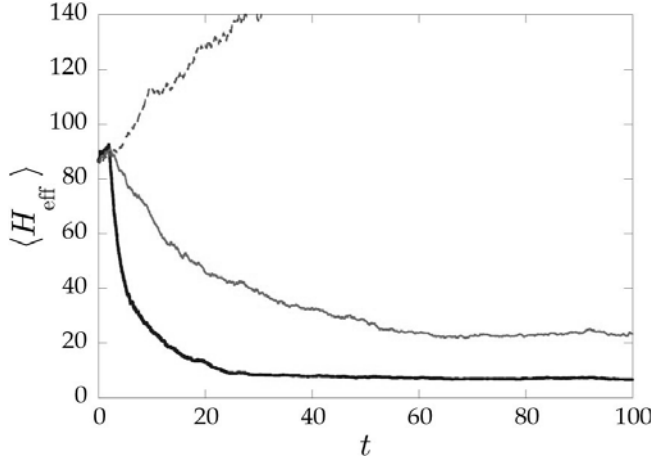
Figure 3. Feedback cooling in cavity QED: Evolution of the mean atomic effective energy, with no cooling (top curve), cooling based on direct feedback of the photocurrent signal (middle), cooling based on feedback with a simple Gaussian state estimator (bottom). Note the improved cooling efficiency in the second case.

the point where the resonators are less than a factor of 10 away from the quantum limit, i.e., the point where the thermal energy is less than the energy of the resonator ground state. Lowering the temperature of the resonators to the mK regime would allow this goal to be reached. In principle, active cooling could achieve this by measuring the resonator position using a SET as described earlier (Fig. 1) and then applying (damping) feedback through the control electrode (A. Hopkins et.al., 2003). Experiments to test this idea are currently in progress.

6. Acknowledgments

References

Peres, A. Quantum Theory: Concepts and Methods. *Kluwer*, 1993.

Maybeck, P.S. Stochastic Models, Estimation and Control. *Academic Press, New York*, 1982; Jacobs, O.L.R. Introduction to Control Theory. *Oxford University Press, Oxford*, 1993.

Unruh, W.G. *Phys. Rev. D*, 14:870, 1976.

Hillery, M., R.O. Connell, M.O. Scully and E.P. Wigner. *Phys. Rep.*, 106:121, 1984.

Zwanzig, R. Nonequilibrium Statistical Mechanics. *Oxford University Press, Oxford*, 2001.

Carmichael, H.J. An Open Systems Approach to Quantum Optics Quantum Noise. *Springer*, 1993; Gardiner, C.W. and P. Zoller. Quantum Noise. *Springer*, 2000; Orszag, M. Quantum Noise, *Springer*, 2000.

Caves, C.M. and G.J. Milburn. *Phys. Rev.A.*, 36:5543. 1987; Milburn, G.J. *Quantum Semiclass. Opt.*, 8:269. 1996; Doherty, A.C. and K. Jacobs. *Phys. Rev. A*, 60:2700, 1999; Warszawski, P. and H.M. Wiseman. *J. Opt. B*, 5:1, 2003.

Doherty, A.C., K. Jacobs and G. Jungman. *Phys. Rev. A*, 63:062306, 2001.

Gillespie, D.T. *Am. J. Phys.*, 64:225, 1996.

Mozyrsky, D. and I. Martin. *Phys. Rev. Lett.*, 89:018301, 2002.

Bhattacharya, T., S. Habib and K. Jacobs. *Phys. Rev. Lett.*, 85:4852, 2000; *Phys. Rev. A*, 67:042103, 2003.

Chirikov, B.V. *Chaos*, 1:95, 1991.

Habib, S., K. Jacobs, H. Mabuchi, R. Ryne, K. Shizume and B. Sundaram. *Phys. Rev. Lett.*, 88:040402, 2002.

Greenbaum, B., S. Habib, K. Shizume and B. Sundaram. *quant-ph*, 0401174.

Habib, S., K. Shizume, W.H. Zurek. *Phys. Rev. Lett.*, 80:4361, 1998.

Kosloff, R. and S.A. Rice. *J. Chem. Phys.*, 74:1340, 1981; Manz, J. *J. Chem. Phys.*, 91:2190, 1989.

Habib, S., K. Jacobs and K. Shizume. *quant-ph*, 0412159 and in preparation.

Mabuch, H. and A.C. Doherty. *Science*, 298:1372, 2002. LaHaye, M.D., O. Buu, B. Camarota and K.C. Schwab. *Science*, 304:74, 2004.

Belavkin, V.P. *Comm. Math. Phys.*, 146:611, 1992; *Rep. Math. Phys.*, 43:405, 1999; Doherty, A.C., S. Habib, K. Jacobs, K. Mabuchi and S.-M. Tan. *Phys. Rev. A*, 62:012105, 2000.

Wiseman, H.M. and G.J. Milburn. *Phys. Rev. Lett.*, 70:548, 1993.

Wiseman, H.M., S. Mancini and J. Wang. *Phys. Rev. A*, 66:013807, 2002.

Ruskov, R. and A.N. Korotkov. *Phys. Rev. B*, 66:041401(R), 2002.

Steck, D.A., K. Jacobs, H. Mabuchi, T. Bhattacharya and S. Habib. *Phys. Rev. Lett.*, 92:223004, 2004.

Hopkins, A., K. Jacobs, S. Habib and K. Schwab. *Phys. Rev. B*, 68:235328, 2003.

Signatures of quantum chaos in open chaotic billiards

Almas F. Sadreev[a,b] and Karl-Fredrik Berggren[a]

(a) Department of Physics and Measurement Technology, Linköping University,
SE-581 83 Linköping, Sweden
e-mail: kfber@ifm.liu.se, almsa@ifm.liu.se
(b) Kirensky Institute of Physics, 660036 Krasnoyarsk, Russia
e-mail: almas@tnp.krasn.ru

Abstract. We discuss signatures of quantum chaos in open chaotic billiards. Solution for such a system are given by complex scattering wave functions $\psi = u + iv$ provided that a steady current flows through the billiard. For slightly opened chaotic billiards the current distributions are simple and universal. It is remarkable, that the resonant transmission through integrable billiards also gives the universal current distribution. Currents induced by the Rashba spin-orbit interaction can flow even in closed billiards. Wave function and current distributions for chaotic billiard with weak and strong spin-orbit interactions have been derived and compared with numerics.

The complex scattering wave function can be specified by nodal points at which $u = 0, v = 0$. They have great physical significance since they are responsible for current vortices. We have calculated distribution functions for nearest distances between nodal points and found that there is a universal form for open chaotic billiards. The form coincides with the distribution for the Berry function and hence, it may be used as a signature of quantum chaos in open systems. All distributions agree well with numerically computed results for transmission through quantum chaotic billiards.

Similarities with classical waves are considered. In particular we propose that the networks of electric resonance RLC circuits may be used to study wave chaos. However, being different from quantum billiards there is a resistance from the inductors which gives rise to heat power and decoherence.

Keywords: distribution functions, transmission, nodal lines

1. Introduction

1.1. Closed Billiards

The nature of quantum chaos in a specific system is traditionally inferred from its classical counterpart. It is an interdisciplinary field that extends into, for example, atomic and molecular physics, condensed matter physics, nuclear physics, and subatomic physics (H.-J. Stöckmann, 1999). The main achievement of this field is the establishment of universal statistics of energy levels: the typical distribution of the spacing of neighbouring levels is Poisson or Gaussian ensembles for integrable or chaotic quantum systems. This statistics is well described by random-matrix theory (RMT). It was first introduced by

Wigner (E.P. Wigner, 1951) to explain the statistical fluctuations of neutron resonances in the compound nucleus. Rather than trying to explain individual eigenfunctions, RMT addresses questions about their statistical behavior. Its original justification was our lack of knowledge of the exact Hamiltonian; RMT assumes maximal ignorance regarding the system's Hamiltonian except that it must be consistent with the underlying symmetries. The theory proceeds to construct ensembles of Hamiltonians classified by their symmetry. Wigner's ideas were followed by those of Porter and Rosenzweig (E.P. Wigner et. al., 1960) and Mehta and Gaudin (M.L. Mehta et. al., 1961; M.L. Mehta, 1991).

Next, consider statistical properties of the eigenfunctions of the chaotic two-dimensional quantum billiards in hard wall approximation

$$-\nabla^2 \psi_n(x,y) = \epsilon_n \psi_n(x,y), \tag{1}$$

where the Dirichlet boundary condition is implied at the boundary Ω of the billiard : $\psi_{|\Omega} = 0$. Here we use Cartesian coordinates x, y which are dimensionless via a characteristic size of the billiard L, and correspondingly $\epsilon_n = k_n^2 = E_n/E_0$, $E_0 = \hbar^2/2mL^2$. Shapiro and Goelman (M. Shapiro et.al., 1984) first presented statistics of the eigenfunctions although their numerical histogram $P(\psi)$ was not compared with the Gaussian distribution. This was done by McDonnell and Kauffmann (S.W. McDonald et.al., 1988) who concluded that the majority ($\approx 90\%$) of the eigenfunctions of the Bunimovich billiard are a Gaussian random field (RGF) for all x, y. Also McDonnell and Kauffmann revealed characteristic complex patterns of disordered, undirectional and non-crossing nodal lines. Such features have also been observed experimentally for microwave cavities (H.-J. Stöckmann, 1999; S. Sridhar et.al., 1992) and acoustic resonators (C. Ellegaard et.al., 2001).

These results nicely agree with the Berry conjecture (M.V. Berry, 1977) of quantum chaos according to which the wave function in the chaotic billiard has to be expressed as a sum over an infinite number of plane waves

$$\psi(x,y) = \sum_j a_j \exp[i\,(\mathbf{k_j}\mathbf{r} + \phi_j)] \tag{2}$$

each having a random amplitude a_j, phase ϕ_j and direction $\mathbf{k}_j$ but equal length $|k_j|^2 = \epsilon$. In closed chaotic billiards we are to take the real part of (2). This leads to a Gaussian amplitude distribution and a spatial correlation function with Bessel function dependence. This conjecture, in fact, was raised by Rayleigh (lord Rayleigh, 1945).

However, there exist also eigenfunctions which behave otherwise. Most of them are localized on families of regular classical trajectories (scars (E.J. Heller, 1984)) or bouncing ball modes (S.W. McDonald

et.al., 1988)). Their number behaves as $N_{bb}(E) = \alpha E^{\delta}$ with $\alpha = 0.2, \delta = 3/4$ (G. Tanner, 1997; A. Bäcker et.al., 1997).

1.2. Open Billiards

The typical way to open a billiard is to attach some reservoirs with continuous energy spectrum, for example, the leads or microwave waveguides, as shown in fig. 3 below. Full information about the scattering properties of the billiard is given by the scattering wave function which is a solution of the Schrödinger equation $H\psi = E\psi$ with the total Hamiltonian

$$H = H_B + H_U + H_L + V, \tag{3}$$

where H_B is the Hamiltonian of the closed quantum system, in the present case the billiard with a spectrum given by eq. (1), $H_U + H_L$ describes two leads (the upper and lower as shown below in fig. 3) with continuous spectrum and $V = V_U + V_L$ is the coupling between the closed system and the leads. The mathematical tool to treat scattering processes is provided by scattering theory (H. Feshbach, 1958; U. Fano, 1961; C. Mahaux et.al., 1969; I. Rotter, 1991) which has been successfully applied to billiards (Y.V. Fyodorov et.al., 1997; F.M. Dittes, 2000; A.F. Sadreev et.al., 2003). Assume, that we know the coupling matrices $W_C(n, p)$, $C = U, L$ of rank $M \times N$ where M is the number of channels in the leads and N is the Hilbert dimension of the billiard. A recipe how to calculate the matrix elements $W_C(n, p)$ for straight leads is given in (F.M. Dittes, 2000; K. Pichugin et.al., 2002; A.F. Sadreev et.al., 2003). Then the spectroscopic properties of the billiard are given by complex eigenvalues z_λ of effective non-hermetian Hamiltonian

$$H_{eff} = H_B - i\pi \sum_{C=U,L} W_C^+ W_C. \tag{4}$$

$Re(z_\lambda)$ defines positions of the resonances, while $Im(z_\lambda)$ gives their widths.

Similar to closed chaotic billiards the idea was to adjust RMT to the effective Hamiltonian $H_{eff} = H - i\Gamma$ (see the pioneering work (J.J.M. Verbaarschot et.al., 1985) and (H.-J. Sommers et.al., 1999) for references). These matrices correspond to GUE with broken time-reversal symmetry. A next natural step was to assume that in the transition region between GOE and GUE, the eigenfunctions are complex and may be thought as columns of the unitary random matrix (G. Lenz et.al., 1992; E. Kanzieper et.al., 1996) $S = S_1 + i\epsilon S_2$, composed of two independent orthogonal matrices. The parameter

$$\epsilon^2 = \frac{\langle Re(\psi)^2 \rangle}{\langle Im(\psi)^2 \rangle} \tag{5}$$

governs the crossover between GOE and GUE. Later different approaches were explored (R. Pnini et.al., 1996; P. Šeba et.al., 1997; H. Ishio et.al., 2001) to give the same probability density distribution $\rho = |\psi|^2$

$$f(\rho) = \mu \exp(-\mu^2 \rho) I_0(\mu \nu \rho), \tag{6}$$

with the following notations

$$\begin{cases} \mu = \frac{1}{2}\left(\frac{1}{\epsilon} + \epsilon\right), \\ \nu = \frac{1}{2}\left(\frac{1}{\epsilon} - \epsilon\right), \end{cases} \tag{7}$$

and $I_0(x)$ is the modified Bessel function of zeroth order.

2. The wave function and current statistics

The scattering wave function $H\psi = E\psi$ can be mapped onto the interior space of the billiard by the projection operator $\psi_B = P_B \psi$ where $P_B = \sum_n |n\rangle\langle n|$. Then this truncated scattering wave function can be expanded in the eigenfunctions of the closed billiard $\psi_n(x,y)$ (A.F. Sadreev et.al., 2003)

$$\psi_B(x,y) = \sum_n c_n \psi_n(x,y). \tag{8}$$

If the contribution of the localized eigenfunctions (scars or bouncing ball modes) in (8) is negligible, then all eigenfunctions $\psi_n(x,y)$ are RGF. The complex coefficients in the superposition, c_n, depend on the energy and the coupling between the billiard and leads and are not random as in the Berry function (2). Nonetheless the superposition of RGFs is also a complex RGF (W. Feller, 1971; M.I. Tribelsky, 2002)

$$\psi_B(x,y) = u(x,y) + iv(x,y). \tag{9}$$

Even for the resonant transmission through the Sinai billiard, computations show that many eigenfunctions contribute to the scattering wave function as shown in fig. 1. An assumption of a complex RGF for the scattering function (9) means that the joint probability density has the form

$$f(u,v) = \frac{1}{2\pi\sqrt{\langle u^2\rangle\langle v^2\rangle - \langle uv\rangle}} \exp\left(-\frac{u^2}{2\langle u^2\rangle} - \frac{v^2}{2\langle v^2\rangle} + \frac{uv}{2\langle uv\rangle}\right). \tag{10}$$

First of all, following (A.I. Saichev et.al., 2002) we perform a phase transformation

$$\psi(\mathbf{x}) \to e^{i\alpha}\psi(\mathbf{x}) = p(\mathbf{x}) + iq(\mathbf{x}) \tag{11}$$
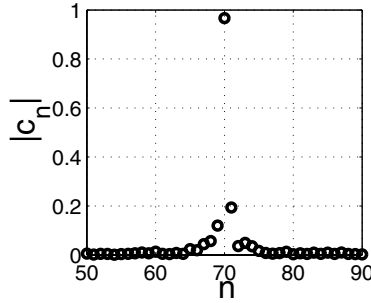
Figure 1. The coefficients $|c_n|$ in the expansion (8) for the resonant transmission through the Sinai billiard with numerical sizes $500 \times 500, R = 50$ with energy $\epsilon = 10.425$.

to new functions $p(\mathbf{x})$ and $q(\mathbf{x})$ with condition that the statistical average $\langle pq \rangle = 0$. This step eliminates phase ambiguity and ensures that RGFs p and q are statistically independent. This phase transformation (11) corresponds to diagonalization of the quadratic form in (10) (A.F. Sadreev et.al., 2004):

$$\begin{cases} f(p,q) = f(p)f(q), \\ f(p) = \frac{1}{\sqrt{2\pi\langle p^2 \rangle}} \exp\left(-\frac{p^2}{2\langle p^2 \rangle}\right), \\ f(q) = \frac{1}{\sqrt{2\pi\langle q^2 \rangle}} \exp\left(-\frac{q^2}{2\langle q^2 \rangle}\right). \end{cases} \tag{12}$$

This step is a matter of convenience which simplifies calculations. For example, calculation of the distribution of intensity $\rho = |\psi_B|^2$ becomes elementary and gives the distribution (6) (A.I. Saichev et.al., 2002).

As for the next tutorial of a RGF we consider current distributions. The expression for current

$$\mathbf{j} = p\nabla q - q\nabla p, \tag{13}$$

shows that the distribution for one component of the current density, say j_x we need the Gaussian probability density $f(p, p_x, q, q_x)$ (K.J. Ebeling, 1984). The density and its corresponding characteristic functions are completely determined by the covariance matrix of the field variables

$$\mathbf{M} = \begin{pmatrix} \langle p^2 \rangle & \langle pq_x \rangle & \langle pq \rangle & \langle pp_x \rangle \\ \langle pq_x \rangle & \langle q_x^2 \rangle & \langle qq_x \rangle & \langle p_x q_x \rangle \\ \langle pq \rangle & \langle qq_x \rangle & \langle q^2 \rangle & \langle qp_x \rangle \\ \langle pp_x \rangle & \langle p_x q_x \rangle & \langle qp_x \rangle & \langle p_x^2 \rangle \end{pmatrix} = \begin{pmatrix} \langle p^2 \rangle & \langle pq_x \rangle & 0 & 0 \\ \langle pq_x \rangle & \langle q_x^2 \rangle & 0 & 0 \\ 0 & 0 & \langle q^2 \rangle & \langle qp_x \rangle \\ 0 & 0 & \langle qp_x \rangle & \langle p_x^2 \rangle \end{pmatrix}. \tag{14}$$

The covariance matrix may be simplified further if we assume that the net current $\langle \mathbf{j} \rangle \approx 0$. As shown in (A.F. Sadreev et.al., 2004) $\langle j_x \rangle = T/L_y$

where T is the transmission probability through the billiard and L_y is its width. We have $\langle j_x \rangle \approx 0$ if the transmission is near zero or the aspect ratio d/L_y is very small; d is the lead's width. Therefore it follows from (13) that for this case $\langle pq_x \rangle \approx \langle qp_x \rangle \approx 0$. Correspondingly the Gaussian probability density factorizes as

$$f(p, p_x, q, q_x) = f(p)f(q)f(p_x)f(q_x), \qquad (15)$$

where

$$\begin{cases} f(p_x) = \frac{1}{\sqrt{2\pi \langle p_x^2 \rangle}} \exp\left(-\frac{p_x^2}{2\langle p_x^2 \rangle}\right), \\ f(q_x) = \frac{1}{\sqrt{2\pi \langle q_x^2 \rangle}} \exp\left(-\frac{q_x^2}{2\langle q_x^2 \rangle}\right). \end{cases} \qquad (16)$$

In particular this is the case for the Berry function (2) with $\langle p^2 \rangle = \langle q^2 \rangle$, $\langle p_x^2 \rangle = \langle q_x^2 \rangle$.

Now it is easy to calculate the current distribution functions. For the x component we have

$$P(j_x) = \langle \delta(j_x - pq_x + qp_x) \rangle = \frac{1}{2\pi} \int_{-\infty}^{\infty} \Theta(a_x)\, e^{-ia_x j_x}\, da_x, \qquad (17)$$

where

$$\Theta(a_x) = \int dp\, dq\, dp_x\, dq_x\, f(p)f(q)f(p_x)f(q_x) e^{ia_x(pq_x - qp_x)} = \frac{1}{1 + a_x^2 \tau^2}, \qquad (18)$$

$$\tau^2 = \langle p^2 \rangle \langle q_x^2 \rangle = \langle q^2 \rangle \langle p_x^2 \rangle = \frac{1}{2} k^2 \langle p^2 \rangle \langle q^2 \rangle = \frac{k^2 \epsilon^2}{2(1 + \epsilon^2)^2} \qquad (19)$$

provided that $\langle p^2 \rangle + \langle q^2 \rangle = 1$ (normalization condition), and ϵ is the parameter of openness of the billiard (5). Finally substituting Eqs. (18) and (19) into (17) we obtain the very simple form of the distribution of the x component of current

$$P(j_x) = \frac{1}{2\tau} \exp\left(-\frac{|j_x|}{\tau}\right). \qquad (20)$$

For the case nonzero net current the distribution takes the following form (K.J. Ebeling, 1984)

$$P(j_x) = \frac{1}{2\tau} \exp\left\{-\frac{|j_x|}{\tau} + \frac{\langle j_x \rangle j_x}{2\tau^2}\right\}. \qquad (21)$$

The distribution of the absolute value of current has also a simple form

$$P(j) = \frac{j}{\tau^2} K_0(j/\tau). \qquad (22)$$
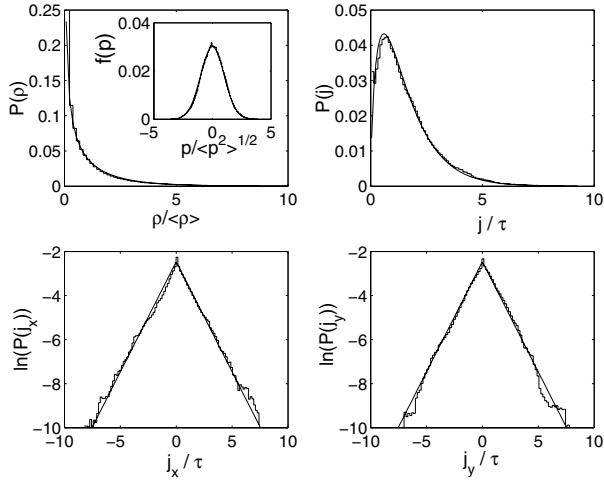
Figure 2. Statistics of current for the transmission through the Sinai billiard for $T \approx 0$. The upper left panel shows the computed distribution for $\rho = |\psi|^2$ together with the Porter-Thomas distribution $P(\rho)$ (solid curve). In the inset in the same panel the computed wave function statistics $f(p)$ for the real part of ψ is compared with a random Gaussian distribution (solid curve).

In the right upper panel the distribution for the current density $P(j)$ is shown together with the theoretical prediction for the case $\langle j_x \rangle = 0$. Lower panels show the computed distributions for the $x-$ and $y-$components of j on a logarithmic scale together with the analytic expression (20) (straight solid lines).

Fig. 2 demonstrates excellent agreement for the numerical statistics of the current with formulas (20) and (22) for a slightly open Sinai billiard. The current distributions might be applicable even for the case of the resonant transmission through integrable billiards (A.F. Sadreev, 2004). For this case the real eigenfunction ψ_n with the eigenenergy $\epsilon \approx \epsilon_n$ is dominant in the scattering wave function (8). However since current is the imaginary part of $\psi^* \nabla \psi$, only ψ_n can not provide the current. We are to take into account a small background of many other non resonant eigenfunctions $\psi_{n'}$, $n \neq n$ (see fig. 1 for an illustration). Therefore the probability current flows only because of the background which may be considered as random noise.

There is a close similarity with planar electromagnetic cavities (H.-J. Stöckmann, 1999). The basic equations take the same form and, in particular, the Poynting vector is the analog of the quantum mechanical current. It is therefore possible to experimentally observe currents, nodal points and streamlines in microwave billiards (M. Barth et.al., 2002; Y.-H. Kim et.al., 2003). The microwave measurements have confirmed many of the predictions of the random Gaussian wave fields described above. For example wave function statistics, current flow and

various correlation functions have been verified. Recently we proposed that the networks of electric resonance RLC circuits may be used to study wave chaos (K.-F. Berggren et.al., 2002; O. Bengtsson et.al.,; E.N. Bulgakov et.al.,).

Statistics of functions and currents in the quantum chaotic billiards with the spin-orbit interaction was considered in (E.N. Bulgakov et.al., 2004). The statistics crucially depends on the constant of the spin-orbit interaction. For small constant the current statistics is described by universal current distributions (20) and (22) although one component of spinor eigenfunctions is not universal. For the strong spin-orbit constant both components of the spinor eigen state are the complex random Gaussian fields. The current statistics is becoming superposition of the distributions (20) because of splitting energy levels by the spin-orbit interaction. For intermediate values of the statistics of the eigen states and currents both are deeply non universal.

3. Statistics of nodal points

For a closed billiard the eigenfunctions ψ_n are real functions. The equation $\psi_n(x,y) = 0$ determines a set of nodal lines which separate nodal domains where ψ_n is of opposite signs. Blum *et al* (G. Blum et.al., 2002) (see also (G. Foltin et.al., 2004)) argued that the statistics of the number of these domains reflects the fundamental difference between integrable and chaotic quantum systems. In (E. Bogomolny et.al., 2002) the distribution of nodal domains was derived analytically based on a simple percolation model. In open system the wave function is then a scattering state with both real and imaginary parts as in (9). Then the equation $\psi_B(x,y) = 0$ gives rise to two separate sets of non-crossing nodal lines at which either u or v vanish. The points at which the two sets of nodal lines intersect are the nodal points (NP). Since at NP $|\psi| = 0$, a phase of the ψ-function $\psi = |\psi|\exp(i\theta)$ becomes unambiguous. Explicit descriptions of NPs as phase singularities or topological charges associated with a complex wave function are given in many articles, for example (P.A.M. Dirac, 1931; J.F. Nye et.al., 1974; J.O. Hirschfelder et.al., 1974; J.O. Hirschfelder, 1977; H. Wu et.al., 1993). As Dirac demonstrated already in 1931 (P.A.M. Dirac, 1931) NPs give rise to a current vortices. Moreover the vortices may be clock wise or anticlock wise, i.e. have ± 1 winding numbers. It was proven (I. Freund et.al., 1994; K.-F. Berggren et.al., 2002) that neighboring NPs on the same nodal line always have opposite winding numbers. Therefore, distribution of NPs is different from the distribution of completely random points.
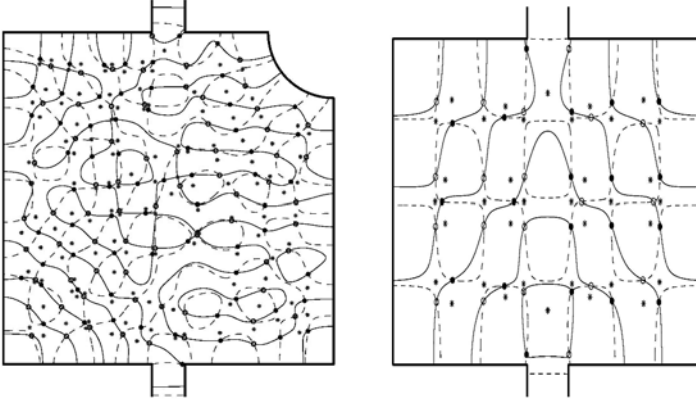
Figure 3. The complexity of nodal lines, nodal points and saddles for the transmission through chaotic (Sinai) (left) and regular billiard (right).

Instead of nodal lines in closed systems we are interested in the statistics of NPs for open chaotic billiards since they form vortex centers and thereby shape the entire flow pattern (K.-F. Berggren et.al., 1999). Thus we will focus on nodal points and their spatial distributions and try to characterize chaos in terms of such distributions. The question we wish to ask is simply if one can find a distinct difference between the distributions for nominally regular and irregular billiards. The answer to this question is clearly positive as it is seen from fig. 3. As shown qualitatively NPs and saddles are both spaced less regularly in chaotic billiard in comparison to the integrable billiard. The mean density of NPs for a complex RGF (9) equals to $k^2/4\pi$ (M.V. Berry et.al., 1986). This formula is satisfied with good accuracy in both chaotic and integrable billiards.

Quantitatively the disorder among points may be expressed through the correlation function of NPs and distribution of nearest distances between them. Let us introduce the density of nodal points as (M.V. Berry et.al., 2000; A.I. Saichev et.al., 2001)

$$d(\mathbf{r}) = |\omega(\mathbf{r}_j)|\delta(u(\mathbf{r}))\delta(v(\mathbf{r})) = \sum_j \delta(\mathbf{r} - \mathbf{r}_j), \qquad (23)$$

where $\mathbf{r}_j$ specify the NPs position, and $\omega(\mathbf{r}) = \nabla u(\mathbf{r}) \times \nabla v(\mathbf{r})$ is the vorticity. Then the correlation function of NPs can be defined as (M.V. Berry et.al., 2000; A.I. Saichev et.al., 2001)

$$G(s) = \langle \sum_{i,j} \delta(\mathbf{r} - \mathbf{r}_j)\delta(\mathbf{r} - \mathbf{r}_j - \mathbf{s}) \rangle. \qquad (24)$$
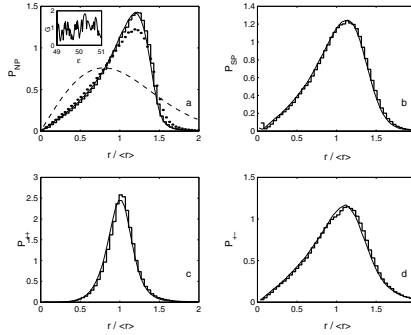
Figure 4. Distributions for separations between the nearest distances nearest NPs, saddle points, NPs with the same (++) and opposite winding numbers (+-) in a chaotic Sinai billiard. The radial distribution of nearest distances for completely random points (26) is shown by the dashed curve in (a). The corresponding distribution for the Berry model function for a chaotic state (2) and random superposition of 16 eigen functions for a rectangular box with the same size and energy are shown by dots and thin curves, respectively.

This was considered by Halperin (B.I. Halperin, 1981) and Liu and Mazenko (F. Liu et.al., 1992). Recently two teams (M.V. Berry et.al., 2000; A.I. Saichev et.al., 2001; M.R. Dennis, 2003) presented different complicated analytical expressions for the correlation function (24). Numerically however they give the same results. Experimental verification was done in microwave billiards (Y.-H. Kim et.al., 2003). A knowledge of the NP correlation function allows one to find the distribution function of nearest distances between NPs (A.I. Saichev et.al., 2001):

$$P_{NP}(r) \approx \frac{4\pi}{\rho^{3/2}} r G(r) \left(1 - \frac{4\pi}{3\rho} \int_0^{\sqrt{\rho} r} G(s) s ds \right)^2 . \qquad (25)$$

It is interesting that the distribution (25) is close to the nearest-neighbour spacing distribution of zeros of random polynomials (P. Leboeuf et.al., 1999). These polynomials approximate the eigenfunctions of the unitary evolution operator of the quantum kicked rotator. It prompts us to consider that the nearest-neighbour spacing distribution of zeros is meaningful not only for the chaotic billiards but for other quantum chaotic systems. Fig. 4 shows numerical results for the transmission through the Sinai billiard (K.-F. Berggren et.al., 2002) compared to the derived distributions. It also shows that nodal points with opposite winding numbers have a tendency to attract each other, while points with the equal winding numbers repel. Hence quantum chaos is not the same as complete randomness. This also evident from the distribution

for nearest neighbors among random points (J.R. Eggert, 1984)

$$P(r) = \frac{\pi}{2} r \exp(-\pi r^2/4). \tag{26}$$

4. Acknowledgments

References

Stöckmann, H.-J. Quantum Chaos: An Introduction *Cambridge University Press, Cambridge, UK*, 1999.

Wigner, E.P. *Ann. Math.*, 53:36, 1951; 62:548, 1955; 65:203, 1957; 67:325, 1958.

Porter, C.E. and N. Rosenzweig. *Phys. Rev.*, 120:1698, 1960.

Mehta, M.L. and M. Gaudin. *Nucl. Phys.*, 18:420, 1960; 25:447, 1961.

Mehta, M.L. Random Matrices. *Academic, New York*, 1991.

Shapiro M., and G. Goelman. *Phys. Rev. Lett.*, 53:1714, 1984.

McDonald, S.W., and A.N. Kaufmann. *Phys. Rev. A.*, 37:3067, 1988.

Sridhar S., and E. Heller. *Phys. Rev. A.*, 46:R1728, 1992.

Ellegaard, C., K. Schaadt, and P. Bertelsen. *Physica Scprita*, 90:223, 2001.

Berry, M.V. *J. Phys. A: Math. Gen.*, 10:2083, 1977.

Rayleigh, Lord. The theory of sound. *Dover Publications, New York*, 1945.

Heller, E.J. *Phys. Rev. Lett.*, 53:1515, 1984.

Tanner, G. *J. Phys. A: Math. Gen.*, 30:2863, 1997.

Bäcker, A., R. Schubert, and P. Stifter. *J. Phys. A: Math. Gen.*, 30:6783, 1997.

Feshbach, H. *Ann. Phys. (NY)*, 5:357, 1958; 19:287, 1962.

Fano, U. *Phys. Rev.*, 124:1866, 1961.

Mahaux C., and H.A. Weidenmüller. Shell Model Approach in Nuclear reactions. *Amsterdam: North Holland*, 1969.

Rotter, I. *Rep. Prog. Phys.*, 54:635, 1991.

Fyodorov, Y.V., and H.J. Sommers. *J. Math. Phys.*, 38:1918, 1997.

Dittes, F.M. *Phys. Rep.*, 339:215, 2000.

Sadreev, A.F., and I. Rotter. *J. Phys. A: Math. Gen.*, 36:11413, 2003.

Pichugin, K., H. Schanz, and P. Šeba. *Phys. Rev. E*, 64:056227, 2002.

Verbaarschot, J.J.M., H.A. Weidenmüller, and M.R. Zirnbauer. *Phys. Rep.*, 129:367, 1985.

Sommers, H.-J., Y.V. Fyodorov, and M. Titov. *J. Phys. A: Math. Gen.*, 32:L77, 1999.

Lenz, G., and K. Życzkowski. *J. Phys. A: Math. Gen.*, 25:5539, 1992.

Kanzieper, E., and V. Freilikher. *Phys. Rev. B*, 54:8737, 1996.

Pnini, R., and B. Shapiro. *Phys. Rev. E*, 54:R1032, 1996.

Šeba, P., F. Haake, M. Kuś, M. Barth, U. Kuhl, and H.-J. Stöckmann. *Phys. Rev. E*, 56:2680, 1997.

Ishio, H., A.I. Saichev, A.F. Sadreev, and K.-F. Berggren. *Phys. Rev. E*, 64:056208, 2001.

Feller, W. An Introduction to Probability Theory and its Applications. *Wiley, New York*, 1971.

Tribelsky, M.I. *Phys. Rev. Lett.*, 89:070201, 2002.

Saichev, A.I., H. Ishio, A.F. Sadreev, and K.-F. Berggren. *J. Phys. A: Math. Gen.*, 35:L87, 2002.

Sadreev, A.F., and K.-F. Berggren. *Phys. Rev. E*, 70:26201, 2004.

Ebeling, K.J. Statistical properties of random wave fields in Physical Acoustics: Principles and Methods. *New York: Academic Press*, 1984.

Sadreev, A.F. *Phys. Rev. E*, 70:16208, 2004.

Barth, M., and H.J. Stöckmann. *Phys. Rev. E*, 65:066208, 2002.

Kim, Y.-H., M. Barth, U. Kuhl, and H.J. Stöckmann. *Progr. Theort. Phys. Suppl.*, 150:105, 2003.

Berggren, K.-F., and A.F. Sadreev. Chaos in quantum billiards and similarities with pure-tone random models in acoustics, microwave cavities and electric networks. Mathematical modelling in physics, engineering and cognitive sciences. *Proc. of the conf. "Mathematical Modelling of Wave Phenomena"*, 7:229, 2002.

Bengtsson, O., J. Larsson, and K.-F. Berggren. *Phys. Rev. E*, 71: April, 2005.

Bulgakov, E.N., D.N. Maksimov, and A.F. Sadreev. *Phys. Rev. E*, 71': April, 2005.

Bulgakov, E.N., and A.F. Sadreev. *Phys. Rev. E*, 70:61414, 2004.

Blum, G., S. Gnutzmann, and U. Smilansky. *Phys. Rev. Lett.*, 88:114101, 2002.

Foltin, G., S. Gnutzmann, and U. Smilansky. *J. Phys. A: Math. Gen.*, 37:11363, 2004.

Bogomolny, E., and C. Schmit. *Phys. Rev. Lett.*, 88:114102, 2002.

Dirac, P.A.M. *Proc. Roy. Soc. (London)*, 133:60, 1931.

Nye, J.F., and M.V. Berry. *Proc. Roy. Soc. (London)*, A336:165, 1974.

Hirschfelder, J.O., A.C. Christoph, and W.E. Palke. *J. Chem. Phys.*, 61:5435, 1974.

Hirschfelder, J.O. *J. Chem. Phys.*, 67:5477, 1977.

Berry, M. "Singularities in waves and rays", in "Physics of Defects". *R. Balian et al., eds. (North Holland, Amsterdam)*, 1981.

Wu, H., and D.W.L. Sprung. *Phys. Lett.*, A183:413, 1993.

Freund, I., and N. Shvartsman. *Phys. Rev. A*, 50:5164, 1994.

Berggren, K.-F., A.F. Sadreev, and A.A. Starikov. *Phys. Rev. E*, 66:16218, 2002.

Berggren, K.-F., K.N. Pichigin, A.F. Sadreev, and A.A. Starikov. *JETP Lett.*, 70:403, 1999.

Berry, M.V., and M. Robnik. *J. Phys. A: Math. Gen.*, 19:1365, 1986.

Berry, M.V., and M.R. Dennis. *Proc. R. Soc. Lond.*, A456:2059, 2000.

Saichev, A.I., K.-F. Berggren, and A.F. Sadreev. *Phys. Rev. E*, 64:036222, 2001; 65:19903, 2003.

Halperin, B.I. Statistical Mechanics of topological defects. *edited by R. Balian, N. Kleman, and J.-P. Poirer (North Holland, Amsterdam*, 1981.

Liu, F. and G.F. Mazenko. *Phys. Rev. B*, 46:5963, 1992.

Dennis, M.R. *J. Phys. A: Math. Gen.*, 36:6611, 2003.

Leboeuf, P., and P. Shukla. *J. Phys. A: Math. Gen.*, 29:4827, 1999.

Eggert, J.R. *Phys. Rev. B*, 29:6664, 1984.

From quantum graphs to quantum random walks

Gregor K. Tanner

School of Mathematical Sciences, University of Nottingham, UK

Abstract. We give a short overview over recent developments on quantum graphs and outline the connection between general quantum graphs and so-called quantum random walks.

1. Introduction

The study of quantum mechanics on graphs has become an important tool for investigating the influence of classical dynamics on spectra, wavefunctions and transport properties of quantum systems. Quantum networks have been used with great success to model quantum phenomena observed in disordered metals and mesoscopic systems (Chalker and Coddington 1988); typical behaviour found in diffusive systems such as localisation - delocalisation transitions (Freche et.al 1999), transport properties (Pascaud and Montambaux 1999) and quantum spectral statistics (Klesse and Metzler 1997) have been studied on graphs in the limit of infinite network size. Kottos and Smilansky (1997, 1999) looked at quantum graph models for general, non-diffusive graphs; this approach was motivated by trying to understand the validity of the Bohigas-Giannoni-Schmit (BGS) conjecture (Bohigas, et.al 1984) in terms of periodic orbit trace formula. The conjecture relates the properties of the classical dynamics of a systems to the spectral statistics of its quantum counterpart and states that for chaotic systems the statistics depends only on the symmetries of the problem and follows random matrix theory (RMT) otherwise.

Making use of the fact that periodic orbit trace formula are exact on quantum graphs and that there are only a finite number of different length scales on a finite graph, a series of remarkable results have been obtained over the last couple of years. A closed form quantisation conditions in terms of periodic orbits has been given by Blümel et.al (2002); Barra and Gaspard (2000) derived an integral expression for the level spacing distribution starting form the periodic orbit trace formula. Furthermore, Schanz and Smilansky (2000) described localisation on one-dimensional chains in terms of combinatorial expression using periodic orbits. The most far reaching development is maybe due to Berkolaiko et.al (2002,2003), who, inspired by work from Sieber (2002)

and Sieber and Richter (2001), derived next to leading oder terms for the formfactor. Extensions to all orders have been given by Müller et.al (2004). Gap conditions given by Tanner (2001) and Gnutzmann and Altland (2004) give lower and upper bounds for the border of universality. For a recent review on quantum graphs see Kuchment (2002).

Quantum dynamics on graphs became an issue also in the context of quantum information. Aharonov et.al (1993) pointed out that a random quantum walk on one dimensional chains can be faster than the corresponding classical random walk. Since then, a whole field has emerged dealing with quantum effects on graphs with properties superiour to the corresponding classical operations. For an introductory overview and further references, see Kempe (2003).

We will in the following give a general definition of quantum graphs and discuss a specific set-up considered by Kottos and Smilansky (1997). We will then review recent developments on the spectral statistics of quantum graph ensembles. Next, we discuss a special class of quantum graph ensembles, so-called regular quantum graphs. These types of graphs can show strong deviations from RMT depending on topological properties imposed on the graph in form of edge-colouring matrices. We will show that such graphs can be interpreted as realisations of quantum random walks on graphs.

2. Quantum graphs - a brief review

2.1. QUANTUM GRAPHS ON LINE GRAPHS

In its most general form, a quantum graph is defined in terms of a (finite) graph G together with a unitary propagator $\mathbf{U}$; it describes the dynamics of "wavefunctions" ϕ on the graph according to

$$\phi_{n+1} = \mathbf{U}\phi_n \, ,$$

such that waves can propagate only between connected vertices. Motivated by physical application we will adopt a construction of quantum graphs in terms of so-called line-graphs as explained below.

A (finite) *directed graph* or *digraph* consists of a finite set of *vertices* and a set of ordered pairs of vertices called *arcs*. We denote by V^G and E^G the set of vertices and arcs of the digraph G, respectively. Given an ordering of the vertices, the *adjacency matrix* of a digraph G on n vertices, denoted by $\mathbf{A}^G$, is the $(0,1)$-matrix where the ij-th element

is defined by

$$A_{ij}^{G} := \begin{cases} 1, & \text{if } (ij) \in E^{G}, \\ 0, & \text{otherwise.} \end{cases} \qquad (1)$$

An *undirected graph* (for short, *graph*) is a digraph whose adjacency matrix is symmetric. The undirected connections between vertices are called edges in this case. The *line digraph* of a digraph G, denoted by LG, is the graph which is obtained when taking the arcs as the new vertices; it is thus defined as $V^{LG} = E^{G}$ and, given $(hi), (jk) \in E^{G}$, the ordered pair $((hi)(jk)) \in E^{LG}$ if and only if $i = j$ (Bang-Jensen and Gutin 2001).

A *quantum graph* associated with a digraph G on n vertices can then be defined in terms of a set of unitary vertex scattering matrices $\sigma^{(j)}$ on vertices $j = 1, \ldots n$ and a set of arc lengths L_{ij} defined for every arc $(ij) \in E^{G}$. Waves propagate freely along the directed arcs, transitions between incoming and outgoing waves at a given vertex j are described by the scattering matrix $\sigma^{(j)}$, see Fig. 1a. The two sets specify a unitary propagator of dimension $n_{E} = |E^{G}|$ defining transitions between arcs $(ij), (i'j') \in E^{G}$ which has the form (Kottos and Smilansky 1997)

$$\mathbf{S}^{G} = \mathbf{D}\,\mathbf{V} \text{ with } D_{(ij)(i'j')} = \delta_{i,i'}\,\delta_{j,j'}\,e^{ikL_{ij}}, \qquad (2)$$

where k is a wave number and

$$V_{(ij)(i'j')} = A_{(ij)(i'j')}^{LG}\sigma_{ij'}^{(j)} \text{ with } A_{(ij)(i'j')}^{LG} = \delta_{j,i'}. \qquad (3)$$

The local scattering matrices $\sigma^{(i)}$ describe the underlying physical process which may be derived from boundary conditions on the vertices. We will construct an example below but may often regard the $\sigma^{(i)}$'s as arbitrary unitaries. Let d_{i}^{-} and d_{i}^{+} be the number of incoming and outgoing arcs of a vertex i, respectively. A sufficient and necessary condition for a digraph G to be quantisable in the way above is then, that for every vertex $i \in V^{G}$, $d_{i}^{+} = d_{i}^{-} = d_{i} = \dim \sigma^{(i)}$ (Pakoński et.al 2003). This means in particular that if G is an undirected graph then it is quantisable.

Kottos and Smilansky (1997) considered solving the 1d Schrödinger equation on an undirected graph assuming free propagation on the arcs and imposing continuity and flux conservation at the vertices. The solution on each arc propagating from vertex $i \to j$ takes on the form

$$\phi(x_{ij}) = \phi_{ij}^{+}e^{ikx_{ij}} = \phi_{ij}^{-}e^{-ik(L_{ij}-x_{ij})},$$

with $\phi_{ij}^{\pm}$ being the outgoing $(+)$ or incoming $(-)$ wave at vertex i or j. Continuity and flux conservation can then be written in terms of the amplitudes $\phi_{ij}^{+}(0)$ and $\phi^{-}(L_{ij})$ at the vertices, that is
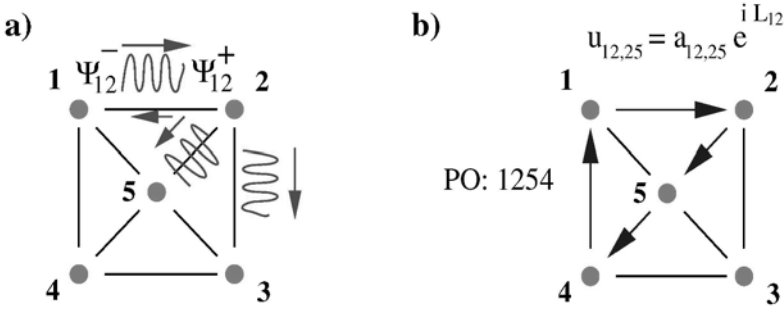
Figure 1. a) Quantum graph; b) periodic path on a graph with quantum weights defined with respect to the line - graph.

$$\text{Continuity: } \phi_{ij}^+ = \phi_{ji}^- = c_i \quad \text{for all } j \text{ with}(i,j) \in E^G$$

$$\text{Flux cons.: } \sum_{j:(ij)\in E^G} \phi_{ij}^+ = \sum_{j:(ji)\in E^G} \phi_{ji}^-$$

These conditions give rise to local scattering matrices σ^l mapping amplitudes ϕ_{il}^- onto ϕ_{lj}^+ at vertex l having the form

$$\sigma_{ij}^{(l)} = -\delta_{ij} + \frac{2}{d_l}. \tag{4}$$

The eigenvalue condition is then given as

$$\det(\mathbf{I} - \mathbf{S}^G(k)) = 0 \tag{5}$$

with $\mathbf{S}^G(k) = \mathbf{D}(k)\mathbf{V}$ as defined in (2), (3). Scattering matrices for more general boundary conditions can be found in Kottos and Smilansky (1999).

The "classical" dynamics corresponding to a quantum graph defined by a unitary propagator $\mathbf{S}^G$ is given by a stochastic process with transition matrix $\mathbf{T}$ defined by

$$\mathbf{S}^G \to \mathbf{T}(\mathbf{S}^G) \qquad \text{with} \quad T(\mathbf{S}^G)_{ij} = |S_{ij}^G|^2 = |V_{ij}|^2. \tag{6}$$

The matrix $\mathbf{T}$ is clearly stochastic, as $\sum_{j=1}^{n_E} T_{ij} = 1$ due to the unitarity of $\mathbf{S}^G$; the set of transition matrices related to a unitary matrix as defined in (6) is a subset of the set of all stochastic transition matrices, referred to as the set of *unitary-stochastic* matrices. The topology of the set in the space of all stochastic matrices is in fact quite complicated, see Pakoński et.al. (2001). In what follows, we will only use that $\mathbf{T}$

has a largest eigenvalue 1 with corresponding eigenvector $\frac{1}{n_E}(1, \ldots, 1)$ which follows from the Frobenius-Perron theorem and $\mathbf{T}$ being unitary-stochastic.

Note that both the quantum mechanics as well as the associated stochastic dynamics relates to transitions between arcs and is thus defined on the line digraph of G.

2.2. Unitary stochastic ensembles and spectral statistics

Inspired by the BGS conjecture for quantum systems, we expect a link between the dynamical properties of the stochastic process $\mathbf{T}$ and the statistical properties of the spectrum of associated unitary matrices $\mathbf{S}^G$. It is thus natural to consider the ensemble of unitary matrices

$$USE_{\mathbf{T}_0} = \left\{ \mathbf{S}^G \text{is quantum graph on } G \,|\, \mathbf{T}(\mathbf{S}^G) = \mathbf{T}_0 \right\} \qquad (7)$$

for a given graph G and a fixed unitary stochastic matrix $\mathbf{T}_0$ associated with a stochastic process on the line-graph of G. Clearly, if $\mathbf{S}^G(k)inUSE_{\mathbf{T}_0}$ for $k = 0$ then it is for all $k \in R$. In fact, if all the arc length L_{ij} are incommensurate, $\mathbf{D}(k)$ sweeps out the space of unitary diagonal matrices of dimension n_E. For practical purposes we will thus often replace averages over a given $USE_{\mathbf{T}}$ by averaging over the space of diagonal unitary matrices $\mathbf{D}$ with $D_{ij} = \delta_{ij} e^{i\varphi_j}$ using the Euclidean measure on the n_E - torus.

Rather than looking at the spectrum obtained from the secular determinant (5), we will here consider the spectrum $\mathbf{S}^G$ for fixed wavenumber k and than average over k. One can write the spectrum in terms of a periodic orbit trace formula reminiscent to the celebrate Gutzwiller trace formula being a semiclassical approximation of the trace of the Green function (Gutzwiller 1990). We write the density of states in terms of the traces of $\mathbf{S}^G$, that is,

$$d(\theta) = \sum_{i=1}^{n_E} \delta(\theta - \theta_i) = \frac{n_E}{2\pi} + \frac{1}{\pi} Re \sum_{n=1}^{\infty} \text{Tr}(\mathbf{S}^G)^n e^{-in\theta}, \qquad (8)$$

where $\{\theta_i\}_{i=1,n_E}$ refers to the eigenphases of $\mathbf{S}^G$. The traces $\text{Tr}(\mathbf{S}^G)^n$ can be given as sum over all periodic paths of length n on the graph, i.e.

$$\text{Tr}(\mathbf{S}^G)^n = \sum_{p}^{(n)} A_p e^{ikL_p}.$$

Describing a given periodic path in terms of its vertex code $(v_1, v_2 \ldots v_n)$, $v_i \in \{1, 2, \ldots n\}$ with $(v_i, v_{i+1}) \in E^G$ being an allowed transitions

between vertices, one obtains for the amplitudes A_p and lengths L_p

$$A_p = \prod_{i=1}^{n} V_{(v_i v_{i+1}),(v_{i+1} v_{i=2})}, \qquad L_p = \sum_{i=1}^{n} L_{v_i v_{i+1}}. \tag{9}$$

where the amplitudes give again transitions between arcs (not vertices). An example of such a periodic path is given in Fig. 1b.

Trace formulas like (8) are a starting point for analysing the statistical properties of quantum spectra. The statistical quantities such as the two-point correlation function can be written in terms of the density of states $d(\theta, N)$, that is,

$$R_2(x) = \frac{1}{\overline{d}^2} < d(\theta) d(\theta + x/\overline{d}) >_{USE_\mathbf{T}, \theta}, \tag{10}$$

where $\overline{d} = N/2\pi$ is the mean level density. The average is taken here over the angle θ as well as over the USE (which is equivalent to energy averaging). The Fourier coefficients of (10) can be written in terms of the traces of $\mathbf{S}$; one obtains

$$K(\tau) = < \frac{1}{N} |\mathrm{Tr} \mathbf{S}^{N\tau}|^2 >_{USE_\mathbf{T}} \tag{11}$$

with $\tau = n/N$ and the average is taken over a USE. The so-called form factor $K(\tau)$ can thus be written as a double sum over periodic paths on the graph

$$K(\tau) = < \frac{1}{N} \sum_{p,p'}^{(n)} A_p A_{p'} e^{i(L_p - L_{p'})} >_{USE_\mathbf{T}} \tag{12}$$

$$\approx g \frac{n}{N} \mathrm{Tr} \mathbf{T}^n + < \sum_{p \neq p'}^{(n)} A_p A_{p'} e^{i(L_p - L_{p'})} >_{USE_\mathbf{T}}. \tag{13}$$

The first term in (13), also called the diagonal term (Berry 1985), originates from periodic orbit pairs (p, p') related through cyclic permutations of the vertex symbol code. There are typically n orbits of that kind and all these orbits have the same amplitude A and phase L. The corresponding periodic orbit pair contributions is (in general) $g \cdot n$ - times degenerate where n is the length of the orbit and g is a symmetry factor ($g = 2$ for time reversal symmetry).

Expanding the random matrix result for the formfactor, one obtains for $0 \leq \tau = n/N \leq 1$

$$K_{CUE}(\tau) = \tau$$

$$K_{COE}(\tau) = 2\tau - \tau \log(1 - 2\tau)$$
$$= 2\tau - 2\tau^2 + 2\tau^3 + \dots.$$
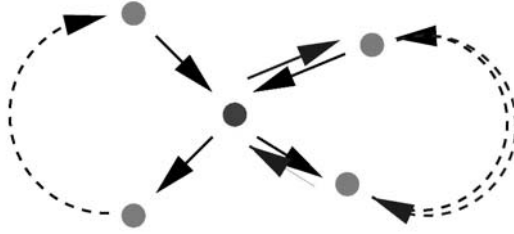
Figure 2. Periodic orbit with one intersection on undirected graphs: two different paths exist having the same length following either the black or blue orbit.

The linear terms are reproduced by the diagonal contribution which gives the important link between the stochastic dynamics and the spectral statistics; it follows from $\lim_{n\to\infty} \mathrm{Tr}\mathbf{T}^n = 1$ given there is a gap between the leading and next-leading eigenvalue of $\mathbf{T}$. Contributions to the double sum in (13) which survive the ensemble average are due to periodic orbit pairs where orbits visit the same arcs along its path but in different order. The simplest examples are "figure eight" orbits of the type shown in Fig. 2 which arise in undirected graphs. Berkolaiko et.al. (2002) could indeed show that orbits of that type give the correct $\mathcal{O}(\tau^2)$ - contributions to the GOE - form factor. In fact, a general scheme emerges relating $\mathcal{O}(\tau^n)$ contributions to periodic orbits with n intersections. This work was inspired by a similar analysis for general quantum systems by Sieber and Richter (2001). The periodic orbit contributions giving the $\mathcal{O}(\tau^3)$ have been worked out by Berkolaiko et.al. (2003) and a general scheme for obtaining higher order terms iteratively has been given by Müller et.al. (2004).

2.3. BORDER OF UNIVERSALITY

In the light of these recent developments, it becomes important to establish the boundaries at which the spectral statistics of quantum graph ensembles (or more general quantum systems) starts to deviate from random matrix behaviour. One can distinguish two different scenarios. Firstly, the properties of the underlying dynamics, that is, the stochastic process $\mathbf{T}$ may be linked to the spectral statistics and may thus provide conditions for the onset of deviations from RMT behaviour; such an approach is in the spirit of the original BGS - conjecture making a connection between classical chaos and random matrix statistics. Secondly, one may consider special phase or length correlations in the quantum graph which could lead to interesting non-universal statistics; in this approach, quantum graph ensemble averages are carried out only over subsets of the full USE.

We will discuss known bounds on the border of universality related to the properties of the stochastic process. An interesting family of quantum graphs which belongs to the second category are so-called regular quantum graphs, which will be treated in more detail in section 3.

2.3.1. *Spectral gap conditions*

When studying the border of universality, we always need to consider the limit of large graphs, that is, $n_E \to \infty$. This limit is in general not well defined, but may often be obvious from the examples considered. We will thus define the semiclassical limit loosely via a family of unitary-stochastic transition matrices $\{\mathbf{T}_{n_E}\}$ and associate USE's and take $n_E \to \infty$. The leading term in (13) then gives a condition for a family to show deviations from RMT statistics in terms of the spectrum of $\mathbf{T}$; the diagonal term must obey

$$1 - \text{Tr}\mathbf{T}^{n_E\tau} \approx e^{-\Delta n_E\tau} \to 0; \quad \text{for} \quad n_E \to \infty$$

in order to match the leading coefficient in the expansion of the RMT form - factor; here Δ is the spectral gap, that is, $\Delta = -\log(1 - |\Lambda_1|)$ with Λ_1 being the next to leading eigenvalue of $\mathbf{T}_{n_E}$) and $\tau = n/n_E$ is fixed. The condition above implies that we expect to see deviations from RMT behaviour to leading order if

$$\Delta \sim n_E^{-\alpha} \quad \text{with} \quad \alpha > 1,$$

that is, whenever the gap closes faster than $1/n_E$ for large system sizes (Tanner 2001). Based on super-symmetric techniques, Gnutzmann and Altland (2004) could give a lower bound by showing that the spectral gap condition guarantees RMT behaviour for $\alpha \leq 1/2$. The border of universality must therefore lie in the range $1/2 < \alpha \leq 1$. Other bounds have been given by Berkolaiko et.al. (2002,2003) which have been derived from higher order terms in the expansion of the form factor. Below we we will give two examples families with $\alpha = 1$ displaying critical behaviour by neither converging to RMT nor to Poisson statistics in the semiclassical limit.

2.3.2. *Quantum star-graphs:*

Quantum star-graphs arise naturally when one quantises a graph with a single central vertex attached to n_E undirected edges, see inset of Fig. 3a. The underlying graph is complete, that is, we can reach every edge from every other edge through the central vertex (ignoring the trivial dynamics on the outer vertices). Typical boundary conditions imposed on the wave equation at the central vertex following Kottos and Smilansky's approach in Sec. 2.1 yield scattering matrices which
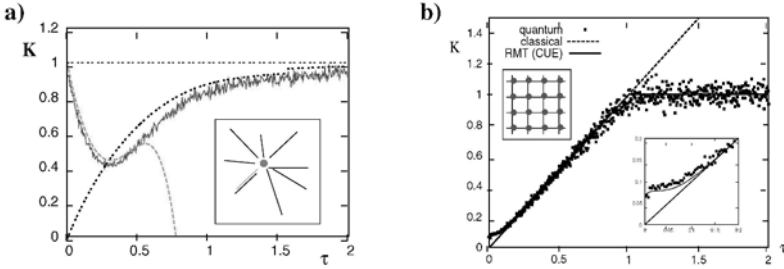
Figure 3. Form factor for a) star graphs: numerics (red) versus the power series expansion (15) (green); b) diffusive network (in 2 d): deviations occur for small τ, see inset.

greatly favour backscattering. The vertex scattering matrix (4) which is essentially equivalent to the matrix $\mathbf{S}$ here is

$$S_{ij} = -\delta_{ij} + \frac{2}{n_E} \ . \tag{14}$$

The Markov processes associated with quantum star graphs correspond to systems of weakly coupled edges. Its dynamical properties are determined by the spectrum of the stochastic matrix associated with (14) which is highly degenerate and can be given explicitly (Kottos and Smilansky 1999), that is,

$$\Lambda_0 = 1, \quad \Lambda_1, \ldots, \Lambda_{n_E-1} = (1 - \frac{4}{n_E}) \approx \frac{4}{n_E} \ .$$

Quantum star-graphs have therefore a critical classical spectrum with a spectral gap vanishing proportional to $1/n_E$; one finds indeed spectral statistics intermediate between Poisson and COE statistics.

The two-point correlation function has been worked out explicitly by Berkolaiko et.al. (2001) and has been shown to coincide with the statistics of so-called Seba billiards, that is, rectangular billiards with a single flux line. The first few terms in a power series expansion of the form factor have been derived by Kottos and Smilansky (1999) and Berkolaiko and Keating (1999) and yield

$$K(\tau) = e^{-4\tau} + 8\tau^3 \frac{32}{3}\tau^4 + \frac{16}{3}\tau^5 + \ldots, \tag{15}$$

see Fig. 3a.

2.3.3. *Diffusive networks*
The quantum mechanics of classically diffusive systems has been studied mainly in the context of Anderson localisation and localisation-delocalisation transitions, see e.g. Dittrich (1996) and Janssen (1998) for recent review articles.

As a simple example, we consider here a quantum graph corresponding to a classical Markov process on a regular lattice in d dimensions, see Fig. 3b for $d = 2$. Choosing a stochastic matrix $\mathbf{T}_d$ with constant transition probabilities $t_{ij} = 1/2d$ between connected edges corresponds to d-dimensional diffusion in the continuum limit $L \to \infty$; here, L is the number of vertices along each direction, that is, the total number of arcs is $n_E = 2dL^d$. Solving the diffusion equation with periodic boundary conditions allows one to recover the low lying part of the spectrum of $\mathbf{T}_d$, that is,

$$\log \Lambda_{\mathbf{m}} = -\frac{4\pi^2 D}{L^2} \sum_{i=1}^{d} m_i^2, \tag{16}$$

with diffusion constant $D = \frac{1}{2d}$ and $\mathbf{m}$ is a d-dimensional integer lattice vector. The influence of the dimension d on the small τ behaviour of the form factor in diffusive systems has been described in detail by, for example, Dittrich (1996) and references therein. In terms of the spectral gap condition, one obtains

$$\Delta_N = \frac{4\pi^2 D}{L^2} = \frac{4\pi^2 (2d)^{2/d-1}}{n_E^{2/d}}$$

that is, we expect universal statistics for $d \geq 3$ only. (Actually, the bound by Gnutzmann and Altland (2004) guarantees random matrix statistics only for $d \geq 4$, numerics suggests however, that $d = 3$ follows RMT already (Tanner 2001)). One finds convergence to the Poisson limit due to Anderson localisation in one dimension (Schanz and Smilansky 2000). The two-dimensional case is critical with $\Delta \sim 1/n_E$ which shows up in the form factor as a plateau for $\tau \to 0$, that is, $\lim_{\tau \to 0} K(\tau) = 1/4\pi$, see Fig. 3b (Tanner 2002).

3. Regular quantum graphs

In the following, we will consider quantum graphs for which the above bounds do not necessarily hold due to length correlations in the graphs, that is, averages are not taken over a full USE. We will actually look at a specific set of such non-generic quantum graphs, namely quantum graphs for which the global propagator $\mathbf{S}$ consists of identical local scattering processes at every vertex. Such graphs have been called *regular quantum graphs* by Severini and Tanner (2004); the name derives from the notation *regular graphs* for graphs which have the same number of incoming and outgoing arcs at every vertex and thus share the property that vertices are locally indistinguishable. We will show that regular

quantum graphs corresponding to the same underlying graph G can behave very differently depending on how the local scattering processes are connected to each other. We will show that a crucial element in this is played by the possible ways regular graphs can be edge-coloured. Regular graphs are in fact another way at looking at *quantum random walks* as will be pointed out at the end of this section.

3.1. REGULAR QUANTUM GRAPHS AND EDGE-COLOURING MATRICES

We will construct a quantum graph on a d-regular digraph G with n vertices for which the wave dynamics at a given vertex of the graph is "locally indistinguishable" from that of any other vertex of the graph. This is done by choosing a unitary d-dim. matrix σ and a set of arc-lengths $L_i, i = 1, \ldots d$ and ascribing the scattering process σ to every vertex in the graph with incoming as well as outgoing arcs chosen from the set of L_i's at every vertex. This is done here by first fixing a so-called *edge-colouring* of the graph (see eg Bollobás 1979), that is, we assign one of d different "colours" to every directed arc of the graph in such a way that no vertex has two incoming or two outgoing arcs of the same colour. Note that there are many different ways to edge-colour a given regular graph for $d \geq 2$. Edge-colouring can be described in terms of a set of n - dimensional permutation matrices $\rho_i, i = 1, \ldots d$ having the property that

$$\sum_{i=1}^{d} \rho_i = \mathbf{A}^G \tag{17}$$

with $\mathbf{A}^G$ being the adjacency matrix of G; the arc (ij) is then assigned the colour k if the (ij) matrix element of ρ_k is non-zero. We refer to the set of ρ_i's as the *edge-colouring matrices* of G[1]. In Fig. 4, an explicit example is shown with

$$\mathbf{A} = \begin{pmatrix} 1 & 1 & 1 & 0 \\ 0 & 1 & 1 & 1 \\ 1 & 1 & 0 & 1 \\ 1 & 0 & 1 & 1 \end{pmatrix}, \quad \rho_1 = \begin{pmatrix} 1 & 0 & 0 & 0 \\ 0 & 0 & 0 & 1 \\ 0 & 1 & 0 & 0 \\ 0 & 0 & 1 & 0 \end{pmatrix},$$

$$\rho_2 = \begin{pmatrix} 0 & 1 & 0 & 0 \\ 0 & 0 & 1 & 0 \\ 0 & 0 & 0 & 1 \\ 1 & 0 & 0 & 0 \end{pmatrix}, \quad \rho_3 = \begin{pmatrix} 0 & 0 & 1 & 0 \\ 0 & 1 & 0 & 0 \\ 1 & 0 & 0 & 0 \\ 0 & 0 & 0 & 1 \end{pmatrix}.$$

---

[1] In Severini and Tanner (2004), these matrices have been called *connectivity matrices*.

$$A = \begin{pmatrix} 1 & 1 & 1 & 0 \\ 0 & 1 & 1 & 1 \\ 1 & 1 & 0 & 1 \\ 1 & 0 & 1 & 1 \end{pmatrix}$$
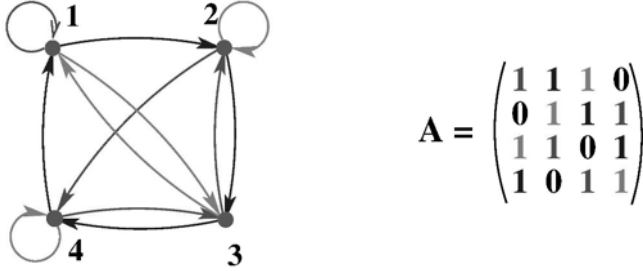
Figure 4. A 3-regular graph of size 4 together with a possible edge-colouring; the edge-colouring matrices correspond to entries having the same colour in the adjacency matrix A of the graph.

The adjacency matrix $\mathbf{A}^{LG}$ of the line-graph of G can then be written in the form (Severini 2003, Severini and Tanner 2004)

$$\mathbf{A}^{LG} = \left(\bigoplus_{i=1}^{d} \rho_i \right) \cdot (\mathbf{J}_d \otimes \mathbf{I}_n) \, something \,, \qquad (18)$$

where $\mathbf{J}_d$ is the $(d \times d)$ matrix with all elements being equal to 1 and $\mathbf{I}_n$ is the identity matrix. We proceed by defining a quantum graph on the line-graph of G in the form of a unitary propagator $\mathbf{S}^G$ as follows:

$$\mathbf{S}^G = \left(\bigoplus_{i=1}^{d} \rho_i \right) \cdot (\mathbf{C} \otimes \mathbf{I}_n) = \begin{bmatrix} C_{11}\,\rho_1 & C_{12}\,\rho_1 & \cdots & C_{1d}\,\rho_1 \\ C_{21}\,\rho_2 & C_{22}\,\rho_2 & \cdots & C_{2d}\,\rho_2 \\ \vdots & \vdots & \ddots & \vdots \\ C_{d1}\,\rho_d & C_{d2}\,\rho_d & \cdots & C_{dd}\,\rho_d \end{bmatrix}, \qquad (19)$$

with $\mathbf{C}(k) = \mathbf{D}(k)\,\sigma$ and $D(k)_{il} = \delta_{jl} e^{ikL_j}$ describing the local scattering process. The d - dimensional matrix $\mathbf{C}$ is also called the *coin* in the context of quantum random walks on graphs (Kempe 2003).

Note that different ways of edge-colouring the graph, that is, different decomposition of A^G in the form (17) lead to different quantum graphs which may have quite different properties as will be shown in the next section; this is in contrast to the representations of the line-graph adjacency matrix (18) which are all equivalent up to relabeling the arcs in the graph. For modifications of this construction for undirected graphs with time reversal symmetry, see Severine and Tanner (2004).

3.2. FROM 'INTEGRABLE' TO 'CHAOTIC' REGULAR QUANTUM GRAPHS - SOME EXAMPLES

In this section, we will show that different ways to edge-colour a graph can indeed lead to very different types of quantum graphs with spectral
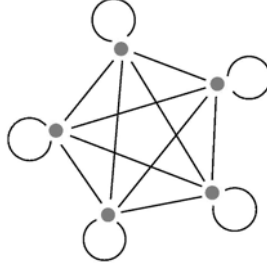
Figure 5. The complete graph K^n with $n = 5$.

statistics ranging from Poisson to CUE. In other words, in regular quantum graphs it is the choice of the edge-colouring matrices ρ_i, a purely topological quantity, which determines the properties of the quantum graph independent of the single vertex scattering processes given through the coin $\mathbf{C}$. We will demonstrate this here for a specific example, namely so called *complete graphs* $G = K^n$ with adjacency matrix $\mathbf{A}^G = \mathbf{J}_n$, that is every vertex is connected to every other vertex, see Fig. 5. (Note that $n_E = n^2$, here). A more general treatment can be found in Severini and Tanner (2004). In the examples discussed below, we make use of the fact that for finite groups Γ of order n, we may write

$$\sum_{i=1}^{n} \rho_i = \mathbf{J}_n \,. \tag{20}$$

where the ρ_i's form a regular representation of Γ. In what follows we will study various decompositions of J_n and see how they effect statistical properties of the spectra of quantum graphs.

3.3. THE CYCLIC GROUP $\mathbb{Z}_n$

We will first consider an abelian group, namely the cyclic group $\mathbb{Z}_n$. The ρ_i's forming a regular representation commute with each other and are of the form

$$(\rho_j)_{kl} = \delta_{k,(l+j) \bmod n} \text{with eigenvalues} \chi_m^j = e^{2\pi i \frac{jm}{n}}, \text{where } j, m = 1, \ldots, n \,. \tag{21}$$

The abelian nature of the group allows one to block-diagonalise the matrix $\mathbf{S}^G$ into n blocks of dimension n each, independent of the coin $\mathbf{C}$. The spectrum of the quantum graph is then given by the spectra of the sub-matrices

$$\mathbf{S}_m^G = \left(\bigoplus_{j=1}^{n} e^{2\pi i \frac{jm}{n}} \right) \cdot \mathbf{C} \quad \text{with} \quad m = 1, \ldots, n \,.$$

The eigenvalues of $\mathbf{S}^G$ are here characterised in terms of two quantum numbers, an 'angular momentum' quantum number m and a second quantum number counting the eigenvalues in each m manifold. If the spectra for different m are uncorrelated, one expects Poisson statistics of the total spectrum in the limit $n \to \infty$.

Figure 6a) shows spectral properties of $\mathbf{S}^G$ with $n = 24$, that is, $\dim S^G = 576$. We plot here the nearest neighbour spacing (NNS) distribution $P(s)$ and the form factor $K(\tau)$. The coin is of the from $C(k) = D(k)\,\sigma$ where the local scattering matrix σ is choosen to be the Fourier matrix and the arc lengths entering the diagonal matrix D are chosen independently and identically distributed in $[0,1]$. The average is, for a fixed choice of the coin, taken by averaging over the wavelength k. The numerical results are shown in Fig. 6a) and suggest indeed Poisson-statistics apart form deviations in the form factor on scales $\tau \leq 1/n$ due to the 'random nature' of the coin.

3.4. The non-abelian case: the symmetric group S_4

Next, we consider a specific example of a non-abelian group, namely the symmetric group S_4 with $n = 24$ elements. By writing the permutation matrices ρ_i forming the regular representation of S_4 in terms of the irreducible representations (for short *irreps*) of S_4, we can again give the propagator $S^{K^{24}}$ in block-diagonal form where the blocks are now of size $n\,d$, with d being the dimension of the irrep under consideration. The group S_4 has 2 one-dimensional, 1 two-dimensional and 2 three-dimensional irreps, and each d - dimensional irrep is contained d times in each ρ_i according to the general formula

$$2 \cdot 1^1 + 1 \cdot 2^2 + 2 \cdot 3^3 = 24.$$

We thus have 5 independent sub-spectra making up the spectrum of the quantum graph $\mathbf{S}^G$ of which two are of dimension $n = 24$, one is of dimension $2 \cdot 24 = 48$ and two are of dimension $3 \cdot 24 = 72$; the latter once are two and three times degenerate, respectively. The huge degeneracy in the spectra can clearly be seen in the spectral statistics; it is manifest in the peak at $s = 0$ in $P(s)$, see Fig. 6b, and leads to

$$[c]cccK(\tau) = (2 \cdot 3^3 + 1 \cdot 2^3 + 2 \cdot 1^3) = 8/3 \text{for } \tau > 3/24\,. \qquad (22)$$

The spectra appear to be uncorrelated otherwise; note however, that the spectrum for each sub-block alone are correlated following CUE statistics, which gives rise to the deviations from purely Poisson behaviour in $P(s)$ (cf. dashed curve) as well as in the behaviour of the form factor for $\tau \leq 3/24$ which is dominated by the sub-spectra of the three dimensional irreps.

(a) The cyclic group (n=24):
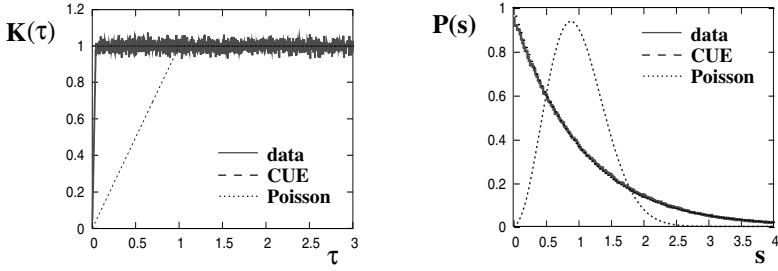
(b) The symmetric group (n=24):
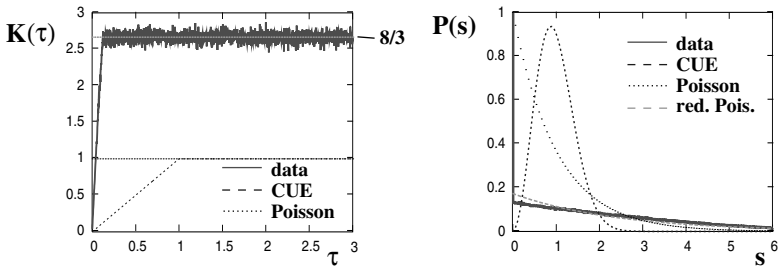
(c) The generic case; only trivial symmetry (n=20):
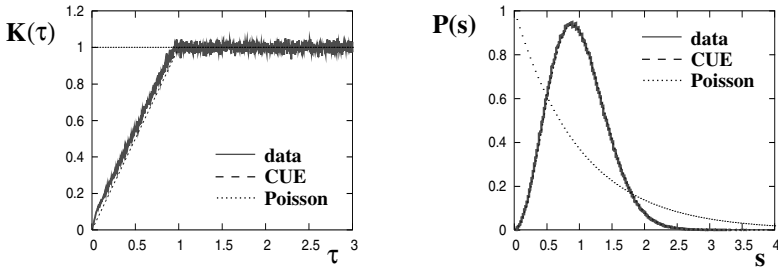
Figure 6. Formfactor $K(\tau)$ and nearest neighbour spacing distribution $P(s)$ for: (a) the ρ_i's form the regular representation of the cyclic group $\mathbb{Z}_{24}$; (b) ρ_i's represent the symmetric group S_4; (c) a 'random' set of ρ_i's without symmetries. The dashed curve in (b) labeled "red. Poisson" corresponds to a distribution of degenerate levels being Poisson distributed otherwise.

3.5. THE GENERIC CASE: NO SYMMETRIES

The overwhelming number of decompositions of the form (20) will of course have no common symmetry, that is, it is not possible to block-diagonalise the ρ_i's simultaneously. We therefore do not expect any

special features in the spectrum. The question remains, however, if the 'randomness' put into the system by choosing a random edge-colouring is enough to produce generic, random matrix type, statistics. After all, these quantum graphs still possess a large degree of degeneracy due to the presence of identical coins at every vertex. A numerical study may thus reveal interesting insights into the range of validity of the RMT - regime. Fig. 6c shows the level statistics for an unstructured choice of edge-colouring matrices which is in good agreement with random matrix theory for the CUE - ensemble [2]. Note that the statistic has been obtained from the spectrum on an $(n^2 \times n^2)$ unitary matrix which has only n^3 non-zero elements of which only n^2 are independent; in addition, there are only n different arcs lengths to choose from for n^2 different arcs. The origin of the universality in the spectral statistics in this type of quantum graphs is here clearly not due to the 'randomness' in the choice of the matrix elements but due to random edge-colouring of the graph alone!

3.6. QUANTUM RANDOM WALKS

In recent years, the study of unitary propagation on graphs has also been looked at from the perspective of devising a quantum version of a random walk. This line of thought arose as part of the effort to build quantum information systems being able to do operations which are impossible or much slower on classical devices. It could indeed be shown that quantum random walks have this property under certain circumstances: quantum walks can be faster for some network geometries (Aharonov et.al. 1993) and can even lead to an exponential speed-up such as for the graph-traversal algorithm by Childs et.al. (2003); for an introductory overview and further references, see Kempe (2003). The generalisation of Grover's algorithm (Grover 1997) to spatial searches on graphs (Shenvi et.al. 2003, Ambianis et.al. 2004, Childs and Goldstone 2004) is another remarkable recent result.

We will not study the properties of quantum random walks here; instead, we would like to point out that the discrete quantum walk modules discussed in the literature are in fact equivalent to regular quantum graphs such as introduced in the previous sections.

In brief, a discrete quantum random walk comprises of an in general d - regular graph G with n vertices (where lattices are favoured in the literature) and a 'spin' degree of freedom, where the spin can take up d different states. A quantum state at a vertex v with spin i is then

---

[2] Deviations in the formfactor for small τ can be attributed to the fact that the spectrum of C itself is always contained in the full spectrum, see Severini and Tanner (2004); this part has been removed in the NNS statistic.

described by $|v, i >$ and the quantum wave function is a superposition of all possible vertex states. The quantum random walk consists of a 'walk' element and a 'quantum coin toss'. The walk is steered by the internal spin states, that is, there exist matrices ρ_i, $i = 1, \ldots d$ which define in which direction the component $|v, i >$ is flowing, that is,

$$\rho_i |v, i >= |v', i >$$

where the internal spin states remains unchanged. The ρ_i's are obviously permutation matrices in the vertex space. The coin toss is simulated by applying a unitary transformation C to the spin states at every vertex, that is,

$$\mathbf{C}|v, i >= |v, \sum_j C_{ij} j >;$$

the coin is unbiased, if $|C_{ij}|^2 = 1/d$ throughout. It is clear from the construction, that one obtains a classical random walk on such a network, if one performs a measurement after every walk by projecting out the spin degrees of freedom.

A full cycle of walk and coin toss is then described by a unitary matrix

$$\mathbf{S}_{QW} = \left(\bigoplus_{i=1}^{d} \rho_i \right) \cdot (\mathbf{C} \otimes \mathbf{I}_n) \tag{23}$$

which has exactly the form of the propagator for regular quantum graphs in Eq. (19). We thus identify the ρ_i's with the edge-colouring matrices and the coin is in fact a local scattering matrix. Writing the components of the wave function in $|v, i >$ notation is thus just a different way of labeling the arcs in the graph and the dynamics takes indeed place on the line-digraph of G.

To demonstrate the mechanism, let us give a specific example: the quantum walk on an infinite line. A popular setting is the following walk:

states: $\quad |i, \uparrow>, |i, \downarrow>, \quad i \in \mathbb{Z}$

walk: $\quad \begin{matrix} |i, \uparrow> \rightarrow |i + 1, \uparrow> \\ |i, \downarrow> \rightarrow |i - 1, \downarrow> \end{matrix}, \quad$ that is, $\quad \rho_\uparrow = \delta_{i,i+1}, \quad \rho_\downarrow = \delta_{i,i-1};$

coin: $\quad \mathbf{C} = \dfrac{1}{\sqrt{2}} \begin{pmatrix} 1 & 1 \\ -1 & 1 \end{pmatrix}.$

A random walk starting in the state $|i, \uparrow>$ then evolves according to

$$|i, \uparrow> \overset{C}{\rightarrow} \frac{1}{\sqrt{2}} (|i, \uparrow> -|i, \downarrow>) \overset{\text{walk}}{\rightarrow} (|i + 1, \uparrow> -|i - 1, \downarrow>) \overset{C}{\rightarrow} \ldots.$$

Continuing this process leads quickly to a probability profile which grows linearly with the number of steps t which is in contrast to the classical spreading for 1d random walks being of the order $\sqrt{t}$ (Kempe 2003). It must be pointed out, however, that this is a pure symmetry effect due the choice of edge-colouring matrices; in the setting chosen here, the two operations $\rho_\uparrow$ and $\rho_\downarrow$ commute. Colouring the arcs in a different way, for example by randomly assigning colours to the arcs, leads to a completely different behaviour which is for a generic choice of **C** similar to that of a quantum graph on a diffusive network as discussed in sec. 2.3. In particular, one finds localisation in one-dimensional chains, that is, a typical wave function will not spread at all!

4. Acknowledgment:

References

Aharonov Y, Davidovich L and Zagury N 1993 Phys. Rev. A bf 48 1687

Ambainis A, Kempe J and Rivosh A 2004 quant-ph/0402107.

Bang-Jensen J and Gutin G, *Digraphs. Theory, algorithms and applications*, Springer Monographs in Mathematics, Springer-Verlag, London, 2001.

Barra F and Gaspard P 2000 *J. Stat. Phys.* **101** 283–320.

Bollobás B, *Graph Theory - An Introductory Course* Springer Graduate Texts in Mathematics, Springer-Verlag, New York, 1979.

Berkolaiko G and Keating J P 1999 *J. Phys. A* **32** 7827.

Berkolaiko G, Bogomolny E B and Keating J P 2001 *J. Phys. A* **34** 335.

Berkolaiko G, Schanz H and Whitney R S 2002 *Phys. Rev. Lett.* **88** 104101.

Berkolaiko G, Schanz H and Whitney R S 2003 *J. Phys. A* **36** 8373.

Berry M V 1985 *Proc. R. Soc. A* **400** 229.

Bohigas O, Giannoni M J and Schmit C 1984 *Phys. Rev. Lett.* **52** 1.

Blümel R, Dabaghian Yu and Jensen R V 2002 *Phys. Rev. Lett.* **88** 044101; Dabaghian Yu and Blümel R 2004 *Phys. Rev. E* **70** 046206.

Chalker J T and Coddington P D 1988 *J. Phys. C* **21** 2665–2679

Childs A M, Cleve R, Deotto E, Fahri E, Gutman S and Spielman D A 2003 *Proc. 35th ACM Symb. on the Theory of Comp. (STOC 2003)* 59; quant-ph/0209131.

Childs A M and Goldstone J 2004

Dittrich T 1996 *Physics Reports* **271** 267.

Freche P, Janssen M and Merkt R 1999 *Phys. Rev. Lett.* **82** 149.

Gnutzmann S and Altland A 2004 *Phys. Rev. Lett.* **93**, 194101.

Grover L K 1997 *Phys. Rev. Lett.* **79** 325. *Phys. Rev. A* **70** 022314.

Gutzwiller M C 1990 *Chaos in Classical and Quantum Mechanics* (Springer, New York).

Janssen M 1998 *Physics Reports* **295** 1.

Kempe J 2003 *Contemporary Physics*, **44** 307.

Klesse R and Metzler M 1995 *Europhys. Lett* **32** 229–234

Klesse R and Metzler M 1997 *Phys. Rev. Lett.* **79** 721–724

Kottos T and Smilansky U 1997 *Phys. Rev. Lett.* **79** 4794.

Kottos T and Smilansky U 1999 *Ann. Phys. NY* **274** 76.

Kuchment P 2002 *Waves in Random Media*, **12**, R1.

Müller S, Heusler S, Braun P, Haake F and Altland A 2004 *Phys. Rev. Lett.* **93**, 014103.

Pakoński P, Życzkowski K and Kuś M 2001 *J. Phys. A* **34** 9303.

Pakoński P, Tanner G and Życzkowski K, 2003 *J. Stat. Phys.* **111**, 1331.

Pascaud M and Montambaux 1999 *Phys. Rev. Lett.* **82** 4512–4515

Shenvi N, Kempe J, Whaley K B 2003 *Phys. Rev. A* **67** 052307.

Sieber M and Richter K 2001 *Physica Scripta* **T90** 128.

Sieber M 2002 *J. Phys. A* **35**, L613.

Severini S 2003, math.CO/0309092.

Severini S and Tanner G 2004 *J. Phys. A* **37** 6675.

Schanz H and Smilansky U 2000 *Phys. Rev. Lett.* **84**, 1427.

Tanner G 2001 *J. Phys. A* **34** 8485.

Semiclassics and propagation of coherent states for spin-orbit coupling problems

Jens Bolte

Abteilung Theoretische Physik, Univ. Ulm,
Albert-Einstein-Allee 11, D-89069 Ulm, Germany

Abstract. The Dirac equation is discussed in a semiclassical context, with an emphasis on the separation of particles and anti-particles. Classical spin-orbit dynamics are obtained as the leading contribution to a semiclassical approximation of the quantum dynamics. In a second part the propagation of coherent states in general spin-orbit coupling problems is studied in two different semiclassical scenarios.

Keywords: Dirac equation, semiclassics, spin-orbit coupling, coherent states

1. Introduction

Spin-orbit coupling problems are of a genuine quantum nature since a priori spin is a quantity that only occurs in quantum mechanics. However, already Thomas (Thomas, 1927) had introduced a classical model for spin precession. Later, Rubinow and Keller (Rubinow and Keller, 1963) derived the Thomas precession from a WKB-like approach to the Dirac equation. They found that although the spin motion only occurs in the first semiclassical correction to the relativistic classical electron motion, it can be expressed in merely classical terms.

Our approach is based on a systematic semiclassical study of the Dirac equation. After separating particles and anti-particles to arbitrary powers in $\hbar$, a semiclassical expansion of the quantum dynamics in the Heisenberg picture is developed. To leading order this method produces classical spin-orbit dynamics for particles and anti-particles, respectively, that coincide with the findings of Rubinow and Keller: Hamiltonian relativistic (anti-) particles drive a spin precession along their trajectories. A modification of that method leads to a semiclassical equivalent of the Foldy-Wouthuysen transformation resulting in relativistic quantum Hamiltonians with spin-orbit coupling.

In a second part we study the propagation of coherent states in general spin-orbit coupling problems with semiclassical means. This is done in two semiclassical scenarios: $\hbar \rightarrow 0$ with either spin quantum number s fixed (as above), or such that $\hbar s = S$ is fixed. In both cases, first approximate Hamiltonians are introduced that propagate coherent states exactly. The full Hamiltonians are then treated as perturbations of the approximate ones. The full quantum dynamics is seen to follow appropriate classical spin-orbit trajectories, with a semiclassical error of size $\sqrt{\hbar}$. As opposed to the first case,

in the second scenario the classical spin motion is found to exert a back re-action on the (anti-) particle trajectories. Finally, it is observed that the semi-classical propagation holds up to the Ehrenfest time, which reads $T_E(\hbar) = |\log \hbar|/6\lambda$ when the classical trajectory is unstable with Lyapunov exponent λ. Full proofs of the results presented here can be found in (Bolte and Glaser, 2004; Bolte and Glaser, 2004; Bolte and Glaser, 2005).

2. Semiclassics for the Dirac equation

We consider particles of spin $1/2$, mass m, and electric charge e in a fixed inertial frame. They shall be exposed to external electromagnetic fields that are static in the given frame,
$$\boldsymbol{E}(\boldsymbol{x}) = -\nabla\phi(\boldsymbol{x})$$
and
$$\boldsymbol{B}(\boldsymbol{x}) = \nabla \times \boldsymbol{A}(\boldsymbol{x}).$$

In relativistic quantum mechanics such particles are described by the Dirac equation

$$\mathrm{i}\hbar\frac{\partial}{\partial t}\Psi(t,\boldsymbol{x}) = \hat{H}_D\,\Psi(t,\boldsymbol{x})\,, \tag{1}$$

where the Dirac-Hamiltonian reads

$$\hat{H}_D = c\boldsymbol{\alpha}\cdot\left(\frac{\hbar}{\mathrm{i}}\nabla - \frac{e}{c}\boldsymbol{A}(\boldsymbol{x})\right) + mc^2\beta + e\phi(\boldsymbol{x})\,. \tag{2}$$

The relations $\alpha_k\alpha_l + \alpha_l\alpha_k = 2\delta_{kl}$, $\alpha_k\beta + \beta\alpha_k = 0$, and $\beta^2 = \mathbb{1}_4$ define the relevant Clifford algebra, for which we choose the Dirac representation. In a phase space language, employing Weyl quantisation, this Hamiltonian can be written as (see, e.g., (Dimassi and Sjostrand, 1999))

$$(\hat{H}_D\psi)(\boldsymbol{x}) = \frac{1}{(2\pi\hbar)^3}\iint \mathrm{e}^{\frac{\mathrm{i}}{\hbar}\boldsymbol{p}\cdot(\boldsymbol{x}-\boldsymbol{y})}\,H_D\big(\tfrac{\boldsymbol{x}+\boldsymbol{y}}{2},\boldsymbol{p}\big)\,\psi(\boldsymbol{y})\,\mathrm{d}p\,\mathrm{d}y\,, \tag{3}$$

where

$$H_D(\boldsymbol{x},\boldsymbol{p}) = \begin{pmatrix} (e\phi(\boldsymbol{x}) + mc^2)\mathbb{1}_2 & (c\boldsymbol{p} - e\boldsymbol{A}(\boldsymbol{x}))\cdot\boldsymbol{\sigma} \\ (c\boldsymbol{p} - e\boldsymbol{A}(\boldsymbol{x}))\cdot\boldsymbol{\sigma} & (e\phi(\boldsymbol{x}) - mc^2)\mathbb{1}_2 \end{pmatrix} \tag{4}$$

is the matrix valued Weyl symbol of the operator $\hat{H}_D$. For each point $(\boldsymbol{x},\boldsymbol{p})$ in phase space this is a hermitian 4×4 matrix with the (twofold degenerate) eigenvalues

$$h_\pm(\boldsymbol{x},\boldsymbol{p}) = \pm\sqrt{(c\boldsymbol{p} - e\boldsymbol{A}(\boldsymbol{x}))^2 + m^2c^4} + e\phi(\boldsymbol{x})\,. \tag{5}$$

The functions $h_\pm(\boldsymbol{x},\boldsymbol{p})$ are the classical relativistic Hamiltonians of spinless particles with positive and negative energies, respectively.

2.1. PARTICLES AND ANTI-PARTICLES

In order to achieve a semiclassical separation of particles and anti-particles one starts with the projection matrices

$$\Pi_0^\pm(\boldsymbol{x}, \boldsymbol{p}) = \frac{1}{2}\Big(\mathbb{1}_4 \pm \frac{\boldsymbol{\alpha} \cdot (c\boldsymbol{p} - e\boldsymbol{A}(\boldsymbol{x})) + \beta mc^2}{\varepsilon(\boldsymbol{x}, \boldsymbol{p})}\Big) \qquad (6)$$

onto the two-dimensional eigenspaces in $\mathbb{C}^4$ corresponding to the eigenvalues (5); here we have introduced

$$\varepsilon(\boldsymbol{x}, \boldsymbol{p}) := \sqrt{(c\boldsymbol{p} - e\boldsymbol{A}(\boldsymbol{x}))^2 + m^2 c^4} \, . \qquad (7)$$

The Weyl quantisations $\hat{\Pi}_0^\pm$ of (6) according to the rule (3), however, are not projection operators on the Hilbert space $\mathcal{H} = L^2(\mathbb{R}^3) \otimes \mathbb{C}^4$, since (see, e.g., (Emmrich and Weinstein, 1996))

$$\big(\hat{\Pi}_0^\pm\big)^2 - \hat{\Pi}_0^\pm = O(\hbar) \quad \text{and} \quad [\hat{H}_D, \hat{\Pi}_0^\pm] = O(\hbar) \, . \qquad (8)$$

One can improve the error to higher orders in $\hbar$ by successively adding $\hbar$-dependent corrections to (6), finally arriving at projection operators $\hat{\Pi}^\pm$ that are Weyl quantisations of (see again (Emmrich and Weinstein, 1996))

$$\Pi^\pm(\boldsymbol{x}, \boldsymbol{p}) \sim \sum_{k=0}^{\infty} \hbar^k \, \Pi_k^\pm(\boldsymbol{x}, \boldsymbol{p}) \, , \qquad (9)$$

and that almost commute with the Dirac-Hamiltonian,

$$[\hat{H}_D, \hat{\Pi}^\pm] = O(\hbar^\infty) \, . \qquad (10)$$

Here $O(\hbar^\infty)$ indicates an error that is smaller than any power of $\hbar$. The operators $\hat{\Pi}^\pm$ also provide a semiclassical resolution of unity,

$$\hat{\Pi}^+ + \hat{\Pi}^- = O(\hbar^\infty) \quad \text{and} \quad \hat{\Pi}^+\hat{\Pi}^- = O(\hbar^\infty) \, . \qquad (11)$$

In the Hilbert space $\mathcal{H}$ one can therefore introduce the subspaces $\mathcal{H}^\pm = \hat{\Pi}^\pm \mathcal{H}$ that are almost invariant under the quantum dynamics generated by the Dirac Hamiltonian (2), since the estimate (10) implies that

$$\mathrm{e}^{-\frac{\mathrm{i}}{\hbar}\hat{H}_D t}\hat{\Pi}^\pm\psi - \hat{\Pi}^\pm \mathrm{e}^{-\frac{\mathrm{i}}{\hbar}\hat{H}_D t}\psi = O(t\hbar^\infty) \, . \qquad (12)$$

Hence, for finite times t any initial vector from $\mathcal{H}^\pm$ remains in this subspace up to an error of the order $\hbar^\infty$. Moreover, for semiclassically large times, $t \ll \hbar^{-N}$ for any $N > 0$, the error is still approaching zero in the semiclassical limit. Since the construction of the projectors $\hat{\Pi}^\pm$ was based on the "classical" projection matrices (6) associated with positive and negative

classical energies, one can interpret the subspaces $\mathcal{H}^{\pm}$ as to contain particle and anti-particle states, respectively. This identification is exact in the absence of external electromagnetic fields, where the Weyl quantisation of (6) already yields the proper projection operators to the particle and anti-particle subspaces.

2.2. CLASSICAL DYNAMICS

The classical motion corresponding to the quantum dynamics generated by the Dirac-Hamiltonian (2) can most conveniently be obtained by considering the limit $\hbar \rightarrow 0$ in the Heisenberg picture: Consider an operator $\hat{B}$ that is a Weyl quantisation of some symbol (see (Dimassi and Sjostrand, 1999))

$$B(\boldsymbol{x}, \boldsymbol{p}; \hbar) \sim \sum_{k=0}^{\infty} \hbar^k \, B_k(\boldsymbol{x}, \boldsymbol{p}) \,, \tag{13}$$

and propagate it to time $t > 0$,

$$\hat{B}(t) = \mathrm{e}^{\frac{\mathrm{i}}{\hbar} \hat{H}_D t} \, \hat{B} \, \mathrm{e}^{-\frac{\mathrm{i}}{\hbar} \hat{H}_D t} \,. \tag{14}$$

Up to a possible error of order $\hbar^{\infty}$ this operator is again a Weyl quantisation of some symbol

$$B(t)(\boldsymbol{x}, \boldsymbol{p}; \hbar) \sim \sum_{k=0}^{\infty} \hbar^k \, B(t)_k(\boldsymbol{x}, \boldsymbol{p}) \,, \tag{15}$$

if and only if the operator $\hat{B}$ satisfies the condition

$$\hat{\Pi}^+ \hat{B} \hat{\Pi}^- = O(\hbar^{\infty}) = \hat{\Pi}^- \hat{B} \hat{\Pi}^+ \,, \tag{16}$$

i.e., if $\hat{B}$ semiclassically does not induce transitions between the particle and anti-particle subspaces, see (Bolte and Glaser, 2004). In that case the coefficients $B(t)_k(\boldsymbol{x}, \boldsymbol{p})$ in the expansion (15) can be determined order by order, with leading term (Bolte and Glaser, 2004; Bolte and Glaser, 2004)

$$B(t)_0(\boldsymbol{x}, \boldsymbol{p}) = \sum_{\nu=+,-} d_\nu^\dagger(\boldsymbol{x}, \boldsymbol{p}, t) \, (\Pi_0^\nu B_0 \Pi_0^\nu)(\boldsymbol{x}_\nu(t), \boldsymbol{p}_\nu(t)) \, d_\nu(\boldsymbol{x}, \boldsymbol{p}, t) \,. \tag{17}$$

In this expression $(\boldsymbol{x}_{\pm}(t), \boldsymbol{p}_{\pm}(t))$ are solutions of the classical equations of motion generated by the Hamiltonians (5), with $(\boldsymbol{x}_{\pm}(0), \boldsymbol{p}_{\pm}(0)) = (\boldsymbol{x}, \boldsymbol{p})$. Moreover, $d_{\pm}(\boldsymbol{x}, \boldsymbol{p}, t)$ are unitary 4×4 matrices that describe the dynamics of the spin degrees of freedom to leading semiclassical order along the trajectories $(\boldsymbol{x}_{\pm}(t), \boldsymbol{p}_{\pm}(t))$ in phase space.

The classical spin motion that follows from the above considerations can be viewed as a dynamics on the sphere S^2 driven by the Hamiltonian dynamics in phase space. To see this one first transforms the (redundant) four-dimensional representation of the matrix degrees of freedom, corresponding

to either positive or negative energies, into a more convenient two-dimensional form. The matrices

$$V_+(\boldsymbol{x},\boldsymbol{p}) = \frac{1}{\sqrt{2\varepsilon(\boldsymbol{x},\boldsymbol{p})(\varepsilon(\boldsymbol{x},\boldsymbol{p})+mc^2)}} \begin{pmatrix} (\varepsilon(\boldsymbol{x},\boldsymbol{p})+mc^2)\mathbb{1}_2 \\ (c\boldsymbol{p}-e\boldsymbol{A}(\boldsymbol{x}))\cdot\boldsymbol{\sigma} \end{pmatrix}$$

$$V_-(\boldsymbol{x},\boldsymbol{p}) = \frac{1}{\sqrt{2\varepsilon(\boldsymbol{x},\boldsymbol{p})(\varepsilon(\boldsymbol{x},\boldsymbol{p})+mc^2)}} \begin{pmatrix} (c\boldsymbol{p}-e\boldsymbol{A}(\boldsymbol{x}))\cdot\boldsymbol{\sigma}) \\ -(\varepsilon(\boldsymbol{x},\boldsymbol{p})+mc^2)\mathbb{1}_2 \end{pmatrix}$$

(18)

provide isometries from $\mathbb{C}^2$ to $\Pi_0^\pm(\boldsymbol{x},\boldsymbol{p})\mathbb{C}^4$, such that $V_\pm V_\pm^\dagger = \Pi_0^\pm$ and $V_\pm^\dagger V_\pm = \mathbb{1}_2$, see (Bolte and Keppeler, 1999; Bolte and Glaser, 2004). That way the expressions $\Pi_0^\nu B_0 \Pi_0^\nu$ occurring in (17) can be converted into the 2×2 matrices

$$V_\pm^\dagger(\boldsymbol{x},\boldsymbol{p})\, B_0(\boldsymbol{x},\boldsymbol{p})\, V_\pm(\boldsymbol{x},\boldsymbol{p})\ . \tag{19}$$

E.g., for the spin operator

$$\boldsymbol{\Sigma} = \begin{pmatrix} \boldsymbol{\sigma} & 0 \\ 0 & \boldsymbol{\sigma} \end{pmatrix} \tag{20}$$

this transformation amounts to

$$V_\pm^\dagger(\boldsymbol{x},\boldsymbol{p})\, \boldsymbol{\Sigma}\, V_\pm(\boldsymbol{x},\boldsymbol{p}) = \boldsymbol{\sigma}\ , \tag{21}$$

which is independent of the phase-space point $(\boldsymbol{x},\boldsymbol{p})$. The leading semiclassical order of the spin operator following from (17) thus reads

$$D_\pm^\dagger(\boldsymbol{x},\boldsymbol{p},t)\,\boldsymbol{\sigma}\, D_\pm(\boldsymbol{x},\boldsymbol{p},t) \tag{22}$$

in two-dimensional form, where the spin propagator $D_\pm(\boldsymbol{x},\boldsymbol{p},t) \in \mathrm{SU}(2)$ is determined by the equation (see (Bolte and Glaser, 2004))

$$\mathrm{i}\hbar\frac{\partial}{\partial t}D_\pm(\boldsymbol{x},\boldsymbol{p},t) = \tfrac{\hbar}{2}\,\boldsymbol{C}_\pm(\boldsymbol{x}_\pm(t),\boldsymbol{p}_\pm(t))\cdot\boldsymbol{\sigma}\, D_\pm(\boldsymbol{x},\boldsymbol{p},t)\ , \tag{23}$$

with $D_\pm(\boldsymbol{x},\boldsymbol{p},0) = \mathbb{1}_2$. Here

$$\boldsymbol{C}_\pm(\boldsymbol{x},\boldsymbol{p}) = \pm\frac{ec}{\varepsilon(\boldsymbol{x},\boldsymbol{p})}\left(\boldsymbol{B}(\boldsymbol{x}) \pm \frac{c\boldsymbol{E}(\boldsymbol{x})\times(c\boldsymbol{p}-e\boldsymbol{A}(\boldsymbol{x}))}{\varepsilon(\boldsymbol{x},\boldsymbol{p})+mc^2}\right) \tag{24}$$

defines a spin Hamiltonian $H_{\mathrm{spin}}^\pm = \tfrac{\hbar}{2}\,\boldsymbol{C}_\pm\cdot\boldsymbol{\sigma}$ at each point $(\boldsymbol{x},\boldsymbol{p})$ in phase space. The spin dynamics (22) is completely determined by a corresponding classical spin motion. The latter follows from expectation values of the operator (22) in spin states $u \in \mathbb{C}^2$ with $\|u\|_{\mathbb{C}^2} = 1$,

$$\boldsymbol{n}_\pm(t) := \langle u, D_\pm^\dagger(\boldsymbol{x},\boldsymbol{p},t)\,\boldsymbol{\sigma}\, D_\pm(\boldsymbol{x},\boldsymbol{p},t)u\rangle_{\mathbb{C}^2}\ , \tag{25}$$

see (Bolte and Keppeler, 1999). Clearly, $\boldsymbol{n}_\pm(t) \in \mathbb{R}^3$ is of unit length and therefore represents a point on the sphere S^2. Its dynamics immediately follows from (23),

$$\dot{\boldsymbol{n}}_\pm(t) = \boldsymbol{C}_\pm(\boldsymbol{x}_\pm(t),\boldsymbol{p}_\pm(t)) \times \boldsymbol{n}_\pm(t)\ . \tag{26}$$

This equation describes the Thomas precession of a classical spin (Thomas, 1927), which is driven by the underlying Hamiltonian dynamics in phase space. In combination the two types of dynamics, Hamiltonian on phase space and driven precession on the sphere, yield the following picture: There is a combined phase space $\mathbb{R}^3 \times \mathbb{R}^3 \times S^2$ with two dynamical systems,

$$(\boldsymbol{x}, \boldsymbol{p}, \boldsymbol{n}) \mapsto (\boldsymbol{x}_\pm(t), \boldsymbol{p}_\pm(t), \boldsymbol{n}_\pm(t)) \,, \tag{27}$$

that each posses the form of a skew product (see (Cornfeld, Fomin and Sinai, 1982)), qualifying them as genuine flows on the combined phase space. These two motions are the classical dynamical systems that in leading semiclassical order correspond to the quantum dynamics generated by the Dirac-Hamiltonian (2). They involve the semiclassical separation of particles from anti-particles and are independently associated with either particles $(+)$ or anti-particles $(-)$.

2.3. SEMICLASSICAL FOLDY-WOUTHUYSEN TRANSFORMATION

In the previous discussion the semiclassical separation of particles and anti-particles employed projection operators and the associated subspaces of the Hilbert space. By suitable choices of bases such a separation can also be constructed with the help of unitary operators rotating the Hamiltonian into a block-diagonal form. Such a procedure is closely analogous to the Foldy-Wouthuysen transformation that provides a similar separation in a non-relativistic limit. A (unitary) semiclassical Foldy-Wouthuysen transformation $\hat{U}_{sc}$ rotates the Dirac-Hamiltonian $\hat{H}_D$ into

$$\hat{U}_{sc}^\dagger \hat{H}_D \, \hat{U}_{sc} = \begin{pmatrix} \hat{H}_D^+ & 0 \\ 0 & \hat{H}_D^- \end{pmatrix} + O(\hbar^\infty) \,, \tag{28}$$

where $\hat{H}_D^\pm$ are Weyl quantisations of symbols

$$H_D^\pm(\boldsymbol{x}, \boldsymbol{p}) \sim \sum_{k=0}^\infty \hbar^k \, H_{D,k}^\pm(\boldsymbol{x}, \boldsymbol{p}) = h_\pm(\boldsymbol{x}, \boldsymbol{p}) + \tfrac{\hbar}{2} \boldsymbol{C}_\pm(\boldsymbol{x}, \boldsymbol{p}) \cdot \boldsymbol{\sigma} + O(\hbar^2) \,, \tag{29}$$

see, e.g., (Cordes, 1983; Bruneau and Robert, 1999; Teufel, 2003). Cutting off this symbol expansion after the two leading terms would yield the relativistic quantum Hamiltonians

$$\pm \sqrt{\left(\tfrac{\hbar c}{i}\nabla - e\boldsymbol{A}(\boldsymbol{x})\right)^2 + m^2 c^4} + e\phi(\boldsymbol{x}) + \tfrac{\hbar}{2}\boldsymbol{C}_\pm(\boldsymbol{x}, \tfrac{\hbar}{i}\nabla) \cdot \boldsymbol{\sigma} \,, \tag{30}$$

separately for particles and anti-particles, with completely relativistic spin-orbit coupling. This has to be compared with the usual non-relativistic Foldy-

Wouthuysen transformation that yields, up to second order in $1/c$, the Pauli-operators

$$\pm\frac{1}{2m}\Big(\frac{\hbar}{\mathrm{i}}\nabla - \frac{e}{c}\boldsymbol{A}(\boldsymbol{x})\Big)^2 + e\phi(\boldsymbol{x}) \mp \frac{e\hbar}{2mc}\boldsymbol{B}(\boldsymbol{x})\cdot\boldsymbol{\sigma}\ , \qquad (31)$$

which are themselves non-relativistic approximations to the operators (30).

3. Propagation of coherent states in spin-orbit coupling problems

Semiclassical studies of the propagation of coherent states have proven useful in many circumstances see, e.g., (Klauder and Skagerstam, 1982; Perelomov, 1986). Here we consider spin-orbit coupling problems that result from the Dirac equation either in a semiclassical or in a non-relativistic approximation (see, e.g., the Hamiltonians (30) and (31)). The Hamiltonians $\hat{H}$ that arise in such a context can be viewed as Weyl quantisations of symbols

$$H(\boldsymbol{x},\boldsymbol{p}) = H_0(\boldsymbol{x},\boldsymbol{p})\mathbb{1}_2 + \tfrac{\hbar}{2}\,\boldsymbol{C}(\boldsymbol{x},\boldsymbol{p})\cdot\boldsymbol{\sigma}\ , \qquad (32)$$

where $H_0(\boldsymbol{x},\boldsymbol{p})$ is a real valued function. This setting allows to cover a wide range of problems including, e.g., spin-orbit couplings of the Rashba-type in semiconductors (see, e.g., (Zaitsev, Frustaglia and Richter, 1982)).

The goal is to investigate solutions to the ("Pauli-type") equation

$$\mathrm{i}\hbar\frac{\partial}{\partial t}\Psi(t,\boldsymbol{x}) = \hat{H}\,\Psi(t,\boldsymbol{x})\ , \qquad (33)$$

in the semiclassical limit, when $\Psi(0,\boldsymbol{x})$ is a coherent state in the translational as well as in the spin degrees of freedom.

3.1. COHERENT STATES

Coherent states for the translational degrees of freedom (in d dimensions) are Gaussians located at a point $(\boldsymbol{q},\boldsymbol{p})$ in phase space. For convenience we choose them as

$$\varphi^B_{(\boldsymbol{q},\boldsymbol{p})}(\boldsymbol{x}) := N_B\,\mathrm{e}^{\frac{\mathrm{i}}{\hbar}\boldsymbol{p}\cdot(\boldsymbol{x}-\boldsymbol{q})+\frac{\mathrm{i}}{2\hbar}(\boldsymbol{x}-\boldsymbol{q})B(\boldsymbol{x}-\boldsymbol{q})}\ , \qquad (34)$$

where B is a complex-symmetric $d \times d$ matrix whose imaginary part is positive-definite, and N_B is a suitable normalisation. It is well known that quadratic Hamiltonians, i.e., Weyl quantisations of

$$H_{\mathrm{osc}}(\boldsymbol{x},\boldsymbol{p}) = \sum_{|\alpha|+|\beta|\leq 2} A_{\alpha\beta}\,\boldsymbol{x}^\alpha\,\boldsymbol{p}^\beta\ , \qquad (35)$$

propagate such coherent states exactly. This means

$$
\mathrm{e}^{-\frac{\mathrm{i}}{\hbar}\hat{H}_{\mathrm{osc}}t}\varphi_{(\boldsymbol{q},\boldsymbol{p})}^{B} = \mathrm{e}^{\frac{\mathrm{i}}{\hbar}\chi(t)}\,\varphi_{(\boldsymbol{q}(t),\boldsymbol{p}(t))}^{B(t)} \ , \tag{36}
$$

where $(\boldsymbol{q}(t),\boldsymbol{p}(t))$ is the classical trajectory generated by (35),

$$
\chi(t) = \int_{0}^{t} \left(\dot{\boldsymbol{q}}\cdot\boldsymbol{p} - H_{\mathrm{osc}}\right)\mathrm{d}t' + \tfrac{\pi}{2}\,\sigma(t) \ , \tag{37}
$$

and

$$
B(t) = \left(\frac{\partial\boldsymbol{p}(t)}{\partial\boldsymbol{p}}B + \frac{\partial\boldsymbol{p}(t)}{\partial\boldsymbol{q}}\right)\left(\frac{\partial\boldsymbol{q}(t)}{\partial\boldsymbol{p}}B + \frac{\partial\boldsymbol{q}(t)}{\partial\boldsymbol{q}}\right)^{-1} \ ; \tag{38}
$$

here $\sigma(t)$ is a suitable Maslov-phase. Spin-coherent states are associated with unitary irreducible representations π_s of the group $\mathrm{SU}(2)$ (see, e.g., (Klauder and Skagerstam, 1982; Perelomov, 1986)). They are labeled by points

$$
\boldsymbol{n} = (\sin\theta\cos\varphi, \sin\theta\sin\varphi, \cos\theta) \tag{39}
$$

on the sphere S^2. Denoting by $|s,s\rangle \in \mathbb{C}^{2s+1}$ a "spin-up" (highest weight) vector and introducing

$$
g_{\boldsymbol{n}} := \begin{pmatrix} \cos\frac{\theta}{2} & -\sin\frac{\theta}{2}\,\mathrm{e}^{-\mathrm{i}\varphi} \\ \sin\frac{\theta}{2}\,\mathrm{e}^{\mathrm{i}\varphi} & \cos\frac{\theta}{2} \end{pmatrix} \ , \tag{40}
$$

a coherent state of spin s is

$$
\phi_{\boldsymbol{n}} = \pi_s(g_{\boldsymbol{n}})\,|s,s\rangle \ . \tag{41}
$$

Spin-Hamiltonians that are linear in the spin operators, $\hat{H}_{\mathrm{spin}} = \boldsymbol{C}(t)\cdot\hat{\boldsymbol{S}}$, propagate spin-coherent states exactly,

$$
\phi_{\boldsymbol{n}} \mapsto \mathrm{e}^{\mathrm{i}s\rho(t)}\,\phi_{\boldsymbol{n}(t)} \ . \tag{42}
$$

Here $\boldsymbol{n}(t)$ is a solution of the classical precession equation

$$
\dot{\boldsymbol{n}}(t) = \boldsymbol{C}(t)\times\boldsymbol{n}(t) \tag{43}
$$

associated with $\hat{H}_{\mathrm{spin}}$, and

$$
\rho(t) = \int_{0}^{t}\left[(\cos\theta - 1)\dot{\varphi} - \boldsymbol{C}\cdot\boldsymbol{n}\right]\mathrm{d}t' \ . \tag{44}
$$

is the corresponding classical action integral.

3.2. SEMICLASSICAL PROPAGATION

Obviously, the above discussion implies that quantum Hamiltonians of the type $\hat{H}_{\text{osc}} + \hat{H}_{\text{spin}}$ propagate initial product coherent states $\varphi^{B}_{(\boldsymbol{q},\boldsymbol{p})} \otimes \phi_{\boldsymbol{n}}$ exactly; however, they do not describe any non-trivial spin-orbit coupling. The time evolution of an initial product coherent states that is generated by some Hamiltonian arising as a Weyl quantisation of (32), which describes genuine spin-orbit coupling, can therefore only be studied in a semiclassical approximation. This procedure is not unique since there are two semiclassical parameters available: $\hbar$ corresponding to the translational part, and $1/s$ associated with the spin. In the following two scenarios will be discussed.

 (i) $\hbar \to 0$ and s fixed,

 (ii) $\hbar \to 0$, $s \to \infty$ such that $\hbar s = S$ fixed.

The first case has already been considered section 2.0; the second case leads to a strong classical spin-orbit coupling, which is reflected in a Hamiltonian nature of the classical combined dynamics. In both situations the procedure is to find a suitable approximate Hamiltonian $\hat{H}_Q(t)$ that propagates coherent states exactly along appropriate classical spin-orbit trajectories $(\boldsymbol{x}(t), \boldsymbol{p}(t), \boldsymbol{n}(t))$. (For problems with only translational degrees of freedom this has been suggested in (Heller, 1975) and proven in (Combescure and Robert, 1997).) Then one treats the full Hamiltonian as a perturbation of the approximate one and calculates the full time evolution in quantum mechanical perturbation theory (via the Dyson series), i.e., one iterates the Duhamel formula

$$\hat{U}(t) = \hat{U}_Q(t) - \tfrac{\text{i}}{\hbar} \int_0^t \hat{U}(t - t') \left(\hat{H} - \hat{H}_Q(t')\right) \hat{U}_Q(t')\, \mathrm{d}t' \qquad (45)$$

for the unitary time-evolution operators up to any given order. The leading expression (45) then allows to estimate

$$\left\| (\hat{U}(t) - \hat{U}_Q(t)) \varphi^{B}_{(\boldsymbol{q},\boldsymbol{p})} \otimes \phi_{\boldsymbol{n}} \right\| \qquad (46)$$

in terms of the semiclassical parameters. This procedure depends on the semiclassical scenario chosen, since estimating the difference (46) requires to consider (Bolte and Glaser, 2005)

$$\hat{\boldsymbol{S}}\phi_{\boldsymbol{n}} = \hbar s\, \boldsymbol{n}\, \phi_{\boldsymbol{n}} + \cdots , \qquad (47)$$

where the dots indicate semiclassically subleading terms. The order in which this expression contributes to (46) therefore depends on the choice $\hbar s = O(\hbar)$, as in case (i), or $\hbar s = S = O(1)$, as in case (ii).

The classical spin-orbit dynamics that emerge from the two semiclassical limits are the following (Bolte and Glaser, 2005): In case (i) one obtains the

combined motion (27) consisting of the Hamiltonian translational dynamics generated by the Hamiltonian $H_0(\boldsymbol{q}, \boldsymbol{p})$ from (32), which drives a spin precession according to (26). Due to the relation (47) scenario (ii) implies a stronger classical spin-orbit coupling that includes a back reaction of the spin on the translational motion. The combined dynamics are Hamiltonian, generated by

$$H_{\mathrm{so}}(\boldsymbol{q}, \boldsymbol{p}, \boldsymbol{n}) = H_0(\boldsymbol{q}, \boldsymbol{p}) + S\,\boldsymbol{n} \cdot \boldsymbol{C}(\boldsymbol{q}, \boldsymbol{p}) \,, \tag{48}$$

so that

$$\begin{aligned}
\dot{\boldsymbol{q}}(t) &= \frac{\partial H_{\mathrm{so}}}{\partial \boldsymbol{p}}(\boldsymbol{q}(t), \boldsymbol{p}(t), \boldsymbol{n}(t)) \,, \\
\dot{\boldsymbol{p}}(t) &= -\frac{\partial H_{\mathrm{so}}}{\partial \boldsymbol{q}}(\boldsymbol{q}(t), \boldsymbol{p}(t), \boldsymbol{n}(t)) \,, \\
\dot{\boldsymbol{n}}(t) &= \boldsymbol{C}(\boldsymbol{q}(t), \boldsymbol{p}(t)) \times \boldsymbol{n}(t) \,.
\end{aligned} \tag{49}$$

In order to define the approximate Hamiltonians $\hat{H}_Q(t)$ one considers suitably truncated Taylor expansions of the symbol (32) about appropriate classical trajectories $(\boldsymbol{x}(t), \boldsymbol{p}(t), \boldsymbol{n}(t))$. Introducing $\boldsymbol{z}(t) = (\boldsymbol{x}(t), \boldsymbol{p}(t))$ and $\boldsymbol{w} = (\boldsymbol{x}, \boldsymbol{\xi})$, in case (i) this reads

$$H_Q^{(i)}(t, \boldsymbol{w}) = \sum_{|\nu| \leq 2} \frac{1}{\nu!} \frac{\partial^{|\nu|} H_0}{\partial \boldsymbol{z}^\nu}(\boldsymbol{z}(t))\,(\boldsymbol{w} - \boldsymbol{z}(t))^\nu + \boldsymbol{C}(\boldsymbol{z}(t)) \cdot \hat{\boldsymbol{S}} \,. \tag{50}$$

Notice that due to (47) the last term is effectively of order $\hbar$. In case (ii) one chooses

$$\begin{aligned}
H_Q^{(ii)}(t, \boldsymbol{w}) ={}& \sum_{|\nu| \leq 2} \frac{1}{\nu!} \frac{\partial^{|\nu|} H_0}{\partial \boldsymbol{z}^\nu}(\boldsymbol{z}(t))\,(\boldsymbol{w} - \boldsymbol{z}(t))^\nu + \boldsymbol{C}(\boldsymbol{z}(t)) \cdot \hat{\boldsymbol{S}} \\
&+ S \sum_{|\nu| = 1, 2} \frac{1}{\nu!} \boldsymbol{n}(t) \cdot \frac{\partial^{|\nu|} \boldsymbol{C}}{\partial \boldsymbol{z}^\nu}(\boldsymbol{z}(t))\,(\boldsymbol{w} - \boldsymbol{z}(t))^\nu \,.
\end{aligned} \tag{51}$$

As opposed to (50), here the term with the spin operator is of effective order one. The Weyl quantisations of (50) and (51) propagate initial coherent states $\varphi_{(\boldsymbol{q}, \boldsymbol{p})}^B \otimes \phi_{\boldsymbol{n}}$ to

$$\mathrm{e}^{\frac{\mathrm{i}}{\hbar} R(t) + \mathrm{i}\frac{\pi}{2}\sigma(t)}\, \varphi_{(\boldsymbol{q}(t), \boldsymbol{p}(t))}^{B(t)} \otimes \phi_{\boldsymbol{n}(t)} \,. \tag{52}$$

The time evolution $B(t)$ of the matrix B is defined as in (38), along the appropriate trajectory $(\boldsymbol{q}(t), \boldsymbol{p}(t))$, and

$$R(t) = \int_0^t \left(\boldsymbol{p} \cdot \dot{\boldsymbol{q}} - H_0 + \hbar s\big((\cos\vartheta - 1)\dot{\varphi} - \boldsymbol{C} \cdot \boldsymbol{n}\big)\right) \mathrm{d}t' \,. \tag{53}$$

In the case (i) this is the action integral of the translational motion plus $\hbar$ times the action of the (driven) spin precession. In contrast, due to the condition

$\hbar s = S$, in the case (ii) this quantity is independent of $\hbar$ and represents the action integral of the classical combined spin-orbit dynamics. In either situation an estimate of the difference (46), based on the relation (45), yields for finite times t,

$$\|(\hat{U}(t) - \hat{U}_Q(t))\varphi^B_{(\boldsymbol{q},\boldsymbol{p})} \otimes \phi_{\boldsymbol{n}}\| \leq C(t)\sqrt{\hbar}\,, \qquad (54)$$

where the t-dependence of $C(t) < \infty$ is determined by the stability of the classical trajectory through $(\boldsymbol{q}, \boldsymbol{p}, \boldsymbol{n})$. Thus, the full time evolution of an initial spin-orbit coherent state follows an appropriate classsical trajectory up to an error of size $\sqrt{\hbar}$. Moreover, if the classical trajectory is unstable with maximal Lyapunov exponent λ, the error on the r.h.s. of (54) vanishes as $\hbar \to 0$ and $t \to \infty$, as long as $t \ll T_E(\hbar)$. Here

$$T_E(\hbar) = \frac{1}{6\lambda}\,|\log \hbar| \qquad (55)$$

denotes the so-called Ehrenfest-time. In the case of a regular trajectory, on a KAM-torus, the same holds up to times $t \ll const.\,\hbar^{-1/8}$.

It is possible to improve the error term in (54) to any desired order $\hbar^{N/2}$ by replacing (45) with its N-th iterate. That way the state that is propagated along classical trajectories is no longer given by the coherent state (52), but by a suitably squeezed version of it. These states possess the same localisation properties as (52), however, their explicit form looks considerably more awkward.

References

Thomas L. H. London Edinburgh Dublin Philos. Mag. J. Sci. **3** (1927) 1.

Rubinow S. I. and Keller J. B. Phys. Rev. **131** (1963) 2789.

Bolte J. and Glaser R. *Commun. Math. Phys.* **247** (2004) 391.

Bolte J. and Glaser R. J. Phys. A: Math. Gen. **37** (2004) 6359.

Bolte J. and Glaser R. Semiclassical propagation of coherent states with spin-orbit interaction, to appear in *Ann. H. Poincaré*.

Dimassi M. and Sjostrand J. Spectral Asymptotics in the Semi-Classical Limit. London Mathematical Society Lecture Notes Series, **268**. Cambridge University Press (Cambridge) (1999).

Emmrich C. and Weinstein A. Commun. Math. Phys. **176** (1996) 701.

Bolte J. and Keppeler S. Ann. Phys. (NY) **274** (1999) 125.

Cordes H. O. Commun. Part. Diff. Eqs. **8** (1983) 1475.

Bruneau V. and Robert D. Ark. Mat. **37** (1999) 1.

Teufel S. Adiabatic Perturbation Theory, Lecture Notes in Mathematics Springer, Berlin, Heidelberg, Vol. 1821, (2003)

Cornfeld I. P., Fomin S. V. and Sinai Ya. G. Ergodic Theory. Springer (Berlin, Heidelberg) (1982).

Klauder J. R. and Skagerstam B. S. (eds.) Coherent States. Applications in Physics and Mathematical Physics. World Scientific (Singapore) (1985).

Perelomov A.   Generalized Coherent States and Their Applications. Springer (Berlin, Heidelberg) (1986).

Zaitsev O., Frustaglia D. and Richter K. Phys. Rev. Lett. **94** (2005) 026809;

Heller E. J. J. Chem. Phys. **62** (1975) 1544.

Combescure M. and Robert D. Asymptot. Anal. **14** (1997) 377.

Lass of inhomogeneously driven dyamical systems: General theory, regular and chaotic properties, applications

Vladimir Damgov

Space Research Institute at the Bulgarian Academy of Sciences
6 Moskovska St., 1000 Sofia, Bulgaria

Abstract.
A generalized model of an oscillator, subjected to the influence of external waves is considered. It is shown that the systems of diverse physical background which this model encompasses by their nature should belong to the broader class of "kick-excited self-adaptive dynamical systems".

A class of kick-excited self-adaptive dynamical systems is formed and proposed. The class is characterized by a nonlinear (inhomogeneous) external periodic excitation (as regards the coordinates of the excited system) and is remarkable for the occurrence of the following objective regularities: the phenomenon of discrete oscillation excitation in macro-dynamical systems having multiple branch attractors and strong self-adaptive stability.

A generalized oscillator-wave model is considered showing that the inhomogeneous external influence is realized naturally and does not require any specific conditions. The article considers also the presence of a small horseshoe in the dynamics of a particle under the action of two waves. Originally the problem comes from the plasma physics in despite of the existence of some other applications of the differential equation we study here.

Keywords: inhomogeneous, dynamical system, chaos

1. Introduction

The main goal of this report is to present a phenomenon of highly general nature manifested in various dynamical systems. We present the occurrence of peculiar "quantization" by the parameter of intensity of the excited oscillations and we show that given unchanging conditions it is possible to excite oscillations with a strictly defined discrete set of amplitudes; the rest of the amplitudes being "forbidden". The realization of oscillations with a specific amplitude from the "permitted" discrete set of amplitudes is determined by the initial conditions. The occurrence of this unusual property is predetermined by the new general initial conditions, i.e. the nonlinear action of the external excited force with respect to the coordinate of the system subjected to excitation.

A striking example of the so formed class of kick-excited self-adaptive dynamical phenomena and systems is the model of a pendulum influenced by quasi-periodic short-term actions, as considered in papers (Damgov, 2004) - (Damgov and Trenchev, 1999).

Quantization (the idea of quantums, photons, phonons, gravitons) is postulated in Quantum Mechanics, while the Theory of Relativity does not derive quantization from geometric considerations. In the case of the established phenomenon the "quantized nature" of portioned energy transfer stems directly from the mechanisms of the process and has a precise mathematical description. The quasi-harmonic oscillator obeys the classical laws to a greater extent than any other system. A number of problems, related to quasi-harmonic oscillators, have the same solution in classical and quantum mechanics.

Here we also consider the generalized "oscillator-wave" model and show that, in this case, the inhomogeneous external influence is realized naturally and does not require any specific conditions. Systems covered by the "oscillation-wave" model immanently belong to the generalized class of kick-excited self-adaptive dynamical systems. We show that under certain condition in the system will arise non-attenuated oscillations with a frequency close to the system's natural frequency and amplitude which belongs to a defined discrete spectrum of possible amplitudes. A second important quality also appears – self-adaptive stability of the excited oscillations with given amplitude for a broad range of the incoming wave's intensity.

Leaving the details, the equation describing the motion of one particle in two electrostatic waves allows perturbation methods to be applied in its study. There are three main types of behavior in the phase space - a limit cycle, formation of a non-trivial bounded attracting set and escape to infinity of the solutions. One of the goals is to determine the basins of attraction and to present a relevant bifurcation diagram for the transitions between different types of motion.

2. A numeric demonstration of the excitation of "quantized" pendulum oscillations

The inhomogeneously AC driven, damped pendulum system can be described by the following equation:

$$\frac{d^2x}{dt^2} + 2\delta\frac{dx}{dt} + \sin x = \varepsilon(x)F_o \sin \nu t, \qquad (1)$$

where the function $\varepsilon(x)$ can be analytically expressed in various ways, such as:

$$\varepsilon(x) = \begin{cases} 1 & for \quad |x| \le d' \\ 0 & for \quad |x| > d' \end{cases}. \qquad (2)$$

or $\varepsilon(x) = e^{\frac{x^2}{2d'^2}}$, $\varepsilon(x) = \begin{cases} \frac{1}{2}\left[1 + \cos\left(\frac{\pi}{d'}x\right)\right] & for \quad |x| \le d' \\ 0 \quad for \quad |x| > d' \end{cases}$ and so on; $d' << 1$ is a parameter limiting the external action on a small part of the trajectory of motion in the system (in the particular case (2) the parameter thereby determines a symmetric zone of action in the area of the lower equilibrium position).

We emphasize the link with the name of the already formed class of kick-excited self-adaptive systems and phenomena: the external force is linked, through the function $\varepsilon(x)$, with the motion coordinate in an adaptive mode, and at the same time it exerts action in the form of short impulses much shorter than the oscillation period of the system.

Results from the computer experiment are presented in (Damgov, 2004; Damgov and Trenchev, 2003): (i) the joint phase portrait of stationary steady motion of the pendulum of four different initial conditions; (ii) an illustration of a bifurcation of tripling the period of oscillations; (iii) the multi-basins of the stationary attractors, or the set of initial conditions that evolve toward each of the fixed points; (iv) the colour images of the basins of the different attractor when changing the control parameter (that is the amplitude of the external exciting force); (v) the multi-bifurcation diagram of the system; (vi) the single segment strange attractors; (vii) the multi- bifurcation diagram of the Duffing oscillator.

3. Model of the interaction of an oscillator with an electromagnetic wave

Analytical approaches applicable for small and large amplitudes (for weak and strong nonlinearity) of the oscillations in a nonlinear dynamic system subjected to the influence of a wave has been developed (Damgov, 2004; Damgov, Trenchev and Sheiretsky, 2003).

The performed analysis shows that the continuous wave having a frequency much larger than the frequency of a given oscillator can excite in it oscillations with a frequency close to its natural frequency and an amplitude belonging to a discrete set of possible stable amplitudes.

The settling of certain particular amplitude depends on the initial conditions. When the motion becomes stationary the amplitude's value practically does not depend on the wave's intensity when the latter changes over a significant range above a certain threshold value. This is reminiscent of Einstein's explanation of the photoelectric effect using Planck's quantization hypothesis. In this case the absorption is also independent of the incoming wave's intensity. Besides, the absorbed

frequencies can be expressed as integer multiples of a certain basic frequency reminding of resonance phenomena.

4. "Quantized" cyclotron motion

When an electromagnetic wave interacts with resonators, the effect of "quantization" of all possible stationary stable oscillating amplitudes arises without the requirement of any specifically organized conditions (like the inhomogeneous action of external harmonic force).

An electric charge, moving on a circular orbit in a homogeneous permanent magnetic field has been considered. When the charge was irradiated by a flat electromagnetic wave having a length commensurable with the orbit's radius, an effect of discretization ("quantization") of the possible stable orbital radii (or motion velocities) was observed (Damgov, 2004; Damgov, Trenchev and Sheiretsky, 2003).

5. General conditions for transition to irregular behaviour in an oscillator under wave action

General conditions for transition to irregular and chaotic behaviour in an oscillator under wave action have been derived using the notion about the Melnikov distance:

$$D(t_o, t_o) = - \int\limits_{-\infty}^{\infty} f_o \wedge f_1 dt = \int\limits_{-\infty}^{\infty} \frac{2F_o}{ch(t-t_o)} \sin[\theta - 2\rho \arcsin(th(t - t_o))]$$

$$+ \frac{4\delta_d}{ch^2(t-t_o)} dt$$

Irregular (chaotic) behaviour occurs for the areas where $D(t_o, t_o)$ passes through zero.

Under the condition $D(t_o, t_o) = 0$ and taking into account that $|\sin(\nu t_o + \theta_o| < 1$ and that $\delta_d > 0$, the general condition for transmission to irregular (chaotic) behaviour in nonlinear oscillator under the wave action takes the form $2\delta_d sh(|\nu| \pi) < \pi \nu^2 |F_o| e^{\nu \frac{\pi}{2}}$.

Obviously this condition is fulfilled in some domains of the space (δ_d, F_o, ν).

6. Presence of a small horseshoe in the dynamics of a particle under the action of two waves

The equation which describes the motion of one particle in two electrostatic waves is given by

$$\ddot{x} = -M \sin x - P \sin(x - t), \qquad (3)$$

where x is the position of the particle measured in the frame of one of the waves, P and M are dimensionless amplitudes of the waves. We shall extend our model introducing a damping term in (4), and we shall also assume that $P << M$. Under these assumptions the equation that governs the motion of the particle can be written as

$$\ddot{x} + \varepsilon \delta \dot{x} + \sin x = \varepsilon f \sin(\nu t - x), \qquad (4)$$

where x is again the position of the particle measured in the frame of one of the waves, whereas δ, f and ν are real non-negative constants. The form of the equation allows perturbation methods to be applied in its study. Our preliminary numerical investigation of (5) revealed very rich dynamics depending on the change of parameters and initial conditions. There are three main types of behaviour in the phase space of (5) that can be observed:
- Approaching a limit cycle;
- Formation of a non-trivial bounded attracting set;
- Escape to infinity of the solutions of (4).

One question which is of natural interest is to determine the basins of attraction, and to present a relevant bifurcation diagram for the transitions between different types of motion. Although there has been reached a significant progress in the understanding of the behaviour of driven non-linear oscillators, there exist some obstacles that prevent clarifying the dynamics of particular examples. In our work we present a rigorous result for existence of horseshoe-like dynamics for (4) and hence for exhibiting the phenomena deterministic chaos. Our result is as follows:

Theorem 1. *The sufficient conditions for transition to chaotic motion in the dynamics of equality (4) is fulfilment of*

$$4\delta < f\pi\nu^2 \left(\frac{1}{\cosh(\pi\nu/2)} - \frac{1}{\sinh(\pi\nu/2)} \right) \qquad (5)$$

or

$$4\delta > f\pi\nu^2 \left(\frac{1}{\cosh(\pi\nu/2)} + \frac{1}{\sinh(\pi\nu/2)} \right) \qquad (6)$$

In next section we shall give a short account of the Melnikov method in a form convenient for our problem. Then we shall prove Theorem 1.

6.1. Short summary of the Melnikov method

We shall explain the Melnikov technique following [11].

6.1.1. *A. General assumptions and geometric structure of the non-perturbed system*

Consider the system of differential equations

$$\dot{x} = J D_x H(x) + \varepsilon g(x, t, \varepsilon), \tag{7}$$

where $(x, t) \in R^2 \times T^1$ and J is the symplectic matrix defined by $J = \begin{bmatrix} 0 & 1 \\ -1 & 0 \end{bmatrix}$.

We get the following structural assumptions:

1. The functions
$$JD_x H : R^2 \longrightarrow R^2$$
$$g : R^2 \times R \times R \longrightarrow R^2 \, ,$$
are defined and at least C^2 differentiable on their respective domains of definition, and that g is periodic in t with period $T = 2\pi/\omega$.

2. The system (7) with $\varepsilon = 0$ is referred as *unperturbed system*. About it we shall assume that it possesses a hyperbolic fixed point $x_{o,h}$ connected to itself by a homoclinic orbit $x_h(t) \equiv (x_h^1(t), x_h^2(t))$.

3. Denote by $W^s(x_{o,h})$ the set of points $x \in R^2$ that approach $x_{o,h}$ as $t \longrightarrow \infty$, and by $W^u(x_{o,h})$ the set of points $x \in R^2$ that approach $x_{o,h}$ as $t \longrightarrow -\infty$, under the action of the unperturbed flow

$$\dot{x} = J D_x H(x) \tag{8}$$

$W^s(x_{o,h})$ is referred as *asymptotically stable manifold* for $x_{o,h}$, and $W^u(x_{o,h})$ is referred as *asymptotically unstable manifold* for $x_{o,h}$. Denote by $\Gamma_{x_{o,h}} \equiv \{x \in R^2 \,|\, x = x_h(t), t \in R\} \cup \{x_{o,h}\} = W^s(x_{o,h}) \cap W^u(x_{o,h}) \cup \{x_{o,h}\}$. We shall assume that interior of $\Gamma_{x_{o,h}}$ is filled with continuous family of periodic orbits $x^a(T)$ of (8) with period T^a, $\alpha \in [-1, 0]$ and $\lim_{a \longrightarrow 0} x^a(t) = x_h(t)$ and $\lim_{a \longrightarrow 0} T^a = \infty$.

When viewed in three-dimensional space $R^2 \times S$, the hyperbolic fixed point $x_{o,h}$ turns to hyperbolic periodic orbit of the system

$$\begin{aligned} \dot{x} &= J D_x H(x) \\ \dot{\theta} &= \omega \end{aligned} \tag{9}$$

and so do $W^s(x_{o,h})$ and $W^u(x_{o,h})$ which turn to two-dimensional asymptotic manifolds $W^s(\gamma(t))$ and $W^u(\gamma(t))$, which coincide along the two-dimensional homoclinic manifold $\Gamma_{\gamma(t)} \equiv \{(x, \theta) \in R^2 \times S \,|\, x = x_h(t), t \in R\} \cup \{x_{o,h} \times S\}$.

6.1.2. *B. Geometric structure of the perturbed phase space.*
Here we shall argue that most of the upper structure goes over for the
perturbed system

$$\begin{aligned}
\dot{x} &= JD_xH(x) + \varepsilon g(x, \theta, \varepsilon) \\
\dot{\theta} &= \omega
\end{aligned} \tag{10}$$

Proposition 1. *For ε sufficiently small the periodic orbit $\gamma(t)$ of (7)
survives as a periodic orbit $\gamma_\varepsilon(t) = \gamma(t) + O(\varepsilon)$, of (10) having the same
stability type as $\gamma(t)$, and depending on ε in a C^2 manner. Moreover,
the local stable and unstable manifolds $W^s_{loc}(\gamma_\varepsilon(t))$ and $W^u_{loc}(\gamma_\varepsilon(t))$ of
$\gamma_\varepsilon(t)$ remain also ε-close to the local stable and unstable manifolds
$W^s_{loc}(\gamma(t))$ and $W^u_{loc}(\gamma(t))$ of $\gamma(t)$, respectively.*
Remark 1. *The concept for local stable and unstable manifolds
becomes clear when one represents the stable and unstable manifolds
of the hyperbolic fixed point (periodic orbit) locally. For details see
(Wiggins, 1989) or (Wiggins, 1988).*

$$W^s(\dot{\gamma_\varepsilon}(t)) \;=\; \bigcup_{t \leq 0}(x, \theta)^t \, (W^s_{loc}(\gamma_\varepsilon(t)))$$

$$W^u(\dot{\gamma_\varepsilon}(t)) \;=\; \bigcup_{t \succeq 0}(x, \theta)^t \, (W^u_{loc}(\gamma_\varepsilon(t)))$$

where we denote by $(x, \theta)^t$ the phase flow of (10).
Consider the following cross-section of the plane $R^2 \times S$

$$\Theta^{\theta_o} = \left\{ (x, \dot{\theta}) \in R^2 \,|\, \theta = \theta_o \right\}$$

Θ^{θ_o} is parallel to the x-plane (and coincides with the x-plane for $\theta_o = 0$).
Note that $\gamma(t) \cap \Theta^{\theta_o} = x_{o,k}$ and $\Gamma_\gamma \cap \Theta^{\theta_o} = \{(x, \theta) \in R^2 \,|\, x = x_{o,k}, \ t \in R\} = \Gamma_{x_{o,h}}$. Consider a trajectory

$$(x_\varepsilon(t), \theta(t)) \tag{11}$$

of the perturbed vector field (10). Then its projection onto Θ^{θ_o} is given
by $(x_\varepsilon(t), \theta_o) = W^s(\gamma_\varepsilon(t)) \cap W^u(\gamma_\varepsilon(t))$. Since $x_\varepsilon(t)$ actually depends
on θ_o(as opposed to $x(t)$, for some solutions $(x(t), \theta(t)$ of (10)), the
perturbed vector field (10) is non-autonomous, which may result in
a very complicated picture of (35) in Θ^{θ_o}, possibly intersecting itself.
The points from the Poincaré map P_ε defined as the successive points of
intersection of the solution $(x_\varepsilon(t), \theta(t))$ with Θ^{θ_o}, will be mapped also
onto this curve. It turns out that these points can form very complicated

(non-trivial) sets due to transversal intersection of the asymptotic manifolds $W^s(\gamma_\varepsilon(t))$ and $W^u(\gamma(t))$. One computable criterion that assures such dynamics is given by:

Proposition 2. *Suppose that we have a point* $(t_o, \theta_o) = (\bar{t}_o, \bar{\theta}_o)$ *such that*

1. $M(\bar{t}_o, \bar{\theta}_o) = 0$,
2. $\left.\frac{\partial M}{\partial t_o}\right|_{(\bar{t}_o, \bar{\theta}_o)} \neq 0$,

where $M(t_o, \theta_o)$ *is the Melnikov vector*

$$M(t_o, \theta_o) = \int\limits_{-\infty}^{\infty} DH(x_h(t).g(x_h(t), \omega t + \theta_o, 0)dt$$

Then $W^s(\gamma_\varepsilon(t))$ *and* $W^u(\gamma_\varepsilon(t))$ *intersect transversely at* $\left(x_h(-\bar{t}_o) + O(\varepsilon), \bar{\theta}_o\right)$ *and consequently (from the S male-Birkhoff homoclinic theorem) for the map* P_ε *there exists an integer* $n > 1$ *that* P_ε^n *has an invariant Cantor set on which it is topologically conjugate to a full shift of* N *symbols.*

6.1.3. C. Proof of Theorem 1

Consider equation (4) written in the form

$$\begin{aligned}
\dot{x}^1 &= x^2 \\
\dot{x}^2 &= \sin x^1 + \varepsilon\left[-\delta x^2 + f\sin(\theta - x^1)\right] \\
\dot{\theta} &= \nu
\end{aligned} \qquad (12)$$

Then the following lemma holds:

Lemma 1. *For* $\varepsilon = 0$ *system (12) contains hyperbolic periodic orbit* $M = \left(\bar{x}^1, \bar{x}^2, \theta(t)\right) = (\pm\pi, 0, vt + \theta_o) \in R^2 \times T^1$

This orbit is connected to itself by a pair of 2-dimensional homoclinic manifolds given by

$$\left(x_\pm^1(t), x_\pm^2(t), \theta(t)\right) = \left(\pm 2\arcsin(\tanh(t - t_o), \pm\frac{2}{\cosh(t - t_o)}, vt + \theta_o\right) \qquad (13)$$

Proof. We easily see that $(\pm\pi, 0)$ is a hyperbolic fixed point of
$$\dot{x}^1 = x^2, \dot{x}^2 = \sin x^1$$
linearizing (12) (for $\varepsilon = 0$) about it. A trivial check gives that (for $\varepsilon = 0$) (13) in solution of (12). Furthermore, using asymptotic of (13) we obtain that it connects $(\pm\pi, 0, vt + \theta_o)$ to itself. This proves the lemma.

Using Proposition 2 and hyperbolicity of (13), we conclude that for $\varepsilon \neq 0$, (13) turns to hyperbolic periodic, orbit which we shall shortly

denote by $\gamma_{\varepsilon,\pm} \equiv (\pm\pi + O(\varepsilon), 0 + O(\varepsilon), vt + \theta_o)$. From Proposition 2 it follows that its asymptotic manifolds $W^s(\gamma_{\varepsilon,\pm}(t))$ and $W^u(\gamma_{\varepsilon,\pm}(t))$ will intersect transversely if the corresponding Melnikov vector

$$M_{\pm}(t_o, \theta_o, \delta, f, v) =$$
$$= \int_{-\infty}^{\infty} \left[-\delta\left(x_{h,\pm}^2(t - t_o)\right)^2 + f \sin\left(vt + \theta_o - x_{h,\pm}^1(t - t_o)\right) x_{h,\pm}^2(t - t_o) \right] dt =$$
$$= \int_{-\infty}^{\infty} \left[-\delta\left(\frac{\pm 2}{\cosh(t-t_o)}\right)^2 + f\left(\frac{\pm 2}{\cosh(t-t_o)}\right) \sin(vt + \theta_o \pm 2\arcsin(\tanh(t - t_o))) \right] dt$$

has a simple zero. Furthermore we fix $\theta = \theta_o$, which defines the cross-section

$$\Theta^{\theta_o} = \{(x_1, x_2, \theta) \,|\, \theta = \theta_o \in [0, 2\pi)\}$$

and consider the Poincaré map $P_{\varepsilon}^{\theta_o} : \Theta^{\theta_o} \to \Theta^{\theta_o}$ generated by the flow (12). In order to make the conclusions we pursue about the dynamics of $P_{\varepsilon}^{\theta_o}$ we need to compute $M_{\pm}(t_o, \theta_o, \delta, f, v)$. After some algebra we obtain for $M_{\pm}$

$$M_{\pm}(t_o, \theta_o, \delta, f, v) = -8\delta \pm 2f \sin(vt_o + \theta_o) [I_1 \mp 2I_2]$$

where

$$I_1 = \int_{-\infty}^{\infty} \frac{1 - \sinh^2\tau}{\cosh^3\tau} \cos(vt)d\tau = v \int_{-\infty}^{\infty} \frac{\sinh\tau}{\cosh^2\tau} \sin(vt)d\tau$$

$$I_2 = \int_{-\infty}^{\infty} \frac{\sinh\tau}{\cosh^3\tau} \sin(vt)d\tau = \frac{v}{2} \int_{-\infty}^{\infty} \frac{\sinh\tau}{\cosh^2\tau} \cos(vt)d\tau$$

The integrals I_1 and I_2 are evaluated by the methods of residues. The standard calculation gives

$$I_1 = \frac{\pi v^2}{\cosh(\pi v/2)}; \text{ and } I_2 = \frac{\pi v^2}{2\sinh(\pi v/2)}.$$

Hence, for the Melnikov vector $M\pm$ we obtain

$$M_{\pm}(t_o, \theta_o, \delta, f, v) = -8\delta \pm 2f\pi v^2 \left[\frac{1}{\cosh(\pi v/2)} \mp \frac{1}{\sinh(\pi v/2)} \right] \sin(vt_o + \theta_o)$$
$$(14)$$

Then fulfillment of (5) assures existence of simple zero for

$$M_{\pm}(t_o, \theta_o, \delta, f, v) = 0$$

and hence transversal intersection of the asymptotically stable manifold $W^s(\gamma_{\varepsilon,+})$ and asymptotically unstable manifold $W^u(\gamma_{\varepsilon,+})$, whereas the fulfillment of (6) assures existence of simple zero for

$$M_-(t_o, \theta_o, \delta, f, v) = 0$$

and hence transversal intersection of $W^u(\gamma_{\varepsilon,-})$ and $W^u(\gamma_{\varepsilon,-})$. Now from Proposition 2 it follows for $\varepsilon > 0$ sufficiently small there exists an integer $n > 1$ such that the map $P_\varepsilon^{\theta_o}$ has an invariant Cantor set, subset of the Poincaré section Θ^{θ_o}, on which the power $(P_\varepsilon^{\theta_o})$ is conjugate to a full shift of N symbols.

The last implies that high sensitiveness of solution to the choice of initial conditions, or equivalently deterministic chaos.

7. General characteristic features of the class of kick-excited self-adaptive dynamical systems. conclusions

The main characteristics and regularities, characterizing the considered class of kick-excited self-adaptive dynamical systems are as follows:

1. The excitation of oscillations with a quasi-natural system frequency and numerous discrete stationary amplitudes, depending only on the initial conditions (i.e. discretization of the processes of absorption by the system of energy, coming from the high-frequency source). A new in principle property is the possibility for excitation of oscillations with the system's natural frequency under the influence of an external high-frequency force on unperturbed linear and conservative linear and non-linear oscillating systems.

2. Adaptive self-control of the energy contribution in the oscillating process, exhibited in the sustaining of a value for the system's oscillation amplitude and frequency which is stable over significant variance of the amplitude of external influence, the quality factor of the oscillator (the load) and other external variables.

The phenomenon of continuous oscillation excitation with an amplitude belonging to a discrete set of stationary amplitudes has been demonstrated on the basis of a common model – an oscillator under wave influence. It is shown that the conditions necessary for the manifestation of this phenomenon are realized in a natural way in an oscillator system interacting with a continuous fall wave.

Here-with is shown the potential for excitation of relatively low frequency continuous oscillations having a discrete amplitude set under the influence of a wave with incompatibly higher frequency. In the

presence of particle flows and fields of different nature, the "oscillator-wave" model realizes (materializes) widely in Nature in a very natural way. Everywhere where waves interact with oscillators, conditions arise for the excitation of oscillations with a discrete sequence of possible stable amplitudes (for example, space ensembles of charged particles under the action of fall waves from the ultraviolet band, the near and the far IR range and the radio-band). In one way or another, the model has been considered by a number of authors, but the most essential feature of behaviour – the "quantization" phenomenon, has escaped their attention.

On the basis of the presented oscillator-wave model it is also possible to create heuristic models of the interaction of electromagnetic waves with plasma particles in the Earth's ionosphere and magnetosphere, heuristic models of the generation of powerful low-frequency waves in the space around the Earth when a cosmic electromagnetic background is present etc. High-efficient sub-millimeter emitter, built on this basis, could be suitable for radio-physical heating of plasma, e.g. in the experiments aimed the achievement of controlable thermonuclear reaction [1].

The main consequence of Theorem 1 is the strong dependence of the solution of (4) on the choice of initial conditions. The phenomenon deterministic chaos arises often in the dynamics of the driven non-linear oscillators. In this regard our result is not surprising. Anyway, we think that it is useful to present such a condition for the parameters of the system which guarantees appearance of a Smale horseshoe like dynamics, since usually the homoclinic bifurcation (due to a simple zero of the Melnikov vector) is one of the first bifurcations that occur in the transition from regular to irregular motion for a given system. We want to emphasis that the homoclinic tangency (predicted with a good accuracy by the Melnikov analysis), as a rule, implies formation of a fractal boundary for the

The method developed of entering energy in oscillation processes and the excitation of "quantized" oscillations in dynamic macro-systems finds and will find in the future applications in the solving of important practical problems in the creation of new methods and mechanisms for the excitation and the sustaining of continuous oscillations and different energy transformations which could be grouped in the following way:

1. Transformation of signals and oscillations of different nature by frequency with a high efficiency at single division of the frequency by ratio of tens, hundreds and thousands.

2. Energy transformation of one kind into another, for example of electric into mechanical and vice-versa as with electric and electro-mechanic transformers, generators of electric signals, transformers of

wave energy, non-traditional methods for the transformation of heat into electric energy etc.

3. Stabilization of different parameters with their change in a wide range (e.g. 50-100-300%), including the voltage stabilizers for microprocessor systems with a wide range of allowed change of the load etc.

4. The development of new base elements for specialized calculating devices possessing a large number of stable discrete states.

5. Intensification of different processes through a special organization of interaction of different oscillation or wave processes such as cavitational destruction, cleaning, emulgation of non-mixing liquids and of substances in the liquid phase, the development of different wave technologies.

6. The modelling of micro- and macro- processes with the methods of classic oscillation theory.

References

Damgov, V. N. Nonlinear and Parametric Phenomena: Theory and Applications in Radiophysical and Mechanical Systems . Monograph. Series A: Monographs (Series of Nonlinear Sciences), Series Editor: prof.Leon O. Chua, University of California, Berkeley, World Scientific: New Jersey, London, Singapore 2004, 570 p., Chapter 10

Damgov, V. and Trenchev Pl. Class of Kick-Excited Self-Adaptive Dynamical Systems: "Quantized" Oscillation Excitation. - "Chaos, Solitons and Fractals". Oxford, Vol. 17, No 1, P. 11, (2003)

Damgov, V. N. "Quantized" Oscillations and Irregular Behaviour of a Class of Kick-Excited Self-Adaptive Dynamical Systems. Progress of Theoretical Physics Suppl, Kyoto, Japan, No. 139, P. 344 (2000)

Damgov, V. and Trenchev Pl. Phenomenon of "Quantized" Oscillation Excitation. Nonlinearity and Disorder: Theory and Applications, F.Abdulaev et al. (Eds), Kluwer Academic Publishers, Netherlends, P. 397 (2001)

Damgov, V. N. and Popov I. "Discrete" Oscillations and Multiple Attractors in Kick-Excited Systems. Discrete Dynamics in Nature and Society, Vol. 4, P. 99 (2000)

Damgov, V.N. "Quantized" Oscillations and Irregular Behaviour of Inhomogeneously Driven, Damped Pendulum. Dynamical Systems and Chaos. World Scientific, London, Vol. 2, P. 558 (1995)

Damgov, V.N. and P.G. Georgiev Amplitude Spectrum of the Possible Pendulum Motions in the Field of an External. Nonlinear to the Coordinate Periodic Force. Dynamical Systems and Chaos, World Scientific, London, Vol. 2, P. 304 (1995)

Damgov V. N and Popov I. Multiple Attractors in a Class of Dynamical Systems. Comptes Rendus de la Academy Bulgare des Science, 52 (No.5-6), 31-34 (1999)

Damgov V .N. and Georgiev G. General Conditions for Resonance Oscillations Excitation Under the Action of External Nonlinear Force. Comptes Rendus de la Academy Bulgare des Science, 52 (No.9-10), 22-25 (1999)

Damgov, V. N, Trenchev Pl. and Sheiretsky K. "Oscillator-Wave" Model: Properties and Heuristic Instances. Chaos, Solitons and Fractals, Oxford, Vol. 17 (2003), P. 41

WIGGINS, S. Introduction to Applied Nonlinear Dynamics and Chaos. Springer-Verlag, New York, Berlin, 1989

WIGGINS, S. Global Bifurcations and Chaos. Springer-Verlag, New York, Berlin, Heidelberg, 1988

Quantum chaos in floppy molecular systems: The LiCN molecule

F. Borondo[(a)] and R.M. Benito[(b)]

(a) Departamento de Química, C–IX
Universidad Autónoma de Madrid
CANTOBLANCO - 28049 Madrid, Spain
(b)Departamento de Física y Mecánica
Escuela Técnica Superior de Ingenieros Agrónomos
Universidad Politécnica de Madrid
28040 Madrid, Spain

Abstract. The development of modern spectroscopic techniques and efficient computational methods have allowed a detailed investigation of highly excited vibrational states of small polyatomic molecules. As excitation energy increases, molecular motion becomes chaotic and nonlinear techniques can be applied to their analysis. The corresponding spectra get also complicated, but some interesting low resolution features can be understood simply in terms of classical periodic motions. In this chapter we describe some techniques to systematically construct quantum wave functions localized on specific periodic orbits, and analyze their main characteristics.

Keywords: Quantum chaos, Scar theory, Semiclassical theories, Excited vibrational states, Vibrational spectroscopy

1. Introduction

The correspondence between classical and quantum mechanics has received much attention since the early days of quantum theory, and more recently in connection to quantum chaos (Reichl, 2004; Gutzwiller, 1990). This implies elucidating which are the classical objects that should be quantized, this being at the heart of every semiclassical theory. Among the different achievements in the field of quantum chaos, random matrix theory (Metha, 1991), with the celebrated Bohigas–Giannoni–Schmit conjecture on spectral statistics (Bohigas, Giannoni and Schmit, 1984), Gutzwiller's semiclassical trace formula able to quantize chaotic systems (Gutzwiller, 1990), and the theory of scars (Kaplan and Heller, 1999) deserve special mention.

The term "scar" was introduced by Heller in his seminal paper (Heller, 1984), to describe the localization of quantum probability density of certain individual eigenfunctions of classical chaotic systems along unstable periodic orbits (PO), and he constructed a theory of scars based on wave packet propagation (Heller, 1991). Another important contribution to this theory is due to Bogomolny (Bogomolny, 1988), who derived an explicit expression for the smoothed probability density over small ranges of space and energy

(i.e. semiclassical average over a large number of eigenfunctions). The corresponding theory for Wigner functions was developed by Berry (Berry, 1989). Resummation techniques have also been applied to provide some information about individual states (Agam and Fishman, 1994), and a systematic method, based on dynamical arguments, was developed (de Polavieja, Borondo and Benito, 1994) to quantify the contribution of the different eigenstates. The influence of homoclinic motion (Tomsovic and Heller, 1991; Wisniacki et al, 2005) and heteroclinic connections (Wisniacki et al, 2004) on scarring has also been considered in the literature.

From the experimental point of view, scars have been observed in microwave cavities (Sridhar, 1991) and mesoscopic devices (Wilkinson, 1996), where they have an enormous practical interest.

In this chapter we present some results obtained by our group on scar theory in the context of molecular vibrations, and in particular for the LiNC/LiCN molecular system. This kind of (generic) systems exhibits a dynamical behavior in which regular and chaotic motions are mixed (Gutzwiller, 1990), a situation which presents significant differences with respect to the completely chaotic case considered in most references cited above, and are very important in many areas of physics and chemistry.

The corresponding classical mechanics is well understood in terms of the Kolmogorov–Arnold–Moser (KAM) theorem (Reichl, 2004). At very low excitation, molecular dynamics take place in the vicinity of Born–Oppenheimer potential energy surface minima, where the motion corresponds to normal modes. The associated spectra are simple, consisting of band progressions easily assignable. As energy increases, anharmonicities and coupling terms grow in importance. Spectra become distorted due to the influence of resonances, and the different peaks can be hierarchically organized in terms of polyads (Kellman, 1995). This reflects the importance of the intramolecular energy transfer processes taking place inside the molecule. At very high excitation energies, the interactions become too large and the picture based on normal mode states is no longer valid. Classically, the motion becomes chaotic, as invariant tori are destroyed following the fate dictated by the KAM theorem. However, the complexity of the emerging chaotic sea is organized by periodic orbits (PO) and their associated manifolds. The corresponding spectra can become very complex, but usually show simple low resolution features related to the above mentioned classical structures (Taylor, 1989). The associated nonlinear dynamical effects control chemically interesting processes, such as intramolecular vibrational relaxation (Uzer and Miller, 1991) or chemical reactivity (Wiggins et al, 2001).

Some recent activity (Keating and Prado, 2001; Backer, Keating and Prado, 2001) related to scarring in generic systems should be mentioned. Special consideration deserves the work of Keating and Prado (Keating and Prado, 2001) who showed, by considering scaling laws in an extension of Bogo-

molny's theory, that scars of quantum eigenfunctions by classical PO may be dramatically enhanced when these orbits undergo bifurcations. These "superscars" manifest as stronger localization on wider regions of configuration space than in the case of the scars corresponding to isolated POs.

2. The system

The example that we have chosen to study is the dynamics of the molecular vibrations of LiNC/LiCN. This system is representative of a large class of triatomic molecules, which exhibit similar dynamical behavior, mainly derived from the large amplitude motion in one of the vibrational modes. This class includes other cyanides, such as HCN/HNC, RbCN/RbNC or KCN, and other similar species, such as HCP, the HO_2 radical or van der Waals complexes. The vibrational motion in the bending coordinate for these systems is very floppy, and then one atom (Li in the case of LiCN) can easily rotate around the remaining (i.e. CN) fragment. In this way, extensive regions of the potential energy surface are sampled, and the effects of anharmonicities and mode couplings are very important. This makes chaos to set in at low values of the excitation energy. Another important dynamical characteristics of our system is that the C–N vibrational frequency is very high, and then it separates effectively from the rest of vibrational modes. Finally, the barrier separating the two stable isomers in LiNC/LiCN is very modest. All these characteristics make the LiNC/LiCN molecule a very interesting dynamical system: It constitutes a generic example in molecular physics, that can be described very realistically, and has been often considered in the past (Borondo and Benito, 1995), specially in relation with the quantum manifestations of classical chaos.

The vibrational dynamics of this system can be adequately studied by a two degrees of freedom model, with the C–N distance kept frozen at its equilibrium value of $r_e = 2.186$ a.u. The vibrational (total angular momentum $J = 0$) Hamiltonian in scattering or Jacobi coordinates is given by

$$H = \frac{P_R^2}{2\mu_1} + \frac{1}{2}\left(\frac{1}{\mu_1 R^2} + \frac{1}{\mu_2 r_e^2}\right)P_\theta^2 + V(R,\theta), \qquad (1)$$

where R is the distance between the center of mass of the CN (anionic) fragment to the Li atom, r the N–C distance, θ the angle formed by the corresponding vectors, and P_R and P_θ the associated conjugate momenta. The reduced masses, μ_1 and μ_2, correspond, respectively, to the Li–CN and C–N fragments. The potential energy surface has been taken from the literature (Essers, Tennyson, and Wormer, 1982) and is presented as a contours plot in Fig. 1. The two stable isomers, LiNC and LiCN, appearing at $\theta = 180°$ and $0°$, respectively, are clearly visible as potential wells. They are separated in
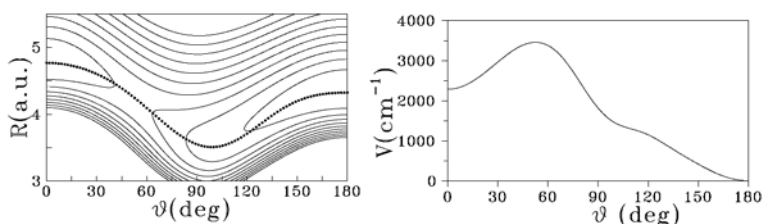
Figure 1. (Left) Potential energy surface for the LiNC/LiCN isomerizing system drawn as a contours plot. The minimum energy path connecting the two stable linear isomers, LiNC ($\theta = 180°$) and LiCN ($\theta = 0$), is shown as a dotted line.
(Right) Energy profile along the minimum energy path.

energy by 2281 cm^{-1}. Relevant information concerning the stationary points of the potential energy surface is summarized in Table I. The minimum energy

Table I. Geometries and energies for the stationary points of the potential energy surface (Essers, Tennyson, and Wormer, 1982) used in our 2D model of the LiNC/LiCN isomerizing system.

Configuration	θ(deg)	R(a.u.)	E(cm^{-1})
Li–NC	180°	4.35	0
Li–CN	0°	4.795	2281.0
saddle	48.41°	4.30	3454.0
"plateau"[a]	110°	3.65	1207.0

[a] See text for details.

path, connecting the two wells, $R_e(\theta)$ has also been plotted superimposed as a dotted line in Fig. 1. The energy profile along this path is shown in the right part the figure.

There exist in the literature more accurate calculations of the LiNC/LiCN potential energy surfaces. Makarewitz and Ha reported in 1995 new improved *ab initio* quantum chemistry calculations including electron correlation at MP4 level (Makarewitz and Ha, 1995). The geometries of the linear minima predicted by these authors are in close agreement with those of Essers *et al.*, but there are significant differences in their relative energies. Another difference is the existence, in the Makarewitz and Ha surfaces, of a stable T–shaped minimum in the region around $(R, \theta) = (3.65 \text{ a.u.}, 110°)$, where the surface of Essers *et al.* only shows a small plateau. However, this feature is dynamically not very significant since the motion around this region gets stabilized by an adiabatic separation mechanism for high value of the excitation in the R coordinate, as it has been demonstrated by us (Borondo,

Zembekov and Benito, 1995). Moreover, there is no experimental evidence of the T–shaped minimum.

3.   Calculations

In this section we describe the numerical methods used to study the classical and quantal dynamics of the LiNC/LiCN system.

3.1.   CLASSICAL CALCULATIONS

The classical vibrational dynamics of the LiNC/LiCN molecular system is followed by using the method of classical trajectories, which in our case are calculated using a fixed step Gear algorithm for the numerical integration of Hamilton equations of motion corresponding to Eq. (1). Most significant vibrational details for this system are obtained by considering the motion along the θ coordinate, which exhibits a rich dynamical behavior (isomerization, anharmonicity, etc.). This dynamics are best monitored by computing a Poincare surface of section (SOS) (Reichl, 2004) taking the sectioning plane lying along the minimum energy path. Accordingly, the values of coordinates (θ, P_θ) are recorded every time that a trajectory passes through $R = R_e(\theta)$. This presents a problem, since R_e depends on θ, thus making the SOS a non-preserving area map. This inconvenience is solved by making the following canonical transformation (Benito et al, 1989):

$$\rho = R - R_e(\theta), \;\; \psi = \theta, \;\; P_\rho = P_R, \;\; \text{and} \;\; P_\psi = P_\theta + P_\rho(dR_e/d\theta). \quad (2)$$

The SOS corresponds then to the conjugate pairs (ψ, P_ψ) at the successive intersections with the $\rho = 0$ plane, *i.e.* $R = R_e(\psi)$, taking only those points for which P_ρ is in a particular branch of the momentum, that is, in a particular solution of the equation:

$$H(\rho = 0, \psi, P_\rho, P_\psi) = E. \quad (3)$$

3.2.   QUANTUM CALCULATIONS

Quantum vibrational energy levels and the corresponding wave functions for Hamiltonian (1) are calculated using the Discrete Variable Representation (DVR) method (Bacic and Lightl, 1986). This procedure is ideally suited for molecules with one or more large amplitude vibrational motions, contrary to traditional variational methods based on finite basis representations (FBR), which are more demanding computationally since they require larger basis sets. The essence of the DVR is an orthogonal transformation into a representation labelled by a discrete set of angles corresponding to the points of

a given quadrature. This transformation presents the additional advantage of allowing an easier way of handling the involved potential matrix elements. In our case we use a discrete representation in the θ coordinate and a function representation of distributed Gaussian basis (DGB) (Hamilton and Lightl, 1986)in the radial coordinate R. A prediagonalization along each θ ray prepares the final basis set, that consisted of 2016 elements rendering the 900 low lying eigenvalues converged to within 0.1 cm^{-1}.

Another way to study the quantum dynamics of a system is to consider quantum phase space representations, that can be compared directly with classical results. Although there is no unique way to define a phase space representation of quantum mechanics, the most popular are the Wigner (Wigner, 1932) and Husimi (Husimi, 1940) functions. The Wigner transform

$$\mathcal{W}(\mathbf{q}, \mathbf{P}) = (2\pi\hbar)^{-N} \int \cdots \int d\mathbf{x} \, \exp(i\mathbf{x} \cdot \mathbf{P}/\hbar) \, \varphi(\mathbf{q} - \mathbf{x}/2)\varphi^*(\mathbf{q} + \mathbf{x}/2) \tag{4}$$

was proposed by this author as a tool to compute quantum corrections to statistical thermodynamics. Although certain properties of the Wigner function support its interpretation as a probability density function in phase space, namely, it gives the correct marginal probability distributions

$$\int d\mathbf{q} \, \mathcal{W}(\mathbf{q}, \mathbf{P}) = |\langle \mathbf{P}|\varphi\rangle|^2, \quad \int d\mathbf{P} \, \mathcal{W}(\mathbf{q}, \mathbf{P}) = |\langle \mathbf{q}|\varphi\rangle|^2, \tag{5}$$

others, in particular the fact that is not everywhere positive, make this interpretation questionable. This problem is due to the uncertainty principle, that precludes the possibility of defining distribution functions at precise points of phase space. A way to overcome this difficulty was devised by Husimi, who proposed the use of a Gaussian smoothing of the Wigner function. The Husimi function defined in this way is everywhere non–negative, and should be understood, consistently with the uncertainty principle, in the following way: $\mathcal{H}$ does not give the probability density at a point in phase space, but the probability density smoothed over a region of volume $\sim \hbar^N$ around that point. Furthermore, it can be shown to be given simply by the expression:

$$\mathcal{H}(\mathbf{q}, \mathbf{P}) = (2\pi\hbar)^{-N}|\langle\chi|\varphi\rangle|^2 \tag{6}$$

where χ is a minimum uncertainty harmonic oscillator coherent state (Zhang, 1990)

$$\chi_{\mathbf{q},\mathbf{P}}(\mathbf{q}', \mathbf{P}') = [(2\pi(\Delta q)^2]^{-N/4} \exp[-(\mathbf{q}' - \mathbf{q})^2/4(\Delta q)^2 + i\mathbf{q}' \cdot \mathbf{P}/\hbar], \tag{7}$$

centered at the phase space point $(\mathbf{q}, \mathbf{P})$. From all these expressions, the Husimi function can be interpreted in a number of ways: as a coherent state representation of quantum mechanics, as a smoothed Wigner distribution, as a coarse graining of phase space, or as the expectation value of the projection operator on a certain state.

The information contained in the Wigner or Husimi functions can be visualized in a number of ways. From the point of view of the present paper the most interesting one is the construction of quantum analogues to the classical Poincare surfaces of section, which hereafter will be called QSOS. This can be accomplished, for example, by projection on suitable planes of phase space, or by integrating out the unwanted coordinates and momenta. In our case we have obtained Husimi based QSOS for the first 900 states of LiNC/LiCN (Borondo and Benito, 1995) using the same definition introduced in the previous subsection,

$$\mathcal{H}_{QSOS}(\psi, P_\psi) = \mathcal{H}[\rho = 0, \psi, P_\rho = P_\rho(E), P_\psi], \qquad (8)$$

calculated by numerical integration of Eq. (6) using the DVR eigenfunctions. We choose isotropic harmonic oscillator coherent states, with width parameters corresponding to the geometric mean of that for the Li–NC bend and the LiNC/LiCN stretch modes, for the calculation of the QSOS. Another computational detail worth mentioning is the fact that for molecular systems like ours and $J = 0$, wave functions are only defined on a half–plane whereas the 2D coherent states are defined on the full (x, y) plane. It is therefore necessary to embed the 2D wave functions into a 3D cartesian space, and calculate overlaps between wave functions $\varphi(R, \theta, \phi)$ (independent of angle ϕ) and 3D harmonic oscillator coherent states centered on the (R, θ) plane with zero momentum out of this plane. Moreover, when comparing $J = 0$ classical and quantum mechanics, we have the problem that the classical Hamiltonian is planar while the quantum is not. To solve these problems, we simply follow the procedure of folding the SOS into the interval $0 \leq \psi \leq \pi$, taking into account the corresponding invariance under the transformation

$$\psi \to 2\pi - \psi \quad P_\psi \to -P_\psi. \qquad (9)$$

A lot of interest has been devoted in the literature to the study of the maxima of quasiprobability densities like $\mathcal{H}_{QSOS}$, paying attention to the relation of these maxima with fixed points and other relevant classical structures of the corresponding SOS in conditions of widespread chaos. The topology of the zeros of this function is also very interesting, specially in connection with the understanding of scarring of vibrational wave functions (Arranz, Borondo, and Benito, 1996; Bacic and Lightl, 2004).

Another popular and convenient way to study the quantum dynamics of a vibrational system is wave packet propagation (Sepulveda and Grossmann, 1996). According to the ideas of Ehrenfest the center of these non–stationary functions follows during a certain time classical paths, thus representing a natural way of establishing the quantum–classical correspondence. In our case the dynamics of wave packets can be calculated quite easily by projection of the initial function into the basis set formed by the stationary eigen-

states of the system, followed by the application of the corresponding evolution operator

$$|\Psi(t)\rangle = e^{-i\hat{H}t/\hbar}|\Psi(0)\rangle = \sum_n |\varphi_n\rangle\langle\varphi_n|\Psi(0)\rangle\, e^{-iE_n t/\hbar}. \qquad (10)$$

This evolution can be studied either in time domain, by following the recurrences of the correlation function:

$$C(t) = \langle\Psi(0)|\Psi(t)\rangle, \qquad (11)$$

or in energy domain through the corresponding spectrum:

$$I(E) = \sum_n |\langle\Psi(0)|\varphi_n\rangle|^2\, \delta(E - E_n), \qquad (12)$$

where the coefficients are known as Franck–Condon factors. It is well known that these two quantities are related by Fourier transform,

$$I(E) = (2\pi\hbar)^{-1} \int_{-\infty}^{+\infty} dt\, e^{iEt/\hbar}\, \langle\Psi(0)|\Psi(t)\rangle. \qquad (13)$$

This equation constitutes the basis of the time–dependent formulation of the spectroscopy (Heller, 1981), that has been widely used also in many fields.

As stated before, wave packets remain for some time close to classical paths, and then can be used to explore which phase space objects are important quantum mechanically. Recurrences in the wave packet motion imprint its signature in the corresponding spectra as low resolution features (Taylor, 1989; Gomez–Llorente and Pollak, 1992). Moreover, the associated wave functions can be calculated easily with a method developed by us (Gomez–Llorente et al, 1992; de Polavieja, Borondo and Benito, 1994). Since they correspond to structures which are not well defined in energy, they must have some sort of resonant–like character. This character can be unveiled by using appropriate calculation techniques that come from resonance theory. For example, one can obtain the corresponding wave functions by Fourier transforming the time–dependent wave packet $|\Psi(t)\rangle$ using a finite time span

$$|\Psi^k\rangle = (2\pi\hbar)^{-1} \int_{-\tau}^{\tau} dt\, |\Psi(t)\rangle\, e^{iE_k t/\hbar}, \qquad (14)$$

where E_k represents is a representative energy of the spectral feature, and τ is related to irs spectral width. In the way that we calculate $|\Psi(t)\rangle$, [i.e. Eq. (10)], this expression reduces to

$$|\Psi^k\rangle = \sum_n |\varphi_n\rangle\langle\varphi_n|\Psi(0)\rangle \frac{\sin[(E_k - E_n)\tau/\hbar]}{\pi(E_k - E_n)}, \qquad (15)$$
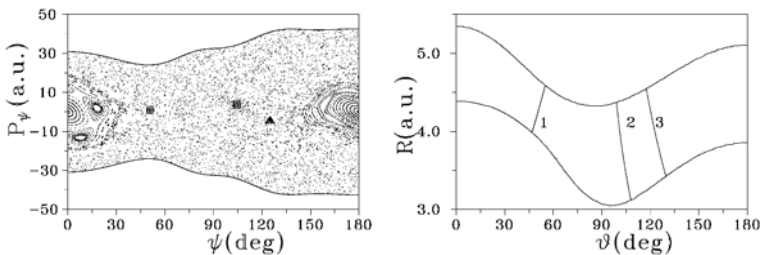
Figure 2. (Left) Composite Poincare surface of section (SOS) for LiNC/LiCN at an excitation energy of $E = 4600$ cm^{-1}. Two islands of regularity are seen corresponding to the two stable linear isomers, LiNC ($\theta = 180°$) and LiCN ($\theta = 0$).
(Right) Three 1:1 periodic orbits (PO) relevant to our work. The corresponding fixed points appear, respectively, as a circle (PO 1), a square (PO 2), and a triangle (PO 3) in the SOS at the left part of the figure.

which can be approximated to

$$|\Psi^k\rangle = \sum_n{}' |\varphi_n\rangle\langle\varphi_n|\Psi(0)\rangle, \tag{16}$$

with the prime indicating that the sum extend only to the states under the k–th band (see examples below). Equation (16) clearly shows the projection character implied in the procedure used to calculate $|\Psi^k\rangle$ (Gomez–Llorente et al, 1992). Moreover, this method can be used to obtain information about the localization process due to scarring of a given PO (de Polavieja, Borondo and Benito, 1994).

4.   Results

In this Section we present some results for LiCN related with the scarring character of some particular POs which connect different branches of the equipotential lines for energies above the isomerization barrier.

4.1.   CLASSICAL RESULTS

To discuss the classical dynamics of the LiNC/LiCN system we present in Fig. 2 a composite Poincare SOS at an excitation energy of 4600 cm^{-1}. This corresponds approximately to the energy of the 100–th vibrational eigenstate, which is well above the isomerization barrier (see Table I). In it, two islands of regularity, corresponding to the two stable linear isomers LiNC ($\theta = 180°$) and LiCN ($\theta = 0$), can be seen embedded in a big area with chaotic dynamics corresponding to isomerizing trajectories, visiting both wells. We have marked the positions of the fixed points of three 1:1 POs, which are relevant
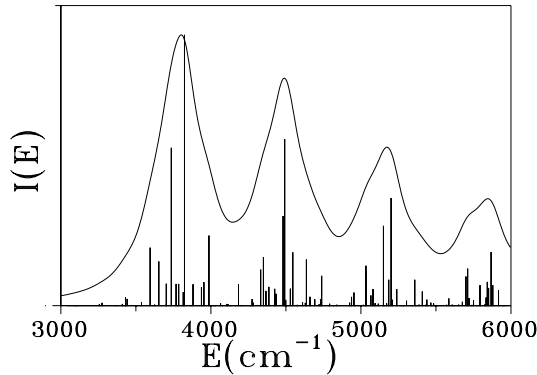
Figure 3. Infinite resolution spectrum (sticks) generated from a Gaussian wave packet launched at the inner turning point of PO 1 in Fig. 2, and low resolution version of it (full line).

to our work. The associated trajectories, which correspond to high excitations in the R coordinate running vertical at an almost constant value of the angular coordinate θ, are shown in the right part of the figure. The first one (PO 1) sits on the saddle point of the potential energy surface (see Table I), while the other two are originated in a saddle node bifurcation at a much lower energy (see details in Ref. (Borondo, Zembekov and Benito, 1996)), being the three of them very relevant in the localization properties of the LiNC/LiCN eigenstates (Arranz et al, 2005).

4.2. Quantum results

Let us now discuss the localizing effect of the POs described above. For this purpose we use the quantum dynamical method presented at the end of Section 3, with allow the construction of wave functions highly localized along the POs. In this sense, we refer to these functions as "scar wave functions".

In Fig. 3 we present the stick spectrum [corresponding to infinite resolution; see eq. (12)] generated from a Gaussian wave packet of the form

$$\langle R, \theta | \Psi(0) \rangle = \left(\frac{4\alpha_R \alpha_\theta}{\pi^2} \right)^{1/4} \exp[-\alpha_R (R - R_0)^2 - \alpha_\theta (\theta - \theta_0)^2] \quad (17)$$

initially located in the inner turning point of PO 1, $(R, \theta)_0 = (3.992 \text{ a.u.}, 46.90°)$, and with values of the parameters $\alpha_R = 16.114$ and $\alpha_\theta = 14.123$. As can be seen, it looks quite complicated and seemingly unassignable, with the separation between levels and intensities distributed according to the laws of random matrix theory (Metha, 1991). On the contrary, when one considers a smoothed (low resolution) version of the spectrum it appears much more regular. For example, we present in full line a convolution of the stick spectrum with a
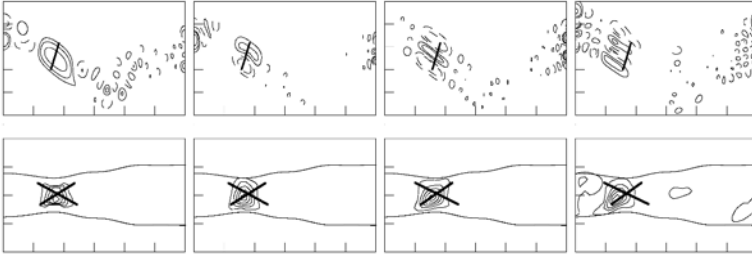
Figure 4. Scar wave functions (upper part) and corresponding Husimi based quantum surfaces of section, QSOS, (lower part) for the four bands observed in the low resolution spectrum in Fig. 3. As can be seen, there appear highly localized along the PO 1 (also plot in the figure) of Fig. 2 and the corresponding fixed points. The horizontal and vertical axes for the wave functions correspond to the θ and R coordinates, spanning the ranges 0–180° and 3–5.5 a.u., respectively while for the QSOS they are ψ and P_ψ spanning 0–180° and –80–80 a.u.

Lorentzian of width 200 cm^{-1}. It consists, in the range of energies shown in the figure, of four equally spaced bands of a certain width, similar to what it is obtained in a typical resonance spectrum. Moreover, the wave functions associated to each of these bands can be computed by means of eq. (16). The results are shown in the upper part of Fig. 4 along with the scarring PO calculated at E=4600 cm^{-1}. As can be seen, they correspond to four scar wave functions with an increasing excitation in a vibrational mode that approximately coincide with the R coordinate. In these functions, the long term contributions [see eqs. (14) and (15)] existing in the corresponding eigenstates which are highly delocalized (in configuration and/or phase space), corresponding to background and/or chaotic states, have disappeared due to a coherence induced by the combined action of the coefficients $\langle \varphi_n | \Psi(0) \rangle$.

In the lower part of the figure we also present Husimi based QSOS. As can be seen, all of them appear located over the fixed point corresponding to the scarring PO. Second, and more important, these functions also spread significantly along the manifolds (incoming and outgoing) associated to the fixed point. This is not surprising since they constitute a dynamically significant picture of the corresponding phase space densities, having been obtained by smoothing the dynamics of a localized wave packet along the scarring PO. As a consequence the scar wave functions constructed by us contains information about the linearized dynamics taking place in the vicinity of the PO on which the initial wave packet is launched. This structure of the QSOS along the manifolds emanating from the fixed point of the scarring PO would be better defined if a longer time, or equivalently a narrower width in the smoothing convoluting Lorentzian function, is used, since in this way a longer exploration of the dynamics of the system would have been allowed to the wave packet.

Finally, let us examine another interesting point in connection with the scar functions that we are studying, which is their projections on the eigen-spectrum of the system. As it is well known (Heller, 1984; Heller, 1991), the existence of scars implies a regularity in the corresponding spectrum, related to the period of the PO (Gutzwiller, 1990; Kaplan and Heller, 1999). In time domain, the dynamics of a packet running along a PO induce recurrences in the autocorrelation function, that when Fourier transformed define an enve-lope in the spectrum. This gives rise to peaks of width proportional to the Lyapunov exponent, at energies given by a Bohr–Sommerfeld quantization condition. Actually, Fig. 3 is a good example of this. In the case of LiCN there exists another additional regularity in the spectrum superimposed to the previous one. This new regularity is originated by the associated homoclinic motion, and is given by the phase space area enclosed by the stable and un-stable manifolds up to the first crossing. This regularity can be unveiled by considering the fluctuations of the spectral widths corresponding to localized wave functions along unstable POs, such as those presented before. For this purpose we calculated the spectral bands originated by PO 3 of Fig. 2. We do not present the corresponding spectrum or wave functions plots, since they are completely similar to those already shown in Fig. 3. The corresponding widths in the eigenvalue spectrum of LiNC/LiCN (stick spectrum) can be easily calculated using the following expression

$$\overline{\sigma}_n = \sqrt{\sum_\mu |\langle \|varphi_\mu|\Psi^n\rangle|^2 (E_\mu - E_n)^2}, \tag{18}$$

computed at a fixed value of the excitation energy ($E = 9197.3$ cm^{-1} in our case (Wisniacki et al, 2005)). This is accomplished by artificially varying the value of $\hbar$ until the center of the desired band coincides with the value of the working energy. By using this procedure we make the spectral features of the system directly comparable with the corresponding classical magni-tudes, which otherwise would vary with the level of excitation. Indeed, as the LiNC/LiCN system is very floppy, its classical dynamics depends very strongly on the energy, as opposed to what happens with mechanically scal-able systems, such as billiards. The values of the $\overline{\sigma_n}$ so obtained are made dimensionless by division by the characteristic energy: $\hbar(n)\omega$,

$$\sigma_n = \frac{\overline{\sigma}_n}{\hbar(n)\omega}. \tag{19}$$

In our case $\omega = 530.8$ cm^{-1} and corresponds to the frequency of PO 3 at $E = 9197.3$ cm^{-1}. The corresponding results for σ_n are presented in Fig. 5. As can be seen, they show a clear increasing linear tendency with and slight oscillatory behavior, σ_{osc}, superimposed. This oscillatory behavior is shown in the right part of the figure, and corresponds to a single frequency
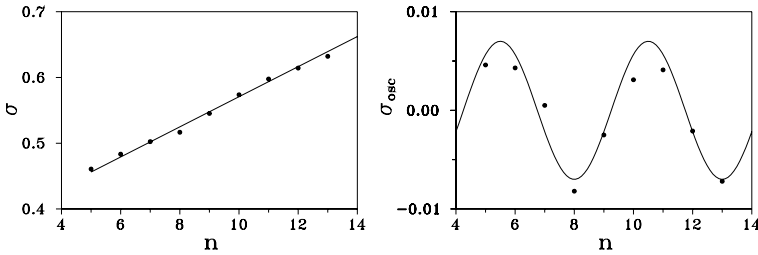
Figure 5. Dimensionless widths (left) and its oscillatory part (right) corresponding to the scar function spectral peaks for periodic orbit number 3 in Fig. 2.

of 17.4 a.u. Moreover, our calculations show that these fluctuations have a surprisingly simple explanation, since they are essentially governed by the quantization of the primary homoclinic dynamics. This result has been thoroughly discussed in Refs. (Wisniacki et al, 2005), specially in the case of the stadium billiard, and can be understood in terms of the coherence of the classical homoclinic motion, which constitutes the natural global extension of the local hyperbolic structure around the PO. As a result the frequency in the oscillations of σ_{osc} coincides very well with the homoclinic area defined by the stable and unstable manifolds emanating from the fixed point of the scarring PO up to the point where they first cross. This result is very important, since it points out to the fact that there may exist properties in the the long term dynamics of chaotic system that can be understood in terms of a small number of classical invariants (see also Ref. (Tomsovic and Heller, 1991).

5. Acknowledgments

References

Reichl, L. E. The Transition to Chaos. (Springer–Verlag, New York, 2004).

Gutzwiller, M. C. Chaos in Classical and Quantum Mechanics Springer–Verlag, New York, 1990.

Metha, M. L. Random Matrices Academic Press, New York, 1991.

Bohigas, Giannoni, O. M.–J. and Schmit, C. Phys. Rev. Lett. **52**, 1 (1984).

Kaplan L. and Heller, E. J. Ann. Phys. **264**, 171 (1998); Kaplan, L. Nonlinearity **12**, R1 (1999).

Heller, E. J. Phys. Rev. Lett. **53**, 1515 (1984).

Heller, E. J. *Chaos and Quantum Physics*, edited by M. J. Giannoni, A. Voros, and J. Zinn–Justin (Elsevier, Amsterdam, 1991).

Bogomolny, E. B. Physica D **31**, 169 (1988).

Berry, M. V. Proc. R. Soc. Lon. A **243**, 219 (1989).

Agam, O. and Fishman, S. Phys. Rev. Lett. **73**, 806 (1994).

de Polavieja, G. G., Borondo, F. and Benito, R. M. Phys. Rev. Lett. **73**, 1613 (1994).

Tomsovic S. and Heller, E. J. Phys. Rev. Lett. **67**, 664 (1991).

Wisniacki, D. A. et al Phys. Rev. Lett. **94**, 054101 (2005); Borondo, F. et al. J. Chem. Phys. **122**, 111101 (2005).

Wisniacki D. A. et al Phys. Rev. E **70**, 035202(R) (2004).

Sridhar, S. Phys. Rev. Lett. **67**, 785 (1991); Dorr, U. et al *ibid.* **80**, 1030 (1998).

Wilkinson, P. B. et al Nature (London) **380**, 608 (1996).

Kellman, M. E. Ann. Rev. Phys. Chem. **46**, 395 (1995).

Taylor, H. S. Acc. Chem. Res. **22**, 264 (1989).

Uzer, T. and Miller, W. H. Phys. Rep. **199**, 72 (1991); Keske, J. C. and Pate, B. H. Annu. Rev. Phys. Chem. **51**, 323 (2000).

Wiggins, S. et al. Phys. Rev. Lett. **86**, 5478 (2001).

Keating, J. P. and Prado, S. D. Proc. R. Soc. Lond. A **457**, 1855 (2001).

Backer, A. Keating, J. P. and Prado, S. D. Nonlinearity **15**, 1417 (2002).

See, for example: Borondo, F. and Benito, R. .M. Frontiers of Chemical Dynamics, edited by E. Yurtsever (Kluwer, Dordrecht, 1995) p. 371; and in *The Physics and Chemistry of Wave Packets*, edited by J. Yeazell and T. Uzer (John Wiley & Sons, New York, 2000) p. 193, and references therein.

Essers, R. Tennyson, J. and Wormer, P. E. S. Chem. Phys. Lett. **89**, 223 (1982).

Makarewitz, J. and Ha, T. Chem. Phys. Lett. **232**, 497 (1995).

Borondo, F. Zembekov A. A. and Benito, R. M. Chem. Phys. Lett. **246**, 421 (1995).

Benito, R. M. et al Chem. Phys. Lett. **161**, 60 (1989).

Bacic, Z. and Light, J. C. J. Chem. Phys. **85**, 4594 (1986).

Hamilton I. P. and Light, J. C. J. Chem. Phys. **84**, 306 (1986).

Wigner, E. Phys. Rev. **40**, 749 (1932).

Husimi, K. Proc. Phys. Math. Soc. Japan **22**, 264 (1940).

Zhang, W.–M. et al Rev. Mod. Phys. **62**, 867 (1990).

Arranz, F. J. Borondo, F. and Benito, R. M. Phys. Rev. E **54**, 2458 (1996).

Arranz, F. J. Benito, R. M. and Borondo, F. J. Chem. Phys. **120**, 6516 (2004).

Sepulveda M. A. and Grossmann, F. Adv. Chem. Phys. **96**, 191 (1996).

Heller, E. J. Acc. Chem. Res. **14**, 368 (1981).

Gomez–Llorente, J. M. and Pollak, E. Ann. Rev. Phys. Chem. **43**, 91 (1992).

Gomez–Llorente, J. M. et al Chem. Phys. Lett. **192**, 430 (1992).

Borondo, F. Zembekov A. A. and Benito, R. M. J. Chem. Phys. **105**, 5068 (1996).

Arranz, F. J. et al J. Chem. Phys. **123**, xxxx (2005).

Modern aspects of the three-body Coulomb problems

Javier Madroñero and Andreas Buchleitner
Max Planck Institute for the Physics of Complex Systems, Dresden

Abstract. We explore quantum aspects of characteristic, highly correlated configurations of doubly excited two-electron atoms, in one, two and three dimensions, along stable and unstable periodic orbits of the classical system. Comparing the autoionization rates of such configurations we find that the two dimensional restriction is in quantitative agreement with the real physical system, whilst the one dimensional model can underestimate the actual decay rates by orders of magnitude. We also study the influence of an additional electromagnetic field on the system. An accurate ab initio quantum treatment of the driven planar atom indicates the existence of nondispersive two-electron wave packets. These highly correlated wave packets arise as a quantum manifestation of regular islands in a mixed classical space, induced by nonlinear resonances between the external field and the unperturbed dynamics of the associated regular configuration of the atom.

Keywords:

1. Introduction

The 3-body Coulomb problem (3BCP) is the microscopic realization of one of the most famous problems of nonlinear physics: the 3-body problem of celestial mechanics, which has attracted the attention of many physicists like Laplace, Lagrange, Poincaré, Einstein, and many others, for several centuries. There the dynamics is in general chaotic with rather small regions of regular motion. The situation does not change much for the 3BCP, and precisely the nonintegrability of the classical dynamics caused the failure of the early quantization schemes at the beginning of the last century. Indeed, after first (unsuccessful) attempts to calculate the helium ground state in the days of Bohr and Sommerfeld it took more than half a century to accurately describe the spectra of 2-electron atoms (see (G. Tanner et.al., 2000) for a historical review).

Notwithstanding, after hydrogen, helium is also the simplest naturally available atomic species, which, in contrast to one electron atoms, exhibits the additional electron-electron interaction, as a source of electronic correlations. Hence, helium is one of the simplest systems where electronic correlations can be studied. Direct manifestations of electronic correlations have been found, e.g., in doubly excited states of helium localized along highly asymmetric, though very stable, frozen planet configurations (FPC) (K. Richter et.al., 1990), or scarred by

unstable periodic orbits of antisymmetric stretch configurations (ASC) (G.S. Ezra et.al., 1991). Even though the complexity of the dynamics of the system is dramatically increased, these correlation effects can prevail under the action of an electromagnetic field: Evidence of highly correlated wave packets propagating along periodic orbits of the FPC has been obtained in one dimensional model calculations (P. Schlagheck et.al., 2003; P. Schlagheck et.al., 2003), when the atom is driven by an electromagnetic field near-resonant with the classical round trip period along the orbit.

Indirect signatures of correlated electron dynamics are provided by the enhancement of the doubly charged ion production in the double ionization process of helium from the ground state by strong laser fields (B. Walker et.al., 1994). Whilst a qualitative description of this phenomenom has been attempted within the framework of several approximate models (P.B. Corkum, 1993; D.N. Fittinghoff et.al., 1992; A. Becker et.al., 2000), we are still lacking a quantitative understanding of the correlated fragmentation process (Th. Weber et.al., 2000; K. Sacha et.al., 2001; V.L.B. de Jesus et.al., 2004).

Such an accurate and clear understanding of the excitation and fragmentation process under external driving requires an accurate theoretical treatment with a minimum of approximations. This, however, defines a formidable theoretical and numerical challenge: even in the simplest case of the field-free, 3D helium atom, the rapid increase of the basis size and of the number of nonzero coupling matrix elements with increasing angular momentum saturates the currently available computing facilities, already at low values of the angular momentum. An additional electromagnetic field will mix almost all the remaining good quantum numbers of the field-free system. The density of states dramatically increases, not only with the excitation of the electrons, but furthermore with the order of the multiphoton excitation process induced by the external drive. Therefore, a fully three dimensional treatment of the driven helium problem, for arbitrary driving frequencies and electronic excitations, still remains beyond reach, even of the largest supercomputers currently available.

For this reason, we will restrict our subsequent approach to planar configurations of the two electrons and of the nucleus, with the polarization axis within this plane. This presents the most accurate quantum treatment of the driven three body Coulomb problem to date, valid in the entire nonrelativistic parameter range, without any adjustable parameter, and with no further approximation beyond the confinement of the accessible configuration space to two dimensions. Whilst this latter approximation certainly does restrict the generality of our model, semiclassical scaling arguments suggest that the unperturbed three

body dynamics is essentially planar at high electronic excitations and small to moderate total angular momenta. The same is true for highly correlated fragmentation processes starting from the atomic ground state (K. Sacha et.al., 2001; J. Madroñero, 2004). Furthermore, the planar three body Coulomb problem has independent realizations in quasi two dimensional semiconductor structures (B. Stébé et.al., 1989), as well as in 2D quantum dots (R.G. Nazmitdinov et.al., 2002).

In the present contribution, we will study the quantum signatures of the FPC and the ASC. In section 2 we briefly sketch our theoretical approach, in section 3 we review the most important aspects of the classical FPC and ASC, and study the implications thereof for the quantum spectrum. In section 4 we consider the quantum aspects of the driven frozen planet configuration. We conclude in section 5.

2. Theory

The Hamiltonian of helium, in the center of mass frame and under the action of an electromagnetic field polarized along the x axis, with field amplitude F and frequency ω, reads, in atomic units,

$$H = \frac{p_1^2}{2} + \frac{p_2^2}{2} - \frac{Z}{r_1} - \frac{Z}{r_2} + \frac{1}{r_{12}} + F(x_1 + x_2)\cos\omega t. \qquad (1)$$

Here r_1 and r_2 are the distances from the electrons to the nucleus, and r_{12} is the inter-electronic distance. Our approach combines the Floquet theorem (J.H. Shirley, 1965), to account for the periodicity of the external perturbation, the complex rotation method (Y.K. Ho, 1983), to extract the atomic decay rates, and the representation of (1) in a suitable basis set (J. Madroñero, 2004; L. Hilico, 2002): subsequent parabolic coordinate transformations completely regularise the Coulomb singularities in this Hamiltonian, and allow to express the associated Floquet eigenvalue problem as a polynomial of finite degree in the creation and annihilation operators of four harmonic oscillators. Therefore the eigenvalue problem can be represented in a basis set defined by the tensor product of Fock states of individual harmonic oscillators, and all matrix elements have analytic expressions which only involve square roots of integer numbers. The final eigenvalue problem contains polynomials of maximal degree 16 in the creation and annihilation operators, with altogether 5472 terms (generated using symbolic calculus). The final matrix is complex symmetric (as a consequence of complex rotation), sparse banded, with 488 nonzero matrix elements in the band. Due to the high density of states the matrices to be diagonalized are rather huge (J. Madroñero et.al., 2004). This requires advanced

techniques of parallel programming, and an efficient implementation of
the Lanczos algorithm (C. Lanczos, 1950; D. Delande et.al., 1991).

3. Classical and quantum aspects of one dimensional configurations of helium

In the FPC both electrons are located on the same side of the nucleus,
with asymmetric excitation. On the first glance, this highly asymmet-
ric structure might appear to be unstable. However, classical studies
(K. Richter et.al., 1990; D. Wintgen et.al., 1992; P. Schlagheck, 1992)
show that, indeed, it is *dynamically stable*: while the inner electron fol-
lows highly eccentric elliptic trajectories which precess around the sym-
metry axis of the configuration, the outer electron is localized around
some equilibrium distance far from the inner electron. It is dynami-
cally stabilized due to the fast oscillation of the latter, which implies a
rapidly oscillating potential experienced by the outer electron, due to
the competition between electron-electron repulsion and the Coulomb
attraction exerted on the outer electron by the screened Coulomb po-
tential of the nucleus. Upon averaging over the characteristic time scale
of the inner electron's motion, the outer electron experiences an effec-
tive, time-independent, weakly attractive potential what determines
the equilibrium distance (V.N. Ostrovsky et.al., 1995; A. Buchleitner
et.al., 2002).

The classical dynamics of the FPC is governed by the Hamiltonian
(1) for $F = 0$ and is regular as evident from the Poincaré surface of
section in Fig. 1(a) (D. Wintgen et.al., 1992; P. Schlagheck, 1992),
where position and momentum of the outer electron are represented
by a point each time when the inner electron collides with the nu-
cleus. Due to the homogeneity of the Hamiltonian (1), the dynamics
remain invariant under scaling transformations (P. Schlagheck et.al.,
2003; J. Madroñero, 2004)

$$
\begin{aligned}
r_i &\rightarrow r_i(N - 1/2)^2 \\
p_i &\rightarrow p_i(N - 1/2)^{-1} \\
E &\rightarrow E(N - 1/2)^{-2},
\end{aligned}
\tag{2}
$$

where N represents an arbitrary, real positive quantity. Since any clas-
sical action scales linearly with N, we identify N with the principal
quantum number of the inner electron. From this property it is possi-
ble to identify intrinsic quantities of the configuration in terms of N.
For instance, the equilibrium position of the outer electron x_{min}, the
frequency ω_I of small oscillations around this point, and the minimum
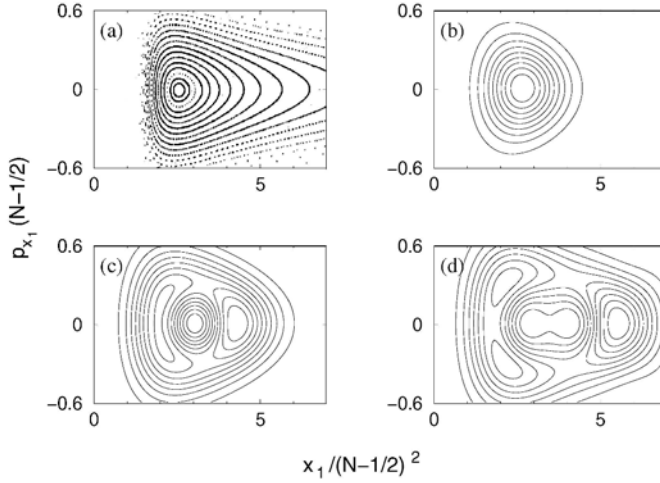
Figure 1. Contour plots of the Husimi distributions of the ground (b), first excited (c) and second excited (d) triplet FPS of the sixth series, compared with the classical phase space of the collinear FPC in (a) (K. Richter et.al., 1990; P. Schlagheck, 1992). The Husimi functions show perfect phase space localization: while the fundamental state (a) is localized at the minimum of the effective potential at 2.6 scaled units, the excited states are localized along frozen planet trajectories with higher energy, with outer turning points (at the maximum of the distribution) at 4.2 (c) and 5.5 (d) scaled units.

electric field F_I necessary to ionize the configuration are respectively given by

$$x_{min} = 2.6\,(N - 0.5)^2, \tag{3}$$
$$\omega_I = 0.3\,(N - 0.5)^{-3}, \tag{4}$$
$$F_I = 0.03\,(N - 0.5)^{-4}. \tag{5}$$

As seen in Fig. 1(a) the phase space of the collinear FPC contains a large region of bound motion. Therefore, it is possible to identify eigenstates in the spectrum which are localized along the frozen planet orbit, even for relatively weak excitations. Indeed, starting from the 3rd. Rydberg series of helium there are subseries of *frozen planet states* (FPS) converging to the associated single ionization thresholds. Figs. 1(b)-(c) show the Husimi function projected on the phase space of the outer electron, for the three lowest planar FPS from the 6th Rydberg series: the fundamental state (b) is localized at the minimum (3) of the effective potential, the excited states are localized along frozen planet trajectories with higher energy. The localization of these states along the periodic orbit is corroborated by the left plot in Fig. 2.
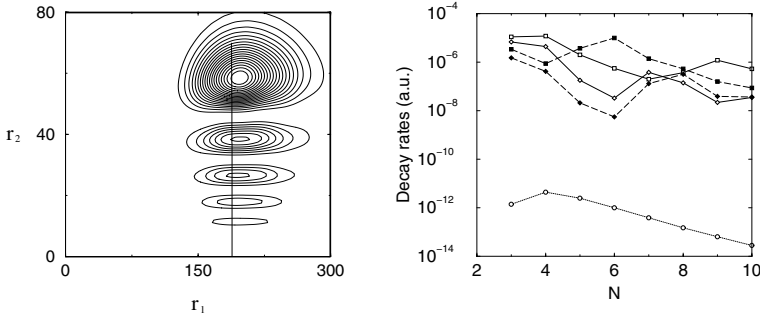
Figure 2. Contour plot (on a linear scale) of the electronic density of the planar frozen planet state in 2D configuration space spanned by the electrons' distances r_1 and r_2 from the nucleus, in the collinear configuration (left). This eigenstate belongs to the $N = 9$ series. The solid line depicts the associated classical periodic orbit. Autoionization rates of frozen planet states of helium (right) in 1D (open circles; the exchange energy vanishes in 1D configuration space, since the electrons are effectively distinguishable (P. Schlagheck, 1992)), 2D (filled squares for singlet, filled diamonds for triplet symmetry), and 3D (open squares for singlet, open diamonds for triplet) configuration space. The much higher rates in two and three dimensions provide a clear proof that autoionization in the longitudinal direction is a slow process, largely dominated by autoionization in the transverse direction, which probes the chaotic domain of phase space.

Indeed, triggered by pioneering experiments (U. Eichmann et.al., 1990), the existence of such states was already demonstrated by earlier accurate 3D (K. Richter et.al., 1990) and 1D (P. Schlagheck et.al., 2003) quantum calculations, though dramatically enhanced ionization rates of the 3D as compared to the 1D eigenstates were found. This contrasts a wide spread argument (D.G. Lappas et.al., 1996), according to which 1D models should exhibit enhanced autoionization rates as compared to the actual 3D problem, since in the 1D case no space is left for the electrons to avoid the detrimental Coulomb singularity of the electron-electron interaction term in (1). On the basis of simulations of the 3D classical dynamics the authors of the 1D calculation (P. Schlagheck et.al., 2003) therefore conjectured that the origin of this counterintuitive effect is caused by a dynamical stabilization mechanism: only not too large transverse deviations from the ideal collinear case maintain the stability – the region of classical stability has a finite extension in the phase space component spanned by the transverse dimension.

If this argument holds true, already the frozen planet configurations of planar helium should exhibit enhanced autoionization rates as compared to the 1D case. In figure 2 (right) we therefore compare the decay rates of our 2D frozen planet states with the earlier 1D and 3D results. Clearly, the 2D rates are of the same order of magnitude as the 3D rates,

and considerably larger than the 1D results. Thus, the present results already confirm the above picture gained from classical calculations, and imply an important caveat for oversimplified 1D models (D.G. Lappas et.al., 1996; M. Lein et.al., 2000) of correlated electronic systems in 3D, where dynamical (and, in fact, often nonlinear) stabilization effects are easily underestimated. On the other hand, since the 2D and 3D rates are essentially identical, our present results also indicate that the planar restriction of the three body Coulomb problem already extracts the most important qualitative (if not quantitative) features of the fragmentation process.

Another well-defined configuration of the classical three body Coulomb problem with unambiguous quantum correspondence is the collinear antisymmetric stretch configuration, where the electrons are located on opposite sides of the nucleus. In contrast to the frozen planet orbit, the antisymmetric stretch is unstable in the axial direction (G.S. Ezra et.al., 1991; P. Schlagheck et.al., 2003), with the two electrons colliding with the nucleus in a perfectly alternating way (Fig. 3 (left)). Hence, already the one dimensional treatment accounts for the dominant classical decay channel of this configuration. As for the frozen planet, there are doubly excited states of helium associated to the periodic orbit of the ASC as illustrated in Fig. 3 (left).
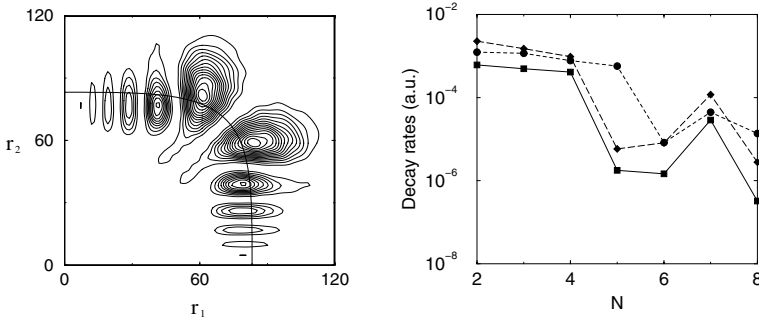

Figure 3. Contour plot of the electronic density of a (triplet) eigenstate strongly scarred by the antisymmetric stretch orbit (left), in 2D configuration space (spanned by the electrons' distances r_1 and r_2 from the nucleus, in the collinear configurations considered here). This eigenstate belong to the $N = 9$ series. The solid lines depict the associated classical periodic orbit. Autoionization rates of antisymmetric stretch singlet states (right) of the Nth autoionizing series of the helium spectrum, in 1D (squares), 2D (circles), and 3D (diamonds) configuration space.

Figure 3 (right) compares the life times of the collinear antisymmetric stretch eigenstates in one, two, and three dimensions, for principal quantum numbers $N = 2 \ldots 8$, and for singlet symmetry. Apart from unsystematic fluctuations – which we attribute to local avoided cross-

ings with other states, a generic phenomenon in the doubly excited energy range and more generally in any chaotic quantum system – the autoionization rates are of the same order of magnitude in all dimensions, with the 1D states almost always slightly more long lived than those in 2D and 3D. This is consistent with our intuition already alluded to above: since the classical antisymmetric stretch configuration decays along the axial degree of freedom, already the 1D model can grasp the dominant fragmentation process, and contributions to the autoionization rates due to transverse tunnelling in the 2D and 3D case are but a small correction. In addition, this observation corroborates that the planar confinement does not imply any severe restriction for the quantitative description of the (auto-)ionization process.

4. Driven frozen planet configuration

So far we have only considered quantum aspects of the field-free three-body Coulomb problem. In the present section we investigate the localization properties of frozen planet states under the influence of a near-resonant external driving field, in more than one dimension. Until now this regime of driven helium has been unaccessible, simply due to the mere size of the corresponding Floquet eigenvalue problem, brought about by the field induced coupling of many angular momentum states, and only a one dimensional approach to this problem can be found (P. Schlagheck et.al., 2003). In the classical case, it is still possible to find classically stable configurations of the driven collinear frozen planet, which manifest as regular resonance islands in the associated mixed regular-chaotic phase space. These islands propagate along the near-resonantly driven periodic orbit of the field free problem, with the frequency of the driving field (Fig. 4 a_{1-3}). Semiclassical arguments (G.P. Berman et.al., 1977; P. Schlagheck et.al., 1999) suggest the existence of quantum eigenstates of the driven system associated with these phase space structures. Indeed, there are eigenstates of driven planar helium which are anchored to the fix points of the phase space. Fig. 4 b_{1-3} shows the projection of the electronic density of the outer electron of a Floquet state on the classical phase space component spanned by x_1 and p_1, for different phases of the driving field. Clearly, this state is entirely associated with the chaotic phase space domain and localized on the unstable (hyperbolic) fix point of the resonance. This wave packet propagates periodically along the near-resonantly driven periodic orbit, without dispersion. Fig. 4 c_{1-3} depicts the electronic density of the outer electron, in configuration space, for a fixed position of the inner electron on the x axis, at some distance close to the maximum of the
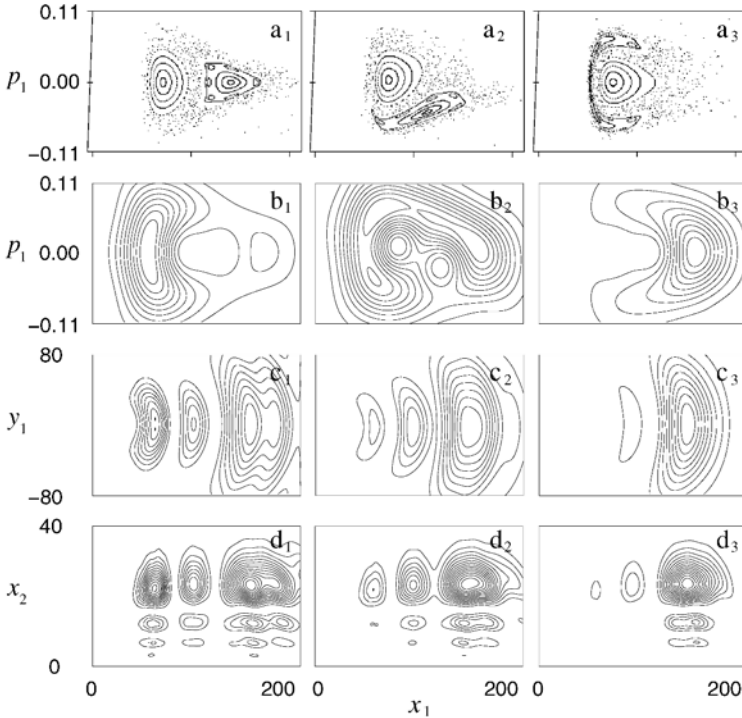
Figure 4. Classical phase space structure of the restricted collinear problem (P. Schlagheck et.al., 2003) ($a_1 - a_3$), as well as the wave packet triplet eigenstate (b, c, d) along the $N = 6$ frozen planet trajectory of 2D helium, under electromagnetic driving at frequency $\omega = 0.2(N - 0.5)^{-3}$ a.u. and amplitude $F = 0.005(N - 0.5)^{-4}$ a.u.. The contour plot of the Husimi distribution projected onto the phase space component spanned by x_1 and p_1 (the position and momentum of the outer electron) is shown for phase $\omega t = 0$ (b_1), $\omega t = \pi/2$ (b_2) and $\omega t = \pi$ (b_3) of the driving field, and compared with the corresponding Poincaré sections ($a_1 - a_3$). Clearly, the electronic density is associated with the chaotic phase space region, localized around the hyperbolic fix point of the 1:1 resonance, and propagates along the near-resonantly driven periodic orbit. $c_1 - c_3$ show the electronic density of the outer electron, for the inner electron fixed at $x_2 \simeq 23$ a.u. The projection of the electronic probability density along the polarization axis of the field is depicted in $d_1 - d_3$.

probability density. The strict correlation between the outer electron's dynamics and the inner electron's position is apparent (there is no dispersion of the wave packet in the transverse direction), and prevails for any other choice of the inner electron's position. This observation finds an alternative expression in the configuration space representation in Fig. 4 d_{1-3}, where the x-coordinates of both electrons are correlated: clearly, the outer electron propagates along the resonantly driven frozen

planet orbit (in phase opposition to the field – hence its locking on the hyperbolic fixed point in phase space), while the inner electron's dynamics remains largely unaffected.

The nondispersive wave packet illustrated here propagates along the $N = 6$ frozen planet trajectory of 2D helium. In this highly excited spectral range we already expect that semiclassical predictions are applicable. In particular, the classical dynamics of the driven frozen planet suggest that the system decays via ionization of a single electron (P. Schlagheck et.al., 2003). Therefore, in our calculations we include only as many Floquet blocks as necessary to reach the next single ionization threshold by absorbing the corresponding number of photons. Even then, the matrices of the associated eigenvalue problem almost saturate one of the largest currently available supercomputers in Germany (RZG, 2005). For lower excitations, where it is possible to reach the double ionization threshold, we do not find significant deviations of the wave packets' lifetimes if we increase the number of Floquet blocks such that the wave packets are also coupled to the double ionization continuum. This has been also observed in the 1D case for higher excitations ($N \sim 10$) (P. Schlagheck, 2005). Therefore, the results presented here provide abundant evidence for the existence of nondispersive two-electron wave packets in helium, with lifetimes of approximate 500 cycles of the driving field.

5. Conclusions

In this paper we examined quantum aspects of special classical configurations of two-electron atoms. In the doubly excited regime, we found quantum states of helium that are localized along 1D periodic orbits of the classical system. A comparison of the decay rates of such states obtained in one, two and three dimensional ab initio calculations allows us to conclude that the dimension of the accessible configuration space *does* matter for the quantitative description of the autoionization process of doubly excited Rydberg states of helium. Whilst 1D models can lead to dramatically false predictions for the decay rates, the planar model allows for a quantitatively reliable reproduction of the exact life times.

For the driven atom, we developed an accurate approach without any adjustable parameter, and with no other approximation than the confinement of the accessible configuration space to two dimensions. This method was successfully applied for the study of the near resonantly driven frozen planet configuration. Floquet states were found that are well localized in the associated phase space and propagate along near-

resonantly driven periodic orbits without any dispersion. Thus, strong evidence for the existence of nondispersive two-electron wave packets in helium, propagating in an effective, molecular-like potential, was given.

References

Tanner, G., K. Richter and J.M. Rost. *Rev. Mod. Phys.*, 72:497, 2000.

Richter, K. and D. Wintgen. *Phys. Rev. Lett.*, 65:1965, 1990.

Ezra, G.S., K. Richter, G. Tanner and D. Wintgen. *J. Phys. B*, 24:L413, 1991.

Schlagheck, P. and A. Buchleitner. *Eur. Phys. J. D*, 22:401, 2003.

Schlagheck, P., D. Pingel and P. Schmelcher *Phys. Rev. A*, 68:053410, 2003.

Walker, B., B. Sheehy, L.F. DiMauro, P. Agostini, K.J. Schafer and K.C. Kulander. *Phys. Rev. Lett.*, 73:1227, 1994.

Corkum, P.B. *Phys. Rev. Lett.*, 71:1994, 1993.

Fittinghoff, D.N., P.R. Bolton, B. Chang and K.C. Kulander. *Phys. Rev. Lett.*, 69:2642, 1992.

Becker, A. and F.H.M. Faisal. *Phys. Rev. Lett.*, 84:3546, 2000.

Weber, Th., H. Giessen, M. Weckenbrock, G. Urbash, A. Staudte, L. Spielberger, O. Jagutzki, V. Mergel, M. Vollmer and R. Döner. *Nature*, 405:658, 2000.

Sacha, K. and B. Eckhardt. *Phys. Rev. A*, 63:043414, 2001.

De Jesus, V.L.B., B. Feuerstein, K. Zrost, D. Fischer, A. Rudenko, F. Afaneh, C.D. Schröter, R. Moshammer and J. Ullrich. *J. Phys. B*, 37:L161, 2004.

Madroñero, J. Spectral structure of planar helium under periodic driving. *Ludwig-Maximilians-Universität München*, 2004.

Stébé, B. and A. Ainane. *Superlattices and Microstruct.*, 5:545, 1989.

Nazmitdinov, R.G., N.S. Simonović and Jan M. Rost. *Phys. Rev. B*, 65:155307, 2002.

Shirley, J.H. *Phys. Rev.*, 138:B979, 1965.

Ho, Y.K. *Phys. Rep.*, 99:1, 1983.

Hilico, L., B. Grémaud, T. Jonckheere, N. Billy and D. Delande. *Phys. Rev. A*, 66:022101, 2002.

Madroñero, J. and A. Buchleitner. *in Proceedings of the Second Joint HLRB and KONWIHR Result and Reviewing Workshop, Springer-Verlag, Berlin*, 2004.

Lanczos, C. *J. Res. Nat. Bur. Standards, Sect. B*, 45:225, 1950.

Delande, D., A. Bommier and J.C. Gay. *Phys. Rev. Lett.*, 66:141, 1991.

Wintgen, D., K. Richter and G. Tanner. *Chaos*, 2:19, 1992.

Schlagheck, P. Das Drei-Körper-Coulombproblem unter periodischem Antrieb. *Technische Universität München*, 1999.

Ostrovsky, V.N. and N.V. Prudov. *J. Phys. B*, 28:4435, 1995.

Buchleitner, A., D. Delande and J. Zakrzewski. *Phys. Rep.*, 368:409, 2002.

Eichmann, U., V. Lange and W. Sandner. *Phys. Rev. Lett.*, 64:274, 1990.

Lappas, D.G., A. Sanpera, J.B. Watson, K. Burnett, P.L. Knight, R. Grobe and J.H. Eberly *J. Phys. B*, 29:L619, 1996.

Lein, M., E.K.U. Gross and V. Engel. *Phys. Rev. Lett.*, 85:4707, 2000.

Berman, G.P. and G.M. Zaslavsky. *Phys. Lett. A*, 61:295, 1977.

Schlagheck, P. and A. Buchleitner. *Physica D*, 131:110, 1999.

RZG 2005.

Schlagheck, P. Private communication. 2005.

Concerning regularities of particle's motion in the electric and thermoelectric fields with distributed potential

V.I. Fedulov

Institute of Power Engineering and Automation,
Uzbek Academy of Sciences,
Academgorodok, Tashkent,
Uzbekistan

Abstract. The subject of this research are the regularities of the particles motion in the electric and thermoelectric fields with distributed potential and the influence of temperature field to the particle motion trajectories in aggregate electric and thermal fields. The analytical solution of the problem of particle motion in thermoelectric field with distributed potential is produced. Common regularities of particle motion and trajectory changes in such fields are derived. It is shown that nonlinear curves give a nonconsiderable part of the trajectory within the macrostructures and so the trajectory shape doesn't considerably influence the electron flow transformation process. Conversely, the trajectory shape does influence the aforesaid processes in micro- and nanostructures defining the specific ways of transformation.

Keywords: Thermoelectric potential field, particles motion, trajectory of electrons.

1. Introduction

The problem of particle motion in stationary potential fields (electric, thermal, gravity fields) commonly comes to the field parameters estimates (the determination of potential function satisfying the Laplace's equation) and a solution of particle motion equation in this field (Landau et. al., 1988; Lorents, 1935). Analytical solution of the motion equation in central forces system is derived for finite quantity of potential distributions. The methods of calculus of approximation can answer only special questions about the particle motion and operate only in specified areas of potential field (Connie et. al., 2003; Leon O. Chua, 2003; Mihael Zitnik, 2003). Because of that, seeking physical systems which have the potential distribution satisfying the Laplaces equation and the equations of motion with known common analytical solution remains essential. One of the examples of such systems is the potential field formed by two electrodes, constant-potential and distributed-potential. This system could be used for measuring and functional transformation of electric signals. During the operation of such a solid-state system (usually using semiconductors) a thermal field appears and forms the thermoelectric field with distributed potential. The superposition of the latter and the original field can cause variation

of the resulting field and distortion of its operational characteristics. On the other hand, the discovery of this effect regularity would make it possible to construct new functional electronics devices. Besides that, a solution of this problem would probably give the generalized idea of particle motion in accelerating and decelerating fields and the way to research the general regularities of electron flow transformation in the devices designed for such aims as determining the magnitude of the signal under study (Fedulov, No.2052823, 1996; Fedulov, No.3659, 1996). The physics of electric signals transformation in such devices differs and naturally requires different methods of transformation process analysis. Temperature dependences of operational characteristics of semiconductor devices (which are representable by macrostructures) are deeply researched and widely described in modern literature (Collinge, 2002). The process of electron flow transformation in these structures depends on its magnitude and doesn't considerably depend on motion trajectory. Oppositely, the electron motion trajectory shape is decisive in micro- and nanostructures (Groves et. al., 2002; Despere et. al., 2002; Al-Qahtani et. al., 2004). Because of that the papers concerning the influence of temperature on electron trajectory shape in micro- and nanostructures are the subject of great interest. The aim of the present article is the research of the regularities of temperature field influence on particle motion trajectory in the aggregate electric and thermal fields.

2. Concerning particle motion regularities in stationary thermoelectric fields

We'll search for a solution of equation of motion in a stationary potential thermoelectric field with distributed potential. Such a field is generated in a plane-parallel structure (Fedulov, 2003) with distributed potential (fig. 1). The potential thermoelectric field in this structure can be described by the following independent expressions:

$$U(x,y) = (U_{max} - U_{min})/l_0 d_0 \cdot x \cdot y = k_e \cdot x \cdot y \qquad (1)$$

$$T(x,y) = (T_{max} - T_{min})/l_0 d_0 \cdot x \cdot y) = k_T \cdot x \cdot y \qquad (2)$$

where l_0, d_0 stand for the length and the width of the structure under study, and U_{min}, U_{max}, T_{min}, T_{max} stand for minimal and maximal values of potential and temperature at the edges of the electrode on $y = d_0$ plane respectively. The distribution of potential and temperature along this electrode is linear: $U_1(x) = U(x,0) = 0$, $U_2(x) = U(x,d_0) = kx$, assuming that $k_e = (U_{max} - U_{min})/l_0 d_0$, and $k_T =$
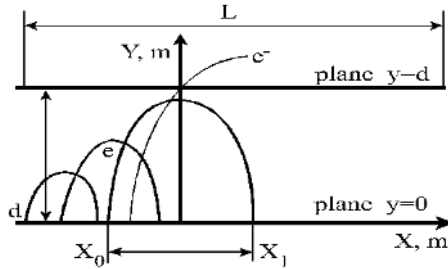
Figure 1. The configuration of the task.

$(T_{max} - T_{min})/l_0 d_0$ stand for potential and temperature distribution coefficients.

The field between the planes with the given potentials will be electrostatic and plane-parallel and satisfies the two-dimensional Laplace's equation

$$\partial^2 U/\partial x^2 + \partial^2 U/\partial y^2 = 0. \tag{3}$$

The intensity of electrical field is determined by the expression:

$$E = -gradU = -k/d(y\vec{x}_0 + x\vec{y}_0). \tag{4}$$

The electric field potential can be found using Eq. (1). The thermoelectric field intensity can be written as [13]:

$$E_T = L_{12}/eL_{11}T \cdot \nabla T = \alpha_T \nabla T \tag{5}$$

Here: E_T is the intensity of the electric field generated by the particle motion in thermal field, L_{11} and L_{12} - Onsagera kinetic coefficients, $\alpha_T = L_{12} \cdot (eL_{11})^{-1} \cdot T^{-1}$ - thermoelectric coefficients.

Then we can rewrite the equation of electron motion in thermal field with distributed potential as following:

$$m\ddot{x} = e \cdot \alpha_T \cdot gradT \tag{6}$$

Since the form of the particle equation of motion in electric potential and thermal fields is alike, both kinds of motion can be described by following equations:

$$\begin{cases} \ddot{x} = -em^{-1}E_x = ay, \\ \ddot{y} = -em^{-1}E_y = ax, \end{cases} \tag{7}$$

The solution can be represented in parametric form as (Fedulov, 2003):

$$\begin{cases} 2px(t) = p(x_0 + y_0)Ch(pt) + (V_{0x} + V_{0y})Sh(pt) \\ \quad +p(x_0 - y_0)Cos(pt) + (V_{0x} + V_{0y})Sin(pt), \\ 2py(t) = p(x_0 + y_0)Ch(pt) + (V_{0x} + V_{0y})Sh(pt) \\ \quad -p(x_0 - y_0)Cos(pt) - (V_{0x} + V_{0y})Sin(pt), \end{cases} \tag{8}$$

$$
\begin{cases}
\qquad 2V_x(t) = p(x_O + y_O)Sh(pt) + (V_{Ox} \\
+V_{Oy})Ch(pt) - p(x_O - y_O)Sin(pt) + (V_{Ox} - V_{Oy})Cos(pt), \\
\qquad 2V_y(t) = p(x_O + y_O)Sh(pt) + (V_{Ox} + V_{Oy})Ch(pt) \\
\qquad +p(x_O - y_O)Sin(pt) - (V_{Ox} - V_{Oy})Cos(pt),
\end{cases}
\tag{9}
$$

where x_0, y_0, V_{0x}, V_{0y} - stand for entry point coordinates and initial velocity components of the electron, e and m - its electric charge and mass, $\alpha_e = p_e^2 = e\cdot k_e/m\cdot d_0$ and $\alpha_T = p_T^2 = e\cdot k_T/m\cdot d_0$ - structure parameters for electric and thermal fields respectively. The Eqs. (8) describe the trajectory of electrons movement in modulating kind, and Eq. (9) - its velocity. Let us assume that Y axis passes the points of equal potentials normally to electrode planes. Electron motion equations in electric and thermal fields only differ in p value. Since the influence of thermal and electric fields on particle trajectory are independent, the resulting trajectory can be regarded as a sum of two trajectories.

3. Concerning the particle motion in macrothermoelectric fields

We can find from expressions Eq. (7) and Eq. (8) the functional dependence between the values of structure's parameter p, the value of electron's entry point into the structure x_0 and y_0 and the values of components of its entry's initial velocity V_{0x} and V_{0y} at which electron remains in structure, or abandons it:

$$
px_0 = 2V_0 Sin(pt + arctg V_{Ox}/V_{Oy})/(e^{pt}) + \sqrt{2}Sin(pt + \pi/4) - (V_{OX} + V_{OY}).
\tag{10}
$$

At $t = 0$, Eq. (8) becomes:

$$
px_0 = V_0 Sin(arctg V_{0X}/V_{0Y}) - (V_{OX} + V_{OY}) = B.
\tag{11}
$$

The Eqs. (10) and (11) functionally connect the p parameter, the initial electron's velocity V_0 and velocity's constituents V_{0x} and V_{0y} in plane-parallel structure with distributed potential with the coordinate of its entry's point x_0, on the electrode with distributed potential. Let us analyze Eq. (10): Under $px_0 \leq B$ the electron will lose the initial kinetic energy completely with generation of electromagnetic radiation (the kinetic energy is absorbed completely). Under these conditions the electron doesn't leave the structure. There is the partial selection of energy under $px_0 \geq B$ and the electron comes beyond the limits of structure. If electron enters the structure normally ($V_{0y} = V_0$, $V_{0x} = V_0$) the boundary condition after that electron leaves the structure can be written as:
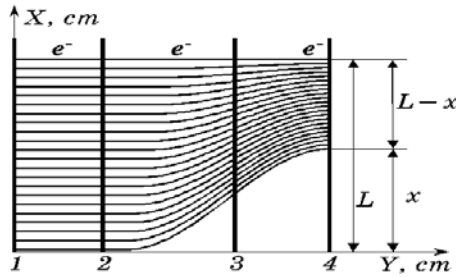
$$
px_0 \geq -V_{OY}
\tag{12}
$$

Figure 2. The measurer macrostructure with distributed potential. 1 − the cathode (emitter), 2 − grids for a measured electrical signal, 3 − grid with a distributed potential and 4 − anode.

Conditions (10), (11) and (12) divide the structure into two areas, one of which behaves as accelerating while another as decelerating. Electron flow passing through this structure is able to leave it when in accelerating area only. Leaving point variations situated in this area can be used for developing devices for measuring the magnitude of electric signal. Voltage measuring devices can be categorized to micro- and macrostructures reasoning from the particle equation of motion form. We'll assume that the electron passage time is greater than the reciprocal of the structure parameter in macrostructures and smaller in microstructures. The voltage measuring method has the variation of electron flow intensity during its path through the structure in its basis in microstructures and trajectory changing in macrostructures. So the influence of thermal field on the electron flow transformation process differs in this structure class. The macrostructure - based voltage measuring device is shown in fig. 2. The essence of this method is judging about the magnitude of the signal under study by the observed changing of electron flow while it passes through the decelerating and accelerating parts of the structure.

The Eq. (12) for this structure can be turned into

$$U_c = (U_{max} - U_{min})/L \cdot x \cdot F(U), \qquad (13)$$

where U_{max}, U_{min} stand for the values of maximal potential and minimal potential, which are applied to the ends of the electrode in the plane $y = d$; L - the length of a structure (m); $F(U)$ - the law of distribution of potential on a grid.

It was demonstrated by research that the rectilinear form of electron flow trajectory is characteristic for macrostructures and the temperature doesn't considerably influence the overall process in this circumstances. At the same time changing of initial particle velocity (by varying the temperature or the potential) just leads to changing of accelerating area width and electron flow intensity near the anode. The influence

of temperature on the technical characteristics of macrostructure-based devices is widely researched (Collinge, 2002; Groves et. al., 2002) and is not reviewed in this paper.

4. Concerning the particle motion in electric and microthermoelectric fields

Particle motion trajectory changing during its pass through the accelerating and decelerating parts of thermoelectric field in microstructure plays the major role in the research and voltage measuring methods development areas. The most characteristic and interesting methods of the design of electric signals measuring and transformation devices are those which utilize the electron motion trajectory changing in the area of S-shape trajectories ("the tunnel effect") originated from the same point (Despere et. al., 2002; Al-Qahtani et. al., 2004). The conditions of existence of such area are researched for the electric field system (Fedulov, 2003), and the electron motion trajectories in this area regarding the initial velocity with constant entry point are shown at Fig. 3. Fig. 4 shows the electron motion trajectories regarding the initial velocity with constant entry point.

Produced process models can be used for the design of measuring devices based on electromagnetic oscillation effect in the first case and based on charged particle lodging area definition in second. The equations decribing the motions in thermoelectric field have the following form:

$$x^2(t) - y^2(t) = \sqrt{2}x_0^2 e^{p_e t} Sinpt(p_e t - \pi/4) \tag{14}$$

$$x^2(t) - y^2(t) = \sqrt{2}x_0^2 e^{p_T t} Sinpt(p_T t - \pi/4) \tag{15}$$

The electron motion trajectories in this area regarding the initial velocity with constant entry point are shown in Fig. 5, and regarding the initial velocity in Fig. 6. This figures display that the thermal velocity component can considerably influence the motion trajectory and naturally the technical characteristics of device.

5. Concerning the regularities of particle motion in the field with distributed potential

While reviewing the operation of measuring and transformation devices based on distributed potential structures utilizing the decelerating (reflective) and accelerating field areas (fig. 4), the problem of its operation
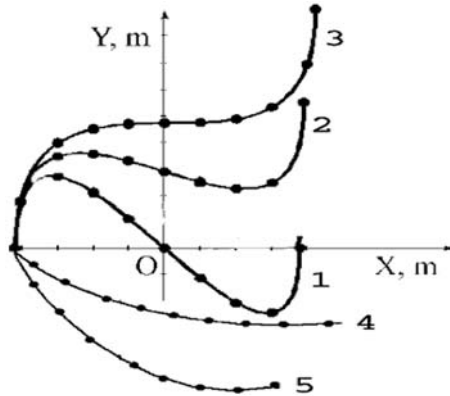
Figure 3. The trajectories of electron's motion in the area of "the tunnel effect" at change of value of its initial speed. 1 − the trajectories of electron's motion in an electric field, 2 and 3 − the trajectory of electron's motion in aggregate electrical and thermal fields, accordingly, under $p_T = 0.25p_e$ and $p_T = 0.5p_e$, 4 and 5 − the trajectory of electron's motion in aggregate electrical and thermal fields, accordingly, under $p_T = -0.25p_e$ and $p_T = -0.5p_e$.
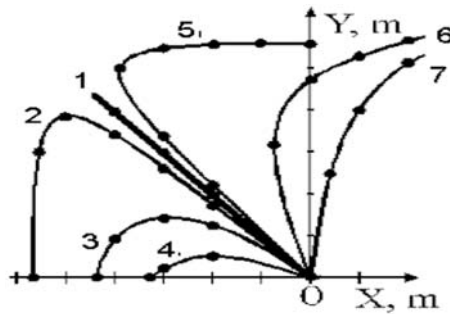

Figure 4. The trajectories of electron's motion exiting from one point, at change of value of initial speed and its components. 1 − the trajectories of electron's motion in an electric field, 2, 3 and 4 − the trajectory of electron's motion in aggregate electrical and thermal fields, accordingly, under $p_T = -0.25p_e$, $p_T = -0.5p_e$ and $p_T = -0.75p_e$, 5, 6 and 7 − the trajectory of electron's motion in aggregate electrical and thermal fields, accordingly, under $p_T = 0.25p_e$, $p_T = 0.5p_e$ and $p_T = 0.75p_e$.

speed (particle pass time) estimation appears. Different field areas define the peculiarities of particle motion in such structures. We'll serialize the velocity expression (9) and limit it to the quadratic terms:

$$V(t) = \sqrt{V_0^2 + 2V_{Oy}p^2 x_O t + 2V_{Ox}V_{Oy}p^2 t^2 + p^4 x_0^2 t^2}. \qquad (16)$$

For a braking site of a field according to expression (10) coordinates of an entry point always have negative value. Then expression (16) will be written as:

$$V(t) = V_0\sqrt{1 - V_{Oy}p^2 x_O t \cdot V_O^{-2}}. \qquad (17)$$
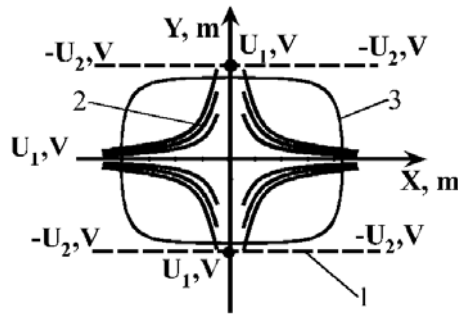
Figure 5. A closed trajectory of electron's motion in structure with symmetric thermoelectric field. 1 − electrode with distributed potential, 2 − the pattern of electrical field, 3 − closed trajectory of the electron.
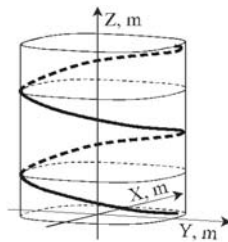

Figure 6. The picture of researched volumetric structure and trajectory of the electron's motion.

The case is interesting, when the spectator is in braking area of a field and researches character of driving of a particle. Researches (Fedulov, No.3659, 1996; Collinge, 2002) have shown, that in a brake field at a given entry point it is possible always to define value of initial entry speed, at which on any site of a trajectory the moving along an axis X will be infinitesimal. And, on the contrary, at any initial speed of a particle it is possible to create such brake field always, at which particle also will make infinitesimal moving along a X axis. Measured value of speed of electron driving in any place of a braking site of a potential field (20) will be always lower than the value of its initial entry speed. Or, in other words it is possible to speak, that the speed of a particle has the finite value, only for its local value. Besides it can appear, that measuring speed of a particle before reflection and after in two close points of brake field (at its infinitesimal moving along an X -axes)) one can have equal values. It can reduce the spectator to conclusion that the speed does not vary (rectilinear uniform driving). The spectator can consider this point as unique. Probably, one cannot speak about the character of particle's driving in all potential field on the basis of experimental definition of local value of particle's speed in braking electric fields only. The coincidence of these values measured in

various moments in close points, can reduce to an incorrect conclusions about the character of the particle driving. Particle's speed measured in another, sufficiently remote point of a trajectory of driving, can be different. The value of speed for an accelerating site of a field can be defined from the expression:

$$V(t) = V_0 \sqrt{1 \pm V_{Oy} p^2 x_O t \cdot V_O^{-2}}. \qquad (18)$$

Coordinate of an entry point under the radical in the (18) has always positive value for accelerating area. And for an area, in which an entry point coordinate has negative value (boundary conditions (10)), the expression under a radical in the (18) has positive value also. Other feature of the particle driving in the field with a distributed potential is that the trajectories of particle motion are curvilinear to sites of acceleration and deceleration (Fedulov, 2003). If one will consider the curvilinear motion of the particle as an approximate uniform driving on rectilinear trajectories, it will appear, that the particle's path on these trajectories are different for identical time. And then any hypothesis is required to explain this effect. In other words there is a danger of different treatment of results of experience, if the conditions and legitimacies of driving of the particle in a concrete potential field are not known for the spectator. These assertions can be confirmed by other reasons also. The process of periodic motion of the particle (acceleration and inhibiting action), in a symmetric electric field with a distributed potential is featured by Eq. (16). This motion can be decomposed into two sorts of motions - accelerated (deceleration and acceleration) driving circumscribed by the equation

$$x^2(t) + y^2(t) = x_0^2/2 \cdot [2Sin^2(pt + \pi/4) - Sh2pt], \qquad (19)$$

and uniformly accelerated driving on an arc of a circle:

$$x^2(t) + y^2(t) = x_0^2/2. \qquad (20)$$

One can see from these expressions, that for identical time of driving (for example, for half of period) the paths of the particle on different trajectories are different. It is possible to tell, that the replacement of driving on curvilinear trajectories on uniform rectilinear driving always will require introducing some correction factor.

6. The particle's motion in a symmetric thermoelectric field

The symmetric thermoelectric field can be created in structure, showed in fig. 5. The trajectories of an electron motion in a symmetric field with a distributed potential are represented there.

There can be closed trajectories of motion in a symmetric potential field under the condition (12). The electron's motion in a symmetrical electrical field is circumscribed by the equation

$$2[x^2(t) + y^2(t) = x_0^2[1 + 2Sin^2(pt + \pi/4) - Sh(2pt)]. \qquad (21)$$

The opportunity of creation of oscillating system in the structure with braking potential field, which were made by the distributed potentials and accelerating potential, is shown. The particle in such the field will make fourfold process of braking and accelerating.

7. The particle's motion in a symmetric volumetric thermoelectric field

The equations for the description of an electron motion in a volumetric thermoelectric field are following:

$$\begin{cases} \ddot{x} = -e/m \cdot E_x = \alpha_Y, \\ \ddot{y} = -e/m \cdot E_y = \alpha_X, \\ \ddot{z} = -e/m \cdot E_z = \alpha_z, \end{cases} \qquad (22)$$

where: $\alpha_z = -e \cdot (U_{max\,z} - U_{min\,z})/m \cdot l_z = -e/m \cdot k_z$, $U_{min\,z}$, $U_{max\,z}$, - minimum and maximum values of a potential on an axes z, $k_z = (T_{max\,z} - T_{min\,z})/l_z$ - distribution coefficient of an electrical potential. Solutions of these equations are the trajectories (fig. 6)

$$\begin{cases} 2 \cdot px(t) = p(x_0 + y_0)Ch(pt) + (V_{0x} + V_{0y})Sh(pt) + \\ \quad p(x_0 - y_0)Cos(pt) + (V_{0x} + V_{0y})Sin(pt), \\ 2 \cdot py(t) = p(x_0 + y_0)Ch(pt) - (V_{0x} + V_{0y})Sh(pt) - \\ \quad p(x_0 - y_0)Cos(pt) - (V_{0x} + V_{0y})Sin(pt), \\ \quad 2 \cdot z(t) = 2 \cdot z_0 + 2 \cdot V_{0z} \cdot + \alpha_z t^2 \end{cases} \qquad (23)$$

For forming of apparent particle's motion in (circular helix) it is necessary to create in addition the tangential constituent of velocity Z - direction. We can create such conditions at the cost of distributed electrical field along Z - axle and then the particle in the submitted structure will move over circular helix.

8. The particle's motion in a non-stationary thermoelectric field

In practice of creation of measuring and transforming instruments on structures with a distributed potential there are tasks about research of trajectories of driving of a particle in a non-stationary thermoelectric field. This task arises in conditions, when a varying potential adds to one of electrodes of structure with a distributed potential. We considered the non-stationary task under condition of a linear dependence between coefficients in a stationary and non-stationary thermoelectric fields. The potential in such a field can be described by the equation

$$U = \alpha_0(1 + \beta t)/d \cdot x \cdot y, \tag{24}$$

where: $\alpha_0 = ek(md)^{-1}$ - coefficients of stationary potential field, β - coefficient of change of a potential in time. An equation of motion looks like:

$$\begin{cases} \ddot{x} = -e/m \cdot E_x = (\alpha_0 + \beta t)y \\ \ddot{y} = -e/m \cdot E_y = (\alpha_0 + \beta)x. \end{cases} \tag{25}$$

We can consider the parameter exchange

$$t = \beta \cdot \alpha^{-1} + z \cdot \beta^{-1/3} \tag{26}$$

and using Airy integration

$$Ai(z) = \frac{1}{\pi} \int_0^\infty \cos(t^3/3 + zt)dt, \tag{27}$$

we get the general solution for eq. (26)

$$\lambda j(z) + \mu h(z) + \xi f(z) + \eta g(z) = 0 \tag{28}$$

where

$$\lambda = -\Gamma(1/3) \cdot 3^{1/3}(v_{0,x} + v_{0,y}) + \Gamma(2/3) \cdot 3^{2/3}\omega(x_0 + y_0) \cdot [2(1-\omega)]^{-1} \tag{29}$$

$$\mu = -\Gamma(1/3) \cdot 3^{1/3}(v_{0,x} + v_{0,y}) + \Gamma(2/3) \cdot 3^{2/3}\omega(x_0 + y_0) \cdot [2(1-\omega)]^{-1} \tag{30}$$

$$\xi = -\Gamma(1/3) \cdot 3^{1/3}(v_{0,x} - v_{0,y}) + \Gamma(2/3) \cdot 3^{2/3}\omega(x_0 + y_0) \cdot [2(1-\omega)]^{-1} \tag{31}$$

$$\eta = -\Gamma(1/3) \cdot 3^{1/3}(v_{0,x} + v_{0,y}) - \Gamma(2/3) \cdot 3^{2/3}\frac{2}{3}3^{\frac{2}{3}}\omega(x_0 - y_0) \cdot [2(1-\omega)]^{-1} \tag{32}$$

Here

$$\Gamma(z) = \int_0^\infty x^{z-1} \cdot e^{-x}dx \tag{33}$$

So, our main purpose is attained, since we have solved the equations of motion for the case, which is one of the most general cases of exactly solvable models. This aim can be enlarged in the sense, that all quadratic cases will be solved in the following papers.

9. The conclusion

The equations of motion of charged particles are output at simultaneous operation of electrical and thermoelectric fields with distributed potentials, and analytical solutions of them are obtained. Essentially variations of a trajectory of charged particles motion under operation of an additional thermoelectric field with a distributed potential are detected. This one can be used to create a new type of measuring instruments and functional converters.

References

Landau, L., E. Lifchic. The theory of a field. *Science, Moscow*, 2:78, 1988.

Lorents, G.A. Electromagnetic phenomena in system moving with any velocity smaller than of moving of light. *in Classics of a relativism edited by V.K. Frederics and D.D. Ivanenko (ONTI - Chief edition of the common - technical literature, Moscow)*, ??:16, 1935.

Connie, J. Chang-Hasnain, Pei-Cheng Ku, Jungho Kim and Shun-Lien Chuang. Variable Optical Buffer Using Slow Light in Semiconductor Nanostructures. *Proceedings of the IEEE*, 91:1884, 2003.

Leon, O. Chua. Nonlinear Circuit Foundations for Nanodevices. Part 1: The Four-Element Torus. *Proceedings of the IEEE*, 91:1830, 2003.

Mihael, Zitnik. Numerical Modelling of Transients in Electrical Systems. *Uppsala*, 2001.

Fedulov, V.I. The method of definition of power. *Patent of Russian Federation No.2052823*, 4, 1996.

Fedulov, V.I. The method of definition of power. *Patent of Uzbekistan No.3659*, 4, 1996.

Collinge, J.-P. Physics of semiconductor Devices. *Kluwer Acad. Publ.*, 436, 2002.

Groves, C., C.N. Harrison, J.P.R. David and G.J. Rees. Temperature dependence of breakdown voltage in $Al_xGa_{1-x}As$. *J. Appl. Phys.*, 96:5017, 2004.

Despere, G. and Th. Jager. Exploitation of thermotunnal effect for energy scavening. *J. Appl. Phys.*, 96:5026, 2004.

Al-Qahtani, H and S.K. Datto Thermoelastic waves in an anisotropic infinite plate. *J. Appl. Phys.*, 96:3645, 2004.

Fedulov, V.I. Concerning Regularities of Particle's Driving in Potential Fields (on example of electron's movement in electrical field with distributed potential) in ARW977788 'Emerging Applications of Vacuum-Arc-Produced Plasma, Ion and Electron Beams'. *edited by E.M. Oks and I.G. Brown (Kluwer Academic Publishers, Dordrecht, the Netherlands)*, 213, 2003.

Ropke, G. Statistiische Mechanik das Nichtgleichgewicht. *WEB Deutcher Verlag fer Vissenshaften Berlin*, 236, 1987.

Theory of relativistic ideal gas for quasi and ordinary particles

Mustaqim Jumaev

Bukhara State University, 11 M.Ikbal Str., 705018, Bukhara, Uzbekistan. E-mail: mjumaev@rambler.ru

Abstract. A theory of relativistic ideal gas (RIG), fluxons and electrons is presented. A distribution function of velocities (FRS) and the equation of state of the RIG are found, together with the distribution function of the observed frequencies.

Keywords: fluxon gas in thermalized Josefson systems; the criteria of degeneracy of the relativistic ideal gas; absolute minimum realization of the most probable state in the equilibrium system; temperature of the primary microwave cosmic background; primary quantum magnetic flow.

1. Introduction

As is well known, the theory of ideal gas (IG) formulated by Maxwell, Boltzmann and Gibbs, consider it as an ensemble of material point particles. The exponent of the distribution function for ensemble particles "is a linear function of the energies, which at the same time are quadratic functions of the momentum". The study of ideal gases has been developed further by Bose, Einstein, Fermi and Dirac who created quantum statistical physics (QSP). Further, soliton theory introduced non-linear modes in statistics. At the present time there does not exist a general soliton statistical theory for the non-linear evolution of systems. In this work we present some generalizations of certain results obtained earlier (Djumaev et al., 1997)-(Jumaev, 2004), where we achieved the idea of a soliton gas and found the statistics of a fluxon gas of thermalized superconductor system (or Josephson system). Using the analogy between solitons (or quasi particles) and particles we generalize this result for relativistic ordinary particles.

This paper is organized as follows. Section 2 presents non-trivial properties of the velocity distribution functions for RIG for quasi and ordinary particles in one dimensions. In section 3 we find the state equation for relativistic ideal gas of both types. Section 4 presents the distribution function for the observed frequency radiation generated for quasi and ordinary particles of the relativistic ideal gas, for fluxons under transfer radiation and radiative atoms of the relativistic ideal gas. Section 5 presents a generalization of the theory of the relativistic ideal gas in three dimensions and the distribution function for particles

in the relativistic ideal gas is found. Section 6 shows formulas for the temperature of relic radiation which is based on the exact Doppler formula and the velocity distribution function for particles forming this radiation is found. In conclusion we formulate the two most important physical results: initial quantum magnetic flow corresponding to the absolute minimal realization of the most probable state, the temperature of relic radiation corresponding also to the initial temperature of the primary cosmic radiation absolute minimal realization observed frequency radiation or in other words, the absolute minimal realization of the most probable state of the considered equilibrium system.

2. Non trivial properties of relativistic DFV

It is known that in order to define the distribution function of many particle systems it is enough to know the distribution function for one particle. Here we use that the mean average quantities for the ensemble are the thermodynamic averages. This is a consequence of the Ergodic theorem which till now is not proved in full mathematical rigor (Gibbs, 1946; Einstein, 1965). The last investigation shows that this property works for systems with elastic interaction and elastic collisions between particles. This gives us non-trivial possibilities to construct non-linear theory of ideal gases as solitons possessing unique properties of elastic interaction between quasi particles.

Earlier the velocity distribution function of quasi particles of a relativistic ideal gas for a one dimensional system, for example, fluxons in thermalized Josephson systems and electrons in a high temperature plasma was found.

Let us introduce non-trivial properties of the distribution function of velocities of a relativistic ideal gas for both cases. For this we remind that the probability to find a particle with velocity between v_x and $v_x + dv_x$ is

$$dW(v_x) = f(v_x)dv_x$$

$$\int f(v_x)dv_x = 1$$

where $f(v_x)$ is the velocity distribution function of particles of the relativistic ideal gas.

A) For quasi particles (fluxon in thermalized Josephson transmision lines (JTL)):

$$f(v_x) = A(1 - \frac{v_x^2}{c^2})^{-3/2}Exp[-a\frac{v_x^2}{c^2}(1 - \frac{v_x^2}{c^2})^{-1}]$$

where c is the Swihart's electromagnetic wave velocity in JTL; a is a parameter; which is defined at the end of the report (see figure 1.a).

B) For ordinary particles (electrons in relativistic plasma)

$$f(v_x) = B(1 - \frac{v_x^2}{c^2})^{-3/2} Exp[-b(1 - \frac{v_x^2}{c^2})^{-1/2}]$$

where x is light's velocities and b is a characteristic parameter which is defined in conclusions of the report (see also figure 1.b).

2.1. THE MOST PROBABLE VELOCITY

In order to define the statistical characteristics of a many particle system, for instance an ideal gas, their distribution function with some defined physical parameters (for example, velocity, momentum, energy, etc) should be fully determined. In particular it is physically important to define the velocity of particles corresponding to the most probable state, which is the maximum of the distribution function.

Using this condition we obtain the following results.

A) For fluxons A is a constant $(A = \sqrt{\frac{a}{\pi}})$ and for $0 < a < 3/2$ there are the three extreme points of the distribution of fluxon velocity (DFV),

$$v_{mp} = \pm c\sqrt{1 - \frac{2}{3}a} \qquad v_{lp} = 0.$$

B) For electrons (constant $B = 1/2cK_1(b)$, where $K_1(b)$ is the modified Bessel function). For $0 < b < 3$, there are three extreme points of DFV :

$$v_{mp} = \pm c\sqrt{1 - \frac{b}{3}} \qquad v_{lp} = 0.$$

where v_{mp} and v_{lp} are the most and least probable velocities for particles of an ideal relativistic gas for fluxons and electrons.

From the physical point of view the condition $a < 3/2$ and $b < 3$ can be interpreted as a criteria for a relativistic ideal gas to be degenerate. In other words, this means that if these conditions are satisfied, there exists a non-zero most probable velocity.

2.2. THE MEAN AVERAGE SQUARE VELOCITY

To define the mean velocity of particles in a relativistic ideal gas, as always, we use that

$$v_{sq} = \sqrt{< v^2 >}.$$

The results obtained are the following.

A) For fluxons:

$$v_{sq} = c[1 - \sqrt{\pi a}e^a erfc(\sqrt{a})]^{1/2}$$

where $erfc(x)$ is the error function.

B) For electrons:

$$v_{sq} = c[1 - \frac{K(b)}{K_1(b)}]^{1/2}$$

where $K(b)$ is the integral function depending on the parameter b.

We have for $a >> 1$ and $b >> 1$ the following results

A) For fluxons:

$$< v_x^2 >= c^2 \frac{1}{2a}.$$

B) For electrons:

$$< v_x^2 >= c^2 \frac{1}{b}.$$

So these coincide with the non relativistic result. Indeed, for a non-relativistic ideal gas theory - Maxwellian theory (for 1D systems)- we obtain

$$< E_k >= \frac{m}{2} < v_x^2 >= \frac{kT}{2}$$

or

$$< v_x^2 >= \frac{kT}{m}$$

So, the characteristic parameters for those systems are

$$a = \frac{E_0}{2kT}, \qquad E_0 = \frac{I_c \Phi}{2\pi},$$

and

$$b = \frac{E_0}{kT}, \qquad E_0 = mc^2.$$

where E_0 is the rest energy for fluxons and electrons, respectively; k is the Boltzman's constant; I_c is the critical superconductivity current, $\Phi = h/2e$ the quantum magnetic flow and T is the absolute temperature for the system.

3. The equation of state for the relativistic ideal gas

We obtain using the relativistic expression for energy and force that

$$< E >= N E_0 < (1 - \beta^2)^{-1/2} >,$$

$$< P >= \frac{n E_0}{3} < \beta^2 (1 - \beta^2)^{-1/2} >,$$

where $\beta = v_x c$, E is the energy and P is the pressure of ideal relativistic gas.

A) For fluxons

$$E = N E_0 \sqrt{\frac{a}{4\pi}} [K_0(\frac{a}{2}) + K_1(\frac{a}{2})] e^{a/2}$$

$$P = n E_0 \sqrt{\frac{a}{4\pi}} [K_0(\frac{a}{2}) - K_1(\frac{a}{2})] e^{a/2}$$

$$\frac{E}{V} - 3P = n E_0 \sqrt{\frac{a}{4\pi}} K_0(\frac{a}{2}) e^{a/2}$$

where n is the number of particles in unit volume (or length) and $K_i(x)$ $(i = 1, 2, 3)$ is the modified Henckel function (or entire Bessel function).

B) For electrons

$$E = N E_0 (\frac{1}{b} + \frac{K_0}{K_1})$$

$$P = \frac{n E_0}{3} (\frac{1}{b} + \frac{K_0}{K_1} - K_0)$$

$$\frac{E}{V} - 3P = n E_0 K_0$$

When $a >> 1$ and $b >> 1$ we obtain that

$$P \approx \frac{n E_0}{3} < \beta_x^2 >$$

that coincides with the equation of state for a non-relativistic ideal gas.

4. The minimally observed signal

The exact Doppler formulas for the relativistic particles

$$\nu = \nu_0 \sqrt{\frac{1-\beta}{1+\beta}}$$

($\beta = v_x c$) where ν and ν_0 are the observer and emission frequencies respectively (for $\beta = 0$). Since the particles in ideal gas are moving with the different velocities, the observer frequency defined by the DFV of particles of IRG. That is

$$\int f(v_x)dv_x = \int f(v_x(\nu))|\frac{dv_x}{d\nu}|d\nu = \int f(\nu)d\nu$$

where $f(\nu)$ is the profile form of the spectral radiation lines or distribution function of the observable frequency radiation.

A) JTL as system of SQUID'S. In this case using last formulas and DFV of fluxons we obtain

$$f(x) = \frac{1}{2}\sqrt{\frac{a}{\pi}}e^{a/2}(1+\frac{1}{x^2})Exp[-\frac{a}{4}(x^2+\frac{1}{x^2})]$$

where $x = (\frac{\nu}{\nu_0})^2$ (see figure 2.a).

B) The form of profile of SRL

$$f(x) = \frac{1}{4K_1(b)}(1+\frac{1}{x^2})Exp[-\frac{b}{2}(x+\frac{1}{x})]$$

where $x = (\frac{\nu}{\nu_0})^2$ (see figure 2.b).

It is easy to get that

$$x_m = \sqrt{\sqrt[3]{\frac{4}{3a}(r+s)} + \sqrt[3]{\frac{4}{3a}(r-s)} - 1/3}$$

with

$$r = \frac{2a}{9} + \frac{1}{2}; \qquad s = \sqrt{\frac{2}{3a}[(a-\frac{13}{16})^2 + \frac{343}{256}]}$$

is the most probable normalized frequency for fluxons and

$$\tilde{x}_m = \frac{1}{2}[\sqrt{2w - (y-z)} - \sqrt{(y-z)}]$$

with

$$y = 2\sqrt[3]{[\sqrt{\frac{1}{27} + \frac{1}{b^4} + \frac{1}{b^2}]}}, \qquad y = 2\sqrt[3]{[\sqrt{\frac{1}{27} + \frac{1}{b^4}} - \frac{1}{b^2}]}$$

$$w = \sqrt{(y-z)^2 + 3yz}.$$

is the analog for radiating particles.

Analysis of the last formula shows that in both cases, in principle, we can observe the minimal intensity of radiation or magnetic flow. This is in agreement with the absolute minimal realization of the most probable state in equilibrium system (see fig 3.a and fig 4.a, fig 3.b and fig 4.b). They are in agreement with the values of the observed distribution function observable frequencies and are equal to $I_m = f(x_m)$ for fluxons and $I_m = f(\tilde{x}_m)$ for radiating particles. For details of statistical characteristics of observable frequencies see reference (Jumaev, 2004).

5. Some physical aspects of theory of relativistic ideal gases

Three dimensional generalization of the theory of relativistic ideal gas.
A) For fluxons

$$f(v) = (\frac{a}{\pi})^{3/2} J Exp[-a\frac{\beta^2}{1-\beta^2}], \qquad \beta = \frac{v}{c}$$

B) For electrons

$$f(v) = \frac{1}{4\pi(mc)^3} \frac{b}{K_2(b)} J Exp[-\frac{b}{\sqrt{1-\beta^2}}], \qquad \beta = \frac{v}{c}$$

where J is given by

$$J = m^3(1-\beta^2)^{-5/2},$$

and is the Jacobian of transformation from momentum to velocities ((Gibbs, 1946)).

6. Statistical properties of the relic radiation

Using the exact Doppler formula and the DFV for particles forming the relic radiation we have obtained that

$$\frac{T}{T_0} = \frac{\nu}{\nu_0} = \frac{\sqrt{1-\beta^2}}{1+\beta cos\theta}$$

where β is the normalized velocities of the particles of an ideal relativistic gas which acts as a source of relic radiation.

In consequence, the statistical characteristic temperature of relic radiation is fully determined in terms of relativistic invariant spectrum of the cosmic microwave background radiation and the distribution velocity function of radiating particles, i.e., is described with the following expression (compare with the results of reference (Einstein, 1965))

$$< \frac{T}{T_0} >= \int \frac{\sqrt{1-\beta^2}}{1+\beta cos\theta} f(\overrightarrow{v})d\overrightarrow{v}$$

where

$$d\overrightarrow{v} = dv_x dv_y dv_z = v^2 dv sin\theta d\theta d\varphi$$

Angular distribution, dispersion and relative fluctuation of the temperature of the relic radiation ((Jumaev, 2004)) is found.

7. Conclusion

As follows from the previous analysis for quasi and ordinary particles gases there exists a critical value of parameters a and b for which the least value of the distribution function for observable frequencies is observed. From the physical point of view this is in agreement with the absolute minimal realization of the most probable state. As in any equilibrium distribution, there is an unique most probable state which the system tends to achieve. In consequence we conclude that the observable temperature of the relic radiation corresponds to this state. Or, what is the same, the temperature of such radiation correspond to the temperature originated in the primary microwave cosmic background and the primitive quantum magnetic flow.

Therefore we can formulate two important results:

A) Primary quantum magnetic flow

$$\Phi_0 = \frac{\Phi}{\sqrt{x_m}} \approx \frac{\Phi}{0.698} \approx 1.433\Phi,$$

see figure 4.a.

B) Temperature of the primary microwave cosmic radiation

$$T_0 = \frac{T}{\sqrt{\tilde{x}_m}} \approx \frac{T}{0.668} \approx 1.497T,$$

see figure 4.b. Here T is the observable temperature of the relic radiation at the present time ($T \approx 2.728K$). In consequence of the last

relation it follows that the temperature of the primary microwave cosmic radiation at the creation of the universe was $T_0 \approx 4.08K$. Then we get the following important conclusion: at temperature T_0 and due to the non linear fluctuation mechanism the vacuum was transformed into matter and radiation.

Discussion of the quantum field and astrophysical aspects of this problem are beyond the thematic of this conference and need special consideration.

References

M. R. Djumaev N. K. Nosirova *Abs. of Int. Sem. on Magn.*, 20-21 (1997).

M.R. Djumaev et al. *Third Int. Conf. Act. Probl. of Nuclear Physics* (1999), pp. 451-452.

M.R. Djumaev et al. *Journal of Tech.Phys.* 70, 5 (2000), 43-47.

M.R. Djumaev *Proc. Int. Conf. "Nonlinearity and Disorder"* (2001), 411-414.

M.R. Jumaev *"Evolution of random pulses at nonlinear systems with fluctuating parameters"-Dissertation for Doctor in Science in Theoretical Physics* (2002)

M.R. Jumaev *NATO Advanced Research Workshop, "Vortex dynamics and high temperature superconductors", Tashkent, Uzbekistan, 16-23 May 2002* (2002).

M.R. Jumaev *"Evolution of random and regular pulses at nonlinear systems with constant and fluctuating parameters", Bukhara, "Universitet"* (2004).

J. Gibbs *"Fundamental principles of statistical mechanics", Moscow-Leningrad, "Gostekhizdat", in Russian* (1946).

A. Einstein *"Theory of special relativity" in Selected Papers, edited by I.E.Tamm (in russian)* (1965).
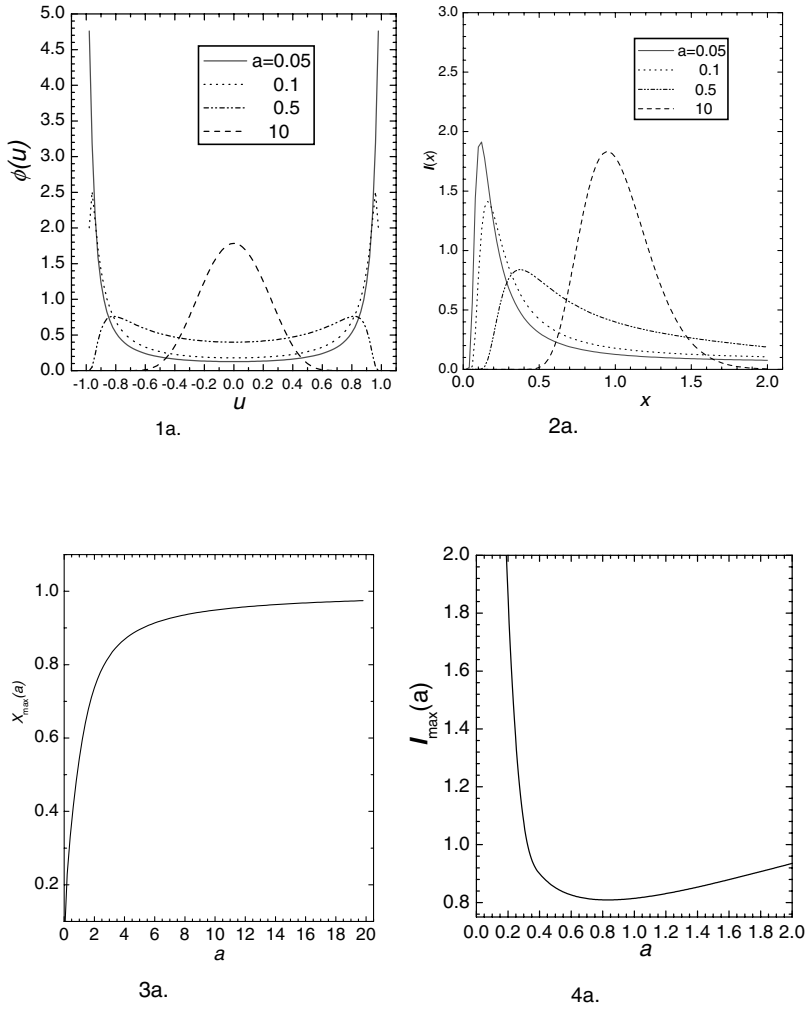
Mustaqim Jumaev

Figure 1. (1a) Distribution function of the velocity for the relativistic ideal gas of gluxions. (2a) Distribution functions of the observable frequencies. (3a) Most probable values of the observable frequencies as function of a. (4a) Absolute minimal realization of most probable states of system.
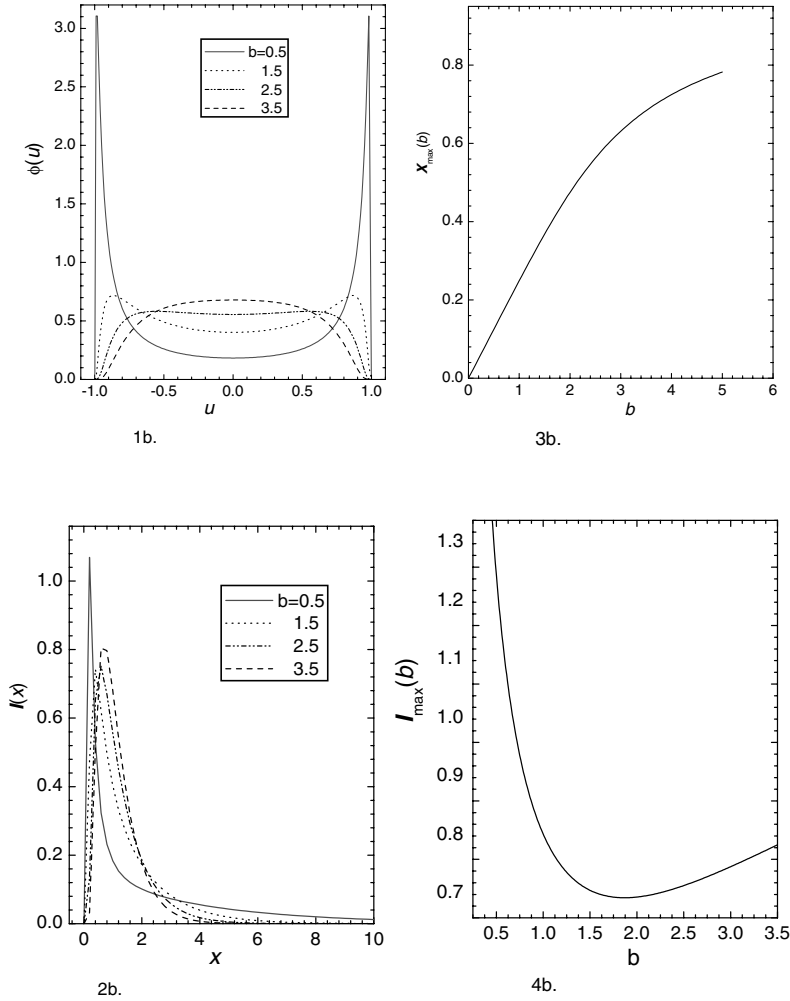
Figure 2. (1b) Distribution function of the velocity for the relativistic electrons. (2b) Distribution functions of the observable frequencies. (3b) Most probable values of the observable frequencies as a function of b. (4b) Absolute minimal realization of most probable states of system.

Finite-temperature quantum billiards

U.R. Salomov[*], D.U. Matrasulov, F.C. Khanna[†] and G.M. Milibaeva
Heat Physics Department of the Uzbek Academy of Sciences,
28 Katartal St., 700135 Tashkent, Uzbekistan

Abstract. A method for the computation of eigenvalues of quantum billiard is offered. This method is based on combining of boundary integral method and thermofield dynamics formalism.

Keywords: Quantum chaos, finite-temperature, quantum billiard

1. Introduction

Quantum chaos problem appeared in early eighties as a quantum mechanics of classically non-integrable systems and has been subject of extensive theoretical and experimental studies (Eckhardt, 1988; Gutzwiller, 1990) For the past decade quantum chaology has got new developments due to the newly appeared area, physics of mesoscopic systems (Richter, 1990; Alhassid, 1990). Remarkable feature of these systems is the fact that because of sizes such systems exhibit quantum as well as classical properties that allows them to be a convenient testing ground for the quantum-classical correspondence. Since nanostructures have also mesoscopic scales these systems are of practical importance, too. Such systems as quantum dots, quantum graphs, and quantum wires are expected to play central role in nanotechnology. Particle dynamics in mesoscopic systems could exhibit strong chaotic dynamics both in classical as well as in quantum regimes. This makes them attractive from the viewpoint of quantum chaology, too. Despite the considerable progress made in the study of dynamical chaos in mesoscopic systems some problems in this area still remain less-studied. Most important of them is the role of finite-temperature in quantum chaos. In this paper we treat quantum billiard problem at finite-temperature.

Another development in the quantum chaos where finite-temperature effects are important is the Quantum field theory. As it is shown by recent studies on the Quantum Chromodynamics (QCD) Dirac operator level statistics (Bittner et.al., 1999), nearest level spacing distribution of this operator is governed by random matrix theory both in confinement and deconfinement phases. In the presence of in-medium effects

---

[*] comments to salukrah@yahoo.com
[†] Physics Department, University of Alberta, Edmonton, T6G 2J1, Canada

these calculations should be performed within a finite-temperature field theory. Also, the spectra of hadrons subjected to the color screening exhibit considerable fluctuations (Gu et.al., 1999).

It should be noted that there is no universal approach for the study of finite-temperature effects in quantum chaos, in particular for quantum billiards. One of the way for introducing temperature in billiards is to consider softer-wall Gaussian boundaries. Relation (Stockmann et. al., 1997) between billiard geometry and the temperature has been considered.

The role of finite temperature in quantum chaos is studied within the imaginary time formalism via quantum action approach (Caron et al 2001).

In this work we use thermofield dynamics formalism (Takahashi et.al., 1996; Das, 1997) and boundary integral method (Li et.al., 1995) to get temperature dependence in the billiard energy level spectrum. Instead of the zero-temperature Green's function we use finite-temperature one which is obtained within the TFD formalism.

2. Zero temperature case

Before proceeding to finite-temperature treatment we briefly describe the boundary integral method for zero-temperature case, which was introduced to solve this type of problem (Berry et al, 1984; Tiago et al, 1997).

The billiard system is described by the following Schrödinger equation:

$$\hat{H}\psi(r) = \left[-\frac{\hbar^2 \nabla^2}{2m} + V(r) \right] \psi(r) = E\psi(r) \tag{1}$$

This differential equation can be replaced by an integral equation using the Green's function from which one can obtain E and $\psi(r)$. For this purpose, the Green's function $G(r, r'; E)$ of the operator $E - \hat{H}$, is defined as a solution of

$$[E - \hat{H}(r)]G(r, r', E) = \delta(r - r') \tag{2}$$

Multiplying eq.1 by $G(r, r'; E)$, eq.2 by $\psi(r)$ and adding the resulting equations yield

$$\psi(r)\delta(r - r') = G(r, r'; E)\hat{H}\psi(r) - \psi(r)\hat{H}G(r, r'; E) \tag{3}$$

and using the expression for the Hamiltonian we have

$$\psi(r)\delta(r - r') = \frac{\hbar^2}{2m}[-G(r, r'; E)\nabla^2\psi(r) + \psi(r)\nabla^2 G(r, r'; E)] \tag{4}$$

recalling the identity $u\nabla^2 v = \nabla(u\nabla v) - \nabla u \nabla v$, valid for any differentiable functions $u(r)$ and $v(r)$ and integration with respect to r over the domain D; applying Green's formula, the integral can be expressed as a line integral along ∂D

$$\psi(r') = \frac{\hbar^2}{2m} \oint_{\partial D} ds(r)[\psi(r)\partial_\nu G(r,r';E) - G(r,r';E)\partial_\nu \psi(r)]$$

where $\partial_\nu = \nu(r)\partial_r$ normal derivative. This is so-called BIE (boundary integral equation). Applying the normal derivative operator $\nu(r')\partial_{r'}$ to both sides of equation which, according to definition:$u(s) = \partial_\nu \psi(r)$ and with boundary conditions: $\psi(r) = 0$, $\partial_\nu \psi(r) = arbitrary$, $\forall r \in \partial D$ finally we arrive at

$$u(r') = -\frac{\hbar^2}{m} \oint_{\partial D} ds(r)u(r)\partial_{\nu'}G(r,r';E)$$

for free particles inside a plane Euclidean billiard with the Green's function given as

$$G(r,r';E) = -\frac{im}{2\hbar^2}H_0^{(1)}(k|r'-r|)$$

and for BIE we have

$$u(r') = -\frac{ik}{2} \oint_{\partial D} ds(r)cos\phi(r,r')u(r)H_1^{(1)}(k|r'-r|)$$

where $cos\phi(r,r') \equiv \nu' \frac{r'-r}{r'-r}$ is the cosine of the angle between the exterior normal vector to ∂D at r' and the unit vector corresponding to $r' - r$.

In order to calculate eigenvalues of energy use is made of the corresponding Boundary Element Equation (BEE) of this BIE. And for matrix elements of BEE we have:

$$C_{ij}(k) = \delta_{ij} + \frac{ik}{2}\Delta s_i cos\phi_{ij}H_1^{(1)}(kr_{ij}) \qquad (5)$$

$$cos\phi(r,r') \equiv \nu_i \frac{\mathbf{r_{ij}}}{r_{ij}}$$

Energy eigenvalues can be determined as the roots of the determinant of C_{ij}

$$det|C_{ij}(k)| = 0$$

3. Finite temperature case

In the case of finite temperature a similar approach can be used based on the boundary integral method, where instead of the zero temperature Green's function, finite-temperature Green's function derived within TFD formalism is used. Introducing finite-temperature within the thermofield dynamics formalism is based on two steps, doubling of the Hilbert space and Bogolyubov transformations (Takahashi et.al., 1996; Ademir, 2005).

In TFD the Green's function is a 2×2 matrix:

$$G_\beta(r, r'; E) = \begin{pmatrix} G_\beta^{11}(r, r'; E) & G_\beta^{12}(r, r'; E) \\ G_\beta^{21}(r, r'; E) & G_\beta^{22}(r, r'; E) \end{pmatrix}$$

where elements are given as

$$G_\beta^{11}(r, r'; E) = G_0(r, r'; E) + v^2(\beta, \omega)(G_0(r, r'; E) - G_0^*(r, r'; E)),$$

$$G_\beta^{22}(r, r'; E) = -G^*(_0r, r'; E) + v^2(\beta, \omega)(G_0(r, r'; E) - G_0^*r, r'; E)),$$

$$G_\beta^{12}(r, r'; E) = G_\beta^{12}(r, r'; E) = v(\beta, \omega)(1 + v^2(\beta, \omega))^{1/2}(G_0(r, r'; E) - G_0^* (r, r'; E)),$$

where $G_0(r, r'; E)$ is the zero-temperature Green's function,

$$v^2(\beta, \omega) = \frac{1}{e^{\beta\omega} - 1} \text{for bosons}$$

$$v^2(\beta, \omega) = \frac{e^{-\beta\omega}}{e^{-\beta\omega} + 1} \text{for fermions.}$$

and G_0^* is the complex conjugate of G_0.

Physical observables are related to $G_\beta^{11}(r, r'; E)$ only. Therefore in the case of the billiard the finite-temperature Green's function is

$$G(r, r'; E) = -\frac{im}{2\hbar^2}(1 + 2v^2(\beta, \omega))H_0^{(1)}(k|r' - r|).$$

Using in-boundary integral method for this Green's function gives us finite-temperature analog of the matrix given in Eq. (5),

$$C_{ij}(k, \beta) = \delta_{ij} + \frac{ik}{2}\Delta s_i cos\phi_{ij}(1 + 2v^2(\beta, \omega)H_1^{(1)}(kr_{ij}). \qquad (6)$$

Then finite-temperature eigenvalues of the quantum billiard can be obtained from the equation

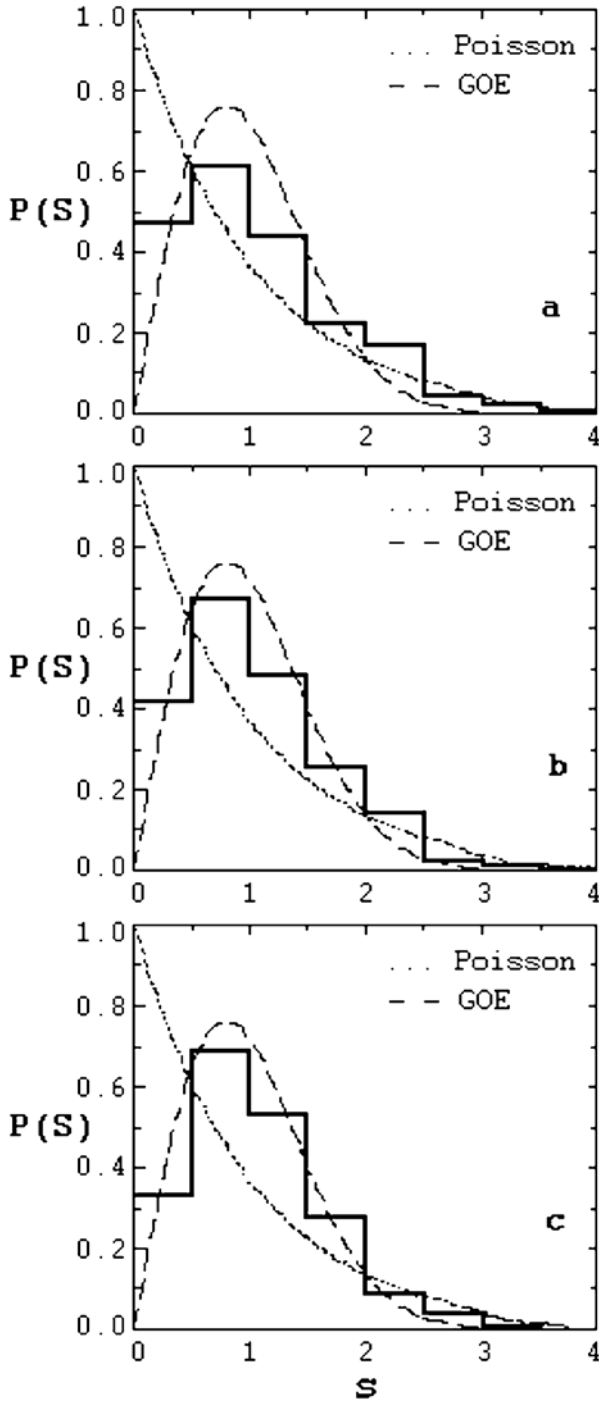$$det|C_{ij}(k, \beta)| = 0. \qquad (7)$$

Figure 1. The nearest neighbor level spacing distribution for various parameter of temperature a) zero temperature case; b) $\beta = 0.1$; c) $\beta = 0.01$;

In Fig.1, the nearest neighbor level spacing distribution which is plotted using the spectra calculated from Eq. 7 is presented. As it can be clear from this plot, the finite-temperature effects lead to histogram more Gaussian, which means strengthening of quantum chaos by finite-temperature. Thus using the thermofield dynamics formalism we have given a prescription for the calculation of finite-temperature energy eigenvalues of the quantum billiard. This method allows us to treat quantum chaos at finite-temperature using billiard models.

4. Acknowledgement

References

Eckhardt, B. *Physics Reports*, 163(4):205-297, 1988.

Gutzwiller, M. C. *Chaos in classical and quantum systems, New York, Springer Verlag*, 1990.

K. Richter, *Semiclassical Theory of Mesoscopic Quantum Systems. Springer, Berlin* 2000.

Y.Alhassid, *Rev.Mod.Phys* **72**, 895, (2000).

Bittner, E., H. Markum and R. Pullrich. *hep-lat/0110222*.

Gu, J.- z., H.- s. Zong, Y.-x. Liu and E.-g. Zhao. *Phys. Rev. C.*, 60(3) 035211, 1999.

Takahashi, Y., H.Umezawa. *Internatinal Journal of Modern Physics A*, 10:1755, 1996.

Das, A. Finite Temperature Field Theory (*World Scientific, New York*, 1997).

Baowen Li and Marko Robnik *chao-dyn/9507002*

Hans-Jurgen Stöckmann, Ulrich Stoffregen and Michael Kollmann Fachbereich, *J. Phys. A: Math. Gen.*, 30 129, 1997. Caron, L. A., H. Jirari, H. Kröger, X.Q. Luo, G. Melkonyan, K.J.M. Moriarty Phys.Lett. A288 (2001) 145-153

Matsubara, T. *Prog. Theoretical Physics*, 14:351, 1955.

da Silva, J. D., F.C.Khanna, A. Matos Neto and A.E.Santana. *Phys. Rev. A*, 66 052101, 2002.

Tiago, M. I., T.O. de Carvalho, and M.A.M. de Aguiar. *Phys. Rev. E.*, 55:65-70, 1997.

Berry, M. V., and M. Wilkinson. *Proc. of Royal Soc. (London)*, 392:15, 1984.

Santana Ademir. *see contribution to this proceedings.*

Chaotic dynamics of the relativistic kicked rotor

G.M. Milibaeva[a] *, D.U. Matrasulov[a], U.R. Salomov[a] and Bala Sundaram[b]

(a) Heat Physics Department of the Uzbek Academy of Sciences,
28 Katartal St., 700135 Tashkent, Uzbekistan
(b)Graduate Faculty in Physics and Department of Mathematics,
City University of New York-CSI,
2800, Victory Boulevard
Staten Island, New York, 10314

Abstract. The relativistic periodically driven classical and quantum rotor problems are studied. Kinetical properties of the relativistic standard map is discussed. Quantum rotor is treated by solving the Dirac equation in the presence of the periodic δ-function potential. The relativistic quantum mapping which describes the evolution of the wave function is derived. The time-dependence of the energy are calculated.

Keywords: Dynamical chaos, kicked rotor, relativistic systems

1. Introduction

Kicked rotor is a paradigm in classical and quantum chaology that allows a treatment of periodically driven systems with great success (Casati et.al., 1979; Izrailev, 1990). Besides being the simplest system whose dynamics is completely described by simple both classical (standard) and quantum mappings it also provides excellent model for many periodically driven systems in atomic and molecular physics. Being quantised such systems exhibit some new feautures compared to classical case. One of these features is the so-called quantum localization phenomenon which means the supression of classical chaos in the quantum case (Izrailev, 1990; Casati et.al., 1987; Casati et.al., 1987a; Casati et.al., 1988).

In the classical case, the evolution of the kicked rotor dynamics is described by the well-known standard map (Chirikov, 1979). This map greatly facilitates the qualitative treatment of the system. A map describing the evolution of the wave function can be obtained in the quantum case, too (Casati et.al., 1979). In spite of the fact, that the first work with detailed treatment of the quantum kicked rotor appeared 23 years ago (Casati et.al., 1979), this system is still studied extensively (Casati et.al., 1987; Izrailev, 1990).

---

* comments to sabmax1@mail.ru

In this work we treat classical and quantum relativistic kicked rotor problem. Using the relativistic standard map, we calculate the average energy of the classical rotor for various values of the relativistic factor. The relativistic quantum rotor is treated using the same approach as in the pioneering work (Casati et.al., 1979).

As is well known (Chirikov, 1979; Izrailev, 1990), the phase-space evolution of the norelativistic classical kicked rotor is described by nonrelativistic standard map. The analysis of this map shows that the motion of the nonrelativistic kicked rotor is accompanied by unlimited diffusion in the energy and momentum. However, this diffusion is suppressed in the quantum case (Casati et.al., 1979; Izrailev, 1990). Such a suppression of diffusive growth of the energy can be observed when one considers the (classical) relativistic extention of the classical standard map (Nomura et.al., 1992) which was obtained recently by considering the motion of the relativistic electron in the field of an electrostatic wave packet. The relativistic generalization of the standard map is obtained recently (Nomura et.al., 1992)

$$P_{n+1} = P_n - \frac{K}{2\pi} \sin(2\pi X_n), \tag{1}$$

$$X_{n+1} = X_n + \frac{P_{n+1}}{\sqrt{1 + \beta^2 P_{n+1}^2}}, \tag{2}$$

where

$$K = \frac{4\pi^2 e E_0 k}{m_0 \omega^2} \qquad \beta = \frac{\omega}{kc}. \tag{3}$$

It is clear that the relativistic standard map depends on two parameters K and β. Here β is defined as a relativistic factor for the group velocity, ω/k.

Being mainly concerned with the derivation and treatment of the dynamical and symmetry properties of the relativistic standard map, some papers (Nomura et.al., 1992) do not concern with the kinetical aspects of this map. However, the kinetical properties are interesting for particle transport and acceleration processes. Here we calculate the time-dependence of the energy for various values of β including the resonance case.

Fig. 1 (a) shows the energy as a function of time for resonance ($\beta = 1/2\pi$) and nonresonance ($\beta = 0.1$) cases.

In the resonance case the diffusive growth of the energy can be observed while it is highly suppressed for the value of $\beta = 0.1$ which is less than $\beta = 1/2\pi$. However, the diffusion is not unlimited even for the resonance case.

Thus the diffusion in the energy of the relativistic kicked rotor described by the relativistic standard map depends on the value of parameter β: for smaller values of β which are close to 0 the growth of the energy is linear and the suppression is not considerable; for intermediate values the energy grows (not linearly) for some time and suppression occurs after that. For higher values (which starts from $\beta = 0.1$) excluding resonance cases the growth of the energy is completely suppressed.

Definition of the relativistic quantum rotor is given earlier (Aldinger et.al., 1983). According to this definition the relativistic quantum rotor is an object having three limits:

i) the elementary limit, in which it is an elementary (pointlike) particle,

ii) the classical limit, in which it coincides with the classical relativistic rotor and,

iii) the nonrelativistic limit, in which it coincides with the nonrelativistic quantum rotor.

Quantum dynamics of the relativistic kicked rotor is described by the following Dirac equation:

$$i\frac{\partial \psi}{\partial t} = \hat{H}\psi \tag{4}$$

where

$$\hat{H} = \alpha_\theta p_\theta + \beta + \varepsilon_0 \delta(t) cos\theta \tag{5}$$

and

$$\delta_T(t) = \sum_{m=-\infty}^{\infty} \delta(t - mT)$$

with T being the period of the kicks. The method to be used for solution of this equation is the same as in (Casati et.al., 1979). The wave function $\psi(\theta, t)$ is expanded in terms of the relativistic free rotor eigenfunctions

$$\psi(\theta, t) = \sum_n A_n(t)\Phi_n \tag{6}$$

Over any period T between delta function kicks the $A_n(t)$ evolves as

$$A_n(t + T) = A_n(t)e^{-iE_nT} = A_n(t)e^{-i\sqrt{1+n^2}T} \tag{7}$$

During the infinitesimal time interval of a kick the Eq. (4) takes the form

$$i\frac{\partial \psi}{\partial t} = -\varepsilon_0 cos\theta \delta_T(t)\psi \tag{8}$$

Integration of this equation over the infinitesimal interval (before and after the kick) $(t + T)$ to $(t + T^+)$ yields

$$\psi(\theta, t + T^+) = \psi(\theta, t + T)e^{ikcos\theta}, \tag{9}$$

where $k = \varepsilon_0 T$. Expanding both sides of this equation in relativistic free rotor eigenfunctions we have

$$\sum_n A_n(t + T^+)\Phi_n(\theta) = \sum_{r,s} A_r(t+T)\Phi_r(\theta)b_s(T)e^{is\theta}. \quad (10)$$

Here we have used the expression

$$e^{ikcos\theta} = \sum_s b_s(k)e^{is\theta}, \quad (11)$$

where

$$b_s(k) = i^s J_s(k) = b_{-s}(k), \quad (12)$$

J_s are the ordinary Bessel function of the first kind.

Multiplying both sides of Eq. (10) and taking into account that

$$\int_0^{2\pi} d\theta \Phi_n^* \Phi_r e^{is\theta} = 2\left(1 + \frac{nr}{(1+E_n)(1+E_r)}\right)\delta_{s,n-r} \quad (13)$$

we get the relativistic quantum mapping

$$A_n(t + T^+) = 2\sum_r A_r(t)b_{n-r}(k)\left(1 + \frac{nr}{(1+E_n)(1+E_r)}\right)e^{-iE_r T} \quad (14)$$

It is clear from these equations that in the nonrelativistic limit ($n, r \ll 1$) the relativistic quantum mapping coincides with its nonrelativistic counterpart (Casati et.al., 1979). Also, the structure of the relativistic mapping shows that there are no resonances in the relativistic case due to the fact that E_n is an irrational number in this case.

The main feature of the quantum kicked rotor is the quantum localization phenomenon, which implies suppression of the diffusive growth of energy of the quantum kicked rotor compared to the energy of the classical rotor (Izrailev, 1990). The time dependence of the energy can be calculated as

$$\langle E \rangle = \sum_n \beta^{-2}\sqrt{\beta^2 n^2 + 1}\rho(n) \quad (15)$$

In Fig.1(b) we compare the time-dependence of the energy for various valus of the relativistic factor, $\beta = c^{-1}$. For smaller values of β it behaves as its nonrelativistic counterpart, while in strongly relativistic regime the saturation occurs quite quickly.

Thus we have treated relativistic kicked rotor problem both in classical and quantum contexts. It is found that in the classical case the diffusion is strongly suppressed in highly relativistic and ultrarelativistic regimes. However, the energy growth can be observed in resonances
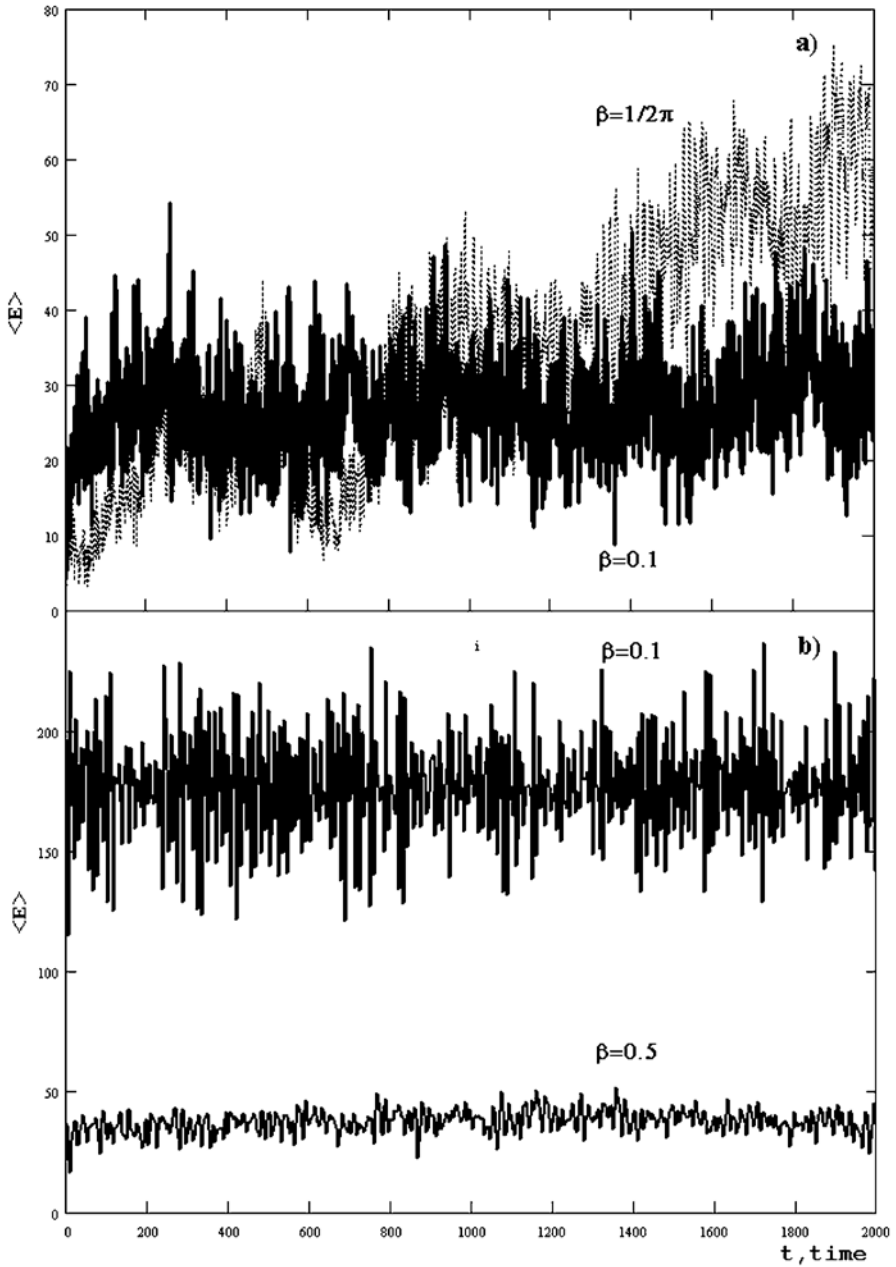
Figure 1. The average energy for various parameter of β a) classical case $\beta = 0.1$, $\beta = 1/2\pi$ (resonance case); b) quantum case $\beta = 0.1$, $\beta = 0.5$ at the fixed $K = 5$.

during a long time period, which is also saturated. In quantum problems the situation is completely different than that in the nonrelativistic case. There is no quantum localization phenomenon in this case. Saturation occurs in quite short time period. Also, the absence of resonance states is a feature of the relativistic quantum kicked problem.

2. Acknowledgements

References

Chirikov, B. V. *Physics Reports*, 52(5):263-379, 1979.

Casati, G., B. Chirikov, F. Izrailev and J.Ford. *Lecture Notes of Physics*, 93(6):334-351, 1979.

Izrailev, F. M. *Physics Reports*, 196(5-6):299-392, 1990.

Casati, G., J. Ford, I. Guarneri and F. Vivaldi. *Physical Review A*, 34(2):1413-1419, 1987.

Casati, G., B. Chirikov, D. Shepelyansky and I. Guarneri. *Physics Reports*, 154(2):77-123, 1987.

Casati, G., I. Guarneri, D. Shepelyanky. *IEEE J.Quantum Electronics*, 24(7):1420-1444, 1988.

Aldinger, R. R., A. Bohm, P. Kielanovski, M. Loewe, P. Magnollay, N.Mukunda. *Phys. Rev. D*, 28(12):3020-3031, 1983.

Nomura, Y. H., Y. Ichikawa, W. Horton. *Phys. Rev. A*, 45(2):1103-1115, 1992.

Arsenovic, D., C. Bozic. *Nuovo Cimento B*, 115(02):185-214, 2000.

Bohm, A. *Phys. Rev. D*, 28(12):3032-3040, 1983.

Hafner, H. and N.J.Ionescu-Pallas. *Acta Physics Austriaca*, 18(6):38, 1964.

Herbert, C., H. *Phys. Rev. D*, 30(12):2683-2689, 1984.

Arkhiezer, A., I., V.B.Berestetsky *Quantum electrodynamics*, Interscience Publishers, 1965.

The largest Lyapunov exponents for the relativistic hydrogen-like atom in a uniform magnetic field

S.K. Avazbaev * D.U. Matrasulov and P.K. Khabibullaev
Heat Physics Department of the Uzbek Academy of Sciences,
28 Katartal St., 700135 Tashkent, Uzbekistan

Abstract. Classical regular and chaotic dynamics of a system is treated on the basis of solution of classical equations of motion. Appropriate scaling of the relativistic Hamiltonian is presented. To determine the degree of chaoticity of the system the largest Lyapunov exponents are calculated as a function of the scaled energy, which includes both the energy and magnetic field strength. It is found that by increasing the scaled energy the motion of the electron becomes more chaotic.

Keywords: Dynamical chaos, Lyapunov exponents

1. Introduction

For the past three decades deterministic classical systems with chaotic dynamics have been the subject of extensive study (Chirikov, 1979)-(Sagdeev et. al., 1988). Dynamical chaos is a phenomenon peculiar to the deterministic systems, i.e. the systems whose motion in some state space is completely determined by a given interaction and the initial conditions. Under certain initial conditions the behaviour of these systems is unpredictable.

Many realistic systems and their models have been considered to study dynamical chaos phenomenon. Such systems as, kicked rotor and various billiard geometries allow one to treat chaotic behavior of deterministic systems successfully.

It should be noted that there is a limited number of works on classical relativistic dynamical chaos (Chernikov et.al., 1989; Drake and et.al., 1996; Matrasulov, 2001). However, the study of the relativistic systems is important both from fundamental as well as from practical viewpoints. Such systems as electrons accelerating in laser-plasma accelerators (Mora, 1993), heavy and superheavy atoms (Matrasulov, 2001) and many other systems in nuclear and particle physics are essentially relativistic systems which can exhibit chaotic dynamics and need to be treated by taking into account relativistic dynamics. Besides that interaction with magnetic field can also strengthen the role of the relativistic effects since the electron gains additional velocity in a magnetic field.

---

* comments to sanat@hpd.uzscinet.uz

Nonrelativistic hydrogen atom in a constant uniform magnetic field is a paradigm of classical chaology (Friedrich and Wintgen, 1989; Delande and Gay, 1986; Schweizer et.al., 1988). In this work we address a relativistic extention of this problem considering relativistic hydrogen-like atom in a constant uniform magnetic field. Dealing with the scaled Hamiltonian we calculate so called largest Lyapunov exponent (LLE), which completely describes the dynamics of the system with 2 degrees of freedom (Meyer, 1986).

2.   The relativistic Hamiltonian

The classical Hamiltonian of the relativistic hydrogen-like atom in a uniform magnetic field is given as (Landau, 1980)

$$H = \sqrt{m_e^2 c^4 + (\vec{p} - \frac{e}{c}\vec{A})^2} - \frac{Ze^2}{r}, \qquad (1)$$

where $\vec{A}$ is the vector potential of the external electromagnetic field. For the case when the field strength B is directed along the z-axis the Hamiltonian (7) can be written as

$$H = \sqrt{m_e^2 c^4 + p^2 + 2m_e \omega L_z + m_e^2 \omega^2 (x^2 + y^2)} - \frac{Ze^2}{r}. \qquad (2)$$

The frequency ω in (2) is half the cyclotron frequency $\omega = \frac{1}{2}\omega_c = \frac{eB}{2m_e c}$, m_e is the mass of the electron, L_z is the z-component of the angular momentum. The Hamiltonian (2) in the relativistic system of units $(m_e = c = \hbar = 1)$ and cylindrical coordinates is

$$H = \sqrt{1 + p_\rho^2 + p_z^2 + \frac{m^2}{\rho^2} + m\gamma + \frac{\gamma^2 \rho^2}{4}} - \frac{Z}{\sqrt{\rho^2 + z^2}}, \qquad (3)$$

$\gamma = B/B_0$ is the field strength written in units of $B_0 = m^2 e^3 c/\hbar = 2.35 \times 10^5 \ T$ and m- is the azimuthal (magnetic) quantum number.

We scale coordinates and momenta to remove γ dependence of the Hamiltonian (3)

$$r = \gamma'^{-1/2}\tilde{r}, \quad p = \sqrt{\tilde{p}^2 \gamma' - 1}, \qquad (4)$$

where $\gamma' = \alpha^2 \gamma$, α is the fine structure constant. This transformation leads to the Hamiltonian

$$\epsilon = \gamma'^{-1/2}H = \sqrt{\tilde{p}_\rho^2 + \tilde{p}_z^2 + \frac{m^2}{\tilde{\rho}^2} + m + \frac{\tilde{\rho}^2}{4}} - \frac{Z}{\sqrt{\tilde{\rho}^2 + \tilde{z}^2}}. \qquad (5)$$

Eq. (5) shows that the classical dynamics depends on the scaled energy $\epsilon = E\gamma'^{-1/2}$. As it is clear from Eq. (5) the Hamiltonian has the singularity at $\tilde{r} = 0$. This singularity can be removed by performing the following transformations

$$e^\nu = \tilde{r} - \tilde{z}, \quad e^\mu = \tilde{r} + \tilde{z},$$

and

$$p_\nu = \frac{d\nu}{d\tau}, \quad p_\mu = \frac{d\mu}{d\tau}.$$

Then new momenta are connected with old ones by the relation

$$\tilde{p}_\rho^2 + \tilde{p}_z^2 = \frac{1}{4} \frac{e^\nu p_\nu^2 + e^\mu p_\mu^2}{(e^\nu + e^\mu)^2}, \tag{6}$$

where the scaled time is given by

$$dt = (e^\nu + e^\mu)^{3/2} d\tau \tag{7}$$

with t, τ being real and scaled times, respectively. Then the Hamiltonian takes the form

$$h = \sqrt{\frac{1}{4}(e^\nu p_\nu^2 + e^\mu p_\mu^2) + (e^\nu + e^\mu)^2 \left[m + \frac{m^2}{e^{\nu+\mu}} + \frac{e^{\nu+\mu}}{4} \right]} - \epsilon(e^\nu + e^\mu) \equiv 2Z. \tag{8}$$

The equations of motion obtained from the Hamiltonian (5) at a fixed value of the scaled energy are equivalent to ones obtained from the Hamiltonian (8).

3. The Method for computing the largest Lyapunov exponent

The most important quantitative measure for the degree of chaoticity is provided by the Lyapunov exponents (LE) (Eckmann and Ruelle, 1985; Wolf et. al., 1985). The LE defines the rate of exponential divergence of initially nearby trajectories, i.e. the sensitivity of the system to small changes in initial conditions. A practical way for calculating the LE is given by Meyer (Meyer, 1986). This method is based on the Taylor-expansion method for solving differential equations. This method is applicable for systems whose equations of motion are very simple and higher-order derivatives can be determined analytically (Schweizer et.al., 1988).

Consider an n-dimensional continous-time dynamical system

$$\frac{dz}{dt} = \mathbf{F}(\mathbf{z}, t), \tag{9}$$

where $\mathbf{z} = (\mathbf{z_1}, \mathbf{z_2}, ..., \mathbf{z_n})$ and $\mathbf{F}$ is an n-dimensional vector field. Let $\mathbf{Z}(t) = \mathbf{z}(t) - \mathbf{z_0}(t)$ denote deviations from the fiducial trajectory $\mathbf{z_0}(t)$. Linearizing Eq. (9) around this trajectory, we obtain

$$\frac{d\mathbf{Z}}{dt} = \mathbf{DF}(\mathbf{z_0}(t), t) \cdot \mathbf{Z}, \tag{10}$$

where $\mathbf{DF}$ denotes the $n \times n$ Jacobian matrix.

Integrating the linearized equations along the fiducial trajectory yields the tangent map $M(\mathbf{z_0}, t)$ which takes the initial variables $\mathbf{Z}^{in}$ into the time-evolved variables $\mathbf{Z(t)} = \mathbf{MZ^{in}}$. Let Λ be a matrix $\Lambda = \lim_{t \to \infty} (M\tilde{M})^{1/2t}$, where $\tilde{M}$ denotes the matrix transpose of M. The Lyapunov exponents then equal the logarithm of the eigenvalues of Λ (Eckmann and Ruelle, 1985).

Using the method described in (Janaki et.al., 1999) we get the following differential equations for the LLE and angles which are also dynamical variables evolving simultaneously with LLE.

$$\dot{\lambda}_L = cos^2\theta_1 cos^2\theta_2 cos^2\theta_3 df_{11} + sin^2\theta_1 cos^2\theta_2 cos^2\theta_3 df_{22}+$$

$$+sin^2\theta_2 cos^2\theta_3 df_{33} + sin^2\theta_3 df_{44} - \frac{1}{2}sin2\theta_1 cos^2\theta_2 cos^2\theta_3(df_{12} + df_{21})-$$

$$-\frac{1}{2}cos\theta_1 sin2\theta_2 cos^2\theta_3(df_{31} + df_{13}) - \frac{1}{2}cos\theta_1 cos\theta_2 sin2\theta_3(df_{41} + df_{14})+$$

$$+\frac{1}{2}sin\theta_1 sin2\theta_2 cos^2\theta_3(df_{32} + df_{23}) + \frac{1}{2}sin\theta_1 cos\theta_2 sin2\theta_3(df_{42} + df_{24})+$$

$$+\frac{1}{2}sin\theta_2 sin2\theta_3(df_{43} + df_{34}), \tag{11}$$

$$\dot{\theta}_1 = -\frac{\dot{Q}_{11}sin\theta_1 + \dot{Q}_{21}cos\theta_1}{cos\theta_2 cos\theta_3}, \tag{12}$$

$$\dot{\theta}_2 = -\frac{\dot{Q}_{31} + \dot{Q}_{41}sin\theta_2 tan\theta_3}{cos\theta_2 cos\theta_3}, \tag{13}$$

$$\dot{\theta}_3 = -\frac{\dot{Q}_{41}}{cos\theta_3}, \tag{14}$$

where df_{ij} - are Jacobian matrix elements and $\dot{Q}_{ij}$ - are functions of angles and Jacobian matrix elements. The largest Lyapunov exponents are calculated by solving these differential equations by the fourth-order Runge-Kutta algorithm.
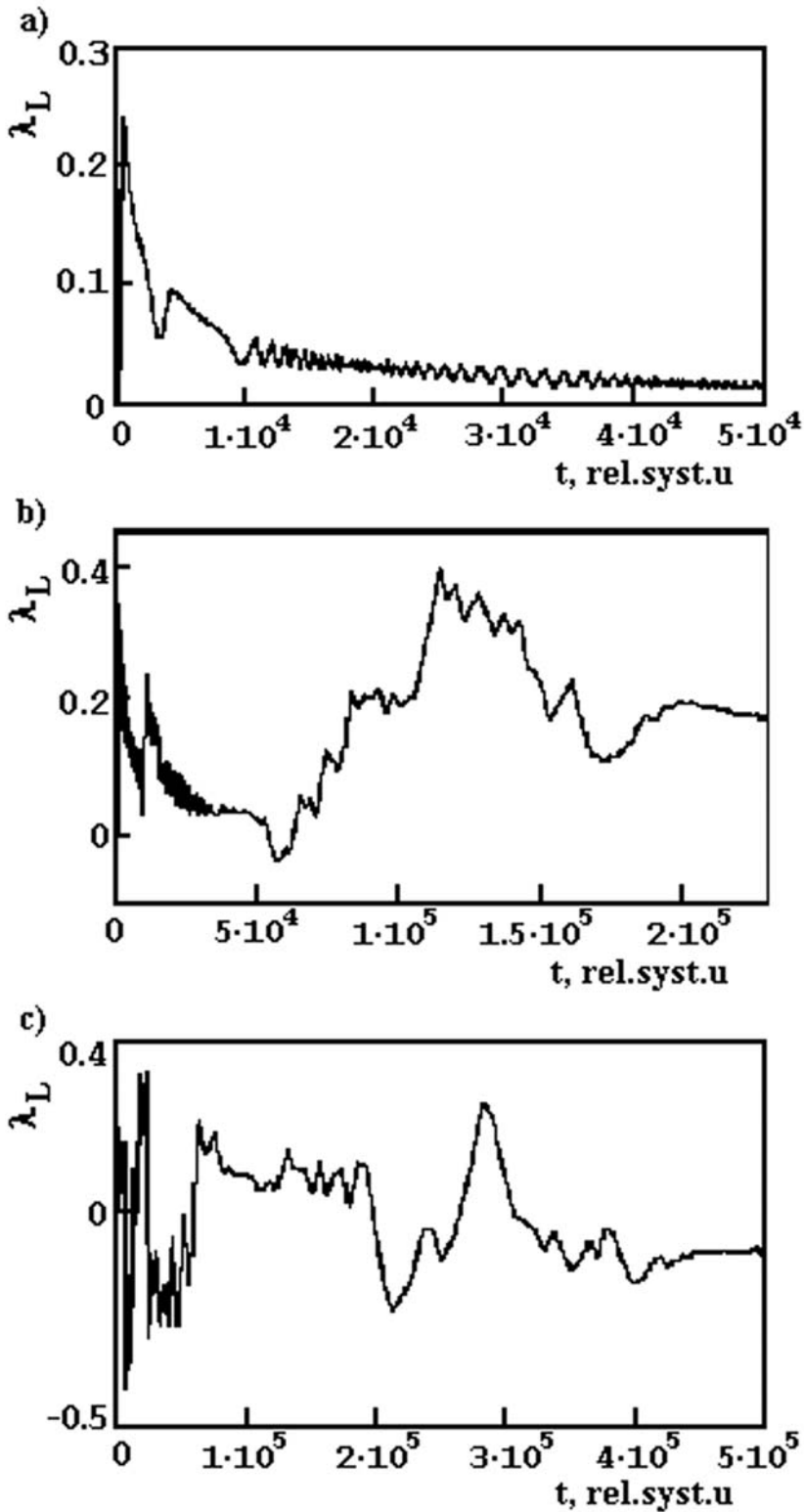
Figure 1. The largest Lyapunov exponents for a) $\epsilon = 10$; b) $\epsilon = 50$; c) $\epsilon = 100$ at the fixed $Z = 50, m = 1$.

4. Results and conclusion

It is clear from Eq.(7) that the real time t flows dynamically. In computing the trajectories with sufficiently small step sizes of τ, the elapsing of real time t was followed by simultaneously integrating the relation (7). Here the real time t will be given in the relativistic system of units. The Lyapunov functions $\lambda_L(t)$ are in units of $1/t$.

In Figs. 1(a)-1(c) the Lyapunov functions are shown for $Z = 50, m = 1$ and different scaled energies. Fig. 1(a) shows results for $\nu = 0$, $\mu = 0$, $\epsilon = 10$. $\lambda_L(t)$ tends to zero indicating that this trajectory is regular. This figure has the same shape as that for the nonrelativistic hydrogen atom in a uniform magnetic field (Schweizer et.al., 1988). In Fig. 1(b) the Lyapunov function for $\nu = 0$, $\mu = 0$, $\epsilon = 50$ is shown. It tends to some positive value, which means that this trajectory is chaotic. While for $\nu = 0$, $\mu = 0$, $\epsilon = 100$ (Fig. 1(c)) we find that the trajectory is unstable.

As follows from the above treatment for higher values of the scaled energy ϵ which includes both the energy and magnetic field strength the behaviour of the system becomes more chaotic, while for the smaller values regular behaviour is observed.

References

Chirikov, B. V. *Physics Reports*, 52(5):263-379, 1979.

Eckhardt, B. *Physics Reports*, 163(4):205-297, 1988.

Sagdeev, R. Z., D. A. Usikov, G. M. Zaslavsky. Nonlinear Physics: From the Pendulum to Turbulence and Chaos. *Harwood Academic Publishers*, New York, 1988.

Chernikov, A. A T. Tel, G. Vattay, G.M. Zaslavsky, *Phys. Rev. A*, 40(7):4072-4076, 1989.

Drake, S. P, C.P. Dettmann, N.E. Frankel and N.J. Cornish. *Phys. Rev. E*, 53(2):1351-1361 (1996).

Antonsen, T. M, Jr. and P. Mora. *Physics of Fluids B*, 5(5):1440, 1993.

Matrasulov, D. U. *Physics of Atomic Nuclei*, 64(2):253-255, 2001.

Friedrich, H. and D. Wintgen. *Physics Reports*, 183:37-79, 1989.

Delande, D. and J.C. Gay. *Phys. Rev. Letters*, 57(16):2006-2009, 1986.

Schweizer, W., R. Niemeier, H. Friedrich, G. Wunner and H. Ruder. *Phys. Rev. A*, 38(4):1724-1733, 1988.

Meyer, H. -D. *Journal of Chemical Physics*, 84(6):3147-3161, 1986.

Landau, L. D. The Classical Theory of Fields: Volume 2 (Course of Theoretical Physics Series). *Butterworth-Heinemann; 4th edition*, 1980.

Eckmann, J.-P and D. Ruelle. *Rev. of Modern Physics*, 57(3):617-656, 1985.

Wolf, A, J. Swift H. Swinney, and J. Vastano. *Physica*, 16D:285, 1985.

Janaki, T. M., G. Rangarajan, S. Habib and R.D. Ryne. *Phys. Rev. E*, 60(6):6614-6626, 1999.

Fundamental Interactions

Thermal field theory:
Algebraic aspects and applications to confined systems

A.E. Santana[a], J.M.C. Malbouisson[b], A.P.C. Malbouisson[c] and
F.C. Khanna[d]

(a) Instituto de Fisica, Universidade de Brasilia,
70910-900, Brasilia, DF, Brazil
Physics Department, Theoretical Physics Institute,
(b) Instituto de Fisica, Universidade Federal da Bahia
Campus de Ondina, 40210-340, Salvador, BA, Brazil
(c) Centro Brasileiro de Pesquisas Fisicas
Rua Dr. Xavier Sigaud, 150, 22290-180, Rio de Janeiro RJ, Brazil
(d) University of Alberta Edmonton, Alberta T6G 2J1 Canada and
TRIUMF 4004, Westbrook mall,
Vancouver, British Columbia V6T 2A3, Canada

Abstract. A resume of recent trends in thermal field theory is presented with
emphasis on algebraic aspects. In this sense, some representations of Lie symme-
tries provide, in particular, a unified axiomatization, via the so-called thermofield
dynamics (TFD) approach, of different methods treating thermal systems. First, a
connection between imaginary and real time formalism is presented, with emphasis
on physical paradigms of thermal physics. The study of Poincare Lie algebra leads
us to a derivation of Liouville-like equations for the scalar and Dirac field, and as an
application the Juttiner distribution for bosons is obtained. Exploring the fact that a
finite temperature prescription results to be equivalent to a path-integral calculated
on $R^{D-1} \times S^1$, where S^1 is a circle of circumference $\beta = 1/T$, a generalization
of the thermal quantum field theory is presented in order to take into account the
space confinement of fields. In other words, we consider the TFD and the Matsubara
mechanism on a $R^{D-N} \times S^{1_1} \times S^{1_2} ... \times S^{1_N}$ topology, describing time (temperature)
and space confinement. The resulting geometrical approach is then applied to analyse
the $3 - D$ $N-$ component Gross-Neveu model compactified in a square of side L,
at a temperature T. The main result is a closed expression for the large-N effective
coupling constant, $g(L, T)$. For large values of the fixed coupling constant, we obtain
simultaneously asymptotic freedom, spacial confinement and a decoupling transition
at a temperature T_d. Taking the Gross-Neveu model as describing the effective
interaction between quarks, the confining length and the deconfining temperature
obtained are of the order of the expected values for hadrons.

Keywords: Thermal Fields, Lie-groups, Compactification, Gross-Neveau model.

Introduction

Just fifty years ago, with an acclaimed paper by Matsubara (T. Mat-
subara, 1955), there was the emergence of a systematic approach for
the quantum field theory at finite temperature ($T \neq 0$), presently well-
known as the *imaginary time* approach. Since then the development

of the thermal field formalism, followed in a broad sense along the lines of the achievements of the $T = 0$ quantum field theory, and its first generalization was carried out by Ezawa, Tomonaga and Umezawa (H. Ezawa et.al., 1957), who extended the Matsubara's work to the relativistic quantum field theory, discovering in particular the periodicity (antiperiodicity) conditions for the Greens's functions of boson (fermion) fields. Many concepts, some originally introduced in $T = 0$ theories, could then be considered with the counterpart ideas at finite temperature; and we can list, for instance, the thermal Ward-Takahashi relations, the Goldstone theorem, KMS (Kubo, Martin, Schwinger) relations, renormalization procedures, the notion of nonabelian gauge field among others, with all its consequences for the particles physics (A.L. Fetter et.al., 1971; J.I. Kapusta, 1989; M. Le Bellac, 1996).

Despite the successes, even with its generalizations, difficulties in thermal field theory remain to be overcome in order to deal with experimental and theoretical demands. In fact, numerous studies, in particular using quantum chromodynamics (A. Smilga, 2001), have been carried out in an attempt to understand, for instance, the quark-gluon plasma at finite temperature; and in this common effort, some underlying aspects have been identified. For example, the coupling constants for π, σ, w and ρ mesons decrease to zero at a certain critical temperature, which are, respectively, given by: $T_c^\pi = 360$ MeV, $T_c^\sigma = 95$ MeV, $T_c^w = 175$ MeV and $T_c^\rho = 200$ MeV. All these results require a general and consistent calculation to establish the phase transition; reinforcing thus the claim for the development of the finite temperature field theory in the context of the standard model, which would provide us with a more definitive answer about the transition from hadrons to quark-gluon plasma. In this realm, effective models have been largely employed in trials to obtain clues to the behaviour of interacting particles. Among them, one recognizes the seminal paper by Dolan and Jackiw (L. Dolan et.al., 1974), which performs the calculations for the effective potential at finite temperature, and the Gross-Neveu model (D.J. Gross et.al., 1974), dealing with the direct four-fermion interaction, which has also been analyzed at finite temperature as an effective model for QCD and for superconducting systems (see for instance (C. de Calan et.al., 1991; H.R. Christiansen et.al., ; J-P. Blaizot et.al.,) and references therein).

Beyond that, despite the numerous instances in high energy physics and in condensed matted physics where (real) time dependance is essential, a nonequilibrium theory has not been fully developed as yet. This difficulty was recognized early as a flaw in the Matsubara equilibrium formalism and has been motivating attempts to construct real-time formalisms at finite temperature (D.N. Zubarev et.al., 1991; R. Floreanini

et.al., 1988; S.P. Kim et.al., ; S.P. Kim et.al., 2000; S. Sengupta et.al., 2003).

One of these real-time method is the closed-time path formulation due to Schwinger and Keldysh (J. Schwinger, 1961). The approach depends on a closed path in the complex-time plane such that the contour goes along the real axis and then back. From this procedure an effective doubling of the degrees of freedom emerges, such that the Green's functions are represented by 2×2 matrices. Actually, this kind of doubling has been recognized as an intrinsic characteristic of real-time theories, providing in turn a correct definition for perturbative series, which is not the case of the Matsubara method (for a detailed discussion see for example (M. Le Bellac, 1996)).

Concepts in quantum field approach have been usually implemented as a matter of fundamental ingredients: a quantum formalism is strongly founded on the basis of algebraic representation (vector space) theory. This suggests that a $T \neq 0$ field theory needs a real-time *operator* structure. Such a theory was presented by Takahashi and Umezawa 30 years ago and they labelled it *Thermofield Dynamics* (TFD) (Y. Takahashi et.al., 1975). As a consequence of the real-time requirement, a doubling is defined in the original Hilbert space of the system, such that the temperature is introduced by a Bogoliubov transformation.

TFD has been developed for practical purposes and some results should be mentioned. The KMS condition follows in TFD after an algebraic analysis; the Goldstone theorem can be proved within this formalism with a quite amazing physical and mathematical appeal and the perturbative scheme can be set up with Feynman rules established to carry out calculations completely in parallel with the zero-temperature quantum field theory (H. Umezawa, 1993). Thus it has been successfully applied to study superconductivity (H. Umezawa et.al., 1982); magnetic systems like ferromagnets and paramagnets (J.P. Whitehead et.al., 1984); quantum optics and transport phenomena (A. Mann et.al., 1989; A. Mann et.al., 1989; S. Chaturvedi et.al., 1999; L.M. Silva et.al., 1997) ; d-branes (M.C.B. Abdala et.al., 2001; M.C.B. Abdala et.al., 2003); among others. Furthermore, the propagators are 2×2 matrices; from this fact the association of the Matsubara and Schwinger-Keldysh methods has been analysed in a unified sense via TFD (H. Chu et.al., 1994).

Formally the thermal theory can be established, via TFD, within c^* algebra (I. Ojima, 1981; A.E. Santana et.al., 1999) and symmetry groups (A.E. Santana et.al., 1999), opening a broad spectrum of possibilities for the study of thermal effects. For instance, the kinectic theory has been formulated for the first time as a representation theory of Lie symmetries (A.E. Santana et.al., 2000) and elements of

the q-group have been considered, where the effect of temperature is related to a deformation in the Weyl-Heisenberg algebra (T. Kopf et.al., 1997; E. Celeghini et.al., 1998).

Exploring topological aspects of a thermal formalism, we can observe that the final prescription results in a scheme of compactification in time of the $T = 0$ theory. That is the Matsubara prescription results are equivalent to a path-integral calculated on $R^{D-1} \times S^1$, where S^1 is a circle of circumference $\beta = 1/T$. As a consequence, the thermal field theory can be thought, in a generalized way, as a mechanism to deal simultaneously with spatial constraints and thermal effects in a field theory model. These ideas have been developed recently for the Matsubara formalism (A.P.C. Malbouisson et.al., 2002; A.P.C. Malbouisson et.al., 2002; J.C. da Silva et.al., 2002) as well as for TFD and applied to the Casimir effect considering the electromagnetic and fermionic fields within a box (see the paper by Khanna et al in this volume and (J.C. da Silva et.al., 2002; H. Queiroz et.al.,)), to the $\lambda\phi^4$ model as the Ginsburg-Landau theory for superconductors (L.M. Abreu et.al., 2005), and to the Gross-Neveu model at $T = 0$ temperature (A.P.C. Malbouisson et.al., 2004).

In this report we will review some algebraic aspects of TFD to construct representations for the Poincaré symmetries leading, in particular, to the kinetic theory and to Liouville-von Neumann equations for the Klein-Gordon and Dirac Field. We emphasize the aspects of unification of different thermal theories and, by exploring the topological nature of such approaches, we address the problem of spatial confinement of fermions at $T \neq 0$. We then generalize the results of Ref. (A.P.C. Malbouisson et.al., 2004) treating the Gross-Neveau model via the Matsubara mechanism taking a path-integral formalism on a $R^{D-d} \times S^{1_1} \times ... \times S^{1_d}$. In the case of $D = d = 3$ we demonstrate that the model presents simultaneouly asymptotic freedom and spacial confinement. Considering such a model as an effective description for the quark interaction, we can take $m \approx 350\,MeV \simeq 1.75\,fm^{-1}$, for the constituent quark mass. Then we find a confining lengh, $L_c \simeq 3.13\,m^{-1} \approx 1.79\,fm$, and a deconfining temperature, $T_d \simeq 127\,MeV$. These values should be compared with the experimentally measured proton charge diameter ($\approx 1.74\,fm$) and the estimated deconfining temperature ($\approx 200\,MeV$) for hadronic matter, respectively. To the best of our knowledge this is the first time that such results are derived analytically.

1. Thermal theories and compactification

In this section we review the construction of thermal theories starting with TFD to show the connection among different methods. A mechanism for space and time compactification of a quantum field theory is then discussed in this context.

1.1. THERMOFIELD DYNAMICS

The ensemble average of an operator, A, in thermal equilibrium is given by

$$\langle A \rangle_\beta = Z^{-1}(\beta) Tr(e^{-\beta H} A), \tag{1}$$

where $Z(\beta)$ is the partition function, $\beta = 1/k_B T$, with k_B being the Boltzmann constant, and H the Hamiltonian. Then assuming that $H|n\rangle = E_n|n\rangle$ and $\langle n|m\rangle = \delta_{nm}$, we write

$$\langle A \rangle_\beta = Z^{-1}(\beta) \sum_n e^{-\beta E_n} \langle n|A|n\rangle. \tag{2}$$

The pertubative techniques of zero temperature field theory can be used in the thermal context if we define a state $|0(\beta)\rangle$ so that (Y. Takahashi et.al., 1975; H. Umezawa, 1993)

$$\langle A \rangle_\beta \equiv \langle 0(\beta)|A|0(\beta)\rangle = Z^{-1}(\beta) \sum_n e^{-\beta E_n} \langle n|A|n\rangle.$$

This can be the case if we consider a product space, $|n, \tilde{m}\rangle = |n\rangle \otimes |\tilde{m}\rangle$, such that, $A|n, \tilde{m}\rangle = (A|n\rangle) \otimes |\tilde{m}\rangle$. Therefore, defining

$$|0(\beta)\rangle = \sum_n f_n(\beta)|n, \tilde{n}\rangle,$$

we can realize in a straightforward way that $|0(\beta)\rangle$ reproduces the statistical average. That is, taking the expectation of an operator A in the state $|0(\beta)\rangle$, we obtain,

$$\begin{aligned} \langle 0(\beta)|A|0(\beta)\rangle &= \sum_{n,m} f_n^*(\beta) f_m(\beta) \langle n, \tilde{n}|A|m, \tilde{m}\rangle \\ &= \sum_{n,m} f_n^*(\beta) f_m(\beta) \langle n|A|m\rangle \delta_{nm}. \\ &= \sum_n f_n^*(\beta) f_n(\beta) \langle n|A|n\rangle. \end{aligned}$$

Comparing with Eq. (2) we have $f_n^*(\beta) f_n(\beta) = Z^{-1}(\beta)\, e^{-\beta E_n}$, which has the solution

$$f_n(\beta) = Z^{-1/2}(\beta)\, e^{-\beta E_n/2}.$$

Hence we introduce a thermal state $|0(\beta)\rangle$ if the degrees of freedom are doubled. Let us explore some preliminary, but not the least, consequences of what we have just introduced, analysing the case of bosons.

Considering a bosonic oscillator characterized by the Hamiltonian $H = wa^\dagger a$, the state $|0(\beta)\rangle$ can be constructed if for each bosonic operator a , another bosonic operator, say $\widetilde{a}$, is introduced such that the tilde and non-tilde variables obey the following algebra

$$[a_k, a^\dagger] = [\widetilde{a}, \widetilde{a}^\dagger] = 1, \quad [a, \widetilde{a}] = [a, \widetilde{a}^\dagger] = 0. \tag{3}$$

This mapping of $a \to \widetilde{a}$ is a consequence of the doubling in the Hilbert space of the original system, $|\phi\rangle \to |\phi, \widetilde{\phi}\rangle = |\phi\rangle \otimes |\widetilde{\phi}\rangle$, which is defined by

$$a|\phi\rangle \;\to\; a|\phi, \widetilde{\phi}\rangle = (a|\phi\rangle) \otimes |\widetilde{\phi}\rangle, \tag{4}$$

$$\widetilde{a}|\widetilde{\phi}\rangle \;\to\; \widetilde{a}|\phi, \widetilde{\phi}\rangle = |\phi\rangle \otimes (\widetilde{a}|\widetilde{\phi}\rangle) \stackrel{def}{=} |\phi\rangle \otimes (\langle\phi|a^\dagger). \tag{5}$$

In this way, the state $|0(\beta)\rangle$ is given by

$$\begin{aligned}
|0(\beta)\rangle &= Z^{-1/2}(\beta) \sum_n \exp(-\beta n\omega/2)|n, \widetilde{n}\rangle \\
&= (1 - e^{\beta\omega}) \exp\{\exp[(-\beta\omega/2)a^\dagger\widetilde{a}^\dagger]\}|0, \widetilde{0}\rangle,
\end{aligned} \tag{6}$$

satisfying $\langle 0(\beta)|0(\beta)\rangle = 1$.

Let us consider in Eq. (1), $A = n = a^\dagger a$. Using Eq. (6) we get

$$n = \langle 0(\beta)\rangle |a^\dagger a|0(\beta)\rangle = \frac{e^{-\beta\epsilon}}{1 - e^{-\beta\epsilon}} = \sum_{n=1}^{\infty} e^{-\beta\varepsilon n}. \tag{7}$$

Notice that, the physical variables are described by non-tilde operators, while the tilde operators, up to now, play a role of ancillary variables only. However, as we will see in Section 3, the full Hilbert space has the original set of non-tilde operators associated to dynamical observables, whilst the tilde operators are connected with the generators of symmetries.

The results derived earlier can be written via a Bogolubov transformation introduced by

$$U(\beta) = e^{-iG}, \tag{8}$$

where $G = -i\theta(\beta)(a^\dagger\widetilde{a}^\dagger - a\widetilde{a})$, such that $\theta(\beta)$ is defined via

$$\cosh\theta(\beta) = \frac{1}{[1 - e^{-\beta\epsilon}]^{1/2}} \equiv u(\beta), \tag{9}$$

$$\sinh\theta(\beta) = \frac{1}{[e^{\beta\epsilon} - 1]^{1/2}} \equiv v(\beta). \tag{10}$$

Using Eq. (8), the thermal state $|0(\beta)\rangle$ is given by $|0(\beta)\rangle = U(\beta)|0, \widetilde{0}\rangle$. On the other hand, thermal operators are introduced by

$$a(\beta) = U(\beta)aU^\dagger(\beta) \quad and \quad \widetilde{a}(\beta) = U(\beta)\widetilde{a}U^\dagger(\beta). \tag{11}$$

It should be noticed that $a(\beta)$ and $\widetilde{a}(\beta)$ satisfy the same algebraic relation as those given in Eq. (3), and also that $a(\beta)|0(\beta)\rangle = \widetilde{a}(\beta)|0(\beta)\rangle = 0$. Then the thermal state $|0(\beta)\rangle$ is a vacuum for $a(\beta)$ and $\widetilde{a}(\beta)$ (otherwise, $|0, \widetilde{0}\rangle$ is the vacuum for the operators a and $\widetilde{a}$). As a result, the thermal vacuum average of a non-thermal operator is equivalent to the Gibbs canonical average in statistical physics. As a consequence, the thermal problem can be treated by a Bogoliubov transformation, such that the thermal state describes a condensate with the mathematical characteristics of a pure state.

At this point it is interesting to introduce a doublet notation that is more adequate to treat with infinite degrees of freedom. Considering then an arbitrary operator A we define

$$(A^a) = \begin{pmatrix} A(\beta) \\ \widetilde{A}^\dagger(\beta) \end{pmatrix}, \quad (A^{a\dagger}) = \left(A^\dagger(\beta) \ , \ \widetilde{A}(\beta) \right). \tag{12}$$

The algebraic rules for the thermal bosonic operators are, therefore, written as $[a^a(\beta), a^{b\dagger}(\beta)] = \delta^{ab}$; $a, b = 1, 2$. The Bogoliubov transformation, Eq. (8), is in turn written as a 2×2 matrix,

$$\mathcal{B} = \begin{pmatrix} u\ (\beta) & -v(\beta) \\ -v(\beta) & u(\beta) \end{pmatrix}, \tag{13}$$

such that from Eq. (11) we have $a^a = (\mathcal{B}^{-1})^{ab}a^b(\beta)$ and $a^{\dagger a} = a^{\dagger b}(\beta)\,\mathcal{B}^{ba}$, that is

$$a = u(\beta)\,a(\beta) + v(\beta)\,\widetilde{a}^\dagger(\beta) \ , \quad \widetilde{a} = u(\beta)\,\widetilde{a}(\beta) + v(\beta)\,a^\dagger(\beta). \tag{14}$$

Notice that the thermal average can be given by taking the vacuum average $|0, \widetilde{0}\rangle$ of a thermal non-tilde variables. For instance for the particular case of the bosonic number operator, $n = a^\dagger a$, the thermal distribution, as in Eq.(7) reads,

$$n(\beta) = \langle 0, \widetilde{0}|a^\dagger(\beta)a(\beta)|0, \widetilde{0}\rangle \equiv \frac{1}{e^{\beta\epsilon} - 1}, \tag{15}$$

which is the boson distribution. The same scheme can be then generalized for a quantum field, a subject treated in the following.

1.2. Thermal Propagators

In the case of the free scalar field, since we have equation of motion for the tilde and non-tilde variables, the β−dependent Klein-Gordon field theory is given by the Lagrangian (Y. Takahashi et.al., 1975; H. Umezawa, 1993)

$$\widehat{L} = \frac{1}{2}\partial_\mu\phi(x;\beta)\partial^\mu\phi(x;\beta) - \frac{m^2}{2}\phi(x;\beta)^2 \tag{16}$$

$$-\frac{1}{2}\partial_\mu\widetilde{\phi}(x;\beta)\partial^\mu\widetilde{\phi}(x;\beta) + \frac{m^2}{2}\widetilde{\phi}(x;\beta)^2, \tag{17}$$

where the metric $g^{\mu\lambda}$ is such that $diag(g^{\mu\lambda}) = (1,-1,-1,-1)$. This Lagrangian gives rise to the equations of motions

$$(\partial_\mu\partial^\mu + m^2)\phi(x;\beta) = 0\,, \qquad (\partial_\mu\partial^\mu + m^2)\widetilde{\phi}(x;\beta) = 0.$$

Therefore, in TFD the Lagrangian can be written as $\widehat{L} = L - \widetilde{L}$ and, in consequence, the Hamiltonian is $\widehat{H} = H - \widetilde{H}$ (this is a general result, which can be used for every field, as we will see in section 3).

The two-point Green function for the β-scalar field is defined, then, by

$$\begin{aligned} G(x - x';\beta)^{(ab)} &= \langle 0,\widetilde{0}|T[\phi(x;\beta)^a\phi(x';\beta)^b|0,\widetilde{0}\rangle \\ &= \frac{1}{(2\pi)^4}\int d^4k\, G(k;\beta)^{ab}e^{ik(x-x')}, \end{aligned} \tag{18}$$

where

$$G(k;\beta)^{(ab)} = \mathcal{B}^{-1}(k_0;\beta)G_o(k)^{ab}\mathcal{B}(k_0;\beta),$$

with

$$\mathcal{B}(k_0,\beta) = \begin{pmatrix} u(k_0,\beta) & -v(k_0,\beta) \\ -v(k_0,\beta) & u(k_0,\beta) \end{pmatrix}, \tag{19}$$

and

$$(G_o(k)^{ab}) = \begin{pmatrix} G_0(k) & 0 \\ 0 & \widetilde{G}_0(k) \end{pmatrix} = \begin{pmatrix} \frac{1}{k^2-m^2+i\epsilon} & 0 \\ 0 & \frac{-1}{k^2-m^2-i\epsilon} \end{pmatrix}. \tag{20}$$

The components of $G(x - x')^{(ab)} = \langle 0,\widetilde{0}|T[\phi(x)^a\phi(x')^b|0,\widetilde{0}\rangle$, for a massless bosonic field can be explicitly written, by using Eq. (20) with $m = 0$, as

$$G_0^{(11)}(x - x') \equiv G_0(x - x') = -\frac{i}{(2\pi)^2}\frac{1}{(x-x')^2 + i\eta}, \tag{21}$$

$$G_0^{(22)}(x - x') \equiv \widetilde{G}_0(x - x') = \frac{i}{(2\pi)^2}\frac{1}{(x-x')^2 - i\eta}, \tag{22}$$

and $G_0^{(12)}(x - x') = G_0^{(21)}(x - x') = 0$. Then we have

$$G(k; \beta)^{(ab)} = \begin{pmatrix} G(k; \beta)^{11} & G(k; \beta)^{12} \\ G(k; \beta)^{21} & G(k; \beta)^{22} \end{pmatrix},$$

with

$$
\begin{aligned}
G(k; \beta)^{11} &= G_0(k) + v^2(k, \beta)[G_0(k) + \widetilde{G}_0(k)], \\
G(k; \beta)^{12} &= G(k; \beta)^{21} = v(k, \beta)[1 + v^2(k, \beta)]^{1/2}[G_0(k) + \widetilde{G}_0(k)], \\
G(k; \beta)^{22} &= \widetilde{G}_0(k) + v^2(k, \beta)[G_0(k) + \widetilde{G}_0(k)].
\end{aligned}
$$

The physical information is given by $G(k; \beta)^{11}$.

Using the definition of $\mathcal{B}(k_0, \beta)$ given in Eq. (19), with

$$n(k_0, \beta) = v(k_0, \beta)^2 = 1/[e^{\beta k_0} - 1], \tag{23}$$

and $u(k_0, \beta)^2 = v(k_0, \beta)^2 + 1 = 1/[1 - e^{-\beta k_0}]$, the components of $G(k; \beta)^{ab}$ read

$$
\begin{aligned}
G(k; \beta)^{(11)} &= \frac{1}{k^2 - m^2 + i\epsilon} - 2\pi i\, n(k_0; \beta)\, \delta(k^2 - m^2), \\
G(k; \beta)^{(22)} &= \frac{-1}{k^2 - m^2 - i\epsilon} - 2\pi i\, n(k_0; \beta)\, \delta(k^2 - m^2), \\
G(k; \beta)^{(12)} &= G(k; \beta)^{21} = -2\pi i\, [n(k_0; \beta) + n(k_0; \beta)^2]^{1/2}\, \delta(k^2 - m^2).
\end{aligned}
$$

Since the non-tilde operators describe physical variables, $G(k; \beta)^{11}$ is the physical propagator to be used to treat the properties of the thermal bosonic system. It is interesting to observe that, except for the non-diagonal elements, this TFD-propagator is equal to the one introduced in the Schwinger-Keldysh approach, which is claimed to be (in this equivalence with TFD) a thermal theory describing linear-response processes only (H. Chu et.al., 1994).

1.3. IMAGINARY TIME FORMALISM AND COMPACTIFICATION

Let us analyse the component $G(k; \beta)^{11}$ closely to address the connection of TFD with the imaginary time formalism. Using the fact that $n(k_0; \beta)$ in Eq. (23) may be written as

$$n(k_0) = \sum_{m=1}^{\infty} \exp(-m\beta k_0),$$

we obtain

$$G(x - x'; \beta)^{11} = \sum_{l=-\infty}^{\infty} G_o(x - x' - i\beta l\widehat{n}), \tag{24}$$

where $\widehat{n} = (1, 0, 0, 0)$ denotes a time-like unit vector and

$$G_o(x - x' - i\beta l\widehat{n}) = \frac{-i}{(2\pi)^2} \frac{1}{(x - x' - i\beta l\widehat{n})^2}.$$

Then the thermal propagator is represented by a sum over free propagators each one displaced in time by the pure complex quantity $i\beta l$. Actually this result can be seen as describing a scalar field constrained in the time axes, now considered as a sum of complex quantities. Each term $G_o(x - x' - i\beta l\widehat{n})$ in $G(x - x'; \beta)^{11}$ is but the contribution of images reflected on the "walls" placed at $\mathrm{Im}(t) = 0$ and $\mathrm{Im}(t) = \beta$. This interpretation is reinforced by a similar expression that can be derived if we consider the field within a slab of two parallel planes, such that for instance one at $z = 0$ and the other at $z = L$ (J.C. da Silva et.al., 2002).

Notice that we can write $iG(k; \beta)^{11} \equiv Tr\{\rho(H; \beta)T[\phi(x)\phi(x')]\}$ (J.I. Kapusta, 1989), where

$$\rho(H; \beta) = \frac{\exp(-\beta H)}{Z}$$

is the canonical density matrix. The periodical conditions of the propagator can be also observed by a general result involving thermal two-point functions. Let us define a two-time correlation function by

$$\langle A_H(t)B_H(t')\rangle = Tr[\rho(\beta)A_H(t)B_H(t')],$$

where $A_H(t)$ and $B_H(t')$ are given in the Heisenberg picture (represented by the index H). Using then the canonical form for $\rho(\beta)$, we have

$$\begin{aligned} \langle A_H(t)B_H(t')\rangle &= \frac{1}{Z}Tr[\exp(-\beta H)A_H(t)B_H(t')] \\ &= \frac{1}{Z}Tr[\exp(-\beta H)A_H(t)\exp(\beta H)\exp(-\beta H)B_H(t')] \\ &= \frac{1}{Z}Tr[A_H(t + i\beta)\exp(-\beta H)B_H(t')]. \end{aligned}$$

Using the trace property of invariance by cyclical transformations, it results in

$$\langle A_H(t)B_H(t')\rangle = \langle B_H(t')A_H(t + i\beta)\rangle.$$

Such equation is termed the KMS (Kubo, Martin and Schwinger) relation and describes the conditions of periodicity to be obeyed by a correlation, in particular the Green functions.

As a consequence, we can reduce the problem of calculating the thermal quantities by taking the generating functional of the $T = 0$

theory and performing the time integration for periodic fields, considering $\tau = it$ instead of t. Then, in the case of bosons, we can write the partition function as (J.I. Kapusta, 1989)

$$\mathcal{Z} = N \int d[\phi] exp \left(\int_0^\beta d\tau \int dx^3 \mathcal{L} \right) \qquad (25)$$

All these results gathered together, for practical proposals, show that we can interpret the effect of temperature as a process of compactification in time. Reversing such an interpretation, we can assume that the final result of a thermal theory is equivalent to a mechanism to describe a quantum field on a torus, $R^{D-1} \times S^1$, where S^1 is a circle of circumference $\beta = 1/T$. This contention is still more appealing if we consider Euclidian theories. However, whether this is so as such, we can think of generalizing this topological interpretation for a more general torus, and consider the scheme for introducing temperature, for more than one dimension. This can then be performed through a proper generalization of either the Bogoliubov transformation in TFD or the substitution of a time integral by a discrete sum over the Matsubara frequencies. Thus, in principle, we would be able to carry out calculations for compactified systems, within some specific geometry, via a simple prescription for changing the Feynman rules. In other words, we assume that to treat a compactified field theory in spatial dimensions and in time (to describe temperature), the Matsubara mechanism can be considered on $R^{D-d} \times S^{1_1} \times ... \times S^{1_d}$. Up to now there is no way to demonstrate this conjecture for the general situation, except considering an immediate generalization of the KMS condition in Euclidean geometries, a result confirmed by the successful use in different physical situations, reproducing some known results and bring new possibilities for calculations (A.P.C. Malbouisson et.al., 2002; A.P.C. Malbouisson et.al., 2002; J.C. da Silva et.al., 2002; L.M. Abreu et.al., 2005; A.P.C. Malbouisson et.al., 2004). Notice that, for some of those situations, it would be very cumbersome, even rather impossible to get some useful information, to depart from the very beginning with the modes of the confined field. A new application of this result is presented in Section 5. (To see how this procedure works in the case of the Bogoliubov transformations see Ref. (J.C. da Silva et.al., 2002) and Khanna *et al* in this Proceedings.)

Similar results can be derived for fermionic fields (H. Queiroz et.al.,). In such a situation, we can start with the propagator given by

$$S(x - x') = -i\gamma^\alpha \partial_\alpha G_0(x - x')$$

where $S(x - x') = -i\langle 0|T[\psi(x)\overline{\psi}(x')]|0\rangle$. In this case $v_k(\beta)$ is defined through the fermion number distribution, that is

$$v(k_0; \beta) = \frac{e^{-\beta k_0/2}}{[1 + e^{-\beta k_0}]^{1/2}}. \tag{26}$$

Observe that we can write

$$v^2(k_0; \beta) = \sum_{l=1}^{\infty} (-1)^{l+1} e^{-\beta k_0 l}; \tag{27}$$

leading to the thermal Green's function,

$$G_0^{11}(k; \beta) = G_0(k) + \sum_{l=1}^{\infty} (-1)^{l+1} e^{-\beta k_0 l} [G_0^*(k) - G_0(k)], \tag{28}$$

such that

$$
\begin{aligned}
G_0^{11}(x - x'; \beta) =\ & G_0(x - x') + \sum_{l=1}^{\infty} (-1)^{l+1} [G_0^*(x' - x - i\beta l \widehat{n}_0) \\
& - G_0(x - x' - i\beta l \widehat{n}_0)].
\end{aligned}
$$

(for the use of such a result, see Khanna et al in this Proceedings)

It is worth emphasizing that for the fermionic field, we have antiperiodic KMS conditions, which when considered in terms of space compactification, coincide with the physical bag-model conditions (A.P.C. Malbouisson et.al., 2004; A. Chodos et.al., 1974; C.A. Lutken et.al., 1988). Such a result will be used in Section 5. Now we will be concerned with the algebraic elements of the thermal theories.

2. Thermal algebraic structure

In this section we develop some preliminary algebraic aspects associated to thermal systems. Our main interest will be the analysis of representations of Lie groups (for a more evolving discussion see (I. Ojima, 1981; A.E. Santana et.al., 1999; A.E. Santana et.al., 2000; T. Kopf et.al., 1997)).

2.1. TFD, *-ALGEBRAS AND q-GROUP

Let us denote by $\mathcal{L}_T = \{A, B, C, ..., \widetilde{A}, \widetilde{B}, \widetilde{C}...\}$ the set of dynamical variables in TFD defined in the Hilbert space $\mathcal{H}$ with elements $|\Phi\rangle = |\phi, \widetilde{\phi}\rangle$. The action of generic operators A and $\widetilde{A}$ on $|\Phi\rangle$ is specified by

$$A|\Phi\rangle \equiv \mathsf{A} \otimes 1(|\phi\rangle \otimes \langle\phi|) = \mathsf{A}^l(|\phi\rangle \otimes \langle\phi|) = (\mathsf{A}|\phi\rangle) \otimes \langle\phi|, \tag{29}$$

$$\widetilde{A}|\Phi\rangle = 1 \otimes \mathsf{A}(|\phi\rangle \otimes \langle\phi|) = \mathsf{A}^r(|\phi\rangle \otimes \langle\phi|) = |\phi\rangle \otimes \langle\phi|\mathsf{A}^\dagger, \tag{30}$$

where the operator A is defined in the usual Hilbert space, $\mathfrak{H}$, such that $|\phi\rangle \in \mathfrak{H}$. The set of operator acting on $\mathfrak{H}$ is denoted by $\mathcal{L}$. The Hilbert space in TFD, $\mathcal{H}$, is given by

$$\mathcal{H} = \mathfrak{H} \otimes \mathfrak{H}^*. \tag{31}$$

Then we find that Eqs. (29) and (30) induce a mapping $\tilde{} : \mathcal{L}_T \mapsto \mathcal{L}_T$, called tilde (or dual) conjugation rules fulfilling the properties:

$$
\begin{aligned}
(AB)^{\tilde{}} &= \widetilde{A}\widetilde{B}, \\
(A + \beta B)^{\tilde{}} &= \widetilde{A} + \beta^* \widetilde{B}, \\
(A^\dagger)^{\tilde{}} &= (\widetilde{A})^\dagger, \\
\widetilde{\widetilde{A}} &= A, \\
[A, \widetilde{B}] &= 0.
\end{aligned}
$$

this set of rules (which can also be derived directly from the Lie algebra representation discussed in Sections (3) and (4)) emerge as a direct consequence of the Tomita-Takesaki (standard) representation of w*-algebra, where the tilde conjugation is the usual anti-linear isometry, ς, such that $\varsigma^2 = 1$, and $\varsigma A \varsigma = \widetilde{A}$. In this standard representation we also have generators of isomorphism $\hat{} : \mathcal{L}_T \to \mathcal{L}_T$ operators of the type

$$\widehat{A} = A - \varsigma A \varsigma = A - \widetilde{A}. \tag{32}$$

Thus TFD is nothing but a simple example of the standard representation of a w*-algebra.

A Hopf algebra emerges by a proper redefinition of the antilinear characteristics of TFD. Consider $\mathfrak{g} = \{g_i, i = 1, 2, 3, ..\}$ be an associative algebra defined on the field of the complex numbers and let $\mathfrak{g}$ be equipped with a Lie algebra structure specified by $g_i \lozenge g_j = C_{ij}^k g_k$, where $\lozenge$ is the Lie product and C_{ij}^k are the structure constants (we are assuming the rule of sum over repeated indeces). Now we take $\mathfrak{g}$ first realized by $\mathcal{L} = \{A_i, i = 1, 2, 3, ..\}$ such that the commutator $[A_i, A_j]$ is the Lie product of elements $A_i, A_j \in \mathcal{L}$. Consider ψ and ϕ two representations of $\mathcal{L}$, such that $\psi(A)$ ($\phi(A)$) are linear operators defined on a representation vector space $\mathfrak{H}_\psi$ ($\mathfrak{H}_\phi$). As a consequence, $\varphi = \psi * \phi$, defined by

$$\varphi(A) = (\psi * \phi)(A) = \psi(A) \otimes 1 + 1 \otimes \phi(A),$$

is a representation of $\mathcal{L}$ as a Lie algebra, since $[\varphi(A_i), \varphi(A_j)] = \varphi[A_i, A_j]$. If $\mathcal{L}$ is equipped with a coproduct defined by $\Delta(A) = A \otimes 1 + 1 \otimes A$, then we can write $(\psi * \phi) = (\psi \otimes \phi) \circ \Delta$. Notice that Δ is not, in general,

defined in the Lie algebra $\mathcal{L}$ but in the (universal) enveloping algebra of A, say $U(A)$.

But some algebraic characteristics of the enveloping algebra can be immediately pointed out. $U(A)$ is a Lie algebra and admits a Hopf structure, which is induced by the product $\Delta(A)$, where the maps of the coalgebra are

$$\Delta(A) = A \otimes 1 + 1 \otimes A, \quad s(A) = -A, \quad \epsilon = 0.$$

Observe that the algebraic structure is respected for such maps; for instance: $[\Delta(A_i), \Delta(A_j)] = \Delta[A_i, A_j]$.

In order to emphasize the Hopf-algebra ingredients attached to the enveloping algebra, it is convenient to define the coproduct by two different maps on A. That is, let Δ be given by $\Delta = \Delta^r + \Delta^l$, where $\Delta^r(A) = 1 \otimes A$ and $\Delta^l(A) = A \otimes 1$. Observe that Δ^l and Δ^r induce two different representations of A, which can be denoted by $\psi \circ \Delta^l$ and $\psi \circ \Delta^r$, both preserving the Lie structure. In the context of antilinear representation, we then reproduce the TFD structure. This result leads to the fact that the temperature has been introduced as a deformation parameter when we consider the Weyl-Heisenberg algebra (E. Celeghini et.al., 1998).

2.2. TFD and Lie Algebras

This w*-algebra structure can be used to develop a representation theory of symmetry groups, taking $\mathcal{H}$ as a representation space for Lie algebras. As before let $\mathfrak{g}$ be a Lie algebra specified by $g_i \Diamond g_j = C_{ij}^k g_k$. A unitary representation of $\mathfrak{g}$ in $\mathcal{H}$ is then given by

$$[A_i, A_j] = iC_{ij}^k A_k, \tag{33}$$
$$[\widetilde{A}_i, \widetilde{A}_j] = -iC_{ij}^k \widetilde{A}_k, \tag{34}$$
$$[A_i, \widetilde{A}_j] = 0. \tag{35}$$

For physical interpretation, this algebra can be rewritten by the use of the hat-operators, the generators of transformation in w*-algebras, as given in the last subsection. Therefore, from Eqs. (33)–(35) we get

$$[A_i, A_j] = C_{ij}^k A_k,$$
$$[\widehat{A}_i, A_j] = C_{ij}^k A_k,$$
$$[\widehat{A}_i, \widehat{A}_j] = C_{ij}^k \widehat{A}_k.$$

Notice that this Lie algebra, to be denoted by $\mathfrak{g}_T$, as a vector space is given by $\mathfrak{g}_T = \mathfrak{g} \oplus \widehat{\mathfrak{g}}$, where $\mathfrak{g}$ $(\widehat{\mathfrak{g}})$ is a sub-vector space of $\mathfrak{g}_T$ given by

the non-hat (hat) operators. Therefore, $\mathfrak{g}_T$ is a particular case of semi-direct product of the two Lie algebras. $\mathfrak{g}$ and $\widehat{\mathfrak{g}}$. In the next section we explore this representation(A.E. Santana et.al., 1999).

3.   Representations of the poincare group in $\mathcal{H}$

The $\mathfrak{g}_T$ Poincaré-Lie algebra, which will be denoted by $\mathfrak{p}_T$, is given by (A.E. Santana et.al., 1999)

$$
\begin{aligned}
{[M_{\mu\nu}, P_\sigma]} &= i(g_{\nu\sigma}P_\mu - g_{\sigma\mu}P_\nu), \ [P_\mu, P_\nu] = 0, \\
{[M_{\mu\nu}, M_{\sigma\rho}]} &= -i(g_{\mu\rho}M_{\nu\sigma} - g_{\nu\rho}M_{\mu\sigma} + g_{\mu\sigma}M_{\rho\nu} - g_{\nu\sigma}M_{\rho\mu}), \\
{[\widehat{M}_{\mu\nu}, P_\sigma]} &= [M_{\mu\nu}, \widehat{P}_\sigma] = i(g_{\nu\sigma}P_\mu - g_{\sigma\mu}P_\nu), \ [\widehat{P}_\mu, P_\nu] = 0, \\
{[\widehat{M}_{\mu\nu}, M_{\sigma\rho}]} &= -i(g_{\mu\rho}M_{\nu\sigma} - g_{\nu\rho}M_{\mu\sigma} + g_{\mu\sigma}M_{\rho\nu} - g_{\nu\sigma}M_{\rho\mu}), \\
{[\widehat{M}_{\mu\nu}, \widehat{P}_\sigma]} &= i(g_{\nu\sigma}\widehat{P}_\mu - g_{\sigma\mu}\widehat{P}_\nu), \ [\widehat{P}_\mu, \widehat{P}_\nu] = 0, \\
{[\widehat{M}_{\mu\nu}, \widehat{M}_{\sigma\rho}]} &= -i(g_{\mu\rho}\widehat{M}_{\nu\sigma} - g_{\nu\rho}\widehat{M}_{\mu\sigma} + g_{\mu\sigma}\widehat{M}_{\rho\nu} - g_{\nu\sigma}\widehat{M}_{\rho\mu}),
\end{aligned}
$$

where $M_{\mu\nu}$ stands for rotations and P_μ for translations.

Introducing, therefore, the Pauli-Lubanski matrices as usual, $w_\mu = \frac{1}{2}\varepsilon_{\mu\nu\rho\sigma}M_{\nu\sigma}P_\rho$, where $\varepsilon_{\mu\nu\rho\sigma}$ is the Levi-Civita symbol, the invariants of $\mathfrak{p}_T$ are

$$
\begin{aligned}
W &= w_\mu w^\mu, & (36) \\
P^2 &= P_\mu P^\mu, & (37) \\
\widehat{W} &= 2\widehat{w}_\mu w^\mu - \widehat{w}_\mu \widehat{w}^\mu = w_\mu w^\mu - \widetilde{w}_\mu \widetilde{w}^\mu, & (38) \\
\widehat{P^2} &= 2\widehat{P}_\mu P^\mu - \widehat{P}_\mu \widehat{P}^\mu = P_\mu P^\mu - \widetilde{P}_\mu \widetilde{P}^\mu, & (39)
\end{aligned}
$$

where

$$
\widehat{w}_\mu = \frac{1}{2}\varepsilon_\mu^{\nu\rho\sigma}(\widehat{M}_{\nu\sigma}P_\rho + M_{\nu\sigma}\widehat{P}_\rho - \widehat{M}_{\nu\sigma}\widehat{P}_\rho).
$$

Let us study now the scalar and spin-1/2 representations.

3.1.   Scalar Representation

Representations for $\mathfrak{p}_T$ can be built from the Casimir invariants, and in this case we can write for the non-tilde variables explicitly

$$
(P^2 - m^2)|\Psi\rangle \rightarrow [(P^2 - m^2)]^l|\Psi\rangle = [(P^2 - m^2) \otimes 1]|\Psi\rangle = 0, \quad (40)
$$

and for the tilde variables

$$
(P^2 - m^2)\widetilde{\ }|\Psi\rangle \rightarrow (P^2 - m^2)^r|\Psi\rangle = [1 \otimes (P^2 - m^2)]|\Psi\rangle = 0.
$$

Here we take

$$|\Psi\rangle = |\phi\rangle \otimes \langle\phi| = |\phi\rangle \otimes |\widetilde{\phi}\rangle, \qquad (41)$$

with $\langle\phi|\phi\rangle = 1$. This fact defines the TFD representation for the states $|\Psi\rangle$. We have, hence, two equations associated with the two invariants $P^2 \equiv \square$ and $\widehat{P^2} \equiv \widehat{\square}$, that is

$$(P^2 - m^2)|\Psi\rangle = (\square - m^2)|\phi\rangle \otimes \langle\phi| = 0, \qquad (42)$$

and

$$\widehat{P^2}|\Psi\rangle = [\square^l - \square^r]|\Psi\rangle = 0, \qquad (43)$$

where

$$\square^l|\Psi\rangle = (\square \otimes 1)|\Psi\rangle = (\square|\phi\rangle)\langle\phi|;$$
$$\square^r|\Psi\rangle = (1 \otimes \square)|\Psi\rangle = |\phi\rangle(\langle\phi|\square).$$

By construction Eq. (38) associated with observables, describes the mass-shell condition, while Eq. (43) is a density matrix equation giving the time-evolution of the state Ψ. That this is so can be seen in the following way. Considering Eqs. (41), let us multiply Eq. (43) by $|\phi\rangle$, that is

$$[\square^l - \square^r]|\Psi\rangle|\phi\rangle = (\square|\phi\rangle\langle\phi| - |\phi\rangle\langle\phi|\square)|\phi\rangle = 0.$$

Since $\langle\phi|\square|\phi\rangle = m^2$ and $\langle\phi|\phi\rangle = 1$, we derive the Klein-Gordon equation, i.e. $(\square - m^2)|\phi\rangle = 0$. Using, on the other hand, the bra vector, $\langle\phi|$, the Klein-Gordon equation in the dual Hilbert space may be obtained from Eq. (43); that is

$$\langle\phi|(\square|\phi\rangle\langle\phi| - |\phi\rangle\langle\phi|\square) = \langle\phi|(m^2 - \square) = 0.$$

This result shows that Eq. (43) is a (square root) density matrix equation for the Klein-Gordan field. This last aspect can be better understood if write $|\Psi\rangle$ as

$$|\Psi\rangle = \rho^{1/2}|1\rangle,$$

such that $[\square^l - \square^r]\rho^{1/2} = 0$. That is

$$[\square, \rho] = [P^\mu P_\mu, \rho] = 0, \qquad (44)$$

where ρ can be interpreted as the density matrix associated to the Klein-Gordon field, whose general form is then given by $\rho(P^\mu)$. We can in addition show that the non-relativistic limit ($c \to \infty$) of Eq. (44) is the usual Liouville-von Neumann equation for the Schrödinger equation.

3.2. Spinor Representation

In order to construct a spinorial density-matrix equation, we can introduce an equation like

$$\widehat{(\gamma^\mu P_\mu)} \ |\Psi\rangle = 0, \tag{45}$$

such that, differently from Eqs. (39), we can write

$$\widehat{(\gamma^\mu P_\mu)} \ \widehat{(\gamma^\mu P_\mu)} = \widehat{P^2}. \tag{46}$$

Therefore we find

$$\begin{aligned}
\widehat{(\gamma^\mu P_\mu)} \ |\Psi\rangle &= [(\gamma^\mu P_\mu) \otimes 1 - 1 \otimes (\gamma^\mu P_\mu)]|\phi\rangle \otimes \langle\bar\phi| \\
&= (\gamma^\mu P_\mu)|\phi\rangle \otimes \langle\bar\phi| - |\phi\rangle \otimes \langle\bar\phi|(\gamma^\mu P_\mu)^\dagger = 0. \tag{47}
\end{aligned}$$

where now $|\Psi\rangle$ is a 16-component spinor, and $|\phi\rangle(\langle\bar\phi|)$ is the 4-component (dual) Dirac spinor. The Liouville von Neumann-like equation for the Dirac field can be then written, in parallel to the Klein- Gordon equation, as

$$[(\gamma^\mu P_\mu), \rho] = 0.$$

Multiplying the rhs of Eq. (47) by $|\phi\rangle$, it results in $(\gamma^\mu P_\mu - m) \ |\phi\rangle = 0$, the Dirac equation. Now, multiplying the lhs of Eq. (47) by $\langle\bar\phi|$ it results in $\langle\bar\phi|(P_\mu\gamma^\mu - m) = 0$, the conjugated Dirac equation. In this sense, in fact, Eq. (47) is a density matrix equation for the Dirac field.

3.3. Interpretation of the Doubling

From these two representations for bosons and fermions, we can infer the meaning of the doubling in the algebraic degrees of freedom arising in $\mathfrak{p}_T = \mathfrak{p} \oplus \widehat{\mathfrak{p}}$. The subalgebra of hat-operators, $\widehat{\mathfrak{p}}$, is interpreted as generators for dynamical symmetries, while the subalgebra of the non-hat operators, say $\mathfrak{p}$, is to be interpreted as describing dynamical observables.

The fact that $\mathfrak{p}_T$ is a semidirect product of these two subalgebras is a necessary condition to support such an interpretation. Indeed, since we have $[\mathfrak{p}, \widehat{\mathfrak{p}}] = \mathfrak{p}$, we see that the role played by the generators of symmetries $\widehat{\mathfrak{p}}$ is to impress dynamical modification on the observables $\mathfrak{p}$ giving rise to other observables. As a consequence, the non-commutativity between the observables is a matter of measurement. In the case we are studying in this section we have $[\mathfrak{p}, \mathfrak{p}] = \mathfrak{p}$ resulting in a quantum theory. For the sake of consistency, we expect to derive a classical TFD theory with an algebra similar to $\mathfrak{p}_T$ but in which $[\mathfrak{p}, \mathfrak{p}] = 0$. (This result has been explored in Ref.(L.M. Silva et.al., 1997))

In this context, a tilde operator, and the tilde conjugation rules are introduced by the difference among a generator of symmetry and

observables, that is $\widetilde{A} = A - \widehat{A}$ (A.E. Santana et.al., 2000). What has been shown, in classical theory as well as in quantum formalisms, is that tilde operators, when used to define the Hamiltonian in TFD (actually, the hat-Hamiltonian), play the role of heat-bath variables. However, if the tilde operators are not interpreted in a proper way, their use would be considered somewhat artificial, and has been, at times, designated as "ghost" variables. But this naive artificiality (sometimes used as a motive to deny the physical content of real-time formalisms) can be treated with the analysis of symmetry, which shows the true content of duplication of the degrees of freedom in thermal theories as we have seen here. Moreover, since there is a connection between the Matsubara formalism and real-time approaches, with such a physical interpretation of the doubling we can better understand the real meaning of working with an imaginary time.

4. Bosonic kinetic theory and juttiner distribution

In this section, using the representation theory introduced before, we analyse the structure of statistical mechanics and kinetic theory for bosons starting from Eq. (44). We consider that Eq. (44) describes the evolution of an ensemble of quantum particles specified through the density operator ρ such that the entropy is given by(A.E. Santana et.al., 1999; A.E. Santana et.al., 2000)

$$S = -k_B Tr\rho \ln \rho, \tag{48}$$

where k_B is the Boltzmann constant. In a stationary case the entropy is an extremum, that is

$$\delta S = 0, \tag{49}$$

under the constraints

$$Tr\rho = 1, \tag{50}$$
$$Tr\rho N = \langle N \rangle, \tag{51}$$
$$Tr\rho P^\nu = \langle P^\nu \rangle, \tag{52}$$

where $\langle N \rangle$, the macroscopic particle number, and $\langle P^\nu \rangle$, the macroscopic four momentum, are assumed to be constant. Then we obtain

$$\beta_o + \beta_\nu p^\nu + \beta_N N - k_B - k_B \ln \rho = 0, \tag{53}$$

where β_o, β_N and β_μ are the Lagrange multipliers attached to the constraints given by Eqs. (50)–(52), respectively. From Eq. (53), we get

$$\rho = \frac{1}{Z} \exp[\frac{1}{k_B}(\beta_\nu P^\nu + \beta_N N)], \tag{54}$$

where

$$Z = \exp(1 - \frac{\beta_o}{k_B}) \qquad (55)$$

is the partition function. Multiplying Eq. (53) by ρ, taking the trace and using Eqs. (50)–(52) and Eq. (55), we derive

$$K_B \ln Z + \beta_\nu \langle P^\nu \rangle + \beta_N \langle N \rangle + S = 0.$$

We obtain a physical interpretation of this approach by a suitable definition of the Lagrange multipliers β_ν and β_N. Thus we assume that

$$\beta_\nu = -k_B \beta U_\nu, \quad \beta_N = k_B \mu \beta,$$

where $\beta = 1/k_B T$, T is the temperature of the rest frame, μ is the chemical potential and U_ν is the macroscopic four-velocity field satisfying the relation $U_\nu U^\nu = 1$. Therefore, ρ in Eq. (54) is given as

$$\rho_o = \frac{1}{Z} \exp[-\beta(U_\nu P^\nu - \mu N)]. \qquad (56)$$

The partition function, Z, is inferred from the normalization of ρ. Thus, Eq. (56) provides a general form to ρ for steady states. Let us analyse this from another point of view.

Using Eq. (43), Eq. (44) can be written as

$$(\partial^{\mu'} \partial_{\mu'} - \partial^\mu \partial_\mu)\rho(x', x) = 0. \qquad (57)$$

In that case, defining the following four-operators by

$$\frac{\partial}{\partial x^\mu} = \frac{1}{\sqrt{2}}(\frac{\partial}{\partial q^\mu} - p^\mu), \quad \frac{\partial}{\partial x'^\mu} = \frac{1}{\sqrt{2}}(\frac{\partial}{\partial q^\mu} + p^\mu), \qquad (58)$$

it is straightforward to show that Eq. (57) is given as

$$p^\mu \frac{\partial}{\partial q^\mu} \rho(q, p) = 0. \qquad (59)$$

This equation can be interpreted as the drift term of a collisionless Boltzmann equation for the one-particle Wigner distribution $\rho(q, p)$. To see that, let us explore the physical meaning of $\rho(q, p)$ in this context. First note that $\rho(q, p)$ is in principle a Lorentz scalar. Thus an invariant solution of Eq. (59) is

$$\rho(q, p) = \int d^4u\, \delta(p^\nu u_\nu) \exp\{-u \cdot q\} g(p, u). \qquad (60)$$

The microscopic nature of $\rho(q, p)$ can be specified through the definition,

$$g(p, u) = \langle a^\dagger(p - \frac{u}{2})\, a(p + \frac{u}{2}) \rangle = Tr\rho a^\dagger(p - \frac{u}{2})\, a(p + \frac{u}{2}), \qquad (61)$$

where $a(p)$ and $a^\dagger(p)$ are boson operators, such that the number and momentum operators can be introduced by

$$N = \int \frac{d^3p}{p^o} a^\dagger(p)a(p), \quad P^\mu = \int \frac{d^3p}{p^o} p^\mu a^\dagger(p)a(p).$$

Using Eq. (56) in Eq. (61), the result is

$$\langle a^\dagger(p - \frac{u}{2})\, a(p + \frac{u}{2})\rangle_o = \langle a(p + \frac{u}{2})a^\dagger(p - \frac{u}{2})\rangle_o \exp(\beta\mu - p^\nu U_\nu)$$

which is derived from the properties of the trace in the equilibrium average represented by $\langle \cdots \rangle_o$. Hence we get

$$\rho(p) = \frac{1}{\exp(\beta p^\nu U_\nu - \beta\mu\langle N\rangle) - 1},$$

that is the Juttiner distribution (S.R. de Groot et.al., 1980). Thus Eq. (61) is an appropriate choice for $g(q,p)$, providing a physical interpretation of the theory in the case of bosons in a steady state.

In a more general treatment, we consider the inclusion of antibosons, such that $g(q,p)$ in Eq. (60) can be defined as

$$g(p,u) = \langle a^\dagger(p - \frac{u}{2})\, a(p + \frac{u}{2})\rangle + \langle \bar{a}^\dagger(p - \frac{u}{2})\, \bar{a}(p + \frac{u}{2})\rangle,$$

where $\bar{a}(p)$ and $\bar{a}^\dagger(p)$ are the momentum-space operators for antibosons. Therefore, the microscopic specification of the operators N and P^ν, in the momentum representation, is

$$N = \int \frac{d^3p}{p^o}[a^\dagger(p)a(p) + \bar{a}^\dagger(p)\bar{a}(p)],$$

$$P^\nu = \int \frac{d^3p}{p^o}p^\nu[a^\dagger(p)a(p) + \bar{a}^\dagger(p)\bar{a}(p)].$$

In particular the macroscopic current density is given by

$$\langle J^\mu \rangle = \int d^3p \frac{1}{p^o}p^\mu \rho(q,p) \tag{62}$$

$$= \int d^3p \frac{1}{p^o}p^\mu \frac{1}{\exp(\beta p^\nu U_\nu - \beta\mu\langle N\rangle) - 1}. \tag{63}$$

The representation of this expression in the coordinate space can be done as usual.

5. Compactification of the Gross-Neveu model

We now apply the generalized Matsubara formalism, discussed earlier, to a fermionic theory aiming to discuss effects of simultaneous spatial confinement and finite temperature. We consider the Wick-ordered massive Gross-Neveu model in a D-dimensional Euclidean space, described by the Lagrangian density (D.J. Gross et.al., 1974)

$$\mathcal{L} = : \bar{\psi}(x)(i\overset{\leftrightarrow}{\nabla} + m)\psi(x) : + \frac{u}{2} \left(: \bar{\psi}(x)\psi(x) :\right)^2 . \tag{64}$$

Here $x \in \mathbf{R}^D$ and $\psi(x)$ is a spin $\frac{1}{2}$ field having N (flavor) components, $\psi^a(x)$ ($a = 1, 2, ..., N$), summation over flavor and spin indices being implicit. We shall consider the large-N limit ($N \to \infty$), which permits considerable simplifications. We use natural units, $\hbar = c = k_B = 1$.

To describe the fully compactified model, with Euclidean coordinates, say x_i, restricted to segments of length L_i ($i = 1, 2, ...D$) and the field $\psi(x)$ satisfying anti-periodic (bag model) boundary conditions, the Feynman rules should be modified following the Matsubara prescription

$$\int \frac{dk_i}{2\pi} \to \frac{1}{L_i} \sum_{n_i=-\infty}^{+\infty} , \qquad k_i \to \frac{2(n_i + \frac{1}{2})\pi}{L_i} . \tag{65}$$

Then the L_i-dependent four-point function at leading order in $1/N$, at zero external momenta, has the formal expression

$$\Gamma_D^{(4)}(0; \{L_i\}, u) = \frac{u}{1 + Nu\Sigma_D(\{L_i\})} , \tag{66}$$

where L_i-dependent Feynman one-loop subdiagram is given by

$$\Sigma_D(\{L_i\}) = \frac{1}{L_1 \cdots L_D} \sum_{\{n_i\}=-\infty}^{\infty} \frac{m^2 - \sum_{i=1}^{D} \nu_i^2}{\left(\sum_{i=1}^{D} \nu_i^2 + m^2\right)^2} \tag{67}$$

and $\nu_i = 2(n_i + \frac{1}{2})\pi/L_i$. Introducing the dimensionless quantities $b_i = (mL_i)^{-2}$ and $q = (2\pi)^{-1}$, one can write

$$\Sigma_D(\{b_i\}) = m^{D-2(s-1)} \sqrt{b_1 \cdots b_D}$$
$$\times \left[q^2 U_D(s; \{b_i\}) + \left(\sum_{i=1}^{D} b_i \frac{\partial}{\partial b_i}\right) \frac{U_D(s-1; \{b_i\})}{s-1} \right]_{s=2} \tag{68}$$

where

$$U_d(\mu; \{b_i\}) = q^{2(\mu-1)} \sum_{\{n_i\}=-\infty}^{\infty} \frac{1}{\left(\sum_{i=1}^{d} b_i(n_i + \frac{1}{2})^2 + q^2\right)^{\mu}} . \tag{69}$$

To calculate $U_d(\mu; \{b_i\})$, the summations over half-integers are transformed into sums over integers, leading to

$$U_d(\mu; \{b_i\}) = 4\pi^{-2(\mu-1)} \left[Z_d^{4q^2}(\mu; b_1, ..., b_d) - \sum_{i=1}^{d} Z_d^{4q^2}(\mu; ..., 4b_i, ...) \right.$$

$$\left. + \sum_{i<j=1}^{d} Z_d^{4q^2}(\mu; ..., 4b_i, ..., 4b_j, ...) - \cdots + (-1)^d Z_d^{4q^2}(\mu; 4b_1, ..., 4b_d) \right],$$

(70)

where $Z_d^{h^2}(\mu; \{a_i\})$ is the multivariable Epstein-Hurwitz *zeta*-function

$$Z_d^{h^2}(\mu; \{a_i\}) \equiv \sum_{\{n_i\}=-\infty}^{\infty} [a_1 n_1^2 + \cdots + a_d n_d^2 + h^2]^{-\mu}$$

$$= \frac{\pi^{d/2}}{\sqrt{a_1 \cdots a_d}\,\Gamma(\mu)} \left[\frac{1}{h^{2\mu-d}} \Gamma\left(\mu - \frac{d}{2}\right) \right.$$

$$+ \sum_{w=1}^{d} 2^{w+1} \sum_{\{\sigma_w\}} \sum_{\{n_{\sigma_l}\}=1}^{\infty} \left(\frac{\pi}{h} \sqrt{\frac{n_{\sigma_1}^2}{a_{\sigma_1}} + \cdots + \frac{n_{\sigma_w}^2}{a_{\sigma_w}}} \right)^{\mu-\frac{d}{2}}$$

$$\left. \times K_{\mu-\frac{d}{2}} \left(2\pi h \sqrt{\frac{n_{\sigma_1}^2}{a_{\sigma_1}} + \cdots + \frac{n_{\sigma_w}^2}{a_{\sigma_w}}} \right) \right].$$

(71)

Here, $\{\sigma_w\}$ represents the set of all combinations of $\{1, 2, ..., d\}$ possessing w elements and $K_\nu(x)$ is the Bessel function of the third kind. This is an analytical extension of the multivariable Epstein-Hurwitz *zeta*-function to the whole complex μ-plane (A.P.C. Malbouisson et.al., 2002). The first term in Eq. (71) leads to a contribution for Σ_D which is divergent for even dimensions $D \geq 2$ due to the pole of the Γ-function. We renormalize Σ_D by subtracting this contribution, corresponding to a finite renormalization when D is odd.

From now on, we restrict ourselves to the case of $D = 3$. Notice that, although the Gross-Neveu model is not perturbatively renormalizable for $D > 2$, it has been shown to exist and has been explicitly constructed for $D = 3$ (C. de Calan et.al., 1991). We will be considering the fermions confined to a square box of side L ($L_1 = L_2 = L$) and at finite temperature $T = \beta^{-1}$, with the confining length $L_3 = \beta$. In this case, using the formula for the Bessel functions $K_{\pm 1/2}(z) = \sqrt{\pi}e^{-z}/\sqrt{2z}$, we obtain the following expression for the L and T-dependent renormalized single-loop subdiagram:

$$\frac{\Sigma_R(L, \beta)}{m} = 2\pi \left[\frac{2}{mL} \log(1 + e^{-mL}) + \frac{1}{m\beta} \log(1 + e^{-m\beta}) + F_1(L, \beta) \right]$$

$$- \frac{4\pi^2 + 1}{4\pi} \left[\frac{e^{-mL}}{1 + e^{-mL}} + \frac{e^{-m\beta}}{1 + e^{-m\beta}} + F_2(L, \beta) \right], \qquad (72)$$

where

$$
\begin{aligned}
F_r(L, \beta) =\ & -2G_r(L, L) + 8G_r(L, 2L) - 8G_r(2L, 2L) - 4G_r(L, \beta) \\
& + 8G_r(2L, \beta) + 8G_r(L, 2\beta) - 16G_r(2L, 2\beta) \\
& + 4H_r(L, L, \beta) - 16H_r(2L, L, 2\beta) - 8H_r(L, L, 2\beta) \\
& + 16H_r(2L, 2L, \beta) + 32H_r(L, 2L, 2\beta) - 32H_r(2L, 2L, 2\beta),
\end{aligned}
$$

with the functions G_r and H_r (for $r = 1, 2$) defined by

$$
G_r(x, y) = \sum_{n,l=1}^{\infty} \left(m\sqrt{x^2 n^2 + y^2 l^2} \right)^{r-2} \exp\left(-m\sqrt{x^2 n^2 + y^2 l^2} \right),
$$

$$
H_r(x, y, z) = \sum_{n,l,k=1}^{\infty} \left(m\sqrt{x^2 n^2 + y^2 l^2 + z^2 k^2} \right)^{r-2}
$$

$$
\times \exp\left(-m\sqrt{x^2 n^2 + y^2 l^2 + z^2 k^2} \right).
$$

Now, taking as usual $Nu = \lambda$ fixed and using Eq. (66), we find the large-N effective renormalized coupling constant as

$$
g(L, \beta, \lambda) = N\Gamma_{3R}^{(4)}(0, L, \beta, u) = \frac{\lambda}{1 + \lambda \Sigma_R(L, \beta)}. \qquad (73)
$$

Since $\lim_{L,\beta \to \infty} \Sigma_R(L, \beta) = 0$, we find that $g(\infty, \infty, \lambda) = \lambda$ is the renormalized fixed coupling constant in free space at zero temperature. On the other hand, for either $L \to 0$ or $\beta \to 0$, $\Sigma_R(L, \beta)$ diverges implying that we have ultraviolet asymptotic freedom for short distances and/or for high temperatures, irrespective of the value of λ.

Consider initially the situation at $T = 0$ ($\beta \to \infty$); the behavior of $\Sigma_R(L)$, in this case, is shown in Fig. 1 A. We find that $\Sigma_R(L)$ is negative for $L > L_c^{min} \simeq 2.29\, m^{-1}$ and reaches a minimum ($\Sigma_R^{min} \simeq -0.0624 m$) for $L = L_c^{max} \simeq 3.13\, m^{-1}$. This implies that, for $\lambda \geq \lambda_c = -(\Sigma_R^{min})^{-1} \simeq 16.03\, m^{-1}$, $\lambda/g(L, \lambda)$ has a non-positive minimum value and vanishes for a length $L_c^{(0)}(\lambda)$ in the interval $\left(L_c^{min}, L_c^{max} \right]$. This divergence of the effective coupling constant as L approaches $L_c^{(0)}(\lambda)$ can be interpreted as the system being confined; that is, in the strong coupling regime (with large enough λ), starting with L small (in the region of asymptotic freedom), the side of the square can not go above the length $L_c^{(0)}(\lambda)$ since $g(L, \lambda) \to \infty$ as $L \to L_c^{(0)}(\lambda)$. Similar behavior has also been found for the 3D Gross-Neveu model compactified in a strip of width L at zero temperature (A.P.C. Malbouisson et.al., 2004).
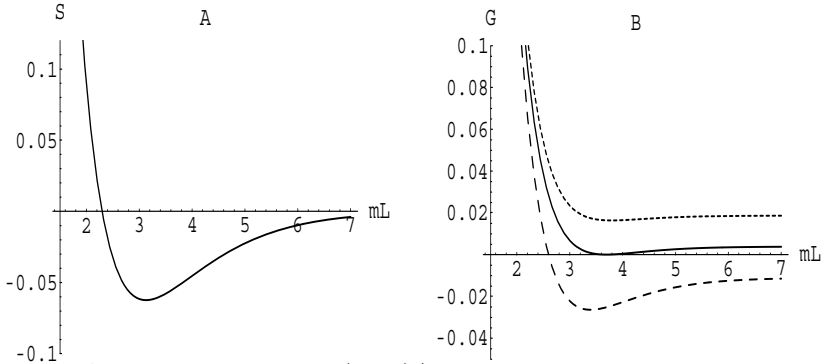
Figure 1. A - Plot of $S = \Sigma_R(L, \infty)/m$ as a function of mL. B - Plot of $G = \lambda/g(L, \beta, \lambda)$ as a function of L, with $\lambda = 25.0\,m^{-1}$, for some values of β: $3.0\,m^{-1}$, $2.34\,m^{-1}$ and $2.2\,m^{-1}$ (dashed, full and dotted lines respectively).

Let us now consider the effect of temperature, taking $\lambda \geq \lambda_c$. For low (fixed) T, $\lambda/g(L, \beta, \lambda)$ vanishes at a value $L_c^{(\beta)}(\lambda) < L_c^{(0)}(\lambda)$, its minimum (negative) value being slightly lower than the zero temperature case. Further raising the temperature, $L_c^{(\beta)}(\lambda)$ and the minimum value of λ/g increase and, at the temperature $T_d(\lambda) = \beta_d^{-1}(\lambda)$, the minimum of $\lambda/g(L, \beta, \lambda)$ vanishes. For $\beta < \beta_d(\lambda)$, $\lambda/g(L, \beta, \lambda)$ becomes positive for all values of L and then the system is unconfined. Thus, $T_d(\lambda)$ corresponds to the deconfining temperature for the given fixed coupling constant $\lambda \geq \lambda_c$. The behavior of λ/g is illustrated in Fig. 1 B.

The above discussion demonstrates analytically that, in the strong coupling regime ($\lambda > \lambda_c$), the compactified 3D Gross-Neveu model presents simultaneously asymptotic freedom and spatial confinement. This means that, if we start with a system of a *fermion-antifermion* pair bounded within a square of side L ($< L_c(\lambda)$) at low enough temperature, it would not be possible to separate them a distance larger than $L_c(\lambda)$. This *spatial* confinement of the pair could be interpreted as the existence of bound ("baryon-like") states, characteristic of the model in the strong coupling regime. By raising the temperature, we find that the spatial confinement disappears at the deconfining temperature $T_d(\lambda)$.

To estimate the values of the confining length and the deconfining temperature, the fermion mass has to be fixed. Since, at most, the Gross-Neveu model can be taken as an effective model for quark interaction, we will choose $m \approx 350\,MeV \simeq 1.75\,fm^{-1}$, the constituent quark mass. Taking for λ the minimum strength for confinement, $\lambda = \lambda_c \simeq 16.03\,m^{-1}$, we have $L_c \simeq 3.13\,m^{-1} \approx 1.79\,fm$. For this case, we find $\beta_d \simeq 2.76\,m^{-1}$ and so the deconfining temperature is $T_d \simeq 127\,MeV$. These values should be compared with the experimentally measured proton charge diameter ($\approx 1.74\,fm$) and the estimated deconfining temperature ($\approx 200\,MeV$) for hadronic matter, respectively

(K. Gawedzki et.al., 1985; Particle Data Group, 2004; S.G. Karshenboim, 1999).

6.   Concluding remarks

In this survey we have presented the main aspects and some of the consequences of the algebraic structure underlying the finite-temperature quantum field theory. The basic approach is the formalism known as thermofield dynamics (TFD), from which the connection among the famous methods of thermal theories has been established. The basic ingredients consist of a doubling in the degrees of freedom, which are indeed a basic fact in every $T \neq 0$ formalism, and Bogolioubov transformations, introducing thermal degrees of freedom. Here such a doubling has been identified with the elements of the standard representation of w*-algebras, the co-product of Hopf algebra, and with a semi-simple Lie algebra. This last content has then been explored to derive density matrix equations for the Klein-Gordon and Dirac Field, and a preliminary analysis of the kinetic theory based on a representation approach.

The underlying topological structure of a thermal formalism is also analysed giving rise to a mechanism of compactification in space and time (in this case describing temperature), which has been applied to study the 3-D Gross-Neveu model. In this case our main result is the observations of asymptotic freedom and confinement, as well as a critical temperature for deconfinement. The results are compared with the experimentally measured proton charge diameter and with the estimated temperature of deconfinement. In both situations we have found very satisfactory agreement. It is worth noticing that this is the first time that all these results are obtained analytically, despite the fact we are treating an effective model for the hadronic matter.

Acknowledgments

References

Matsubara, T. *Prog. Theor. Phys.*, 14:351, 1955.

Ezawa, H., Y. Tomonaga and H. Umezawa. *N. Cimento Ser. X*, 5:810, 1957.

Fetter, A.L. and J.D. Walecka. Quantum Theory of Many-Particles Systems. *McGraw-Hill, New York*, 1971.

Kapusta, J.I. Finite-Temperature Field Theory. *Cambridge University Press, Cambridge*, 1989.

Bellac, M. Le. Thermal Field Theory. *Cambridge University Press, Cambridge*, 1996.

Smilga, A. Lectures on QCD. *World Scientific, Singapore*, 2001.

Dolan, L. and R. Jackiw. *Phys. Rev. D*, 9:3320, 1974.

Gross, D.J. and A. Neveu. *Phys. Rev. D*, 10:4410, 1974.

De Calan, C., P.A. Faria da Veiga, J. Magnen and R. Séneor. *Phys. Rev. Lett.*, 66:3233, 1991.

Christiansen, H.R., A.C. Petkou, M.B. Silva Neto and N.D. Vlachos. Thermodynamics of the $2+1$ dimensional Gross-Neveu model with complex chemical potential. *hep-th/9911177*.

Blaizot, J-P., R.M. Galain and N. Wschebor. The Gross-Neveu model at finite temperature at next to leading order in the $1/N$ expansion. *hep-ph/0212084*.

Zubarev, D.N. and M.V. Tokarshuk. *Theor. Math. Phys.*, 88:876, 1991.

Floreanini, R. and R. Jackiw. *Phys. Rev. D.*, 37:2206, 1988; Eboli, O., R. Jackiw and S.-Y. Pi. *Phys. Rev. D*, 37:3557, 1989.

Kim, S.P. and F.C. Khanna. TFD of Time Dependent Boson and Fermion Systems. *quant-ph/0308053*.

Kim, S.P., A.E. Santana and F.C. Khanna. *Phys. Lett. A*, 272:46, 2000.

Sengupta, S., S.P. Kim and F.C. Khanna. *Phys. Rev. D*, 68:105014, 2003.

Schwinger, J. *J. Math. Phys.*, 2:407, 1961; Keldysh, L.V. JETP, 20:1018, 1965.

Takahashi, Y. and H. Umezawa. *Coll. Phenomena*, 2:55, 1975; *Reprinted in Int. J. Mod. Phys.*, 10:1755, 1996.

Umezawa, H. Advanced Field Theory: Micro, Macro and Thermal Physics. *AIP, New York*, 1993.

Umezawa, H., H. Matsumoto and M. Tachiki. Thermofield Dynamics and Condensed States. *North-Holland, Amsterdam*, 1982.

Whitehead, J.P., H. Matsumoto and H. Umezawa. *Phys. Lett. A*, 103:408, 1984.

Mann, A. and M. Revzen. *Phys. Lett. A*, 134:273, 1989.

Mann, A., M. Revzen, H. Umezawa and Y. Yamanaka. *Phys. Lett. A*, 140:475, 1989.

Chaturvedi, S., V. Srinivasan and G.S. Agarwal. *J. Phys. A: Math. Gen.*, 32:1909, 1999.

Silva, L.M., A.E. Santana and J.D.M. Vianna. *Braz. J. Phys.*, 27:619, 1997.

Abdala, M.C.B., A.L. Gadelha and I.V. Vancea. *Phys. Rev. D*, 64:086005, 2001.

Abdala, M.C.B., A.L. Gadelha and I.V. Vancea. *Int. J. Mod. Phys. A*, 18:2109, 2003.

Chu, H. and H. Umezawa. *Int. J. Mod. Phys. A*, 9:2363, 1994.

Ojima, I. *Ann. Phys. (N.Y.)*, 137:1 1981.

Santana, A.E., A. Matos Neto, J.D.M. Vianna and F.C. Khanna. *Int. J. Theor. Phys.*, 38:641, 1999.

Santana, A.E. and F.C. Khanna. *Phys. Let. A*, 203:68, 1995.

Santana, A.E., A. Matos Neto, J.D.M. Vianna and F.C. Khanna. *Physica A*, 280:405, 2000.

Kopf, T., A.E. Santana and F.C. Khanna. *J. Math. Phys.*, 38:4071, 1997.

Celeghihi E., et.al. *Phys. Lett. A*, 244:455, 1998.

Malbouisson, A.P.C. and J.M.C. Malbouisson. *J. Phys. A: Math. Gen.*, 35:2263, 2002.

Malbouisson, A.P.C., J.M.C. Malbouisson and A.E. Santana. *Nucl. Phys. B*, 631:83, 2002.

Da Silva, J.C., F.C. Khanna, A. Matos Neto and A.E. Santana. *Phys. Rev. A*, 66:052101, 2002.

Abreu, L.M., C. de Calan, A.P.C. Malbouisson, J.M.C. Malbouisson and A.E.Santana. *J. Math. Phys.*, 46:12304, 2005.

Malbouisson, A.P.C., J.M.C. Malbouisson, A.E. Santana and J.C. da Silva. *Phys. Lett. B*, 583:373, 2004.

Queiroz, H., J.C. da Silva, F. C. Khanna, J. M. C. Malbouisson, M. Revzen and A.E. Santana. Thermofield Dynamics and Casimir Effect for Fermions. *Ann. Phys. (N.Y.)*, 317:220, 2005.

Chodos, A., R.L. Jaffe, K. Johnson, C.B. Thorn and V.F. Weisskopf. *Phys. Rev D*, 9:3471, 1974.

Lutken, C.A. and F. Ravndal. *J. Phys. A: Math. Gen.*, 21:L793, 1988.

De Groot, S.R., W.A. Van Leeuwen and Ch.G. Van Weert. Relativistic Kinetic Theory - Principles and Applications. *North-Holland, New York*, 1980.

Gawedzki, K. and A. Kupianen. *Nucl. Phys. B*, 262:33, 1985.

Particle Data Group. *Phys. Lett. B*, 592:1, 2004.

Karshenboim, S.G. *Can. J. Phys.*, 77:241, 1999.

Thermofield dynamics:
Generalized Bogoliubov transformations
and applications to Casimir effect

F.C. Khanna[(a)], J.M.C. Malbouisson[b] and A.E. Santana[(c)]

(a) Physics Department, Theoretical Physics Institute,
University of Alberta Edmonton, Alberta T6G 2J1 Canada and
TRIUMF 4004, Westbrook mall,
Vancouver, British Columbia V6T 2A3, Canada
(b) Instituto de Fisica, Universidade Federal da Bahia
40210-340, Salvador, BA, Brazil
(c) Instituto de Fisica, Universida de Brasilia,
70910-900, Brasilia, DF, Brazil

Abstract. Within the context of the Thermofield Dynamics, we introduce generalized Bogoliubov transformations which accounts simultaneously for spatial compactification and thermal effects. As a specific application of such a formalism, we consider the Casimir effect for Maxwell and Dirac fields at finite temperature. Particularly, we determine the temperature at which the Casimir pressure for a massless fermionic field in a cubic box changes its nature from attractive to repulsive. This critical temperature is approximately $100\,MeV$ when the edge of the cube is of the order of the confining length ($\approx 1\,fm$) for baryons.

Keywords: Thermofield dynamics, Bogoliubov transformation, Compactification, Casimir effect.

Introduction

The Thermofield Dynamics (TFD) formalism (Y. Takahashi et.al., 1975; H. Umezawa et.al., 1982; H. Umezawa, 1993) relies on two basic ingredients: first, the doubling of the original Fock space of the system leading to an expanded space $\mathcal{H}_T = \mathcal{H} \otimes \tilde{\mathcal{H}}$; this doubling is carried out by associating to each operator a acting on $\mathcal{H}$ two operators in $\mathcal{H}_T$, $A = a \otimes \mathbf{1}$ and $\tilde{A} = \mathbf{1} \otimes a$, which are connected by the tilde (dual) conjugation rules $(A_i A_j)\tilde{} = \tilde{A}_i \tilde{A}_j$, $(cA_i + A_j)\tilde{} = c^* \tilde{A}_i + \tilde{A}_j$, $(A_i^\dagger)\tilde{} = (\tilde{A}_i)^\dagger$ and $(\tilde{A}_i)\tilde{} = -\xi A_i$, with $\xi = -1$ for bosons and $\xi = +1$ for fermions. The physical variables are described by nontilde operators. Second, a Bogoliubov transformation, $B(\alpha)$, introducing a rotation in the tilde and nontilde variables, in such a way that thermal effects emerge from a condensate state. In the standard doublet notation (H. Umezawa,

1993), we write

$$(A^r(\alpha)) = \begin{pmatrix} A(\alpha) \\ \xi \widetilde{A}^\dagger(\alpha) \end{pmatrix} = B(\alpha) \begin{pmatrix} A \\ \xi \widetilde{A}^\dagger \end{pmatrix}, \tag{1}$$

$(A^r(\alpha))^\dagger = \left(A^\dagger(\alpha), \, \widetilde{A}(\alpha) \right)$, with the Bogoliubov transformation given by

$$B(\alpha) = \begin{pmatrix} u(\alpha) & -v(\alpha) \\ \xi v(\alpha) & u(\alpha) \end{pmatrix}, \tag{2}$$

where $u^2(\alpha) + \xi v^2(\alpha) = 1$. The usual parametrization of the Bogoliubov transformation in TFD is obtained by setting $\alpha = \beta = T^{-1}$ and by requiring that $\langle 0, \tilde{0} | a^\dagger(\alpha) a(\alpha) | 0, \tilde{0} \rangle$ (with $a^\dagger$ and a being the creation and the annihilation operators) gives either the Bose or the Fermi distribution; therefore

$$u(\beta) = \left(1 + \xi e^{-\beta\varepsilon} \right)^{-\frac{1}{2}} \quad , \quad v(\beta) = \left(e^{\beta\varepsilon} + \xi \right)^{-\frac{1}{2}}. \tag{3}$$

The TFD formalism permits the discussion of several aspects in quantum mechanics, as for example, the thermal coherent states of an oscillator.

In this talk, we consider the TFD approach for free fields aiming to extend the Bogoliubov transformation to account also for spatial compactification effects. The main application of our general discussion is the Casimir effect for cartesian confining geometries at finite temperature.

1.   Free massless fields in TFD

The formalism can be extended for a quantum field with the TFD Lagrangian density given by $\mathcal{L}_T = \mathcal{L} - \widetilde{\mathcal{L}}$, where $\widetilde{\mathcal{L}}$ is a replica of $\mathcal{L}$ for the tilde fields so leading to similar equations of motion. For the purpose of our applications, we shall restrict our analysis to free massless fields. Thus, considering the free-massless boson (Klein-Gordon) field, the two-point Green function in the doubled space is given by

$$\begin{aligned} G_0^{(ab)}(x - x') &= \langle 0, \tilde{0} | T\phi(x)^a \phi(x')^b | 0, \tilde{0} \rangle \\ &= \frac{-1}{(2\pi)^4} \int d^4 k \; G_0^{(ab)}(k) \; e^{-ik \cdot (x - x')}, \end{aligned} \tag{4}$$

where (remember that $\xi = -1$ whenever we refer to bosons)

$$G_0^{(ab)}(k) = \begin{pmatrix} G_0(k) & 0 \\ 0 & \xi G_0^*(k) \end{pmatrix} = \begin{pmatrix} \frac{1}{k^2 + i\epsilon} & 0 \\ 0 & \frac{-\xi}{k^2 - i\epsilon} \end{pmatrix}. \tag{5}$$

In the configuration space, we have explicitly

$$G_0(x - x') = \frac{-i}{(2\pi)^2} \frac{1}{(x - x')^2 - i\varepsilon}. \tag{6}$$

Also, the doubled free-photon propagator is given by

$$iD_{\mu\nu}^{(ab)}(x - x') = \langle 0, \tilde{0}|T[A_\mu^a(x)A_\nu^b(x')]|0, \tilde{0}\rangle = g_{\mu\nu}G_0^{(ab)}(x - x'). \tag{7}$$

On the other hand, for the free-massless Dirac field, the doubled Green function is given by

$$S_0^{(ab)}(x - x') = \begin{pmatrix} S_0(x - x') & 0 \\ 0 & -S_0^*(x' - x) \end{pmatrix}, \tag{8}$$

where $S_0(x - x') = -i\langle 0|T[\psi(x)\overline{\psi}(x')]|0\rangle = -i\gamma_\mu\partial^\mu G_0(x - x')$. The α-dependent Green functions in all cases are obtained through the Bogoliubov transformations (2) (carrying a label k for each field mode) acting on $G_0^{(ab)}(k)$:

$$G_0^{(ab)}(k; \alpha) = B_k^{-1(ac)}(\alpha)G_0^{(cd)}(k)B_k^{(db)}(\alpha); \tag{9}$$

explicitly, the components of $G_0^{(ab)}(k; \alpha)$ are given by

$$G_0^{11}(k; \alpha) = G_0(k) + \xi v_k^2(\alpha)[G_0^*(k) - G_0(k)], \tag{10}$$
$$G_0^{12}(k; \alpha) = G_0^{21}(k; \alpha) = \xi v_k(\alpha)u_k(\alpha)[G_0^*(k) - G_0(k)], \tag{11}$$
$$G_0^{22}(k; \alpha) = \xi G_0^*(k) + v_k^2(\alpha)[G_0(k) - G_0^*(k)]. \tag{12}$$

Notice that, taking $\xi = +1$, we obtain the auxiliary doubled two-point function which must be used for calculating the fermionic propagator.

We shall be concerned with the doubled operators describing the energy-momentum tensor of the free Maxwell and Dirac fields; according to the tilde conjugation rules, we have, respectively:

$$T_{\mathrm{M}}^{\mu\nu(ab)} = -F^{\mu\lambda(ab)}F_\lambda^{\nu(ab)} + \frac{1}{4}g^{\mu\nu}F_{\lambda\rho}^{(ab)}F^{\rho\lambda(ab)}, \tag{13}$$

$$T_{\mathrm{D}}^{\mu\nu(ab)} = \frac{i}{2}(\overline{\psi}^a\gamma^\mu\partial^\nu\psi^b - \partial^\nu\overline{\psi}^a\gamma^\mu\psi^b), \tag{14}$$

where $F_{\mu\nu}^{(ab)} = \partial_\mu A_\nu^a - \partial_\nu A_\mu^b$ is the electromagnetic field tensor. In all cases, the α-dependent energy-momentum tensors are obtained from these expressions replacing the fields by the Bogoliubov transformed counterparts. Actually, to treat thermal (and space confinement) effects, we will consider the renormalized vacuum expectation value of

the α-dependent energy-momentum tensor defined, by subtracting the value corresponding to the free space at zero temperature, as

$$\mathcal{T}^{\mu\nu(ab)}(x;\alpha) = \langle 0, \tilde{0}|T^{\mu\nu(ab)}(x;\alpha)|0, \tilde{0}\rangle - \langle 0, \tilde{0}|T^{\mu\nu(ab)}(x)|0, \tilde{0}\rangle. \quad (15)$$

In fact, we will be interested in calculating only the (11)-component, which corresponds to the physical energy-momentum tensor.

Let us now consider the thermal effects by taking $\alpha = \beta = T^{-1}$. Notice, initially, that $v_k^2(\alpha)$ (given in Eq. (3) for one mode, with $k_0 = \varepsilon$) can be written, for both boson ($\xi = -1$) and fermion ($\xi = +1$) fields, as

$$v_k^2(\beta) = \sum_{l=1}^{\infty} (-\xi)^{l+1} e^{-\beta k_0 l}, \quad (16)$$

so that Eq. (10) becomes

$$G_0^{11}(k;\beta) = G_0(k) + \sum_{l=1}^{\infty} (-\xi)^{l+1} e^{-\beta k_0 l}[G_0^*(k) - G_0(k)]. \quad (17)$$

Taking the inverse Fourier transform, we obtain

$$\bar{G}_0^{11}(x - x';\beta) = \sum_{l=1}^{\infty} (-\xi)^{l+1} \left[G_0^*(x' - x - i\beta l \hat{n}_0) \right.$$
$$\left. - G_0(x - x' - i\beta l \hat{n}_0) \right], \quad (18)$$

where $\bar{G}_0^{11}(x-x';\beta) = G_0^{11}(x-x';\beta) - G_0(x-x')$ and $\hat{n}_0 = (1,0,0,0)$ is a time-like vector. This expression is useful for calculating $\mathcal{T}^{\mu\nu(11)}(x;\beta)$.

Consider, for example, the electromagnetic field. In this case, we have

$$\langle 0, \tilde{0}|T_M^{\mu\nu(ab)}(x;\beta)|0, \tilde{0}\rangle = -i \left\{ \Gamma^{\mu\nu}(x, x') G^{(ab)}(x - x';\beta) \right.$$
$$\left. + 2\left(\hat{n}_0^{\mu}\hat{n}_0^{\nu} - \frac{1}{4}g^{\mu\nu} \right) \delta(x - x')\delta^{ab} \right\} \Bigg|_{x \to x'},$$

where $\Gamma^{\mu\nu}(x, x') = 2(\partial^{\mu}\partial'^{\nu} - \frac{1}{4}g^{\mu\nu}\partial^{\rho}\partial'_{\rho})$. This leads to

$$\mathcal{T}_M^{\mu\nu(11)}(\beta) = -i \left\{ \Gamma^{\mu\nu}(x, x') \bar{G}_0^{11}(x - x';\beta) \right\} \Big|_{x \to x'}$$
$$= -\frac{2}{\pi^2} \sum_{l=1}^{\infty} \frac{g^{\mu\nu} - 4\hat{n}_0^{\mu}\hat{n}_0^{\nu}}{(\beta l)^4} = \frac{-\pi^2}{45\beta^4}(g^{\mu\nu} - 4\hat{n}_0^{\mu}\hat{n}_0^{\nu}), \quad (19)$$

where we have used the Riemann *zeta*-function $\zeta(4) = \sum_{l=1}^{\infty} l^{-4} = \pi^4/90$. As expected, $E(T) = \mathcal{T}_M^{00(11)}(\beta) = \frac{1}{15}\pi^2 T^4$ gives the correct energy density of the photon gas at temperature T, the blackbody

radiation. Similar result can be obtained for the free-massless fermionic field. In this case, we have

$$\langle 0, \tilde{0} | T_{\mathrm{D}}^{\mu\nu(ab)}(x; \beta) | 0, \tilde{0} \rangle = \gamma^\mu \partial^\nu S^{(ab)}(x - x')|_{x' \to x}$$
$$= -4i\partial^\mu \partial^\nu G_0^{(ab)}(x - x')|_{x' \to x},$$

leading to

$$\mathcal{T}_D^{\mu\nu(11)}(\beta) = -4i\partial^\mu\partial^\nu [\bar{G}_0^{11}(x - x'; \beta)]_{x' \to x}$$
$$= \frac{4}{\pi^2} \sum_{l=1}^{\infty} (-1)^l \left[\frac{g^{\mu\nu} - 4\widehat{n}_0^\mu \widehat{n}_0^\nu}{(\beta l)^4} \right]. \tag{20}$$

From this tensor, using that $\sum_{l=1}^{\infty}(-1)^l l^{-4} = -7\pi^4/720$ we recover the well known result for the internal energy density of the Dirac field at temperature T, $E(T) = \mathcal{T}_D^{00(11)}(\beta) = \frac{7\pi^2}{60}T^4$.

The main goal of this talk is to show that the Bogoliubov transformation of TFD can be generalized to account for spatial compactification and thermal effects simultaneously. These ideas are then applied to the Casimir effect in various cases.

2. Generalized Bogoliubov transformations

The preceding results show that the equilibrium TFD is equivalent to the Matsubara imaginary-time formalism (for a detailed discussion, see the chapter by Santana et. al. in this Proceedings). Matsubara formalism has been used also to consider spatial compactification in field theoretical models (A.P.C. Malbouisson et.al., 2002; A.P.C. Malbouisson et.al., 2002; A.P.C. Malbouisson et.al., 2004).

Similarly, confined fields can be treated with TFD by choosing appropriately the parameter α entering in the Bogoliubov transformation (J.C. da Silva et.al., 2002; H. Queiroz et.al., 2005). To see how this works, replace β and k_0 in Eq. (16) by $\alpha = i2L$ and k_3, corresponding to confinement along the z-axis, writing

$$v_k^2(L) = \sum_{l=1}^{\infty} (-\xi)^{l+1} e^{-i2Lk_3 l}. \tag{21}$$

Using this v_k^2 in Eq. (10) and performing the inverse Fourier transform, we get

$$\bar{G}_0^{11}(x - x'; L) = \sum_{l=1}^{\infty} (-\xi)^{l+1} [G_0^*(x' - x - 2Ll\widehat{n}_3)$$
$$- G_0(x - x' - 2Ll\widehat{n}_3)] \tag{22}$$

where $\bar{G}_0^{11}(x - x'; L) = G_0^{11}(x - x'; L) - G_0(x - x')$ and $\widehat{n}_3 = (0, 0, 0, 1)$. For this situation, similar steps as those leading to Eqs. (19) and (20) give

$$\mathcal{T}_M^{\mu\nu(11)}(L) = -\frac{2}{\pi^2} \sum_{l=1}^{\infty} \frac{g^{\mu\nu} + 4\widehat{n}_3^\mu \widehat{n}_3^\nu}{(2Ll)^4} = -\frac{\pi^2}{720L^4}(g^{\mu\nu} + 4\widehat{n}_3^\mu \widehat{n}_3^\nu), \quad (23)$$

$$\mathcal{T}_D^{\mu\nu(11)}(L) = \frac{4}{\pi^2} \sum_{l=1}^{\infty} (-1)^l \left[\frac{g^{\mu\nu} + 4\widehat{n}_3^\mu \widehat{n}_3^\nu}{(2Ll)^4} \right] = -\frac{7\pi^2}{2880}[g^{\mu\nu} + 4\widehat{n}_3^\mu \widehat{n}_3^\nu]. \quad (24)$$

The Casimir effect for the electromagnetic field between parallel metallic plates can be obtained from Eq. (23); the Casimir energy and pressure are

$$E(L) = \mathcal{T}_M^{00(11)}(L) = -\frac{\pi^2}{720L^4} \ , \quad P(L) = \mathcal{T}_M^{33(11)}(L) = -\frac{\pi^2}{240L^4} \ .$$

Similarly, from Eq. (24), we find the Casimir energy and pressure for the Dirac field confined between parallel plates, with anti-periodic boundary conditions, as:

$$E(L) = \mathcal{T}_D^{00(11)}(L) = -\frac{7\pi^2}{2880L^4} \ ; \quad P(L) = \mathcal{T}_D^{33(11)}(L) = -\frac{7\pi^2}{960L^4} \ .$$

These results demonstrate explicitly the usefulness of the Bogoliubov transformation to treat confined fields in the context of TFD. From the above considerations, a question emerges naturally: what should be the appropriate generalization of the Bogoliubov transformation to account for simultaneously space compactification and thermal effects?

Such a generalization must reproduce, for example, the known results for the Casimir effect in the case of the parallel plates geometry at finite temperatures. Since energy is an additive quantity, we expect to have L- and T-dependent contributions plus a mixed (LT-dependent) contribution representing the interference of the two effects. In the next Section, we will show that the proper extension of expressions (16) and (21), for this case, is

$$
\begin{aligned}
v_k^2(\beta, L) = & \sum_{l_0=1}^{\infty} (-\xi)^{l_0+1} e^{-\beta k_0 l_0} + \sum_{l_3=1}^{\infty} (-\xi)^{l_3+1} e^{-i2Lk_3 l_3} \\
& + 2 \sum_{l_0, l_3=1}^{\infty} (-\xi)^{l_0+l_3+2} e^{-\beta k_0 l_0 - i2Lk_3 l_3} \ .
\end{aligned}
\quad (25)
$$

To treat the general situation, compatible with cartesian geometries, we will consider the (1+N)-dimensional Minkowski space. Then, taking

$\alpha = (\alpha_0, \alpha_1, \alpha_2, ..., \alpha_N)$, we write

$$v_k^2(\alpha) = \sum_{s=1}^{N+1} \sum_{\{\sigma_s\}} \left(\prod_{n=1}^{s} f(\alpha_{\sigma_n}) \right) 2^{s-1}$$

$$\times \sum_{l_{\sigma_1},...,l_{\sigma_s}=1}^{\infty} (-\xi)^{s+\sum_{r=1}^{s} l_{\sigma_r}} \exp\{-\sum_{j=1}^{s} \alpha_{\sigma_j} l_{\sigma_j} k_{\sigma_j}\}, \quad (26)$$

where $f(\alpha_j) = 0$ for $\alpha_j = 0$, $f(\alpha_j) = 1$ otherwise and $\{\sigma_s\}$ denotes the set of all combinations with s elements, $\{\sigma_1, \sigma_2, ...\sigma_s\}$, of the first $N + 1$ natural numbers $\{0, 1, 2, ..., N\}$, that is all subsets containing s elements, which we choose to write in an ordered form with $\sigma_1 < \sigma_2 < \cdots < \sigma_s$. Inserting this $v_k^2(\alpha)$ into Eq. (10) and taking the inverse Fourier transform, we obtain

$$\bar{G}_0^{11}(x - x'; \alpha) = \sum_{s=1}^{N+1} \sum_{\{\sigma_s\}} \left(\prod_{n=1}^{s} f(\alpha_{\sigma_n}) \right) \sum_{l_{\sigma_1},...,l_{\sigma_s}=1}^{\infty} (-\xi)^{s+\sum_{r=1}^{s} l_{\sigma_r}}$$

$$\times 2^{s-1} \left[G_0^*(x' - x - i\sum_{j=1}^{s} \eta_{\sigma_j} \alpha_{\sigma_j} l_{\sigma_j} \widehat{n}_{\sigma_j}) \right.$$

$$\left. - G_0(x - x' - i\sum_{j=1}^{s} \eta_{\sigma_j} \alpha_{\sigma_j} l_{\sigma_j} \widehat{n}_{\sigma_j}) \right] \Bigg|_{x' \to x} , \quad (27)$$

where $\eta_{\sigma_j} = +1$, if $\sigma_j = 0$, and $\eta_{\sigma_j} = -1$ for $\sigma_j = 1, 2, ..., N$. To get the physical situation of finite temperature and spatial confinement, α_0 has to be taken as a positive real number while α_n, for $n = 1, 2, ..., N$, must be pure imaginary of the form $i2L_n$; in these cases, one finds that $\alpha_j^{*2} = \alpha_j^2$.

Considering such choices for the parameters α_j and using the explicit form of $\bar{G}_0^{11}(x - x'; \alpha)$ in the 4-dimensional space-time (corresponding to $N = 3$), we obtain the renormalized α-dependent energy-momentum tensor in the general case, for both Maxwell and Dirac fields:

$$\mathcal{T}_M^{\mu\nu(11)}(\alpha) = -i \left\{ \Gamma^{\mu\nu}(x, x') \bar{G}_0^{11}(x - x'; \alpha) \right\} \Big|_{x \to x'}$$

$$= -\frac{2}{\pi^2} \sum_{s=1}^{4} \sum_{\{\sigma_s\}} \left(\prod_{n=1}^{s} f(\alpha_{\sigma_n}) \right) 2^{s-1}$$

$$\times \sum_{l_{\sigma_1},...,l_{\sigma_s}=1}^{\infty} \left[\frac{g^{\mu\nu}}{[\sum_{j=1}^{s} \eta_{\sigma_j}(\alpha_{\sigma_j} l_{\sigma_j})^2]^2} \right.$$

$$\left. - \frac{2\sum_{j,r=1}^{s}(1 + \eta_{\sigma_j}\eta_{\sigma_r})(\alpha_{\sigma_j} l_{\sigma_j})(\alpha_{\sigma_r} l_{\sigma_r})\widehat{n}_{\sigma_j}^{\mu}\widehat{n}_{\sigma_r}^{\nu}}{[\sum_{j=1}^{s} \eta_{\sigma_j}(\alpha_{\sigma_j} l_{\sigma_j})^2]^3} \right]; \quad (28)$$

$$
\begin{aligned}
\mathcal{T}_D^{\mu\nu(11)}(\alpha) &= -4i\partial^\mu\partial^\nu[\bar{G}_0^{11}(x-x';\alpha)]_{x'\to x} \\
&= -\frac{4}{\pi^2}\sum_{s=1}^{4}\sum_{\{\sigma_s\}}\left(\prod_{n=1}^{s}f(\alpha_{\sigma_n})\right)\sum_{l_{\sigma_1},\dots,l_{\sigma_s}=1}^{\infty}(-1)^{s+\sum_{r=1}^{s}l_{\sigma_r}} \\
&\quad \times 2^{s-1}\left[\frac{g^{\mu\nu}}{[\sum_{j=1}^{s}\eta_{\sigma_j}(\alpha_{\sigma_j}l_{\sigma_j})^2]^2}\right.\\
&\quad \left.-\frac{2\sum_{j,r=1}^{s}(1+\eta_{\sigma_j}\eta_{\sigma_r})(\alpha_{\sigma_j}l_{\sigma_j})(\alpha_{\sigma_r}l_{\sigma_r})\widehat{n}_{\sigma_j}^{\mu}\widehat{n}_{\sigma_r}^{\nu}}{[\sum_{j=1}^{s}\eta_{\sigma_j}(\alpha_{\sigma_j}l_{\sigma_j})^2]^3}\right]. \quad (29)
\end{aligned}
$$

Notice that the results obtained so far (Eqs. (19) and (23) for the Maxwell field and Eqs. (20) and (24) for the Dirac field) are particular cases of the above expressions, corresponding to $\alpha = (\beta, 0, 0, 0)$ and $\alpha = (0, 0, 0, i2L)$ respectively. Another important aspect is that $\mathcal{T}^{\mu\nu(11)}(\alpha)$ is traceless in both cases, as it should be. Now, we will apply these general results to some specific examples.

3. Casimir effect for parallel plates at finite temperature

As a first example of developments of the last Section, we now consider the electromagnetic field satisfying Dirichlet boundary conditions on parallel planes (metallic plates), normal to the z-direction, at finite temperature. In this case, $v_k^2(\alpha)$ is given by Eq. (25) with $\xi = -1$ (corresponding to the choice $\alpha = (\beta, 0, 0, i2L)$) and Eq. (28) reduces to

$$
\begin{aligned}
\mathcal{T}_M^{\mu\nu(11)}(\beta, L) = -\frac{2}{\pi^2}\left\{\sum_{l_0=1}^{\infty}\frac{g^{\mu\nu}-4\widehat{n}_0^{\mu}\widehat{n}_0^{\nu}}{(\beta l_0)^4}+\sum_{l_3=1}^{\infty}\frac{g^{\mu\nu}+4\widehat{n}_3^{\mu}\widehat{n}_3^{\nu}}{(2Ll_3)^4}\right.\\
\left.+2\sum_{l_0,l_3=1}^{\infty}\frac{(\beta l_0)^2[g^{\mu\nu}-4\widehat{n}_0^{\mu}\widehat{n}_0^{\nu}]+(2Ll_3)^2[g^{\mu\nu}+4\widehat{n}_3^{\mu}\widehat{n}_3^{\nu}]}{[(\beta l_0)^2+(2Ll_3)^2]^3}\right\}(30)
\end{aligned}
$$

It follows then that the Casimir energy $(\mathcal{T}_M^{00(11)})$ and pressure $(\mathcal{T}_M^{33(11)})$ are given by (J.C. da Silva et.al., 2002)

$$
E(\beta, L) = \frac{\pi^2}{15\beta^4} - \frac{\pi^2}{720L^4} + \frac{4}{\pi^2}\sum_{l_0,l_3=1}^{\infty}\frac{3(\beta l_0)^2-(2Ll_3)^2}{[(\beta l_0)^2+(2Ll_3)^2]^3}, \quad (31)
$$

$$
P(\beta, L) = \frac{\pi^2}{45\beta^4} - \frac{\pi^2}{240L^4} + \frac{4}{\pi^2}\sum_{l_0,l_3=1}^{\infty}\frac{(\beta l_0)^2-3(2Ll_3)^2}{[(\beta l_0)^2+(2Ll_3)^2]^3}. \quad (32)
$$

The first two terms of these expressions reproduce Eqs. (19) and (23), giving the blackbody and the Casimir contributions for the energy

and the pressure, separately. The last term represents the interplay between the two effects. These results have been obtained before with the use of mode-sum techniques and the image method (L.S. Brown et.al., 1969; G. Plunien et.al., 1986). Thefore, they constitute a clear indication that our generalization of the Bogoliubov transformation has the correct form.

We notice that the positive blackbody contributions for E and P dominate in the high-temperature limit, while the energy and the pressure are negative for low T. From Eq. (32), we can determine the critical curve $(\beta_c = \chi_0 L)$ for the transition from negative to positive values of P, by searching for the value of the ratio $\chi = \beta/L$ for which the pressure vanishes; this value, χ_0, is the solution of the transcendental equation

$$\frac{\pi^2}{45}\frac{1}{\chi^4} - \frac{\pi^2}{240} + \frac{4}{\pi^2}\sum_{l,n=1}^{\infty}\frac{(\chi l)^2 - 3(2n)^2}{[(\chi l)^2 + (2n)^2]^3} = 0, \qquad (33)$$

given, numerically, by $\chi_0 \simeq 1.316$.

Such an analysis can be extended to cases where two or more spatial dimensions are compactified. This will be explored in the next Section for the fermionic effect.

4. Casimir effect for fermions

We initially consider the massless Dirac field confined between parallel planes. In this case, we take $\alpha = (\beta, 0, 0, i2L)$ and $\xi = +1$ in Eq. (29) leading to

$$\mathcal{T}_D^{\mu\nu(11)}(\beta, L) = \frac{4}{\pi^2}\left\{\sum_{l_0=1}^{\infty}\frac{[g^{\mu\nu} - 4\widehat{n}_0^{\mu}\widehat{n}_0^{\nu}]}{(-1)^{l_0}(\beta l_0)^4} + \sum_{l_3=1}^{\infty}\frac{[g^{\mu\nu} + 4\widehat{n}_3^{\mu}\widehat{n}_3^{\nu}]}{(-1)^{l_3}(2Ll_3)^4}\right.$$

$$\left. - 2\sum_{l_0,l_3=1}^{\infty}\frac{(\beta l_0)^2[g^{\mu\nu} - 4\widehat{n}_0^{\mu}\widehat{n}_0^{\nu}] + (2Ll_3)^2[g^{\mu\nu} + 4\widehat{n}_3^{\mu}\widehat{n}_3^{\nu}]}{(-1)^{l_0+l_3}[(\beta l_0)^2 + (2Ll_3)^2]^3}\right\}; \quad (34)$$

the Casimir energy and pressure are readily obtained as:

$$E(\beta, L) = \frac{7\pi^2}{60\beta^4} - \frac{7\pi^2}{2880L^4} - \frac{8}{\pi^2}\sum_{l_0,l_3=1}^{\infty}(-1)^{l_0+l_3}\frac{3(\beta l_0)^2 - (2Ll_3)^2}{[(\beta l_0)^2 + (2Ll_3)^2]^3}; (35)$$

$$P(\beta, L) = \frac{7\pi^2}{180\beta^4} - \frac{7\pi^2}{960L^4} + \frac{8}{\pi^2}\sum_{l_0,l_3=1}^{\infty}(-1)^{l_0+l_3}\frac{(\beta l_0)^2 - 3(2Ll_3)^2}{[(\beta l_0)^2 + (2Ll_3)^2]^3}. (36)$$

Again, taking the limit $L \to \infty$, we regain the Stefan-Boltzmann contribution alone, while making $\beta \to \infty$ the Casimir term at zero temperature is recovered. The third term, which stands for the correction

of temperature, remains finite as $\beta \to 0$ and so, as expected, the high temperature limit is dominated by the positive contribution of the Stefan-Boltzmann term. These results for the fermionic Casimir effect for parallel plates can be also obtained, using mode-summation techniques, with the field satisfying anti-periodic (bag model) boundary conditions (C.A. Lutken et.al., 1984).

As before, for any given value of L, the pressure changes from negative to positive when the temperature is raised. The critical curve for this transition is $\beta_c = \chi_0 L$, where χ_0 is the value of ratio $\chi = \beta/L$ for which the pressure vanishes, that is the solution of the transcendental equation

$$\frac{7\pi^2}{180}\frac{1}{\chi^4} - \frac{7\pi^2}{960} + \frac{8}{\pi^2}\sum_{l,n=1}^{\infty}(-1)^{l+n}\frac{\chi^2 l^2 - 12n^2}{[\chi^2 l^2 + 4n^2]^3} = 0; \qquad (37)$$

numerically, we find $\chi_0 \simeq 1.382$.

To show how powerful our method is, let us consider fermions confined in a tridimensional box at finite temperature. The energy-momentum tensor is a long expression for the general case of a parallelepiped box, but it follows from Eq. (29) that the Casimir energy for a cubic box of edge L is given by

$$
\begin{aligned}
E_B(\beta, L) \; = \; & \frac{7\pi^2}{60}\frac{1}{\beta^4} - \left(\frac{7\pi^2}{960} + \frac{\mathcal{C}}{2\pi^2}\right)\frac{1}{L^4} \\
& + \frac{24}{\pi^2}\sum_{l,n=1}^{\infty}(-1)^{l+n}\frac{3\beta^2 l^2 - 4L^2 n^2}{[\beta^2 l^2 + 4L^2 n^2]^3} \\
& - \frac{48}{\pi^2}\sum_{l,n,r=1}^{\infty}(-1)^{l+n+r}\frac{3\beta^2 l^2 - 4L^2(n^2 + r^2)}{[\beta^2 l^2 + 4L^2(n^2 + r^2)]^3} \\
& + \frac{32}{\pi^2}\sum_{l,n,r,q=1}^{\infty}(-1)^{l+n+r+q}\frac{3\beta^2 l^2 - 4L^2(n^2 + r^2 + q^2)}{[\beta^2 l^2 + 4L^2(n^2 + r^2 + q^2)]^3},
\end{aligned}
$$
$$(38)$$

where the constant $\mathcal{C}$ is defined by

$$\mathcal{C} = 3\sum_{l,n=1}^{\infty}\frac{(-1)^{l+n}}{(l^2 + n^2)^2} - 2\sum_{l,n,r=1}^{\infty}\frac{(-1)^{l+n+r}}{(l^2 + n^2 + r^2)^2} \simeq 0.707. \qquad (39)$$

Again, as $\beta \to 0$, the Stefan-Boltzmann term dominates, while in the limit $\beta \to \infty$, we find the Casimir energy at zero temperature, the second term in the right hand side of Eq. (38).

The pressure can also be obtained directly from Eq. (29). Notice that, in the case of a cubic box, by symmetry we have $\mathcal{T}_D^{11(11)} =$

$\mathcal{T}_D^{22(11)} = \mathcal{T}_D^{33(11)}$. In terms of L and $\chi = \beta/L$, the pressure can be written as

$$
\begin{aligned}
P_B(\chi, L) = & \; \frac{1}{L^4} \left\{ \frac{7\pi^2}{180} \frac{1}{\chi^4} - \left(\frac{7\pi^2}{2880} + \frac{\mathcal{C}}{6\pi^2} \right) \right. \\
& + \frac{16}{\pi^2} \sum_{l,n=1}^{\infty} \frac{(-1)^{l+n}}{[\chi^2 l^2 + 4n^2]^2} + \frac{8}{\pi^2} \sum_{l,n=1}^{\infty} (-1)^{l+n} \frac{\chi^2 l^2 - 12n^2}{[\chi^2 l^2 + 4n^2]^2} \\
& - \frac{16}{\pi^2} \sum_{l,n,r=1}^{\infty} \frac{(-1)^{l+n+r}}{[\chi^2 l^2 + 4n^2 + 4r^2]^2} \\
& - \frac{32}{\pi^2} \sum_{l,n,r=1}^{\infty} (-1)^{l+n+r} \frac{\chi^2 l^2 + 4n^2 - 12r^2}{[\chi^2 l^2 + 4n^2 + 4r^2]^2} \\
& \left. + \frac{32}{\pi^2} \sum_{l,n,r,q=1}^{\infty} (-1)^{l+n+r+q} \frac{\chi^2 l^2 + 4n^2 + 4r^2 - 12q^2}{[\chi^2 l^2 + 4n^2 + 4r^2 + 4q^2]^2} \right\}.
\end{aligned}
\tag{40}
$$

For a fixed value of L, as $\beta \to \infty$ ($T = 0$), the pressure is negative, given by $P_B(L) \simeq -0.036 L^{-4}$, corresponding to an attractive force between opposite faces of the cube. On the other hand, $P_B(\beta) \approx 7\pi^2/(180\beta^4) > 0$ as $\beta \to 0$ and, therefore, a transition from negative to positive values of the pressure occurs by raising the temperature. The critical temperature for such a transition depends on L and is determined by the value of χ (χ_0) for which $P_B(\chi, L) = 0$; numerically, we find $\chi_0 = 2.283$ and the critical curve is given by

$$
T_c(L) = \frac{1}{\chi_0 L} \simeq \frac{1}{2.283 L}.
\tag{41}
$$

From this expression we can obtain the value of T_c corresponding to a given value of L. For $L \simeq 1\,fm$, which is a value of the order of confining lengths for hadrons, we obtain $T_c \simeq 0.438\,fm^{-1} \simeq 87.6\,MeV$. This gives us a crude estimate of the Casimir contribution of a single quark flavor for the deconfining transition for hadrons.

5. Concluding remarks

We have shown that generalizations of the TFD Bogoliubov transformation allow a calculation, in a very direct way, of the Casimir effect at finite temperature for cartesian confining geometries. This approach is applied to both bosonic and fermionic fields, making very clear the

differences between these cases. It is worth to emphasize that the procedure developed here is simpler and more direct than the standard techniques, such as the sum of modes and the image method.

It is important to stress that use of the generalised Bogoliubov transformatin provides an elegant physical interpretation of the Casimir effect as a consequence of the condensation in the vacuum of the fermion or the boson field. The method can be extended to other geometries such as spherical or cylindrical.

It is interesting to note that we have calculated the casimir pressure at finite temperature for parallel plates, a square wave-guide and a cubic box. For a fermion field in a cubic box with an edge of 1.0 fm, which is of the order of the nuclear dimensions, the critical temperature is 100 MeV. Such a result will have implications for confinement of quarks in nucleons. However such an analysis will require a realistic calculation, a spherical geometry, with full account of color and flavor degrees of freedom of quarks and gluons.

Acknowledgments

References

Takahashi, Y. and H. Umezawa. *Coll. Phenomena*, 2:55, 1975; *Reprinted in Int. J. Mod. Phys.*, 10:1755, 1996.

Umezawa, H., H. Matsumoto and M. Tachiki. Thermofield Dynamics and Condensed States. *North-Holland, Amsterdan*, 1982.

Umezawa, H. Advanced Field Theory: Micro, Macro and Thermal Physics. *AIP, New York*, 1993.

Malbouisson, A.P.C. and J.M.C. Malbouisson. *J. Phys. A: Math. Gen.*, 35:2263, 2002.

Malbouisson, A.P.C., J.M.C. Malbouisson and A.E. Santana. *Nucl. Phys. B*, 631:83, 2002.

Malbouisson, A.P.C., J.M.C. Malbouisson, A.E. Santana and J.C. da Silva. *Phys. Lett. B*, 583:373, 2004.

Da Silva, J.C., F.C. Khanna, A. Matos Neto and A.E. Santana. *Phys. Rev. A*, 66:052101, 2002.

Queiroz, H., J.C. da Siva, F.C. Khanna, J.M.C. Malbouisson, M. Revzen and A.E. Santana. *Annals of Physics*, to appear., 2005.

Brown L.S. and G.J. Maclay. *Phys. Rev.* 184:1272, 1969.

Plunien, G., B. Müeller and W. Greiner. *Phys. Rep.*, 134:87, 1986.

Lutken, C.A. and F. Ravndal. *J. Phys. G: Nucl. Phys.*, 10:123, 1984.

A force from nothing onto nothing: Casimir effect between bubbles in the Fermi sea

Andreas Wirzba

Institut für Kernphysik (Theorie), Forschungszentrum Jülich
D-52425 Jülich, Germany

Abstract.
   We report on a new force that acts on cavities (literally empty regions of space) when they are immersed in a background of non-interacting fermionic matter fields. The interaction follows from the obstructions to the (quantum mechanical) motions of the fermions in the Fermi sea caused by the presence of bubbles or other (heavy) particles immersed in the latter, as, for example, nuclei in the neutron sea in the inner crust of a neutron star.

   This effect resembles the traditional Casimir effect, which describes the attraction between two parallel metallic mirrors in vacuum. Here, however, the fluctuating (bosonic) electromagnetic fields are replaced by fermionic matter fields. Furthermore, the Casimir energy is inferred from the geometry-dependent part of the density of states, and its sign is not fixed, but oscillates according to the relative arrangement and distances of the cavities.

   In fact, with the help of Krein's trace formula, the quantum field theory calculation is mapped onto a quantum mechanical billiard problem of a point-particle scattered off a finite number of non-overlapping spheres or disks; i.e. classically hyperbolic (or even chaotic) scattering systems.

   This topic is relevant to the physics of neutron stars (nuclei or quark bubbles embedded in a neutron gas), to dilute Bose-Einstein-condensate bubbles inside the background of a Fermi-Dirac condensate, to buckyballs in liquid mercury and to superconducting droplets in a Fermi liquid.

Keywords: Casimir effect, Fermi sea, scattering problem, Krein formula

1. Introduction

1.1. THE ORIGINAL CASIMIR EFFECT

In 1948 the Dutch physicist H.B.G. Casimir predicted a remarkable effect (Casimir, 1948): two parallel, very closely spaced, flat, uncharged, metallic plates of separation L attract each other in vacuum with a force per area A

$$\frac{F^{\parallel}(L)}{A} = -\frac{\hbar c}{L^4}\frac{\pi^2}{240} \approx -1.3 \times 10^{-7}\frac{1}{L^4}\mathrm{N}\frac{\mu\mathrm{m}^4}{\mathrm{cm}^2}\,. \tag{1}$$

The corresponding Casimir energy is given by

$$\mathcal{E}^{\parallel}(L) = -\frac{\hbar c}{L^3}\frac{\pi^2}{720}A\,. \tag{2}$$

Note that the Casimir force does not depend on any material constants, but is solely formulated in terms of fundamental constants, namely the velocity of

light, c, and Planck's constant, $\hbar = h/2\pi$. In contrast to the long-range $1/L^2$ behavior of the Coulomb force, the *Casimir force* varies more rapidly with distance, i.e. as $1/L^4$. Whereas it is negligible at a separation of more than $1\,\mu\text{m}$, the negative pressure between the plates at a separation of e.g. $10\,\text{nm}$ has already the magnitude of one atmosphere.

The origin of this force can be traced back to the zero-point fluctuations of the electromagnetic field which are modified by the addition of the two plates relative to the free case. This induces the following *change* in the energy of the vacuum:

$$\sum\!\!\!\!\!\!\int \tfrac{1}{2}\hbar\omega_k\big|_{\text{plates}(L)} - \sum\!\!\!\!\!\!\int \tfrac{1}{2}\hbar\omega_k\big|_{\text{free}}, \tag{3}$$

where the summation/integration accounts for all the zero-point modes (labeled by the wave number k, for instance) and ω_k is the eigenfrequency of the modes. As the linear dimension of the plates is of the size of hundred(s) of μm, whereas the separation is less than $1\,\mu\text{m}$, the Casimir effect belongs to the mesoscopic manifestations of quantum fluctuations. It is related to the van der Waals force; note, however, that the latter is attractive at the considered ranges.

Only in the last decade the Casimir effect has been *quantitatively* confirmed in experiment, see the pioneering experiment of S. Lamoureaux in 1997 (Lamoureaux, 1997) and of U. Mohideen and A. Roy in 1998 (Mohideen and Roy, 1998). On February 9, 2001 the Casimir effect even made it into the science section of the *New York Times*. In fact, the Casimir effect was not confirmed for the original geometry of two parallel plates, which in real life are very hard to align in such a way that they stay parallel, but for the much simpler geometry of a sphere (or part of sphere) of radius a opposite to one plate (Lamoreaux, 1999). For such a system, independently of the alignment of the plate, there always exists a minimal separation L. Of course the force (1) has to be readjusted: under the so-called *proximity force approximation* (Derjaguin, Abrikosova and Lifshitz, 1956) it is given by the following expression

$$F^{\text{o}|}(L) = 2\pi a\,\frac{E^{\|}(L)}{A} = 2\pi a\,\frac{-\hbar c}{L^3}\,\frac{\pi^2}{720}\,. \tag{4}$$

1.2. Casimir effect and vacuum energy in quantum field theory

We teach our students that the infinite zero-point energy that arises when a free relativistic scalar (or Dirac-) field theory is canonically quantized can be subtracted (discarded) by a suitable redefinition of the energy-origin; in other words, by normal ordering. However, the energy-origin can be re-defined only once, *and* only in homogenous space (i.e. without boundary conditions) *and*

without gravity. Therefore, the Casimir energy (density) should be defined as the difference of a (properly regularized) eigen-mode sum of a *constrained* quantum field theory minus the eigen-mode sum of the corresponding *free* theory:

$$\varepsilon_C \;=\; \lim_{V\to\infty} \frac{\mathcal{E}_C}{V} \qquad (V : \text{quantization box})$$

$$= \lim_{\Lambda\to\infty} \lim_{V\to\infty} \underbrace{(-1)^{2S}}_{\text{statistics}} \left(\sideset{}{}\sum_{k,\nu_{\text{deg}}} \tfrac{1}{2}\hbar\omega_k|_{V,\Lambda,C} - \sideset{}{}\sum_{k,\nu_{\text{deg}}} \tfrac{1}{2}\hbar\omega_k|_{V,\Lambda,\emptyset} \right) , \quad (5)$$

where the constraint(s) can arise from the presence of gravity (e.g. non-flat metric), external fields (e.g. anomalies), internal fields (e.g. non-perturbative vacuum of quantum chromodynamics (QCD) versus its perturbative one) or from the presence of geometry-dependent boundary conditions (e.g. two plates, two half-spheres, etc.). Here Λ stands for an UV-cutoff, the labels C and $\emptyset$ indicate the presence or absence of a constraint, respectively. The degeneracy factor ν_{deg} accounts for spin and internal quantum numbers, while the spin-statistic factor $(-1)^{2S}$ (with S the spin (helicity) quantum number of the modes) signals that fluctuating relativistic (fermionic) spin-one-half modes acquire an additional minus sign.

2. Generalizations of the concept of Casimir energy

2.1. GEOMETRY DEPENDENCE OF THE CASIMIR ENERGY

Before 1968 everybody expected that the Casimir forces, similarly to the van der Waals forces, always are attractive, as it is indeed the case for two parallel plates, a plate and a sphere or two opposing spheres. Casimir even got inspired by this to suggest in 1953 the following idea of stabilizing the electron (Casimir, 1953): Assume that the electron has the form of a thin spherical shell of radius a, with its electric charge e uniformly distributed over the whole shell. Then, according to Casimir, the arising repulsive static Coulomb energy

$$\mathcal{E}_{em} = \frac{e^2}{2a} \qquad (6)$$

ought to be compensated by an attractive Casimir-type energy of the form

$$\mathcal{E}_C \stackrel{?}{=} -C\,\frac{\hbar c}{2a^3}\,4\pi a^2\,, \qquad (7)$$

which, in similarity to Eq. (2), is assumed to be negative, proportional to the area, here $4\pi a^2$, and inversely proportional to the third power of the distance scale, here a^{-3}. Now if the coefficient C happens to be the fine-structure

constant $e^2/4\pi\hbar c$, both energies would balance independently of the radius a. Unfortunately this intriguing way of determining the fine structure constant as 'an exercise in calculating Bessel functions' (paraphrasing Feynman) is incorrect, as shown by T. Boyer in 1968 (Boyer, 1968): the Casimir force for a spherical shell is repulsive. Balian and Bloch confirmed this in the seventies in their calculations for the total energy of the modes inside a cavity (Balian and Bloch, 1970): the sign of this energy characteristically depends on the geometry of the cavity.

2.2. UTILIZING THE GEOMETRY DEPENDENCE OF THE CASIMIR ENERGY

Let us now invert the logic and define the Casimir energy as the energy resulting from the *geometry-dependent* part of the density of states (d.o.s.) – a concept that is closely related to the shell correction energy in nuclear physics:

$$\rho(E) \equiv \sum_{E_k} \delta(E - E_k) = \rho_0(E) + \rho_{\text{bulk}}(E) + \delta\rho_C(E, \textit{geom.-dep.}) \,, \quad (8)$$

where $\{E_k\}$ are the eigenenergies of the modes, ρ_0 is the d.o.s. of the homogeneous background, ρ_{bulk} is the bulk d.o.s. that sums up the excluded volume effects, surface contributions and Friedel oscillations due to the introduction of each of the obstacles separately, and $\delta\rho_C$ is the Casimir-effect related *geometry-dependent* part of the d.o.s. that takes into account the relative geometric arrangement of the obstacles. The integrated density of states (or number of states, N.o.s) reads as usual

$$\mathcal{N}(E) \equiv \sum_{E_k} \Theta(E - E_k) = \int_0^E dE' \, \rho(E') \,. \quad (9)$$

Now the Casimir energy can be extracted from the *geometry-dependent* part of the density of states as a simple integral

$$\mathcal{E}_C \equiv \int dE \, E \, \delta\rho_C(E, \textit{geom.-dep.}) = -\int dE \, \mathcal{N}_C(E, \textit{geom.-dep.}) \,. \quad (10)$$

2.3. GENERALIZATION OF THE CASIMIR ENERGY CONCEPT TO MATTER FIELDS

Let us assume that space is not "filled" with fluctuating electromagnetic modes, but with a gas of *non-interacting* (non-relativistic) fermions.

Under this scenario we have the following similarities with the ordinary Casimir effect: In both cases, there exist modes sums $\sum \hbar\omega_k$ with *constant*

degeneracy factors. The constant weight of the fluctuating electromagnetic modes can be traced back to the two helicity states of the photon. The constancy in the degeneracy of the fermionic matter modes, on the other hand, follows from Pauli's exclusion principle, where the pertinent weight can be formulated in terms of spin and isospin factors.

However, the Casimir mode summation of matter fields differs from the one of fluctuating fields by the presence of a further independent scale, namely the Fermi energy (i.e., the chemical potential μ at zero temperature) in addition to the geometric size and distance scales (e.g. the area A and the plate separation L).

In the following we will consider the case of matter fields (non-relativistic fermions) located in the space between voids or cavities, such that the matter fields will build up a quantum pressure on the voids. Even if we assume that the matter fields are non-interacting, an *effective* interaction between the empty regions of space will still arise in the background of the fermionic matter fields, since the cavities – depending on their geometric arrangement – can shield the free movement of the matter modes.

Applications of this scenario exist e.g. for the inner crust of neutron stars. Inside the neutron star, with increasing distance from the star's surface, the nuclei start to loose neutrons due to the increasing pressure and density. The folklore is that below saturation density, between $\rho \approx 0.03\,\mathrm{fm}^{-3}$ and $0.1\,\mathrm{fm}^{-3}$, there exists a chain of phases (Baym, Bethe and Pethick, 1971): The lowest density phase consists of spherical nuclei (or nuclear drops) embedded in a homogeneous low-density background of neutrons. With increasing density, further inside the inner crust, the spherical bubbles fuse to form rods. More deeper inside the inner crust the rods fuse to form plate-like structures surrounded by a low-density background of neutrons. At even higher densities, again deeper inside the inner crust, the low-density background phase is compressed to tubes, surrounded now by a high-density nuclear background phase. Then these tubes spallate into low-density bubbles surrounded by the high-density background. Eventually the density at about $0.1\,\mathrm{fm}^{-3}$ is high enough, such that the low-density bubbles are squeezed to zero size and a *uniform* high-density nuclear phase emerges. Note that the liquid drop model was used to predict these various phases via the interplay between the Coulomb and surface energy terms and that the phase differences are of the order of a few keV/fm^3. Aurel Bulgac and Piotr Magierski, however, showed that the neglected shell correction energies of the surrounding background phases in the presence of bubbles and cylindrical tubes (in other words, the Casimir energies) are of the same order of magnitude (Bulgac and Magierski, 2001). They argued that a chaotic transition between the low-density nuclei phase and the high-density uniform phase is rather more likely than the above-mentioned regular chain between the so-called

meatball, *spaghetti*, and *lasagne* phases which received their descriptive nick-names from the Italian cuisine.

The investigation of bubbles inside a Fermi gas background is also of relevance for the inner *core* of neutron stars; namely, under the assumption that quark droplets will form, there exists a similar pattern with the quark droplet phase taking over the role of the embedded nuclei.

Finally, also in the laboratory the study of the interaction of cavities inside a uniform fermionic background is of importance (Bulgac and Wirzba., 2001). Examples are C_{60} buckyballs immersed in liquid mercury. The liquid metal itself serves only as free-moving shapeable neutral background which provides the Fermi gas environment by its conductance electrons, in which the buckyballs "drill" the voids. Another example would be buckyballs in liquid ^{3}He as Fermi gas. Finally, in the future, boson condensate cavities immersed in dilute atomic Fermi condensates could serve as further system with which the effective interactions of cavities inside a Fermi gas can be studied in the lab.

3. Casimir calculation mapped to a scattering problem

Note that the Casimir calculation under the presence of fermionic (non-relativistic) matter fields simplifies enormously since the presence of the second scale, the chemical potential $\mu = \hbar^2 k_F^2 / 2m$ or the Fermi momentum k_F, provides for a natural UV-cutoff, $\Lambda_{UV} \equiv \mu$ and $k_{UV} \equiv k_F$. Therefore the Casimir energy for fermions between two impenetrable (parallel) planes at a distance L is simply given as

$$\mathcal{E}_C = \mu \, F(k_F L) \,, \tag{11}$$

namely in terms of the product of the chemical potential times a finite function of the dimensionless argument $k_F L$.

For more complicated geometries, the computations become more and more involved as it is the case for the ordinary electromagnetic Casimir effect. However, Casimir calculations of a finite number of immersed non-overlapping *spherical* voids or rods, i.e. spheres and cylinders in 3 dimensions or disks in 2 dimensions, are still doable. In fact, these calculations simplify because of Krein's trace formula (Krein, 2004; Beth and Uhlenbeck, 1937)

$$\delta\rho(E) = \bar{\rho}(E) - \bar{\rho}_0(E) = \frac{1}{2\pi i} \frac{d}{dE} \text{tr} \ln S_n(E) \,, \tag{12}$$

which links the variation in the level density $\delta\rho(E)$ (the difference of the total density of states and the background one) to the energy-variation of the phase shift $\frac{1}{2i} \ln \det S_n(E)$ of the n-sphere/disk scattering matrix $S_n(E)$. Note that the level densities on the left hand side are averaged over an energy-interval larger than the mean-level spacing in the volume V of the entire system

in order to match the *continuous* expression on the right hand side. Thus the Casimir calculation can be mapped to a quantum mechanical "billiard" problem: the quantum mechanics of a classically hyperbolic or even chaotic scattering of a point-particle off an assemble of n non-overlapping spheres (or disks) (Eckhardt, 1987; Gaspard and Rice, 1989; Cvitanovic and Eckhardt, 1989; Henseler, Wirzba and Guhr, 1997).

In this way, the geometry-dependent Casimir fluctuations can be extracted from the *multiple*-scattering part of the scattering matrix. The determinant of the n-sphere/disk S-matrix can be separated into a product of the determinants of the 1-sphere/disk S-matrices $S_1(E, a_i)$, where a_i are the radii of the single scatterers, and the ratio of the determinant of the multi-scattering matrix $M(k)$ and its complex conjugate (A. Wirzba., 1999):

$$\det S_n(E) = \prod_{i=1}^{n} \det S_1(E, a_i) \frac{\det (M(k^*))^{\dagger}}{\det M(k)} . \tag{13}$$

Here the energy E and the wave number k are related as $E = \hbar^2 k^2 / 2m$. When inserted into Krein's formula, the product over the single-scatterer determinants generates just the bulk (or Weyl term) contribution to the density of states

$$\bar{\rho}_{\text{bulk}}(E, \{a_i\}) \equiv \sum_{i=1}^{n} \bar{\rho}_{\text{Weyl}}(E, a_i) = \frac{1}{2\pi i} \frac{d}{dE} \sum_{i=1}^{n} \ln \det S_1(E, a_i) , \tag{14}$$

which takes care of the excluded volume terms and the surface terms (including Friedel oscillations). The geometry-dependent part of the d.o.s. is therefore given by a modified Krein equation (Bulgac and Wirzba., 2001) which is formulated in terms of the multi-scattering matrix instead of the full S-matrix

$$\delta \bar{\rho}_C(E, \{a_i\}, \{\vec{r}_{ij}\}) = \bar{\rho}(E) - \bar{\rho}_0(E) - \sum_{i=1}^{n} \bar{\rho}_{\text{Weyl}}(E, a_i)$$

$$= -\frac{1}{\pi} \text{Im} \left(\frac{d}{dE} \ln \det M(E) \right) , \tag{15}$$

where $\vec{r}_{ij}$ are the relative separation vectors between the centers of the spheres (or disks). The pertinent Casimir energy can then be read off from the energy integral

$$\mathcal{E}_C = \int_0^{\mu} dE \, (E - \mu) \, \delta \bar{\rho}_C = -\int_0^{\mu} dE \, \overline{\mathcal{N}}_C . \tag{16}$$

Note that the chemical potential μ serves here as a UV cutoff. Thus the integral is finite. Even if $\mu \to \infty$, the integral is at least conditionally convergent, because of the oscillating nature of $\delta \bar{\rho}_C(E)$ as a function of E. Note that it does not matter whether a canonical-ensemble formulation or a

grandcanonical-ensemble formulation is used to calculate the Casimir energy. In the former the total number of fermions of the geometry-dependent system is the same as the one of the reference system (which is defined by infinitely far separated cavities)

$$N = \int_0^{\mu} dE \left(\bar{\rho}_0 + \bar{\rho}_{\text{bulk}} + \delta\bar{\rho}_C \right) = \int_0^{\mu_0} dE \left(\bar{\rho}_0 + \bar{\rho}_{\text{bulk}} \right), \qquad (17)$$

whereas the chemical potentials μ and μ_0 are different in general. In the latter formulation the chemical potentials of both systems are the same. The results of both formulations merge when the system volume V of the non-interacting fermionic background fields is taken to infinity (Bulgac and Wirzba., 2001).

4. The calculation

The problem is not simplified by Eq. (15), since there exists a closed-form expression for the multi-scattering matrix for n spheres in terms of spherical Bessel and Hankel functions, spherical harmonics and 3j-symbols, where l, l' and m, m' are total angular momentum and z-projection quantum numbers, respectively (Henseler, Wirzba and Guhr, 1997):

$$
\begin{aligned}
M_{lm,l'm'}^{jj'} &= \delta^{jj'}\delta_{ll'}\delta_{mm'} + (1 - \delta^{jj'})\, i^{2m+l'-l}\sqrt{4\pi(2l+1)(2l'+1)} \\
&\quad \times \left(\frac{a_j}{a_{j'}}\right)^2 \frac{j_l(ka_j)}{h_{l'}^{(1)}(ka_{j'})} \sum_{\tilde{l}=0}^{\infty} \sum_{\tilde{m}=-l'}^{l'} \sqrt{2\tilde{l}+1} \\
&\quad \times i^{\tilde{l}} \begin{pmatrix} \tilde{l} & l' & l \\ 0 & 0 & 0 \end{pmatrix} \begin{pmatrix} \tilde{l} & l' & l \\ m-\tilde{m} & \tilde{m} & -m \end{pmatrix} \\
&\quad \times D_{m',\tilde{m}}^{l'}(j,j')\, h_{\tilde{l}}^{(1)}(kr_{jj'})\, Y_{\tilde{l}}^{m-\tilde{m}}(\hat{r}_{jj'}^{(j)})
\end{aligned}
\qquad (18)
$$

The indices $j, j' = 1, 2, \cdots, n$ are the labels of the n spheres of radii a_j and mutual separation $r_{jj'}$. The vectors $\hat{r}_{jj'}^{(j)}$ are the unit vectors pointing from the origin of sphere j (as measured in its local coordinate system) to the origin of sphere j'. The local coordinate system of sphere j' is mapped onto the one of sphere j with the help of the rotation matrix $D_{m',\tilde{m}}^{l'}(j,j')$.

For small scatterers the expression of the multi-scattering matrix simplifies, since only s-wave scattering is important

$$M^{jj'}(E) \approx \delta^{jj'} - (1 - \delta^{jj'}) \underbrace{f_j(E)}_{s\text{-wave}} \frac{\exp(ikr_{jj'})}{r_{jj'}} + \mathcal{O}(p\text{-wave}), \qquad (19)$$

where spherical waves modulated by an s-wave amplitude propagate between the spheres j and j'. This leads to the following expression for the integrated

d.o.s. in the case of two small spherical cavities of common radius a and center-to-center separation r (Bulgac and Wirzba., 2001):

$$\mathcal{N}_C^{oo}(E) = -\frac{1}{\pi}\mathrm{Im}\ln\det M^{oo}(E) \approx \nu_{\mathrm{deg}}\frac{a^2}{\pi r^2}\sin[2(r-a)k] + \mathcal{O}\left((ka)^3\right),$$
(20)

where ν_{deg} is the spin/isospin–degeneracy factor. This expression should be compared with the semiclassical approximation that sums up all partial waves

$$\mathcal{N}_{C,scl}^{oo}(E) = \nu_{\mathrm{deg}}\frac{a^2}{4\pi r(r-2a)}\sin[\underbrace{2(r-2a)k}_{S_{po}(k)/\hbar}].$$
(21)

In fact, the latter is the leading contribution to Gutzwiller's trace formula (Gutzwiller, 1990), namely the contribution of the two-bounce periodic orbit between the two spheres without repetition, with the action $S_{po}(k)=2(r-2a)k$ where $2(r-2a)$ is the length of the geometric path. Note that the semiclassical result is suppressed by a factor of $1/4$ in comparison to the small-scatterer one.

As shown in Ref. (Bulgac and Wirzba., 2001) the semiclassical result is a very good approximation of the full quantum mechanical result calculated from the exact expression (18) of the two-sphere scattering matrix when plugged into the modified Krein formula (15).

Therefore the Casimir energy for the two spherical cavities inside a non-relativistic non-interacting fermion background can be approximated in terms of a spherical Bessel function j_1 as

$$\mathcal{E}_C^{oo} = -\int_0^{\mu(k_F)} dE\,\mathcal{N}_C^{oo}(E) \approx -\nu_{\mathrm{deg}}\,\mu\frac{a^2}{2\pi r(r-2a)}j_1[2(r-2a)k_F], (22)$$

which is valid for $k_F a > 1$. Note that this expression is long-ranged, i.e. $1/L^3$ with $L = r - 2a$, in comparison to the molecular van der Waals energies. For the sphere-plate system the Casimir energy reads instead

$$\mathcal{E}_C^{o|} \approx -\nu_{\mathrm{deg}}\,\mu\frac{a}{2\pi(r-a)}j_1[2(r-a)k_F],$$
(23)

which scales even as $1/L^2$ with $L = r - a$. Note that in both cases, the two-sphere system or the sphere-plate system, the Casimir energy does not have a fixed sign in contrast to the standard Casimir effect with fluctuating electromagnetic or scalar fields between these obstacles. Instead the sign of the Casimir energy oscillates as a function of the action of the two-bounce orbit. Therefore, under an increase of the distance between the cavities, the Casimir energy, which starts out to be attractive, can be made repulsive, and under a further increase of this distance, it can become attractive again, with a decreased strength of course. The reason for this new type of behavior of a Casimir energy is the presence of a new scale in addition to the length

scales, namely the chemical potential μ. In fact, the strength of this fermionic Casimir energy scales with the strength of the chemical potential and therefore with the UV-cutoff of the theory. Also this behavior distinguishes the fermionic Casimir effect from the standard Casimir effect: the latter is governed by the infrared behavior of the corresponding density of states.

In Ref. (Bulgac and Wirzba., 2001) the Casimir energy was also calculated for three and even four spherical cavities inside the non-relativistic fermion background, where the spheres were centered at the vertices of an equilateral triangle or tetrahedron, respectively. In agreement with the semiclassical scenario we expect the presence of many-cavity contributions to the Casimir energy. However, as shown in Ref. (Bulgac and Wirzba., 2001) the three- and four-body contributions in the equilateral triangle case and in the equilateral tetrahedron case are completely dominated by the pairwise two-body contributions. This does not come as a surprise if one takes the semiclassical periodic orbit picture into account, namely the increase of the instabilities of the periodic orbits with increasing bounce number: as every billiard player knows, it is difficult to make long shots and even more difficult to make shots with many bounces – the slightest error would ruin the shot. Since the pairwise interactions dominate and since these interactions oscillate with increasing distance between the cavities, systems with a large number of cavities will arrange themselves as superlattices with discrete lattice constants determined by the minima of the two-cavity Casimir energy.

5. Summary

We have shown that there exists an effective interaction between voids inside a Fermi gas background, even if the fermions are non-interacting. This new form of Casimir energy is neither attractive nor repulsive, but oscillates according to the relative arrangement of the cavities. The Casimir contributions can well be approximated semiclassically. Furthermore, there exist many-body Casimir contributions in n-sphere systems. However, these terms are short-ranged and dominated by long-ranged two-body interactions – even for small separations or small scatterers. In Ref. (Bulgac and Wirzba., 2001) only results for symmetric arrangements of spheres were presented. However, tests of various asymmetrical configurations of three and four spheres show the same general pattern: the integrated d.o.s. $\mathcal{N}_C(E)$ can be represented fairly accurately as a *sum* of the corresponding pairwise contributions. The spheres can be replaced with other objects, if the curvature radii are larger than the Fermi wave length. The effects of finite surface thickness can be considered as Weyl-term contributions and do not affect the geometrical Casimir part if the objects do not overlap. In the case of point scatterers (curvature radii smaller

than the Fermi wave length) the pairwise additivity is reasonably well satisfied as well. The most important application are nuclei immersed in neutron gas in a neutron star crust: The Casimir interactions are of the same order of magnitude ($\sim$ keV/fm^3) as the energy differences between various liquid drop phases (Bulgac and Magierski, 2001). Since the Casimir interaction between bubbles is oscillating and rather long-ranged (in comparison to van der Waals terms), disordered lattices are expected as emerging structures. The disorder can be further enhanced by finite temperature T and corrugated surfaces. The most promising case in the laboratory are buckyball-lattices in liquid mercury or liquid ^{3}He.

In Ref. (Bulgac, Magierski and Wirzba, 2004) new results for superconducting grains embedded in a normal Fermi gas were presented. The pairing interaction induces an enhancement of the Casimir contributions, because of the dominance of the particle-hole terms over the particle-particle and hole-hole contributions. Semiclassically, this can be explained by the focusing (and only for large separations defocusing) nature of the Andreev reflections (Andreev, 1964) in comparison to specular reflections at normal impenetrable boundaries.

Finally note that the map method onto a scattering problem can be generalized from the Casimir effect in the Fermi sea to other systems; it is especially applicable for the case of a fluctuating scalar field between two spheres or a sphere and a plate (with Dirichlet boundary conditions) (Gies, Langfeld and Moyaerts, 2003). Whereas the s-wave approximation in the small-scatterer limit does not affect the fermionic Casimir energy, as it is governed by the UV part of the d.o.s. (i.e. by the contribution at the chemical potential), it is essential for the large distance physics of the fluctuating-scalar Casimir effect, as the latter is governed by the infrared behaviour of the d.o.s. Remember the relative factor of four between the s-wave and semiclassical result of the two-cavity d.o.s. The same expressions are valid for the d.o.s. of the fluctuating-scalar Casimir effect. Therefore, we expect that the Casimir energy for two far separated Dirichlet spheres is enhanced by a factor of four relative to the result of the proximity force approximation which is only valid for small separations. For the sphere-plate configuration the corresponding enhancement for large separations is a factor of two, because only one sphere is involved. In the case of the electromagnetic Casimir effect, the s-wave dominance at large separation should probably be replaced by a p-wave dominance, since the charge-neutrality of the sphere forbids a monopole term, whereas a dipole contribution is allowed.

6. Acknowledgments

The author wishes to thank his collaborators Aurel Bulgac (University of Washington, Seattle, USA) and Piotr Magierski (Warsaw University of Technology, Warsaw, Poland). The author also wishes to thank the organizers of the NDFI workshop, Prof. Faqir Khanna and Dr. Davron Matrasulov, the workshop secretary Ms. Olga Karpova, and the Uzbek colleagues and students for their kind hospitality and help before, during and after the workshop.

References

Casimir H. B. G. Proc. K. Ned. Akad. Wet. **51**, 793 (1948).

Lamoureaux S. Phys. Rev. Lett., **78**, 5 (1997); **81**, 5475(E) (1998).

Mohideen U. and Roy A. Phys. Rev. Lett., **81**, 4549 (1998).

Lamoreaux S. K. Am. J. Phys. **67**, 850 (1999); Elizalde E. and Romeo A. Am. J. Phys. **59**, 711 (1991); Bordag M., Mohideen U. and Mostepanenko V. M. Phys. Rept., **353**, 1 (2001).

Derjaguin B. V., Abrikosova I. I. and Lifshitz E. M. Q. Rev. **10**, 295 (1956); Blocki J., Randrup J., Swiateck W. J. and Tsang C. F. Ann. Phys. (N.Y.) **105**, 427 (1977).

Casimir H. B. G. Physica **19**, 846 (1953).

Boyer T. H. Phys. Rev. **174**, 1764 (1968).

Balian R. and Bloch C. Ann. Phys. (N.Y.) **60**, 401 (1970); Balian R. and Bloch C. Ann. Phys. (N.Y.) **85**, 514 (1974); Balian R. and Duplantier B. Ann. Phys. (N.Y.) **112**, 165 (1978).

Baym G., Bethe H. A. and Pethick C. Nucl. Phys. **A175**, 225 (1971); Ravenhall D. G., Pethick C. J. and Wilson J. R. Phys. Rev. Lett. **50**, 2066 (1983).

Bulgac A. and Magierski P. Nucl. Phys. **A683**, 695 (2001); Erratum Nucl. Phys. **A703**, 892 (2002); Phys. Scripta **T90**, 150 (2001).

Bulgac A. and Wirzba A. Phys. Rev Lett. **87**, 120404 (2001); Physics News Update, No 556, #1, Sep. 13, 2001.

Krein M. G. Mat. Sborn. (N.S.) **33**, 597 (1953); Sov. Math.-Dokl. **3**, 707 (1962); Birman M. Sh. and Krein M. G. Sov. Math.-Dokl. **3**, 740 (1962); Thirring W. Quantum Mechanics of Atoms and Molecules, Springer–Verlag, New York (1981), ch. 3.6; Birman M. Sh. and Yafaev D. R. *St. Petersburg Math. J.* **4**, 833 (1993).

Beth E. and Uhlenbeck G. E. Physica **4**, 915 (1937); Huang K. Statistical Mechanics, John Wiley & Sons, New York (1987), ch. 10.3; Friedel J. Nuovo Cim. Ser. 10 Suppl. **7**, 287 (1958).

Eckhardt B. J. Phys. **A 20**, 5971 (1987).

Gaspard P. and Rice S. A. J. Chem. Phys. **90**, 2225 (1989); **90**, 2242 (1989); **90**, 2255 (1989).

Cvitanovic P. and Eckhardt B. Phys. Rev. Lett. **63**, 823 (1989); Eckhardt B. et al Pinball scattering Quantum chaos between order and disorder, eds G. Casati and B. Chirikov (Cambridge University press, Cambridge, 1995) P. 405.

Henseler M., Wirzba A. and Guhr T. Ann. Phys. (N.Y.) **258**, 286 (1997)

Wirzba A. Phys. Rept. **309**, 1 (1999)

Gutzwiller M. C. Chaos in Classical and Quantum Mechanics (Springer, New York, 1990).

Bulgac A., Magierski P. and Wirzba A. cond-mat/0406255.

Andreev A. F. Zh. Eksp. Teor. Phys. **46**, 1823 (1964) [JETP **19**, 1228 (1964)]; De Gennes P. G. Superconductivity of Metals and Alloys, (Addison-Wesley, Reading, 1998); Blonder G. E. et al. Phys. Rev. B **25**, 4515 (1982).

Gies H., Langfeld K. and Moyaerts L. JHEP **0306**, 018 (2003); Jaffe R. L. and Scardicchio A. Phys. Rev. Lett. **92**, 070402 (2004); Scardicchio A. and Jaffe R. L. Nucl. Phys. **B704**, 552 (2005).

Let us add that the cause of chaos is the non-linearity of the underlying equations. In general relativity the Einstein field equations are non-linear and one expects that chaos should emerge in a natural way. In fact, several authors have investigated chaotic behavior in classical relativistic systems.

We are interested in the quantum case and want to investigate whether a quantum system possesses a chaotic counterpart. A billiard is a good example where one can study the connection between classical and quantum chaos. The classical billiard is a point particle moving freely in a domain with elastic reflections at the boundary. The quantum billiard is the corresponding quantum system described by the stationary Schrödinger equation with Dirichlet boundary conditions.

The question arises how one can characterize the spectra of such systems. The answer is given by the distribution $P(s)$ of the spacings s between adjacent eigenvalues. For a regular system the distribution is of Poisson type,

$$P(s) = e^{-s},$$

whereas for a chaotic system it is given by the Wigner distribution

$$P(s) = \frac{\pi}{2} s \, e^{-\frac{\pi}{4} s^2}.$$

We shall come back to this question in more detail below.

In order to understand the connection between classical and quantum mechanics a central role is played by the Bohigas-Giannoni-Schmit conjecture. The conjecture states that the spectral fluctuations of a quantum system whose classical counterpart is chaotic can be described by random-matrix theory.

Figure 1. Nearest-neighbor spacing distributions of eigenvalues for a circle (left) and the Bunimovich stadium (right). Taken from Ref. (McDonald and Kaufman, 1979).
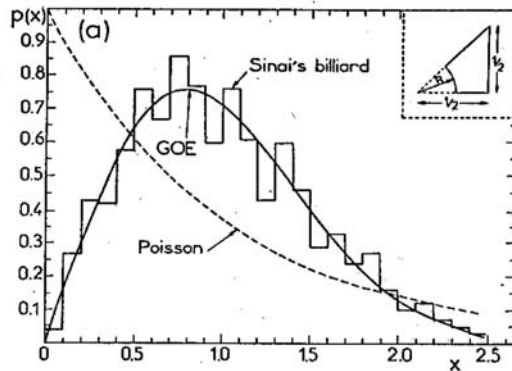
Figure 2. Nearest-neighbor spacing distributions of eigenvalues for the Sinai billiard with the Wigner surmise compared to the Poisson distribution. The histogram comprises about 1000 consecutive eigenvalues. Taken from Ref. (Bohigas, Giannoni and Schmit, 1984).

Very accurate results were obtained for the classically chaotic Sinai billiard by Bohigas, Giannoni, and Schmit (see Fig. 2) which led them to the important conclusion (Bohigas, Giannoni and Schmit, 1984): Spectra of time-reversal invariant systems whose classical analogues are K systems show the same fluctuation properties as predicted by the Gaussian orthogonal ensemble (GOE) of random-matrix theory

(RMT). K systems are most strongly mixing classical systems with a positive Kolmogorov entropy. The conjecture turned out valid also for less chaotic (ergodic) systems without time-reversal invariance leading to the Gaussian unitary ensemble (GUE).

2. Random matrix theory

In lack of analytical or numerical methods to obtain the spectra of complicated Hamiltonians, Wigner and Dyson analyzed ensembles of random matrices and were able to derive mathematical expressions. A Gaussian random matrix ensemble consists of square matrices with their matrix elements drawn from a Gaussian distribution

$$p(x) = \frac{1}{\sqrt{2\pi}\sigma} \exp\left(-\frac{x^2}{2\sigma^2}\right) . \tag{1}$$

One distinguishes between three different types depending on space-time symmetry classified by the Dyson parameter $\beta_D = 1, 2, 4$ (Guhr, Muller-Groeling and Weidenmuller, 1998). The Gaussian orthogonal ensemble (GOE, $\beta_D = 1$) holds for time-reversal invariance and rotational symmetry of the Hamiltonian

$$H_{mn} = H_{nm} = H_{nm}^* . \tag{2}$$

When time-reversal invariance is violated and

$$H_{mn} = [H^\dagger]_{mn} , \tag{3}$$

one obtains the Gaussian unitary ensemble (GUE, $\beta_D = 2$). The Gaussian symplectic ensemble (GSE, $\beta_D = 4$) is in correspondence with time-reversal invariance but broken rotational symmetry of the Hamiltonian

$$H_{nm}^{(0)} \mathbb{1}_2 - i \sum_{\gamma=1}^{3} H_{nm}^{(\gamma)} \sigma_\gamma , \tag{4}$$

with $H^{(0)}$ real and symmetric and $H^{(\gamma)}$ real and antisymmetric.

The functional form of the distribution $P(s)$ of the neighbor spacings s between consecutive eigenvalues for the Gaussian ensembles can be approximated by

$$P_{\beta_D}(s) = a_{\beta_D}\, s^{\beta_D} \exp\left(-b_{\beta_D}\, s^2\right) , \tag{5}$$

which is known as the Wigner surmise and reads for example in the case $\beta_D = 2$ (GUE)

$$P(s) = \frac{32}{\pi^2}\, s^2 \exp\left(-\frac{4}{\pi}\, s^2\right)\ . \tag{6}$$

If the eigenvalues of a system are completely uncorrelated one ends up with a Poisson distribution for their neighbor spacings

$$P(s) = \exp\left(-s\right)\ . \tag{7}$$

An interpolating function between the Poisson and the Wigner distribution is given by the Brody distribution (Brody, 1973) reading for the GOE case

$$P(s,\omega) = \alpha\,(\omega+1)s^\omega \exp\left(-\alpha\, s^{\omega+1}\right)\ , \qquad \alpha = \Gamma^{\omega+1}\left(\frac{\omega+2}{\omega+1}\right)\ , \tag{8}$$

with $0 \leq \omega \leq 1$.

Remarkably, the Wigner distribution could be observed in a number of systems by physical experiments and computer simulations evading the whole quantum world from atomic nuclei to the hydrogen atom in a magnetic field to the metal-insulator transition (Guhr, Muller-Groeling and Weidenmuller, 1998). In this contribution we address the situation in QCD and in hadrons.

3. Quantum chromodynamics

The Lagrangian $\mathcal{L}^{\mathrm{QCD}}$ of quantum chromodynamics (QCD) consists of a gluonic part $\mathcal{L}_{\mathrm{G}}^{\mathrm{QCD}}$ and a part $\mathcal{L}_{\mathrm{F}}^{\mathrm{QCD}}$ from the quarks

$$\begin{aligned}
\mathcal{L}^{\mathrm{QCD}} &= \mathcal{L}_{\mathrm{G}}^{\mathrm{QCD}} + \mathcal{L}_{\mathrm{F}}^{\mathrm{QCD}} \\
&= -\frac{1}{4}F_{\mu\nu}^a(x)F_a^{\mu\nu}(x) + \sum_{f=1}^{N_f} \bar{\psi}_f(x)(i\slashed{D} - m_f)\psi_f(x)\ ,
\end{aligned} \tag{9}$$

with the Dirac spinor ψ_f, the quark mass m_f, the number of flavors N_f, and the generalized field strength tensor

$$F_a^{\mu\nu}(x) = \partial^\mu A_a^\nu(x) - \partial^\nu A_a^\mu(x) - gf_{abc}A_b^\mu(x)A_c^\nu(x)\ , \tag{10}$$

where the gauge field A_a^μ with the SU(3) indices $a, b, c = 1,\ldots,8$, the coupling constant g and the structure constants f_{abc} of SU(3) enter. The main object of study is the eigenvalue spectrum of the Dirac operator of QCD in 4 dimensions

$$\frac{\lambda^a}{2} = \gamma_\mu\partial_\mu + ig\gamma_\mu A_\mu^a\frac{\lambda^a}{2}\ , \tag{11}$$

with the λ_a the generators of the SU(3) color-group (Gell-Mann matrices). Discretizing the Dirac operator on a lattice in Euclidean space-time and applying the Kogut-Susskind (staggered) prescription, leads to the matrix

$$(M_{\text{KS}})^{aa'}_{xx'} = \frac{1}{2a} \sum_{\mu} \left[\delta_{x+\hat{\mu},x'} \; \Gamma_{x\mu} \; U^{aa'}_{x\mu} - \delta_{x,x'+\hat{\mu}} \; \Gamma_{x'\mu} \; U^{\dagger \; aa'}_{x'\mu} \right] \; , \quad (12)$$

where

$$U_{x\mu} = \exp\left(ig A^a_\mu(x) \frac{\lambda^a}{2} \right) \quad (13)$$

are the gauge field variables on the lattice and $\Gamma_{x\mu}$ a representation of the γ_μ-matrices.

In random matrix theory (RMT), one has to distinguish several universality classes which are determined by the symmetries of the system. For the case of the QCD Dirac operator, this classification was done in Ref. (Verbaarschot, 1994). Depending on the number of colors and the representation of the quarks, the Dirac operator is described by one of the three chiral ensembles of RMT. As far as the fluctuation properties in the bulk of the spectrum are concerned, the predictions of the chiral ensembles are identical to those of the ordinary ensembles in Sect. 2 (Fox and Kahn, 1964). In Ref. (Halasz and Verbaarschot, 1964), the Dirac matrix was studied for color-SU(2) using both Kogut-Susskind and Wilson fermions which correspond to the chiral symplectic (chSE) and orthogonal (chOE) ensemble, respectively. Here (Pullirsch et al, 1998), we additionally study SU(3) with Kogut-Susskind fermions which corresponds to the chiral unitary ensemble (chUE). The RMT result for the nearest-neighbor spacing distribution can be expressed in terms of so-called prolate spheroidal functions, see Ref. (Mehta, 1991). A very good approximation to $P(s)$ is provided by the Wigner surmise for the unitary ensemble,

$$P_{\text{W}}(s) = \frac{32}{\pi^2} s^2 e^{-4s^2/\pi} \; . \quad (14)$$

We generated gauge field configurations using the standard Wilson plaquette action for SU(3) with and without dynamical fermions in the Kogut-Susskind prescription. We have worked on a $6^3 \times 4$ lattice with various values of the inverse gauge coupling $\beta = 6/g^2$ both in the confinement and deconfinement phase. We typically produced 10 independent equilibrium configurations for each β. Because of the spectral ergodicity property of RMT one can replace ensemble averages by spectral averages if one is only interested in bulk properties.

The Dirac operator, $D = \partial + igA$, is anti-Hermitian so that the eigenvalues λ_n of iD are real. Because of $\{D, \gamma_5\} = 0$ the non-zero λ_n occur in pairs of opposite sign. All spectra were checked against the analytical sum rules $\sum_n \lambda_n = 0$ and $\sum_{\lambda_n > 0} \lambda_n^2 = 3V$, where V is the lattice volume. To construct the nearest-neighbor spacing distribution from the eigenvalues, one first has to "unfold" the spectra (Bohigas and Giannoni, 1984).

Confinement $\beta = 5.2$
$ma = 0.05$

Deconfinement $\beta = 5.4$
$ma = 0.05$
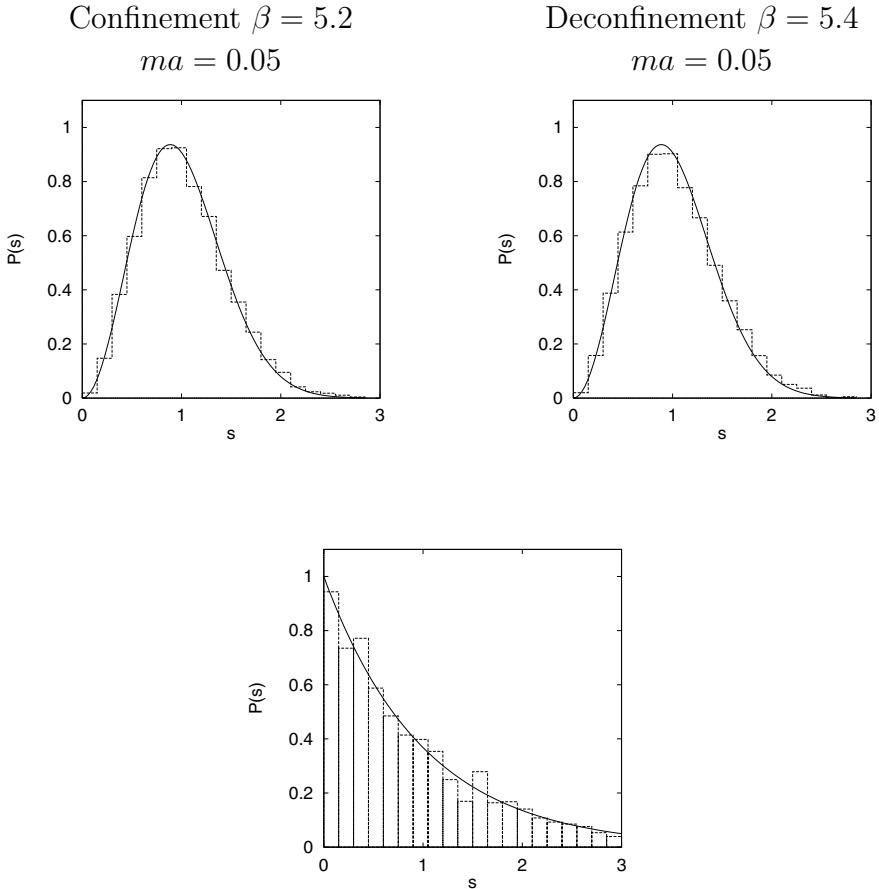
Figure 4. Nearest-neighbor spacing distribution $P(s)$ for the free Dirac operator on a $53 \times 47 \times 43 \times 41$ lattice compared with a Poisson distribution, e^{-s}.

Figure 3 compares $P(s)$ of full QCD with $N_f = 3$ flavors and quark mass $ma = 0.05$ to the RMT result. In the confinement as well as in the deconfinement phase we observe agreement with RMT up to very high β (not shown). The observation that $P(s)$ is not influenced by the presence of dynamical quarks is expected from the results of Ref. (Fox and Kahn, 1964), which apply to the case of massless quarks. Our
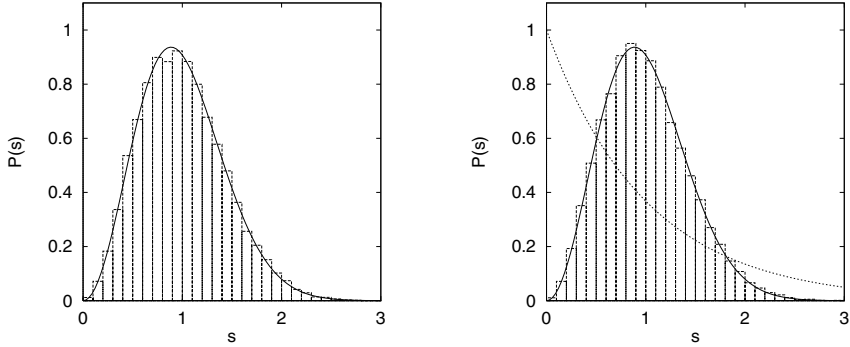
Figure 5. Nearest-neighbor spacing distribution $P(s)$ for U(1) gauge theory on an $8^3 \times 6$ lattice in the confined phase (left) and in the Coulomb phase (right). The theoretical curves are the chUE result, Eq. (14), and the Poisson distribution, $P_P(s) = \exp(-s)$.

results, and those of Ref. (Halasz and Verbaarschot, 1964), indicate that massive dynamical quarks do not affect $P(s)$ either.

No signs for a transition to Poisson regularity are found. The deconfinement phase transition does not seem to coincide with a transition in the spacing distribution. For very large values of β far into the deconfinement region, the eigenvalues start to approach the degenerate eigenvalues of the free theory, given by $\lambda^2 = \sum_{\mu=1}^{4} \sin^2(2\pi n_\mu/L_\mu)/a^2$, where a is the lattice constant, L_μ is the number of lattice sites in the μ-direction, and $n_\mu = 0, \ldots, L_\mu - 1$. In this case, the nearest-neighbor spacing distribution is neither Wigner nor Poisson. It is possible to lift the degeneracies of the free eigenvalues using an asymmetric lattice where L_x, L_y, etc. are relative primes and, for large lattices, the distribution is then Poisson, $P_P(s) = e^{-s}$, see Fig. 4.

We have also investigated the staggered Dirac spectrum of 4d U(1) gauge theory which corresponds to the chUE of RMT but had not been studied before in this context. At $\beta_c \approx 1.01$ U(1) gauge theory undergoes a phase transition between a confinement phase with mass gap and monopole excitations for $\beta < \beta_c$ and the Coulomb phase which exhibits a massless photon for $\beta > \beta_c$. As for SU(2) and SU(3) gauge groups, we expect the confined phase to be described by RMT, whereas free fermions are known to yield the Poisson distribution (see Fig. 4). The question arose whether the Coulomb phase would be described by RMT or by the Poisson distribution (Berg et al, 1999). The nearest-neighbor spacing distributions for an $8^3 \times 6$ lattice at $\beta = 0.9$ (confined phase) and at $\beta = 1.1$ (Coulomb phase), averaged over 20 independent configurations, are depicted in Fig. 5. Both are consistent with the chUE of RMT.

4. Hadrons

Taking the experimentally measured mass spectrum of hadrons up to 2.5 GeV from the Particle Data Group, Pascalutsa (2003) could show that the hadron level-spacing distribution is remarkably well described by the Wigner surmise for $\beta = 1$ (see Fig. 6). This indicates that the fluctuation properties of the hadron spectrum fall into the GOE universality class, and hence hadrons exhibit the *quantum chaos* phenomenon. One then should be able to describe the statistical properties of hadron spectra using RMT with random Hamiltonians from GOE that are characterized by good time-reversal and rotational symmetry.
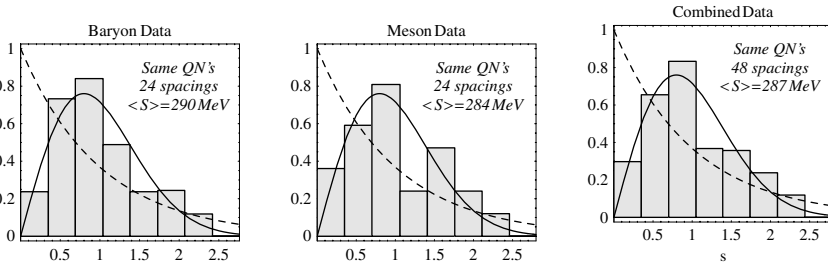
Figure 6. Histograms of the nearest-neighbor mass spacing distribution for hadron states with same quantum numbers. Curves represent the Poisson (dashed) and Wigner (solid) distributions. Taken from Ref. (Pascalutsa, 2003).

In order to test this experimental finding we are comparing with the eigenvalues of a Hamiltonian for a realistic quark model, namely the Goldstone-boson-exchange (GBE) constituent quark model (Glozman et al, 1998). It includes the kinetic energy in relativistic form

$$H_0 = \sum_{i=1}^{3} \sqrt{\vec{p}_i^2 + m_i^2}, \tag{15}$$

with m_i the masses and $\vec{p}_i$ the 3-momenta of the constituent quarks. The interaction between two constituent quarks i, j

$$V(ij) = V_{\text{conf}}(ij) + V_\chi(ij) \tag{16}$$

is given by a confinement potential in linear form

$$V_{\text{conf}}(ij) = V_0 + Cr_{ij} \tag{17}$$
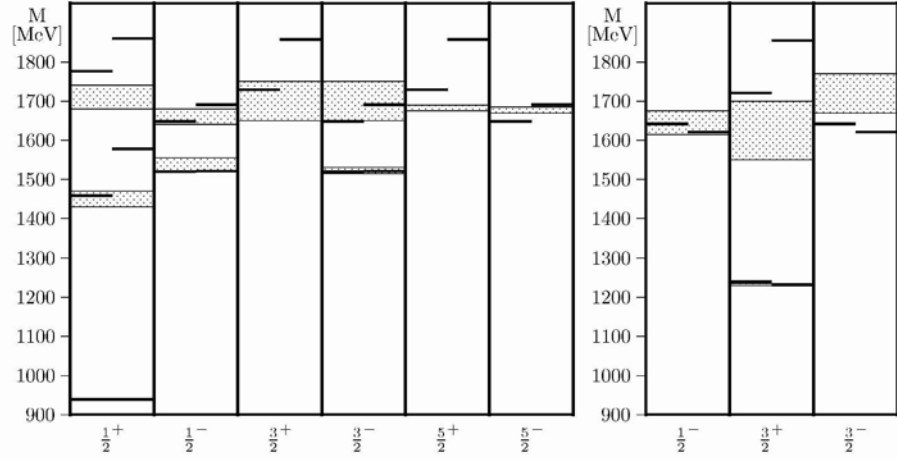
Figure 7. Low lying nucleon (left plot) and delta (right plot) states with total spin and parity J^π. The left and right bars are the theoretical energies predicted from the GBE and OGE models as described in the text, respectively. The shaded boxes represent the experimental energies with their uncertainties (Eidelman et al, 2004).

and a hyperfine interaction consisting of only the spin-spin part of the pseudoscalar-meson-exchange potentials

$$V_\chi(ij) = \Big[\sum_{F=1}^{3} V_\pi(r_{ij})\lambda_i^F \lambda_j^F + \sum_{F=4}^{7} V_K(r_{ij})\lambda_i^F \lambda_j^F$$
$$+ V_\eta(r_{ij})\lambda_i^8 \lambda_j^8 + \tfrac{2}{3} V_{\eta'}(r_{ij})\Big]\, \vec{\sigma}_i \cdot \vec{\sigma}_j. \tag{18}$$

Here r_{ij} is the distance between the quarks, $\vec{\sigma}_i$ are the Pauli spin matrices and λ_i the Gell-Mann flavor matrices of the individual quarks. This kind of interaction is motivated by the spontaneous breaking of chiral symmetry. As a consequence constituent quarks and Goldstone bosons should be the appropriate effective degrees of freedom at low energies. Baryons are then assumed to be bound states of three con-fined constituent quarks with a hyperfine interaction relying on the exchange of the Goldstone bosons. Due to the specific flavor dependence in Eq. (18) a reasonable agreement between the spectra of the low lying light and strange baryon states calculated from the model and the experimental spectra could be achieved. In particular the ordering of the excited states with respect to their parities comes out correctly as is demonstrated in Fig. 7. It is interesting to notice that both the experiment and the numerical treatment have their problems to resolve the higher excited states.

In order to investigate the influence of the hyperfine interaction we also analyze the nearest-neighbor spacings obtained with the confine-

ment potential without the hyperfine interaction V_χ and with a model consisting of a different kind of hyperfine interaction which is based on one-gluon exchange (OGE). This was traditionally used in constituent quark models and has a flavor independent spin-spin potential. Therefore it has principal problems in reproducing the phenomenological ordering of the low lying excited nucleon states. Nevertheless, for comparison we consider here a simple version of such a model, i.e., a reparametrization of the Bhaduri, Cohler, and Nogami model consisting of a potential of the form

$$V(ij) = V_0 + Cr_{ij} - \frac{2b}{3r_{ij}} + \frac{\alpha_s}{9m_i m_j}\Lambda^2 \frac{e^{-\Lambda r_{ij}}}{r_{ij}}\vec{\sigma}_i \vec{\sigma}_j, \qquad (19)$$

and also a relativistic kinetic energy term in its Hamiltonian (Theussl et al, 2001). The spectra of the low lying nucleon and delta states calculated with this model are inserted in Fig. 7.

In Fig. 8 we present our theoretical results of the nearest-neighbor spacing distribution for the nucleon and the delta. Both the hyperfine interaction of either Goldstone-boson exchange and one-gluon exchange type yield spacing distributions corresponding to the GOE. One observes a preference for the GOE from the linear rise at the origin while the other ensembles are quadratic or quartic (cf. Eq. 5). It turns out that the linear confinement potential alone without reproducing the spectra yields eigenvalues with reduced correlations between their neighbors and thus leading to a Poisson distribution, as seen clearly from the nucleon in Fig. 8.

5.   Conclusion

We have outlined the universal applicability of random-matrix theory and have presented our studies of quantum chromodynamics and hadrons. Concerning QCD, we were able to demonstrate that the nearest-neighbor spacing distribution $P(s)$ of the eigenvalues of the Dirac operator agrees perfectly with the RMT prediction both in the confinement and quark-gluon plasma-phase. This means that QCD is governed by quantum chaos in both phases. We could show that the eigenvalues of the free Dirac theory yield a Poisson distribution related to regular behavior. Our investigations tell us that the critical point of the spontaneous breaking of chiral symmetry does not coincide with a chaos-to-order transition. Concerning quarks building hadrons, we employed a relativistic quark potential model allowing for meson exchange or one-gluon exchange. Computing the spectrum of the nucleon and delta baryon indicates a spacing distribution, $P(s)$, favoring the GOE
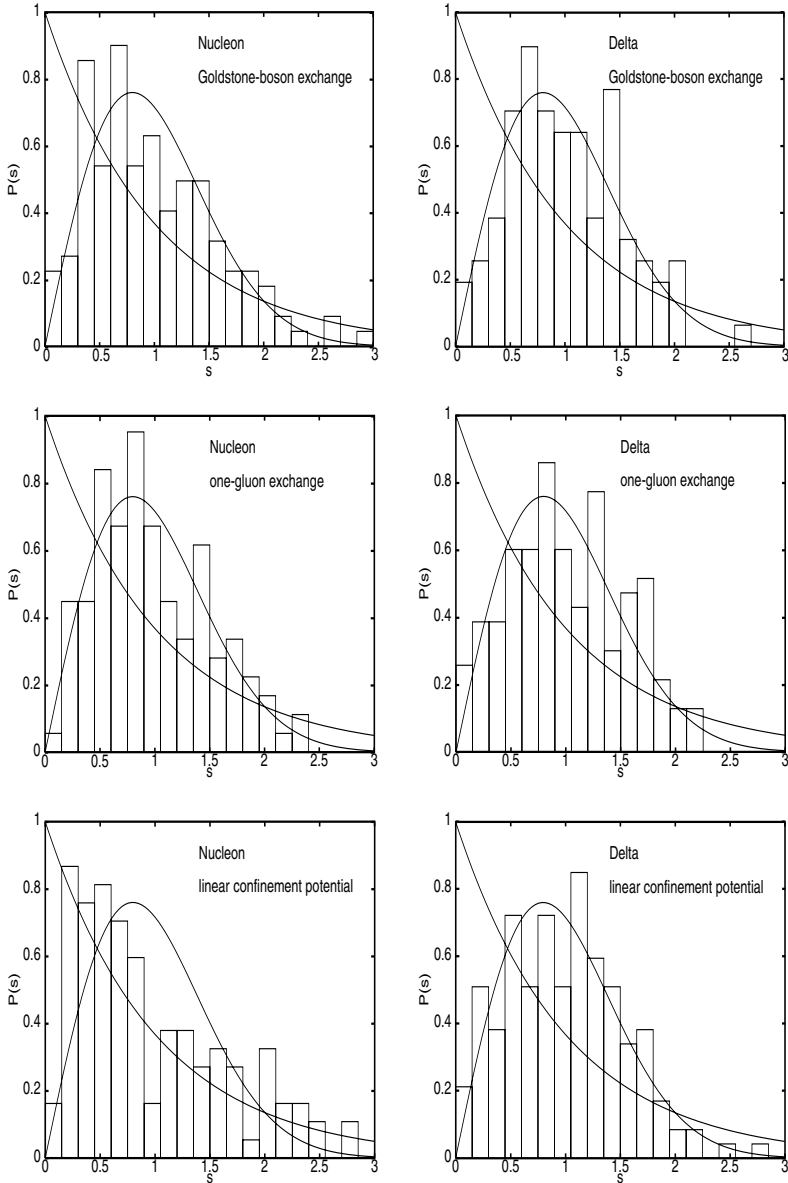
Figure 8. Histograms of the nearest-neighbor spacing distribution for the nucleon (left plots) and the delta (right plots). The data is for Goldstone-boson exchange and for one-gluon exchange compared to a pure linear confinement potential of the same strength. Curves represent the Poisson and the GOE-Wigner distributions.

of RMT. A linear confinement potential alone without reproducing the level ordering is not enough to obtain the correct fluctuations between the eigenvalues. Our results are in agreement with an analysis of the experimental mass spectrum of hadrons from the Particle Data Tables. Invoking the Bohigas-Giannoni-Schmit conjecture, we conclude that not only the quarks but also the hadrons show evidence of quantum chaos.

6.   Acknowledgments

References

McDonald S. W. and Kaufman A. N. Phys. Rev. Lett. 42 (1979) 1189.

Casati G., Valz-Gris F. and Guarneri I. Lett. Nuovo Cimento 28 (1980) 279.

Berry M. V. Ann. Phys. (NY) 131 (1981) 163.

Robnik M. J. Phys. A 17 (1984) 1049.

Seligman T. H., Verbaarschot J. J. M. and Zirnbauer M. R. Phys. Rev. Lett. 53 (1984) 215; Seligman T. H., Verbaarschot J. J. M. and Zirnbauer M. R. J. Phys. A 18 (1985) 2751.

Bohigas O., Giannoni M. J. and Schmit C. Phys. Rev. Lett. 52 (1984) 1.

Guhr T., Muller-Groeling A. and Weidenmuller H. A. Phys. Rep. 299 (1998) 189.

Brody T. A. Lett. Nuovo Cimento 7 (1973) 482.

Verbaarschot J. J. M. Phys. Rev. Lett. 72 (1994) 2531.

Fox D. and Kahn P. B. Phys. Rev. 134 (1964) B1151; Nagao T. and Wadati M. J. Phys. Soc. Jpn. 60 (1991) 3298; 61 (1992) 78; 61 (1992) 1910.

Halasz M. A. and Verbaarschot J. J. M. Phys. Rev. Lett. 74 (1995) 3920; Halasz M. A., Kalkreuter T. and Verbaarschot J. J. M. Nucl. Phys. B (Proc. Suppl.) 53 (1997) 266.

Pullirsch R., Rabitsch K., Wettig T. and Markum H. Phys. Lett. B 427 (1998) 119.

Mehta M. L. Random Matrices, 2nd Ed. (Academic Press, San Diego, 1991).

Bohigas O. and Giannoni M. J. Springer Lect. Notes Phys. 209 (1984) 1.

Berg B.A., Markum H. and Pullirsch R. Phys. Rev. D 59 (1999) 097504.

Pascalutsa V. Eur. Phys. J. A 16 (2003) 149.

Glozman L. Y. et al. Phys. Rev. D 58 (1998) 094030.

Eidelman S. et al.[Particle Data Group Collaboration] Phys. Lett. B 592 (2004) 1.

Theussl L. et al Eur. Phys. J. A 12 (2001) 91.

QCD instanton vacuum effective action

M.M. Musakhanov

Department of Physics, Pusan National University,
609-735 Pusan, Republic of Korea
& Theoretical Physics Dept, Uzbekistan National University,
Tashkent 700174, Uzbekistan

Abstract. Low-momentum quark determinant and effective action in the presence of current quark mass and external flavor fields is derived. The results of the calculations of various correlators are briefly presented. We conclude that, this approach is a reliable tool for the hadron physics, especially including strange quarks.

Keywords: QCD, instanton, vacuum, quark, action, chiral symmetry.

Introduction

Classical vacuum in non-abelian gauge theory is infinitely degenerate and numbered by Chern-Simons number N_{CS} of vacuum gauge fields A_i^a:

$$N_{CS} = \int d^3x \; K_0 = \frac{1}{16\pi^2} \int d^3x \; \epsilon^{ijk} \left(A_i^a \partial_j A_k^a + \frac{1}{3} \epsilon^{abc} A_i^a A_j^b A_k^c \right).$$

Since under large gauge transformations: $A_i \Rightarrow U^\dagger A_i U + iU^\dagger \partial_i U$, $N_{CS} \Rightarrow N_{CS} + N_W$ where N_W is the winding number of the gauge transformation:

$$N_W = \frac{1}{24\pi^2} \int d^3x \; \epsilon^{ijk} \left[(U^\dagger \partial_i U)(U^\dagger \partial_j U)(U^\dagger \partial_k U) \right],$$

N_{CS} can be considered as a collective coordinate. Potential energy density as a function of N_{CS} is periodical. Instanton is a classical path in Euclidean time corresponding to quantum tunneling from one minimum of the potential energy to the neighbor one. On this path the action is minimal($= 8\pi^2/g^2$) and gauge fields are *self-dual*: $G_{\mu\nu}^a = \tilde{G}_{\mu\nu}^a$. The explicit expression for the instanton in the singular Lorenz gauge:

$$A_\mu^a = \frac{2\rho^2 O^{ab} \bar{\eta}_{\nu b}^\mu (x-z)_\mu}{(x-z)^2 [\rho^2 + (x-z)^2]}, \quad O^{ab} = Tr(U^\dagger t^a U \sigma^b), \quad O^{ab} O^{ac} = \delta^{bc}.$$

Instanton collective coordinates are
$$4(\text{position}) + 1(\text{size}) + (4N_c - 5)(\text{color orientations}) = 4N_c.$$

Without any doubt instantons are a very important component of the QCD vacuum. Simplest version of the instanton vacuum model

corresponds to $A = \sum_I A^I + \sum_{\bar{I}} A^{\bar{I}}$. The main properties of the instanton vacuum are given by the average instanton size ρ and interinstanton distance R. In 1982 Shuryak (E.V. Shuryak, 1982) fixed them phenomenologically as

$$\rho = 1/3\,fm, \quad R = 1\,fm. \tag{1}$$

From that time the validity of such parameters was confirmed by theoretical variational calculations (D. Diakonov et.al., 1984) and recent lattice simulations of the QCD vacuum (see (T. De Grand et.al., 1998; M.C. Chu et.al.,1994; T. DeGrand, 2001; P. Faccioli et.al., 2003; J. Negele, 1999)). The following figure represent results of lattice calculations (J. Negele, 1999).
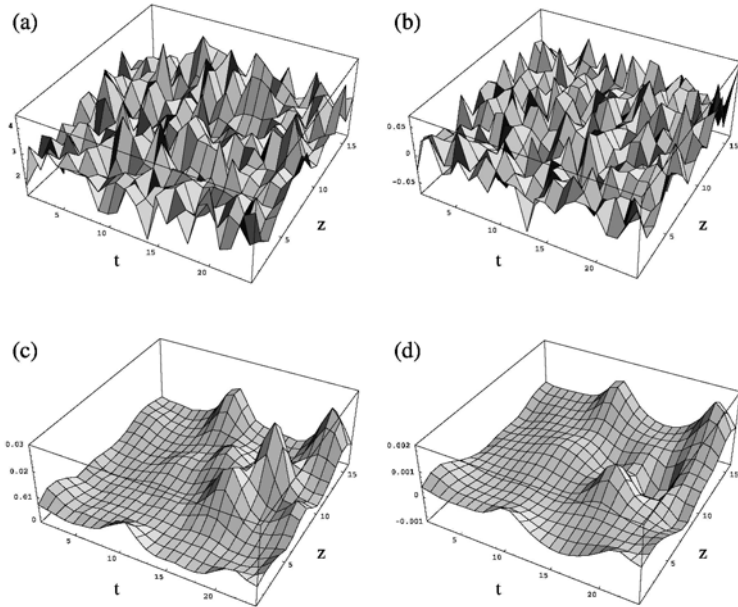
It was found that normal zero-point oscillations lie on top of large gluon fluctuations – instantons and anti-instantons with random positions and sizes. The left column – action density and the right column – topological charge density. Here instantons are peaks and anti-instantons are holes.

The presence of instantons in QCD vacuum very strongly affects light quark properties, owing consequent generation of quark-quark interactions. These effects lead to the formation of the massive constituent interacting quarks. This implies spontaneous breaking of chiral symmetry (SBCS), which leads to the collective massless excitations of

the QCD vacuum–pions. The most important degrees of freedom in low-energy QCD are these quasiparticles. So instantons play a leading role in the formation of the lightest hadrons and their interactions, while the confinement forces are rather unimportant, probably.
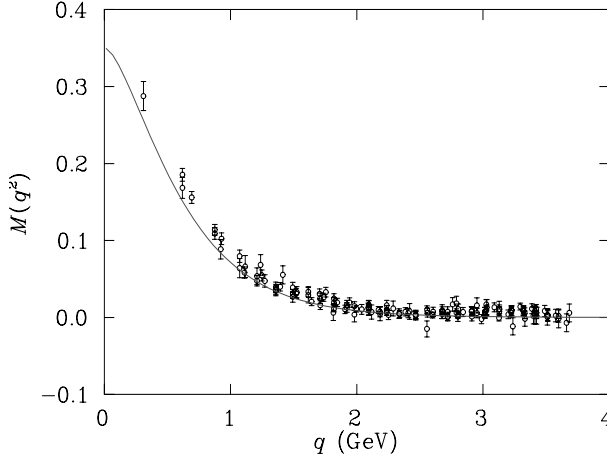
The figure represents dynamical quark mass $M(p)$ from a lattice simulation (P. Bowman et.al., 2004). Here solid curve: from instantons vacuum model **no fitting** (D. Diakonov et.al., 1986). So, rescattering of massless quarks on an instanton vacuum leads to the dynamical quark mass $M(p)$, which is perfectly confirmed by lattice calculations.

The properties of the quasiparticles are described by the low-momentum $(p < \rho^{-1})$ part of total quark determinant $\mathrm{D_{low}}$ (in the field of N_+ instantons and N_- antiinstantons), calculated first by Lee and Bardeen (C. Lee et.al., 1979):

$$\mathrm{D_{low}} = \det B, \ B_{ij} = im\delta_{ij} + a_{ji}, \tag{2}$$

and a_{ij} is the overlapping matrix element of the quark zero-modes $\Phi_{\pm,0}$ generated by instantons(antiinstantons)(in general, we define $\Phi_{\pm,n}$ by the equation $(i\hat{\partial} + \hat{A}_\pm)\Phi_{\pm,n} = \lambda_n \Phi_{\pm,n}$, where $A_{\mu,\pm}$ is a instanton (antiinstanton) field and it was assumed the convention $\lambda_0 = 0$). This matrix element is nonzero only between instantons and antiinstantons (and vice versa) due to specific chiral properties of the zero-modes and equal to

$$a_{-+} = - < \Phi_{-,0} | i\hat{\partial} | \Phi_{+,0} > . \tag{3}$$

The overlapping of the quark zero-modes provides the propagation of the quarks by jumping from one instanton to another one. So, $\mathrm{D_{low}}$ was reduced to the determinant of the finite matrix in the space of

only zero-modes[1]. This result was reproduced further by another methods (D. Diakonov et.al., 1986), (T. Schafer et.al., 1998).

The fermionic determinant Det_{low} averaged over instanton & anti-instanton positions, orientations and sizes leads to a partition function of light quarks Z. Then the properties of the hadrons and their interactions are concentrated in the QCD effective action written in terms of the quasiparticles. This approach leads to the Diakonov-Petrov(DP) effective action (D.I. Diakonov et.al., 1996). It was shown that DP effective action is a good tool in the chiral limit but fails beyond this limit, checked by the calculations of the axial-anomaly low energy theorems (M.M. Musakhanov et.al., 1997; E. Di Salvo et.al., 1998).

In detyB we observe the competition between current mass m and overlapping matrix element $a \sim \rho^2 R^{-3}$. With typical instanton sizes $\rho \sim 1/3 fm$ and inter-instanton distances $R \sim 1 fm$, a is of the order of the strange current quark mass, $m_s = 150\, MeV$. So in this case it is very important to take properly into account the current quark mass.

Within this approach it was proposed so called improved effective action which is more properly takes into account current quark masses and satisfies axial-anomaly low energy theorems also beyond the chiral limit (M.M. Musakhanov, 1999) at least at $O(m)$.

In the present work we refine the calculations D_{low} and derive the QCD low-energy effective action not only with an account of current quark masses but also other external $\hat{V} = \hat{v} + \hat{a}\gamma_5 + s + p\gamma_5$ fields, where $\hat{v} = \gamma_\mu v_\mu$, $\hat{a} = \gamma_\mu a_\mu$. v_μ and a_μ are vector and axial fields, s and p are scalar and pseudoscalar fields. They also may have flavor content. We calculate this one via fermionic quasiparticle–constituent quark representation of D_{low} which provides easy way for the averaging over instanton collective coordinates – positions and orientations (M.M. Musakhanov et.al., 1997). This one provides a consistent way for the calculation of various correlators.

We present in brief the results of the calculations of quark condensate, $\tilde{G}G \rightarrow 2\ photons$ correlator and QCD vacuum magnetic susceptibility.

Low-momentum part of the quark determinant

The total quark determinant $\equiv (i\hat{\partial} + \hat{A} + \hat{V} + im)$ should be split into two parts, i.e. low and high momentum (with respect to some auxiliary parameter lying inside of an interval, $R^{-1} \ll M_1 \ll \rho^{-1}$):

---

[1] The fermionic determinant is $\sim m^{|N_+ - N_-|}$ and strongly suppress the fluctuations of $|N_+ - N_-|$. Therefore in final formulas we will assume $N_+ = N_- = N/2$.

Det = Det$_{\text{low}}\times_{\text{high}}$ (D. Diakonov et.al., 1986). The fermion determinant can be rewritten as a product

$$= \frac{(i\hat{\partial} + \hat{A} + \hat{V} + im)(i\hat{\partial} + \hat{V} + iM)}{(i\hat{\partial} + \hat{A} + \hat{V} + iM)(i\hat{\partial} + \hat{V} + im)} = \text{Det}_{\text{high}} \cdot \text{Det}_{low}, \qquad (4)$$

where

$$\text{Det}_{\text{high}} = \frac{(i\hat{\partial} + \hat{A} + \hat{V} + iM_1)(i\hat{\partial} + \hat{V} + iM)}{(i\hat{\partial} + \hat{A} + \hat{V} + iM)(i\hat{\partial} + \hat{V} + iM_1)},$$

$$\text{Det}_{\text{low}} = \frac{(i\hat{\partial} + \hat{A} + \hat{V} + im)(i\hat{\partial} + \hat{V} + iM_1)}{(i\hat{\partial} + \hat{A} + \hat{V} + iM_1)(i\hat{\partial} + \hat{V} + im)}. \qquad (5)$$

So, $_{high}$ gets a contribution from fermion modes with Dirac eigenvalues from the interval M_1 to the Pauli–Villars mass M, and Det$_{low}$ considers eigenvalues less than M_1. The product of these determinants is independent on the scale[2] M_1. But, we may calculate both of them only approximately. In (D. Diakonov et.al., 1986) it was demonstrated a weak dependence of the product on M_1 in the wide range of M_1 which serves as a check of the approximations.

The high-momentum part Det$_{\text{high}}$ can be written as a product of the determinants in the field of individual instantons, while the low-momentum one Det$_{\text{low}}$ has to be treated approximately, would-be zero modes being taken into account only.

Thus, according to this prescription, in the present case we have to calculate the low-momentum part of the quark determinant in the presence of instantons and also external $\hat{V} = \hat{v} + \hat{a}\gamma_5 + s + p\gamma_5$ fields, and then average it over the collective coordinates of the instantons to find low-energy QCD partition function as a functional of the external fields $\tilde{Z}[m, \hat{V}]$. We specify $\hat{v} = \gamma_\mu v\_mu$, $\hat{a} = \gamma_\mu a_\mu$, where v_μ and a_μ are vector and axial fields, s and p are scalar and pseudoscalar fields they also may have flavor content. We assume that v_μ and a_μ has a trivial topological properties and their topological charges are equal to zero. We are starting from the total quark propagator in the fields of the instanton ensemble A and external fields $\hat{V}$:

$$\tilde{S} = (i\hat{\partial} + g\hat{A} + \hat{V} + im)^{-1}. \qquad (6)$$

Here we assume that with above mentioned average size of instantons $\rho \sim 1/3\ fm$ and average inter-instanton distance $r \sim 1\ fm$ total instanton field A may be approximated by the sum of single instantons

---

[2] Certainly, $\frac{(i\hat{\partial}+\hat{V}+im)}{(i\hat{\partial}+\hat{V}+iM_1)}$ and $\frac{(i\hat{\partial}+\hat{V}+iM_1)}{(i\hat{\partial}+\hat{V}+iM)}$ must be properly normalized to free fields case.

A_i. Also we define quark propagator in the field of single instanton A_i and external fields $\hat{V}$:

$$\tilde{S}_i = \frac{1}{i\hat{\partial} + g\hat{A}_i + \hat{V} + im} \tag{7}$$

and only in the external fields $\hat{V}$ and free one:

$$\tilde{S}_0 = \frac{1}{i\hat{\partial} + \hat{V} + im}, \quad S_0 = \frac{1}{i\hat{\partial} + im}. \tag{8}$$

Then, the quark propagator $\tilde{S}$ can be expanded with respect to a single instanton:

$$\tilde{S} = \tilde{S}_0 + \sum_i (\tilde{S}_i - \tilde{S}_0) + \sum_{i \neq j} (\tilde{S}_i - \tilde{S}_0)\tilde{S}_0^{-1}(\tilde{S}_j - \tilde{S}_0) + ... \tag{9}$$

We rewrite $\tilde{S}_i$ and S_0 in another form

$$\tilde{S}_i = L_i \frac{1}{i\hat{\partial} + g\hat{A}_i + \hat{V}_i' + im} L_i^{-1} \tag{10}$$

$$\tilde{S}_0 = L_i \frac{1}{i\hat{\partial} + \hat{V}_i' + im} L_i^{-1} = L_i S_{0i}' L_i^{-1} \tag{11}$$

where $\hat{V}' = L^\dagger(i\hat{\partial} + \hat{V})L$ and L is P ordered exponential gauge factor:

$$L_i(x, z_i) = Pexp(i \int_{z_i}^x d\xi_\mu v_\mu(\xi) + \gamma_5 a_\mu(\xi)) \tag{12}$$

Here x_i is an instanton position.

We do not include fields s and p into L-factor since they transform homogenously under local gauge transformations.

The main assumption of previous works (D. Diakonov et.al., 1986; D.I. Diakonov et.al., 1996) (see also review (T. Schafer et.al., 1998)) was that at very small m the quark propagator in the single instanton field A_i may be approximated as:

$$S_I(m \sim 0) \approx \frac{1}{i\hat{\partial}} + \frac{|\Phi_{0I} >< \Phi_{0I}|}{im} \tag{13}$$

It gives proper value for the $< \Phi_{0I}|S_I(m \sim 0)|\Phi_{0I} >= \frac{1}{im}$, but in $S_I(m \sim 0)|\Phi_{0I} >= \frac{|\Phi_{0I}>}{im} + \frac{1}{i\hat{\partial}}|\Phi_{0I} >$ second extra term has a wrong chiral properties. We may neglect this only for the $m \sim 0$.

Our assumption for non-small m case is:

$$S_I \approx S_0 + S_0 i\hat{\partial} \frac{|\Phi_{0I} >< \Phi_{0I}|}{c_I} i\hat{\partial} S_0, \quad S_0 = \frac{1}{i\hat{\partial} + im} \tag{14}$$

where

$$c_I = - < \Phi_{0I}|i\hat{\partial}S_0i\hat{\partial}|\Phi_{0I} >= im < \Phi_{0I}|S_0i\hat{\partial}|\Phi_{0I} > \qquad (15)$$

The matrix element $< \Phi_{0I}|S_I|\Phi_{0I} >= \frac{1}{im}$, more over

$$S_I|\Phi_{0I} >= \frac{1}{im}|\Phi_{0I} >, \quad < \Phi_{0I}|S_I =< \Phi_{0I}|\frac{1}{im} \qquad (16)$$

as it must be.

In the presence of the external fields $\hat{V}$ the extension of our assumption is:

$$\tilde{S}_i \equiv L_i S_i' L_i^{-1} = \tilde{S}_{0i} + \tilde{S}_{0i}L_i i\hat{\partial}\frac{|\Phi_{0i} >< \Phi_{0i}|}{-b_i}i\hat{\partial}L_i^{-1}\tilde{S}_{0i} \qquad (17)$$

where

$$b_i =< \Phi_{0i}|i\hat{\partial}(L_i^{-1}\tilde{S}_0L_i - \frac{1}{i\hat{\partial}})i\hat{\partial}|\Phi_{0i} > \qquad (18)$$

Then, Eq. (6) for the total propagator leads to:

$$\tilde{S} = \tilde{S}_0 + \tilde{S}_0 \sum_{i,j} L_i i\hat{\partial}|\Phi_{i0} > (\frac{1}{-D} + \frac{1}{-D}C\frac{1}{-D} + ...)_{ij} < \Phi_{0j}|i\hat{\partial}L_j^{-1}\tilde{S}_0$$

$$= \tilde{S}_0 + \tilde{S}_0 \sum_{i,j} L_i i\hat{\partial}|\Phi_{i0} > (\frac{1}{-V - T})ij < \Phi_{0j}|i\hat{\partial}L_j^{-1}\tilde{S}_0 \qquad (19)$$

where

$$V_{ij} + T_{ij} =< \Phi_{0i}|i\hat{\partial}(L_i^{-1}\tilde{S}_0L_j)i\hat{\partial}|\Phi_{0j} > \qquad (20)$$
$$D_{ij} = \delta_{ij}V_{ij} \equiv b_i\delta_{ij}, \quad C_{ij} = (1 - \delta_{ij})V_{ij} \qquad (21)$$

It is natural to introduce

$$|\phi_0 >= \frac{1}{i\hat{\partial}}Li\hat{\partial}|\Phi_0 > . \qquad (22)$$

It is easy to prove that the function $|\phi_0 >$ has the same chiral properties as the zero-mode function $|\Phi_0 >$. Then

$$\tilde{S} - \tilde{S}_0 = -\tilde{S}_0 \sum_{i,j} i\hat{\partial}|\phi_{i0} >< \phi_{0i}|(\frac{1}{V + T})|\phi_{j0} >< \phi_{0j}|i\hat{\partial}\tilde{S}_0 \qquad (23)$$

with

$$V + T = i\hat{\partial}\tilde{S}_0i\hat{\partial}. \qquad (24)$$

Then, from Eq. (9) and V+T we get

$$(\tilde{S} - \tilde{S}_0) = -\sum_{i,j} < \phi_{0,j,f,g_1}|i\hat{\partial}(\tilde{S}_0^2)_{g_1g_2}i\hat{\partial}|\phi_{0,i,g_2,g_3} > \qquad (25)$$

$$\times < \phi_{0,i,g_3,g_4}|(\frac{1}{i\hat{\partial}\tilde{S}_0i\hat{\partial}})_{g_4g_5}|\phi_{0,j,g_5,f} >$$

Introducing now the operator

$$\tilde{B}(m)_{ij}^{fg} = <\phi_{0,i,f,f_1}|(i\hat{\partial}\tilde{S}_0 i\hat{\partial})_{f_1 g_1}|\phi_{0,j,g_1,g}> \tag{26}$$

it is easy to show that

$$\int_{M_1}^{m} idm'(\tilde{S}(m') - \tilde{S}_0(m')) = \tag{27}$$

$$= \sum_{i,j} \int_{\tilde{B}(M_1)}^{\tilde{B}(m)} d\tilde{B}(m')_{ij}^{fg} (\frac{1}{\tilde{B}(m')})_{ji}^{gf} = \ln \frac{\tilde{B}(m)}{\tilde{B}(M_1)}$$

Here ˜ means the trace on the flavor and only on zero-mode ($|\Phi_{0j}>$) space.

Then the desired low-momentum part of fermionic determinant is

$$\text{Det}_{\text{low}}[\hat{V}, m] = \det \tilde{B}(m) \tag{28}$$

We see that $\tilde{B}$ is the extension of Lee-Bardeen's matrix B, taking into account the presence of the external fields $\hat{V}$ and with an account of the quark current mass m without making expansion over current mass m and also extended to a few flavors case.

If we had turned off the external fields $\hat{V}$ and expanded over m keeping only $O(m)$ term we would have obtained the same quark determinant Det_{low} given by (C. Lee et.al., 1979).

Next problem is to average Det_{low} over instanton collective coordinates to get quark partition function $Z[\hat{V}, m]$.

As a first step for solving this problem, by introducing the Grassmanian ($N_f \times N_+, N_f \times N_-$) variables $\bar{\Omega}_i^f, \Omega_j^g$, we represent

$$\det \tilde{B} = \int d\Omega d\bar{\Omega} \exp(\bar{\Omega}\tilde{B}\Omega), \tag{29}$$

where

$$\bar{\Omega}\tilde{B}\Omega = \sum_{i,j,f,f_1,g_1,g} \bar{\Omega}_i^f i < \phi_{0,i,f,f_1}|i\hat{\partial}\tilde{S}_{0,f_1,g_1} i\hat{\partial}|\phi_{0,j,g_1,g}> \Omega_j^g \tag{30}$$

and to introduce $N_f \times N_+, N_f \times N_-$ sources η_i^f and $\bar{\eta}_j^g$ defined as:

$$\bar{\eta}_i^{f_1} = \sum_f \bar{\Omega}_i^f < \phi_{0,i,f,f_1}|i\hat{\partial}, \eta_j^{g_1} = \sum_g i\hat{\partial}|\phi_{0,j,g_1,g}> \Omega_j^g \tag{31}$$

Then, $(\bar{\Omega}\tilde{B}\Omega)$ can be rewritten as

$$(\bar{\Omega}\tilde{B}\Omega) = \bar{\eta}\tilde{S}_0\eta = \sum_{i,j,f,g} \bar{\eta}_j^f (\frac{1}{i\hat{\partial} + \hat{V} + im})_{ij}^{fg} \eta_i^g. \tag{32}$$

This Eq. (32) provides the representation of $\det \tilde{B}$ as a path integral over N_f constituent quark fields $\psi_f(x)$

$$\tilde{B} = \int d\Omega d\bar{\Omega} \exp(\bar{\Omega}B\Omega) = \left((i\hat{\partial} + \hat{V} + im)\right)^{-1} \prod_{i,f} \int d\Omega_i^f d\bar{\Omega}_i^f$$

$$\times \prod_f D\psi_f D\psi_f^\dagger \exp \int dx [\sum_{f,g} \psi_f^\dagger(x)(i\hat{\partial} + \hat{V} + im)_{fg}\psi_g(x)$$

$$+ \sum_{i,f} (\bar{\eta}_i^f(x)\psi_f(x) + \psi_f^\dagger(x)\eta_i^f(x))] \tag{33}$$

The integration over Grassmanian variables Ω and $\bar{\Omega}$ provides finally the fermion representation of the low-momentum part of the quark determinant:

$$\text{Det}_{\text{low}}[\hat{V}, m] = \int D\psi D\psi^\dagger \exp \left(\int dx \sum_{f,g} \psi_f^\dagger (i\hat{\partial} + \hat{V} + im)_{fg}\psi_g \right)$$

$$\times \prod_f \left\{ \prod_+^{N_+} V_{+,f}[\psi^\dagger, \psi] \prod_-^{N_-} V_{-,f}[\psi^\dagger, \psi] \right\} , \tag{34}$$

where

$$\tilde{V}_{\pm,f}[\psi^\dagger, \psi] = \sum_{f_1,f_2} \int d^4x \left(\psi_{f_1}^\dagger(x) L_{f_1 f}(x, z) \, i\hat{\partial} \Phi_{\pm,0}(x; \xi_\pm) \right)$$

$$\int d^4y \left(\Phi_{\pm,0}^\dagger(y; \xi_\pm)(i\hat{\partial} L_{f f_2}^+(y, z)\psi_{f_2}(y) \right). \tag{35}$$

It is obvious that $\tilde{V}_{\pm,f}[\psi^\dagger, \psi]$ describes the nonlocal interaction between constituent quarks generated by instantons. Since the range of integration in Eq.(35) is cut at ρ (it is defined by zero-mode functions $\Phi_{\pm,0}$) the range of the nonlocality is ρ.

Note that external v_μ and a_μ fields gauges not only the kinetic term of the QCD low-energy effective action but also its interaction term $\tilde{V}_{\pm,f}[\psi^\dagger, \psi]$ in Eq. (35). The reason is obvious: It is the nonlocal interaction induced by instantons. The external v_μ and a_μ fields are present here due to the factor L attached to each fermionic line. This factor provides us a gauge invariance of the interaction term $\tilde{V}_{\pm,f}[\psi^\dagger, \psi]$ under the gauge transformation.

QCD low-energy effective action

The remaining problem is to average the quark determinant over collective coordinates $\xi_{\pm}$. It is a rather simple procedure, since the low density of the instanton medium $(\pi^2 \left(\frac{\rho}{R}\right)^4 \sim 0.1)$ allows us to average over positions and orientations of the instantons independently. Then

$$\tilde{W}_{\pm} = \int d^4\xi_{\pm} \prod_f \tilde{V}_{\pm,f}[\psi^{\dagger}\psi] = \int d^4z \det_f i\tilde{J}_{\pm}(z) \tag{36}$$

and

$$\tilde{J}_{\pm}(z)_{fg} = \frac{(2\pi\rho)^2}{N_c} \int \frac{d^4k d^4l}{(2\pi)^8} \exp(-i(k-l)z) \tag{37}$$

$$\times \psi_f^{\dagger}(k) F((k+v(z)\pm a(z))^2) \frac{1 \pm \gamma_5}{2} F(l+v(z)\pm a(z))^2)\psi_g(l).$$

Form-factor $F(k)$ is in fact a normalized zero-mode. It has explicit form:

$$F(k) = -\frac{d}{dt}[I_0(t)K_0(t) - I_1(t)K_1(t)]_{t=\frac{|k|\rho}{2}} \tag{38}$$

In Eq. (37) soft external v_{μ} and a_{μ} fields, carrying momentum $q \ll \rho^{-1}$, were assumed. Then, they are present inside of the form-factor F in above mentioned form. If v, a external fields are flavor matrices then form-factor F also becomes matrix $N_f \times N_f$. So, we get the partition function $\tilde{Z}[m, \hat{V}]$, where $\tilde{W}_{\pm}$ are multi-quark interaction terms in the presence of current quark mass m and external fields $\hat{V}$.

The next step – the exponentiation provide us the QCD low-energy effective action $SS[\psi^{\dagger}, \psi, \lambda_{\pm}]$ in terms of the constituent quarks ψ and couplings $\lambda_{\pm}$:

$$\tilde{Z}[m, \hat{V}] = \int d\lambda_+ d\lambda_- D\psi D\psi^{\dagger} \exp(-S[\psi^{\dagger}, \psi, \lambda_{\pm}]) \tag{39}$$

$$-S[\psi^{\dagger}, \psi, \lambda_{\pm}] = \int d^4x\, \psi^{\dagger}(i\hat{\partial} + \hat{V} + im)\psi \tag{40}$$

$$+ \sum_{\pm}(\lambda_{\pm} \int d^4z \det i\tilde{J}_{\pm}(z) + N_{\pm} \ln \frac{N_{\pm}}{K\lambda_{\pm}} - N_{\pm})].$$

Interaction term in Eq. (39) has $2N_f$ quark legs [3]. In $N_f = 2$ case it resembles NJL-type models, except very important difference – there is we have to integrate over the couplings $\lambda_{\pm}$.

---

[3] In $\tilde{Z}$ K is an unessential constant, which makes log expression dimensionless.

As a further step, it is natural to make bosonization, using auxiliary meson fields $\Phi_{\pm}(x)$, which provide:

$$Z[m, \hat{V}] = \int d\lambda_+ d\lambda_- D\Phi_+ D\Phi_- \exp\left(-S[\lambda_+, \Phi_+; \lambda_-, \Phi_-]\right), \quad (41)$$

where

$$S[\lambda_+, \Phi_+; \lambda_-, \Phi_-] = -\sum_{\pm} \left(N_{\pm} \ln \frac{N_{\pm}}{K\lambda_{\pm}} - N_{\pm} \right) \quad (42)$$

$$+ \int d^4x \sum_{\pm} (N_f - 1)(\det \Phi_{\pm})^{\frac{1}{N_f - 1}},$$

$$- \ln \frac{\hat{p} + im + \hat{V} + i\sum_{\pm} \lambda_{\pm}^{N_f^{-1}} \frac{(2\pi\rho)^2}{N_c} F(P_{\pm})\Phi_{\pm} \frac{1\pm\gamma_5}{2} F(P_{\pm})}{\hat{p} + im + \hat{V}}.$$

means $\int d^4x_c Df$, $p = i\partial, P_{\pm} = p + v \pm a$.

Without external fields ($\hat{V} = 0$) and at $N\pm = N/2$ the common saddle-point on all variables is given by the equation:

$$\frac{N}{V} = 4N_c \int \frac{d^4k}{(2\pi)^4} \frac{M_f F^2(k)(m_f + M_f F^2(k))}{k^2 + (m_f + M_f F^2(k))^2} \quad (43)$$

The saddle-point equation leads to the momentum dependent dynamical quark mass $M_f(k) = M_f F^2(k)$. M_f here is a function of current mass m_f (M.M. Musakhanov, 2002). It was found that that $M[m]$ is a decreasing function and for the strange quark with $m_s = 0.15\,GeV$ $M_s \sim 0.5\,M_{u,d}$. This result in a good correspondence with (P. Pobylitsa, 1989), where another method was completely applied – direct sum is of planar diagrams.

Correlators

The following is the list of recent applications of described approach to the calculations of various correlators:

 — Most simple correlator – quark condensate:

$$< \bar{q}_f q_f >= -i < \psi_f^\dagger \psi_f >= -\frac{1}{Z[m]} \frac{\partial Z[m]}{\partial m} \quad (44)$$

was considered in (M.M. Musakhanov, 2002). It was found that $| < \bar{q}q > |$ is a decreasing function of m. So, strange quark condensate $< \bar{q}_s q_s >\sim 0.5 < \bar{q}_{u,d} q_{u,d} >$.

‒ In order to check the gauging method, applied here, by axial-anomaly low-energy theorem, $\tilde{G}G \to 2\ photons$ correlator (M.M. Musakhanov et.al., 2003) was calculated . It was found that this gauged QCD low-energy effective action perfectly satisfies the theorem (M.M. Musakhanov et.al., 2003).

‒ Recently QCD vacuum magnetic susceptibility was calculated and is defined as:

$$\langle 0|\psi_f^\dagger \sigma_{\mu\nu}\psi_f|0\rangle_F = e_f\, \chi_f\, \langle i\psi_f^\dagger\psi_f\rangle_0\, F_{\mu\nu}, \tag{45}$$

where e_f denotes the quark electric charge, $F_{\mu\nu}$ - external electromagnetic field. For different flavors, the following magnetic susceptibility was found: $\chi_{u,d}\langle i\psi_{u,d}^\dagger\psi_{u,d}\rangle_0 \sim 40 \sim 45\,\mathrm{MeV}$, while $\chi_s\langle i\psi_s^\dagger\psi_s\rangle_0 \simeq 6 \sim 10\,\mathrm{MeV}$ (H.C. Kim et.al.,).

Now the calculations of Gasser-Leutwyler couplings of their phenomenological chiral lagrangian (H.C. Kim et.al., 1984) and related with this problem the meson loops calculations are in progress. First results show exact reproducing of the famous chiral log terms in various correlators.

Conclusion

Proposed approach provides reliable tool in hadron physics with the promising perspective of the application to strange quarks.

Acknowledgement

References

Shuryak, E.V. *Nucl. Phys. B*, 203:93, 1982.

Diakonov, D. and V. Petrov. *Nucl. Phys. B*, 245:259, 1984.

De Grand, T., A. Hasenfratz and T. Kovacs. *Progr.Theor. Phys. Suppl.*, 131:573, 1998.

Chu, M.C., J.M. Grandy, S. Huang and J.W. Negele. *Phys. Rev. D*, 49:6039, 1994.

DeGrand, T. *Phys. Rev. D*, 64:094508, 2001.

Faccioli, P. and T.A. DeGrand. *Phys. Rev. Lett.*, 91:182001, 2003.

Negele, J. *Nucl. Phys. Proc. Suppl.*, 73:92, 1999.

Bowman, P. et.al. *Nucl. Phys. Proc. Suppl.*, 128:23, 2004.

Diakonov, D. and V.Y. Petrov. *Nucl. Phys. B*, 272:457, 1986.

Lee, C. and W.A. Bardeen. *Nucl. Phys. B*, 153:210, 1979.

Schafer, T. and E.V. Shuryak. *Rev. Mod. Phys.*, 70:323, 1998.

Musakhanov, M.M. and F.C. Khanna. *Phys. Lett. B*, 395:298, 1997.

Diakonov, D.I., M.V. Polyakov and C. Weiss. *Nucl. Phys. B*, 461:539, 1996.

Di Salvo, E. and M.M. Musakhanov. *Europ. Phys. J. C*, 5:501, 1998.

Musakhanov, M.M. *Europ. Phys. J. C*, 9:235, 1999.

Musakhanov, M.M. *Nucl. Phys. A*, 699:340, 2002.

Pobylitsa, P. Quarks in the instanton vacuum I. Quark propagator. *Phys.Lett. B*, 226:387, 1989; *LINP*, preprint 1598, 1990.

Musakhanov, M.M. and H.C.Kim. *Phys.Lett. B*, 572:181, 2003.

Kim, H.C., M.M. Musakhanov and M. Siddikov. *arXiv:hep-ph/0411181*.

Gasser, J. and H. Leutwyler. *Ann.Phys.*, 158:142, 1984. arXiv:hep-ph/0411181.

New Casimir energy calculations for single cavities

H. Ahmedov and I. H. Duru[a],
(a) Feza Gürsey Institute, P.O. Box 6, 81220,
Çengelköy, Istanbul, Turkey

Abstract. Casimir energy calculations are presented for the massless scalar field for pyramidal and conical wedges and cavities.

1. Introduction

Having new three dimensional geometries in hand for which the Casimir energies can be calculated is of interest. We may hope that for some of these geometries the experiments may be performed. [1] In the light of rapid advancements in nanotechnology our hope is well justified. We also think that in nanostructures the Casimir energy can not be neglected. Note that for a cavity with a typical size r, the Casimir energy (in $\hbar = c = 1$ units) is of the order $\frac{10^{-1}}{r}$. For nanometer value $r = 10^{-7} cm$, (with $1eV \cong 0, 5 \times 10^5 cm^{-1}$) this energy is $E \simeq 100 eV$ which is of considerable magnitude.

In the coming sections we present the Casimir energy calculations for a pyramidal wedge and then for a pyramidal cavity and a conical cavity. We give the details for the former one, and for the conical cavity we simply present the results.

2. Pyramidal region

We first consider the pyramidal wedge defined by the planes

$$P_1: \ x_1 = x_3, \quad P_2: \ x_2 = 0. \quad P_3: \ x_1 = x_2; \quad x_1 > 0, \ x_2 > 0, \ x_3 > 0 \tag{1}$$

Reflection operators with respect to these planes are

$$q_1 = \begin{pmatrix} 0 & 0 & 1 \\ 0 & 1 & 0 \\ 1 & 0 & 0 \end{pmatrix}, q_2 = \begin{pmatrix} 1 & 0 & 0 \\ 0 & -1 & 0 \\ 0 & 0 & 1 \end{pmatrix}, q_3 = \begin{pmatrix} 0 & 1 & 0 \\ 1 & 0 & 0 \\ 0 & 0 & 1 \end{pmatrix} \tag{2}$$

---

[1] We like to remind that so far all the experiments performed are with geometries involving two bodies (A. Wirzba., 2004). Single cavity experiment has not been performed.

The above reflections generate a group G of order 48

$$G = \{g_j, \; ig_j; \; j = 0, 1 \ldots 23\} \tag{3}$$

where the elements g_j form the Octahedral group of order 24 with g_0 being the unit element and

$$g_i = \begin{pmatrix} -1 & 0 & 0 \\ 0 & -1 & 0 \\ 0 & 0 & -1 \end{pmatrix} \tag{4}$$

is the parity operator (2).

The Green function for the massless scalar field in the region defined by (1) is given by

$$K(x, y) = \sum_{j=0}^{23} [G(g_j x, y) - G(ig_j x, y)], \tag{5}$$

with $G(x, y)$ being the free space Green function

$$G(x, y) = \frac{1}{4\pi^2} \frac{1}{|\; x - y \;|^2}. \tag{6}$$

Here x and y are four vectors with interval $|\; x - y \;|^2 = |\; \vec{x} - \vec{y} \;|^2$ $- (x_0 - y_0)^2$; and the group elements g_j, ig_j act only on the spatial components. Since the sum in, Eq. (5) involves all the elements of the group G and since q_1, q_2, q_3 are the group elements, one can easily show the relations

$$K(q_1 x, y) = K(q_2 x, y) = K(q_3 x, y) = -K(x, y) \tag{7}$$

which guarantee the satisfaction of the Dirichlet boundary conditions on the surfaces P_1, P_2, P_3.

The satisfaction of the required equation ($\eta = diag(-1, 1, 1, 1)$)

$$\eta^{\mu\nu} \frac{\partial^2}{\partial x^\mu \partial x^\nu} K(x, y) = \delta(x - y) \tag{8}$$

is guaranteed if the region between the planes defined in (1) is the fundamental domain of the group G, i.e., if every point in the domain is the representative of the different orbit of G (2).

We employ conformally coupled energy momentum tensor for the massless scalar field

$$T_{\mu\nu} = \lim_{x \to y} [\frac{2}{3} \partial_\mu^y \partial_\nu^x - \frac{1}{6} (\partial_\mu^x \partial_\nu^x + \partial_\mu^y \partial_\nu^y) - \frac{\eta_{\mu\nu}}{6} \eta^{\sigma\rho} \partial_\sigma^y \partial_\rho^x$$

$$+ \frac{\eta_{\mu\nu}}{24} \eta^{\sigma\rho} (\partial_\sigma^x \partial_\rho^x + \partial_\sigma^y \partial_\rho^y)] K(x, y) \tag{9}$$

The energy density $T(x) \equiv T_{00}$ is given by:

$$T(x) = \frac{1}{12\pi^2} \sum_{j=1}^{23} [T(g_j) - T(ig_j)], \tag{10}$$

where

$$T(g) = \left(\frac{tr(g) - 1}{|\vec{\eta}|^4} - 2\frac{|((1+g)\vec{\eta}|^2}{|\vec{\eta}|^6}\right); \qquad \vec{\eta} = (1-g)\vec{x} \tag{11}$$

with g standing for both g_j and ig_j. Note that we omit $j = 0$ in (10) which is required for renormalization. The other singularities i.e., the surface and the vertex ones are all taken care of with the employment of the conformal formula of Eq. (9) (3).

3. Pyramidal cavity

We add to the planes P_1, P_2, P_3 the forth one $P_4 : x_3 = a$. Reflection with respect to the P_4 plane is given by

$$q_4 \begin{pmatrix} x_1 \\ x_2 \\ x_3 \end{pmatrix} = \begin{pmatrix} x_1 \\ x_2 \\ 2 - x_3 \end{pmatrix} \tag{12}$$

Since we have a compact region (all the momenta are now discrete) it is more convenient to employ the energy spectrum formulation to obtain the Casimir energy. The wave function for the massless scalar field in the cavity is

$$\Psi(\vec{x}) = \Omega \sum_{j=1}^{23} [e^{i(\vec{p}, g_j \vec{x})} - e^{i(\vec{p}, ig_j \vec{x})}] \tag{13}$$

or

$$\Psi_{\vec{p}}(\vec{x}) = -8i\Omega[\sin p_1 x_1 \sin p_2 x_2 \sin p_3 x_3 - \sin p_1 x_1 \sin p_2 x_3 \sin p_3 x_2 + c.p.] \tag{14}$$

where Ω is the normalization. Dirichlet boundary condition

$$\Psi_{\vec{p}}(\vec{x}) \mid_{P_4} = 0 \tag{15}$$

forces the momenta to the integer values

$$p_1 = \frac{\pi}{a}n, \quad p_2 = \frac{\pi}{a}m, \quad p_3 = \frac{\pi}{a}k. \tag{16}$$

Inspection of (14) reveals that coordinates x_1, x_2, x_3 and the corresponding momenta p_1, p_2, p_3 appear in exactly the same manner, thus

the momentum space is just a replica of the configuration space. We then employe the properties

$$\Psi_{g_j\vec{p}}(\vec{x}) = \Psi_{\vec{p}}(\vec{x}) \quad \Psi_{i\vec{p}}(\vec{x}) = \Psi_{\vec{p}}(\vec{x}) \tag{17}$$

which imply the hierarchy of the quantum numbers

$$k > n > m > 0. \tag{18}$$

The energy density in the pyramidal cavity is then given by

$$T(x) = \frac{\pi}{2a} \sum_{k=3}^{\infty} \sum_{n=2}^{k-1} \sum_{m=1}^{n-1} \sqrt{n^2 + m^2 + k^2} \mid \Psi_{\vec{p}}(\vec{x}) \mid^2 . \tag{19}$$

After integrating over the volume of cavity $\int_0^a dx_3 \int_0^{x_3} dx_1 \int_0^{x_1} dx_2$ we obtain the total energy in the cavity

$$E_{pyr} = \frac{1}{6}E_1 - \frac{1}{2}E_2 - \frac{6 + 4\sqrt{2}}{16}E_3 \tag{20}$$

Here E_1, E_2 and E_3 are the Casimir energies for the cube with sides a, for the rectangle with sides a, $\frac{a}{\sqrt{2}}$ and for the one dimensional system of length a (Mostepanenko and Trunov, 1997) :

$$E_1 = \frac{\pi}{2a} \sum_{n,m,k=1}^{\infty} \sqrt{n^2 + m^2 + k^2} \simeq -\frac{0,015}{a} \tag{21}$$

$$E_2 = \frac{\pi}{2a} \sum_{n,m=1}^{\infty} \sqrt{n^2 + 2m^2} \simeq \frac{0,045}{a} \tag{22}$$

$$E_3 = \frac{\pi}{2a} \sum_{n=1}^{\infty} n \simeq -\frac{0,131}{a} \tag{23}$$

Inserting the above known results into Eq. (20) we get the positive result

$$E_{pyr} \simeq \frac{0,069}{a} > 0 \tag{24}$$

Note that for nanometer sizes i.e. for $a = 10^{-7} cm$, the above energy (in $\hbar = c = 1$ unit, $1eV \cong 0,5 \times 10^5 cm^{-1}$) is

$$E_{pyr} \simeq 35eV \tag{25}$$

which is of considerable size.

4. A conical cavity

Consider the space between the following planes

$$P_1: \ x_1 = x_2, \quad P_2: \ x_2 = 0, \quad P_3: \ x_2 = x_3; \quad x_1, x_2, x_3 > 0 \qquad (26)$$

together with the boundary conditions for the Green function:

$$K(x,y)|_{\vec{x} \in P_2} = 0 \qquad (27)$$

and

$$K(x,y)|_{\vec{x} \in P_1} = K(x,y)|_{g\vec{x} \in P_3} \qquad (28)$$

where

$$g = \begin{pmatrix} 0 & 0 & 1 \\ 1 & 0 & 0 \\ 0 & 1 & 0 \end{pmatrix} \qquad (29)$$

is the rotation matrix around $\vec{n} = (1,1,1)$ (the intersection of P_1, P_2) by $\frac{2\pi}{3}$. The region we obtain is then a conical wedge (Ahmedov and Duru, 2004). We then consider the fourth and fifth planes

$$P_4: \ x_1 = a, \quad P_5: \ x_3 = a. \qquad (30)$$

with Dirichlet boundary conditions on them. The resulting space is then a conical cavity with height $h = \frac{2\sqrt{2}}{3}a$ and opening angle $\beta = \arcsin \frac{1}{3}$ (Ahmedov and Duru, 2004).

The total Casimir energy for the massless scalar field in this conical cavity is again positive:

$$E_{con} \simeq \frac{0,085}{a} > 0 \qquad (31)$$

5. Discussion

We still do not know what is the connection between the sign and the magnitude of Casimir energy and the shapes and the dimension of the cavity or the space.

The short calculations we presented here are all 3-dimensional cavities with trivial topology (For example of not like the region between co-axial cylinders or cones, co-centric spheres or tori (Ahmedov and Duru, 2003)). The known results (including the present ones) for three dimensional cavities are

$$Cube \ of \ sides \ 2b \qquad E_{cub} \simeq -\frac{0,007}{b} < 0$$

$$Sphere \ of \ radius \ b \qquad E_{sph} \simeq \frac{0,046}{b} > 0$$

$$Pyramid \ located \ in \ the \ cube \quad E_{pyr} \simeq \frac{0,069}{b} > 0$$

$$Conical \ cavity \ of \ height \ b \quad E_{con} \simeq \frac{0,080}{b} > 0 \qquad (32)$$

We choose the distance b to make the sizes of the cavities to be comparable to each other (the details are given in (Ahmedov and Duru, 2004)).

The above short list does not offer a hint about the sign of the effect. All of the cavities including ours are of special types; i.e., the angles are fixed. Thus we still do not know about the dependence on the shape deformations.

If on the other hand we compare the three positive results of equal volume, we observe that the energy for the pyramidal and conical cavities are about half of the sphere of equal volume

$$E_{con} \simeq 0,54E_{sph}$$
$$E_{pyr} \simeq 0,51E_{sph} \qquad (33)$$

The above results can be qualitatively understood. In spherical cavity , the semi classical paths can bounce back from any point of the wall. However a path ending for example at the summit of the conical cavity has no direction to be reflected back. Thus one can speculate that the configuration space available for a field in the conical cavity is less than the spherical cavity.

6. Acknowledgment

References

Wirzba, A. Talk in these proceedings. *NDFI03*,

Ahmedov, H. and Duru, I. H. Casimir Energy for a Wedge with Three Surfaces and for a Pyramidal Region. *math-ph/0407030* , in J. Math. Phys

Birrel, N. D. and Davies, P. C.V. Quantum Fields in Curved Spaces. *Cambridge University Press*, (1982).

Mostepanenko, V. M. and Trunov, N. N. The Casimir Effect and its Applications. *Oxford University Press*, New York, 1997.

Ahmedov, H. and Duru, I. H. Casimir Energy in a Conical Wedge and a Conical Cavity. *math-ph/0408199* , in J. Math. Phys

Ahmedov, H. and Duru, I. H. Casimir Energy in a Conical Wedge and a Conical Cavity. *J. Math. Phys.*, **44**, 5487 (2003).

Quantum field theory for nonequilibrium phase transitions

Sang Pyo Kim
Kunsan National University
Kunsan 573-701, Korea

Abstract. We review the recent development of quantum dynamics for nonequilibrium phase transitions. To describe the detailed dynamical processes of nonequilibrium phase transitions, the Liouville-von Neumann method is applied to quenched second order phase transitions. Domain growth and topological defect formation is discussed in the second order phase transitions. Thermofield dynamics is extended to nonequilibrium phase transitions. Finally, we discuss the physical implications of nonequilibrium processes such as decoherence of order parameter and thermalization.

Keywords: Nonequilibrium phase transitions, Liouville-von Neumann approach, domain growth, topological defect formation.

1. Introduction

When the symmetry of a system is broken explicitly, the system undergoes a phase transition (T.W.B. Kibble et.al., 1976; A. Vilenkin et.al., 1994). The phase transition proceeds in either equilibrium or nonequilibrium, depending on whether the thermal relaxation time is shorter or longer than the dynamical time of the evolution. Particularly, a quenched system undergoes nonequilibrium phase transition when the quench time is shorter than the relaxation time. For instance, the universe would have undergone a supercooling process due to the rapid expansion and thereby a sequence of nonequilibrium phase transitions in the early universe. Another example would be the rapid cooling of quark-gluon plasma in the Heavy Ion Collision or the liquid helium He^3 and He^4, where domain walls and vortices (strings) may be formed. These are the cases to which nonequilibrium but not equilibrium phase transitions should be applied.

The finite-temperature field theory has been the most popular approach to equilibrium phase transitions (L. Dolan et.al., 1974). The effective potential of quantum fluctuations around a classical background provides a convenient tool to describe phase transitions. The symmetry breaking or restoration mechanism can be illustrated by a scalar field model with broken symmetry

$$V(\phi) = -\frac{m^2}{2}\phi^2 + \frac{\lambda}{4!}\phi^4. \qquad (1)$$

Thermal fluctuations, however, may contribute to the classical potential to restore the broken symmetry when the thermal energy is sufficient enough to overcome the potential energy barrier between the true and false vacua. The renormalized effective potential for the background field ϕ_c is then given by

$$V_{\text{eff}}(\phi_c) \equiv \text{Tr}(\hat{\rho}V) = \frac{1}{2}\Big(-m_R^2 + \frac{\lambda_R}{24}T^2\Big)\phi_c^2 + \frac{\lambda_R}{4!}\phi_c^4. \qquad (2)$$

In terms of a critical temperature T_c, the potential takes the form

$$V_{\text{eff}}(\phi_c) = \frac{1}{2}(T^2 - T_c^2)\phi_c^2 + \frac{\lambda_R}{4!}\phi_c^4. \qquad (3)$$

Therefore, the system restores the broken symmetry when $T > T_c$ but breaks the symmetry when $T < T_c$ (L. Dolan et.al., 1974).

However, long wavelength modes suffer from instability during the phase transition and grow exponentially. Thus the effective action gains an imaginary part, which gives the decay rate of the false vacuum (E.J. Weinberg et.al., 1987). Hence, the finite-temperature effective action alone may not be enough to describe the dynamical processes of phase transitions. Kibble (T.W.B. Kibble et.al., 1976) found the correlation length of domains (regions of the same phase) by comparing the thermal energy with the free energy of domains at the Ginzburg temperature, $k_b T_c \approx \xi^3(T_G)\Delta F(T_G)$. In this situation, since the field can jump over the potential barrier to other configurations, topological defects lose stability. Whereas, Zurek (T.W.B. Kibble et.al., 1976) incorporated the dynamics into equilibrium process by introducing the equilibrium correlation length and relaxation time that increase, respectively, as $\xi = \xi_0|(T_c - T)/T_c|^{-\nu}$ and $\tau = \tau_0|(T_c - T)/T_c|^{-\mu}$, where μ and ν are model-dependent parameters. Near the critical temperature T_c, the process critically slows down and the correlation length indefinitely increases. Therefore, there is a time t_* when the correlation length freezes: $|t_*| = \tau(t_*)$. Thus, the Kibble-Zurek mechanism dynamically determines the domain size in terms of the quench rate as $\xi(t_*) \approx \tau_Q^{\nu/(1+\mu)}$.

To describe nonequilibrium phase transitions, there have been developed many methods such as the closed-time path integral by Schwinger and Keldysh (J. Schwinger et.al., 1961), the Hartree-Fock or mean field method (A. Ringwald, 1987), and the $1/N$-expansion method (F. Cooper et.al., 1997;2000). In this talk, we shall employ the so-called Liouville-von Neumann (LvN) method to describe nonequilibrium phase transitions (S.P. Kim et.al., 2000;2002;2001; S.P. Kim et.al., 2003). The LvN method is a canonical method that first finds invariant operators for the quantum LvN equation and then solves exactly the

functional Schrödinger equation (H.R. Lewis et.al., 1969). Compared with the other methods, this canonical method has an advantage that it can be directly applied to time-dependent systems and density operators can be readily found. We also extend thermofield dynamics (TFD) (Y. Takahashi et.al., 1975;1996;1982;1993) to time-dependent systems by combining the LvN equation with the basic notions of thermofield dynamics (S.P. Kim et.al.,). The new formalism is applied to a time-dependent oscillator by using the time-dependent creation and annihilation operators that satisfy the LvN equation. Finally, we discuss decoherence of long wavelength modes and thermalization during phase transitions.

2. Quantum field theory for nonequilibrium phase transitions

As a field model for nonequilibrium phase transitions of second order, we consider a scalar field potential

$$V(\phi) = \frac{1}{2}m^2(t)\phi^2 + \frac{\lambda}{4!}\phi^4, \tag{4}$$

where m^2 changes signs from m_i^2 to $-m_f^2$. For a quench time scale τ, the adiabatic quench process with $|\Delta m^2| \ll \tau$ is distinguished from the rapid quench process with $|\Delta m^2| \gg \tau$. A simple analytical model is provided by (S.P. Kim et.al., 2000;2002;2001)

$$m^2(t) = m_1^2 - m_0^2 \tanh\left(\frac{t}{\tau}\right), \quad (m_0 > m_1) \tag{5}$$

where $m^2 \to m_0^2 + m_1^2$ for $t \to -\infty$ and $m^2 \to -(m_0^2 - m_1^2)$ for $t \to +\infty$. Figure 1 shows the evolution of the potential with the mass given in Eq. (5). In the limiting case of $\tau \to 0$, one has the instantaneous quench, $m_i^2 = m_0^2 + m_1^2$ for $t < 0$ and $m_f^2 = -(m_0^2 - m_1^2)$ for $t > 0$. The field model can readily be generalized to an expanding universe

$$H(t) = \int d^3x \Big[\frac{\pi_\phi^2}{2R^3(t)} + R^3(t)\Big(\frac{(\nabla\phi)^2}{2R^2(t)} + V(\phi)\Big) \Big], \tag{6}$$

where R is the scale factor of the Friedmann-Robertson-Walker (FRW) universe. The Minkowski spacetime is the special case of $R = 1$. In the Hartree-Fock or mean-field approximation, the field ϕ is divided into a classical background field ϕ_c with the equation of motion

$$\ddot{\phi}_c + 3\frac{\dot{R}}{R}\dot{\phi}_c - \nabla^2\phi_c + \Big(m^2(t) + \frac{\lambda}{6}\phi_c^2 + \frac{\lambda}{2}\langle\phi_f^2\rangle\Big)\phi_c = 0, \tag{7}$$

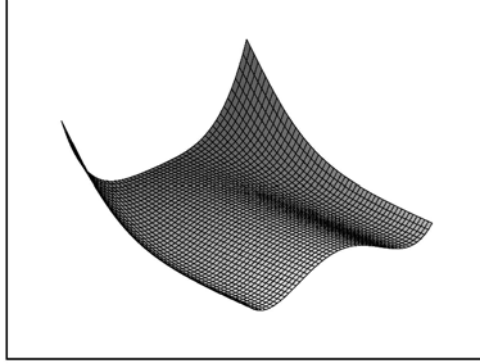*Figure 1.* The quenched potential $V(\phi) = \frac{1}{2}\left[m_1^2 - m_0^2 \tanh\left(\frac{t}{\tau}\right)\right]\phi^2 + \frac{\lambda}{4!}\phi^4$. The time direction is from the upper left to the lower right and the ϕ-direction from the lower left to upper right. Classically, the field rolls down from the false vacuum at the bottom of the upper left to the true vacua in the lower left or upper right. The field fluctuates around such configurations.

and quantum fluctuations with the equation of motion

$$\ddot{\phi}_f + 3\frac{\dot{R}}{R}\dot{\phi}_f - \nabla^2\phi_f + \left(m^2(t) + \frac{\lambda}{2}\phi_c^2 + \frac{\lambda}{4}\phi_f^2\right)\phi_f = 0. \tag{8}$$

In the functional Schrödinger-picture, wave functionals carry all information of quantum states in real time (K. Freese et.al., 1985;1988). The wave functionals satisfy the functional Schrödinger equation

$$i\frac{\partial}{\partial t}\Psi(\phi, t) = \hat{H}(\phi, -i\delta/\delta\phi, t)\Psi(\phi, t). \tag{9}$$

The wave functionals are equipped with an inner product on each spacelike hypersurface Σ_t

$$\langle\Psi_1|\Psi_2\rangle = \int \mathcal{D}[\phi]\Psi_1^*(\phi, t)\Psi_2(\phi, t). \tag{10}$$

Each operator acts on a wave functional as

$$\hat{\mathcal{O}}(\phi, \pi)|\Psi(\phi, \pi)\rangle \rightarrow \hat{\mathcal{O}}(\phi, -i\delta/\delta\phi)\Psi(\phi, t). \tag{11}$$

The evolution of the wave functional may be found in terms of the Green function

$$\Psi(\mathbf{x}, t) = \int G(\mathbf{x}, t; \mathbf{x}_0, t_0)\Psi(\mathbf{x}_0, t_0)d\mathbf{x}_0 dt_0, \tag{12}$$

where the wave functional implicitly depends on the space through $\phi(\mathbf{x})$. The Hamiltonian may be separated into a quadratic part, an exactly solvable one, and a perturbation part:

$$\hat{H}(t) = \hat{H}_0(t) + \lambda\hat{H}_P(t). \tag{13}$$

Here $\hat{H}_0$ includes not only the quadratic potential term but also some contribution from nonlinear terms a la the Hartree-Fock or mean-field approximation. Introducing a Green function for $\hat{H}_0$

$$\Big(i\frac{\partial}{\partial t} - \hat{H}_0(\mathbf{x}, t)\Big)G_0(\mathbf{x}, t; \mathbf{x}', t') = \delta(\mathbf{x} - \mathbf{x}')\delta(t - t'), \qquad (14)$$

we write the wave functional in terms of G_0 as

$$\Psi(\mathbf{x}, t) = \Psi_0(\mathbf{x}, t) + \lambda \int G_0(\mathbf{x}, t; \mathbf{x}', t')\hat{H}_P(\mathbf{x}', t')\Psi(\mathbf{x}', t')d\mathbf{x}'dt', \quad (15)$$

where Ψ_0 is a wave functional for $\hat{H}_0$. The wave functional Ψ can be put recursively into the righthand side of Eq. (15) to result in a series expansion (S.P. Kim et.al., 2003)

$$\begin{aligned}\Psi(1) &= \Psi_0(1) + \lambda \int G_0(1, 2)\hat{H}_P(2)\Psi_0(2)\\ &+ \lambda^2 \int \int G_0(1, 2)\hat{H}_P(2)G_0(2, 3)\hat{H}_P(3)\Psi_0(3) + \cdots, \quad (16)\end{aligned}$$

where (i) denotes $(\mathbf{x}_i, t_i)$. Up to this stage, the quantum field theory works for phase transitions exactly in the same manner as for ordinary quantum field theory.

3. LvN method for nonlinear quantum fields

Recently we have developed another canonical method, the so-called LvN or invariant method, based on the quantum LvN equation (S.P. Kim et.al., 2000;2002;2001; S.P. Kim et.al., 2003)

$$i\frac{\partial}{\partial t}\hat{\mathcal{O}}(\phi, -i\delta/\delta\phi, t) + [\hat{\mathcal{O}}(\phi, -i\delta/\delta\phi, t), \hat{H}(\phi, -i\delta/\delta\phi, t)] = 0. \quad (17)$$

The idea of the LvN method for quantum systems first introduced by Lewis and Riesenfeld (H.R. Lewis et.al., 1969) is to solve Eq. (17) and then find the solution to the Schrödinger equation as an eigenstate of the operator in Eq. (17). In quantum field theory the wave functional to the Schrödinger equation is directly given by the wave functional of the operator

$$\hat{\mathcal{O}}(\mathbf{x}, t)\Psi_\varphi(\mathbf{x}, t) = \varphi(\mathbf{x})\Psi_\varphi(\mathbf{x}, t). \quad (18)$$

Note that the eigenvalue $\varphi(\mathbf{x})$ does not depend on time, which is a consequence of Eq. (17). In particular, for a quadratic Hamiltonian, the operator satisfying Eq. (17) can be obtained explicitly. This canonical method has an advantage that quantum statistical information can

be naturally incorporated into the dynamics even for nonequilibrium systems.

We now turn to the potential (4) for nonequilibrium phase transition. We separate the Hamiltonian density $\mathcal{H}$ into a quadratic part $\mathcal{H}_0$ and a perturbation part $\mathcal{H}_P$:

$$
\begin{aligned}
\mathcal{H}_0(t) &= \frac{\pi^2}{2R^3} + \frac{(\nabla\phi)^2}{2R} + \frac{R^3}{4}(2m^2 + \lambda\langle\phi^2\rangle)\phi^2, \\
\mathcal{H}_P(t) &= \frac{R^3}{4!}(\phi^4 - 6\langle\phi^2\rangle\phi^2).
\end{aligned} \tag{19}
$$

We use the Fourier-cosine and sine modes of the field redefined as

$$
\phi_{\mathbf{k}}^{(+)}(t) = \frac{1}{\sqrt{2}}[\phi_{\mathbf{k}}(t) + \phi_{-\mathbf{k}}(t)], \quad \phi_{\mathbf{k}}^{(-)}(t) = \frac{i}{\sqrt{2}}[\phi_{\mathbf{k}}(t) - \phi_{-\mathbf{k}}(t)]. \tag{20}
$$

For simplicity reason, a compact notation $\alpha, \beta, \cdots$, will be used for $\{\mathbf{k}, (\pm)\}$. Then the total Hamiltonian in a symmetric state takes the form

$$
H(t) = \sum_\alpha \Big[\frac{\pi_\alpha^2}{2R^3} + \frac{R^3}{2}\omega_\alpha^2(t)\phi_\alpha^2\Big] + \frac{\lambda R^3}{4!}\Big[\sum_\alpha \phi_\alpha^4 + 3\sum_{\alpha\neq\beta}\phi_\alpha^2\phi_\beta^2\Big], \tag{21}
$$

where ω_α^2 is a time-dependent frequency squared

$$
\omega_\alpha^2(t) = m^2(t) + \frac{\mathbf{k}^2}{R^2}. \tag{22}
$$

We further separate the quadratic part of the Hamiltonian

$$
H_0(t) = \sum_\alpha \frac{\pi_\alpha^2}{2R^3} + \frac{R^3}{2}\Omega_\alpha^2(t)\phi_\alpha^2, \quad \Omega_\alpha^2(t) = m^2(t) + \frac{\mathbf{k}^2}{R^2} + \frac{\lambda}{2}\sum_\beta\langle\phi_\beta^2\rangle. \tag{23}
$$

Note that the quadratic part simply consists of decoupled oscillators.

We first find the Green function G_0 for $\hat{H}_0$ and then obtain perturbatively the wave functional for the total Hamiltonian. In fact, each mode of the quadratic part $\hat{H}_0$ can be solved exactly in terms the time-dependent creation and annihilation operators (S.P. Kim et.al., 2000;2002;2001; S.P. Kim et.al., 2003)

$$
\hat{a}_\alpha^\dagger(t) = -i[\varphi_\alpha(t)\hat{\pi}_\alpha - R^3\dot{\varphi}_\alpha(t)\hat{\phi}_\alpha], \quad \hat{a}_\alpha(t) = i[\varphi_\alpha^*(t)\hat{\pi}_\alpha - R^3\dot{\varphi}_\alpha^*(t)\hat{\phi}_\alpha], \tag{24}
$$

which satisfy the LvN equation with $\hat{H}_\alpha$

$$
i\frac{\partial}{\partial t}\hat{a}_\alpha^\dagger(t) + [\hat{a}_\alpha^\dagger(t), \hat{H}_\alpha(t)] = 0, \quad i\frac{\partial}{\partial t}\hat{a}_\alpha(t) + [\hat{a}_\alpha(t), \hat{H}_\alpha(t)] = 0. \tag{25}
$$

Then the auxiliary field φ_α satisfies the mean-field equation

$$\ddot{\varphi}_\alpha + 3\frac{\dot{R}}{R}\dot{\varphi}_\alpha + \Omega_\alpha^2\varphi_\alpha = 0. \tag{26}$$

Indeed, these operators satisfy the usual commutation relations at equal times

$$[\hat{a}_\alpha(t), \hat{a}_\beta^\dagger(t)] = \delta_{\alpha\beta}, \tag{27}$$

when the Wronskian condition meets

$$R^3(\dot{\varphi}_\alpha^*\varphi_\alpha - \varphi_\alpha^*\dot{\varphi}_\alpha) = i. \tag{28}$$

In the oscillator representation, we express $\hat{H}_0$ and $\hat{H}_P$ in terms of $\{\hat{a}_\alpha^\dagger, \hat{a}_\alpha\}$ in Eq. (24), but drop all c-number terms.

The essential point of the LvN method is that the number states of $\hat{a}_\alpha^\dagger$ and $\hat{a}_\alpha$

$$\hat{N}_\alpha(t)|n_\alpha, t\rangle_0 = \hat{a}_\alpha^\dagger(t)\hat{a}_\alpha(t)|n_\alpha, t\rangle_0 = n_\alpha|n_\alpha, t\rangle_0, \tag{29}$$

are exact quantum states of the time-dependent Schrödinger equation. The quantum state of the field itself is then a product of each mode state. For instance, the Gaussian vacuum state of the field is given by

$$|0, t\rangle_0 = \prod_\alpha |0_\alpha, t\rangle_0. \tag{30}$$

We now find the Green function for $\hat{H}_\alpha$

$$G_{0\alpha}(\phi_\alpha, t; \phi_\alpha', t') = \sum_{n_\alpha} \langle\phi_\alpha|n_\alpha, t\rangle_0 \, _0\langle n_\alpha, t'|\phi_\alpha'\rangle, \tag{31}$$

and the Green function for $\hat{H}_0$

$$G_0(\mathbf{x}, t; \mathbf{x}', t'\rangle = \prod_\alpha G_{0\alpha}(\phi_\alpha, t; \phi_\alpha', t'). \tag{32}$$

The wave functional for the total Hamiltonian (21) can be obtained perturbatively by substituting Eqs. (32) and $\hat{H}_P$ in the oscillator representation into Eq. (16).

4. Extension of TFD to nonequilibrium systems

Takahashi and Umezawa introduced thermofield dynamics (TFD), a canonical formalism, for finite temperature theory (Y. Takahashi et.al., 1975;1996;1982;1993). TFD keeps the analogy with the zero-temperature field theory by describing thermal state, a mixed state, as a thermal

vacuum, a pure state in an extended Hilbert space. That is, TFD doubles the degrees of freedom by introducing a fictitious Hamiltonian without any interaction with the system and uses the extended Hilbert space of the system plus the fictitious system. Recently TFD has been extended to time-dependent quantum systems by using the basis of time-dependent creation and annihilation operators satisfying the LvN equation (S.P. Kim et.al.,). Thus, the LvN method provides a direct extension of TFD to time-dependent systems with minimal modification.

As a simple model, we confine our attention just to a single mode $H_\alpha(t)$ of the Hamiltonian (23). Note that neither any instantaneous eigenstate of $\hat{H}_\alpha(t)$ is an exact quantum state nor $e^{-\beta \hat{H}_\alpha(t)}$ is a density operator. To calculate the thermal expectation value of an operator $\hat{A}$, one needs either the Heisenberg operator $\hat{A}_H$ or the density operator $\hat{\rho}_\alpha(t) = \hat{U}_\alpha \hat{\rho}_\alpha \hat{U}_\alpha^\dagger$. Now we use the time-dependent creation and annihilation operators (24), invariant operators, to construct the Fock space.

To extend TFD to the time-dependent system $\hat{H}_\alpha$, we introduce a fictitious Hamiltonian

$$\hat{\tilde{H}}_\alpha(t) = \frac{\hat{\tilde{\pi}}_\alpha^2}{2R^3} + \frac{R^3}{2}\Omega_\alpha^2 \hat{\tilde{\phi}}_\alpha^2. \qquad (33)$$

Here and hereafter the tilde conjugation rule, $(cA)\tilde{} = c^* \tilde{A}$, will be used. The time-dependent creation and annihilation operators for the fictitious Hamiltonian (33) are obtained by applying the tilde conjugation rule to Eq. (24)

$$\hat{\tilde{a}}_\alpha^\dagger(t) = i[\varphi_\alpha^*(t)\hat{\tilde{\pi}}_\alpha - R^3 \dot{\varphi}_\alpha^*(t)\hat{\tilde{\phi}}_\alpha], \; \hat{\tilde{a}}_\alpha(t) = -i[\varphi_\alpha(t)\hat{\tilde{\pi}}_\alpha - R^3 \dot{\varphi}_\alpha(t)\hat{\tilde{\phi}}_\alpha]. \qquad (34)$$

In fact, the $\hat{\tilde{a}}_\alpha^\dagger(t)$ and $\hat{\tilde{a}}_\alpha(t)$ satisfy the LvN equation for the fictitious Hamiltonian (33). The equal-time commutator $[\hat{\tilde{a}}_\alpha(t), \hat{\tilde{a}}_\alpha^\dagger(t)] = 1$ also holds.

The Hilbert space of the total system, $\hat{H}_{\rm tot}(t) = \hat{H}_\alpha(t) - \hat{\tilde{H}}_\alpha(t)$, consists of

$$|n_\alpha, \tilde{m}_\alpha, t\rangle = |n_\alpha, t\rangle \otimes |\tilde{m}_\alpha, t\rangle = \frac{\hat{a}_\alpha^{\dagger n}(t)}{\sqrt{n_\alpha!}} \frac{\hat{\tilde{a}}_\alpha^{\dagger m}(t)}{\sqrt{m_\alpha!}}|0_\alpha, \tilde{0}_\alpha, t\rangle. \qquad (35)$$

The density operator in the extended Hilbert space is given by

$$\hat{\rho}_{\rm tot}(t) = \hat{\rho}_\alpha(t) \otimes \hat{\tilde{\rho}}_\alpha(t) = \frac{1}{Z_\alpha^2} e^{-\beta\hbar\omega_\alpha[\hat{a}_\alpha^\dagger(t)\hat{a}_\alpha(t) - \hat{\tilde{a}}_\alpha^\dagger(t)\hat{\tilde{a}}_\alpha(t)]}. \qquad (36)$$

The thermal expectation value of the operator $\hat{A}$ of the system now takes the form

$$\langle \hat{A} \rangle = \mathrm{Tr}[\hat{\rho}_{\mathrm{tot}}(t)\hat{A}] = \langle 0_\alpha(\beta), t|\hat{A}|0_\alpha(\beta), t\rangle, \tag{37}$$

where the thermal vacuum state is given by

$$|0_\alpha(\beta), t\rangle = \frac{1}{Z_\alpha^{1/2}} \sum_{n_\alpha=0} e^{-\beta\hbar\omega_\alpha n_\alpha/2} \frac{1}{n_\alpha!} \hat{a}_\alpha^{\dagger n}(t)\hat{\tilde{a}}_\alpha^{\dagger n}(t)|0_\alpha, \tilde{0}_\alpha, t\rangle. \tag{38}$$

Defining the time- and temperature-dependent annihilation and creation operators through the Bogoliubov transformation

$$\begin{aligned}
\hat{a}_\alpha(\beta, t) &= \cosh\theta_\alpha(\beta)\hat{a}_\alpha(t) - \sinh\theta_\alpha(\beta)\hat{\tilde{a}}_\alpha^{\dagger}(t),\\
\hat{\tilde{a}}_\alpha(\beta, t) &= \cosh\theta_\alpha(\beta)\hat{\tilde{a}}_\alpha(t) - \sinh\theta_\alpha(\beta)\hat{a}_\alpha^{\dagger}(t),
\end{aligned} \tag{39}$$

we find that the thermal state is the time- and temperature-dependent vacuum

$$\hat{a}_\alpha(\beta, t)|0_\alpha(\beta), t\rangle = \hat{\tilde{a}}_\alpha(\beta, t)|0_\alpha(\beta), t\rangle = 0. \tag{40}$$

At each moment, the thermal vacuum state still keeps the same boson distribution

$$\langle 0_\alpha(\beta), t|\hat{a}_\alpha^{\dagger}(t)\hat{a}_\alpha(t)|0_\alpha(\beta), t\rangle = \sinh^2\theta_\alpha(\beta) = \frac{1}{e^{\beta\hbar\omega_\alpha} - 1}. \tag{41}$$

Using TFD we are able to find the thermal expectation values of operators. In general, through the Bogoliubov transformation from $\{\hat{a}_\alpha^{\dagger}(t), \hat{a}_\alpha(t)\}$ to $\{\hat{a}_\alpha^{\dagger}(\beta, t), \hat{a}_\alpha(\beta, t)\}$, we find the formula

$$\langle F(\hat{a}_\alpha^{\dagger}(t), \hat{a}_\alpha(t))\rangle_{\mathrm{T}} = \langle 0_\alpha(\beta), t|F(\cosh\theta_\alpha \hat{a}_\alpha^{\dagger}(\beta, t) + \sinh\theta_\alpha\hat{\tilde{a}}_\alpha(\beta, t),$$
$$\cosh\theta_\alpha\hat{a}_\alpha(\beta, t) + \sinh\theta_\alpha\hat{\tilde{a}}_\alpha^{\dagger}(\beta, t))|0_\alpha(\beta), t\rangle. \tag{42}$$

For instance, we obtain the thermal correlation function of high moments

$$\langle \hat{\phi}_\alpha^{2n} \rangle_{\mathrm{T}} = \frac{(2n)!}{2^n n!} (\varphi_\alpha^* \varphi_\alpha)^n (1 + 2\sinh^2\theta_\alpha(\beta))^n. \tag{43}$$

5. Domain growth and topological defects

Now we study the effects of the dynamical processes of nonequilibrium phase transitions on domain growth and topological defects. The quench models describe such nonequilibrium processes, which can be

treated exactly for the free theory and approximately for the self-interacting theory. Before the onset of the phase transitions, the mass term dominates over the last term in Eq. (23) from the quantum corrections. It is thus justified to use approximately the free theory after the onset of phase transition until it crosses the inflection point or spinodal line. This is also true for the quench process lasting for an indefinitely long period. We first consider the free theory in the Minkowski spacetime and then discuss the effect of nonlinear terms.

The free theory for the quench models is provided by the potential (4), where $\lambda = 0$ and $m^2(t)$ changes signs either instantaneously or for a finite period. In the Minkowski spacetime, we can apply the LvN method simply by letting $R = 1$. Before the phase transition ($m_i = (m_0^2 + m_1^2)^{1/2}$), all the modes are stable and oscillate around the true vacuum:

$$\varphi_{i0\mathbf{k}}(t) = \frac{1}{\sqrt{2\omega_{i\mathbf{k}}}}e^{-i\omega_{i\mathbf{k}}t}, \quad \omega_{i\mathbf{k}} = (\mathbf{k}^2 + m_i^2)^{1/2}. \tag{44}$$

The two-point correlation function is the Green function at equal times

$$G_0(\mathbf{x}, \mathbf{x}', t) = \langle\hat{\phi}(\mathbf{x}, t)\hat{\phi}(\mathbf{x}', t)\rangle_0 = G_0(\mathbf{x}, t; \mathbf{x}', t) \tag{45}$$

with respect to the Gaussian vacuum or thermal equilibrium.

Either in the instantaneous quench or in the finite quench, short wavelength modes with $k > m_f = (m_0^2 - m_1^2)^{1/2}$ are still stable even after the phase transition and oscillate around the false vacuum as

$$\varphi_{f\mathbf{k}} = \frac{\alpha_{\mathbf{k}}e^{-i(\mathbf{k}^2 - m_f^2)^{1/2}t}}{\sqrt{2}(\mathbf{k}^2 - m_f^2)^{1/2}} + \frac{\beta_{\mathbf{k}}e^{i(\mathbf{k}^2 - m_f^2)^{1/2}t}}{\sqrt{2}(\mathbf{k}^2 - m_f^2)^{1/2}}, \tag{46}$$

where $|\alpha_{\mathbf{k}}|^2 - |\beta_{\mathbf{k}}|^2 = 1$. Whereas, long wavelength modes with $k < m_f$ become unstable after the phase transition and exponentially grow as

$$\varphi_{f\mathbf{k}} = \frac{\mu_{\mathbf{k}}e^{(m_f^2 - \mathbf{k}^2)^{1/2}t}}{\sqrt{2}(m_f^2 - \mathbf{k}^2)^{1/2}} + \frac{\nu_{\mathbf{k}}e^{-(m_f^2 - \mathbf{k}^2)^{1/2}t}}{\sqrt{2}(m_f^2 - \mathbf{k}^2)^{1/2}}, \tag{47}$$

where $\mu_{\mathbf{k}}^*\nu_{\mathbf{k}} - \mu_{\mathbf{k}}\nu_{\mathbf{k}}^* = i$.

The coefficients $\mu_{\mathbf{k}}$ and $\nu_{\mathbf{k}}$ are obtained from the exact solutions of Eq. (26) in terms of the hypergeometric function (S.P. Kim et.al., 2000;2002;2001). Using the exact solutions, we obtain the two-point thermal correlation function during the the quench ($-\tau < t < \tau$)

$$G_{m,T}(r, t) \simeq G_{m,T}(0, t)\frac{\sin\left(\frac{\sqrt{\tau t}}{m_0}r\right)}{\frac{\sqrt{\tau t}}{m_0}r}\exp\left(-\frac{r^2}{8\frac{\sqrt{\tau t}}{m_0}}\right). \tag{48}$$

Thus, the domain size is scaled by the Cahn-Allen scaling relation

$$\xi_D(t) = 2\Big(\frac{2\tau t}{m_0^2}\Big)^{1/4}.$$ (49)

After the quench $(t \gg \tau)$, the two-point thermal correlation function is given by

$$G_{f_U,T}(r,t) \simeq G_{f_U,T}(0,t)\frac{\sin\Big(\sqrt{\frac{m_f}{2\tilde{t}}}r\Big)}{\sqrt{\frac{m_f}{2\tilde{t}}}r}\exp\Big(-\frac{m_f r^2}{8\tilde{t}}\Big),$$ (50)

where

$$\tilde{t} = t - \frac{\tau^3 m_0^2}{4}[\zeta(3) - 1].$$ (51)

Then the Cahn-Allen scaling relation for the domain size takes another form

$$\xi_D(t) = \Big(\frac{8\tilde{t}}{m_f}\Big)^{1/2}.$$ (52)

The power of the scaling relation is the same as the instantaneous quench, except for a time-lag proportional to the cube of the quench duration τ.

6. Decoherence of order parameter and thermalization

Quantum phase transitions can be successfully described by quantum field theory. It is the long wavelength modes that play a pivotal role in the dynamical process of phase transitions and thus determine the growth of domains. In classical theory an order parameter plays a similar role in phase transitions. So it is legitimate to expect some relation between long wavelength modes in quantum theory and the order parameter in classical theory. We shall show that the long wavelength modes constitute just an order parameter, which describes the dynamical process. For this order parameter to behave classically, the quantum states of long wavelength modes should lose quantum coherence and also follow their classical trajectories (S.P. Kim et.al., 2000;2002;2001; F.C. Lombardo et.al., 2000;2001;2003). This is known as the quantum-to-classical transition in more general context (D. Guilini et.al., 1996).

In the phase transition model (4) long wavelength modes are coupled to short wavelengths modes by nonlinear couplings (21). It is not known whether this model can be solved exactly except for numerical methods.

Instead of this nonlinear coupling, a linear coupling provides an exactly solvable model with the Hamiltonian (S.P. Kim et.al., 2000;2002;2001)

$$H(t) = \frac{1}{2}\pi_1^2 + \frac{1}{2}\omega_1^2(t)\phi_1^2 + \frac{1}{2}\pi_2^2 + \frac{1}{2}\omega_2^2(t)\phi_2^2 + \lambda\phi_1\phi_2. \qquad (53)$$

Here ϕ_1 and ϕ_2 are the long and short wavelength modes, respectively. To model the instantaneous quench, we assume $\omega_1^2(t) = -\bar{\omega}_1^2$ and $\omega_2^2(t) = \bar{\omega}_2^2$ when $t > 0$. Thus, ϕ_1 becomes unstable but ϕ_2 remains stable even after the phase transition.

The Hamiltonian (53) has a Gaussian wave function of the form

$$\Psi_0(\phi_1, \phi_2, t) = N(t) \exp\Big[-\{A_1(t)\phi_1^2 + \lambda B(t)\phi_1\phi_2 + A_2(t)\phi_2^2\}\Big]. \quad (54)$$

Here N is the normalization constant and the coefficients A_1, A_2 and B will be determined by Schrödinger equation. We are interested in the reduced density matrix for the long wavelength mode ϕ_1, which is obtained by integrating the density matrix $\Psi_0(\phi_1', \phi_2', t)\Psi_0^*(\phi_1, \phi_2, t)$ over the short wavelength mode $\phi_2 = \phi_2'$. Then the reduced density matrix for the long wavelength mode can be written in the form

$$\rho_{\rm R}(\phi_1', \phi_1) = \tilde{N}(t) \exp[-\Gamma_c\phi_{1c}^2 - \Gamma_\delta\phi_{1\delta}^2 - \Gamma_m\phi_{1c}\phi_{1\delta}], \qquad (55)$$

where $\phi_{1c} = (\phi_1' + \phi_1)/2$ and $\phi_{1\delta} = (\phi_1' - \phi_1)/2$ and $\tilde{N}$ is another normalization constant. The measures for quantum decoherence and classical correlation are given by

$$\delta_{QD} = \frac{1}{2}\sqrt{\frac{\Gamma_c}{\Gamma_\delta}}, \quad \delta_{CC} = \sqrt{\frac{\Gamma_c^2\Gamma_\delta^2}{\Gamma_m^*\Gamma_m}}. \qquad (56)$$

A quantum state loses quantum coherence (decoheres) when $\delta_{QD} \ll 1$ and recovers classical correlation when $\delta_{CC} \ll 1$ (M. Morikawa, 1990). A system is classically correlated when its wave functions are peaked along classical trajectories. And it decoheres when each trajectory loses quantum coherence with its neighbors. Quantum decoherence is realized when the diagonal term ϕ_c of the density matrix dominates over the off-diagonal term ϕ_δ.

Before the phase transition ($t < 0$), the measures for decoherence and classical correlation are exactly found

$$\delta_{QD} = \frac{1}{2}\left(1 - \frac{\lambda^2}{\Omega_1\Omega_2(\Omega_1 + \Omega_2)^2}\right)^{1/2}, \quad \delta_{CC} = \infty, \qquad (57)$$

where

$$\Omega_1^2 = \omega_1^2 - \left(\frac{\lambda}{\Omega_1 + \Omega_2}\right)^2, \quad \Omega_2^2 = \omega_2^2 - \left(\frac{\lambda}{\Omega_1 + \Omega_2}\right)^2. \qquad (58)$$

On the other hand, after the phase transition, in the weak coupling limit ($\lambda \ll \bar{\omega}_1, \bar{\omega}_2$), the measures for quantum decoherence and classical correlation are given approximately by

$$\delta_{QD} = \frac{\lambda}{2}\sqrt{\frac{5\bar{\omega}_2^2(\bar{\omega}_1 - \bar{\omega}_2)}{2\bar{\omega}_1(\bar{\omega}_1^2 + \bar{\omega}_2^2)^2}}, \quad \delta_{CC} = \frac{5\lambda^6}{4}\frac{|\bar{\omega}_1 - \bar{\omega}_2|}{\bar{\omega}_1^2(\bar{\omega}_1^2 + \bar{\omega}_2^2)^5}. \tag{59}$$

Therefore, we conclude that the long wavelength mode neither decoheres nor is classically correlated before the phase transition. However, after the phase transitions, the unstable long wavelength mode becomes classical, gaining both quantum decoherence and classical correlation. Thus an order parameter appears from long wavelength modes (S.P. Kim et.al., 2000;2002;2001).

Finally, we discuss the effect of nonlinear coupling on domain growth, decoherence, and thermalization. As the wave functionals Ψ_0 of $\hat{H}_0$ are easily found, Eq. (16) leads to the wave functional beyond the Hartree approximation. Putting the perturbation terms (19) into Eq. (16), we first find the wave functional of the form

$$\Psi = \Psi_0^{(0)} + \sum_{n=1}^{\infty} \lambda^n \Psi_0^{(n)}, \tag{60}$$

from which the Green function follows. The wave functionals $\Psi_0^{(n)}$ include various types of nth order multiple scattering. One effect of the nth order multiple scattering is that the correlation length beyond the Hartree approximation has an additional factor (S.P. Kim et.al., 2003)

$$\xi(t) = (2n + 1)^{1/2}\xi_D(t). \tag{61}$$

The activation of each order of quantum contributions depends on the period for the field rolling from the false vacuum into the true one. The multiple scattering of unstable long wavelength modes with infinitely large number of short wavelength modes (environment) provides a very efficient mechanism for decoherence (F.C. Lombardo et.al., 2000;2001;2003). It is highly likely that since the quadratic part, $\hat{H}_0$, alone cannot lead to thermalization after phase transition, the multiple scattering via $\hat{H}_P$ may result in energy transfer among long and short wavelength modes as well as decoherence and thus lead to thermalization.

7. Summary

We applied the Liouville-von Neumann (LvN) method, a canonical
method, to nonequilibrium quantum phase transitions. The essential
idea of the LvN method is first to solve the LvN equation and then
to find exact wave functionals of time-dependent quantum systems.
The LvN method has several advantages that it can easily incorpo-
rate thermal theory in terms of density operators and that it can
also be extended to thermofield dynamics (TFD) by using the time-
dependent creation and annihilation operators, invariant operators.
Combined with the oscillator representation, the LvN method provides
the Fock space of a Hartree-Fock type quadratic part of the Hamil-
tonian, and further allows to improve wave functionals systematically
either by the Green function or perturbation technique. In this sense
the LvN method goes beyond the Hartree-Fock approximation.

The field model studied for nonequilibrium phase transitions is the
quenched ϕ^4-theory with a quench time scale, where the mass changes
sign during the quench process. This model is a quantum model for the
classical Ginzburg-Landau theory for spinodal decomposition. Phase
transitions occur nonequilibrium when the quench (dynamical) time
scale is shorter than the thermal relaxation time scale. Some interesting
results are growth of domain sizes, topological density and decoherence
of an order parameter. We find that the domains have the Cahn-
Allen scaling relation in the instantaneous quench and different scaling
behaviors in finite quench. Further, the nonlinear effect leads to a
multiple-scaling relation of domains beyond the Hartree-Fock approx-
imation. Another interesting consequence of multiple scattering via
the nonlinear interaction is that long wavelength modes become classi-
cal, losing quantum coherence and gaining classical correlation, during
phase transitions. It is highly likely that the energy transfer among
long and short wavelength modes and decoherence of long wavelength
modes may lead to thermalization.

Acknowledgments

References

Kibble, T.W.B. *J. Phys. A*, 9:1387, 1976; Zurek, W.H. *Nature*, 317:505, 1985.

Vilenkin, A. and E.P.S. Shellard. Cosmic Strings and Other Topological Defects. *Cambridge Univ. Press, Cambridge*, 1994.

Dolan, L. and R. Jackiw. *Phys. Rev. D*, 9:3320, 1974.

Weinberg, E.J. and A. Wu. *Phys. Rev. D*, 36:2474, 1987.

Schwinger, J. *J. Math. Phys.*, 2:407, 1961; Keldysh, L.V. *Sov. Phys. JETP*, 20:1018, 1965.

Ringwald, A. *Phys. Rev. D*, 36:2598, 1987; Boyanovsky, D., D.-S. Lee and A. Singh. *Phys. Rev. D*, 48:800, 1993; Rivers, R.J. *Int. J. Theor. Phys.*, 39:1623, 2000; Cormier, D. and R. Holman. *Phys. Rev. D*, 62:023520, 2000; Destri, C. and E. Manfredini. *Phys. Rev. D*, 62:025008, 2000.

Cooper, F., S. Habib, Y. Kluger and E. Mottola. *Phys. Rev. D*, 55:6471, 1997; Destri, C, and E. Manfredini. *Phys. Rev. D*, 62:025007, 2000; Baacke, J. and K. Heitmann. *Phys. Rev. D*, 62:105022, 2000.

Kim, S.P. and C.H. Lee. *Phys. Rev. D*, 62:125020, 2000; Kim, S.P. and C.H. Lee. *Phys. Rev. D*, 65:045013, 2002; Kim, S.P., S. Sengupta and F.C. Khanna. *Phys. Rev. D*, 64:105026, 2001.

Kim, S.P. and F.C. Khanna. Non-Gaussian Effects on Domain Growth. *hep-ph*, 0011115 (unpublished); Sengupta, S., F.C. Khanna and S.P. Kim. *Phys. Rev. D*, 68:105014, 2003; Kim, S.P. Dynamical Theory of Phase Transitions and Topological Defect Formation in the Early Universe. *hep-ph*, 0401095.

Lewis, H.R. and W.B. Riesenfeld. *J. Math. Phys.*, 10:1458, 1969.

Takahashi, Y. and H. Umezawa. *Collect. Phenem.*, 2:55, 1975; *Reprinted in Int. J. Mod. Phys. B*, 10:1755, 1996; Umezawa, H., H. Matsumoto and M. Tachiki. Thermofield Dynamics and Condensed States. *North-Holland, Amsterdam*, 1982; Umezawa, H. Advanced Field Theory: Micro, Macro and Thermal Physics. *AIP, New York*, 1993.

Kim, S.P. and F.C. Khanna. Thermo Field Dynamics of Time-Dependent Boson and Fermion System. *quant-ph*, 0308053, (unpublished).

Freese, K., C.T. Hill and M. Mueller. *Nucl Phys. B*, 255:693, 1985; Éboli, O., R. Jackiw and S.-Y. Pi. *Phys. Rev. D*, 37:3557, 1988.

Lombardo, F.C., F.D. Mazzitelli and D. Moteoliva. *Phys. Rev. D*, 62:045016, 2000; Lombardo, F.C., F.D. Mazzitelli and R.J. Rivers. *Phys. Lett. B*, 523:317, 2001; Lombardo, F.C., F.D. Mazzitelli and R.J. Rivers. *Nucl. Phys. B*, 672:462, 2003.

Giulini, D., E. Joos, C. Kiefer, J. Kupsch, I.-O. Stamatescu and H.D. Zeh. Decoherence and the Appearance of a Classical World in Quantum Theory. *Springer, Berlin*, 1996.

Morikawa, M. *Phys. Rev. D*, 42:2929, 1990.

The $\phi \to \omega\pi^0$ decay in the Chiral model

Kamil Nasriddinov[a], Boris Kuranov, and Nurmukhammad Iskandarov[b]

Tashkent State Pedagogical University named after Nizami, Yusuf Khos Khojib-103,700100,Tashkent,Uzbekistan[a], Institute of Nuclear Physics Uzbek Academy of Sciences Ulugbek 702132, Tashkent, Uzbekistan[b]

Abstract. The $\phi \to \omega\pi^0$ decay is studied using the method of phenomenological chiral Lagrangians. Obtained in the framework of this method the expression of weak hadronic currents between vector and pseudoscalar mesons has been checked and it is shown that this decay channel proceeds only due to the $\phi - \rho$ - mixing diagram.

Keywords: decay, mixing

Recently, experimental evidence (Achasov,1999) of the G-parity violating $\phi \to \omega\pi^0$ decay with the partial widths

$$B(\phi \to \omega\pi^0) = (4.8^{+1.9}_{-1.7} \pm 0.8) * 10^{-5}$$

has been observed. At present the world average (Nagiwara, (2002)) for this decay channel is estimated to be

$$B(\phi \to \omega\pi^0) = (5.2^{+1.3}_{-1.1}) * 10^{-5}.$$

Here, we consider the $\phi \to \omega\pi^0$ decay by the method of phenomenological chiral Lagrangians(PCL's)(Weinberg,1967). Studies of this decay channel is of interest in this model for the following reasons:
First, this decay channel is a unique "laboratory" for verification of weak hadron currents between pseudoscalar and vector meson states which was obtained earlier (Nasriddinov, 1998) within the formalism of phenomenological chiral Lagrangians

$$I^i_\mu = gF_\pi \vartheta^a_\mu \varphi^b f_{abi}, \tag{1}$$

g is the "universal" coupling constant fixed from the experimental $\rho \to \pi\pi$ decay widht $g^2/4\pi = 3.2$, $F_\pi = 93 MeV$, ϑ^a_μ and φ^b are the fields of the 1^- and 0^- mesons, respectively, and f_{abi} are the structure constants of the $SU(3)$ group (a,b ,i = 1,...,8).
Second, this decay allows to study the nature of ρ, ω and $\phi-$ meson mixing. Note,that in references (Nasriddinov, 1994; Nasriddinov, 2001) the problems of $\pi^0 - \eta$ - and $\omega - \phi$ mixings have been studied on the basis of this model as well and obtained reasonable results for the τ-lepton decay probabilities. In this calculation, we used $\omega - \phi$-mixing

(Nagiwara,2002)in the form

$$\phi = \omega_8 cos\theta_V - \omega_1 sin\theta_V$$

$$\omega = \omega_8 sin\theta_V + \omega_1 cos\theta_V$$

According to the expression for weak hadronic currents between pseudoscalar and vector meson states (1), the Born amplitude of this decay is equal to zero, since the structure constants $f_{13i} = f_{83i} = 0$, (in other words, the current I_μ^i responsible for the direct $\phi \to \omega\pi^0$ decay (FIG.1) is zero).

According to the method of phenomenological chiral Lagrangians (PCL's), this decay channel would originate via the intermediate $\bar{D}^{0*}$ − meson state (FIG. 2). In this case the weak interaction Lagrangian between ϕ and $\bar{D}^{0*}$ mesons has the form given (Kalinovsky,1988) as

$$L_W^{(\Delta C=1)} = (1/2)^{-1/2}G_F h_5(-\sqrt{3}I_\mu^8)I_\mu^{9-i10} + H.c.,$$

where $G_F = 10^{-5}/m_p^2$ is the Fermi constant, h_5=0.285 is the factor that describes deviations from the 20−plet dominance and which is determined by the angles of current rotation about 7th and 10th axes in the SU(4) space, and

$$I_\mu^8 = (\sqrt{2}/g_\rho)m_\vartheta^2\vartheta_\mu^8 = (\sqrt{2}/g_\rho)m_\phi^2\phi_\mu cos\theta_V.$$

$$I_\mu^{9-i10} = (\sqrt{2}/g_\rho)m_D^2\bar{D}_\mu^{0*}.$$

In the PCL the strong interaction Lagrangian of vector mesons with vector and pseudoscalar mesons has the form

$$L_S(vv\varphi) = -1/4g_{vv\varphi}\varepsilon_{\mu va\beta}(d_{kln} + if_{kln})(\partial_\mu V_v^k \partial_\alpha V_\beta^l \varphi^n), \qquad (2)$$

where $g_{vv\varphi} = (3g^2)/16\pi^2 F_\pi$ is the coupling constant; d_{kln} and f_{kln} are the symmetric and anti-symmetric structure constants of the SU(3) group, respectively. Taking into account

$$\bar{D}^{0*} = (1/2i)^{-1/2}(\vartheta_9 - i\vartheta_{10}),$$

$$\pi^0 = \varphi^3,$$

it should be noted, that all structure constants responsible for this interaction equal zero

$$f_{391} = f_{3101} = f_{398} = f_{3108} = d_{391} = d_{3101} = d_{398} = d_{3108} = 0.$$

Therefore, the second diagram does not give any contribution to $\phi \to \omega\pi^0$ decay.

The next diagram (FIG. 3) also does not contribute to the partial width for the $\phi \to \omega\pi^0$ decay. In this case the Lagrangian of the strong coupling of axial-vector mesons to vector and pseudoscalar mesons is derived in a similar way and has the form (Nasriddinov, 1994)

$$Ł_S(0^-, 1^+, 1^-) = -F_\pi g^2 \varphi^l a^i_\mu \vartheta^k_\mu f_{lki},\tag{3}$$

where a^i_μ are the fields of 1^+ mesons.

The structure constants of the SU(3) group responsible for this transition are equal to zero $f_{391} = f_{3101} = f_{398} = f_{3108} = 0$. It should be noted that the diagrams 2 and 3 do not contribute to the partial width of the $\phi \to \omega\pi^0$ decay channel which is obvious also due to the hadronic flavor conservation principle. According to the expression (2), also the anomalous diagram (FIG.4.) does not contribute to the partial width of the $\phi \to \omega\pi^0$ decay because

$$d_{311} = d_{388} = 0.$$

Finally the diagram with the intermediate ω meson (FIG. 5) does not contribute to the partial width of this decay channel also because of these structure constants.

Within the method of phenomenological chiral Lagrangians(PCL's), the partial width of the $\phi \to \omega\pi^0$ decay is therefore given by the diagrams with $\phi - \rho$ and $\omega - \rho$ mixings (FIG.6 and FIG.7). In this case all the structure constants are equal to zero except

$$d_{331} = (1/2)^{-1/2}, d_{338} = (1/3)^{-1/2}.$$

Note, that we studied (Nasriddinov, 1998) the $\tau^- \to \pi^- \eta\nu_\tau$ decay of the τ lepton in the framework of this method with taking into account the isotopic spin violation of chiral symmetry in the Oakes scheme.In this case the $\pi^0 - \eta$ - mixing Lagrangian has the form

$$L_{\pi^0/\eta} = (-1/3)^{-1/2} m^2_{\pi^0} \pi^0 \eta.\tag{4}$$

It was shown, that this decay channel was suppressed with respect to the $\tau^- \to \pi^- \pi^0 \nu_\tau$ decay by a factor 10^{-4}. Therefore, it is natural that the $\phi \to \omega\pi^0$ decay is strongly suppressed because of $\phi - \rho$ and $\omega - \rho$ mixings.

According to (2), the Lagrangians describing ρ -meson interaction with ω and π^0 mesons (FIG. 6), and ϕ-meson interaction with ρ and π^0 mesons (FIG.7) have the forms, respectively

$$L_s(\rho \to \omega\pi^0) = -\frac{1}{4}(\frac{1}{\sqrt{3}} sin\theta_V + \frac{1}{\sqrt{2}} cos\theta_V \times$$

$$g_{vv\varphi}\varepsilon_{\mu\nu\alpha\beta}(\partial_\mu\omega_\nu\partial_\alpha\rho_\beta\pi^0), \tag{5}$$

$$L_s(\phi \to \rho\pi^0) = -\frac{1}{4}(\frac{1}{\sqrt{2}}sin\theta_V - \frac{1}{\sqrt{3}}cos\theta_V)\times$$

$$g_{vv\varphi}\varepsilon_{\mu\nu\alpha\beta}(\partial_\mu\phi_\nu\partial_\alpha\rho_\beta\pi^0). \tag{6}$$

At $\theta_V = 39^0$ the factors of these Lagrangians are equal,respectively

$$\frac{1}{4}(\frac{1}{\sqrt{3}}sin\theta_V + \frac{1}{\sqrt{2}}cos\theta_V) = 0,23$$

$$\frac{1}{4}(\frac{1}{\sqrt{2}}sin\theta_V - \frac{1}{\sqrt{3}}cos\theta_V) = 0,0005$$

Therefore, the contribution of the diagram with $\omega-\rho$ mixing (FIG.7) is negligible with respect to the contribution of the diagram with $\phi-\rho$ mixing (FIG.6). Thus,the decay width of the $\phi \to \omega\pi^0$ decay mainly is defined by the diagram with $\phi - \rho$ mixing (FIG. 6).

Here, we estimate the contribution of this diagram to the partial width of the $\phi \to \omega\pi^0$ decay using the $\pi^0 - \eta$ mixing Lagrangian (4) by making the substitutions $\pi^0 \to \rho$, and $\eta \to \phi$

$$L_{\phi\rho} = \frac{m_\rho^2}{\sqrt{3}}\phi\rho \tag{7}$$

The decay rate is given by

$$\Gamma = \frac{1}{3}\frac{1}{2m}|M|^2\,\Phi, \tag{8}$$

where m is the ϕ-meson mass. The amplitude of the $\phi \to \omega\pi^0$ decay will be determined in accordance with (5) and (7),and has the form

$$M = \frac{1}{2\sqrt{3}}(\frac{1}{\sqrt{3}}sin\theta_V + \frac{1}{\sqrt{2}}cos\theta_V)^2\times$$

$$g_{vv\varphi}\frac{m_\rho^2}{m^2 - m_\rho^2}\left[m^2m_\omega^2 - \left(\frac{m^2 + m_\omega^2 - m_\pi^2}{2}\right)^2\right]$$

The phase space has the form

$$\Phi = \frac{1}{8\pi m^2}\left[m^2 - (m_\omega + m_\pi)^2\right]^{1/2}[m^2 - (m_\omega - m_\pi)^2]^{1/2}$$

where m_ω, m_π and m_ρ are the masses of ω, π^0 and ρ mesons, respectively. According to (8) the decay rate has the form

$$\Gamma = \frac{1}{4608\pi m^3}(\frac{1}{\sqrt{3}}sin\theta_V + \frac{1}{\sqrt{2}}cos\theta_V)^2 g_{vv\varphi}^2(\frac{m_\rho^2}{m^2 - m_\rho^2})^2$$

$$\times \left[m^2 - (m_\omega + m_\pi)^2 \right]^{3/2} \left[m^2 - (m_\omega - m_\pi)^2 \right]^{3/2} \tag{9}$$

It follows that the decay rate of the $\phi \to \omega\pi$ decay is

$$\Gamma(\phi \to \omega\pi) = 0.27 MeV,$$

here we have taken into account only the contribution of the intermediate $\rho(770)$ meson state. The decay rate with taking into account the contributions of intermediate $\rho(1450)$ and $\rho(1700)$ meson states is

$$\Gamma(\phi \to \omega\pi) = 0.77 MeV,$$

For the partial decay rate we obtain

$$B(\phi \to \omega\pi) = 0.18,$$

that is four orders of magnitude large than the experiment (Nagiwara, (2002)).Therefore, our estimation of the $\phi \to \omega\pi^0$ decay rate using $\pi^0 \to \eta$ mixing Lagrangian is inconsistent with experimental data and study of this process in the framework of the $\phi - \rho$ mixing is of interest. In summary, we have studied the $\phi \to \omega\pi^0$ decay in terms of chiral Lagrangians,and we have shown that there is no direct $\phi \to \omega\pi^0$ decay (as was indicated earlier (Achasov,1999)); therefore, this decay channel with G-parity violation will originate mainly from $\phi - \rho$ - mixing. Therefore, the $\phi \to \omega\pi^0$ decay is a unique "laboratory" for studying of the nature of the $\rho - \omega - \phi$ - mixing. At present the investigation of this mixing in the framework of phenomenological chiral Lagrangians is in progress.

References

Achasov M. N. et al. *Phys. Lett.* B449, 122 (1999).

Nagiwara K. et al. Particle Data Group. *Phys. Rev.* D 66, 1 (2002), p. 31.

Weinberg S. *Phys. Rev. Lett.* 18, 188 (1967).

Nasriddinov K. R. and Merkulova T.A. *Phys. Rev.* D 57, 6860 (1998) .

Nasriddinov K. R. *Phys. Atom. Nucl.* 57, 1077 (1994).

Nasriddinov K. R. et al. *Phys. Atom. Nucl.* 64, 1326 (2001).

Kalinovsky Yu.L. et al. *Phys. Lett.* B211, 350 (1988).

Kamil Nasriddinov, Boris Kuranov and Nurmukhammad Iskandarov
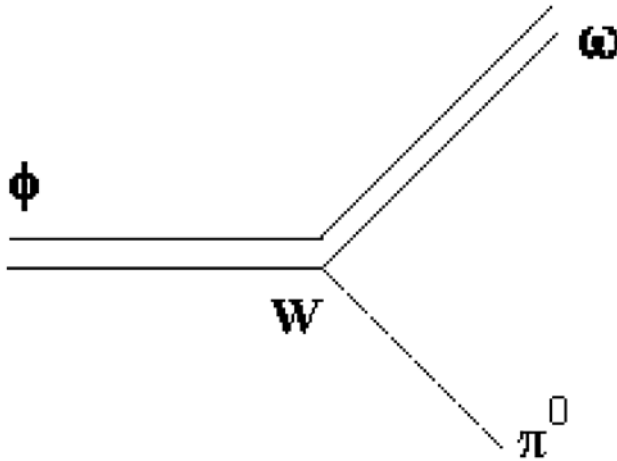
Figure 1. The main diagram for the $\phi \to \omega \pi^0$ decay, (W) weak-interaction vertex.
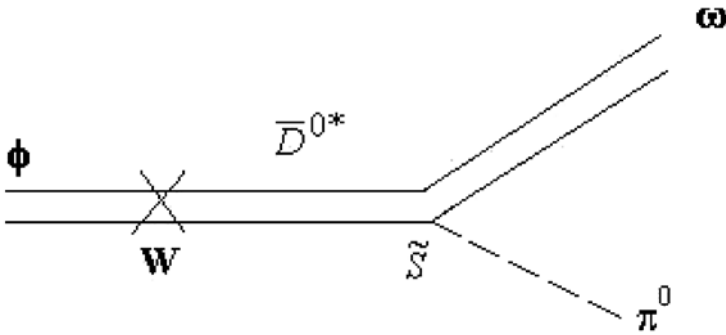
Figure 2. The diagram with the intermediate $\bar{D}^{0*}$ − meson, ($\tilde{S}$) anomalous strong-interection vertex.
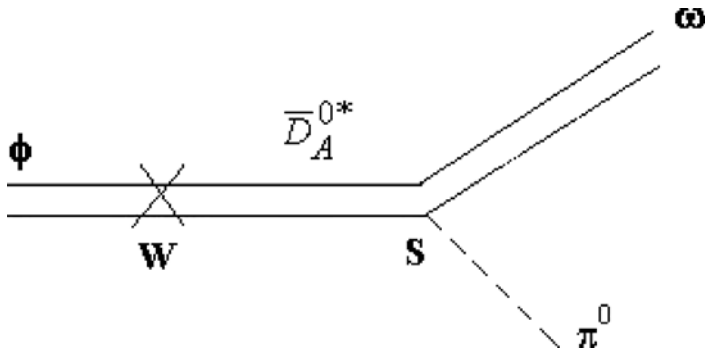
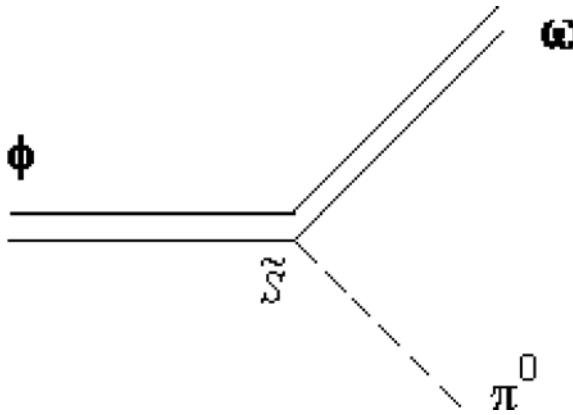*Figure 3.* The diagram with the intermediate $\bar{D}_A^{0*}$ - meson, (S) strong-interection vertex.

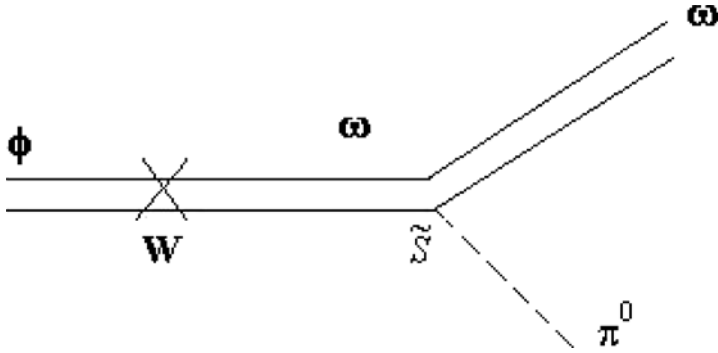*Figure 4.* The anomalous diagram for the $\phi \to \omega\pi^0$ decay

Figure 5. The diagram with the intermediate ω - meson.
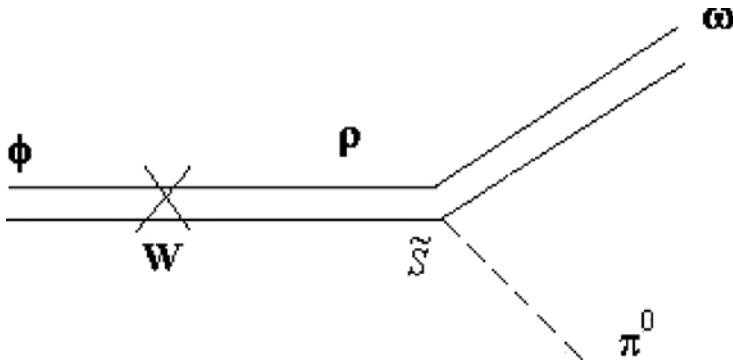
Figure 6. The diagram with the $\rho - \phi$ - mixing
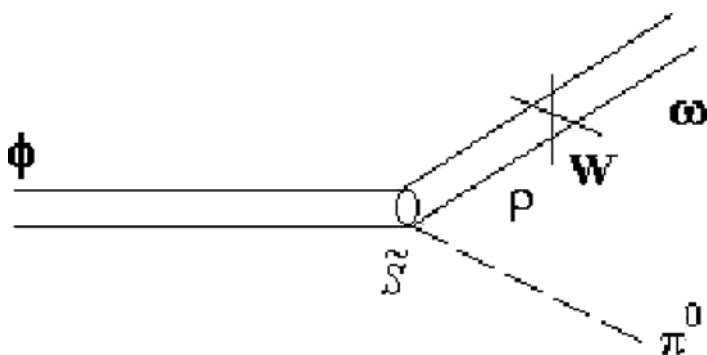
Figure 7. The diagram with the $\rho - \omega$ - mixing

Ginzburg Landau theory of superconductivity: Beyond the post Gaussian approximation

Abdulla Rakhimov[a], Jae Hyung Yee [b] and Chul Koo Kim.[b]

Institute of Nuclear Physics Uzbek Academy of Sciences Ulugbek 702132, Tashkent, Uzbekistan[a], Institute of Physics and Applied Physics, Younsei University, Seoul, 120−749, Korea [b]

Abstract. The post Gaussian effective potential in $D = 3$ and $D = 2+2\epsilon$ are evaluated for the Ginzburg−Landau theory of superconductivity. It is shown that, the next order correction to the Gaussian approximation of the Ginzburg−Landau parameter κ is significant. This strongly indicates that strong correlations play dominant role in high T_c superconductivity. In $D = 2 + 2\epsilon$ fractal dimensions Ginzburg Landau parameter turned out to be sensitive to ϵ and the contribution of the post Gaussian term is larger than that for $D = 3$. Adjusting ϵ to the recent experimental data on $\kappa(T)$ for $high − T_c$ cuprate superconductor $Tl_2Ca_2Ba_2Cu_3O_{10}(T\ell − 2223)$, we find that $\epsilon = 0.21$ is the best choice for this material. These results clearly show that, in order to understand $high − T_c$ superconductivity, it is necessary to include the fluctuation contribution as well as the contribution from the dimensionality of the sample. The method gives a theoretical tool to estimate the effective dimensionality of the samples.

Keywords: superconductivity, fractal dimensions, $Ginzburg − Landau$ model, non-berturbative approach

Introduction

The Ginzburg−Landau (GL) theory of superconductivity (Ginzburg, 1950) was proposed long before the famous BCS microscopic theory of superconductivity was discovered. A few years after the appearance of the BCS theory, Gorkov derived (Gorkov,1958) the GL theory from the BCS theory. Amazingly, the GL theory has played a significant role in understanding superconductivity up to now. It is highly relevant for the description of $high − T_c$ superconductors, even though the original BCS theory is inadequate to treat these materials. The success of the GL theory in the study of modern problems of superconductivity lies in its universal effective character in which the details of the microscopic model are unimportant.

Even at the level of mean field approximation (MFA), the GL theory gives significant information such as penetration depth (l) and coherence length (ξ) of the superconducting samples. Many unconventional properties of superconductivity connected with the break down of the simple MFA has been studied both analytically (Tesanovich, 1999)

303

and numerically using the GL theory (Nguyen, 1999).Particularly, the fluctuations of the gauge field were studied recently by Camarda et.al. (Camarda, 2003) and Abreu et.al. (Abreu) in the Gaussian approximation of the field theory. The effective mass parameters of the Gaussian effective potential (GEP), Ω and Δ, were interpreted as inverses of the coherence length $\xi = 1/\Omega$ and of the penetration depth $l = 1/\Delta$, respectively.

In refs (Kim,2004 Kim, 2005) we take one step further estimating corrections to the Gaussian effective potential for the $U(1)$ scalar electrodynamics where it represents the standard static GL effective model of superconductivity. Although it was found that, in the covariant pure $\lambda\phi^4$ theory in $3+1$ dimensions,corrections to the GEP are not large (Stancu,1990), we do not expect them to be negligible in three dimensions for high T_c superconductivity, where the system is strongly correlated.

Apart from the strong correlation, another important factor, which one should consider for high T_c superconductivity, is the dimensionality of the system. It is well known that, most of the high T_c superconducting materials have layered structures, which strongly suggests two $-$ dimensional nature of high T_c superconductivity. In order to test relative importance of the dimensionality contribution compared to the post Gaussian corrections, we shall also study the case of fractal dimension, $D = 2 + 2\varepsilon$.

The paper is organized as follows: in Section II the GL action is introduced and the post Gaussian approximation is applied; in Section III we discuss the input parameters of the model; in Section IV the theoretical results for $D = 3$ and $D = 2+2\epsilon$ will be compared to existing high T_c experimental data; in Section V we bring a brief summary.

1. Post Gaussian effective potential

We start with the Hamiltonian of the GL model in Euclidean D $-$ dimensional space given by (Kleinert)

$$H' = \frac{1}{T_c}\int d^D x \left\{ \frac{1}{4}F_{ij}^2 + \frac{1}{2}\,|\,(\partial_i - ie\mu^{(3-D)/2}\vec{A})\psi\,|^2 + \frac{1}{2}m^2\psi^2 + \lambda\mu^{(3-D)}\,|\,\psi\,|^4 \right\} \tag{1}$$

where ψ and $\vec{A}$ are the complex scalar and the static electromagnetic fields, respectively; m, λ and e are the input parameters of the model.[1] We introduce natural units employing ξ_0 (coherence length at zero

---

[1] μ is introduced to make λ and e dimensionless.

temperature) and T_c as length and energy scale, respectively, through the transformations :

$$
\begin{array}{ccc}
m \to m\xi_0^{-1}, & \mu \to \mu\xi_0^{-1}, & x \to x\xi_0, \\
e^2 \to e^2\xi_0^{-1}T_c^{-1}, & \lambda \to \lambda\xi_0^{-1}T_c^{-1}, \\
\psi \to \psi\xi_0^{(1-D/2)}T_c^{1/2}, & \vec{A} \to \vec{A}\xi_0^{(1-D/2)}T_c^{1/2}.
\end{array} \tag{2}
$$

Eq.(1) is now rewritten as,

$$
\begin{array}{c}
H' = \int d^D x \{\frac{1}{2} \mid \vec{\nabla} \times \vec{A} \mid^2 + \frac{1}{2} \mid (\partial_i - ie\mu^{(3-D)/2}\vec{A})\psi \mid^2 \\
+ \frac{1}{2}m^2\psi^2 + \lambda\mu^{(3-D)} \mid \psi \mid^4 \}.
\end{array} \tag{3}
$$

In accordance with refs.(camarda 2003,abreu),we apply tranverse unitary gauge and express the partition function as

$$
Z = \int D_\phi DA_T \exp\{-\int d^D x H + \int d^D x j\phi + (\vec{j}_A\vec{A})\} \tag{4}
$$

where the Hamiltonian density is [2]

$$
H = \frac{1}{2}(\vec{\nabla} \times \vec{A})^2 + \frac{1}{2}(\vec{\nabla}\phi)^2 + \frac{1}{2}m^2\phi^2 + \lambda\phi^4 + \frac{1}{2}e^2\phi^2 A^2 + \frac{1}{2\epsilon}(\vec{\nabla}\vec{A})^2. \tag{5}
$$

We have introduced a gauge fixing term, with the limit $\epsilon \to 0$ being taken after the calculations are carried out.In Eq.(5) $\vec{A}$ stands for the transverse gauge field and ϕ is defined as $\psi = \phi\exp(i\gamma)$. To obtain the free energy density, $V_{eff} = \mathcal{F}/\mathcal{V}$ (effective potential), we introduce a shifted field $\phi \to \phi + \phi_0$ and split the Hamiltonian into two parts:

$$
H = H_0 + H_{int}, \tag{6}
$$

where H_0 is the sum of two free field terms describing a vector field $\vec{A}$ with mass Δ_0 and a real scalar field ϕ with mass Ω_0:

$$
H_0 = \frac{1}{2}(\vec{\nabla} \times \vec{A})^2 + \frac{1}{2}\Delta_0^2\vec{A}^2 + \frac{1}{2\epsilon}(\vec{\nabla}\vec{A})^2 + \frac{1}{2}(\vec{\nabla}\phi)^2 + \frac{1}{2}\Omega_0^2\phi^2. \tag{7}
$$

The interaction term then reads

$$
H_{int}(\phi, A) = \sum_{n=0}^{4} v_n\phi^n - \frac{1}{2}\Delta_0^2\vec{A}^2 + \frac{1}{2}e^2\vec{A}^2(\phi + \phi_0)^2, \tag{8}
$$

where

$$
\begin{array}{cc}
v_0 = \frac{1}{2}m^2\phi_0^2 + \lambda\mu^{(3-D)}\phi_0^4, & v_1 = m^2\phi_0 + 4\lambda\mu^{(3-D)}\phi_0^3, \\
v_2 = \frac{1}{2}(m^2 - \Omega_0^2) + 6\lambda\mu^{(3-D)}\phi_0^2, & v_3 = 4\lambda\mu^{(3-D)}\phi_0, \\
& v_4 = \lambda\mu^{(3-D)}.
\end{array} \tag{9}
$$

---

[2] From now on, we denote $\lambda\mu^{(3-D)}$ and $e^2\mu^{(3-D)}$ as λ and e^2, respectively, for simplicity.

Now performing explicit Gaussian integration in Eq.(4),one obtains

$$
\begin{aligned}
Z &= \exp\{-\int d^D x H_{int}(\delta/\delta j, \delta/\delta j_A)\} \int D\phi DA exp\{ \\
&\quad -\int d^D x H_0 + j\phi + \vec{j}_A \vec{A})\} \\
&= [\det D_0^{-1}]^{-\frac{1}{2}} [\det G_0^{-1}]^{-\frac{1}{2}} \exp\{-\int d^D x H_{int}(\delta/\delta j, \delta/\delta j_A)\} \\
&\quad \times exp\{jD_0 j/2\} exp\{j_A G_0 j_A/2\},
\end{aligned}
\tag{10}
$$

where in momentum space

$$
D_0(p) = 1/(p^2 + \Omega_0^2), \quad G_0(p) = 2/(p^2 + \Delta_0^2). \tag{11}
$$

To calculate the partition function in post Gaussian approximation,by isolating cactus-type diagrams we use the method introduced in refs. (Rakhimov 2004,Lee1997) and introduce the so called primed derivatives:

$$
\begin{aligned}
(\tfrac{\delta}{\delta j(x)})' &\equiv \hat{A}_x^{(1)} = \tfrac{\delta}{\delta j(x)}, \quad \tfrac{\delta}{\delta j_A(x)})' \equiv \hat{B}_x^{(1)} = \tfrac{\delta}{\delta j_A(x)}, \\
(\tfrac{\delta^2}{\delta j^2(x)})' &\equiv \hat{A}_x^{(2)} = \tfrac{\delta^2}{\delta j^2(x)} - D_0(x,x), \\
(\tfrac{\delta^2}{\delta j_A^2(x)})' &\equiv \hat{B}_x^{(2)} = \tfrac{\delta^2}{\delta j^2(x)} - G_0(x,x), \\
(\tfrac{\delta^3}{\delta j^3(x)})' &\equiv \hat{A}_x^{(3)} = \tfrac{\delta^3}{\delta j^3(x)} - 3D_0(x,x)R(x), \\
(\tfrac{\delta^3}{\delta j_A^3(x)})' &\equiv \hat{B}_x^{(3)} = \tfrac{\delta^3}{\delta j_A^3(x)} - 3G_0(x,x)R_A(x), \\
(\tfrac{\delta^4}{\delta j^4(x)})' &\equiv \hat{A}_x^{(4)} = \tfrac{\delta^4}{\delta j^4(x)} - 6D_0(x,x)\tfrac{\delta^2}{\delta j^2(x)} + 3D_0^2(x,x) \\
(\tfrac{\delta^4}{\delta j_A^4(x)})' &\equiv \hat{B}_x^{(4)} = \tfrac{\delta^4}{\delta j_A^4(x)} - 6G_0(x,x)\tfrac{\delta^2}{\delta j_A^2(x)} + 3G_0^2(x,x),
\end{aligned}
\tag{12}
$$

where $R(x) = \int d^D y D_0(x,y)j(y)$ and $R_A(x) = \int d^D y G_0(x,y)j_A(y)$, so that

$$
\begin{aligned}
\hat{A}_x^{(n)} \exp\{jD_0 j/2\} &= R_n exp\{jD_0 j/2\}, \\
\hat{B}_x^{(n)} \exp\{j_A G_0 j_A/2\} &= R_A^n \exp\{j_A G_0 j_A/2\}.
\end{aligned}
\tag{13}
$$

Now it can be shown that (Rakhimov 2004, Lee1997), the Gaussian part of Z can easily be isolated as follows:

$$
\begin{aligned}
Z &= Z_G \Delta Z \\
Z_G &= \exp\{-I_1(\Omega) - \tfrac{1}{2}I_1(\Delta) - v_0 - v_2 I_0(\Omega) + 3v_4 I_0^2(\Omega) \\
&\quad + \Delta_0^2 + e^2 I_0(\Omega) - e^2 \phi_0^2)I_0(\Delta)\} \\
\Delta Z &= exp\{-v_2 \hat{A}^{(2)} - v_3 \hat{A}^{(3)} - v_4 \hat{A}^{(4)} \\
&\quad -\tfrac{1}{2}(e^2 \phi_0^2 - \Delta_0^2)\hat{B}^{(2)} - e^2 \phi_0 \hat{B}^{(2)}\hat{A}^{(1)} \\
&\quad -\tfrac{1}{2}e^2 \hat{B}^{(2)}\hat{A}^{(2)}) exp\{jDj/2\} exp_{j_A} Gj_A/2\}
\end{aligned}
\tag{14}
$$

where new correlation functions $D(p) = 1/(p^2 + \Omega^2)$ and $G(p) = 2/(p^2 + \Delta^2)$ include modified masses:

$$
\Omega^2 = \Omega_0^2 + 12v_4 I_0(\Omega) + 2e^2 I_0(\Delta), \quad \Delta^2 = \Delta_0^2 + e^2 I_0(\Omega). \tag{15}
$$

In the above, following integrals are introduced

$$I_0(M) = \int \frac{d^D p}{(2\pi)^D} \frac{1}{(M^2+p^2)}, I_1(M) = \frac{1}{2} \int \frac{d^D p}{(2\pi)^D} \ln(M^2 + p^2). \qquad (16)$$

From Eqs.(2.14),(15) and (9),one gets the following Gaussian effective potential:

$$\begin{aligned}
V_G &= -lnZ_G = I_1(\Omega) + \tfrac{1}{2}I_1(\Delta) + v_0 + v_2 I_0(\Omega) \\
&\quad -3v_4 I_0^2(\Omega) - (\Delta_0^2 + e^2 \mathbf{I}_0 \Omega - e^2 \phi_0^2)\mathbf{I}_0(\Delta) \\
&= I_1(\Omega) + \tfrac{1}{2}I_1(\Delta) + \tfrac{1}{2}m^2 \phi_0^2 + \lambda \phi_0^4 \\
&\quad +\tfrac{1}{2}\mathbf{I}_0(\Omega)[m^2 - \Omega^2 + 6\lambda \mathbf{I}_0(\Omega) + 12\lambda \phi_0^2 \\
&\quad +I_0(\Delta)[-(\Delta_0^2) + e^2 \mathbf{I}_0(\Omega) + e^2 \phi_0^2].
\end{aligned} \qquad (17)$$

Note that, the last equation is exactly the same as it is in refs. (camarda 2003, abreu). The post Gaussian effective potential

$$V_{eff} = V_G + \Delta V_G \qquad (18)$$

includes a correction part ΔV_G :

$$\begin{aligned}
\Delta V_G &= -ln\Delta Z = -ln\{exp[-\delta \hat{W}] \\
&\quad \times exp\{jDj/2\}exp\{j_A G j_A/2\} \mid_{j=0,j_A=0}\} \\
&= -ln\{1 - \delta \hat{W} exp\{jDj/2\}exp\{j_A G j_A/2\} \mid_{j=0,j_A=0} \\
&\quad +\tfrac{\delta^2 \hat{W}^2}{2!} exp\{jDj/2\}exp\{j_A G j_A/2\} \mid_{j=0,j_A}= 0 + \dots,\} \\
&\equiv \delta \Delta V_G^{(1)}(B) + \delta^2 \Delta V_G^{(2)}(B) + \dots, \\
\hat{W} &= v_2 \hat{A}^{(2)} + v_3 \hat{A}^{(3)} + v_4 \hat{A}^{(4)} + \tfrac{1}{2}(e^2 \phi_0^2 - \Delta_0^2)\hat{B}^{(2)} \\
&\quad +e^2 \phi_0 \hat{B}^{(2)} \tfrac{\delta}{\delta j} + \tfrac{1}{2}e^2 \hat{B}^{(2)} \hat{A}^{(2)}.
\end{aligned} \qquad (19)$$

Here we have introduced an auxiliary expansion parameter δ to be set equal to unity after calculations, similar to δ expansion method (de Souza,2002).The first order term $\Delta V_G^{(1)}(B)$ in this equation will not contribute to the effective potential, i.e., $\Delta V_G^{(1)}(B) = 0$,due to the relations (13).The next term of order δ^2 gives the first nontrivial contribution to the post Gaussian effective potential.The explicit calculations give

$$\begin{aligned}
\Delta V_G &= [-\tfrac{1}{2}e^4 I_2(\Delta) - 18I_2(\Omega)\lambda^2]\phi_0^4 + \{-3\lambda I_2(\Omega) \\
&\quad \times[-\Omega^2 + m^2 + 2I_0(\Delta)e^2 + 12\lambda I_0(\Omega)] \\
&\quad -e^2 I_2(\Delta)[-\Delta^2 + e^2 I_0(\Omega)] - 8\lambda^2 I_3(\Omega,\Omega) \\
&\quad -\tfrac{2}{3}e^4 I_3(\Delta,\Omega)\}\phi_0^2 - \tfrac{1}{8}I_2(\Omega)[-\Omega^2 + m^2 + 2I_0(\Delta)e^2 \\
&\quad +12\lambda I_0(\Omega)]^2 - \tfrac{1}{2}I_2(\Delta)[-\Delta^2 + e^2 I_0(\Omega)]^2 - \tfrac{1}{12}e^4 I_4(\Delta,\Omega) - \tfrac{1}{2}\lambda^2 I_4(\Omega,\Omega)
\end{aligned} \qquad (20)$$

where following loop integrals were introduced,

$$
\begin{aligned}
I_2(M) &= \tfrac{2}{(2\pi)^D} \int \tfrac{d^D k}{(k^2+M^2)^2} \\
I_3(M_1, M_2) &= \tfrac{1}{(2\pi)^{2D}} \int \tfrac{d^D k\, d^D p}{(k^2+M_1^2)(p^2+M_1^2)((k+p)^2+M_2^2)}, \\
I_4(M_1, M_2) &= \tfrac{1}{(2\pi)^{3D}} \int \tfrac{d^D k\, d^D p\, d^D q}{(k^2+M_1^2)(p^2+M_1^2)(q^2+M_2^2)} \\
&\quad \times \tfrac{1}{((k+p+q)^2+M_2^2)}.
\end{aligned}
\tag{21}
$$

For $D = 3$, and $D = 2 + 2\epsilon$ these integrals were calculated with dimensional regulariztion in refs.(Braaten,1995) and (Kim 2004, Kim 2005) respectively. The parameters Ω and Δ are determined by the principle of minimal sensitivity(PMS) :

$$
\begin{aligned}
\tfrac{\partial V_{eff}}{\partial \Omega} &= F_\Omega(m\lambda, \epsilon, \bar{\Omega}, \bar{\Delta}, \bar{\phi}_0) = 0. \\
\tfrac{\partial V_{eff}}{\partial \Delta} &= F_\Delta = (m\lambda, \epsilon, \bar{\Omega}, \bar{\Delta}, \bar{\phi}_0) = 0,
\end{aligned}
\tag{22}
$$

where the optimal values of Ω and Δ are denoted by $\bar{\omega}$ and $\bar{\Delta}$, respectively, and $\bar{\phi}_0$ is a stationary point defined from the equation:

$$
\frac{\partial V_{eff}}{\partial \phi_0} = F_\phi(m, \lambda, \epsilon, \bar{\Omega}, \bar{\Delta}, \bar{\phi}_0) = 0.
\tag{23}
$$

The explicit expressions for $F_\Omega(m, \lambda, \epsilon, \bar{\Omega}, \bar{\Delta}, \bar{\phi}_0)$, $F_\Delta(m, \lambda, \epsilon, \bar{\Omega}, \bar{\Delta}, \bar{\phi}_0)$, $F_\phi(m, \lambda, \epsilon, \bar{\Omega}, \bar{\Delta}, \bar{\phi}_0))$ are rather long and may be found in refs.(Kim 2004, Kim 2005). Here we note that, in the Gaussian approximation, for $D = 3$ the gap equations (22) are reduced to simple forms:

$$
\begin{aligned}
\tfrac{\partial V_G}{\partial \Omega} &= \bar{\Omega}^2 \pi - 6\bar{\Omega}\lambda - \bar{\Delta}e^2 + 2m^2\pi = 0 \\
\tfrac{\partial V_G}{\partial \Omega} &= 8\bar{\Delta}^2\pi\lambda - e^4\bar{\Delta} - 4\bar{\Omega}e^2\lambda + 2e^2 m^2\pi = 0.
\end{aligned}
\tag{24}
$$

2. Input parameters

The solutions of the Eqs.(22) are related to the experimentally measured GL parameter κ as $\kappa = \ell/\xi = \bar{\Omega}/\bar{\Delta}$. We make an attempt to reproduce recent experimental data on $\kappa(T)$ (Brandstatter,1994) for $high - T_c$ cuprate superconductor $Tl_2Ca_2Ba_2Cu_3$ $O_{10}(T\ell - 2223)$.

For this purpose, we adopt usual linear T dependence of parametrization of m and λ as:

$$
\begin{aligned}
m^2 &= m_0^2(1 - \tau) + \tau m_c^2, \\
\lambda &= \lambda_0(1 - \tau) + \tau \lambda_c, \\
\tau &= T/T_c.
\end{aligned}
\tag{25}
$$

and calculate κ by solving nonlinear equations (22) (or (24) in Gaussian case).Due to the parametrization (25), the model has in general six input parameters: m_0^2, λ_0, m_c^2,λ_c,ϵ and e.The last parameter is related directly to the electron charge: $e^2 = 16\pi\alpha k_B T_c \xi_0/\hbar c$, where $\alpha = 1/137$, ξ_0 is a coherence length at $T = 0$, and T_c the critical temperature. The experimental values for the cuprate $T\ell - 2223$ are $\xi_0 = 1.36nm$ and $T_c = 121.5K$. The parameters m_0^2 and λ_0 are fitted to the expeimental values of ξ and ℓ at zero temperature: $\xi_0 = 1.36nm$, $\ell_0 = 163nm$.In dimensionless units, (2),we have $\bar{\Omega}_0 = \bar{\Omega}(\tau = 0) = 1$ and $\Delta_0 = \Delta\tau = 0) = \xi_0/l_0 = 0.0083$ which are used to calculate m_0^2 and λ_0 from coupled equations (22) (or (24) in the Gaussian case).The parameters m_c^2c and λ_c are fixed in the similar way. Actually the quantum fluctuations shift m_c^2 from its zero value given by MFA. On the other hand, the exact experimental values of m_c^2 and λ_c are unknown, since the GL parameter at $T = T_c$ is poorly determined. For this reason, we used the experimental values of ξ_c and ℓ_c at very close points to the critical temperature taking $\tau_c = 0.98$ which gives $\bar{\Omega}_c = \bar{\Omega}(\tau_c) = 1/\xi_c = 0.128$ and $\bar{\Delta}_c = \bar{\Delta}(\tau_c) = 1/\ell_c = 0.0043$. Then solving the equations (22) (or (24) in the Gaussian case) with respect to m_c andλ_c, we fix the input parameters. Note that,for $D = 2 + 2\epsilon$ the above procedure was repeated for each guessed value of ϵ.In Table I the input parameters for the Gaussian and the post Gaussian cases for D=3 are summarized.

Table I. Input parameters of the GL model for $D = 3$ (All parameters are given in dimensionless units. See Eq.(2).

	m_0^2	λ_0	m_c^2	λ_c
Gaussian	-0.456	0.046	0.0013	0.002
Post. Gaussian	-0.525	0.050	0.0017	0.008

3. Results and discussions

3.1. The effect of fluctuations

After having fixed the input parameters, the temperature dependence of $\bar{\Omega}(\tau)$, $\Delta(\tau)$ as well as the GL parameter $\kappa = \bar{\Omega}(\tau)/\Delta(\tau)$ are established by solving the gap equations (22) and (24) numerically for the Gaussian and the post Gaussian approximations, respectively.The results are presented in Fig.1,where solid curve corresponds to the post
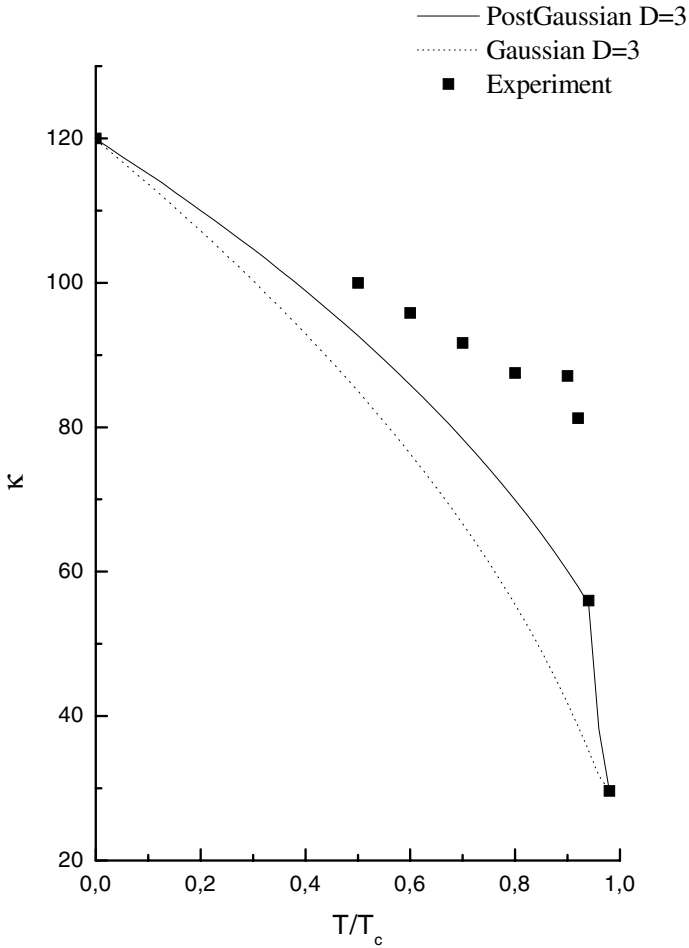
Figure 1. The GL parameter, κ,in the Gaussian (the dotted line) and post Gaussian approximations (the solid kine) in $D = 3$.

Gaussian and dotted one to the Gaussian approximation.It is seen from the figure that corrections to the Gaussian approximation are significant, and in the right direction, although the discrepancy from the experimental values is still substantial.

On the other hand,a better agreement with the experiment has been obtained even on the level of the Gaussian approximation by the authors of ref. (Camarda,2003).However, they introduced a cut off

parameter Λ as a characteristic energy scale of the sample to make the divergent integrals I_0 and I_1 finite.We beleive that, the better agreement is a result of introducing this rather arbitrary additional parameter. It should be noted that,in the present approach for $D = 3$ there is no such additional adjustable parameter.Here we used dimensional regularization [3] in which we put $\mu = \bar{\Omega}_0$. As it is expected, the behavior of $\kappa(\tau)$ does not depend on μ:Another value of μ, e.g. $\mu = 2\bar{\Omega}_0$ leads to another set of input parameters $\{m_02, m_c, \lambda_0, \lambda_0\}$, but to the same behavior for $\kappa(\tau)$.

Clearly, the solutions of nonlinear gap equations are not unique. In numerical calculations we separated the physical solutions by observing the sign of $\bar{\phi}_0^2$ and that of the effective potential at the stationary point:$V_{eff}(\bar{\phi}_0)$. The temperature dependence of these two quantities are presented in Fig. 2. It is seen that $\bar{\phi}_0^2$ (solid line) is positive in the large range of τ and goes to zero when τ is close to $\tau = 1$. Similarly, the depth of the effective potential at the stationary point, $V_{eff}(\bar{\phi}_0)$, becomes shallow when $\tau \to 1$ and vanishes at $T = T_c$.

3.2. THE EFFECT OF DIMENSIONALITY

All the above numerical calculations were made in D=3 dimension. On the other hand it is widely known that, most of high T_c cuprates have layered structures with 2D CuO_2 planes which play an essential role in the high T_c superconductivity.Therefore, it is nessesary to consider the dimensional contribution in the calculation.For this purpose,we consider the case of $D = 2 + 2\epsilon$ ($\epsilon \neq 0$) in the post Gaussian approximation.In this case the optimal values of m and λ also depend on ϵ. Using Eq.(25) and the procedure outlined above one finds the ϵ dependence of m_0^2 presented in Fig.3 (solid line).

One notes that,for small values of ϵ ($0 < \epsilon \leq 0.048$) m^2 becomes positive. Bearing in mind that, in the GL model the phase transition occurs where m^2 changes sign (or more exactly the superconductive phase holds only for $m^2 < 0$),it shows that,in the present approximation scheme, there is no phase transition in $D = 2 + 2\epsilon$ dimension for very small values of ϵ.Note that, λ remains positive on the whole range of ϵ.

For $\epsilon \geq 0.1$,there is a possibility to adjust ϵ to the recent experimental data on $\kappa(T)$ (Brandstatter,1994) for $high - T_c$ cuprate superconductor $Tl_2Ca_2Ba_2Cu_3O_{10}(T\ell - 2223)$. Our calculations show that,the best choice of ϵ is found to be $\epsilon = 0.21$.The appropriate $\kappa(\tau)$ is presented in Fig.4 (solid line).The dashed line in this figure shows $\kappa(\tau)$ for $D = 3$. This fitting process allows us to get an estimation on the effective dimensionality of the $high - T_c$ superconducting materials.

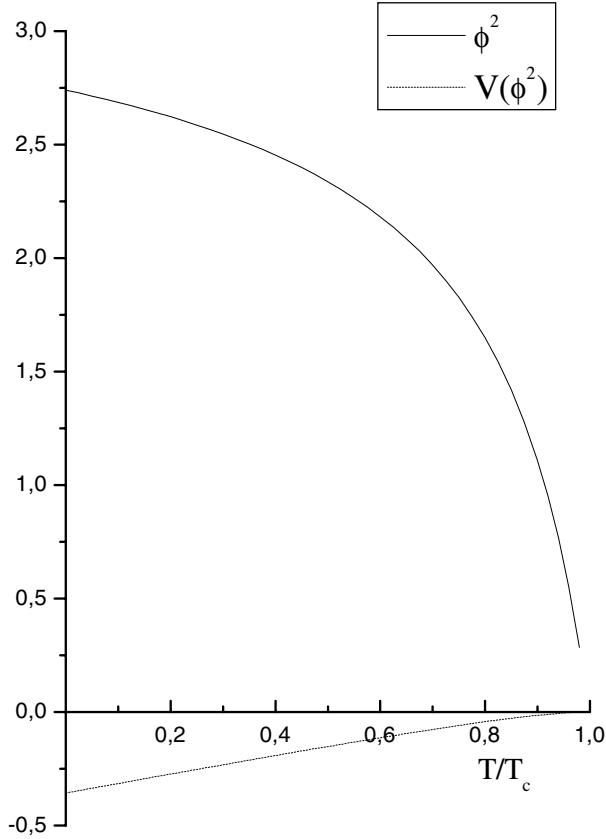[3] see ref.(Kim, 2004) for appropriate counter terms

Figure 2. The stationary point $\bar{\phi}_0^2$ and the depth of the post Gaussian effective potential at the stationary point vs.temperature.

4. Summary

In this report we have carried out calculations of the Ginzburg $-$ Landau effective potential beyond the Gaussian approximation.The result is used to obtain the Ginzburg-Landau parameter,κ, and compared with existing high T_c superconductivity data.It is shown that the post Gaussian correction which is believed to originate from strong correla-
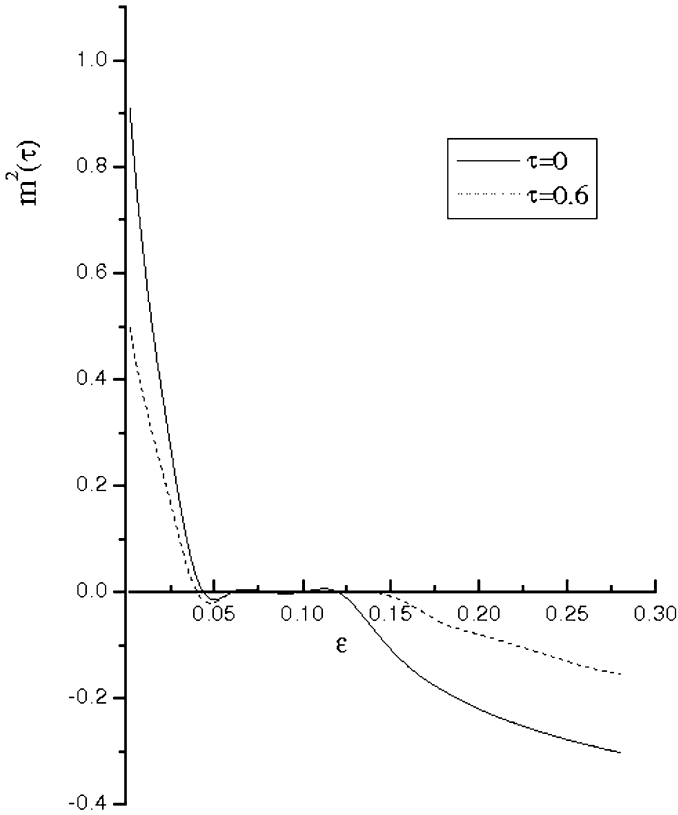
Figure 3. The parameter m^2 of the GL model v.s. ϵ in fractal dimension $D = 2 + 2\epsilon$. The solid and dashed lines are for the temperatures $T = 0$ and $T = 0.6T_c$, respectively.

tion is substantial. We have studied also the role of dimensionality of high T_c superconducting materials. In order to estimate the contribution from the quasi two dimensionality, we have carried out calculations for $D = 2 + 2\epsilon$ case, letting ϵ as a free (but small) paramtere.It has been shown that the GL parameter is rather sensitive to ϵ when the loop corrections to the simple Gaussian approximation are taken into
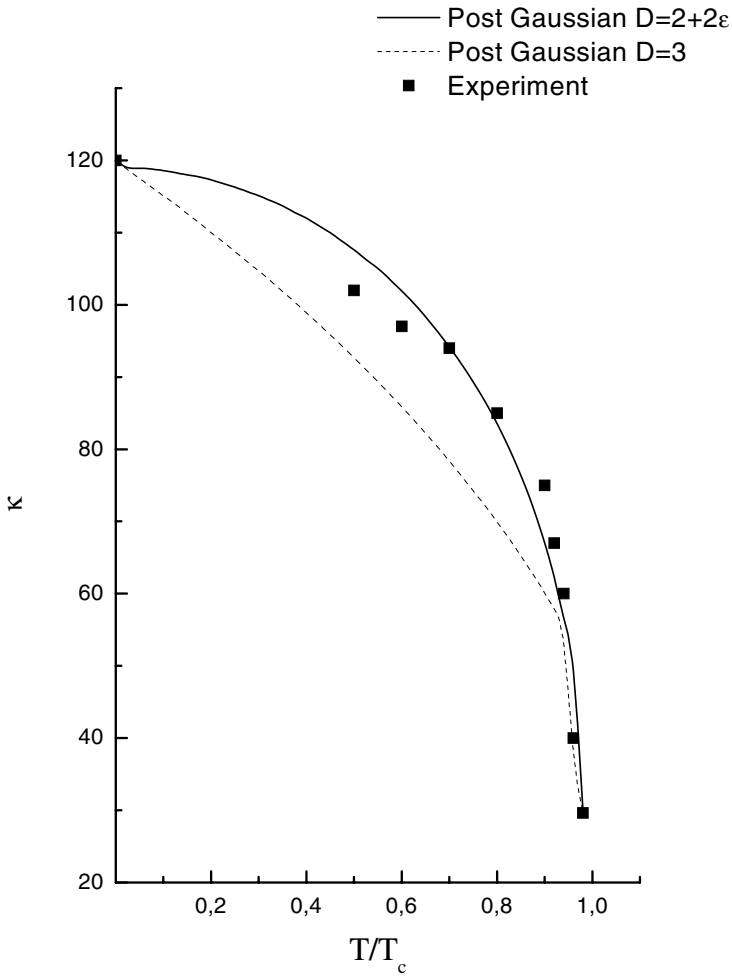
Figure 4. The GL parameter, κ, in $D = 2 + 2\epsilon$ (solid line) and in $D = 3$ (dashed line) cases calculated in the PostGaussian approximation.

account.The optimal value of ϵ for the cuprate $(T\ell - 2223)$ is found to be $\epsilon = 0.21$. It would be interesting to estimate optimal ϵ in fractal dimensions for other cuprates also.

Acknowledgments

References

Ginzburg V. L. and Landau L.D. *Zh. Eksp. Teor. Fiz.* 20, 1064, (1950).

Gorkov, L.P. *.Sov. Phys. JETP* 7, 505 (1958).

Gorkov, L.P. *.Sov. Phys. JETP* 9, 1364 (1959).

Tesanovich Z. *.Phys. Rev. B* 59, 6449 (1999)(and references there in).

Nguyen A. K. and Sudbo A. *.Phys. Rev. B* 60, 15307 (1999).

Camarda M., Angilella G.G.N, Pucci R. and Siringo F. *.Eur.Phys.J.* B33, 273 (2003).

Abreu L.M., Malbouisson A.P.C. and Roditi I. "GAUGE FLUCTUATIONS IN SUPERCONDUCTING FILMS.". *.cond-mat/0305366.*

Kim C.K., Rakhimov A. and Yee J.H. *.Eur. Phys. J.* B39, 301(2004)

Kim C.K., Rakhimov A. and Yee J.H. *.Phys. Rev. B.* 71, 024518, (2005).

Stancu I.and Stevenson P.M. *.Phys. Rev. D.* D42, 2710, (1990).

Kleinert H. *.Gauge Fields in Condensed Matter*, Vol. 1: Superflow and Vortex Lines, World Scientific , Singapore,1989.

Rakhimov A. and Yee J.H. *Int. J. Mod. Phys..* A19, 1589 (2004).

Lee G.H.and Yee J.H. *Phys. Rev. D.* D56, 6573, (1997).

de Souza F. Cruz, Pinto M.B., Ramos R. and Sena P. *Phys. Rev. A.* 65, 053613, (2002), and references therein.

Braaten E. and Nieto A. *Phys. Rev. D.* 51, 6990, (1995).

Davydychev A.I. and Kalmykov M.Yu *Nucl. Phys.* B605, 266, (2001).

Rajantie A. K. *Nucl. Phys.* B480, 729, (1996).

Brandstatter G. Sauerzopf F.M., Weber H.W, Ladenberger F. and Schwarzmann E. *Physica C.* 235, 1845, (1994).

Brandstatter G., Sauerzopf F.M. and Weber H.W. *Phys. Rev.* B55, 11693, (1997).

Chiku S. and Hatsuda T. *Phys. Rev.* D58, 076001, (1998).

Banerjee N. and Malik S. *Phys. Rev.* D43, 3368, (1991).

The s-wave πd scattering length from πd atom using effective field theory

B.F. Irgaziev and B.A. Fayzullaev
Theoretical Physics Department,
National University of Uzbekistan,
700174 Tashkent, Uzbekistan

Abstract. The $\pi^- d$ atom strong energy-level shift in the $1s$ state is derived by using the effective field theory. Taking into account the large value of radius of pionic deuterium and short radius of strong interaction between pion and deuteron we have considered deuteron as a particle described by a vector field. Pion is described by a scalar field. To obtain non-relativistic Hamiltonian for πd system Foldy-Wouthuysen transformation has been derived for the vector field. The strong interaction between pion and deuteron has been taken of zero-range. We have found the Deser type formula for relation between the strong energy-level shift and the s-wave πd scattering length.

Keywords: Pionic atoms, non-relativistic Hamiltonian, scattering length, energy shift.

1. Introduction

Recently, substantial progress has been made in developing Chiral perturbation theory (ChPT) for pionic nucleon (πN) system (Mojzis, 1998; Fettes, Meissner and Steininger, 1998; Fettes and Meissner, 2000; Fettes and Meissner, 2001; Gasser J. et al, 2002). In this context the precision X-ray experiments on pionic hydrogen and pionic deuterium were carried out by ETH Zurich-Neuchâtel-PSI collaboration (Schröder et al, 2001). The $s-$wave πN scattering lengths are important for testing of various theoretical consideration like the Goldberger-Miyazawa-Oehme sum rule (Golberger, Miyazawa and Oehme, 1955) determining the $\pi\pi N$ coupling constant. The sigma term, which is used for lattice and ChPT calculation, is sensitively affected by the isoscalar scattering length. The πN and πd scattering lengths are determined directly from the phase shift analysis and from the X-ray experiments on pionic atoms using the Deser formula (Deser et al, 1954).

The extraction of the s-wave scattering length from the X-ray experiments gives errors less than the phase shift analysis. The accuracy of the modern level of experimental analysis of the parameters of pionic hydrogen reached by the PSI Collaboration is about 1% for the strong energy shift and 2% for the width of the energy level of the ground state

of pionic hydrogen (Anagnostopoulos et al., 2003). The NPE measurement (A. Wirzba., 1998) of the pionic deuterium atomic level strong shift yields for the πd scattering length $a_{\pi d} = [-0.0261(\pm 0.0005) + i0.0063(\pm 0.0007)]m_{\pi}^{-1}$, where m_{π} is the pion mass. Note the imaginary part of the πd scattering length is approximately four times less than its real part. Such results for $\pi^- d$ scattering can be explained by the fact that the absorption channel $\pi^- d \rightarrow nn$ and the radiative absorption channel $\pi^- d \rightarrow \gamma nn$ give very small contribution to the scattering length. Also $\pi^- d \rightarrow \pi^0 nn$ channel, which is open at threshold, is suppressed by the centrifugal barrier. Indeed, 96% of the deuteron state is the $^3S_1$ state, therefore according to Pauli principle the $^3S_1$ state is forbidden for nn system and the $^1S_0$ state is not available if there is no spin flip. In a series of papers (Peresypkin and Petrov, 1974; Afnan and Thomas, 1974; Mizutani and Koltun, 1977; Deloff, 2001) the determination of the pion-deuteron scattering length was considered by solving the Faddeev equations and the Lippman-Schwinger equation (Baru, Kudryavtsev and Tarasov, 2004). There has been remarkable recent progress in developing the effective field theories to problems relevant to the πN (Lyubovitskji and Rusetsky, 2000; Ivanov et al, 2003) and πd (Beane et al, 1998; Borasoy and Griesshammer, 2001; Beane et al, 2003; Beane and Savage, 2003) scattering length. The main results obtained from calculation of the πd scattering length are the following: (a) in all theoretical calculations isospin symmetry of the strong interactions is assumed; (b) the $\pi^- d$ scattering length can be extracted from the $1s$ energy shift of pionic deuterium using the Deser formula; (c) the electromagnetic contribution to the difference of the real parts of the scattering length of π^+ and π^- is of order of the experimental error in the scattering length. The aim of this paper is to establish the precise relation between the strong energy-level shift of the $\pi^- d$ atom in the $1s$ state, and strong πd scattering length using the effective field theory. In the present paper we show how to obtain the nonrelativistic Hamiltonian for πd system from the relativistic equations of motion for the scalar and vector fields by taking into account the electromagnetic interaction. The strong interaction is taken in the zero-range approach.

2. Nonrelativistic limits for the scalar and vector fields

The problem of nonrelativistic limit description for fundamental particles and their interactions may be solved in different ways. Although in all methods of nonrelativistic expansion the first terms of the Hamiltonians coincide, however the difference begins to arise at transition to the higher orders of expansion. The method of Foldy-Wouthuysen

transformation is one of the safest method for solving this problem (Bjorken and Drell, 1964). This method was mainly used for spinor and scalar particles. In our task we need in nonrelativistic Hamiltonian for massive vector field (deuteron is considered as a fundamental particle) interacting with electromagnetic and scalar (pion) fields. In this approach suggested by us the equations of motion are basic for producing nonrelativistic Hamiltonian.

We would like to point out some steps of derivation of the nonrelativistic limit Hamiltonians by means of the Foldy-Wouthuyisen transformation (Bjorken and Drell, 1964). The method is based on the transformation of a relativistic equation of motion to the Schrödinger equation form.

The equation of motion for the scalar particle in the electromagnetic field is

$$\left(D^2 + m^2\right)\varphi = 0, \quad \text{or} \quad D_0^2\varphi = \left(\mathbf{D}^2 - m^2\right)\varphi, \tag{1}$$

where we use the standard notations

$$D_\mu = \partial_\mu - ieA_\mu, \quad D_0 = \partial_0 - ieA_0, \tag{2}$$

$$\mathbf{D} = -\nabla - ie\mathbf{A}, \quad \vec{\pi} = i\mathbf{D} = \mathbf{p} + e\mathbf{A}, \tag{3}$$

and A_μ is the electromagnetic potential, $\vec{\pi}$ is the generalized momentum. Determining the "big" and "small" components of φ by equations

$$\theta = \varphi + \frac{i}{m}D_0\varphi, \quad \chi = \varphi - \frac{i}{m}D_0\varphi, \tag{4}$$

we get

$$iD_0\theta = m\theta - \frac{\mathbf{D}^2}{2m}\left(\theta + \chi\right), \quad iD_0\chi = -m\chi + \frac{\mathbf{D}^2}{2m}\left(\theta + \chi\right), \tag{5}$$

or

$$i\partial_t\Phi = H\Phi, \quad \Phi = \begin{pmatrix} \theta \\ \chi \end{pmatrix}. \tag{6}$$

where

$$H = m\eta - eA_0 - \eta\frac{\mathbf{D}^2}{2m} - \rho\frac{\mathbf{D}^2}{2m} = m\eta - eA_0 + \eta\frac{\vec{\pi}^2}{2m} + \rho\frac{\vec{\pi}^2}{2m}, \tag{7}$$

$$\eta = \begin{pmatrix} 1 & 0 \\ 0 & -1 \end{pmatrix}, \quad \rho = \begin{pmatrix} 0 & 1 \\ -1 & 0 \end{pmatrix}. \tag{8}$$

This Hamiltonian we should transform to separate the states with positive energy from those of negative ones. Substituting

$$\Phi = e^{-iS}\Phi' \tag{9}$$

into Eq. (6) we obtain

$$i\partial_t \Phi' = H'\Phi', \tag{10}$$

where

$$H' = e^{iS}\left(H - \partial_t S\right)e^{-iS}. \tag{11}$$

Using standard expansion formula for S and excluding the terms containing ρ from the expansion, we get the new Hamiltonian up to the accuracy $O(1/m^4)$ (Wirzba and Drell, 1964):

$$H' = \eta\left(m + \frac{\vec{\pi}^2}{2m} - \frac{\vec{\pi}^4}{8m^3}\right) - eA_0 - \frac{ie}{16m^4}[\vec{\pi}^2, \vec{\pi} \cdot \mathbf{E}]. \tag{12}$$

Now we can proceed to a massive vector field theory. A massive particle of spin 1 has three degrees of freedom, so, it may be considered as spatial part of a four vector ψ_μ. In Ref. (Corben and Schwinger, 1940) a general theory describing particles of unit spin and arbitrary magnetic moment was developed and applied to the motion of such particles in the electromagnetic field. For our purpose we use the equations of motion given in Ref. (Wentzel, 1949; Pauli, 1941). The massive four-dimensional vector field ψ_ν is described by

$$\psi_{\mu\nu} = D_\mu\psi_\nu - D_\nu\psi_\mu, \quad D^\mu\psi_{\mu\nu} + M^2\psi_\nu - ie\kappa F_{\nu\mu}\psi^\mu = 0, \tag{13}$$

where M is mass of the vector particle,

$$F_{\nu\mu} = \partial_\mu A_\nu - \partial_\nu A_\mu \tag{14}$$

is the strength tensor of the electromagnetic field,

$$D_\mu = \partial_\mu - ieA_\mu \tag{15}$$

is the electromagnetic covariant derivative and κ is the anomaly part of magnetic moment of the particle. Acting on the second equation by D^ν we get the following constraint:

$$D^\mu\psi_\mu = -\frac{ie}{2M^2}F^{\mu\nu}\psi_{\mu\nu} + \frac{ie\kappa}{M^2}D^\mu(F_{\mu\nu}\psi^\nu). \tag{16}$$

Let us rewrite Eq. (13) as

$$D^2\psi_\nu - D_\nu D^\mu\psi^\mu + M^2\psi_\nu - ie\mu F_{\nu\mu}\psi^\mu = 0, \tag{17}$$

where $\mu = 1 + \kappa$ is the full magnetic moment of the vector particle. Using the constraint (16) we get

$$
\begin{aligned}
D_0^2\psi_\nu =& \left(\mathbf{D}^2 - M^2\right)\psi_\nu + ie\mu F_{\nu\mu}\psi^\mu \\
&- \frac{ie}{2M^2}\left[D_\nu(F^{\mu\nu}\psi_{\mu\nu}) - 2\kappa D_\nu D^\mu(F_{\mu\lambda}\psi^\lambda)\right].
\end{aligned} \tag{18}
$$

Further we replace the zero component of ψ_ν through its spatial part :

$$\psi_0 = \frac{1}{M^2 - \mathbf{D}^2}\left[ie(1+\kappa)\mathbf{E}\cdot\vec{\psi} + D_0 D^i \psi_i\right],\qquad(19)$$

where ψ_i is spatial component of $\vec{\psi}$. Using the following notations

$$\Psi_i = \begin{pmatrix} \zeta_i \\ \chi_i \end{pmatrix},\quad \zeta_i = \psi_i + \frac{i}{M}D_0\psi_i,\quad \chi_i = \psi_i - \frac{i}{M}D_0\psi_i,\qquad(20)$$

and the procedure of the Foldy-Wouthuysen transformation as for the scalar field we obtain the system of equations

$$i\partial_0 \Psi_i = H_i^j \Psi_j,\quad i,j = 1,2,3,\qquad(21)$$

where the Hamiltonian is equal to

$$
\begin{aligned}
H_{ij} &= \left(M\eta - eA_0 + \eta\frac{\vec{\pi}^2}{2M} - \eta\frac{\vec{\pi}^4}{8M^3}\right)\delta_{ij} + \frac{ie\mu}{2M}\eta\varepsilon_{ikj}B^k \\
&\quad - \frac{ie}{2M^2}\left[(2-\mu)\pi_i E_j + \mu E_i \pi_j\right] \\
&\quad + \frac{ie}{2M^3}\eta\left[\varepsilon_{klj}\pi^i\left(B^k\pi^l + (\mu-1)\pi^k B^l\right) + \cdots\right],\qquad(22)
\end{aligned}
$$

where we include terms up to order $O(1/M^3)$. In Eq. (22) E_i and B_i are the components of an electric field intensity $\mathbf{E}$ and a magnetic field of flux density $\mathbf{B}$ respectively.

Let us estimate magnitudes of terms included in the nonrelativistic Hamiltonians (12) and (22) assuming that the pion and deuteron are in the 1s bound state and they move relative to each other with momentum p in the center of mass system. It is well known that the binding energy of $\pi^- d$ atom is about 3 keV therefore we obtain $p/m \sim 6.6\cdot10^{-3}$ for pion and $p/M \sim 5\cdot10^{-4}$ for deuteron. The strong energy-level shift in $\pi^- d$ atom is about $\varepsilon \sim 3$ eV. Therefore we have to take into account the terms of the Hamiltonians which give contributions of the same order like ε. Assuming the Bohr radius of the atom to be $R_b \sim 200$ fm, i.e., $1/R_b \sim 1$ MeV, we arrive at values: the first relativistic correction $p^4/(8m^3)$ for pion has magnitude $\sim 3\cdot10^{-2}$ eV and the Darwin term (the last term in Eq. (12)) has magnitude $7\cdot10^{-7}$ eV; the kinetic energy of the deuteron is about $2\cdot10^2$ eV, the relativistic correction for deuteron $p^4/(8M^3) \sim 1.3\cdot10^{-5}$ eV, the term of order $1/M$ describing interaction of the magnetic moment of deuteron with magnetic field vanishes in the quantum mechanics case, because we consider 1s state of the atom, the contribution of other terms of order $1/M^2$ and $1/M^3$

are $\sim 7 \cdot 10^{-4}$ eV and $\sim 5 \cdot 10^{-9}$ eV respectively. Taking into account these estimations we conclude that the last term in Eq. (12) and the terms of order $1/M^2$ and higher are not important and we can omit all relativistic corrections for deuteron. We underline that in the nonrelativistic limit the down components in the wave functions Eq. (6) and (20) go to zero.

Now we can write down the total Hamiltonian including into consideration the strong πd interaction and the Hamiltonian of the electromagnetic field. We take the density of the Hamiltonian the strong πd interaction in the zero range approach:

$$\mathcal{H}_S = -d_{\pi d} \vec{\Psi}_d^\dagger \Phi_\pi^\dagger \vec{\Psi}_d \Phi_\pi, \tag{23}$$

where Φ_π and $\vec{\Psi}_d$ denote the non-relativistic field operator of pion and deuteron respectively, $d_{\pi d}$ is the coupling constant which does not depend on the spin projection of the deuteron. The electromagnetic Lagrangian is

$$L_{em} = -\frac{1}{4} F_{\mu\nu}^2 = -\mathbf{E} \cdot \partial_0 \mathbf{A} + A_0 \mathrm{div}\mathbf{E} - \frac{1}{2}(\mathbf{E}^2 + \mathbf{B}^2), \tag{24}$$

i.e.,

$$\mathcal{H}_{em} = \frac{1}{2}(\mathbf{E}^2 + \mathbf{B}^2) \tag{25}$$

is the (density) of the electromagnetic Hamiltonian and A_0 is a Lagrange multiplier (it is not a dynamical variable).

To obtain the total Hamiltonian for πd system, in the Coulomb gauge we exclude the A_0 field by using the equations of motion, and neglect high-dimensional operators that arise as a result of this operation. The result for the canonical Hamiltonian of the non-relativistic πd system can be written as

$$\mathbf{H} = \mathbf{H}_0 + \mathbf{H}_{\mathrm{C}} + \mathbf{H}_{\mathrm{R}} + \mathbf{H}_\gamma + \mathbf{H}_{\mathrm{S}} = \mathbf{H}_0 + \mathbf{H}_{\mathrm{C}} + \mathbf{V}, \tag{26}$$

where $\mathbf{H}_0$ is the free Hamiltonian describing non-relativistic pions and deuterons. Further, $\mathbf{H}_\Gamma = \int d^3\mathbf{x}\, \mathcal{H}_\Gamma$, $\Gamma = \mathrm{C}, \mathrm{R}, \mathrm{S}, \gamma$, and

$$\mathcal{H}_{\mathrm{C}} = e^2 (\vec{\Psi}_d^\dagger \vec{\Psi}_d) \triangle^{-1} (\Phi_\pi^\dagger \Phi_\pi), \tag{27}$$

$$\mathcal{H}_{\mathrm{R}} = -\Phi_\pi^\dagger, \frac{\nabla^4}{8m^3} \Phi_\pi, \quad \mathcal{H}_{\mathrm{S}} = -d_{\pi d} \vec{\Psi}_d^\dagger \vec{\Psi}_d \Phi_\pi^\dagger \Phi_\pi, \tag{28}$$

$$\mathcal{H}_\gamma = -\frac{ie}{2M} \vec{\Psi}_d^\dagger (\nabla \mathbf{A} + \mathbf{A}\nabla) \vec{\Psi}_d + \frac{ie}{2m} \Phi_\pi^\dagger (\nabla \mathbf{A} + \mathbf{A}\nabla) \Phi_\pi. \tag{29}$$

3. Energy shift of pionic deuterium atom

We consider the problem of s-state energy shift according to the perturbation theory. Such analysis was performed for the pionic hydrogen in Ref. (Lyubovitskji and Rusetsky, 2000). Let $\mathbf{H}_0 + \mathbf{H}_C$ be the unperturbed Hamiltonian, whereas $\mathbf{V}$ is considered as a perturbation. The ground-state solution of the unperturbed Schrödinger equation in the center of mass (CM) system frame $(\tilde{E}_1 - \mathbf{H}_0 - \mathbf{H}_C)|\Psi_0(\mathbf{0})\rangle = 0$, with $\tilde{E}_1 = M + m + E_1$, is given by

$$|\Psi_0(\mathbf{0})\rangle = \int \frac{d^3\mathbf{p}}{(2\pi)^3}\, \Psi_0(\mathbf{p})\, b^\dagger(\mathbf{p})\, a^\dagger(-\mathbf{p})\,|0\rangle\,, \qquad (30)$$

where $a^\dagger(\mathbf{p})$ and $b^\dagger(\mathbf{p})$ denote creation operators for non-relativistic π^- and deuteron acting on the Fock space vacuum, and $\Psi_0(\mathbf{p})$ stands for the non-relativistic Coulomb wave function of $1S$ state in the momentum space, E_1 is the non-relativistic binding energy of pionic deuterium.

We are going to evaluate the energy-level shift of the ground state due to the perturbation Hamiltonian $\mathbf{V}$ as in Ref. (Lyubovitskji and Rusetsky, 2000). Let us define the free and Coulomb Green operators by the expressions $\mathbf{G}_0(z) = (z - \mathbf{H}_0)^{-1}$ and $\mathbf{G}(z) = (z - \mathbf{H}_0 - \mathbf{H}_C)^{-1}$, respectively. Further, we define the "Coulomb-pole removed" Green function as $\hat{\mathbf{G}}(z) = \mathbf{G}(z)(1 - \mathbf{\Pi})$, where $\mathbf{\Pi}$ denotes the projector onto the Coulomb ground state Ψ_0 (30). The πd scattering states in the sector with the total charge 0 are defined as $|\mathbf{P}, \mathbf{p}\rangle = b^\dagger(\mathbf{p}_1)\, a^\dagger(\mathbf{p}_2)\,|0\rangle$ ($\mathbf{p}_1$ and $\mathbf{p}_2$ denote momenta of deuteron and pion, respectively). The CM and relative momenta are defined by $\mathbf{P} = \mathbf{p}_1 + \mathbf{p}_2$, $\mathbf{p} = (m\,\mathbf{p}_1 - M\,\mathbf{p}_2)/(M+m)$. We remove the CM momenta from the matrix elements of any operator $\mathbf{R}(z)$ by introducing the notation

$$\langle \mathbf{P}, \mathbf{q}|\mathbf{R}(z)|\mathbf{0}, \mathbf{p}\rangle = (2\pi)^3 \delta^3(\mathbf{P})\,(\mathbf{q}|\mathbf{r}(z)|\mathbf{p})\,. \qquad (31)$$

The "Coulomb-pole removed" transition operator satisfies the equation

$$\mathbf{M}(z) = \mathbf{V} + \mathbf{V}\hat{\mathbf{G}}(z)\mathbf{M}(z)\,. \qquad (32)$$

According to the Feshbach's formalism (Feshbach, 1958; Feshbach, 1962) the scattering operator $\mathbf{T}(z)$ develops the pole at $z = \bar{z}$ where $\bar{z}$ is the solution of the following equation

$$\bar{z} - \tilde{E}_1 - (\Psi_0|\mathbf{m}(\bar{z})|\Psi_0) = 0\,, \qquad (33)$$

where $(\mathbf{p}|\Psi_0) = \Psi_0(\mathbf{p})$ and $\mathbf{m}(z)$ is related to $\mathbf{M}(z)$ through the definitions (31).

In order to get the shift of the ground-state energy, the quantity $\mathbf{m}(z)$ is calculated perturbatively from Eq. (32) by the iteration series

at accuracy $O(\alpha^2)$. Using the explicit expression of $\mathbf{V}$ given by Eq. (26), replacing $\hat{\mathbf{G}}(z)$ by $\mathbf{G}_0(z)$ whenever possible, and retaining only those terms that contribute at the accuracy we are working, the operator $\mathbf{M}(z)$ can be written in the form $\mathbf{M}(z) = \mathbf{U}(z) + \mathbf{W}(z)$, where

$$\mathbf{U}(z) = \mathbf{H}_{\mathrm{R}} + \mathbf{H}_\gamma \mathbf{G}_0(z)\mathbf{H}_\gamma, \quad \mathbf{W}(z) = \mathbf{H}_{\mathrm{S}} + \mathbf{H}_{\mathrm{S}}\hat{\mathbf{G}}(z)\mathbf{H}_{\mathrm{S}}. \tag{34}$$

At the accuracy $O(\alpha^2)$, the energy of the bound state is equal to $\bar{z} = \tilde{E}_1 + \Delta E_1^{\mathrm{em}} + \epsilon_{1s}$, where

$$\Delta E_1^{\mathrm{em}} = \mathrm{Re}\,(\Psi_0|\mathbf{u}(\tilde{E}_1)|\Psi_0) + E^{\mathrm{vac}}, \quad \epsilon_{1s} = \mathrm{Re}\,(\Psi_0|\mathbf{w}(\tilde{E}_1)|\Psi_0). \tag{35}$$

Here $\mathbf{u}(z)$, $\mathbf{w}(z)$ are related to $\mathbf{U}(z)$, $\mathbf{W}(z)$ through the definitions (31) and E^{vac} stands for the contribution due to the electron vacuum polarization which is added "by hand". The results of calculations for the matrix elements determining the energy-label shift are the same as in Ref. (Lyubovitskji and Rusetsky, 2000):

$$\mathrm{Re}\,(\Psi_0|\mathbf{u}(\tilde{E}_1)|\Psi_0) = -\frac{5}{8}\,\alpha^4\mu_{\pi d}^4\,\frac{M^3 + m^3}{M^3 m^3} - \frac{\alpha^4\mu_{\pi d}^3}{Mm},$$

$$\mathrm{Re}\,(\Psi_0|\mathbf{w}(\tilde{E}_1)|\Psi_0) = \frac{\alpha^3\mu_{\pi d}^3}{\pi}\left[-d_{\pi d}\right.$$

$$\left. + d_{\pi d}^2\left(\xi + \frac{\alpha\mu_{\pi d}^2}{\pi}\left(\ln\alpha - 1\right)\right)\right], \tag{36}$$

where $\mu_{\pi d}$ is the reduced mass of the πd system, and

$$\xi = \frac{\alpha\mu_{\pi d}^2}{2\pi}\left\{(\mu^2)^{d-3}\left(\frac{1}{d-3} - \Gamma'(1) - \ln 4\pi\right) + \ln\frac{(2\mu_{\pi d})^2}{\mu^2} - 1\right\}. \tag{37}$$

Here d and μ denote the dimension of space and the scale of the dimensional regularization used as in Ref. (Lyubovitskji and Rusetsky, 2000), respectively.

The energy shift (order α^2) due to the vacuum polarization contribution is given by the well-known expression (Lyubovitskji and Rusetsky, 2000). The calculation of the electromagnetic energy-level shift is now complete.

We present our results in a convenient form

$$\tilde{E}_1 + \Delta E_1^{\mathrm{em}} = E^{\mathrm{KG}} + E^{\mathrm{vac}} + E^{\mathrm{rel}}, \tag{38}$$

where

$$E^{\mathrm{KG}} = -\frac{1}{2}\,\mu_{\pi d}\alpha^2\left(1 + \frac{5\alpha^2}{4}\right), \tag{39}$$

$$E^{\mathrm{rel}} = \frac{7}{8}\,\alpha^4\,\frac{\mu_{\pi d}^3}{Mm}. \tag{40}$$

Table I. Contributions to the electromagnetic binding energy
of the $\pi^- p$ and $\pi^- d$ atoms (eV)

Type of contribution	Notation	$\pi^- p$	$\pi^- d$
Point Coulomb, KG equation	E^{KG}	-3235.156	-3459.0
Vacuum polarization, order α^2	E^{vac}	-3.241	-3.732
Relativistic recoil	E^{rel}	0.047	0.021

In Table I we present various contributions to the electromagnetic
energy-level shift of $\pi^- p$ and $\pi^- d$ atoms. As can be seen from Table I,
the calculated values of the electromagnetic shifts for $\pi^- p$ and $\pi^- d$
atoms are close to each other.

4.   *s*-wave scattering length and the Deser's type formula

In order to complete the calculation of the strong energy-level shift,
one has to match at the accuracy $O(\alpha)$ the particular combination of
the non-relativistic coupling $d_{\pi d}$. Therefore we consider the scattering
operator

$$\mathbf{T}_{\mathrm{R}}(z) = \mathbf{V}_{\mathrm{R}} + \mathbf{V}_{\mathrm{R}}\mathbf{G}_{\mathrm{R}}(z)\mathbf{T}_{\mathrm{R}}(z),$$

$$\mathbf{V}_{\mathrm{R}} = \mathbf{H}_{\mathrm{C}} + \mathbf{H}_{\gamma} + \mathbf{H}_{\mathrm{S}}, \quad \mathbf{G}_{\mathrm{R}}(z) = (z - \mathbf{H}_0 - \mathbf{H}_{\mathrm{R}})^{-1}. \quad (41)$$

In the scattering operator $\mathbf{T}_{\mathrm{R}}(z)$, all kinematical insertions con-
tained in $\mathbf{H}_{\mathrm{R}}$ are summed up in the external lines (see (Antonelli et
al, 2001) for details). We calculate the matrix element of the scattering
operator $\mathbf{T}_{\mathrm{R}}(z)$ between the $\pi^- d$ states at $O(\alpha)$. After removing the
CM momentum, the spin-nonflip part of this matrix element on energy
shell is equal to

$$(\mathbf{q}|\mathbf{t}_{\mathrm{R}}(z)|\mathbf{p}) = -\frac{4\pi\alpha}{|\mathbf{q} - \mathbf{p}|^2} - \frac{4\pi\alpha}{4Mm}\frac{(\mathbf{q} + \mathbf{p})^2}{|\mathbf{q} - \mathbf{p}|^2}$$

$$+ e^{2i\alpha\theta_{\mathrm{C}}(|\mathbf{p}|)}\,(\mathbf{q}|\bar{\mathbf{t}}_{\mathrm{R}}(z)|\mathbf{p}), \quad (42)$$

where the (divergent) Coulomb phase in the dimensional regularization
scheme is given by

$$\theta_{\mathrm{C}}(|\mathbf{p}|) = \frac{\mu_{\pi d}}{|\mathbf{p}|}\,\mu^{d-3}\left(\frac{1}{d-3} - \frac{1}{2}(\Gamma'(1) + \ln 4\pi)\right) + \frac{\mu_{\pi d}}{|\mathbf{p}|}\ln\frac{2|\mathbf{p}|}{\mu}, \quad (43)$$

and

$$\mathrm{Re}\,(\mathbf{q}|\bar{\mathbf{t}}_R(z)|\mathbf{p}) \;=\; -\frac{\pi\alpha\mu_{\pi d}d_{\pi d}}{|\mathbf{p}|} \tag{44}$$

$$+\;\frac{\alpha\mu_{\pi d}^2 d_{\pi d}^2}{\pi}\,\ln\frac{|\mathbf{p}|}{\mu_{\pi d}} - d_{\pi d} + d_{\pi d}^2\xi + \cdots,$$

where ellipses stand for the terms that vanish at threshold. The first two terms in Eq. (45) are arisen due to the electromagnetic interactions between deuteron and pion, the sum of two next terms is amplitude of scattering due to the strong interaction at threshold.

Therefore for the regular part of the s-wave scattering length we have

$$-\frac{2\pi}{\mu_{\pi d}}\mathcal{A}_{\pi d} = -d_{\pi d} + d_{\pi d}^2\xi. \tag{45}$$

Finally compare Eq. (45) with Eq. (36) where we take into account all terms at accuracy $O(\alpha^2)$ we obtain the relation between the regular part of the s-wave πd scattering length and the strong energy-level shift of $\pi^- d$ atom:

$$\epsilon_{1s} = -2\alpha^3\mu_{\pi d}^2\,\mathcal{A}_{\pi d}\,, \tag{46}$$

where the ultraviolet divergence contained in the quantity ξ, has been cancelled.

5. Discussion and conclusion

From the measurement of the $3p - 1s$ X-ray transition of pionic deuterium the $\pi^- d$ scattering length has been determined. The strong energy-level shift can be defined by

$$\epsilon_{1s} = E_{3p-1s}^{mag} - E_{3p-1s}^{meas}\,, \tag{47}$$

where E_{3p-1s}^{mag} is the electromagnetic transition energy calculated in the absence of the strong interaction (the strong interaction in the $3p$ state is negligible), E_{3p-1s}^{meas} is the measured transition energy.

In order to combine the results from pionic hydrogen and pionic deuterium, establishing a relation between $\mathcal{A}_{\pi d}$ and πN isoscalar and isovector lengths b_0 and b_1 is the important problem. This relation can be expressed as

$$\mathcal{A}_{\pi d} = \frac{1 + m/m_N}{1 + m/M}2b_0 + \mathcal{A}_{\pi d}^{(\text{higher order})}\,, \tag{48}$$

where the first term is the scattering amplitude in the impulse approximation, $2b_0$ is the sum of the amplitude for $\pi^- p$ and $\pi^- n$ elastic

scattering, m_N is the nucleon mass. The second term is dominant and it includes all remaining (higher order) contributions. The results presented in Ref. (Schröder et al, 2001) shows that the s-wave double scattering gives the most contribution while the multiple scattering and form factor correction are much smaller. On the basis of the solution of the Faddeev equation obtained in Ref. (Deloff, 2001) we get

$$
\begin{aligned}
\mathcal{A}_{\pi d} \;=\; & \frac{2\mu_{\pi d}}{m}\left[\tilde{b}_0 + (\tilde{b}_0^2 - \tilde{b}_1^2)\left\langle \frac{e^{-\kappa r}}{r}\right\rangle \right. \\
& \left. +\; (\tilde{b}_0 + \tilde{b}_1)^2(\tilde{b}_0 - 2\tilde{b}_1)\left\langle \frac{e^{-2\kappa r}}{r^2}\right\rangle \right],
\end{aligned}
\tag{49}
$$

where $\kappa = \sqrt{2\mu_{np}\epsilon_d}$ (ϵ_d is the binding energy of the deuteron, μ_{np} is reduced mass for proton and neutron) and $\tilde{b}_j = (1 + m/m_N)b_0$. The expectation values of $e^{-\kappa r}/r$ and $e^{-2\kappa r}/r^2$ are taken with respect to the deuteron wave function. The calculations of the expectation value $\langle 1/r \rangle$ performed by the various NN potentials gave 20% discrepancy for its value (Deloff, 2001). That means it is necessary to calculate the expectation value with a potential which has the right behavior at short distances.

6. Acknowledgments

References

Mojzis M. Elastic πN scattering to $O(p^3)$ in heavy baryon chiral perturbation theory, Eur.Phys. J. C 2 (1), 181-195 (1998)

Fettes N., Meissner U. G., Steininger S. Pion-nucleon scattering in chiral perturbation theory (I): Isospin-symmetric case. Nucl. Phys.A 640, 199-234 (1998)

Fettes N., Meissner U. G. Pion-nucleon scattering in chiral perturbation theory II: Fourth order calculation. Nucl. Phys. A 676, 311-338 (2000)

Fettes N., Meissner U. G. Towards an understanding of isospin violation in pion-nucleon scattering, Phys. Rev. C 63, 045201-045211 (2001).

Gasser J. et al Ground-state energy of pionic hydrogen to one loop. Eur. Phys. J. C 26, 13-24 (2002).

Schröder H. Ch. et al., The pion-nucleon scattering lengths from pionic hydrogen and deuterium, Eur. Phys. J. C 21, 473-488 (2001)

Golberger M. L., Miyazawa H. and Oehme R. Application of Dispersion Relations to Pion-Nucleon Scattering, Phys. Rev. 99, 986-988 (1955)

Deser S., Goldberger M. L., Baumann K. and Thirring W. Energy Level Displacements in Pi-Mesonic Atoms, Phys. Rev. 96, 774-776 (1954)

Anagnostopoulos D. F. et al., Precision measurements in pionic hydrogen, Nucl. Phys. A 721, 849-852 (2003).

Hauser P. et al., New precision measurement of the pionic deuterium s-wave strong interaction parameters, Phys. Rev. C 58, R1869-R1872, (1998).

Peresypkin V.V. and Petrov N. M. Low-energy elastic scattemng of pions by the deuteron, Nucl. Phys. A 220, 277-283 (1974)

Afnan I. R. and Thomas A. W. Faddeev approach to pion production and pion-deuteron scattering, Phys. Rev. C 10, 109-125 (1974)

Mizutani T. and Koltun D. S. Coupled channel theory of pion-deuteron reaction applied to threshold scattering, Annals Phys. 109, 1, (1977)

Deloff A. Determination of πN scattering lengths from pionic hydrogen and pionic deuterium data, Phys. Rev. C 64, 065205, (2001)

Baru V. V., Kudryavtsev A. E. and Tarasov V. E. On rescattering effects in reaction $\pi^- d \to \pi^- d$. Phys.Atom.Nucl. 67, 743, (2004).

Lyubovitskji V. E. and Rusetsky A. $\pi^- p$ atom in ChPT: strong energy-level shift. Phys. Lett. B 494, 9, (2000)

Ivanov A. N. et al, On pionic hydrogen. Quantum field theoretic, relativistic covariant and model independent approach arXiv: nucl-th/0306047.

Beane S. R., Bernard V., Lee T. S. H., Meissner U. G. The isoscalar S-wave pi-N scattering length a^+ from π-deuteron scattering, Phys.Rev. C 57, 424, (1998)

Borasoy B. and Griesshammer H. W. The S Wave Pion Deuteron Scattering Length in Effective Field Theory. arXiv: nucl-th/0105048.

Beane S. R. et al. The S-Wave Pion-Nucleon Scattering Lengths from Pionic Atoms using Effective Field Theory, Nucl.Phys. A 720, 399, (2003)

Beane S. R. and Savage M. J. Pions in the Pionless Effective Field Theory. Nucl.Phys. A 717, 104, (2003)

Bjorken J. and Drell S. Relativistic quantum mechanics, McGraw-Hill, New York, (1964)

Corben H. C. and Schwinger J. The Electromagnetic Properties of Mesotron, Phys. Rev. 58, 953, (1940)

Wentzel G. Quantum Theory of Fields New York, Interscience Publisher. Inc., (1949).

Pauli W. Relativistic Field Theories of Elementary Particles. Rev. Mod. Phys. 13, 203, (1941)

Feshbach H. A Unified Theory of Nuclear Reactions, Ann. Phys. 5, 357, (1958)

Feshbach H. A Unified Theory of Nuclear Reactions. II. Ann. Phys., 19, 287, (1962)

Antonelli V. et al. Effective Lagrangians in bound state calculations. Annals Phys. 286, 108, (2001)

Sigg D. et al. Electromagnetic correction to the s-wave scattering lengths in pionic hydrogen, Nucl. Phys. A 609, 310, (1996)

Spectra of quarkonia at finite-temperature

Kh.T. Butanov[a], D.U. Matrasulov[a], Kh.Yu. Rakhimov[a] and F.C. Khanna[b]

(a) Heat Physics Department of the Uzbek Academy of Sciences,
28 Katartal St., 700135 Tashkent, Uzbekistan
(b) Physics Department University of Alberta
Edmonton Alberta, T6G 2J1 Canada
and TRIUMF, 4004 Wersbrook Mall,
Vancouver, British Columbia, Canada, V6T2A3

Abstract. Finite-temperature mass spectra of heavy quarkonia are calculated using an approach based on the thermofield dynamics formalism. Schrödinger operator for heavy quarkonium is represented in a temperature-dependent form using doubling procedure and Bogolyubov transformations. Energy eigenvalues of the quarkonium are calculated by diogonalization of this operator on doubled harmonic oscillator basis.

Keywords: Quarkonia, mass spectra, in medium effects.

Accurate theoretical prediction of mass spectra and other properties of hadrons containing heavy quarks is important for mass spectra of hadrons for forthcoming experiments on the study of their properties. At present such facilities as Tevatron, LHC and JHF will have the opportunity to produce hadrons with one or more heavy quarks. The successful experiments at the Collider Detector at Fermilab Collaboration on the observation of the B_c meson (Abe et. al., 1998) gives some hope to observe heavy quarkonia, also.

Heavy flavored hadrons which can be observed experimentally are heavy-light mesons, single- and doubly heavy quarkonia. Properties of these quarkonia have been studied theoretically very extensively (Fleck et. al., 1989; Kiselev et. al., 1999; Gershtein et. al., 2000; Matrasulov et. al., 2000). Studying a larger set of flavored hadrons, including quarkonia with two heavy quarks, and also exploring their properties in dense matter allows to test the relevant aspects of the QCD forces acting in these systems under varying conditions.

At present a considerable amount of data is available for heavy flavored mesons, and it is expected that the experimental observation of heavy flavored hadrons at modern hadron colliders with high luminosity such as Tevatron, LHC and RHIC will further increase our knowledge of this family of hadrons.

Despite the considerable progress made in the spectroscopy of hadrons containing heavy quarks within the framework of potential models and other approaches, most of the work on the calculation of mass spectra

of such hadrons are made without proper account of in-medium effects
such as color screening and finite-temperature effects. However, in the
realistic cases such hadrons interact with nuclear or quark-gluon matter
that leads to these effects in their mass spectra.

In this work we treat finite-temperature effects in the spectra of
heavy quarkonia. As a tool for taking into account finite-temperature
effects we use, a real time finite-temperature field theory, thermofield
dynamics (TFD).

The main idea of TFD is the following (Santana, 2004): for a given
Hamiltonian which is written in terms of annihilation and creation
operators, one applies a doubling procedure which implies extending
the Fock space, formally written as $H_T = H \otimes \tilde{H}$. The physical vari-
ables are described by the non-tilde operators. In a second step, a
Bogolyubov transformation is applied which introduces a rotation of
the tilde and non-tilde variables and transforms the non-thermal vari-
ables into temperature-dependent form. This formalism can be applied
to quite a large class of systems whose Hamiltonian operators can be
represented in terms of annihilation and creation operators.

In the present work we will apply this formalism to the quantum-
mechanical Hamiltonian of the heavy quarkonium.

The Schödinger equation for heavy quarkonium can be written as

$$i\frac{\partial \Psi}{\partial t} = H\Psi$$

where H is the quarkonium Hamiltonian

$$H = -\frac{\Delta}{2} - \frac{\alpha_s}{r} + \lambda r - \frac{4}{3}V_0,$$

with $\alpha_s = \frac{4}{3}Z$,

Multiplying both sides of this equation by r^2 and introducing the
following time scaling

$$\tau = r^{-2}t$$

we have

$$i\frac{\partial \Psi}{\partial \tau} = [-r^2\frac{\Delta}{2} - \alpha_s r + \lambda r^3 - \frac{4}{3}V_0 r^2]\Psi$$

By standard substitution

$$\Psi(r,\theta,t) = e^{-iE\tau}\Psi(r,\theta)$$

we can obtain stationary (time-independent) Schrödinger equation for
quarkonium system as:

$$[-r^2\frac{\Delta}{2} - \alpha_s r + \lambda r^3 - \frac{4}{3}V_0 r^2]\Psi = E\Psi$$

Separating angular and radial variables we get

$$\left[-\frac{1}{2}\frac{d}{dr}(r^2\frac{d}{dr}) + \frac{1}{2}l(l+1) - \alpha_s r + \lambda r^3 - \frac{4}{3}V_0 r^2 \right]\Psi = E\Psi$$

Now, introducing annihilation and creation operators as

$$a = \frac{1}{\sqrt{2}}\frac{d}{dr} + \frac{1}{\sqrt{2}}r \quad a^\dagger = -\frac{1}{\sqrt{2}}\frac{d}{dr} + \frac{1}{\sqrt{2}}r$$

we can write this equation in terms of these operators:

$$[-\frac{1}{8}(a-a^\dagger)(a+a^\dagger)^2(a-a^\dagger) - \frac{\alpha_s}{\sqrt{2}}(a+a^\dagger) + \frac{\lambda}{2\sqrt{2}}(a+a^\dagger)^3 + \frac{1}{2}l(l+1) - \frac{2}{3}V_0$$
$$\left(a+a^\dagger\right)^2]\Psi = E\Psi \tag{1}$$

Now applying TFD prescription (Santana, 2004) which consist of the following doubling

$$\hat{H} = H - \tilde{H}, \tag{2}$$

and Bogolyubov transformations which are given by

$$a = a(\beta)cosh\theta + \tilde{a}^\dagger(\beta)sinh\theta$$

$$a^\dagger = a^\dagger(\beta)cosh\theta + \tilde{a}(\beta)sinh\theta$$

$$\tilde{a} = a^\dagger(\beta)sinh\theta + \tilde{a}(\beta)cosh\theta$$

$$\tilde{a}^\dagger = a(\beta)sinh\theta + \tilde{a}^\dagger((\beta)cosh\theta$$

where

$$\beta = \frac{\omega}{k_B T}, \qquad sinh^2\theta = \left(e^\beta - 1\right)^{-1}.$$

The quarkonium Hamiltonian can be written in a temperature-dependent form as

$$H = -\frac{1}{8}\{A_1 A_2 A_2 A_1 cosh^4\theta + B_1 B_2 B_2 B_1 sinh^4\theta + [A_1 A_2 B_2 A_1 + A_1 B_2 A_2 A_1 -$$
$$A_1 A_2 A_2 B_1 -$$
$$-B_1 A_2 A_2 A_1]cosh^3\theta sinh\theta + [B_1 A_2 B_2 B_1 + B_1 B_2 A_2 B_1 - B_1 B_2 B_2 A_1 - A_1 B_2$$
$$B_2 B_1]cosh\theta sinh^3\theta +$$
$$+[A_1 B_2 B_2 A_1 - A_1 A_2 B_2 B_1 - A_1 B_2 A_2 B_1 + B_1 A_2 A_2 B_1 - B_1 A_2 B_2 A_1 - B_1 B_2$$
$$A_2 A_1]cosh^2\theta sinh^2\theta\} -$$
$$-\frac{\alpha_s}{\sqrt{2}}[A_2 cosh\theta + B_2 sinh\theta] + \frac{\lambda}{2\sqrt{2}}[A_2 A_2 A_2 cosh^3\theta + B_2 B_2 B_2 sinh^3\theta +$$
$$+(A_2 A_2 B_2 + A_2 B_2 A_2 + B_2 A_2 A_2)cosh^2\theta sinh\theta + (B_2 B_2 A_2 + B_2 A_2 B_2 + A_2 B_2$$
$$B_2)cosh\theta sinh^2\theta] -$$
$$-\frac{2}{3}V_0\left(A_2 A_2 cosh^2\theta + B_2 B_2 sinh^2\theta + (A_2 B_2 + B_2 A_2)cosh\theta sinh\theta\right)$$

where

$$A_1 = a(\beta) - a^\dagger(\beta), \qquad A_2 = a(\beta) + a^\dagger(\beta),$$

$$B_1 = \tilde{a}(\beta) - \tilde{a}^\dagger(\beta) \qquad B_2 = \tilde{a}(\beta) + \tilde{a}^\dagger(\beta)$$

Temperature-dependent energy spectrum can be found by numerically diagonalizing of the following matrix:

$$E = \langle n`, \tilde{n}` \mid H(\theta, a(\beta), a^\dagger(\beta), \tilde{a}(\beta), \tilde{a}^\dagger(\beta)) \mid \tilde{n}, n \rangle =$$

$$= \frac{1}{8}(K - L + M) - \frac{\alpha_s}{\sqrt{2}}N + \frac{\lambda}{2\sqrt{2}}O - \frac{2}{3}V_0 P,$$

where

$$K = \left(cosh^4\theta + sinh^4\theta\right)\left(2n^2 + 2n + 3)\delta_{n,n'} - \right.$$

$$\left. -\sqrt{n(n-1)(n-2)(n-3)}\delta_{n,n'-4} + \sqrt{(n+1)(n+2)(n+3)(n+4)}\delta_{n,n'+4}\right),$$

$$L = \left(cosh^3\theta sinh\theta + cosh\theta sinh^3\theta\right)\left(4n^2\delta_{n,n'-1} + 4(n+1)^2\delta_{n,n'+1}\right),$$

$$M = 2cosh^2\theta sinh^2\theta\left((4n^2 + 4n - 1)\delta n, n' + \right.$$

$$\left. + \left(n(n-1) - \sqrt{n(n-1)}\right)\delta_{n,n'-2} + \left((n+1)(n+2) - \sqrt{(n+1)(n+2)}\delta_{n,n'+2}\right)\right),$$

$$N = (cosh\theta + sinh\theta)(\sqrt{n}\delta_{n,n'-1} + \sqrt{n+1}\delta_{n,n'+1}),$$

$$O = (cosh^3\theta + sinh^3\theta)\left(3n\sqrt{n}\delta_{n,n'-1} + 3(n+1)\sqrt{n+1}\delta_{n,n'+1} + \right.$$

$$\left. + \sqrt{n(n-1)(n-2)}\delta_{n,n'-3} + \sqrt{(n+1)(n+2)(n+3)}\delta_{n,n'+3}\right),$$

$$P = \left(\sqrt{n(n-1)}\delta_{n,n'-2} + \sqrt{(n+1)(n+2)}\delta_{n,n'+2}\right)\left(cosh^2\theta + sinh^2\theta\right) +$$

$$+ 2\left(n\delta_{n,n'-1} + (n+1)\delta_{n,n'+1}\right)cosh\theta sinh\theta$$

In tables 1 and 2 finite-temperature mass spectra of charmonium and bottomonium obtained by diogonalizing this matrix are presented. As is clear from these tables, taking account of finite-temperature leads to considerable increasing of the binding energy and masses. Thus, applying thermofield dynamics formalism to quantum mechanical Hamiltonian of quarkonium we have estimated mass spectra of the heavy quarkonia taking into account in medium effect, finite-temperature.

Table I. The mass spectrum of $c\bar{c}$ charmonium (in GeV) at zero and finite temperature (K); $m_c = 1.5 GeV$, $\alpha_s = 0.4$, $\lambda = 0.1111 GeV^2$, $V_0 = 0.1 GeV$. n is the radial quantum number.

n	$T = 0K$	$T = 0.724 10^{14} K$	$T = 0.724 10^{15} K$
1	3.048681	3.641026	3.861899
2	3.616962	4.532977	4.835608
3	3.961313	5.290853	5.872907
4	4.691352	6.192815	7.025122
5	5.426366	7.513399	8.655732
6	6.269434	8.918955	10.37917
7	7.428792	10.51625	12.30986

The approach presented in this work can be also extended to the case of Dirac and Klein-Gordon operators, too in order to calculate finite-temperature spectra of heavy-light and hybrid mesons.

Acknowledgements

Table II. The mass spectrum of $b\bar{b}$ bottomonium (in GeV) at zero and finite temperature (K); $m_b = 4.88 GeV$, $\alpha_s = 0.4$, $\lambda = 0.0105 GeV^2$, $V_0 = 0.1 GeV$. n is the radial quantum number.

n	$T = 0K$	$T = 0.72410^{14}K$	$T = 0.72410^{15}K$
1	9.918375	10.13224	10.54522
2	11.04372	12.07665	13.27507
3	11.96444	14.64021	16.03880
4	13.53718	16.96896	20.61091
5	16.04498	20.03971	25.17539
6	18.38532	24.23369	30.52363
7	21.77419	28.90877	36.74519

References

CDF Collaboration, F. Abe et.al. Observation of the B_c meson in $p\bar{p}$ collisions at $\sqrt{s}$=1.8 TeV. *Physical Review Letters*, 81:2432, 1998. Measurement of the B^- and B^0 meson lifetimes using semileptonic decays. *Physics Review D*, 58:092002, 1998.

Fleck, S. and J.M. Richard. *Progress of Theoretical Physics*, 82:760, 1989.

Kiselev, V.V., A.K. Likhoded and A.I. Onishchenko. *Physics Review D*, 60:014007, 1999.

Gershtein, S.S., V.V. Kiselev, A.K. Likhoded and A.I. Onishchenko. *Physics Review D*, 62:054021, 2000.

Matrasulov, D.U., M.M. Musakhanov and T. Morii. *Physics Review C*, 61:045204, 2000.

Karsch, F. Lattice QCD at high temperature and density. *Lect. Notes Phys.* , 583:209, 2002.

Kaczmarek, O, F. Karsch, E. Laermann and M. Lutgemeier, *Physics Review D*, 62:034021, 2000.

A.E. Santana, This proceeding, 2004

Das, A. *Finite Temperature Field Theory*. World Scientific Publishing Co Pte Ltd, 1997.

Matsui, T. and H. Satz. J/Ψ suppression by quark-gluon plasma formation. *Physics Letters B*, 178:416, 1986.

Karsch, F., H. Satz and Mehr. *Z. Phys. C*, 37:617, 1988.

Digal, S., P. Petreczky and H. Satz. *Physics Review D*, 64:094015, 2001.

Chaotization of the periodically driven quarkonia

Davron Otajanov[a] , Faqir Khanna[b] and Davron Matrasulov[a]
(a) Heat Physics Department of the Uzbek Academy of Sciences,
28 Katartal St.,700135 Tashkent, Uzbekistan
(b) Physics Department University of Alberta
Edmonton Alberta, T6G 2J1 Canada
and TRIUMF, 4004 Wersbrook Mall,
Vancouver, British Columbia, Canada, V6T2A3

Abstract. Classical regular and chaotic dynamics of the particle bound in the Coulomb plus linear potential under the influence of time-periodical perturbations is treated using resonace analysis. Critical value of the external field at which chaotization will occur is evaluated analytically based on the Chirikov criterion of stochasticity.

Keywords: quarkonia, quarks

1. Introduction

Dynamical chaos in periodically driven systems has become attractive topic in many areas of contemporary physics such as atomic, molecular, nuclear and particle physics. Dynamical systems which can exhibit chaotic dynamics can be divided into two classes: time independent and time-dependent systems. Billiards, atoms in a constant magnetic field, celestial systems with chaotic dynamics are time independent systems, whose dynamics can be chaotic.

A convenient testing ground for the theoretical and experimental study of chaos in the time-dependent dynamical systems is the highly excited hydrogen atom in a monochromatic field. A theoretical analysis, of the behaviour of a classical hydrogen atom interacting with monochromatic field, based on the resonance overlap criterion, shows that for some critical value of the external field strength ϵ_{cr}, the electron enters into chaotic regime of motion, marked by unlimited diffusion along orbits, leading to ionization. Experimentally this phenomenon was first observed by Bayfield and Koch. Theoretical explanation of this phenomenon was given later by several authors. Such an ionization was called chaotic or diffusive ionization. During the last three decades chaotic ionization of nonrelativistic atom was investigated by many authors theoretically as well as experimentally.

335

In this paper we consider the QCD counterpart of this problem. Namely, we address the problem of regular and chaotic motion in periodically driven quarkonium. Using resonance analysis based on the Chirikov criterion of stochasticity we estimate critical values of the external field strength at which quarkonium motion enters into chaotic regime.

Quarkonium in a monochromatic field can be considered as an analog of the hydrogen atom in a monochromatic field, in which Coulomb potential is replaced by Coulomb plus confining potential.

2.   One-dimensional model

For simplicity we consider a one-dimensional model with a potential

$$V(x) = \begin{cases} -\frac{Z}{x} + \lambda x & for \ x > 0 \\ \\ \infty & for \ x \le 0 \end{cases},$$

where $Z = \frac{4}{3}\alpha_s$ α_s being the strong coupling constant and λ gives strength of the confining potential.

As is well known, in the case of the hydrogen atom interacting with a monochromatic field, one-dimensional model provides an excellent description of the experimental chaotization thresholds for real three-dimensional hydrogen atom (Jensen, 1984).

The Hamiltonian of the periodically driven quarkonium is given by

$$H = \frac{p^2}{2} - \frac{Z}{x} + \lambda x + \epsilon x cos\omega t, \tag{1}$$

with ϵ and ω being the field strength and frequency, respectively.

Formally the unperturbed Hamiltonian is equivalent to the Hamiltonian of the hydrogen atom in constant homogenious electric field. Chaotic dynamics of hydrogen atom in constant electric field under the influence of time-periodic field was treated earlier (Berman et. al, 1985; Stevens and Sundaram1987). To treat nonlinear dynamics of this system under the influence of periodic perturbations we need to rewrite (1) in action-angle variables. Action can be found using its standard definition:

$$n(E) = \frac{1}{2\pi} \int_c^a p dx = \sqrt{2\lambda} \int_c^a \sqrt{\frac{(a-x)(x-c)}{x}} dx, \tag{2}$$

where the momentum p is given by

$$p = \sqrt{2(E - V(x))}, \tag{3}$$

and the constants a and c given as

$$a = \frac{E + \sqrt{E^2 + 2Z\lambda}}{2\lambda}, \quad c = \frac{E - \sqrt{E^2 + 2Z\lambda}}{2\lambda}$$

are turning points of the particle. Since $c < 0$ for the action we have

$$n(E) = \frac{1}{2\pi} \int_0^a p\,dx = B\sqrt{a + \frac{1}{a}} \cdot \left[\left(a - \frac{1}{a}\right) E(k) + \frac{1}{a} K(k) \right]. \quad (4)$$

where

$$B = \frac{2\sqrt{2}}{3\pi\lambda^{\frac{1}{4}}},$$

here $E(k)$ and $E(k)$ are the elliptic integrals (Abramowitz and Stegun, 1964) and

$$k^2 = \frac{a^2}{a^2 + 1} - (1 + \frac{1}{a^2})^{-1}. \quad (5)$$

Here we consider the two limit cases: $a \gg 1$ and $a \ll 1$.

For the first case $(a \gg 1)$ we have:

$$E \equiv H_0 = Z^2 A n^{2/3} \cdot \left[1 - \frac{\lambda ln 4 B^{-2/3} n^{2/3}}{A^2 n^{4/3}} \right], \quad (6)$$

with

$$A = \left(\frac{3\pi\lambda^{\frac{2}{3}}}{2\sqrt{2}} \right).$$

The corresponding proper frequency is

$$\omega_0 = \frac{2}{3} Z^2 \left[\frac{A}{n^{1/3}} + \frac{\lambda}{A n^{5/3}} [\ln(4A\sqrt{\lambda}n^{2/3})] - 1 \right] \quad (7)$$

For the case $a \ll 1$ we have:

$$E \equiv H_0 = 0.5 Z^2 (9.7\lambda n^2 - n^{-2}); \quad (8)$$

The proper frequency for this Hamiltonian is

$$\omega_0 = Z^2 (n^{-3} + 9.7 n\lambda). \quad (9)$$

The total Hamiltonian can be written as

$$H = H_0 + \epsilon \sum x_k cos(k\theta - \omega t), \quad (10)$$

with

$$x_k(n) = - \int_0^{2\pi} x(n, \theta) e^{ik\theta} d\theta \quad (11)$$

being Fourier amplitude of the perturbation. For $a \ll 1$ we have an estimate for the Fourier component

$$x_k(n) \approx -\frac{4E(n)}{\lambda}\frac{1}{k}\sin^2\frac{\pi k\sqrt{\lambda}}{2}. \tag{12}$$

For $a \gg 1$ we have

$$x_k(n) = -\frac{2An^{2/3}}{\pi^2\lambda k^2}. \tag{13}$$

It is well known that the phase-space trajectories of the regular motion lie on tori (so-called KAM tori). According to Kolmogorov-Arnold-Moser theorem for sufficiently small fields most of the trajectories remain regular. If the value of the external perturbation exceeds some value, which is called the critical field strength, KAM tori start to break down and chaotization of the motion will occur (Zaslavsky, 1988). In Fig. 1 the phase-space portrait of the periodically driven quarkonium is plotted for the following values of parameters: $Z = 0.15$, $\lambda = 0.4$, $\omega = 10^{-5}$ and $\epsilon = 4 \cdot 10^{-4}$. Eight regular and two chaotic trajectories are shown. The values of these parameters are written in the system of units where $m_q = \bar{h} = 1$, where m_q is the quark mass, c is the light speed. The values are chosen to have chaotic as well as regular behaviour. Fig.2 represents the phase-space portrait of the periodically driven quarkonium for $a \ll 1$ case for the values of parameters $Z = 0.15$, $\lambda = 10$, $\omega = 10^{-5}$ and $\epsilon = 4 \cdot 10^{-3}$. Again, the system of units $m_q = \bar{h} = 1$ is used.

To estimate the critical value of the external filed strength ϵ_{cr} we use Chirikov's resonance overlap criterion (Zaslavsky, 1988; Jensen, 1984), which can be written as:

$$s = \frac{\Delta\nu_k + \Delta\nu_{k+1}}{\omega_0(k+1) - \omega_0(k)}, \tag{14}$$

with

$$\Delta\nu_k = (\frac{\epsilon x_k}{\omega_0'})$$

being the width of the k-th resonance (Zaslavsky, 1988) and

$$\omega_0' = d\omega_0/dn.$$

From the resonance condition we have

$$\omega_0(k) - \omega_0(k+1) = \frac{\omega}{k} - \frac{\omega}{k+1} = \frac{\omega}{k(k+1)}.$$

Applying this criterion to the quarkonium Hamiltonian (10) we have for $a \gg 1$

$$\epsilon_{cr} = \frac{0.07Z^2\omega\pi^2\lambda}{n^2} \cdot \frac{k(k+1)}{(k+1)^2+k^2} \times \left\{1 + \frac{\lambda}{A^2 n^{\frac{4}{3}}}\left[5\ln\left(4A\lambda^{-\frac{1}{2}}n^{\frac{2}{3}}\right) - 7\right]\right\} \tag{15}$$

and for $a \ll 1$:

$$\epsilon_{cr} = \frac{0.3\omega\alpha}{k(k+1)n^2} \cdot \frac{29\alpha n^4 - 9}{29\alpha n^4 - 3} \times \left[\frac{1}{k}\sin^2(k\sqrt{\alpha}\frac{\pi}{2}) + \frac{1}{k+1}\sin^2((k+1)\sqrt{\alpha}\frac{\pi}{2})\right]^{-1}$$
(16)

In Table 1 the values of the critical field for both approximations for $u\bar{u}$, $d\bar{d}$, $s\bar{s}$, $c\bar{c}$ and $b\bar{b}$ quarkonia at the following values of parameters: $\omega = 10^9 Hz$, $\alpha_s = 0.112$(Barnett et. al, 1996), $\lambda = 0.2 Gev^2$, $n = 10$. are presented. For light (u, d, s) quarkonia we use formula (15) and formula (16) for bottomium and charmonium.

3. Three-dimensional model

The Hamiltonian for the three-dimensional model is

$$H_0 = \frac{p_r^2}{2} - \frac{Z}{r} + \lambda r + \frac{L^2}{r^2}.$$

where L is the orbital angular momentum and p_r is the radial momentum.

The action can be expressed in terms of elliptic integrals:

$$n = \int_c^a pdr = \int_c^a \sqrt{2(E - \frac{L^2}{r^2} + \frac{Z}{r} - \lambda r)}dr =$$

$$\left[(2Z/3 - L^2/c + Ec/3)K(k) + E(a-c)/3E(k)+\right.$$

$$\left. +L^2(c^{-1} - b^{-1})\prod(\beta^2, k)\right]g/\sqrt{\lambda}$$
(17)

with a and c being the turning points, $K, E, \prod$ are complete elliptic integrals of the first, second and third kind, respectively (Abramowitz and Stegun, 1964), and the constants are given as
$k^2 = (a-b)/(a-c)$, $\beta = ck^2/b$, $g = 2/\sqrt{a-c}$.

Applying resonance overlap criterion to this Hamiltonian we get the following estimate for the critical field strength:

$$\epsilon_{cr} = \frac{0.07\alpha\omega}{k(k+1)\pi n^2}\left(1 - \frac{\pi L}{n}\right)\left\{\sqrt{\frac{16\pi^2}{9} + \frac{1}{k^2}} + \sqrt{\frac{16\pi^2}{9} + \frac{1}{(k+1)^2}}\right\}^{-1}$$

$$\times \left[1 - \frac{L^2}{4\pi^4 n^2}\right].$$
(18)

This estimate for the critical field assumes that n is large. If the external field strength has the value exceeding ϵ_{cr}, breaking of KAM surfaces in

Table I. The values of the critical field strength for various quarkonia.

Quarkonium	Quark mass	Critical field (V/cm)		
	(in MeV)	$n = 5$	$n = 7$	$n = 10$
$u\bar{u}$	5	$2.124 \cdot 10^8$	$1.084 \cdot 10^8$	$5.31 \cdot 10^7$
$d\bar{d}$	10	$2.231 \cdot 10^5$	$1.138 \cdot 10^5$	$5.578 \cdot 10^4$
$s\bar{s}$	150	$1.047 \cdot 10^5$	$5.34 \cdot 10^4$	$2.617 \cdot 10^4$
$c\bar{c}$	1500	49.167	25.045	12.258
$b\bar{b}$	4800	1.224	0.624	0.306

the phase space will occur and and the quarkonium diffuses in action and the motion becomes chaotic.

Thus we have treated the chaotic dynamics of the quarkonium in a time periodic field. Using the Chirikov's resonance overlap criterion we obtain estimates for the critical value of the external field strength at which chaotization of the quarkonium motion will occur. The experimental realization of the quarkonium motion under time periodic perturbation could be performed in several cases: in laser driven mesons and in quarkonia in the hadronic or quark-gluon matter.

References

Sagdeev, R. Z., D. A. Usikov, G. M. Zaslavsky. Nonlinear Physics: from pendulum to turbulence and chaos. *Academic Publisher*, New York, 1988.

Izrailev, G. M. *Physics Reports*, 196:299, 1990.

Jensen, R. V. *Physics Review A*, 30:386, 1984.

Zaslavsky, G. M. Stochastic Behaviour of Dynamical Systems. New York, Harwood. 1985. *IEEE J. Quant. Electronics*, 24:1420, 1988.

Mukherjee S. N. et. al. *Phys. Rev.*. 231:203, 1993.

Zhu, X. Q., F. C. Khanna, R. Gurishankar and R. Teshima. *Phys. Rev. D*, 47:1155, 1993.

Phys. Rev. C, 60:035211, 1999.

Bittner, E., Harald Markum and Reiner Pullrich Quantum chaos in physical systems: from super conductors to quarks. *hep-lat/0110222*

Berman, G. P., G. M. Zaslavskii, and A. R. Kolovskii. *Sov. Phys. JETP*, 61:925, 1985.

Mark J. Stevens and Bala Sundaram. *Phys. Rev. A*, 36:417, 1987.

Abramowitz, M. A., and I. A. Stegun. Handbook of mathematical functions. *National Bureo of Standards*, Washington D.C., 1964.

Particle Data Group, R.M.Barnett et. al. *Phys. Rev. D*, 54:1, 1996.

Quantum chaos at finite temperature

D.U. Matrasulov[a] *, U.R. Salomov[a], F.C.Khanna[b] and A. Santana[c]

(a)Heat Physics Department of the Uzbek Academy of Sciences,
28 Katartal St., 700135 Tashkent, Uzbekistan
(b)Physics Department University of Alberta
Edmonton Alberta, T6G 2J1 Canada
and TRIUMF, 4004 Wersbrook Mall,
Vancouver, British Columbia, Canada, V6T2A3
(c) Instituto de Fisica, Universidade Federal, Campus de Ondina,
402-10 340, Salvador, Bahia Brazil

Abstract. Quantum chaos at finite-temperature is studied using a simple paradigm, two-dimensional coupled nonlinear oscillator. As an approach for the treatment of the finite-temperature a real-time finite-temperature field theory, thermofield dynamics, is used. It is found that increasing the temperature leads to a smooth transition from Poissonian to Gaussian distribution in nearest neighbor level spacing distribution.

Recent years there has been a growing interest in quantum chaos in mesoscopic system theory, field theories and particle physics. Recent studies of spectral statistics of the QCD Dirac operator showed that the low-lying spectrum is governed by the Random Matrix Theory and related to symmetries both in confinement and deconfinement phases. Recent treatment of the charmonium spectral statistics and its dependence on color screening has established quantum chaotic behaviour (Gu et.al., 1999). It is supposed that such a behaviour could be the reason for J/Ψ suppression (Gu et.al., 1999). Despite the considerable progress made in the study of quantum chaos in field theories, particle physics and related areas, all those investigations are restricted only to zero-temperature cases. However, the role of finite-temperature is important since the behavior of hadrons in quark-gluon or in nuclear matter, electrons in quantum dots, and other mesoscopic systems could strongly depend on the environment and heat bath effects (Hallman et.al., 2002).

In this work we give a simple presciption for the treatment of finite-temperature effects in quantum chaos using a well-known paradigm of nonlinear dynamics, nonlinear oscillator.

To introduce temperature we use the thermofield dynamics (TFD) formalism (Takahashi et.al., 1996; Das, 1997). TFD is a real time finite-temperature field theory. In TFD the central idea is the doubling of the Hilbert space of states. The operators on this doubled space

---

are doubled. Bogolyubov transformations define a pure vacuum state. The operators at finite-temperature are related to the operators at zero temperature by Bogolyubov transformations. For our purposes, i.e. for treating quantum chaos in gauge fields, TFD is a convenient approach compared to other finite-temperature field theories, such as Matsubara formalism (Matsubara, 1955) or Schwinger-Keldysh formalism (Das, 1997) The possibility of representing the nonlinear oscillator Hamiltonian in terms of annihilation and creation operators makes TFD a useful tool to explore finite-temperature effects in the energy fluctuations.

The quantum Hamiltonian we wish to treat is given by

$$\hat{H} = \frac{P_1^2}{2} + \frac{P_2^2}{2} + \omega^2(q_1^2 + q_2^2) + \gamma^2 q_1^2 q_2^2 \qquad (1)$$

Introducing annihilation and creation operators

$$\hat{a}_k = \sqrt{\frac{\omega}{2}}\hat{q}_k + i\sqrt{\frac{1}{2\omega}}\hat{p}_k \quad \hat{a}_k^+ = \sqrt{\frac{\omega}{2}}\hat{q}_k - i\sqrt{\frac{1}{2\omega}}\hat{p}_k$$

the Hamiltonian can be represented as

$$H = \omega(a_1 a_1^+ + a_2 a_2^+ + 1) + \frac{\gamma^2}{4\omega^2}(a_1 + a_1^+)^2(a_2 + a_2^+)^2 \qquad (2)$$

Operators $\hat{a}_k$ and $\hat{a}_l^+$ satisfy the commutation relations $[\hat{a}_k, \hat{a}_l^+] = \delta_{kl}, \quad k, l = 1, 2.$

The eigenvalues of this Hamitonian can calculated by numerical diagonalization of the truncated matrix of the quantum system in the basis of the harmonic oscillator wave functions. The matrix elements of H_0 and V are

$$< n_1', n_2'|H_0|n_1, n_2 > = \omega(n_1 + n_2 + 1)\delta_{n_1'n_1}\delta_{n_2'n_2},$$

and

$$< n_1', n_2'|V|n_1, n_2 > = \frac{\gamma^2}{4\omega^2}\{\sqrt{n_1(n_1 - 1)}\delta_{n_1'n_1-2} +$$

$$\sqrt{n_1(n_1 - 1)}\delta_{n_1'n_1+2} + (2n_1 + 1)\delta_{n_1'n_1}\}$$

$$\times\{\sqrt{n_2(n_2 - 1)}\delta_{n_2'n_2-2} +$$

$$\sqrt{n_2(n_2 - 1)}\delta_{n_2'n_2+2} + (2n_2 + 1)\delta_{n_2'n_2}\}$$

The numerical procedure for diagonalization of this matrix is described by Salasnich (Salasnich, 1997). We use the same method in the case of finite-temperature calculations.

Now we extend this result to the case of finite temperature using TFD Formalism. In TFD the thermal average of any operator is equal to the expectation value between the pure vacuum state $|0(\beta)>$ defined by applying Bogolyubov tranformations to the usual vacuum state . Applying donbling and Bogoliubov transformations, we can write the Hamiltonian in the temperature dependant form.

Thus the anharmonic oscillator Hamiltonian in TFD is given as

$$\hat{H} = H - \tilde{H} \tag{3}$$

where H is given by eq.2 and $\tilde{H}$ is given as

$$\tilde{H} = \omega(\tilde{a}_1 \tilde{a}_1^+ + \tilde{a}_2 \tilde{a}_2^+ + 1) + \frac{g^2}{8\omega^2}(\tilde{a}_1 + \tilde{a}_1^+)^2(\tilde{a}_2 + \tilde{a}_2^+)^2$$

First we need to rewrite the non-tilde part of the Hamiltonian in the temperature-dependent form using the Bogolyubov transformations which are given by

$$a_k = a_k(\beta)cosh\theta + \tilde{a}_k^+(\beta)sinh\theta$$

$$a_k^+ = a_k^+(\beta)cosh\theta + \tilde{a}_k(\beta)sinh\theta$$

$$\tilde{a}_k = a_k^+(\beta)sinh\theta + \tilde{a}_k(\beta)cosh\theta$$

$$\tilde{a}_k^+ = a_k(\beta)sinh\theta + \tilde{a}_k^+(\beta)cosh\theta$$

where

$$\beta = \frac{\omega}{k_B T}$$

where tilde and non-tilde creation and annihilation operators satisfy the following commutation relations:

$$[a_k(\beta), a_l^+(\beta)] = \delta_{kl} \quad [\tilde{a}_k(\beta), \tilde{a}_l^+(\beta)] = \delta_{kl}$$

$l, k = 1, 2$, and $sinh^2\theta = (e^\beta - 1)^{-1}$. All other commutation relations are zero.

Then the temperature-dependent forms of H_0 and $\tilde{H}_0$ are

$$H_0 = \omega\{(F_1 + F_2)cosh^2\theta +$$

$$(L_1 + L_2)sinh^2\theta + (S_1 + S_2)cosh\theta sinh\theta + 1\},$$

$$\tilde{H}_0 = \omega\{(F_1 + F_2)sinh^2\theta +$$

$$(L_1 + L_2)cosh^2\theta + (S_1 + S_2)cosh\theta sinh\theta + 1\},$$

where

$$F_k = a_k^+(\beta)a_k(\beta),$$

$$L_k = \tilde{a}_k(\beta)\tilde{a}_k^+(\beta),$$

$$S_k = a_k^+(\beta)\tilde{a}_k^+(\beta) + \tilde{a}_k^+(\beta)a_k(\beta),$$

For V and $\tilde{V}$ we have

$$V = \frac{\gamma^2}{4\omega^2}\{A_1 cosh^2\theta + B_1 cosh\theta sinh\theta +$$

$$C_1 sinh^2\theta\}\{A_2 cosh^2\theta + B_2 cosh\theta sinh\theta + C_2 sinh^2\theta\}$$

$$\tilde{V} = \frac{\gamma^2}{4\omega^2}\{A_1 sinh^2\theta + B_1 cosh\theta sinh\theta + C_1 cosh^2\theta\}\times$$

$$\times\{A_2 sinh^2\theta + B_2 cosh\theta sinh\theta + C_2 cosh^2\theta\},$$

where

$$A_k = (a_k(\beta) + a_k^+(\beta))^2,$$

$$B_k = (a_k(\beta) + a_k^+(\beta))(\tilde{a}_k^+(\beta) + \tilde{a}_k(\beta)) +$$

$$(\tilde{a}_k^+(\beta) + \tilde{a}_k(\beta))(a_k(\beta) + a_k^+(\beta)),$$

and

$$C_k = (\tilde{a}_k^+(\beta) + \tilde{a}_k(\beta))^2.$$

Diagonalizing this matrix numerically we obtain the finite-temperature energy eigenvalues of the anharmonic system.

One of the main characteristics of the statistical properies of the spectra is the level spacing distribution (Eckhardt, 1988; Gutzwiller, 1990) function. In this work we calculate the nearest-neighbor level-spacing distribution (Eckhardt, 1988; Gutzwiller, 1990).

The nearest neighbor level spacings are defined as $S_i = \tilde{E}_{i+1} - \tilde{E}_i$, where $\tilde{E}_i$ are the energies of the unfolded levels, which are obtained by the following way: The spectrum $\{E_i\}$ is separated into smoothed average part and fluctuating parts. Then the number of levels below E is counted and the following staircase function is defined:

$$N(E) = N_{av}(E) + N_{fluct}(E).$$

The unfolded spectrum is finally obtained with the mapping

$$\tilde{E}_i = N_{av}(E_i).$$

Then the nearest level spacing distribution function $P(S)$ is defined as the probability of S lying within the infinitesimal interval $[S, S+dS]$.

For the quantum systems which are chaotic in the classical limit this distribution function is the same as that of the random matrices

(Eckhardt, 1988). For systems which are regular in the classical limit its behaviour is close to a Poissonian distribution function.

For Hamiltonians invariant under rotational and time-reversal transformations the corresponding ensemble of matrices is called the Gaussian orthogonal ensemble (GOE). It was established that GOE describes the statistical fluctuation properties of a quantum system whose classical analog is completely chaotic.

In Fig. 1 level spacing distributions for different temperatures are plotted ($\omega = 0.01$ and θ) for the energy spectrum calculated by diagonalizing of the matrix R. It is clear from this plot that the system is regular at $\theta = 0$. However, the increase of temperature leads to a chaotization of the system and $P(S)$ becomes closer to the Gaussian distribution.

Thus increasing the temperature leads to a smooth transition from a Poissonian to a Gaussian form in the level spacing distribution. This fact makes finite-temperature treatment more interesting from the viewpoint of quantum chaology.

1. Acknowledgement

References

Salasnich, L. *Modern Physics Letter A*, 12:1473-1479, 1997.

Eckhardt, B. *Physics Reports*, 163(4):205-297, 1988.

Gutzwiller, M. C. *Chaos in classical and quantum systems, New York, Springer Verlag*, 1990.

Gu, J.- z., H.- s. Zong, Y.-x. Liu and E.-g. Zhao. *Phys. Rev. C*, 60(3) 035211, 1999.

Bittner, E., H. Markum and R. Pullrich. *Quantum chaos in physical systems: from superconductors to quarks*, hep-lat/0110222.

Hallman, T. J., D.E.Kharzeev, J.T.Mitchell and T.Ullrich . *Nuclear Physics*, A698, 2002.

Takahashi, Y., H.Umezawa. *Int. J. of Mod. Physics A*, 10:1755, 1996.

Das, A. Finite Temperature Field Theory (*World Scientific, New York*, 1997).

Matsubara, T. *Prog. Theoretical Physics*, 14:351, 1955.
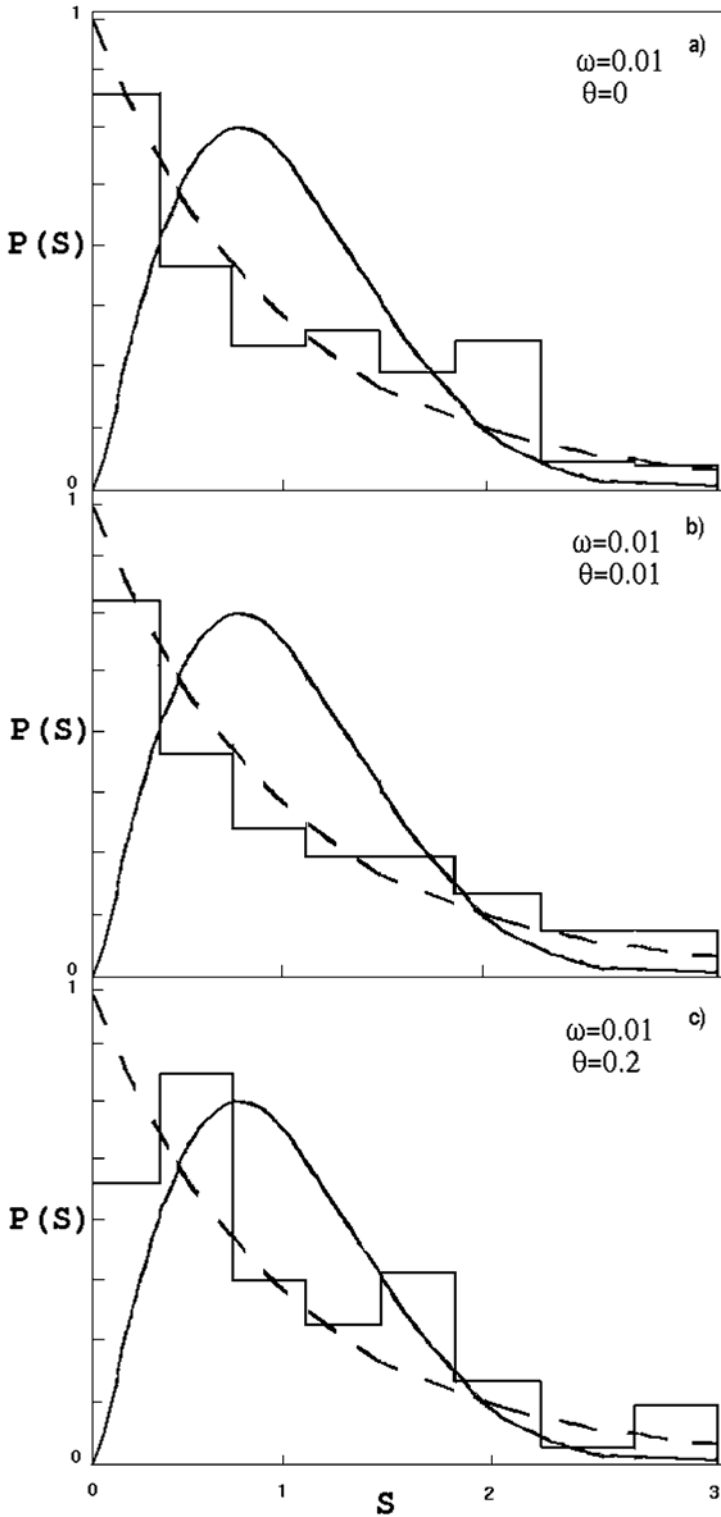
Figure 1. The level spacing distributions for different temperatures a) $\theta = 0$ (zero-temperature case); b) $\theta = 0.01$; c) $\theta = 0.2$ at the fixed $\omega = 0.01$.

Index